INTRODUCTION TO RADAR SYSTEMS

THIRD EDITION

Merrill I. Skolnik

Tata McGraw-Hill Publishing Company Limited
NEW DELHI

McGraw-Hill Offices
New Delhi New York St Louis San Francisco Auckland Bogotá
Caracas Kuala Lumpur Lisbon London Madrid Mexico City Milan
Montreal San Juan Santiago Singapore Sydney Tokyo Toronto

TK
6575
.S477
2003

Tata McGraw-Hill

INTRODUCTION TO RADAR SYSTEMS

Copyright © 2001, 1980, 1962 by The McGraw-Hill Companies, Inc. All rights reserved. No part of this publication may be reproduced or distributed in any form or by any means, or stored in a database or retrieval system, without the prior written permission of the publisher, with the exception that the program listings may be entered, stored, and executed in a computer system, but they may not be reproduced for publication

Tata McGraw-Hill Edition 2001

Eighth reprint 2003
RALQCRYDRQDQB

Reprinted in India by arrangement with The McGraw-Hill Companies, Inc., New York

Sales territories: India, Nepal, Bangladesh, Sri Lanka and Bhutan

ISBN 0-07-044533-8

Published by Tata McGraw-Hill Publishing Company Limited,
7 West Patel Nagar, New Delhi 110 008, and printed at
Pushp Print Services, Delhi 110 053

The McGraw-Hill Companies

BRIEF CONTENTS

CONTENTS

PREFACE

The technology and applications of radar have continued to grow since the previous edition of this book was published in 1980. Among the many new radar systems that have appeared since then are:

- Enhanced meteorological radars (Nexrad, Terminal Doppler Weather Radar, Wind Profiler, TRMM satellite weather radar, and airborne wind-shear detection radar)
- Planetary exploration (Magellan for Venus; Cassini for Titan, a moon of Saturn)
- Interferometric SAR, for three-dimensional images of a scene and for detection of slowly moving surface targets
- Inverse synthetic aperture radar, ISAR (APS-137 for the recognition of ships)
- Ground penetrating radar
- Serial production of phased array radars (Patriot, Aegis, Pave Paws, and B-1B bomber)
- Active-aperture phased arrays
- Ballistic missile defense radars (GBR and Arrow)
- HF over-the-horizon radars (ROTHR and Jindalee)
- Battlefield surveillance (JSTARS)
- Radars for the remote sensing of the environment
- Improved air-traffic control radars
- New multifunction airborne military fighter/attack radars with sophisticated doppler processing

In addition, there have been extensive advances in the use of digital technology for signal processing, data processing, and radar control; significant improvements in the use of doppler for detecting small moving targets in heavy clutter; better understanding of the characteristics of radar echoes from the ground and the sea; automation of the detection decision and information extraction; target recognition; advancement of solid-state transmitters as well as electron power tubes; and development of unattended, highly reliable radar systems. Furthermore, the need for significant improvements in military radar is driven by advances in stealth (low cross-section targets), high-speed attackers at low as well as high altitude, and the increased capability of electronic warfare techniques.

The third edition of *Introduction to Radar Systems*, like its prior two editions, is based on a one-year graduate course designed to introduce the fundamentals of radar and the systems aspects of radar. The book also can be used for self-study, and it is a reference tool suitable for engineers and managers working in the various areas that contribute to the development, procurement, manufacture, and application of radar and related systems.

An examination of the catalogs of most engineering schools will show there are very few courses concerned with the *systems* that are the reason electrical engineering exists at all. The heart of engineering is the system designed to perform some useful function.

Radar is a classic example of an electronic engineering system that utilizes many of the specialized elements of technology practiced by electrical engineers, including signal processing, data processing, waveform design, electromagnetic scattering, detection, parameter estimation, information extraction, antennas, propagation, transmitters, and receivers. These topics, as they affect radar systems, are part of the discussion of radar in this text. Some are touched on lightly, others are discussed in more detail.

The book also includes such specific radar topics as the range equation needed for the basic understanding of radar as well as serve as a tool for system design; the use of the doppler frequency shift to separate moving target echoes from echoes received from the stationary (clutter) environment, as in moving target indication (MTI) radar and pulse doppler radar; the tracking of targets with monopulse and conical scan radars; target tracking with surveillance radars; detection of radar signals; the matched filter which maximizes the signal-to-noise ratio; accuracy of radar measurements; and the characteristics of echoes from the natural environment that affect the performance of radar.

This third edition, just as was the second edition, has been extensively revised. Almost every paragraph has had changes or has been replaced in its entirety. The order of the chapters has been rearranged to reflect how the author covers the material in his own graduate course. The first term (Chaps. 1 through 4) introduces many of the basic concepts of radar through the development of the very important and widely used radar range equation, the use of the doppler frequency shift to extract weak moving-target echo signals from much stronger land and sea clutter echoes, and the use of radar for tracking moving targets. Most of Chap. 8, on the propagation of radar waves, usually is included in the first term, and is discussed as part of the radar equation of Chap. 2. The second term (Chaps. 5 to 7 and 9) covers the detection of signals in noise, extraction of information from radar signals, waveforms, detection of targets when clutter rather than noise is the dominant factor that limits radar performance, and the many variations of the radar antenna. When time permits, the radar transmitter and receiver are discussed, as well as a review of several major radar applications (not part of the book). Sometimes, the subject of transmitters or receivers is introduced in the first term by asking the student to provide a short paper on some aspect of either of these radar subsystems.

A number of the topics in the second edition have been expanded in this third edition because of the availability of new information and because of their increased importance. Because of the publisher's need to keep the book to a reasonable size, several topics had to be removed to accommodate the expansion of others. Some of the topics left out are those that have become obsolete; for example, several methods for phase shifting in phased-array antennas and various types of dispersive delay lines for FM pulse compression. Chapter 3 of the second edition, on CW and frequency modulated radar, has been omitted because of the decreasing utilization of this type of radar. Low-power CW and frequency modulated CW radars will still be used for some special applications, and are briefly included at the end of the current Chap. 3; but long-range, high-power CW radars, with their need to employ separate and isolated antennas for transmitting and receiving, have been largely replaced by the pulse doppler radar that uses a single antenna. Another deletion is the entire last chapter of the second edition. That chapter consisted of short summaries of various system topics such as synthetic aperture radar, HF over-the-horizon radar, air-surveillance radar, height finder and 3D radar, electronic counter-

countermeasures, bistatic radar, and millimeter wave radar. Although these are still important radar topics, they could not be part of this edition if advances in other radar topics were to be included. There are other radar system applications that would be worth discussing, but it is difficult to cover adequately all the important aspects of radar in one volume.

In the first edition there was a single chapter on radar antennas. In the second edition, antennas were covered in two chapters: one on reflector antennas and the other on phased arrays. In this third edition, the subject is again covered in one chapter, which is the longest chapter in the book. By covering antennas in one chapter instead of two, it was easier to treat subjects common to both reflectors and arrays. The antenna chapter is also large because of the distinctive and significant role that the antenna plays in radar.

There are more topics included in this text than can be covered in the usual two-term graduate course. Many of the topics are included for the benefit of the practicing engineer or manager who uses this text as a reference. Thus, the instructor should select which topics to omit, depending on the objectives of the particular course.

It is recognized that the mks system of units is commonly used in university courses and in most of the world; but in this edition the use of mixed units is continued since it seems to be the current practice found in engineering, especially in the United States. (International air-traffic control systems, for example, still give the range in nautical miles and the altitude in feet.) Also, in this book when a value of some quantity is quoted from a published paper, the units found in that paper are used rather than converted to other units. Someday all units will likely be mks, but until that time the engineer should be acquainted with mixed units since they are still found in practice.

The decibel, or dB, is used throughout radar engineering, and it is used widely in this text. Some students do not seem to be too practiced in its use. As a reminder, dB is defined as 10 times the log of a *power* ratio or a parameter related to a power unit (such as antenna gain). If a ratio of two powers is always taken when considering dB, there never need be confusion as to whether the multiplying constant is 10 or is 20; it will always be 10. Also one has to be careful about using equations when some parameters are given in dB but in the equation the parameter is a numeric. The dB has to be converted to a numeric rather than substitute the dB value directly into the equation.

This edition includes problems and questions at the end of each chapter for the benefit of readers (as well as instructors) using this book as a graduate text for a course in radar. They should also be an aid in self-study for the working engineer. Being a systems-oriented course, it is difficult to provide the type of problems usually found in the problem-solving courses often taught in engineering schools. In some of the problems or questions, the methods or equations leading to the answers can be found in the text and help reinforce what has been covered. Other problems, however, attempt to extend the material in the text so the reader will have to stretch his or her own thinking in seeking an answer. A solutions manual for these problems and questions should be available from the publisher, McGraw-Hill.

In my own radar course, I have found the comprehensive term paper to be an important learning tool. I usually try to provide a relatively straightforward concept-design task that the student is not likely to find in the published literature. (This has gotten harder to do as radar progresses over the years.) A term paper has always been assigned in the

second term. Sometimes I have included a paper in the first term on a simpler topic than used in the second term. Term paper topics I have used or considered in the past are also listed in the solutions manual.

As with the other two editions, I have tried to include adequate references to acknowledge the sources of my information and to indicate where the reader interested in digging further might obtain more information on a particular topic. The *Radar Handbook*, also published by McGraw-Hill, is a good source for more advanced information about many of the topics included in this book. Each chapter of the *Radar Handbook* was written by one or more accomplished experts in the particular field covered by the chapter.

In the first edition (1962) of *Introduction to Radar Systems*, almost all of the references were "recent" since radar was relatively new. The early publications on radar began to appear in the literature in the middle to late 1940s, about 15 or 16 years prior to the publication of the first edition. Therefore, the first edition contained many "up to date" references. In this third edition, I have attempted to provide recent references, when they exist, along with early ones; but this was not always possible since some subjects, still of importance, have matured and have not been extended in recent years. Thus there are a number of references in this edition that are 30 to 40 years old. Some were included in the first or second editions, but a few of the older references were not in either of the previous editions since the subjects they cover lay dormant for many years until technology and/or the need for them caught up.

A book of this nature, which covers many diverse topics on many aspects of radar, depends on technical publications in the open literature written by radar engineers. I have relied on such publications in preparing this book, and it is with gratitude that I acknowledge the significant help I have received from the vast literature on radar that now exists.

Merrill I. Skolnik

chapter

1

An Introduction to Radar

1.1 BASIC RADAR

Radar is an electromagnetic system for the detection and location of reflecting objects such as aircraft, ships, spacecraft, vehicles, people, and the natural environment. It operates by radiating energy into space and detecting the echo signal reflected from an object, or target. The reflected energy that is returned to the radar not only indicates the presence of a target, but by comparing the received echo signal with the signal that was transmitted, its location can be determined along with other target-related information. Radar can perform its function at long or short distances and under conditions impervious to optical and infrared sensors. It can operate in darkness, haze, fog, rain, and snow. Its ability to measure distance with high accuracy and in all weather is one of its most important attributes.

The basic principle of radar is illustrated in Fig. 1.1. A transmitter (in the upper left portion of the figure) generates an electromagnetic signal (such as a short pulse of sinewave) that is radiated into space by an antenna. A portion of the transmitted energy is intercepted by the target and reradiated in many directions. The reradiation directed back towards the radar is collected by the radar antenna, which delivers it to a receiver. There it is processed to detect the presence of the target and determine its location. A single antenna is usually used on a time-shared basis for both transmitting and receiving when the radar waveform is a repetitive series of pulses. The range, or distance, to a target is found by measuring the time it takes for the radar signal to travel to the target and return back to the radar. (Radar engineers use the term *range* to mean *distance,* which is

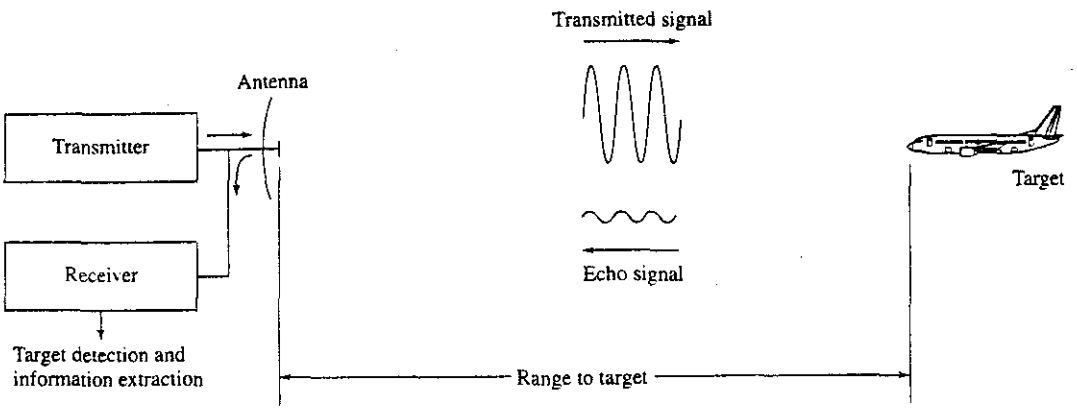

Figure 1.1 Basic principle of radar.

not the definition of range found in some dictionaries.*) The target's location in angle can be found from the direction the narrow-beamwidth radar antenna points when the received echo signal is of maximum amplitude. If the target is in motion, there is a shift in the frequency of the echo signal due to the doppler effect. This frequency shift is proportional to the velocity of the target relative to the radar (*also called the radial velocity*). The doppler frequency shift is widely used in radar as the basis for separating desired moving targets from fixed (unwanted) "clutter" echoes reflected from the natural environment such as land, sea, or rain. Radar can also provide information about the nature of the target being observed.

The term *radar* is a contraction of the words *ra*dio *d*etection *a*nd *r*anging. The name reflects the importance placed by the early workers in this field on the need for a device to detect the presence of a target and to measure its range. Although modern radar can extract more information from a target's echo signal than its range, the measurement of range is still one of its most important functions. There are no competitive techniques that can accurately measure long ranges in both clear and adverse weather as well as can radar.

Range to a Target The most common radar signal, or waveform, is a series of short-duration, somewhat rectangular-shaped pulses modulating a sinewave carrier. (This is sometimes called a *pulse train.*) The range to a target is determined by the time T_R it takes the radar signal to travel to the target and back. Electromagnetic energy in free space travels with the speed of light, which is $c = 3 \times 10^8$ m/s. Thus the time for the signal to travel to a target located at a range R and return back to the radar is $2R/c$. The range to a target is then

$$R = \frac{cT_R}{2} \qquad [1.1]$$

*Webster's New Collegiate Dictionary defines *range* as "the horizontal distance to which a projectile can be propelled" or "the horizontal distance between a weapon and target." This is not how the term is used in radar. On the other hand, the dictionary defines *range finder* as "an instrument . . . to determine the distance to a target," which is its meaning in radar.

With the range in kilometers or in nautical miles, and T in microseconds, Eq. (1.1) becomes

$$R(\text{km}) = 0.15\ T_R\ (\mu\text{s}) \qquad \text{or} \qquad R(\text{nmi}) = 0.081\ T_R\ (\mu\text{s})$$

Each microsecond of round-trip travel time corresponds to a distance of 150 meters, 164 yards, 492 feet, 0.081 nautical mile, or 0.093 statute mile. It takes 12.35 μs for a radar signal to travel a nautical mile and back.

Maximum Unambiguous Range Once a signal is radiated into space by a radar, sufficient time must elapse to allow all echo signals to return to the radar before the next pulse is transmitted. The rate at which pulses may be transmitted, therefore, is determined by the longest range at which targets are expected. If the time between pulses T_p is too short, an echo signal from a long-range target might arrive *after* the transmission of the next pulse and be mistakenly associated with that pulse rather than the actual pulse transmitted earlier. This can result in an incorrect or ambiguous measurement of the range. Echoes that arrive after the transmission of the next pulse are called *second-time-around echoes* (or *multiple-time-around echoes* if from even earlier pulses). Such an echo would appear to be at a closer range than actual and its range measurement could be misleading if it were not known to be a second-time-around echo. The range beyond which targets appear as second-time-around echoes is the *maximum unambiguous range*, R_{un}, and is given by

$$R_{\text{un}} = \frac{cT_p}{2} = \frac{c}{2f_p} \qquad [1.2]$$

where T_p = pulse repetition period = $1/f_p$, and f_p = pulse repetition frequency (prf), usually given in hertz or pulses per second (pps). A plot of the maximum unambiguous range as a function of the pulse repetition frequency is shown in Fig. 1.2. The term *pulse repetition rate* is sometimes used interchangeably with *pulse repetition frequency*.

Radar Waveforms The typical radar utilizes a pulse waveform, an example of which is shown in Fig. 1.3. The peak power in this example is P_t = 1 MW, pulse width τ = 1 μs, and pulse repetition period T_p = 1 ms = 1000 μs. (The numbers shown were chosen for illustration and do not correspond to any particular radar, but they are similar to what might be expected for a medium-range air-surveillance radar.) The pulse repetition frequency f_p is 1000 Hz, which provides a maximum unambiguous range of 150 km, or 81 nmi. The average power (P_{av}) of a repetitive pulse-train waveform is equal to $P_t\tau/T_p = P_t\tau f_p$, so the average power in this case is $10^6 \times 10^{-6}/10^{-3} = 1$ kW. The *duty cycle* of a radar waveform is defined as the ratio of the total time the radar is radiating to the total time it could have radiated, which is $\tau/T_p = \tau f_p$, or its equivalent P_{av}/P_t. In this case the duty cycle is 0.001. The energy of the pulse is equal to $P_t\tau$, which is 1 J (joule). If the radar could detect a signal of 10^{-12} W, the echo would be 180 dB below the level of the signal that was transmitted. A short-duration pulse waveform is attractive since the strong transmitter signal is not radiating when the weak echo signal is being received.

With a pulse width τ of 1 μs, the waveform extends in space over a distance $c\tau$ = 300 m. Two equal targets can be recognized as being resolved in range when they

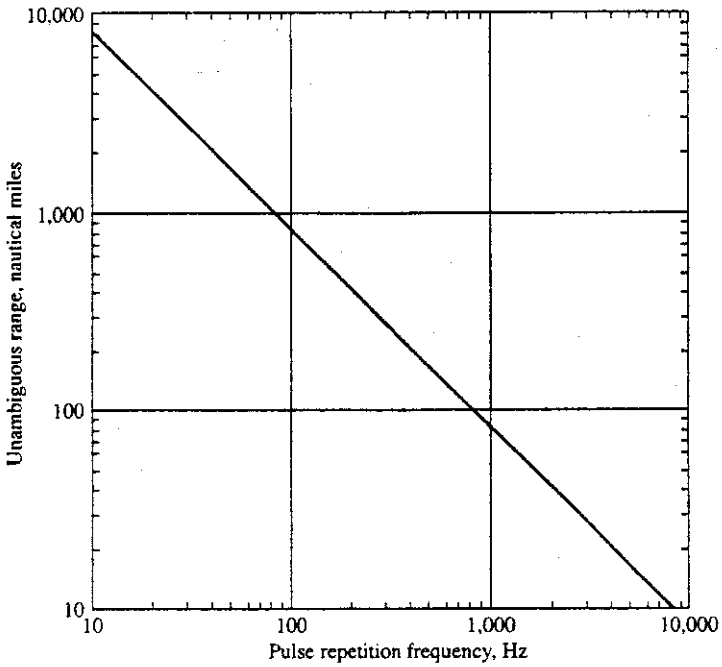

Figure 1.2 Plot of Eq. (1.2), the maximum unambiguous range R_{un} as a function of the pulse repetition frequency f_p.

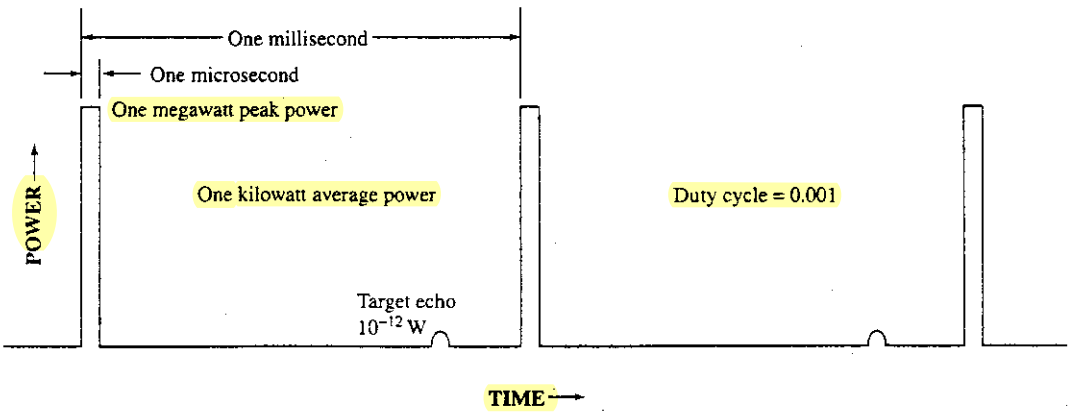

Figure 1.3 Example of a pulse waveform, with "typical" values for a medium-range air-surveillance radar. The rectangular pulses represent pulse-modulated sinewaves.

are separated a distance half this value, or $c\tau/2$. The factor of one-half results from the two-way travel of the radar wave. For example, when $\tau = 1$ μs, two equal size targets can be resolved if they are separated by 150 m.

A very long pulse is needed for some long-range radars to achieve sufficient energy to detect small targets at long range. A long pulse, however, has poor resolution in the range dimension. Frequency or phase modulation can be used to increase the spectral width of a long pulse to obtain the resolution of a short pulse. This is called *pulse compression*, and is described in Sec. 6.5. Continuous wave (CW) waveforms have also been used in radar. Since they have to receive while transmitting, CW radars depend on the doppler frequency shift of the echo signal, caused by a moving target, to separate in the frequency domain the weak echo signal from the large transmitted signal and the echoes from fixed clutter (land, sea, or weather), as well as to measure the radial velocity of the target (Sec. 3.1). A simple CW radar does not measure range. It can obtain range, however, by modulating the carrier with frequency or phase modulation. An example is the frequency modulation (FM-CW) waveform used in the radar altimeter that measures the height (altitude) of an aircraft above the earth.

Pulse radars that extract the doppler frequency shift are called either *moving target indication* (MTI) or *pulse doppler* radars, depending on their particular values of pulse repetition frequency and duty cycle. An MTI radar has a low prf and a low duty cycle. A pulse doppler radar, on the other hand, has a high prf and a high duty cycle. Both types of doppler radars are discussed in Chap. 3. Almost all radars designed to detect aircraft use the doppler frequency shift to reject the large unwanted echoes from stationary clutter.

1.2 THE SIMPLE FORM OF THE RADAR EQUATION

The radar equation relates the range of a radar to the characteristics of the transmitter, receiver, antenna, target, and the environment. It is useful not only for determining the maximum range at which a particular radar can detect a target, but it can serve as a means for understanding the factors affecting radar performance. It is also an important tool to aid in radar system design. In this section, the simple form of the radar range equation is derived.

If the transmitter power P_t is radiated by an isotropic antenna (one that radiates uniformly in all directions), the *power density* at a distance R from the radar is equal to the radiated power divided by the surface area $4\pi R^2$ of an imaginary sphere of radius R, or

$$\text{Power density at range } R \text{ from an isotropic antenna} = \frac{P_t}{4\pi R^2} \qquad [1.3]$$

Power density is measured in units of watts per square meter. Radars, however, employ *directive* antennas (with narrow beamwidths) to concentrate the radiated power P_t in a particular direction. The *gain* of an antenna is a measure of the increased power density radiated in some direction as compared to the power density that would appear in that

direction from an isotropic antenna. The maximum gain G of an antenna may be defined as

$$G = \frac{\text{maximum power density radiated by a directive antenna}}{\text{power density radiated by a lossless isotropic antenna with the same power input}}$$

The power density at the target from a directive antenna with a transmitting gain G is then

$$\text{Power density at range } R \text{ from a directive antenna} = \frac{P_t G}{4\pi R^2} \qquad [1.4]$$

The target intercepts a portion of the incident energy and reradiates it in various directions. It is only the power density reradiated in the direction of the radar (the echo signal) that is of interest. The *radar cross section of the target* determines the power density returned to the radar for a particular power density incident on the target. It is denoted by σ and is often called, for short, *target cross section, radar cross section,* or simply *cross section.* The radar cross section is defined by the following equation:

$$\text{Reradiated power density back at the radar} = \frac{P_t G}{4\pi R^2} \cdot \frac{\sigma}{4\pi R^2} \qquad [1.5]$$

The radar cross section has units of area, but it can be misleading to associate the radar cross section directly with the target's physical size. Radar cross section is more dependent on the target's shape than on its physical size, as discussed in Sec. 2.7.

The radar antenna captures a portion of the echo energy incident on it. The power received by the radar is given as the product of the incident power density [Eq. (1.5)] times the effective area A_e of the receiving antenna. The effective area is related to the physical area A by the relationship $A_e = \rho_a A$, where ρ_a = antenna aperture efficiency. The received signal power P_r (watts) is then

$$P_r = \frac{P_t G}{4\pi R^2} \cdot \frac{\sigma}{4\pi R^2} \cdot A_e = \frac{P_t G A_e \sigma}{(4\pi)^2 R^4} \qquad [1.6]$$

The maximum range of a radar $R_{\max}$ is the distance beyond which the target cannot be detected. It occurs when the received signal power P_r just equals the minimum detectable signal $S_{\min}$. Substituting $S_{\min} = P_r$ in Eq. (1.6) and rearranging terms gives

$$R_{\max} = \left[\frac{P_t G A_e \sigma}{(4\pi)^2 S_{\min}}\right]^{1/4} \qquad [1.7]$$

This is the fundamental form of the *radar range equation.* (It is also called, for simplicity, the *radar equation* or *range equation.*) The important antenna parameters are the transmitting gain and the receiving effective area. The transmitter power P_t has not been specified as either the average or the peak power. It depends on how $S_{\min}$ is defined. In this text, however, P_t denotes the peak power.

If the same antenna is used for both transmitting and receiving, as it usually is in radar, antenna theory gives the relationship between the transmit gain G and the receive effective area A_e as[1,2]

$$G = \frac{4\pi A_e}{\lambda^2} = \frac{4\pi \rho_a A}{\lambda^2} \qquad [1.8]$$

where λ = wavelength. (Wavelength $\lambda = c/f$, where c = velocity of propagation and f = frequency.) Equation (1.8) can be substituted in Eq. (1.7), first for A_e and then for G, to give two other forms of the radar equation

$$R_{\max} = \left[\frac{P_t G^2 \lambda^2 \sigma}{(4\pi)^3 S_{\min}}\right]^{1/4} \tag{1.9}$$

$$R_{\max} = \left[\frac{P_t A_e^2 \sigma}{4\pi \lambda^2 S_{\min}}\right] \tag{1.10}$$

These three forms of the radar equation [Eqs. (1.7), (1.9), and (1.10)] are basically the same; but there are differences in interpretation. For example, from Eq. (1.9) it might be concluded that the maximum range varies as $\lambda^{1/2}$, but Eq. (1.10) indicates the variation with range as $\lambda^{-1/2}$, which is just the opposite. On the other hand, Eq. (1.7) gives no explicit wavelength dependence for the range. The correct interpretation depends on whether the antenna gain is held constant with change in wavelength, or frequency, as implied by Eq. (1.9); or the effective area is held constant, as implied by Eq. (1.10). For Eq. (1.7) to be independent of frequency, two antennas have to be used. The transmitting antenna has to have a gain independent of wavelength and the receiving antenna has to have an effective aperture independent of wavelength. (This is seldom done, however.)

These simplified versions of the radar equation do not adequately describe the performance of actual radars. Many important factors are not explicitly included. The simple form of the radar range equation predicts too high a value of range, sometimes by a factor of two or more. In Chap. 2 the simple form of the radar equation is expanded to include other factors that allow the equation to be in better agreement with the observed range performance of actual radars.

1.3 RADAR BLOCK DIAGRAM

The operation of a pulse radar may be described with the aid of the simple block diagram of Fig. 1.4. The transmitter may be a *power amplifier*, such as the klystron, traveling wave tube, or transistor amplifier. It might also be a power oscillator, such as the magnetron. The magnetron oscillator has been widely used for pulse radars of modest capability; but the amplifier is preferred when high average power is necessary, when other than simple pulse waveforms are required (as in pulse compression), or when good performance is needed in detecting moving targets in the midst of much larger clutter echoes based on the doppler frequency shift (the subject of Chap. 3). A power amplifier is indicated in Fig. 1.4. The radar signal is produced at low power by a *waveform generator*, which is then the input to the power amplifier. In most power amplifiers, except for solid-state power sources, a modulator (Sec. 10.7) turns the transmitter on and off in synchronism with the input pulses. When a power oscillator is used, it is also turned on and off by a *pulse modulator* to generate a pulse waveform.

The output of the transmitter is delivered to the *antenna* by a waveguide or other form of transmission line, where it is radiated into space. Antennas can be mechanically steered parabolic reflectors, mechanically steered planar arrays, or electronically steered phased arrays (Chap. 9). On transmit the parabolic reflector focuses the energy into a narrow

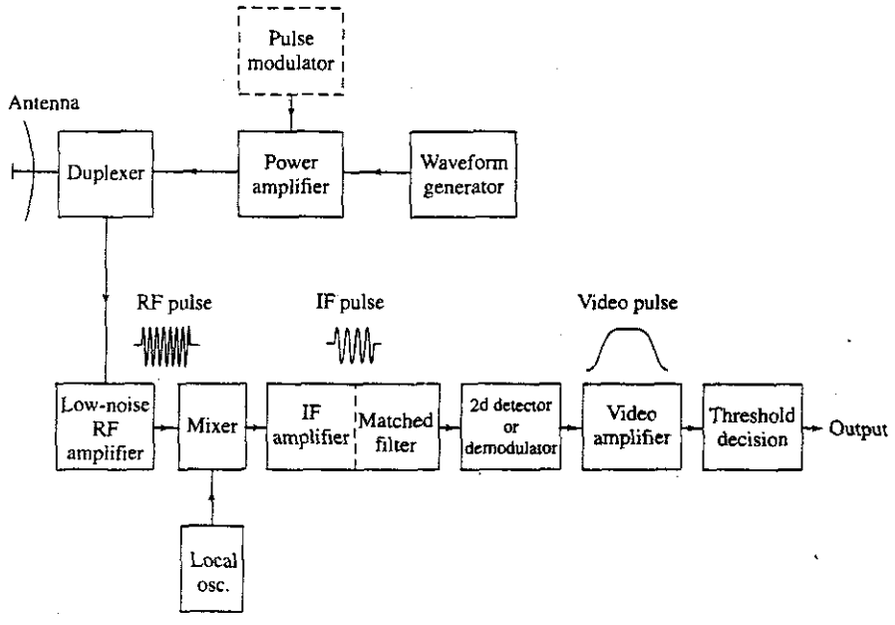

Figure 1.4 Block diagram of a conventional pulse radar with a superheterodyne receiver.

beam, just as does an automobile headlight or a searchlight. A phased array antenna is a collection of numerous small radiating elements whose signals combine in space to produce a radiating plane wave. Using phase shifters at each of the radiating elements, an electronically steered phased array can rapidly change the direction of the antenna beam in space without mechanically moving the antenna. When no other information is available about the antenna, the beamwidth (degrees) of a "typical" parabolic reflector is often approximated by the expression $65\ \lambda/D$, where D is the dimension of the antenna in the same plane as the beamwidth is measured, and λ is the radar wavelength. For example, an antenna with a horizontal dimension $D = 32.5$ wavelengths has an azimuth beamwidth of 2°. At a frequency of 3 GHz ($\lambda = 10$ cm), the antenna would be 3.25 m, or 10.7 ft, in extent. The rotation of a surveillance radar antenna through 360° in azimuth is called an antenna *scan*. A typical scan rate (or rotation rate) for a long-range civil air-traffic control air-surveillance radar might be 6 rpm. Military air-surveillance radars generally require a higher rotation rate.

The *duplexer* allows a single antenna to be used on a time-shared basis for both transmitting and receiving. The duplexer is generally a gaseous device that produces a short circuit (an arc discharge) at the input to the receiver when the transmitter is operating, so that high power flows to the antenna and not to the receiver. On reception, the duplexer directs the echo signal to the receiver and not to the transmitter. Solid-state ferrite circulators and receiver protector devices, usually solid-state diodes, can also be part of the duplexer.

The receiver is almost always a *superheterodyne*. The input, or RF,* stage can be a low-noise transistor amplifier. The mixer and local oscillator (LO) convert the RF signal

*In electrical engineering, RF is an abbreviation for *radio frequency*; but in radar practice it is understood to mean *radar frequency*. RF also is used to identify that portion of the radar that operates at RF frequencies, even though the inclusion of "frequencies" in this expression might seem redundant.

to an intermediate frequency (IF) where it is amplified by the IF amplifier. The signal bandwidth of a superheterodyne receiver is determined by the bandwidth of its IF stage. The IF frequency, for example, might be 30 or 60 MHz when the pulse width is of the order of 1 μs. (With a 1-μs pulse width, the IF bandwidth would be about 1 MHz.) The IF amplifier is designed as a *matched filter* (Sec. 5.2); that is, one which maximizes the output peak-signal-to-mean-noise ratio. Thus the matched filter maximizes the detectability of weak echo signals and attenuates unwanted signals. With the approximately rectangular pulse shapes commonly used in many radars, conventional radar receiver filters are close to that of a matched filter when the receiver bandwidth B is the inverse of the pulse width τ, or $B\tau \approx 1$.

Sometimes the low-noise input stage is omitted and the mixer becomes the first stage of the receiver. A receiver with a mixer as the input stage will be less sensitive because of the mixer's higher noise figure; but it will have greater dynamic range, less susceptibility to overload, and less vulnerability to electronic interference than a receiver with a low-noise first stage (Sec. 11.3). These attributes of a mixer input stage might be of interest for military radars subject to the noisy environment of hostile electronic countermeasures (ECM).

The IF amplifier is followed by a crystal diode, which is traditionally called the *second detector,* or *demodulator.* Its purpose is to assist in extracting the signal modulation from the carrier. The combination of IF amplifier, second detector, and video amplifier act as an *envelope detector* to pass the pulse modulation (envelope) and reject the carrier frequency. In radars that detect the doppler shift of the echo signal, the envelope detector is replaced by a *phase detector* (Sec. 3.1), which is different from the envelope detector shown here. The combination of IF amplifier and video amplifier is designed to provide sufficient amplification, or gain, to raise the level of the input signal to a magnitude where it can be seen on a display, such as a cathode-ray tube (CRT), or be the input to a digital computer for further processing.

At the output of the receiver a decision is made whether or not a target is present. The decision is based on the magnitude of the receiver output. If the output is large enough to exceed a predetermined threshold, the decision is that a target is present. If it does not cross the threshold, only noise is assumed to be present. The threshold level is set so that the rate at which false alarms occur due to noise crossing the threshold (in the absence of signal) is below some specified, tolerable value. This is fine if the noise remains constant, as when receiver noise dominates. If, on the other hand, the noise is external to the radar (as from unintentional interference or from deliberate noise jamming) or if clutter echoes (from the natural environment) are larger than the receiver noise, the threshold has to be varied adaptively in order to maintain the false alarm rate at a constant value. This is accomplished by a *constant false alarm rate* (CFAR) receiver (Sec. 5.7).

A radar usually receives many echo pulses from a target. The process of adding these pulses together to obtain a greater signal-to-noise ratio before the detection decision is made is called *integration.* The integrator is often found in the video portion of the receiver.

The *signal processor* is that part of the radar whose function is to pass the desired echo signal and reject unwanted signals, noise, or clutter. The signal processor is found in the receiver before the detection decision is made. The matched filter, mentioned previously, is an example of a signal processor. Another example is the doppler filter that

separates desired moving targets (whose echoes are shifted in frequency due to the doppler effect) from undesired stationary clutter echoes.

Some radars process the detected target signal further, in the *data processor,* before displaying the information to an operator. An example is an *automatic tracker,* which uses the locations of the target measured over a period of time to establish the track (or path) of the target. Most modern air-surveillance radars and some surface-surveillance radars generate target tracks as their output rather than simply display detections. Following the data processor, or the decision function if there is no data processor, the radar output is displayed to an operator or used in a computer or other automatic device to provide some further action.

The signal processor and data processor are usually implemented with digital technology rather than with analog circuitry. The analog-to-digital (A/D) converter and digital memory are therefore important in modern radar systems. In some sophisticated radars in the past, the signal and data processors were larger and consumed more power than the transmitter and were a major factor in determining the overall radar system reliability; but this should not be taken as true in all cases.

A typical radar display for a surveillance radar is the PPI, or *plan position indicator* (the full term is seldom used). An example is shown in Fig. 1.5. The PPI is a presentation

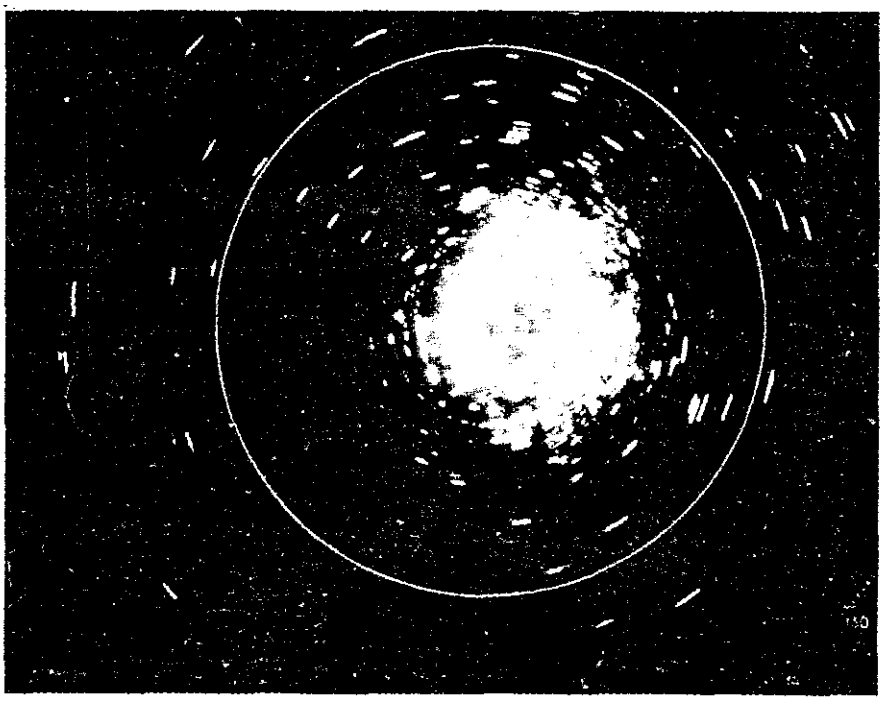

Figure 1.5 Example of a PPI (plan position indicator) display. This is the output of an L-band radar with an antenna beam-width of 3°, without MTI processing. The range ring has a radius of 50 nmi. Clutter is seen in the near vicinity of the radar. Aircraft approaching an airport are seen in the northwest direction.

(Courtesy of George Linde of the Naval Research Laboratory.)

that maps in polar coordinates the location of the target in azimuth and range. The PPI in the past has been implemented with an intensity-modulated CRT. The amplitude of the receiver output modulates (turns on or off) the electron-beam intensity (called the z-axis of the CRT) as the electron beam is made to sweep outward (the range coordinate) from the center of the tube. The sweep of the electron beam rotates in angle in synchronism with the pointing of the antenna beam. A B-scope display is similar to a PPI except that it utilizes a rectangular format, rather than the polar format, to display range versus angle. Both the PPI and the B-scope CRT displays have limited dynamic range since they are intensity modulated. An A-scope is sometimes used for special purposes. It is an amplitude-modulated rectangular display that presents the receiver output on the y-axis and the range (or time delay) on the x-axis. (An example is shown in Fig. 7.21.) It is more suited for tracking radar or continuous staring applications than as a display for surveillance radar.

The early radars displayed to an operator *raw video*, which is the output of the radar receiver without further processing (with the exception of the matched filter). Modern radars usually present *processed video*, which is the output of the radar after signal processing and threshold detection or after automatic tracking. Only processed target detections or target tracks are presented. This relieves the burden on the operator, but processed video can also eliminate information about the environment and unusual operational situations that a trained and alert operator might be able to recognize and interpret.

Radars can operate in various modes by radiating different frequencies, with different polarizations. (The polarization of the radar wave is defined by the direction of the electric field vector.) The radar can also employ various waveforms with different pulse widths, pulse repetition frequencies, or other modulations; and different forms of processing for suppressing different types of clutter, interference, and jamming. The various waveforms and processing need to be selected wisely. A trained operator can fulfill this function, but an operator can become overloaded. When there are many available system options, the radar can be designed to automatically determine the proper mode of operation and execute what is required to implement it. The mode of radar operation is often changed as a function of the antenna look-direction and/or range, according to the nature of the environment.

1.4 RADAR FREQUENCIES

Conventional radars generally operate in what is called the *microwave* region (a term not rigidly defined). Operational radars in the past have been at frequencies ranging from about 100 MHz to 36 GHz, which covers more than eight octaves. These are not necessarily the limits. Operational HF over-the-horizon radars operate at frequencies as low as a few megahertz. At the other end of the spectrum, experimental millimeter wave radars have been at frequencies higher than 240 GHz.

During World War II, letter codes such as *S*, *X*, and *L* were used to designate the distinct frequency bands at which microwave radar was being developed. The original purpose was to maintain military secrecy; but the letter designations were continued after the war as a convenient shorthand means to readily denote the region of the spectrum at which

a radar operated. Their usage is the accepted practice of radar engineers. Table 1.1 lists the radar-frequency letter-band designations approved as an IEEE Standard.[3] These are related to the specific frequency allocations assigned by the International Telecommunications Union (ITU) for radiolocation, or radar. For example, *L* band officially extends from 1000 MHz to 2000 MHz, but *L*-band radar is only allowed to operate within the region from 1215 to 1400 MHz since that is the band assigned by the ITU.

There have been other letter-band designations, but Table 1.1 is the only set of designations approved by the IEEE for radar. It has also been recognized by being listed in the U. S. Department of Defense Index of Specifications and Standards.[4] A different set of letter bands has been used by those working in electronic warfare. It was originally formulated by the U.S. Department of Defense for use only in conducting electronic countermeasure exercises.[5] Sometimes it is incorrectly extended to describe radar frequencies, but the use of the electronic warfare letter bands for radar can be confusing and it is not appropriate. (There may be *J*-band jammers, but according to the IEEE Letter-Band Standards there are no *J*-band radars.) Usually the context in which the nomenclature is employed can aid in distinguishing whether the letters refer to radar or to EW.

Table 1.1 IEEE standard radar-frequency letter-band nomenclature*

Band Designation	Nominal Frequency Range	Specific Frequency Ranges for Radar based on ITU Assignments in Region 2
HF	3–30 MHz	
VHF	30–300 MHz	138–144 MHz 216–225 MHz
UHF	300–1000 MHz	420–450 MHz 850–942 MHz
L	1–2 GHz	1215–1400 MHz
S	2–4 GHz	2300–2500 MHz 2700–3700 MHz
C	4–8 GHz	5250–5925 MHz
X	8–12 GHz	8500–10,680 MHz
K_u	12–18 GHz	13.4–14.0 GHz 15.7–17.7 GHz
K	18–27 GHz	24.05–24.25 GHz
K_a	27–40 GHz	33.4–36 GHz
V	40–75 GHz	59–64 GHz
W	75–110 GHz	76–81 GHz 92–100 GHz
mm	110–300 GHz	126–142 GHz 144–149 GHz 231–235 GHz 238–248 GHz

*From "IEEE Standard Letter Designations for Radar-Frequency Bands," IEEE Std 521–1984.

Letter-band nomenclature is not a substitute for the actual numerical frequencies at which a radar operates. The specific numerical frequencies of a radar should be used whenever appropriate, but the letter designations of Table 1.1 should be used whenever a short notation is desired.

1.5 APPLICATIONS OF RADAR

Radar has been employed to detect targets on the ground, on the sea, in the air, in space, and even below ground. The major areas of radar application are briefly described below.

Military Radar is an important part of air-defense systems as well as the operation of offensive missiles and other weapons. In air defense it performs the functions of surveillance and weapon control. Surveillance includes target detection, target recognition, target tracking, and designation to a weapon system. Weapon-control radars track targets, direct the weapon to an intercept, and assess the effectiveness of the engagement (called *battle damage assessment*). A missile system might employ radar methods for guidance and fuzing of the weapon. High-resolution imaging radars, such as synthetic aperture radar, have been used for reconnaissance purposes and for detecting fixed and moving targets on the battlefield. Many of the civilian applications of radar are also used by the military. The military has been the major user of radar and the major means by which new radar technology has been developed.

Remote Sensing All radars are remote sensors; however, this term is used to imply the sensing of the environment. Four important examples of radar remote sensing are (1) weather observation, which is a regular part of TV weather reporting as well as a major input to national weather prediction; (2) planetary observation, such as the mapping of Venus beneath its visually opaque clouds; (3) short-range below-ground probing; and (4) mapping of sea ice to route shipping in an efficient manner.

Air Traffic Control (ATC) Radars have been employed around the world to safely control air traffic in the vicinity of airports (Air Surveillance Radar, or ASR), and en route from one airport to another (Air Route Surveillance Radar, or ARSR) as well as ground-vehicular traffic and taxiing aircraft on the ground (Airport Surface Detection Equipment, or ASDE). The ASR also maps regions of rain so that aircraft can be directed around them. There are also radars specifically dedicated to observing weather (including the hazardous downburst) in the vicinity of airports, which are called Terminal Doppler Weather Radar, or TDWR. The Air Traffic Control Radar Beacon System (ATCRBS and Mode-S) widely used for the control of air traffic, although not a radar, originated from military IFF (Identification Friend or Foe) and uses radar-like technology.

Law Enforcement and Highway Safety The radar speed meter, familiar to many, is used by police for enforcing speed limits. (A variation is used in sports to measure the speed of a pitched baseball.) Radar has been considered for making vehicles safer by warning

of pending collision, actuating the air bag, or warning of obstructions or people behind a vehicle or in the side blind zone. It is also employed for the detection of intruders.

Aircraft Safety and Navigation The airborne weather-avoidance radar outlines regions of precipitation and dangerous wind shear to allow the pilot to avoid hazardous conditions. Low-flying military aircraft rely on terrain avoidance and terrain following radars to avoid colliding with obstructions or high terrain. Military aircraft employ ground-mapping radars to image a scene. The radio altimeter is also a radar used to indicate the height of an aircraft above the terrain and as a part of self-contained guidance systems over land.

Ship Safety Radar is found on ships and boats for collision avoidance and to observe navigation buoys, especially when the visibility is poor. Similar shore-based radars are used for surveillance of harbors and river traffic.

Space Space vehicles have used radar for rendezvous and docking, and for landing on the moon. As mentioned, they have been employed for planetary exploration, especially the planet Earth. Large ground-based radars are used for the detection and tracking of satellites and other space objects. The field of radar astronomy using Earth-based systems helped in understanding the nature of meteors, establishing an accurate measurement of the Astronomical Unit (the basic yardstick for measuring distances in the solar system), and observing the moon and nearby planets before adequate space vehicles were available to explore them at close distances.

Other Radar has also found application in industry for the noncontact measurement of speed and distance. It has been used for oil and gas exploration. Entomologists and ornithologists have applied radar to study the movements of insects and birds, which cannot be easily achieved by other means.

Some radar systems are small enough to be held in one's hand. Others are so large that they could occupy several football fields. They have been used at ranges close enough to almost touch the target and at ranges that reach to the planets.

1.6 THE ORIGINS OF RADAR[6,7,8]

The basic concept of radar was first demonstrated by the classical experiments conducted by the German physicist Heinrich Hertz from 1885 to 1888.[9] Hertz experimentally verified the predictions of James Clerk Maxwell's theory of the electromagnetic field published in 1864. Hertz used an apparatus that was similar in principle to a pulse radar at frequencies in the vicinity of 455 MHz. He demonstrated that radio waves behaved the same as light except for the considerable difference in frequency between the two. He showed that radio waves could be reflected from metallic objects and refracted by a dielectric prism.

Hertz received quick and widespread recognition for his work, but he did not pursue its practical applications. This was left to others. The potential of Hertz's work for the

detection and location of reflecting objects—which is what radar does—was advanced by another German, Christian Hulsmeyer. In the early 1900s he assembled an instrument that would today be known as a monostatic (single site) pulse radar. It was much improved over the apparatus used by Hertz. In 1904 he obtained a patent in England[10] and other countries. Hulsmeyer's radar detected ships, and he extensively marketed it for preventing collisions at sea. He demonstrated his apparatus to shipping companies and to the German Navy. Although it was a success and much publicized, there apparently was no interest for a ship collision-avoidance device. His invention and his demonstrations faded from memory and were all but forgotten. Radar would have to be rediscovered a few more times before it eventually became an operational reality.

During the 1920s other evidence of the radar method appeared. S. G. Marconi, the well-known pioneer of wireless radio, observed the radio detection of targets in his experiments and strongly urged its use in a speech delivered in 1922 before the Institute of Radio Engineers (now the IEEE).[11] Apparently unaware of Marconi's speech, A. Hoyt Taylor and Leo C. Young of the U.S. Naval Research Laboratory in Washington, D.C. accidentally observed, in the autumn of 1922, a fluctuating signal at their receiver when a ship passed between the receiver and transmitter located on opposite sides of a river. This was called a *CW wave-interference system*, but today it is known as *bistatic CW radar*. (*Bistatic* means the radar requires two widely separated sites for the transmitter and receiver.) In 1925, the pulse radar technique was used by Breit and Tuve of the Carnegie Institution in Washington, D.C. to measure the height of the ionosphere. The Breit and Tuve apparatus was indeed a radar, but it was not recognized at the time that the same principle might be applied for the detection of ships and aircraft.[12] There were additional reported detections of aircraft and other targets by the CW wave-interference (bistatic radar) method in several countries of the world; but this type of radar did not have, and still doesn't have, significant utility for most applications.

It was the appearance of the heavy military bomber aircraft in the late 1920s and early 1930s that eventually gave rise to operational military radar. After World War I, the bomber was transformed from a fabric-coated biplane with open cockpit to an all-metal, single-wing aircraft with enclosed cockpit, which flew at high altitude over long distance with a heavy bomb load. Long-range warning of the approach of the heavy bomber became an important military need. In most of the countries that responded to this threat, the possible detection methods examined were similar even though the developments were covered by secrecy. Sound locators were the first of the sensors to be examined. They were deployed in many armies up to the start of World War II even though they were recognized much earlier to be inadequate for the task. Attempts were made to detect the spark-plug ignition noise radiated at radio frequencies by the aircraft engine; but they were abandoned once it was realized that the radiated noise could be suppressed by proper shielding. Infrared was examined but it did not have adequate range capability; it was not all-weather; and it did not determine the range of the target. The bistatic CW radar then followed from the accidental detection of aircraft, ships, or other targets as they passed between the transmitter and receiver of a radio system. This two-site configuration was cumbersome and merely acted as a trip wire to detect the passage of a target as it crossed the line connecting transmitter and receiver. The radar method did not become truly useful until the transmitter and receiver were colocated at a single site and pulse waveforms were used.

In the 1930s, radar was rediscovered and developed almost simultaneously and essentially independently in the United States, United Kingdom, Germany, Soviet Union, France, Italy, Japan, and Netherlands. These radars operated at frequencies much lower than those generally used in modern radar. Most early radars employed frequencies in the vicinity of 100 to 200 MHz; but the British Chain Home radars operated at 30 MHz, the low end of the pre-war radar spectrum, while the German 600-MHz Wurzburg radars represented the highest frequencies used operationally early in the war. The technologies employed in these early radars were mostly bold extensions of then current leading-edge technology from the field of radio communications. Compared to microwave radars, they had some limitations, but they did their intended job well.

United States The U.S. Naval Research Laboratory tried to initiate bistatic CW radar development in 1922 and later in 1931; but it was in 1934 that serious effort started when A. Hoyt Taylor and Leo C. Young realized that a single site, pulse radar was necessary for success. By the time of the Japanese attack on the United States at Pearl Harbor on December 7, 1941, 132 radar sets were delivered to the U.S. Navy and 79 were installed on various ships.[13] Twenty of these were the 200 MHz CXAM placed on battleships, aircraft carriers, and cruisers. The Navy radars in the Pacific during the Battle of Midway in 1942 were instrumental in allowing the United States to use its limited forces effectively against the Japanese Navy, which did not have a similar radar capability.

The U.S. Army initiated pulse-radar development in the spring of 1936. At the time of Pearl Harbor, it had developed and deployed overseas a number of 200-MHz SCR-268 antiaircraft searchlight-control radars. The Army also received 112 production units of the 100-MHz SCR-270 long-range air-search radar, one of which detected the Japanese attack on Pearl Harbor. (Radar did its job at Pearl Harbor, but the command and control system to utilize the information was lacking.)

United Kingdom In the mid-1930s, the British felt the urgency of the approaching war far more than did the United States. Although the United Kingdom started later that the United States, they turned on their first operational radar system, the 30-MHz Chain Home radar, by the end of the summer of 1938 (a year before the start of World War II on September 3, 1939). The Chain Home system of radars remained in operation for the entire duration of the war. These early radars have been given much credit for helping turn back the major German air attacks on the British Isles during what was called the Battle of Britain in the late summer of 1940. By 1939, the British also developed a 200-MHz airborne-intercept radar for the detection and intercept of hostile aircraft, especially at night and during conditions of poor visibility. This radar was later modified to detect surface ships and submarines. A highly significant advance in radar technology was made with the British invention of the high-power microwave magnetron in 1940, which opened the higher frequencies to radar. Being overextended by the everyday needs of fighting a major war, the British disclosed the magnetron to the United States in the fall of 1940 for its further development. The cavity magnetron provided the basis for the extensive and rapid development of microwave radar at the MIT Radiation Laboratory and the Bell Telephone Laboratories during World War II, as well as the development of microwave radar in the United Kingdom.

Germany The country of Hertz and Hulsmeyer also had to rediscover radar. By the end of 1940, Germany had three major operational radars:

- The 125-MHz Freya air-search radar was originally developed for the Navy, but the German Air Force also became interested in it as a transportable ground-based early warning radar. Orders were placed for its production by the German Air Force in 1939 and it was employed as a Ground Control of Intercept radar for the control of night fighters. By the start of the war, however, only eight Freyas were available.
- The Wurzburg fire-control radar was used in conjunction with the Freya and similar air-search radars. The 565-MHz radar was introduced in the spring of 1940, and by the end of the war over 4000 Wurzburg radars were procured.
- The 500-MHz Seetakt shipboard radar for ranging on ships to control gunfire was installed by the German Navy on four major ships during 1937–1938. It was used as early as 1937 in support of the rebel side during the Spanish Civil War. The Seetakt was the first military radar deployed operationally by any country. (It took a long time for the British to recognize the existence of the Seetakt radars. One of the German ships carrying this radar was sunk by the British Navy in shallow water off Montevideo in South America in December 1939. Its radar antenna remained visible above the water. Although a British radar expert inspected the antenna and reported it to be part of a radar, the British Admiralty did not pay attention.[14]) Over 100 Seetakt sets were in production at the beginning of the war.

In 1940, Germany probably was ahead of all other countries in radar technology, something the United States and the United Kingdom did not realize until after the end of the war in 1945. Neither the United States nor the United Kingdom had at that time an operational shipboard radar like the Seetakt, and the Wurzburg was considerably in advance of any Allied equivalent.[15] The German military, however, did not exploit their early technical advantage. They realized their mistake when the British commenced large-scale bomber raids on their country. When the Germans finally acted, it was too late to catch up with the fast-moving British and Americans.

USSR The Soviet Union started the pursuit of radar early in the 1930s, and had production radars available by the time of the German invasion of their country in June 1941. Both production radars and development radars were employed for the air defense of Leningrad and Moscow. The first production radar, the RUS-1, was a bistatic CW system that operated at 75 MHz with a 35-km separation between the transmitter and receiver. As mentioned previously, the bistatic radar was not all that might be desired of a sensor system; so at the start of hostilities, the Soviets moved these radars "to the east" and deployed the monostatic truck-mounted RUS-2 pulse-radar system, also at 75 MHz, with a range of 150 km. The German invasion forced the relocation of the major Soviet radar development institutions, which seriously reduced further development.

Italy The Italians did not believe in the importance of radar until their decisive naval defeat in March 1941 by the British Navy in the night Battle of Cape Matapan, where British radar found and fired upon the surprised Italian ships during darkness. This defeat led to

the Italian production of a series of 200-MHz shipboard radars, called the Owl. A significant number were installed on Italian ships. Italian work on radar essentially ceased in 1943 when the country was invaded by the Allies (the United Kingdom and United States).

France As did other countries, the French investigated CW wave-interference (bistatic) radar in the 1930s. They carried the bistatic method further than other countries and installed a system early in the war. It was deployed as a triple fence laid out in a Z-pattern so as to obtain the direction of travel, speed, and altitude of an aircraft target. In the mid-1930s, the French received much publicity for the civilian application of a CW obstacle-detection radar installed on a luxury ocean liner. In 1939, development finally began on a 50-MHz pulse radar, but the occupation of France by the Germans in 1940 virtually closed down their radar development.

Japan The Japanese discovered and developed the microwave magnetron before the British. Although they had a number of different microwave magnetron configurations, they never were able to convert this capability to microwave radars that were comparable to those of the Allies. The Japanese explored bistatic radar in 1936 and deployed it for the defense of their homeland during the war. They initiated pulse radar in 1941, much later than other countries, after the Germans disclosed to them the British use of VHF pulse radar. Japan increased their efforts in radar after being surprised by its successful use at night by the U.S. Navy during the Battle of Guadalcanal in October 1942. Although the Japanese possessed the microwave magnetron and had a fine technical capability, they failed to employ radar as effectively as did other countries because of the dominance of the military over the civilian engineers and scientists in technical matters, the excessive secrecy imposed, and a shortage of engineers and materials.[16,17]

Netherlands Even a small country such as the Netherlands produced radar in time for World War II. A naval UHF pulse radar for air defense was configured, and production of 10 prototypes was started. A demonstration was planned for the military on May 10, 1940, but this turned out to be the day of the German invasion of their country. Nevertheless, the Netherlands managed to put one of their radars, known as the Type 289, on a Dutch ship in combat during the war (operating out of the United Kingdom).

Microwave Magnetron As mentioned, a major advance in radar was made with the invention of the high-power microwave cavity magnetron at the University of Birmingham in England early in World War II. The magnetron dramatically changed the nature of radar as it existed up to that time by allowing the development of radars with small antennas that could be carried on ships and aircraft, and by land-mobile systems. Most countries involved in early radar research recognized the importance of obtaining high power at microwave frequencies and tried to push the conventional magnetron upwards in power, but it was the British who succeeded and insured its use in operational radar. The MIT Radiation Laboratory was organized by the United States in the fall of 1940 to pursue development of microwave radar based on the use of the British magnetron. They were highly successful in applying the new microwave technology to military radar for air, land, and sea.[6] The Radiation Laboratory developed more than 100 different radar systems

during the war years for such purposes as early warning of air attack, antiaircraft fire control, air intercept, blind bombing, and ship detection.

After World War II During the war, radar technology and systems grew rapidly, but there was still much left to do. In the years that immediately followed the war, radar development was mainly concentrated on the things that were not completed during the war. Since that time, radar capability has continued to advance. The following is a list of some of the many major accomplishments of radar:[8]

- The use of the doppler effect in the *MTI* (moving target indication) pulse radar was perfected to separate desired aircraft targets from undesired large ground echoes.
- *High-power stable amplifiers* such as the klystron, traveling wave tube, and solid-state transistor allowed better application of the doppler effect, use of sophisticated waveforms, and much higher power than could be obtained with the magnetron.
- Highly accurate angle tracking of targets became practical with *monopulse radar.*
- *Pulse compression* allowed the use of long waveforms to obtain high energy and simultaneously achieve the resolution of a short pulse by internal modulation of the long pulse.
- The airborne *synthetic aperture radar* (SAR) provided high resolution map-like imaging of ground scenes.
- Airborne radars using doppler processing methods gave rise to *airborne MTI and pulse doppler radars,* which were able to detect aircraft in the midst of heavy ground clutter.
- The electronically steered *phased array antenna* offered rapid beam steering without mechanical movement of the antenna.
- *HF over-the-horizon radar* extended the detection range for aircraft by a factor of ten, to almost 2000 nmi.
- Radar became more than a "blob" detector by extracting information from the echo signal to provide *target recognition.*
- Radar has become an important tool for the meteorologist and as an aid for safe and efficient air travel by observing and measuring precipitation, warning of dangerous wind shear and other hazardous weather conditions, and for providing timely measurements of the vertical profile of wind speed and direction.
- The rapid advances in digital technology made many theoretical capabilities practical with *digital signal processing* and *digital data processing.*

New technology, new radar techniques, and new radar applications have fueled the continuous growth of radar since its inception in the 1930s. At the time this is written, growth in radar is continuing and is expected to continue. Illustrations of a small sample of various types of radars are shown in Figs. 1.6 to 1.15. Some of these, such as the airport surveillance radar and the airport surface detection equipment, might be familiar to the reader since they can be seen at major airports. Others shown here are not so usual and are included to indicate the diversity found in radar systems. Additional examples of radar systems will be found in Chapters 3, 4, and 9.

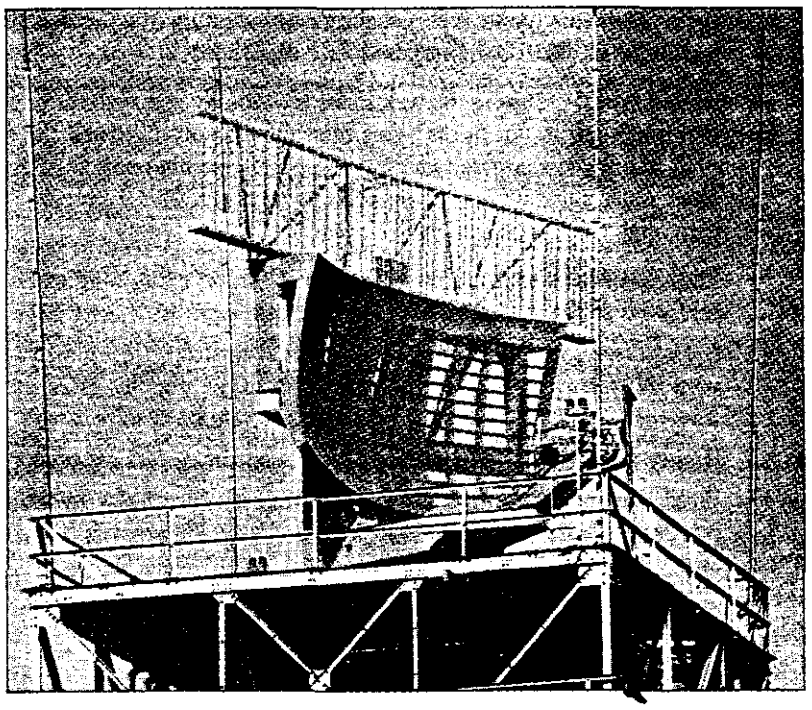

Figure 1.6 The airport surveillance radar, ASR-9, which operates at S band (2.7 to 2.9 GHz) with a klystron transmitter having a peak power of 1.3 MW. Pulse width is 1.0 μs. The antenna has a beamwidth of 1.4°, a gain of 34 dB, and rotates at 12.5 rpm. There are two vertical feeds for this antenna that produce two beams that overlap in elevation. The array antenna on top of the ASR-9 reflector antenna is for the FAA Air Traffic Control Radar Beacon System (ATCRBS). Airport surveillance radars have a range of about 50 to 60 nmi and provide coverage of the air traffic in the vicinity of airports. This radar is similar to the ASR-12 radar, except that the ASR-12 employs a solid-state transmitter and requires different waveforms to accommodate the high duty factor required when using a solid state transmitter.
(Courtesy of Northrop Grumman Corporation.)

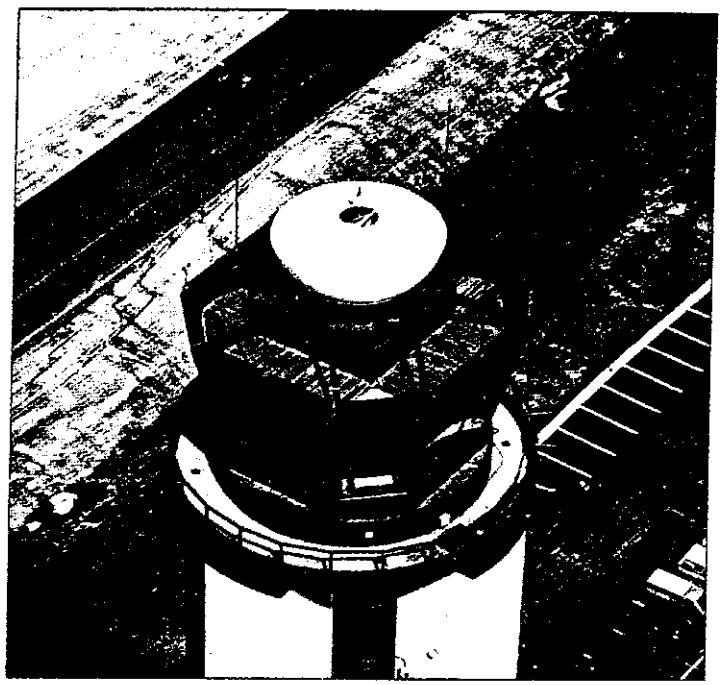

Figure 1.7 This ASDE-3 airport surface detection equipment is shown located on the control tower at the Pittsburgh International Airport. It produces a high-resolution ground map of the airport so as to monitor and expedite the movement of airport vehicle traffic and taxiing aircraft. This K_u-band radar operates from 15.7 to 17.7 GHz with a peak power of 3 kW, 40 ns pulse width, and 16 kHz pulse repetition frequency. The antenna and its rotodome rotate together at 60 rpm. The antenna gain is 44 dB, the azimuth beamwidth is 0.25° (a very narrow beamwidth for a radar), and its elevation beamwidth is 1.6°. It radiates circular polarization and has pulse-to-pulse frequency agility over 16 pulses, both of which help to increase the detectability of aircraft and vehicles in the rain. The display range is from 600 to 7300 m. The hole seen at the top of the rotodome in this figure is an access hatch that is not usually open. (It was open when this picture was made to allow a surveying instrument to be used for precisely locating the antenna.) Four lightning rods are shown around the rotodome.
(Courtesy of Northrop Grumman Corporation Norden Systems.)

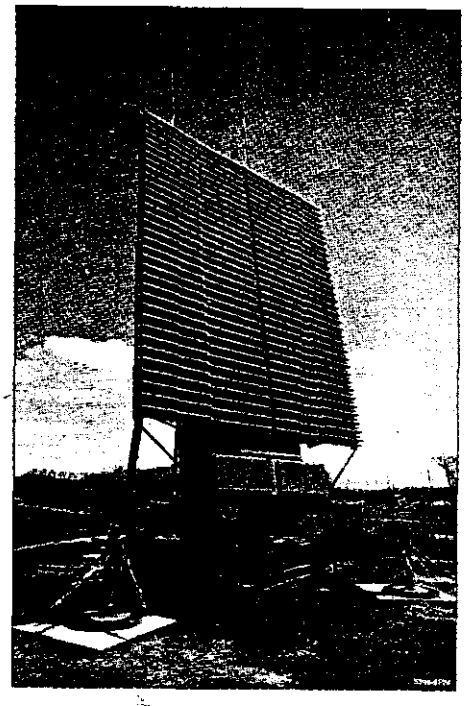

Figure 1.8 The TPS-117 is a transportable 3D military air-surveillance radar with an antenna that is 5.70 m (18.7 ft) high and 4.75 m (15.6 ft) wide and has a gain of 36 dB. It operates at *L* band over a 14 percent bandwidth centered at 1.3 GHz. Its planar phased array antenna rotates in azimuth at 6 rpm while electronically scanning its pencil beam over an elevation angle from 0 to 20°. The azimuth beamwidth is 3.4° and elevation beamwidth is 2.7°. For long range the radar employs a pulse width of 410 μs, compressed to 0.8 μs by means of linear frequency modulation pulse compression. Its solid-state transmitter is distributed over the 34 rows of the antenna, and produces 3.4 kW average power with 19 kW peak power. It can be assembled within three-quarters of an hour by a crew of eight. *(Courtesy of Lockheed Martin. Copyright 1999.)*

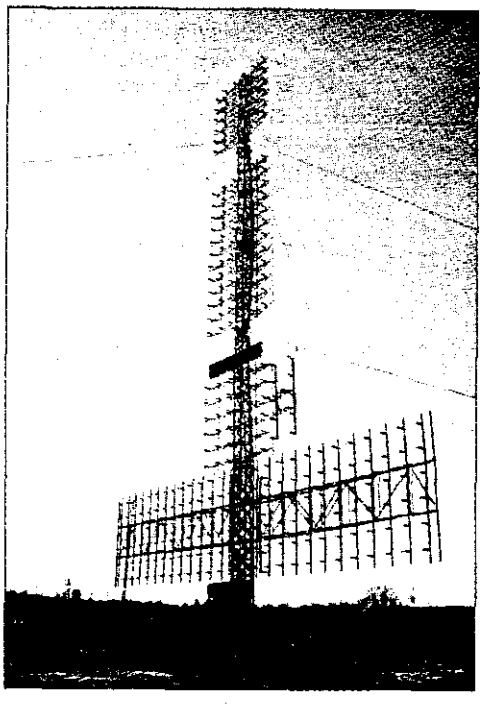

Figure 1.9 This is the 55G6U VHF (180 to 220 MHz) 3D radar, a Russian long-range air-surveillance radar developed by the Nizhny Novgorod Scientific-Research Radiotechnical Institute. The horizontal antenna structure of this radar, which is 27 m wide by 6 m high (89 by 20 ft), obtains the range and the azimuth angle of detected targets. The vertical antenna structure is 30 m high by 6 m wide (98 by 20 ft) and is electronically steered to provide the elevation (and the height) of targets. The antenna assembly extends about 42 m (138 ft) above the surface of the ground. It rotates at 6 rpm. Its accuracy in range is 100 m, in azimuth it is 0.2°, and in elevation the accuracy is 400 m. This large radar is transportable and can be deployed or redeployed in 22 hours. (Courtesy of A. A. Zachepitsky, Designer General, Scientific Research & Manufacturing, Nizhny Novgorod, Russia.)

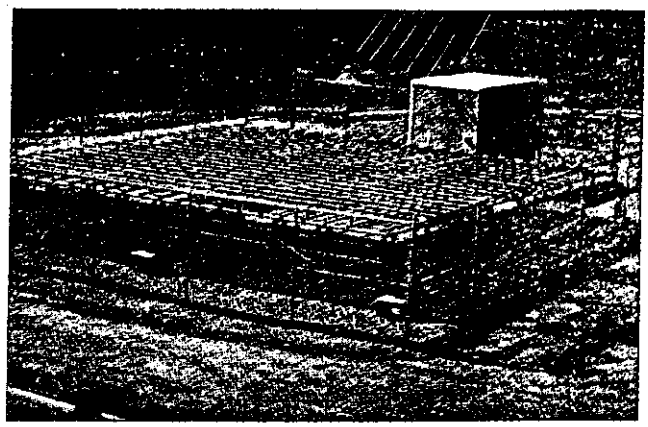

Figure 1.10 A UHF (404 MHz) vertically looking *wind-profiler radar* that provides the speed and direction of the wind as a function of altitude. The phased array antenna is 12 m by 12 m and has a beamwidth of 4°. Three beams are generated. One looks vertically, a second is tilted 15° to the north, and the third is tilted 15° to the east. The orientation of these three beams allows the horizontal and vertical components of the wind direction and speed to be determined. This radar obtains an echo from the clear air, which is due to the random inhomogeneities of the atmosphere caused by turbulence. The radar has an average power of 2.2 kW and a peak power of 16 kW. It can measure winds up to an altitude of 16 km. Wind profilers are important not only for weather observation and forecasting, but also for efficient (greater fuel savings) and safe routing of aircraft. This radar requires no on-site personnel for its operation or maintenance. (Courtesy of D. W. van de Kamp and the NOAA Forecast Systems Laboratory, with the help of M. J. Post.)

Figure 1.11 The Path Finder Utility Mapping System is a ground-penetrating radar shown here being pushed by an operator to locate underground cable, pipes, power lines, and other buried objects. Operator is seen using a wearable computer with a heads-up display that provides 3D data. Depth of penetration varies with soil conditions but is about 2 to 3 m in many types of soil. This is an example of an ultrawideband radar operating in the VHF and lower UHF region of the spectrum. (Courtesy of Geophysical Survey Systems, Inc., North Salem, NH.)

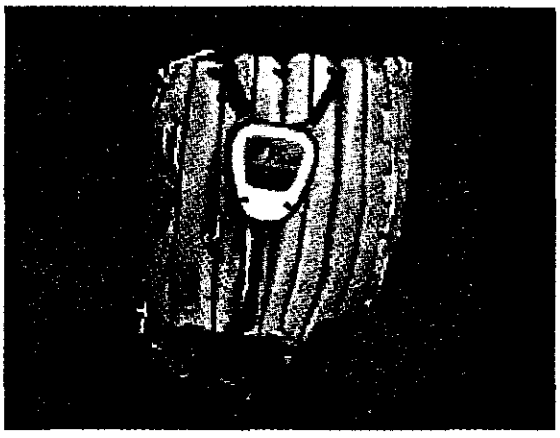

Figure 1.12 The Glove Radar is perhaps the smallest and cheapest radar one can buy. It is shown here attached to the back of a baseball glove to measure the speed of an approaching ball just before it is caught. It is 2.5 in. wide, 3.5 in. long, and 1.25 in. thick. Weight is 3 oz. An LCD displays speed in miles per hour. The frequency is 5.6 GHz and the CW transmitter power is 1 mW. [Courtesy of Al Dilz and Sport Sensors, Inc., Cincinnati, OH.]

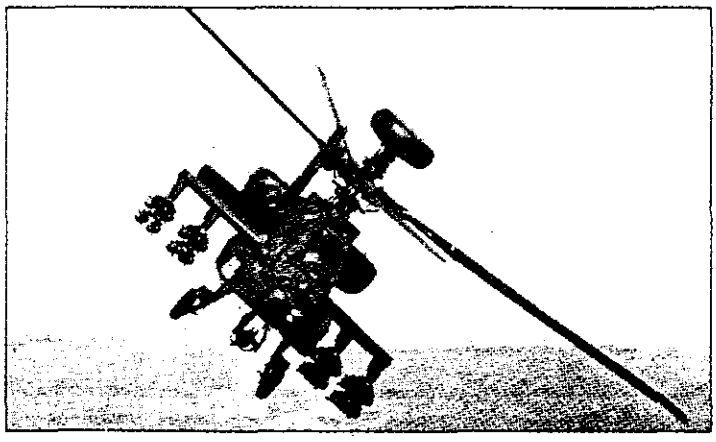

Figure 1.13 The Longbow K_u band (35 GHz) fire control radar for the U.S. Army's Apache helicopter shown mounted in a radome on top of the helicopter mast that rotates the blades. [Courtesy of Northrop Grumman Corporation.]

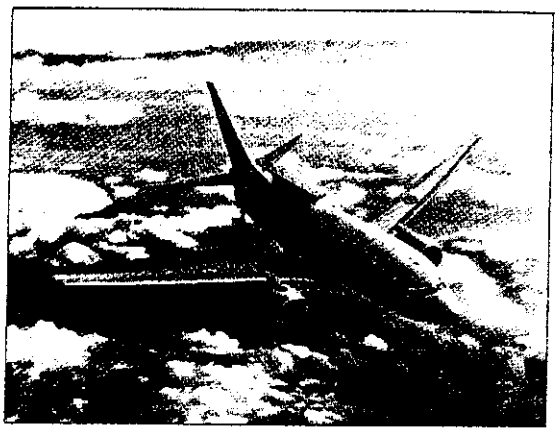

Figure 1.14 *L*-band electronically scanned 360° Wedgetail airborne early warning and control (AEW&C) radar mounted on a 737–700 aircraft. It was developed for the Royal Australian Air Force. The "top hat" on top the aircraft provides a practical solution for fore and aft coverage while maintaining the low drag profile of the dorsal array system.
(Photo: The Boeing Co.)

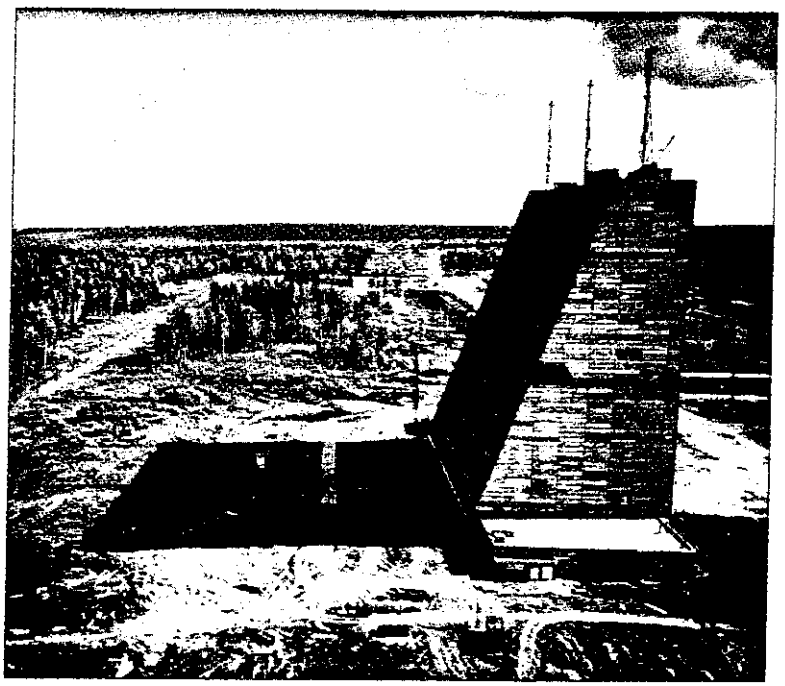

Figure 1.15 A long-range VHF Soviet space-surveillance radar that was located at Krasnoyarsk in central Siberia. The 30-story high receiving phased array antenna is shown on the right. It is approximately the size of a football field. The 11-story transmitting phased array antenna is barely visible in the background. This radar was later dismantled, but it is similar to other large phased array radars developed and operated by the former Soviet Union.
(Courtesy of William J. Broad of the *New York Times*.)

REFERENCES

1. Kraus, J. D. *Antennas.* 2nd ed. New York: McGraw-Hill, 1988, Sec. 2.22.
2. Silver, S. *Microwave Antenna Theory and Design.* MIT Radiation Laboratory Series, vol. 12. New York: McGraw-Hill, 1949, Sec. 6.4.
3. IEEE Standard Letter Designations for Radar-Frequency Bands, IEEE Std 521-1984.
4. DoD Index of Specifications and Standards, Supplement Part II, 1 March 1984, p. 101.
5. Performing Electronic Countermeasures in the United States and Canada, *U.S. Navy OPNAVINST* 3430.9B, 27 Oct. 1969. Similar versions issued as *U.S. Air Force* AFR 55–44, *U.S. Army* AR 105–86, and *U.S. Marine Corps* MCO 3430.1.
6. Guerlac, H. *Radar in World War II.* American Institute of Physics, Tomash Publishers, 1987.
7. Swords, S. S. *Technical History of the Beginnings of Radar.* London: Peter Peregrinus, 1986.
8. Skolnik, M. I. "Fifty Years of Radar." *Proc. IEEE,* vol. 73 (February 1985), pp. 182–197.
9. Hertz, H. *Electric Waves.* New York: Dover Publications, 1962. (Republication of the work first published in 1893 by Macmillan and Company.)
10. British Patent 13,170 issued to Christian Hulsmeyer, Sept. 22, 1904, entitled "Hertzian-Wave Projecting and Receiving Apparatus Adapted to Indicate or Give Warning of the Presence of a Metallic Body, Such as a Ship or a Train, in the Line of Projection of Such Waves."
11. Marconi, S. G. "Radio Telegraphy." *Proc. IRE,* vol. 10, no. 4 (1992), p. 237.
12. Oral history of Leo C. Young, recorded October 15, 1953, regarding the origin of radar at the Naval Research Laboratory, from the *Rear Admiral Stanford C. Hopper collection of the Library of Congress, History of Naval Radio,* LWO 4934 R23B, Reels 150 and 151.
13. Allison, D. K. "New Eye for Navy Radar: The Origin of Radar at the Naval Research Laboratory." *Naval Research Laboratory Report 8466,* Washington, D.C., Sept. 28, 1981.
14. House, D. *Radar at Sea.* Annapolis, MD: Naval Institute Press, 1993, pp. 45–49.
15. Price, A. *Instruments of Darkness.* New York: Charles Scribner's, 1978, p. 61.
16. Nakajima, S. "The History of Japanese Radar Development to 1945." In *Radar Development to 1945,* Russel Burns, Ed. London: Peter Peregrinus, 1988, pp. 243–258.
17. Nakagawa, Y. *Japanese Radar and Related Weapons of World War II.* Laguna Hills, CA: Aegean Park Press, 1997.

PROBLEMS

1.1 *a.* What should be the pulse repetition frequency of a radar in order to achieve a maximum unambiguous range of 60 nmi?
b. How long does it take for the radar signal to travel out and back when the target is at the maximum unambiguous range?
c. If the radar has a pulse width of 1.5 μs, what is the extent (in meters) of the pulse energy in space in the range coordinate?
d. How far apart in range (meters) must two equal-size targets be separated in order to be certain they are completely resolved by a pulse width of 1.5 μs?
e. If the radar has a peak power of 800 kW, what is its average power?
f. What is the duty cycle of this radar?

1.2 A ground-based air-surveillance radar operates at a frequency of 1300 MHz (L band). Its maximum range is 200 nmi for the detection of a target with a radar cross section of one square meter ($\sigma = 1$ m^2). Its antenna is 12 m wide by 4 m high, and the antenna aperture efficiency is $\rho_a = 0.65$. The receiver minimum detectable signal is $S_{\min} = 10^{-13}$ W. Determine the following:
a. Antenna effective aperture A_e (square meters) and antenna gain G [numerically and in dB, where G (in dB) = 10 $\log_{10}$ G (as a numeric)].
b. Peak transmitter power.
c. Pulse repetition frequency to achieve a maximum unambiguous range of 200 nmi.
d. Average transmitter power, if the pulse width is 2 μs.
e. Duty cycle.
f. Horizontal beamwidth (degrees).

1.3 *a.* What is the peak power of a radar whose average transmitter power is 200 W, pulse width of 1 μs, and a pulse repetition frequency of 1000 Hz?
b. What is the range (nmi) of this ground-based air-surveillance radar if it has to detect a target with a radar cross section of 2 m^2 when it operates at a frequency of 2.9 GHz (S band), with a rectangular-shaped antenna that is 5 m wide, 2.7 m high, antenna aperture efficiency ρ_a of 0.6, and minimum detectable signal $S_{\min}$ equal to 10^{-12} W (based on P_t in the radar equation being the peak power)?
c. Sketch the received echo signal power as a function of range from 10 to 80 nmi.

1.4 The moon as a radar target may be described as follows: average distance to the moon is 3.844×10^8 m (about 208,000 nmi); experimentally measured radar cross section is 6.64×10^{11} m^2 (mean value over a range of radar frequencies); and its radius is 1.738×10^6 m.
a. What is the round-trip time (seconds) of a radar pulse to the moon and back?
b. What should the pulse repetition frequency (prf) be in order to have no range ambiguities?
c. For the purpose of probing the nature of the moon's surface, a much higher prf could be used than that found in (b). How high could the prf be if the purpose is to observe the echoes from the moon's front half?

d. If an antenna with a diameter of 60 ft and aperture efficiency of 0.6 were used at a frequency of 430 MHz with a receiver having a minimum detectable signal of 1.5×10^{-16} W, what peak power is required? Does your answer surprise you; and if so, why?

e. The radar cross section of a smooth perfectly conducting sphere of radius a is πa^2. What would be the radar cross section of the moon if it were a sphere with a perfectly smooth, conducting surface? Why might the measured cross section of the moon (given above) be different from this value?

1.5 A radar mounted on an automobile is to be used to determine the distance to a vehicle traveling directly in front of it. The radar operates at a frequency of 9375 MHz (*X* band) with a pulse width of 10 ns (10^{-8} s). The maximum range is to be 500 ft.

a. What is the pulse repetition frequency that corresponds to a range of 500 ft?

b. What is the range resolution (meters)?

c. If the antenna beamwidth were 6°, what would be the cross-range resolution (meters) at a range of 500 ft? Do you think this value of cross-range resolution is sufficient?

d. If the antenna dimensions were 1 ft by 1 ft and the antenna efficiency were 0.6, what would be the antenna gain (dB)?

e. Find the average power required to detect a 10 m^2 radar cross section vehicle at a range of 500 ft, if the minimum detectable signal is 5×10^{-13} W.

1.6 Determine (a) the peak power (watts) and (b) the antenna physical area (m^2) which make the cost of the following radar a minimum:

Frequency: 1230 MHz (*L* band)

Antenna aperture efficiency: 0.6

Receiver minimum detectable signal: 3×10^{-13} W

Unit cost of transmitter: $2.20 per watt of peak power

Unit cost of antenna: $1400 per square meter of physical area

Cost of receiver and other items: $1,000,000

The radar must detect a target of 2 m^2 cross section at a range of 200 nmi.

(You will have to use one of the simple forms of the radar range equation.)

c. What is the cost of the antenna and the cost of the transmitter?

d. In a new radar design, how would you try, as a first attempt, to allocate the costs between the antenna and the transmitter (based only on the answers to the above problem)?

1.7 Who invented radar? (Please explain your answer.)

1.8 Three variants of the simple form of the radar equation have been given. In Eq. (1.9) the wavelength is in the numerator, in Eq. (1.10) the wavelength is in the denominator, and in Eq. (1.7), there is no explicit indication of wavelength. How would you respond to the question: "How does the radar range vary with the radar wavelength, everything else being the same?"

1.9 If the weight of a transmitter is proportional to the transmitter power (i.e., $W_T = k_T P_t$) and if the weight of an antenna is proportional to its volume (so that we can say its weight is proportional to the 3/2 power of the antenna aperture area A, or $W_A = k_A A^{3/2}$), what is the relationship between the weight of the antenna and the weight of the transmitter that makes the total weight $W = W_T + W_A$ a minimum, assuming a fixed range? (You will need the simple form of the radar equation to obtain a relationship between P_t and A.)

chapter

2

The Radar Equation

2.1 INTRODUCTION

The simple form of the radar equation, derived in Sec. 1.2, expressed the maximum radar range R_{max} in terms of the key radar parameters and the target's radar cross section when the radar sensitivity was limited by receiver noise. It was written:*

$$R_{max} = \left[\frac{P_t G A_e \sigma}{(4\pi) 2 S_{min}} \right]^{1/4} \qquad [2.1]$$

where

P_t = transmitted power, W
G = Antenna gain
A_e = Antenna effective aperture, m^2
σ = Radar cross section of the target, m^2
S_{min} = Minimum detectable signal, W

Except for the target's radar cross section, the parameters of this simple form of the radar equation are under the control of the radar designer. It states that if long ranges are desired, the transmitted power should be large, the radiated energy should be concentrated into a narrow beam (large transmitting gain), the echo energy should be received by a large antenna aperture (also synonymous with large gain), and the receiver should be sensitive to weak signals.

*This can also be written in terms of gain or effective aperture by using the relationship $G = 4\pi A_e/\lambda^2$.

In practice, however, this simple form of the radar equation does not adequately predict the range performance of actual radars. It is not unusual to find that when Eq. (2.1) is used, the actual range might be only half that predicted.[1] The failure of the simple form of the radar equation is due to (1) the statistical nature of the minimum detectable signal (usually determined by receiver noise), (2) fluctuations and uncertainties in the target's radar cross section, (3) the losses experienced throughout a radar system, and (4) propagation effects caused by the earth's surface and atmosphere. The statistical nature of receiver noise and the target cross section requires that the maximum radar range be described probabilistically rather than by a single number. Thus the specification of range must include the probability that the radar will detect a specified target at a particular range, and with a specified probability of making a false detection when no target echo is present. The range of a radar, therefore, will be a function of the *probability of detection*, P_d, and the *probability of false alarm*, P_{fa}.

The prediction of the radar range cannot be performed with arbitrarily high accuracy because of uncertainties in many of the parameters that determine the range. Even if the factors affecting the range could be predicted with high accuracy, the statistical nature of radar detection and the variability of the target's radar cross section and other effects make it difficult to accurately verify the predicted range. In spite of it not being as precise as one might wish, the radar equation is an important tool for (1) assessing the performance of a radar, (2) determining the system trade-offs that must be considered when designing a new radar system, and (3) aiding in generating the technical requirements for a new radar procurement.

In this chapter, the simple radar equation will be extended to include many of the important factors that influence the range of a radar when its performance is limited by receiver noise. A pulse waveform will be assumed, unless otherwise noted. In addition to providing a more complete representation of the radar range, this chapter introduces a number of basic radar concepts.

A thorough discussion of all the factors that influence the prediction of radar range is beyond the scope of a single chapter. For this reason, many subjects may appear to be treated lightly. More detailed information can be found in some of the subsequent chapters and in the references listed, especially those by Lamont Blake.[2,3]

2.2 DETECTION OF SIGNALS IN NOISE

The ability of a radar receiver to detect a weak echo signal is limited by the ever-present noise that occupies the same part of the frequency spectrum as the signal. The weakest signal that can just be detected by a receiver is the *minimum detectable signal*. In the radar equation of Eq. (2.1) it was denoted as S_{min}. Use of the minimum detectable signal, however, is not common in radar and is not the preferred method for describing the ability of a radar receiver to detect echo signals from targets, as shall be seen in Sec. 2.3.

Detection of a radar signal is based on establishing a threshold at the output of the receiver. If the receiver output is large enough to exceed the threshold, a target is said to be present. If the receiver output is not of sufficient amplitude to cross the threshold, only

noise is said to be present. This is called *threshold detection.* Figure 2.1 represents the output of a radar receiver as a function of time. It can be thought of as the video output displayed on an A-scope (amplitude versus time, or range). The fluctuating appearance of the output is due to the random nature of receiver noise.

When a large echo signal from a target is present, as at *A* in Fig. 2.1, it can be recognized on the basis of its amplitude relative to the rms noise level. If the threshold level is set properly, the receiver output should not normally exceed the threshold if noise alone were present, but the output would exceed the threshold if a strong target echo signal were present along with the noise. If the threshold level were set too low, noise might exceed it and be mistaken for a target. This is called a *false alarm.* If the threshold were set too high, noise might not be large enough to cause false alarms, but weak target echoes might not exceed the threshold and would not be detected. When this occurs, it is called a *missed detection.* In early radars, the threshold level was set based on the judgment of the radar operator viewing the radar output on a cathode-ray tube display. In radars with automatic detection (electronic decision making), the threshold is set according to classical detection theory described later in this chapter.

The output that is shown in Fig. 2.1 is assumed to be from a *matched-filter* receiver. A matched filter, as was mentioned in Sec. 1.3, is one that maximizes the output signal-to-noise ratio. (This is discussed in detail in Sec. 6.2). Almost all radars employ a matched filter or a close approximation. A matched filter does not preserve the shape of the input waveform. For example, a rectangular-like pulse will be somewhat triangular in shape at the output of the matched filter. For this reason the receiver output drawn in this figure is more a series of triangular-like pulses rather than rectangular. The fact that the matched filter changes the shape of the received signal is of little consequence. The filter is not designed to preserve the signal shape, but to maximize detectability.

A threshold level is shown in Fig. 2.1 by the long dash line. If the signal is large enough, as at *A*, it is not difficult to decide that a target echo signal is present. But consider the two weaker signals at *B* and *C*, representing two target echoes of equal amplitude. The noise accompanying the signal at *B* is assumed to be of positive amplitude and adds to the target signal so that the combination of signal plus noise crosses the threshold and is declared a target. At *C* the noise is assumed to subtract from the target signal, so that the resultant of signal and noise does not cross the threshold and is a missed

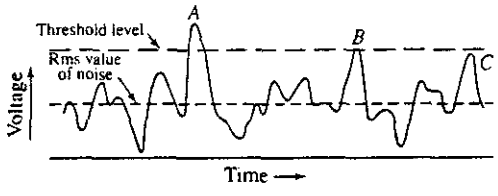

Figure 2.1 Envelope of the radar receiver output as a function of time (or range). *A*, *B*, and *C* represent signal plus noise. *A* and *B* would be valid detections, but *C* is a missed detection.

detection. The ever-present noise, therefore, will sometimes enhance the detection of marginal signals, but it may also cause loss of detection.

The signal at C would have been detected if the threshold were lower. But too low a threshold increases the likelihood that noise alone will exceed the threshold and be improperly called a detection. The selection of the proper threshold is therefore a compromise that depends upon how important it is to avoid the mistake of (1) failing to recognize a target signal that is present (missed detection) or (2) falsely indicating the presence of a target signal when none exists (false alarm).

The signal-to-noise ratio, as has been mentioned, is a better measure of a radar's detection performance than is the minimum detectable signal. The relationship between the two is developed next.

2.3 RECEIVER NOISE AND THE SIGNAL-TO-NOISE RATIO

At microwave frequencies, the noise with which the target echo signal competes is usually generated within the receiver itself. If the radar were to operate in a perfectly noise-free environment so that no external sources of noise accompany the target signal, and if the receiver itself were so perfect that it did not generate any excess noise, there would still be noise generated by the thermal agitation of the conduction electrons in the ohmic portion of the receiver input stages. This is called *thermal noise* or *Johnson noise.* Its magnitude is directly proportional to the bandwidth and the absolute temperature of the ohmic portions of the input circuit. The available thermal-noise power (watts) generated at the input of a receiver of bandwidth B_n (hertz) at a temperature T (degrees Kelvin) is[4]

$$\text{available thermal-noise power} = kTB_n \qquad [2.2]$$

where k = Boltzmann's constant = 1.38×10^{-23} J/deg. (The term *available* means that the device is operated with a matched input and a matched load.) The bandwidth of a superheterodyne receiver (and almost all radar receivers are of this type) is taken to be that of the IF amplifier (or matched filter).

In Eq. (2.2) the bandwidth B_n is called the *noise bandwidth,* defined as

$$B_n = \frac{\int_0^\infty |H(f)|^2 \, df}{|H(f_0)|^2} \qquad [2.3]$$

where $H(f)$ = frequency-response function of the IF amplifier (filter) and f_0 = frequency of the maximum response (usually occurs at midband). Noise bandwidth is not the same as the more familiar half-power, or 3-dB, bandwidth. Equation (2.3) states that the noise bandwidth is the bandwidth of the equivalent rectangular filter whose noise-power output is the same as the filter with frequency response function $H(f)$. The *half-power bandwidth,* a term widely used in electronic engineering, is defined by the separation between the points of the frequency response function $H(f)$ where the response is reduced 0.707 (3 dB in power) from its maximum value. Although it is not the same as the noise bandwidth, the half-power bandwidth is a reasonable approximation for many practical radar

receivers.[5,6] Thus the half-power bandwidth B is usually used to approximate the noise bandwidth B_n, which will be the practice in the remainder of the chapter.

The noise power in practical receivers is greater than that from thermal noise alone. The measure of the noise out of a real receiver (or network) to that from the ideal receiver with only thermal noise is called the *noise figure* and is defined as

$$F_n = \frac{\text{noise out of practical receiver}}{\text{noise out of ideal receiver at std temp } T_0} = \frac{N_{\text{out}}}{kT_0BG_a} \qquad [2.4]$$

where N_{out} = noise out of the receiver, and G_a = available gain. The noise figure is defined in terms of a standard temperature T_0, which the IEEE defines as 290 K (62°F). This is close to room temperature. (A standard temperature assures uniformity in measurements that might be made at different temperatures.) With this definition, the factor kT_0 in the definition of noise figure is 4×10^{-21} W/Hz, a quantity easier to remember than Boltzmann's constant. The available gain G_a is the ratio of the signal out, S_{out}, to the signal in, S_{in}, with both the output and input matched to deliver maximum output power. The input noise, N_{in}, in an ideal receiver is equal to kT_0B_n. The definition of noise figure given by Eq. (2.4) therefore can be rewritten as

$$F_n = \frac{S_{\text{in}}/N_{\text{in}}}{S_{\text{out}}/N_{\text{out}}} \qquad [2.5]$$

This equation shows that the noise figure may be interpreted as a measure of the degradation of the signal-to-noise ratio as the signal passes through the receiver.

Rearranging Eq. (2.5), the input signal is

$$S_{\text{in}} = \frac{kT_0BF_nS_{\text{out}}}{N_{\text{out}}} \qquad [2.6]$$

If the minimum detectable signal S_{min} is that value of S_{in} which corresponds to the minimum detectable signal-to-noise ratio at the output of the IF, $(S_{\text{out}}/N_{\text{out}})_{\text{min}}$, then

$$S_{\text{min}} = kT_0BF_n\left(\frac{S_{\text{out}}}{N_{\text{out}}}\right)_{\text{min}} \qquad [2.7]$$

Substituting the above into Eq. (2.1), and omitting the subscripts on S and N, results in the following form of the radar equation:

$$R_{\text{max}}^4 = \frac{P_tGA_e\sigma}{(4\pi)^2kT_0BF_n(S/N)_{\text{min}}} \qquad [2.8]$$

For convenience, R_{max} on the left-hand side is usually written as the fourth power rather than take the fourth root of the right-hand side of the equation.

The minimum detectable signal is replaced in the radar equation by the *minimum detectable signal-to-noise ratio* $(S/N)_{\text{min}}$. The advantage is that $(S/N)_{\text{min}}$ is independent of the receiver bandwidth and noise figure; and, as we shall see in Sec. 2.5, it can be expressed in terms of the probability of detection and the probability of false alarm, two parameters that can be related to the radar user's needs.

The signal-to-noise ratio in the above is that at the output of the IF amplifier, since maximizing the signal-to-noise ratio at the output of the IF is equivalent to maximizing the video output where the threshold decision is made.[7]

Before continuing the development of the radar equation, it is necessary to digress and briefly review the concept of the *probability density function* in order to describe the signal-to-noise ratio in statistical terms. Those familiar with this subject can omit the next section.

2.4 PROBABILITY DENSITY FUNCTIONS

In this section, we introduce the concept of the probability density function and give some examples that are important in the detection of radar signals.

Noise is a random phenomenon; hence, the detection of signals in the presence of noise is also a random phenomenon and should be described in probabilistic terms. *Probability* is a measure of the likelihood of the occurrence of an event. The scale of probability ranges from 0 to 1. (Sometimes probabilities are expressed in percent—from 0 to 100 percent—rather than 0 to 1.) An event that is certain has a probability of 1. An impossible event has a probability 0. The intermediate probabilities are assigned so that the more likely an event, the greater is its probability. Probabilities represent discrete events. Continuous functions, such as random noise, are represented by the *probability density function*, abbreviated *pdf*.

Consider the variable x as representing the value of a random process such as a noise voltage or current. Imagine each x to define a point on a straight vertical line corresponding to the distance from a fixed reference point. The distance x from the reference point might represent the value of the noise voltage or noise current. Divide the line into small segments of length Δx and count the number of times that x falls within each interval. The probability density function is then defined as

$$p(x) = \lim_{\substack{\Delta x \to 0 \\ N \to \infty}} \frac{(\text{number of values within } \Delta x \text{ at } x)/\Delta x}{\text{total number of values} = N} \qquad [2.9]$$

Thus $p(x)$ expresses probability as a density rather than discrete values, and is more appropriate for continuous functions of time as is noise in a radar receiver.

The probability that a particular value of x lies within the infinitesimal interval dx centered at x is simply $p(x)dx$. The probability that the value of x lies within the finite range from x_1 to x_2 is found by integrating $p(x)$ over the range of interest, or

$$\text{probability } (x_1 < x < x_2) = \int_{x_1}^{x_2} p(x)\, dx \qquad [2.10]$$

The probability density function, by definition, is always positive. Since every measurement must yield some value, the integral of the probability density function over all values of x must equal unity; that is,

$$\int_{-\infty}^{\infty} p(x)\, dx = 1 \qquad [2.11]$$

This condition is used to normalize the pdf. The average value of a variable function $\phi(x)$ that is described by the probability density function $p(x)$ is

$$\langle \phi(x) \rangle_{av} = \int_{-\infty}^{\infty} \phi(x) p(x)\, dx \qquad [2.12]$$

This follows from the definitions of an average value and the probability density function. From the above, the mean, or average, value of x is

$$\langle x \rangle_{av} = m_1 = \int_{-\infty}^{\infty} x p(x)\, dx \qquad [2.13]$$

and the mean square value of x is

$$\langle x^2 \rangle_{av} = m_2 = \int_{-\infty}^{\infty} x^2 p(x)\, dx \qquad [2.14]$$

The quantities m_1 and m_2 are called the *first* and *second moments* of the random variable x. If x represents an electric voltage or current, m_1 is the d-c component. It is the value read by a direct-current voltmeter or ammeter. The mean square value m_2 of the current, when multiplied by the resistance, gives the average power. (In detection theory, it is customary to take the resistance as 1 ohm, so that m_2 is often stated to be the average power.) The *variance* σ^2 is the mean square deviation of x about its mean m_1 and can be expressed as

$$\sigma^2 = \langle (x - m_1)^2 \rangle_{av} = \int_{-\infty}^{\infty} (x - m_1)^2 p(x)\, dx = m_2 - m_1^2 \qquad [2.15]$$

It is sometimes called the *second central moment.* If the random variable x is a noise current, the product of the variance and resistance is the mean power of the a-c component. The square root of the variance is the *standard deviation* and is the root mean square (rms) of the a-c component. It is usually designated as σ. We next consider four examples of probability density functions.

Uniform pdf This is shown in Fig. 2.2a and is defined as

$$p(x) = k \qquad \text{for } a < x < a + b$$
$$= 0 \qquad \text{for } x < a \text{ and } x > a + b$$

where k is a constant. It describes the phase of a random sinewave relative to a particular origin of time, where the phase of the sinewave is, with equal probability, anywhere from 0 to 2π radians. The uniform pdf also describes the distribution of the round-off (quantizing) error in numerical computations and in analog-to-digital converters.

The constant k is found to be equal to $1/b$ by requiring that the integral of the probability density function over all values of x equal unity [Eq. (2.11)]. From Eq. (2.13) the average value of the uniform distribution is $a + (b/2)$, which could have been found from inspection in this simple example. The variance from Eq. (2.15) equals $b^2/12$.

Gaussian pdf The gaussian pdf is important in detection theory since it describes many sources of noise, including receiver thermal noise. Also, it is more convenient to

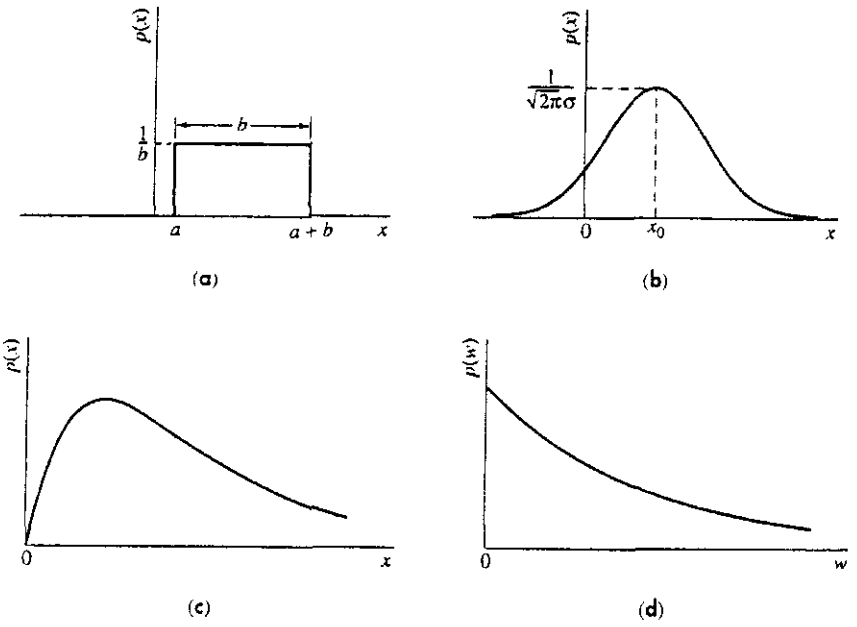

Figure 2.2 Examples of probability density functions. (a) uniform; (b) gaussian; (c) Rayleigh (voltage); (d) Rayleigh (power), or exponential.

manipulate mathematically than many other pdfs. The gaussian probability density function has a bell-shaped appearance, Fig. 2.2b, and is given by

$$p(x) = \frac{1}{\sqrt{2\pi\sigma^2}} \exp\left[-\frac{(x - x_0)^2}{2\sigma^2}\right] \qquad [2.16]$$

where exp [·] is the exponential function, σ^2 is the variance of x, and x_0 is the mean value of x.

The ability of the gaussian pdf to represent many statistical phenomena is a consequence of the *central limit theorem.* It states that, under very general assumptions, the probability density function of the sum of a large number of independently distributed quantities approaches the gaussian pdf no matter what the individual pdfs might be.

Rayleigh pdf This is of interest for radar since the envelope of a narrowband filter (such as the IF filter of a radar receiver) is described by the Rayleigh pdf when the input noise voltage is gaussian. The statistical behavior of the radar cross section of some types of targets and some types of clutter also fit this pdf. It is given as

$$p(x) = \frac{2x}{m_2} \exp\left(-\frac{x^2}{m_2}\right) \qquad x \geq 0 \qquad [2.17]$$

where $m_2 = \langle x^2 \rangle_{av}$ is the mean square value of x. The Rayleigh pdf is shown in Fig. 2.2c. It is a one-parameter pdf (the mean square value), and has the property that its standard deviation is equal to $\sqrt{(4/\pi) - 1} = 0.523$ times the mean value.

Exponential pdf When x^2 in the Rayleigh pdf is replaced by w, the pdf becomes

$$p(w) = \frac{1}{w_0} \exp\left(-\frac{w}{w_0}\right) \qquad w \geq 0 \tag{2.18}$$

where w_0 is the mean value of w. This is the *exponential* pdf, but is sometimes called the *Rayleigh-power* pdf, Fig. 2.2d. If the parameter x in the Rayleigh pdf is the voltage, then w represents the power and w_0 is the average power. The standard deviation of the exponential pdf is equal to the mean.

Other pdfs Later in this chapter the Rice, log normal, and chi-square pdfs will be mentioned as statistical models describing the fluctuations of the target's radar cross section. Section 7.5 provides further discussion of probability density functions as applied to the statistics of clutter. (Clutter is the echo from land, sea, or weather that interferes with the detection of desired targets.)

Statistical phenomena can also be represented by the probability distribution function $P(x)$, which is related to the probability density function $p(x)$ by

$$P(x) = \int_{-\infty}^{x} p(x)\,dx \quad \text{or} \quad p(x) = \frac{d}{dx}P(x) \tag{2.19}$$

Example of the Use of Probability Density Functions The following is a simple example of the use of probability density functions. It involves the calculation of the mean value (d-c component) of the voltage output of a half-wave linear rectifier when the input is gaussian noise voltage of zero mean (thermal noise).[8] The answer itself is of little consequence for our interest in radar detection, but the method used is similar to the more complicated procedures for finding the statistical outputs of a radar receiver mentioned in the next section.

The probability density function (pdf) of the zero-mean gaussian noise voltage x at the input is

$$p(x)\,dx = \frac{1}{\sqrt{2\pi}\sigma} \exp\left(-\frac{x^2}{2\sigma^2}\right) dx \qquad -\infty < x < \infty$$

The output y of a half-wave rectifier for an input x is given as

$$y = ax \qquad x \geq 0,$$

and

$$y = 0 \qquad x < 0$$

where a = constant. To find the mean value of the output, we have to find the pdf at the output. There are three components to the output pdf. The first component is the probability that the rectifier output, $y > 0$, will lie between y and $y + dy$. It is the same as the probability that x lies between x and $x + dx$ when $x > 0$. Thus,

$$p(y)\,dy = p(x)\,dx = \frac{1}{\sqrt{2\pi}a\sigma} e^{-\frac{y^2}{2a^2\sigma^2}} dy \qquad y > 0$$

The second component is the probability that $y = 0$, which is the same as the probability that $x < 0$, which is 1/2 (since half the time the noise voltage is negative and is not passed by the half-wave rectifier). This is represented by $(1/2)\delta(y)$, where $\delta(y)$ is the delta function which has the value 1 when $y = 0$, and is 0 otherwise. The third component is when $y < 0$. There is no output from a rectifier when $y < 0$, thus the probability is 0 that $y < 0$. Combining the three components gives

$$p(y)\,dy = \frac{1}{\sqrt{2\pi}a\sigma} e^{-\frac{y^2}{2a^2\sigma^2}}\,dy + \frac{1}{2}\delta(y)\,dy + 0 \qquad y \geq 0$$

The d-c component is $m_1 = \int_{-\infty}^{\infty} yp(y)\,dy$, or

$$m_1 = \frac{1}{\sqrt{2\pi}a\sigma}\int_0^{\infty} ye^{-\frac{y^2}{2a^2\sigma^2}}\,dy + \frac{1}{2}\int_{-\infty}^{\infty} y\delta(y)\,dy$$

The second integral containing the delta function is zero, since $\delta(y)$ has a value only when $y = 0$. The first integral is easily evaluated. The result is the d-c component, which is $a\sigma/\sqrt{2\pi}$.

In this example we started with the pdf describing the input and found the pdf describing the output. In the next section we will follow a similar procedure to find the probabilities of detection and false alarm, but will only provide the answers rather than go through the more elaborate mathematical derivation.

2.5 PROBABILITIES OF DETECTION AND FALSE ALARM

Next it is shown how to find the minimum signal-to-noise ratio required to achieve a specified probability of detection and probability of false alarm. The signal-to-noise ratio is needed in order to calculate the maximum range of a radar using the radar range equation as was given by Eq. (2.8). The basic concepts for the detection of signals in noise may be found in a classical review paper by Rice[9] or one of several texts on detection theory.[10]

Envelope Detector Figure 2.3 shows a portion of a superheterodyne radar receiver with IF amplifier of bandwidth B_{IF}, second detector,* video amplifier with bandwidth B_v, and a threshold where the detection decision is made. The IF filter, second detector, and video filter form an *envelope detector* in that the output of the video amplifier is the envelope, or modulation, of the IF signal. (An envelope detector requires that the video bandwidth $B_v \geq B_{IF}/2$ and the IF center frequency $f_{IF} >> B_{IF}$. These conditions are usually met in

*The diode stage in the envelope detector of a superheterodyne receiver has traditionally been called the *second detector* since the mixer stage, which also employs a diode, was originally called the first detector. The mixer stage is no longer known as the first detector, but the name second detector has been retained in radar practice to distinguish it from other forms of detectors used in radar receivers (such as phase detectors and phase-sensitive detectors).

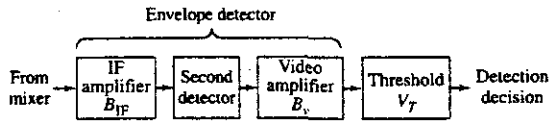

Figure 2.3 Portion of the radar receiver where the echo signal is detected and the detection decision is made.

radar.) The envelope detector passes the modulation and rejects the carrier. The second detector is a nonlinear device (such as a diode). Either a linear or a square-law detector characteristic may be assumed since the effect on the detection probability is relatively insensitive to the choice. (A square-law characteristic is usually easier to handle mathematically, but a linear law is preferred in practice since it allows a larger dynamic range than the square law.) The bandwidth of the radar receiver is the bandwidth of the IF amplifier. The envelope of the IF amplifier output is the signal applied to the threshold detector. When the receiver output crosses the threshold, a signal is declared to be present.

Probability of False Alarm The receiver noise at the input to the IF filter (the terms *filter* and *amplifier* are used interchangeably here) is described by the gaussian probability density function of Eq. (2.16) with mean value of zero, or

$$p(v) = \frac{1}{\sqrt{2\pi\Psi_0}} \exp\left(-\frac{v^2}{2\Psi_0}\right) \qquad [2.20]$$

where $p(v)\,dv$ is the probability of finding the noise voltage v between the values of v and $v + dv$ and Ψ_0 is the mean square value of the noise voltage (mean noise power). S. O. Rice has shown in a *Bell System Technical Journal* paper[9] that when gaussian noise is passed through the IF filter, the probability density function of the envelope R is given by a form of the Rayleigh pdf:

$$p(R) = \frac{R}{\Psi_0} \exp\left(-\frac{R^2}{2\Psi_0}\right) \qquad [2.21]$$

The probability that the envelope of the noise voltage will exceed the voltage threshold V_T is the integral of $p(R)$ evaluated from V_T to ∞, or

$$\text{Probability } (V_T < R < \infty) = \int_{V_T}^{\infty} \frac{R}{\Psi_0} \exp\left(-\frac{R^2}{2\Psi_0}\right) dR = \exp\left(\frac{-V_T^2}{2\Psi_0}\right) \qquad [2.22]$$

This is the *probability of a false alarm* since it represents the probability that noise will cross the threshold and be called a target when only noise is present. Thus, the probability of a false alarm, denoted P_{fa}, is

$$P_{fa} = \exp\left(-\frac{-V_T^2}{2\Psi_0}\right) \qquad [2.23]$$

By itself, the probability of false alarm as given by Eq. (2.23) does not indicate whether or not a radar will be troubled by excessive false indications of targets. The time between false alarms is a better measure of the effect of noise on radar performance.

Figure 2.4 illustrates the occurrence of false alarms. The average time between crossings of the decision threshold when noise alone is present is called the *false-alarm time*, T_{fa}, and is given by

$$T_{fa} = \lim_{N\to\infty} \frac{1}{N}\sum_{k=1}^{N} T_k \qquad [2.24]$$

where T_k is the time between crossings of the threshold V_T by the noise envelope. The false-alarm time is something a radar customer or operator can better relate to than the probability of false alarm. The false-alarm probability can be expressed in terms of false-alarm time by noting that the false-alarm probability P_{fa} is the ratio of the time the envelope is actually above the threshold to the total time it could have been above the threshold, or

$$P_{fa} = \frac{\sum_{k=1}^{N} t_k}{\sum_{k=1}^{N} T_k} = \frac{\langle t_k \rangle_{av}}{\langle T_k \rangle_{av}} = \frac{1}{T_{fa}B} \qquad [2.25]$$

where t_k and T_k are shown in Fig. 2.4, and B is the bandwidth of the IF amplifier of the radar receiver. The average duration of a threshold crossing by noise $\langle t_k \rangle_{av}$ is approximately the reciprocal of the IF bandwidth B. The average of T_k is the *false-alarm time*, T_{fa}. Equating Eqs. (2.23) and (2.25) yields

$$T_{fa} = \frac{1}{B} \exp\left(\frac{V_T^2}{2\psi_0}\right) \qquad [2.26]$$

A plot of T_{fa} as a function of $V_T^2/2\Psi_0$ is shown in Fig. 2.5. If, for example, the bandwidth of the IF amplifier were 1 MHz and the average time between false alarms were specified to be 15 min, the probability of a false alarm is 1.11×10^{-9}. The threshold voltage,

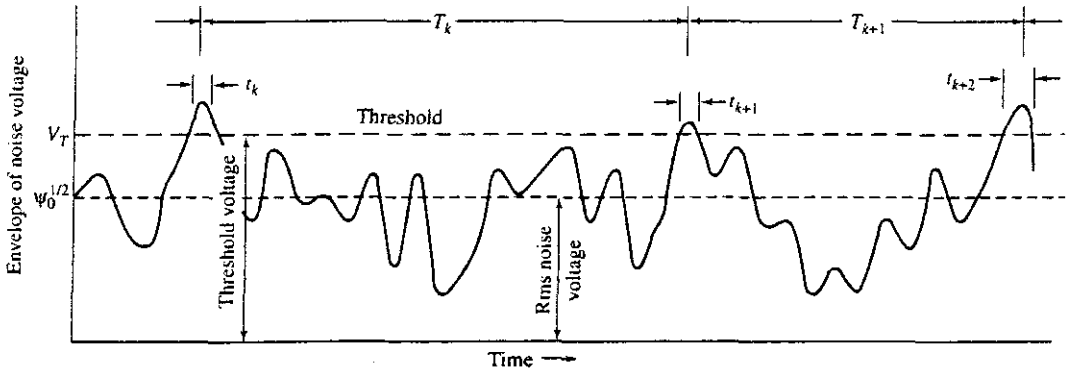

Figure 2.4 Envelope of the receiver output with noise alone, illustrating the duration of false alarms and the time between false alarms.

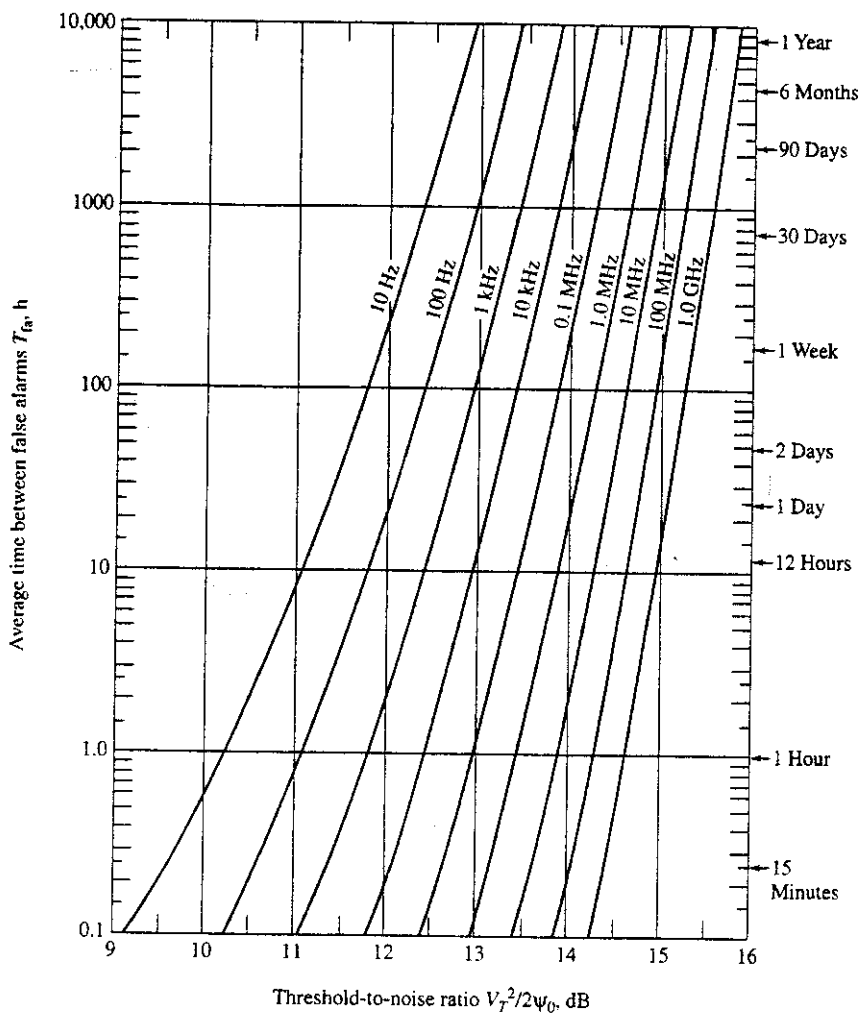

Figure 2.5 Average time between false alarms as a function of the threshold level V_T and the receiver bandwidth B; Ψ_0 is the mean square noise voltage.

from Eq. (2.26), is 6.42 times the rms value of the noise voltage, or the power ratio V_T^2/Ψ_0 is 16.2 dB.

The false-alarm probabilities of radars are generally quite small since a decision as to whether a target is present or not is made every $1/B$ second. The bandwidth B is usually large, so there are many opportunities during one second for a false alarm to occur. For example, when the bandwidth is 1 MHz (as with a 1-μs pulse width) there are 1 million decisions made every second as to whether noise or signal plus noise is present. If there were to be, on average, one false alarm per second, the false-alarm probability would be 10^{-6} in this specific example.

The exponential relationship between the false-alarm time T_{fa} and the threshold level V_T [Eq. (2.26)] results in the false-alarm time being sensitive to small variations in the threshold. For example, if the bandwidth were 1 MHz, a value of $10 \log(V_T^2/2\Psi_0) = 13.2$

dB results in a false-alarm time of about 20 min. A 0.5-dB decrease in the threshold to 12.7 dB decreases the false-alarm time by an order of magnitude, to about 2 min.

If the threshold is set slightly higher than required and maintained stable, there is little likelihood of false alarms due to thermal noise. In practice, false alarms are more likely to occur from clutter echoes (ground, sea, weather, birds, and insects) that enter the radar and are large enough to cross the threshold. In the specification of the radar's false-alarm time, however, clutter is almost never included, only receiver noise.

Although the crossing of the threshold by noise is called a false alarm, it is not necessarily a *false-target report.* Declaration of a target generally requires more than one detection made on multiple observations by the radar (Sec. 2.13). In many cases, establishing the track of a target is required before a target is declared as being present. Such criteria can allow a higher probability of false alarm for each detection; hence, the threshold can be lowered to improve detection without obtaining excessive false-target reports. In the present chapter, however, most of the discussion relating to the radar equation concerns a detection decision based on a single crossing of the threshold.

If the receiver were turned off (or gated) for a small fraction of the time, as it normally would be during the transmission of the radiated pulse, the false-alarm probability will be *increased* by the fraction of time the receiver is not operative. This assumes the false-alarm time remains constant. The effect of gating the receiver off for a short time seldom needs to be taken into account since the resulting change in the probability of false alarm and the change in the threshold level are small.

Probability of Detection So far, we have discussed only the noise input at the radar receiver. Next, consider an echo signal represented as a sinewave of amplitude A along with gaussian noise at the input of the envelope detector. The probability density function of the envelope R at the video output is given by[9]

$$p_s(R) = \frac{R}{\Psi_0} \exp\left(-\frac{R^2 + A^2}{2\Psi_0}\right) I_0\left(\frac{RA}{\Psi_0}\right) \qquad [2.27]$$

where $I_0(Z)$ is the modified Bessel function of zero order and argument Z. For large Z, an asymptotic expansion for $I_0(Z)$ is

$$I_0(Z) = \frac{e^Z}{\sqrt{2\pi Z}}\left(1 + \frac{1}{8Z} + \cdots\right) \qquad [2.28]$$

When the signal is absent, $A = 0$ and Eq. (2.27) reduces to Eq. (2.21), the pdf for noise alone. Equation (2.27) is called the *Rice probability density function.*

The probability of detecting the signal is the probability that the envelope R will exceed the threshold V_T (set by the need to achieve some specified false-alarm time). Thus the probability of detection is

$$P_d = \int_{V_T}^{\infty} p_s(R)\, dR \qquad [2.29]$$

When the probability density function $p_s(R)$ of Eq. (2.27) is substituted in the above, the probability of detection P_d cannot be evaluated by simple means. Rice[9] used a series approximation to solve for P_d. Numerical and empirical methods have also been used.

The expression for P_d, Eq. (2.29), along with Eq. (2.27), is a function of the signal amplitude A, threshold V_T, and mean noise power Ψ_0. In radar systems analysis it is more convenient to use signal-to-noise power ratio S/N than $A^2/2\Psi_0$. These are related by

$$\frac{A}{\Psi_0^{1/2}} = \frac{\text{signal amplitude}}{\text{rms noise voltage}} = \frac{\sqrt{2}\ (\text{rms signal voltage})}{}$$

$$= \left(2\frac{\text{signal power}}{\text{noise power}}\right)^{1/2} = \left(\frac{2S}{N}\right)^{1/2}$$

The probability of detection P_d can then be expressed in terms of S/N and the ratio of the threshold-to-noise ratio $V_T^2/2\Psi_0$. The probability of false alarm, Eq. (2.23) is also a function of $V_T^2/2\Psi_0$. The two expressions for P_d and P_{fa} can be combined, by eliminating the threshold-to-noise ratio that is common to each, so as to provide a single expression relating the probability of detection P_d, probability of false alarm P_{fa}, and the signal-to-noise ratio S/N. The result is plotted in Fig. 2.6.

Albersheim[11,12] developed a simple empirical formula for the relationship between S/N, P_d, and P_{fa}, which is

$$S/N = A + 0.12AB + 1.7B \qquad [2.30]$$

where

$$A = ln\ [0.62/P_{fa}] \quad \text{and} \quad B = ln\ [P_d/(1 - P_d)]$$

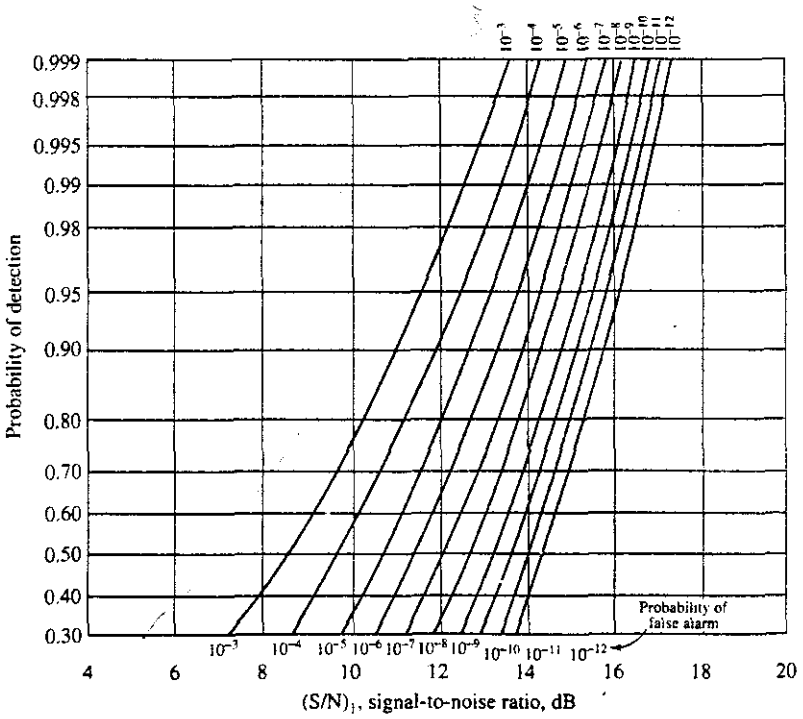

Figure 2.6 Probability of detection for a sinewave in noise as a function of the signal-to-noise (power) ratio and the probability of false alarm.

The signal-to-noise ratio in the above is a numeric, and not in dB; and ln is the natural logarithm. Equation (2.30) is said to be accurate to within 0.2 dB for P_{fa} between 10^{-3} and 10^{-7}, and P_d between 0.1 and 0.9. (It is probably suitable for rough calculations for even greater values of P_d and lower values of P_{fa}.) From such an expression or from a graph such as Fig. 2.6, the minimum signal-to-noise ratio required for a particular probability of detection and a specified probability of false alarm can be found and entered into the radar range equation. The above applies for a single pulse. The case for multiple pulses is given later.

The detection probability and the false-alarm probability are specified by the system requirements as derived from the customer's needs. From the specified detection and false-alarm probabilities, the minimum signal-to-noise ratio is found. For example, suppose that the average time between false alarms is required to be 15 min. If the bandwidth were 1 MHz, Eq. (2.25) gives a false-alarm probability of 1.11×10^{-9}. Figure 2.6 indicates that a signal-to-noise ratio of 13.05 dB is required for a probability of detection of 0.50, 14.7 dB for $P_d = 0.90$, and 15.75 dB for $P_d = 0.99$. Thus, a change of less than 3 dB can mean the difference between highly reliable detection (0.99) and marginal detection (0.50).

At first glance one might be inclined to think that the signal-to-noise ratios required for reliable detection in the above example are relatively high. They are of this magnitude because in the above example it is required that, on average, there be no more than one false alarm every 900 million possible detection decisions. Compared to telecommunications services, however, the signal-to-noise ratios for radar are relatively low. For TV the signal-to-noise ratio is said[13] to be 40 dB; there is some snow with 35 dB; objectionable interference at 30 dB; and the picture is all snow with 25 dB. Telephone service is said to require a signal-to-noise ratio of 50 dB. By comparison, radar detection is highly efficient.

The material in this section assumed only a single pulse was being used for detection. Most radars, however, utilize more than one pulse to make the detection decision, as will be discussed next.

2.6 INTEGRATION OF RADAR PULSES

The number of pulses returned from a point target by a scanning radar with a pulse repetition rate of f_p Hz, an antenna beamwidth θ_B degrees, and which scans at a rate of $\dot{\theta}_s$ degrees per second is

$$n = \frac{\theta_B f_p}{\dot{\theta}_s} = \frac{\theta_B f_p}{6\omega_r} \qquad [2.31]$$

where ω_r = revolutions per minute (rpm) if a 360° rotating antenna. The number of pulses received n is usually called *hits per scan* or *pulses per scan*. It is the number of pulses within the one-way beamwidth θ_B. Example values for a long-range ground-based air-surveillance radar might be 340-Hz pulse repetition rate, 1.5° beamwidth, and an antenna rotation rate of 5 rpm (30°/s). These numbers, when substituted into Eq. (2.31), yield $n = 17$ pulses per scan. (If n is not a whole number it can be either rounded off or the number can be used as is. It will make little difference in the calculation of radar range whichever you choose to do, unless n is small.)

The process of summing all the radar echoes available from a target is called *integration* (even though an *addition* is actually performed). Many techniques have been considered in the past to provide integration of pulses. A common integration method in early radars was to take advantage of the persistence of the phosphor of the cathode-ray-tube display combined with the integrating properties of the eye and brain of the radar operator. Analog storage devices, such as narrowband filters, can act as integrators; but they have been replaced with digital methods.

Integration that is performed in the radar receiver before the second detector (in the IF) is called *predetection integration* or *coherent integration.* Predetection integration is theoretically lossless, but it requires the phase of the echo signal pulses to be known and preserved in order to combine the sinewave pulses in phase without loss. Integration after the second detector is known as *postdetection integration* or *noncoherent integration.* It is easier to accomplish than predetection integration since the phases of the echoes are not preserved and only the envelopes of the pulses need be aligned to perform addition. There is a theoretical integration loss, however, with the use of postdetection integration.

If n pulses, all of the same signal-to-noise ratio, were perfectly integrated by an ideal lossless predetection integrator, the integrated signal-to-noise (power) ratio would be exactly n times that of a single pulse. Therefore, in this case, we can replace the single-pulse signal-to-noise ratio $(S/N)_1$ in the radar equation with $(S/N)_n = (S/N)_1/n$, where $(S/N)_n$ is the required signal-to-noise ratio per pulse when there are n pulses integrated predetection without loss. If the same n pulses were integrated by an ideal postdetection device, the resultant signal-to-noise ratio would be less than n times that of a single pulse. This loss in integration efficiency is caused by the nonlinear action of the second detector, which converts some of the signal energy to noise energy in the rectification processes. An integration efficiency for postdetection integration may be defined as

$$E_i(n) = \frac{(S/N)_1}{n(S/N)_n} \qquad [2.32]$$

where the symbols have been defined in the above. The improvement in signal-to-noise ratio when n pulses are integrated is called the *integration improvement factor* $I_i(n) = nE_i(n)$. It can also be thought of as the *equivalent number of pulses integrated* $n_{eq} = nE_i(n)$. For postdetection integration n_{eq} is less than n; for ideal predetection integration $n_{eq} = n$. Thus for the same integrated signal-to-noise ratio, postdetection integration requires more pulses than predetection, assuming the signal-to-noise ratio per pulse in the two cases is the same.

The postdetection integration efficiency and the required signal-to-noise ratio per pulse $(S/N)_n$ may be found by use of statistical detection theory, similar to that outlined in the previous section. This was originally undertaken for radar application in the classic work of J. I. Marcum.[14] (His work originally appeared in 1954 as a highly regarded, widely distributed, but not generally available, Rand Corporation report.) Marcum defined an integration loss in dB as $L_i(n) = 10 \log [1/E_i(n)]$. The integration loss and the integration improvement factor are plotted in Fig. 2.7. They vary only slightly with probability of detection or probability of false alarm.

Marcum used the *false-alarm number* n_f in his calculations rather the probability of false alarm. His false-alarm number is the reciprocal of our false-alarm probability

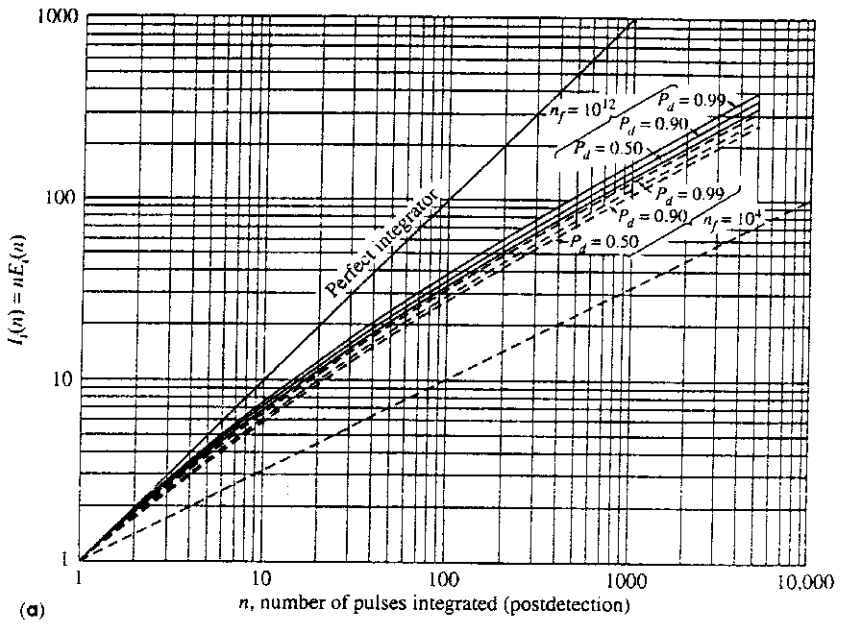

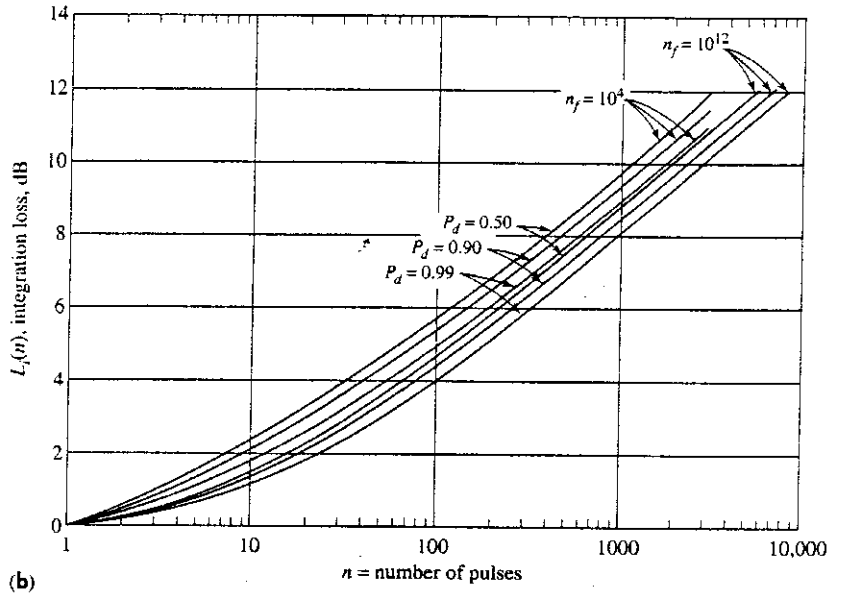

Figure 2.7 (a) Integration-improvement factor (or equivalent number of pulses integrated) for a square-law detector, where P_d = probability of detection, n_f = false-alarm number = $1/T_{fa}B$, T_{fa} = average time between false alarms, B = receiver bandwidth; (b) integration loss as a function of n, the number of pulses integrated, P_d, and n_f.
[(After Marcum,[14] courtesy *IRE Trans.*)

defined by Eqs. (2.23) and (2.25). On average, there will be one false-alarm decision out of n_f possible decisions within the false-alarm time T_{fa}. In other words, the average number of possible decisions between false alarms is n_f. If τ is the pulse width and T_p is the pulse repetition period = $1/f_p$, then the number of possible decisions n_f in the time T_{fa} is equal to the number of range intervals per pulse period (T_p/τ) times the number of pulse periods per second (f_p) times the false-alarm time (T_{fa}). Combining the above, we get $n_f = (T_p/\tau) \times f_p \times T_{fa} = T_{fa}/\tau$. Since $\tau \approx 1/B$, where B = bandwidth, the false-alarm number is $n_f = T_{fa}B = 1/P_{fa}$.

The above assumed that the radar made decisions at a rate equal to the bandwidth B. If the radar integrates n pulses per scan before making a target detection decision, then the rate at which decisions are made is B/n. This results in a false-alarm probability n times as great as when decisions are made at a rate B times per second. This does not mean there will be more false alarms when n pulses are integrated since we have assumed that the average time between false alarms remains the same when pulses are integrated. The rate at which detection decisions are made is lower. The above is another reason why false-alarm probability is not as good a descriptor of false alarms as is the average false-alarm time. A probability by itself has little meaning unless the rate at which events occur is known.

Following the practice of Marcum, P_{fa} will be taken in this text as the reciprocal of $T_{fa}B = n_f$, even when n pulses are integrated. Some authors, on the other hand, prefer to define a false-alarm number $n'_f = n_f/n$ that accounts for the number of pulses integrated. Therefore, caution should be exercised when using different authors' computations or different computer programs for finding the signal-to-noise ratio as a function of probability of detection and probability of false alarm (or false-alarm number). There is no standardization of definitions. Correct values of signal-to-noise ratio for use in the radar equation can be obtained from most sources provided the particular assumptions used by the sources are understood.

The solid straight line in Fig. 2.7a represents a perfect lossless predetection integrator. When only a few pulses are integrated (implying large signal-to-noise ratio per pulse), Fig. 2.7a shows that the performance of the postdetection integrator is not much different from the predetection integrator. When a large number of pulses are integrated (small signal-to-noise ratio per pulse), the difference between predetection and postdetection integration is more pronounced.

The dash straight line in this figure is proportional to $n^{1/2}$. In the early days of radar it was thought that the integration improvement factor of a radar operator viewing a cathode-ray-tube display, such as a PPI, was equal to $n^{1/2}$. This is not necessarily correct. The $n^{1/2}$ relation was based on an incorrect theory and poor displays. When individual pulses are displayed so that they do not overlap or saturate the phosphor screen, the integration improvement achieved by an operator can be equivalent to that predicted by the Marcum theory for signal integration outlined in this chapter.[15]

The radar equation when n pulses are integrated is

$$R_{max}^4 = \frac{P_t G A_e \sigma}{(4\pi)^2 k T_0 B F_n (S/N)_n} \qquad [2.33]$$

where the parameters are the same as previously used, except that $(S/N)_n$ is the signal-to-noise ratio of each of the n equal pulses that are integrated. Also, the half-power

bandwidth B is used instead of the noise bandwidth B_n, as mentioned in Sec. 2.3. To employ this form of the equation it is necessary to have, for each value of n, a set of curves for $(S/N)_n$ similar to those of Fig. 2.6 for $n = 1$. Such curves are available[16] but are not necessary since only Figs. 2.6 and 2.7 are needed. Substituting Eq. (2.32) for $(S/N)_n$ into (2.33) gives

$$R_{\max}^4 = \frac{P_t G A_e \sigma n E_i(n)}{(4\pi)^2 k T_0 B F_n (S/N)_1} \qquad [2.34]$$

The value of $(S/N)_1$ is found from Fig. 2.6, and the integration improvement factor $nE_i(n)$ is found from Fig. 2.7a.

An approximation for the signal-to-noise ratio per pulse is given by an empirical formula due to Albersheim,[11,12] which is an extension of Eq. (2.30).

$$(S/N)_n = -5 \log_{10} n + \left(6.2 + \frac{4.54}{\sqrt{n - 0.44}}\right) \times \log_{10} (A + 0.12AB + 1.7B) \qquad [2.35]$$

where the signal-to-noise ratio per pulse $(S/N)_n$ is in dB, n is the number of independent (pulse) samples integrated, and A and B are the same as defined for Eq. (2.30). This equation is said to have an error of less than 0.2 dB over the range of $n = 1$ to $n = 8096$, $P_d = 0.1$ to 0.9, and $P_{fa} = 10^{-3}$ to 10^{-7}. (As noted with Eq. (2.30), Eq. (2.35) is probably a good approximation for rough calculations when P_d is even greater and P_{fa} is even lower than the above.)

The discussion of integration loss or efficiency in this section is theoretical loss. In addition, there can be loss due to the actual method used for implementing the integration process in a radar.

2.7 RADAR CROSS SECTION OF TARGETS

The radar cross section σ is the property of a scattering object, or target, that is included in the radar equation to represent the magnitude of the echo signal returned to the radar by the target. In the derivation of the simple form of the radar equation in Sec. 1.2 the radar cross section was defined in terms of Eq. (1.5), which was

$$\text{Reradiated power density back at the radar} = \frac{P_t G}{4\pi R^2} \cdot \frac{\sigma}{4\pi R^2} \qquad [1.5]$$

A definition of the radar cross section found in some texts on electromagnetic scattering is

$$\sigma = \frac{\text{power reflected toward source/unit solid angle}}{\text{incident power density}/4\pi} = 4\pi R^2 \frac{|E_r|^2}{|E_i|^2} \qquad [2.36]$$

where R is the range to the target, E_r is the electric field strength of the echo signal back at the radar, and E_i is the electric field strength incident on the target. It is assumed in the above that the target is far enough from the radar that the incident wave can be considered to be planar rather than spherical. Equation (2.36) is equivalent to the simple form

of the radar equation derived in Sec. 1.2. Sometimes the radar cross section σ is said to be a (fictional) area that intercepts a part of the power incident at the target which, if scattered uniformly in all directions, produces an echo power at the radar equal to that produced at the radar by the real target. Real targets, of course, do not scatter the incident energy uniformly in all directions.

The power scattered from a target in the direction of the radar receiver, and hence the radar cross section, can be calculated by solving Maxwell's equations with the proper boundary conditions applied or by computer modeling. The radar cross section can also be measured, based on the radar equation, using either full-size or scale models of targets.

Radar cross section depends on the characteristic dimensions of the object compared to the radar wavelength. When the wavelength is large compared to the object's dimensions, scattering is said to be in the *Rayleigh region.* It is named after Lord Rayleigh who first observed this type of scattering in 1871, long before the existence of radar, when investigating the scattering of light by microscopic particles. The radar cross section in the Rayleigh region is proportional to the fourth power of the frequency, and is determined more by the volume of the scatterer than by its shape. At radar frequencies, the echo from rain is usually described by Rayleigh scattering.

At the other extreme, where the wavelength is small compared to the object's dimensions, is the *optical region.* Here radar scattering from a complex object such as an aircraft is characterized by significant changes in the cross section when there is a change in frequency or aspect angle at which the object is viewed. Scattering from aircraft or ships at microwave frequencies generally is in the optical region. In the optical region, the radar cross section is affected more by the shape of the object than by its projected area.

In between the Rayleigh and the optical regions is the *resonance region* where the radar wavelength is comparable to the object's dimensions. For many objects, the radar cross section is larger in the resonance region than in the other two regions. These three distinct scattering regions are illustrated by scattering from the sphere described next.

Simple Targets The sphere, cylinder, flat plate, rod, ogive, and cone are examples of simple targets. Analytical expressions exist for the radar cross sections of some of these objects. Sometimes the radar cross sections of complex targets can be calculated by describing the target as a collection of simple shapes whose cross sections are known. The total cross section is obtained by summing vectorially the contributions from the individual simple shapes. A few examples will be presented to illustrate the nature of radar cross section behavior.

Sphere The sphere is the simplest object for illustrating radar scattering since it has the same shape no matter from what aspect it is viewed. Its calculated radar cross section is shown in Fig. 2.8 as a function of $2\pi a/\lambda$, the circumference measured in wavelengths, where a is the radius of the sphere and λ is the radar wavelength. The cross section in this figure is normalized by the projected physical area of the sphere, πa^2. The three different scattering regions that characterize the sphere are labeled in the figure. In the Rayleigh region where $2\pi a/\lambda << 1$, the radar cross section is proportional to f^4, where f = frequency = c/λ, and c = velocity of propagation.

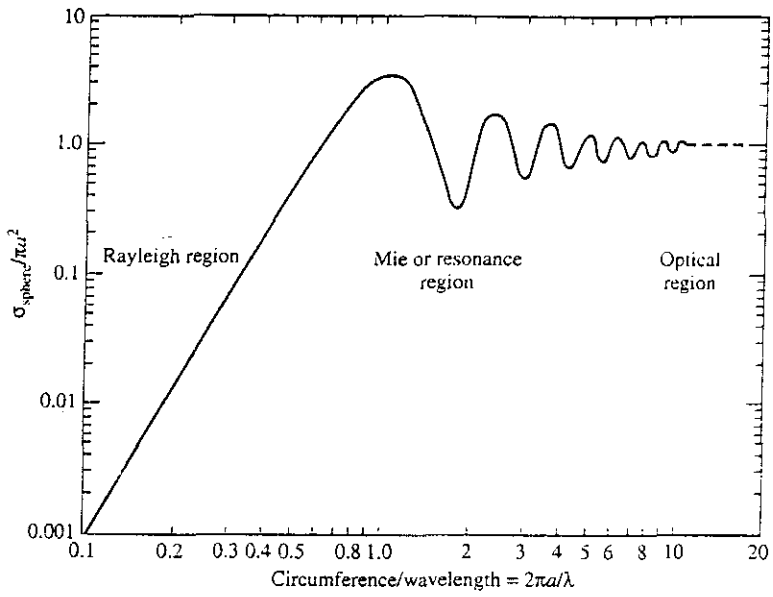

Figure 2.8 Normalized radar cross section of a sphere as a function of its circumference ($2\pi a$) measured in wavelengths.
a = radius;
λ = wavelength.

In the optical region, $2\pi a/\lambda >> 1$, the radar cross section approaches the physical area of the sphere as the frequency is increased. This unique circumstance can mislead one into thinking that the geometrical area of a target is a measure of its radar cross section. It applies to the sphere, but not to other targets. In the optical region, scattering does not take place over the entire hemisphere that faces the radar, but only from a small bright spot at the tip of the smooth sphere. It is more like what would be seen if a polished metallic sphere, such as a large ball bearing, were photographed with a camera equipped with a flash. The only illumination is at the tip, rather than from the entire hemispherical surface. A diffuse sphere or rough-surface sphere, such as a white billiard ball, would reflect from its entire surface, as does the full moon when viewed visually.

The radar cross section of the sphere in the *resonance region* oscillates as a function of frequency, or $2\pi a/\lambda$. Its maximum occurs at $2\pi a/\lambda = 1$, and is 5.6 dB greater than its value in the optical region. The first null is 5.5 dB below the optical region value. Changes in cross section occur with changing frequency because there are two waves that interfere constructively and destructively. One is the direct reflection from the front face of the sphere. The other is the *creeping wave* that travels around the back of the sphere and returns to the radar where it interferes with the reflection from the front of the sphere. The longer the electrical path around the sphere, the greater the loss, so the smaller will be the magnitude of the fluctuation with increasing frequency.

Figure 2.9 illustrates the backscatter that would be produced by a very short pulse radar that can resolve the specular echo reflected from the forward part of the sphere from the creeping wave which travels around the back of the sphere. The incident waveform in this figure is a shaped pulse of sinewave of the form $0.5[1 + \cos(\pi t/t_0)]$, where the pulse extends from $-t_0$ to $+t_0$.[17] The radius of the sphere in this example is equal to the

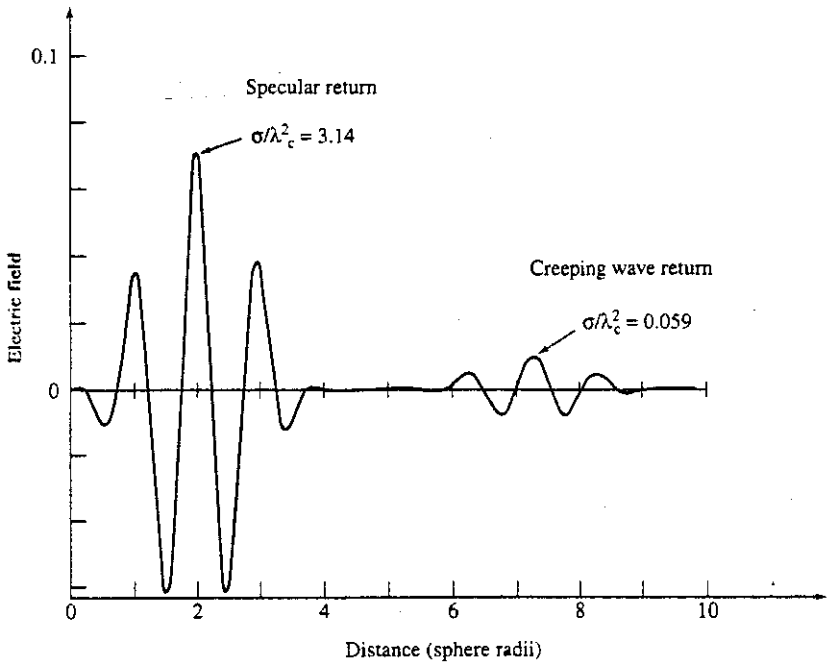

Figure 2.9 Backscattered electric field from a short pulse scattered from a conducting sphere showing the specular return from the front of the sphere and the creeping wave that travels around the back. Radius of sphere is equal to the radar wavelength λ_c.
[From J. Reinstein,[17] © 1965 IEEE.]

carrier wavelength λ_c, and the pulse width $2t_0 = 4\lambda_c$. The creeping wave lags the specular return by the time required to travel one-half the circumference of the sphere plus the diameter.

The behavior of other simple reflecting objects as a function of frequency is similar to that of the sphere, but with some differences.[18–20] It is only the sphere, however, that has a radar cross section independent of viewing aspect and polarization. (With apologies to the avant-garde writer Gertrude Stein, a sphere is a sphere is a sphere—no matter how you look at it.)

Long Thin Wire or Rod (and the Surface Traveling Wave) The experimentally measured radar cross section of a long, thin wire is shown in Fig. 2.10.[21] The wire in this case is 16.5λ long and 0.01λ in diameter. When viewed broadside ($\theta = 90°$) the radar cross section is relatively large. As the viewing angle θ departs from 90°, the cross section decreases rapidly, as expected from classical physical optics scattering theory. However, as the viewing angle decreases, an angle is reached where the backscatter levels off and then increases. This is due to a surface traveling wave, which is not predicted from physical optics theory.

This behavior was first demonstrated experimentally with a long thin rod by Leon Peters.[22] The incident electromagnetic wave couples onto the wire which then travels the length of the rod and reflects from the discontinuity at the far end. In addition to the wire

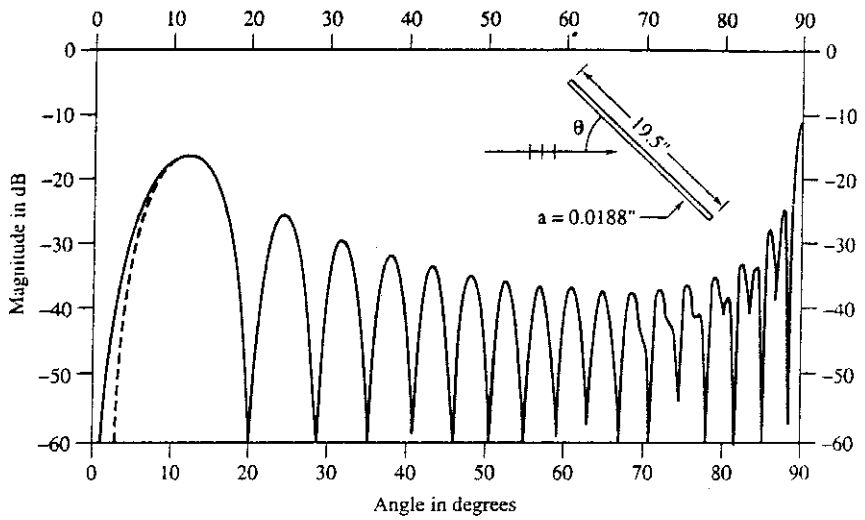

Figure 2.10 Theoretical backscattered field from a long, perfectly conducting thin wire 16.5 wavelengths long and 0.01 wavelength in diameter. Perpendicular incidence is at $\theta = 90°$. Solid curve is an approximate theory from Shamansky et al.; dashed curve is a method of moments solution. Wire dimensions shown in the figure are in inches and the frequency was 10 GHz. (From Shamansky et al.,[21] © 1989 IEEE.)

or rod, a surface traveling wave can occur with objects such as the flat plate, ogive, and the wing of an aircraft. The traveling wave is launched when the incident electric field has components perpendicular and parallel to the surface and lies in the plane of incidence defined by the surface normal and the direction of incidence. A surface traveling wave is not excited if there is no electric field component in the plane of incidence. (In the geometry of Fig. 7.2, vertical polarization, when the electric field is vertical, can excite a traveling wave, but horizontal polarization cannot.) The effect of the traveling wave is prominent when the grazing angle is small and when there is a discontinuity at the far end of the body that reflects the traveling wave back to the radar. According to Knott et al.,[23] the traveling-wave mechanism even has an effect near broadside incidence, as can be seen in Fig. 2.10. (The creeping wave, mentioned previously, is also an example of a surface traveling wave.) The traveling-wave portion of the echo is reduced if the surface is made of resistive material which causes attenuation as the wave travels down the surface and back.

Flat Plate and Corner Reflector At normal incidence (broadside) the radar cross section of a flat plate of area A in the optics region is $4\pi A^2/\lambda^2$, which can give quite large values for a modest size plate. For example, at 3-cm wavelength (X band), a square plate 0.3 m on a side (about one foot) has a radar cross section of 113 m^2 when viewed normal to the surface. The magnitude of the backscatter from a flat plate drops off rapidly with angle from the normal. The radar cross section of a dihedral or a trihedral corner reflector of projected area A is also given by the same expression as the flat plate, but it applies over a much larger viewing angle. (A dihedral corner reflector is a structure formed by two flat faces perpendicular to one another which returns the incident wave back to its

source. A trihedral corner reflector is made up of three faces mutually perpendicular to each other.)

A flat plate may be a simple structure, but its scattering behavior is not simple. Figure 2.11 is the measured cross section of a square flat plate 5λ on a side for vertical and horizontal polarization.[24,25] (The polarization of a radar wave is defined by the orientation of the electric field. Vertical polarization, for example, is when the electric field is in the vertical direction.) Note that there is a traveling-wave backscatter component. Also shown in this figure are theoretical predictions based on two different scattering theories. The theoretical prediction of scattering from this simple object does not account for the experimental observations at angles far from normal incidence.

Cone-Sphere This is a cone whose base is capped with a sphere. The first derivatives of the cone and the sphere contours are equal at the join between the two (that it, the generatrix of the cone is tangent to the sphere at the cone-sphere junction). Figure 2.12 is a plot of the calculated nose-on radar cross section of a cone-sphere with 30° cone angle as a function of $2\pi a/\lambda$, where a is the radius of the sphere.[26] An example of the radar cross section as a function of aspect angle for a cone-sphere with 25° cone angle is shown in Fig. 2.13.[27]

The cross section of the cone-sphere can be very low from nose-on to near normal incidence on the side of the cone. It is a shape sometimes considered for low cross-

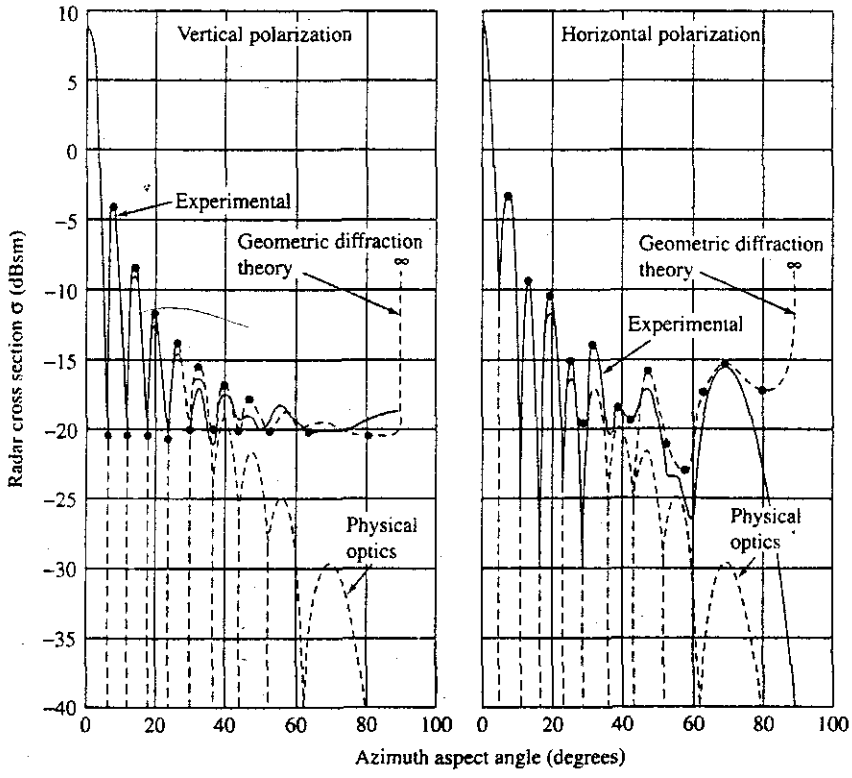

Figure 2.11 Measured radar cross section of a square flat plate, 5 wavelengths on a side compared with predictions based on physical optics and geometric diffraction theory, for vertical and horizontal polarizations. Perpendicular incidence is at 0°. The ordinate is in dBsm, which is dB relative to one square meter. (From Ross,[24] © 1966 IEEE.)

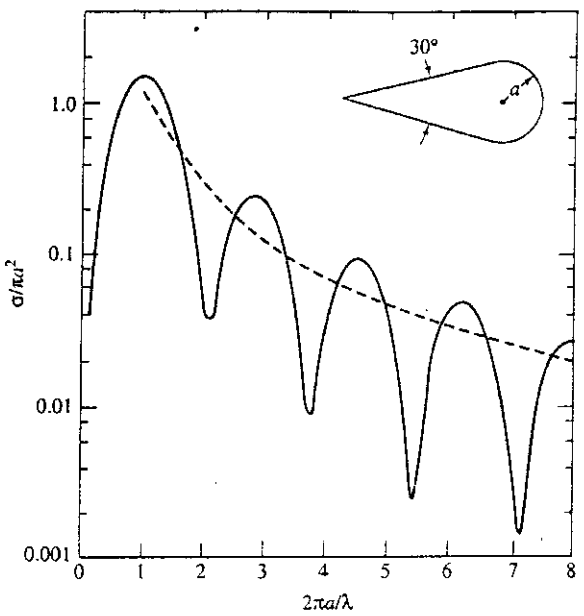

Figure 2.12 Theoretical normalized nose-on radar cross section of a cone-sphere based on an approximate impulse analysis; 15° half cone-angle (30° included cone-angle), a = radius of the sphere, and λ = wavelength. The dashed curve represents the approximation $\sigma \approx 0.1\ \lambda^2$.
[(After David Moffatt,[26] Ohio State University.)

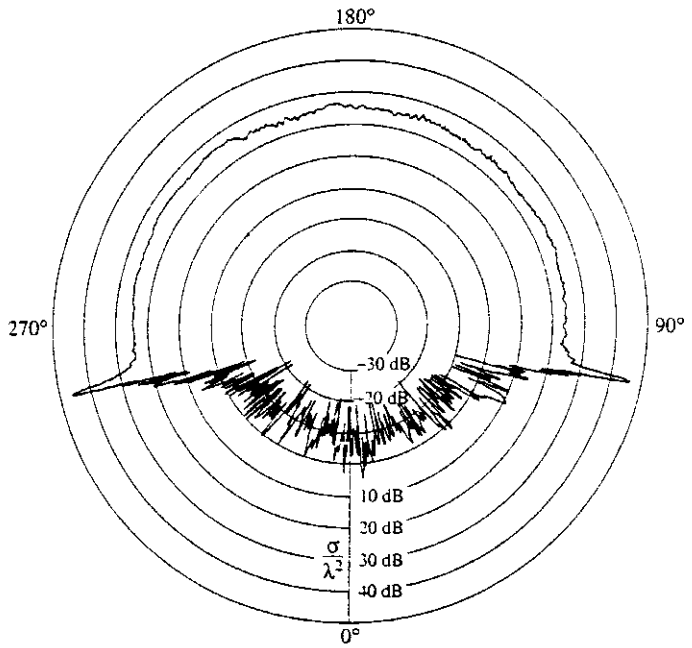

Figure 2.13 Measured radar cross section (σ/λ^2 given in dB) of a large cone-sphere with 25° cone angle and radius of spherical base = 10.4λ, for perpendicular polarization (electric field is perpendicular to the plane containing the direction of propagation and the cone axis; sometimes called horizontal polarization). For large cones the differences between perpendicular and parallel polarization are small.
[(From Pannell et al.[27] MIT Lincoln Laboratory.)

section (stealth) ballistic missile reentry vehicles. From the nose-on aspect, the radar cross section does not depend significantly on the cone angle or the volume. From the rear, the cross section is that of a sphere; hence, it is much larger than the cross section viewed from the front. A large value of cross section also occurs when the radar views the cone perpendicular to its surface. These features can be seen in Fig. 2.13. An approximate expression for estimating the radar cross section from the nose-on direction, when convenience is more important than accuracy, is $0.1\lambda^2$. This is shown by the dashed curve of Fig. 2.12.

The cone-sphere is a good example to illustrate some of the fundamental characteristics of radar scattering. Radar backscattering from metallic objects is due to discontinuities comparable to the radar wavelength and from discontinuities in the surface curvature. In the cone-sphere, echoes come from the tip and the join between the cone and the sphere, as well as from a creeping wave that travels around the sphere. The first derivatives of the cone and the sphere at the join are usually equal, but the curvature is not continuous. There is no backscatter from the sides of the cone when viewed nose-on, assuming the surface of the cone is smooth compared to the wavelength. In practice, the tip will not be of zero radius, but will be rounded. With very low cross-section targets, this rounding, even if small, can contribute to the total cross-section of the cone-sphere so that the cross section no longer varies as λ^2 for small wavelengths. With sufficiently small wavelength where the surface roughness is a significant fraction of the wavelength, scattering will be affected by the roughness and the ability to mechanically maintain the shape of the object with high precision (relative to a wavelength). The result of the rounded tip, the surface roughness, and the imprecision of the target surface contour is that the cone-sphere cross section will no longer decrease with increasing frequency, but will level off and even increase at the higher frequencies where these other factors dominate.

Effect of Target Shape In the optical region where the wavelength is small compared to the object's dimensions, the shape of a scattering object has far greater effect on its radar cross section than does its physical size. For example, at a frequency of 3 GHz (*S* band) a corner reflector (or a flat plate) of physical area 1 m^2 has a radar cross section of about 1000 m^2 (rounding off to keep the example simple). On the other hand, a cone-sphere with a 1 m^2 projected area has a radar cross section at 3 GHz equal to 0.001 m^2 (based on the approximation $\sigma \approx 0.1\lambda^2$). Thus there is a million-to-one difference in the radar cross section of two objects, even though each has the same projected area.

Complex Targets The radar cross section of complex targets such as aircraft, missiles, ships, ground vehicles, fabricated structures, buildings, and terrain can vary considerably depending on the viewing aspect and frequency. The variability results from the multiple individual scatterers that constitute the object. Each individual scatterer of a complex target produces an echo signal characterized by an amplitude and a phase. These echo signals combine at the radar to produce a resultant signal. A change in the relative phases of the echo signals from the individual scatterers will occur if the relative positions of the scatterers change with viewing aspect or there is a change in radar frequency. An example of the variation of radar cross section as a function of aspect angle from a "simple" complex target is shown in Fig. 2.14. The target consists of two equal scattering objects,

such as small spheres, separated in (a) by one wavelength and in (b) by four wavelengths. If the cross section of each of the two equal scatterers is σ_0, the resultant cross section σ_r of the two scatterers considered as one target is

$$\frac{\sigma_r}{\sigma_0} = 2\left[1 + \cos\left(\frac{4\pi l}{\lambda}\sin\theta\right)\right] \qquad [2.37]$$

where l is the separation and θ is the viewing angle with respect to the normal of the line joining the two scatterers. The value of σ_r in this example varies from a minimum of zero to a maximum of four times the cross section σ_0 of an individual scatterer. As the separation in wavelengths between the two scatterers becomes larger, the scattering lobes become narrower and more numerous.

Although this is a rather simple example of a complex target, its behavior is indicative of more complicated targets. Practical targets are composed of many individual scatterers, each with different scattering properties. Also, there may be interactions between the individual scatterers, such as multiple scattering in a corner reflector, which further complicate cross-section characteristics.

Aircraft An example of the variation of the backscatter from a propeller-driven aircraft, the two-engine B-26 medium bomber which saw much service in World War II, is shown in Fig. 2.15.[28] The aircraft was mounted on a turntable in surroundings free from other reflecting objects and was illuminated by a radar operating at 3 GHz (*S* band). The aircraft's propellers were running during the measurement and produced a modulation of the order of 1 to 2 kHz. Changes in the radar cross section by as much as 15 dB can occur for a change in aspect of only 1/3 degree. The maximum echo signal occurred in the vicinity of broadside, where the projected area of the aircraft was largest and there were large, relatively flat surfaces that produced a large return.

The following description of the major scattering features of a jet aircraft is based on information found in Knott, Shaeffer, and Tuley[29] and in Crispin and Siegel.[30] The radar cross section of a jet aircraft from the nose-on aspect is determined to a large extent by reflections from the jet engines and their intake ducts. The compressor blades on the rotating jet engines can also modulate the echo, just as do the propellers of a prop aircraft.

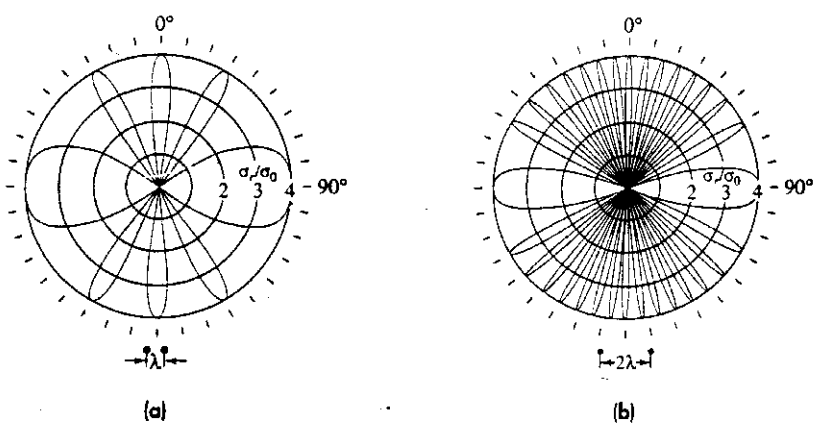

Figure 2.14 Polar plot of the radar cross section σ_r of a two-scatterer "complex" target when each scatterer has a cross section σ_0 [plot of Eq. (2.37)]. (a) separation $l = \lambda$; (b) $l = 4\lambda$.

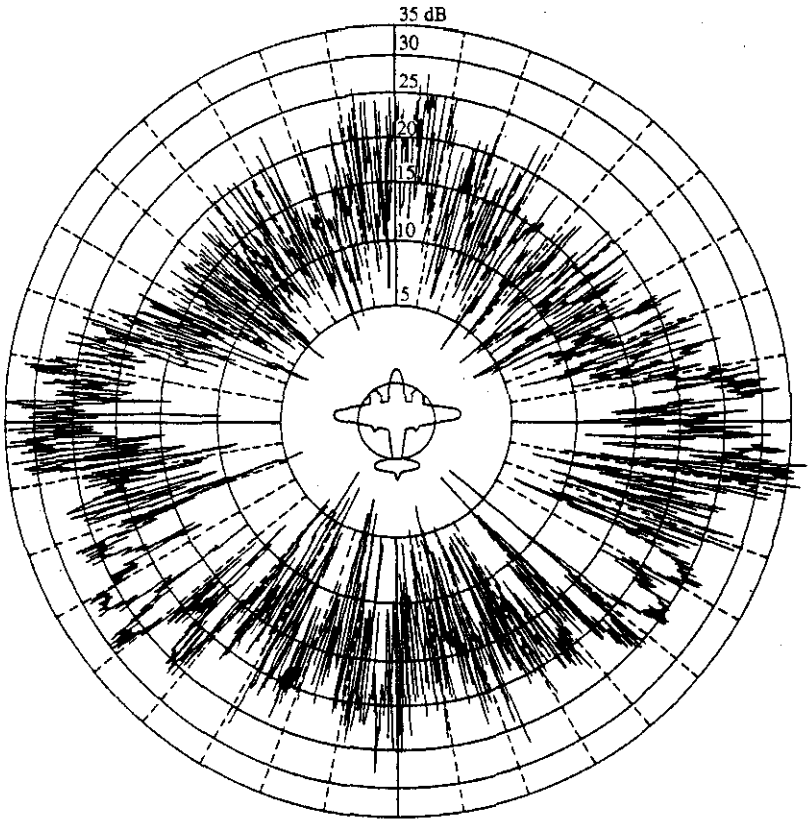

Figure 2.15 Backscatter from a full-scale B-26 two-engine (propeller driven) medium-bomber aircraft at 10-cm wavelength as a function of azimuth angle. This figure has appeared in many books on radar and radar scattering since it is one of the few examples readily available in the literature of the measurement of backscatter from a full-size aircraft without averaging over a range of angles.
(From Ridenour,[28] courtesy McGraw-Hill Book Company, Inc.)

If there is a radar antenna in the nose, the cross section can be large when the aircraft's radar antenna is pointing in the direction of the viewing radar. At angles a few degrees off the nose, the cross section generally decreases until echoes from the leading edge of the wing become important. If the radius of curvature of the leading edge of the wing is more than a few wavelengths, the echo from the wing can be significant for any polarization. If this condition is not met, the echo from the leading edge of the wing is larger when the incident radar polarization is parallel to the edge of the wing (horizontal polarization) than when it is perpendicular. If the wing is viewed from slightly below or slightly above and perpendicular to its trailing edge, a traveling wave can be induced and there can be a radar echo due to reflection from the trailing edge of the wing. This traveling-wave echo can be larger for vertical polarization than horizontal.

In the vicinity of broadside, the fuselage and the engine nacelles are the main sources of backscatter. At broadside the vertical stabilizer also can contribute to the echo. If the aircraft is viewed from considerably above the plane of the wing, there can be significant backscatter from the corner reflector formed by the wing and the fuselage. There can also be a strong echo from the corner reflector formed by the vertical fin and the horizontal stabilizer. From the vicinity of the tail-on aspect, the trailing edge of the wings contribute to the echo. Echoes are also obtained near tail-on from the engine exhaust ducts. External weapons and fuel tanks of military aircraft also contribute to the radar cross section.

An example of the radar cross section of a one-fifteenth scale model Boeing 737 commercial jet aircraft is shown in Fig. 2.16.[31] The cross section in the ordinate is in dBsm, which is decibels relative to one square meter. The values shown are for the scale model at the measured frequency of 10 GHz. At the full-scale frequency of 667 MHz, the values of cross section given by the ordinate in this figure should be increased by 23.5 dB.

The most realistic method for obtaining the radar cross section of aircraft is to measure the actual aircraft in flight. The dynamic radar cross-section measurement facility of the U.S. Naval Research Laboratory[32] was able to measure the backscatter signals from aircraft at *L, S, C, and X bands with horizontal or vertical linear polarization, circular polarization*, as well as the cross (orthogonal) polarizations on receive. Pulse-to-pulse radar measurements were recorded, but for convenience in presenting the data, the cross-section values plotted usually were an average of a large number of values taken within a 10 by 10° aspect angle. Examples are given in Fig. 2.17.

An unusual method for obtaining the scattering characteristics of aircraft in flight is the airborne synthetic aperture radar utilized by Metratek, Inc. of Reston, Virginia.[33] This is a high-resolution multifrequency imaging radar mounted on the tail of an A-3 aircraft to provide 300° coverage. The aircraft carrying the radar is maneuvered from side to side to obtain good resolution in the cross-range dimension by means of synthetic aperture processing. It has been used to image large (200-ft) aircraft in flight with high

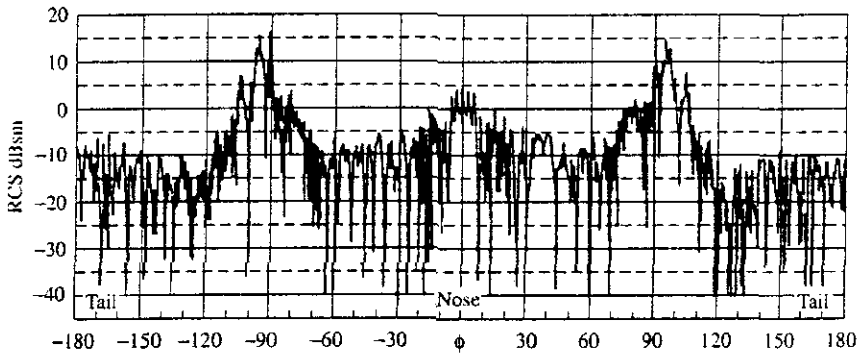

Figure 2.16 Measured radar cross section of a one-fifteenth scale model Boeing 737 commercial jetliner at the model frequency of 10 GHz with vertical polarization. The full-scale measurement would correspond to a frequency 15 times lower, which is 667 MHz. The cross section at the full-scale frequency is 23.5 dB greater than the ordinate values shown in the figure. Model was measured on a pulse-gated compact range.
(From N. A. Howell,[31] © 1970 IEEE.)

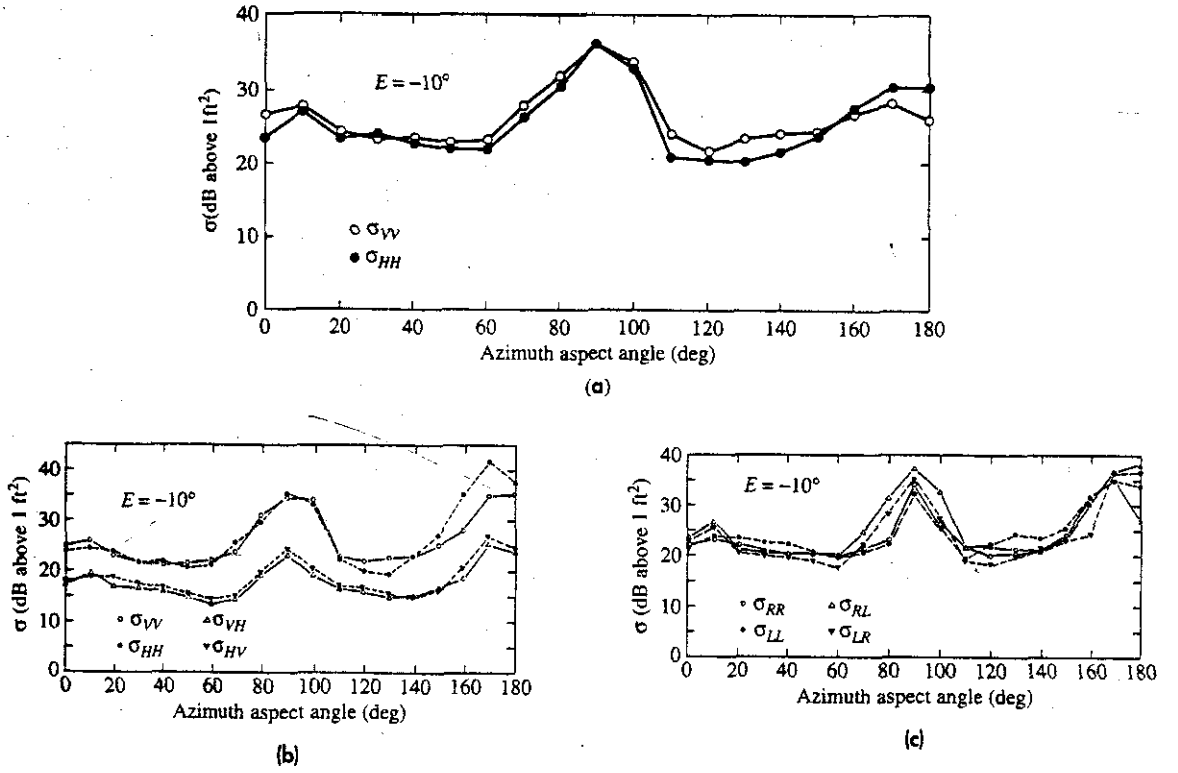

Figure 2.17 Measured radar cross section of the C-54 aircraft at a constant elevation angle of −10° measured from the aircraft. (The C-54 was a military version of the four-piston-engine DC-4 commercial aircraft with a wing span of 36 m and a length of 29 m.) Values are averaged over a 10 by 10° aspect angle. (a) 1300 MHz, linear polarization; (b) 9225 MHz, linear polarization; (c) 9225 MHz, circular polarization. The first subscript is the polarization transmitted, the second subscript is the polarization received; V = vertical, H = horizontal, R = right-hand (clockwise rotation) circular, L = left-hand (counterclockwise) circular polarization. Note that the ordinate is the cross section in dB above 1 ft². Subtract 10 dB for dB above 1 m².
[Courtesy of I. D. Olin and F. D. Queen, Naval Research Laboratory.]

resolution from VHF to at X band. An example of an aircraft image is shown in Fig. 2.18. A similar radar system mounted in the nose of a TA-3B has been reported by Hughes Aircraft Co.[34] The nose mounting permits the rear of the target aircraft to be imaged better than can a rear-mounted radar. The advantage of the high-resolution imaging method is that the individual scatterers which contribute to the backscatter can be readily recognized and their contribution to the total cross section determined.

Although the cross section of aircraft can fluctuate over a large range of values (perhaps as much as 60 dB around the entire target[29]), its average value in the microwave region usually does not vary significantly with frequency. Aircraft cross sections, however, are often larger at lower frequencies (such as VHF) than at microwave frequencies. A military propeller aircraft, such as the old AD-4B,* had a measured cross section

*The AD-4B was a 1950s propeller-engine naval attack bomber with a 50-ft wing span and 39-ft length.

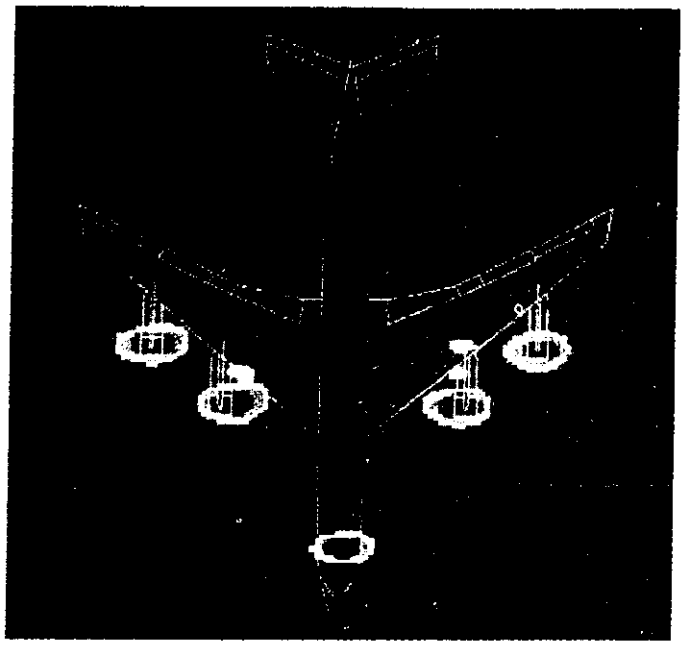

Figure 2.18 Air-to-air radar image of a KC-135, a military version of the 707 aircraft showing its major scattering centers at VHF.[33] The outline of the aircraft is shown for comparison. Resolution is about 4 ft. Aspect is nose-on and elevation angle is zero. (Courtesy of Ray Harris, Metrotek, Inc.)

approximately five times as great at VHF than at L band. At HF, the cross section of large aircraft might be more than an order of magnitude greater than at microwave frequencies.

Ships A "folk theorem" for the radar cross section of a ship is that the cross section in square meters can be approximated by the ship's displacement in tons. (The origin of this is uncertain, but the author believes he first learned of it many years ago from the General Electric Co. of Valley Forge, Pennyslvania.) Thus a 10,000-ton ship might be said to have a radar cross section of the order of 10,000 m^2. This empirical relationship is a convenient measure when no better information is available, when a single number is acceptable to describe the cross section, and when the grazing angle is not near zero degrees.

At low grazing angles near zero degrees, the median (50th percentile) value of the radar cross section can be expressed by the empirical relation[35]

$$\sigma = 52 f^{1/2} D^{3/2} \qquad [2.38]$$

where σ = radar cross section in square meters, f = radar frequency in megahertz, and D is the ship's (full load) displacement in kilotons. This value of cross section was the average taken about the port and starboard bow and quarter aspects of a number of ships (omitting the peak at broadside). Measurements on which this expression is based were at X, S, and L bands, with conventional naval ship displacements from 2000 to 17,000 tons. A plot of this equation is shown in Fig. 2.19 for the three frequencies for which measurements were taken. The values of ship cross sections at zero grazing angle are much

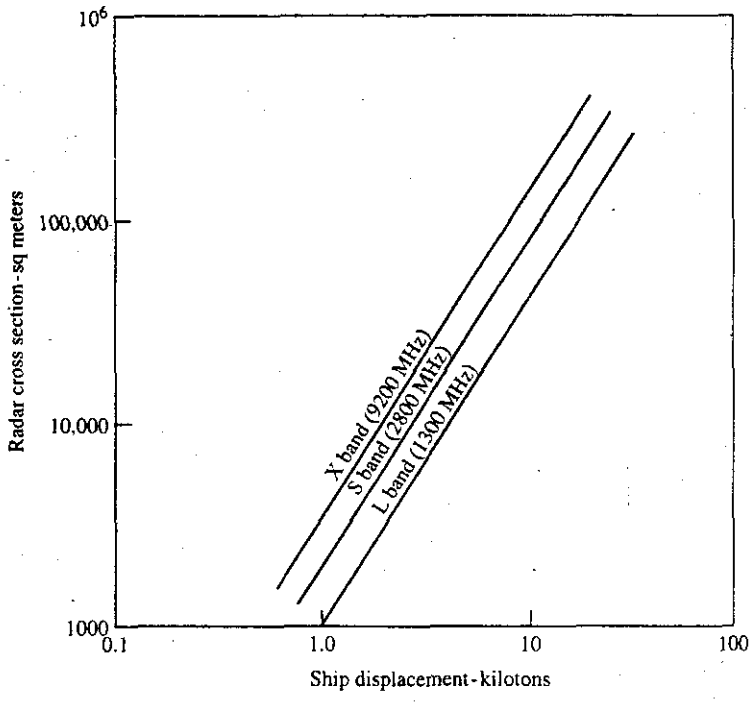

Figure 2.19 Estimate of the median value of the radar cross section of ships at grazing incidence, averaged over the bow and quarter aspects. Based on the empirical relation of Eq. (2.38).

higher than the cross sections at higher grazing angles. At zero degrees a ship's superstructure presents many vertical surfaces and corner reflectors, both of which have large backscatter echoes. An example of the measured radar cross section at grazing incidence of a 16,000-ton naval auxiliary ship is shown in Fig. 2.20.

Other Targets Missile cross sections can vary over large values depending on the type of missile. A ballistic missile with its tanks attached can be large, but the ballistic missile reentry vehicle, a small cruise missile, or antiship missile can be many orders of magnitude smaller. The range profile of a small missile viewed along its longitudinal axis is shown in Fig. 2.21.[36] The radar resolution is 0.2 m. The various scattering centers and their relative cross sections are indicated.

Automobiles generally can have a surprisingly large radar cross section. From the front the cross section might vary from 10 to 200 m^2 at X band, with 100 m^2 being a typical value.[37] This has been attributed to the flat surfaces, such as the engine's radiator, that the radar can view. Not all automobiles should be expected to have these large values, however.

The average radar cross section of small pleasure boats 20 to 30 ft in length might be in the vicinity of a few square meters at X band.[38] Boats from 40 to 50 ft in length might have a cross section of the order of 10 m^2. The measured radar cross section of a man[39] over frequencies from UHF to X band has been reported to vary from 0.03 to 1.9 m^2, with a value of one square meter usually stated as being "typical." Values of the radar cross sections of rain, snow, birds, and insects are given in Chap. 7.

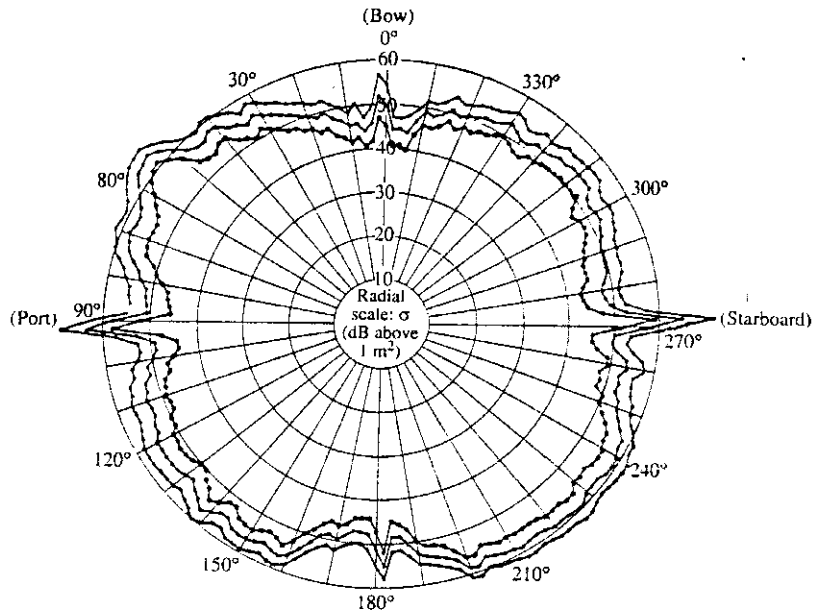

Figure 2.20 Azimuth variation of the radar cross section of a large naval auxiliary ship at *X* band, horizontal polarization, showing 20th, 50th, and 80th percentiles.

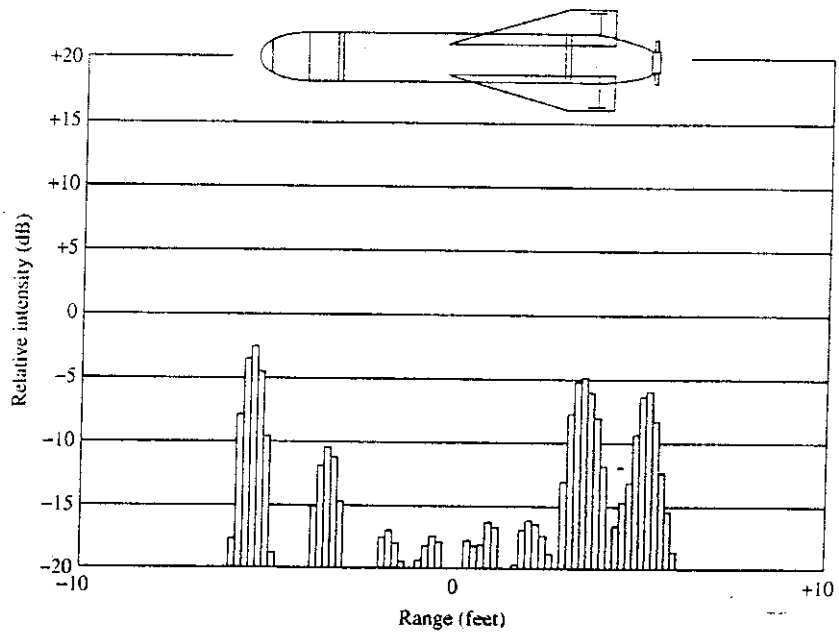

Figure 2.21 High-resolution range profile (backscatter) of a small missile, showing the individual scattering centers.
[From D. L. Mensa,[36] Reprinted with permission from Artech House, Inc., Norwood, MA, USA.]

There have been many cross section measurements of military aircraft, missiles, helicopters, and ships. This type of information, however, is usually not available for public release so there is only meager data available in the published literature on the radar scatter from current operational targets.

It has been seen in this section that the radar cross section of radar targets can vary with aspect, frequency, and polarization. A single number is not a complete measure of radar cross section. There are times, however, when a single number is desired to describe a class of radar target. Table 2.1 lists "example" single values of radar cross sections at microwave frequencies for various classes of targets. Within each class, of course, there can be wide variations in the single-value cross section given here.

There is no standard agreed-upon method for specifying the single-value cross section of a target (probably because a single number by itself is seldom used to describe a target). The average (mean) value or the median value might be taken. These depend on the probability density function that describes the fluctuations of the cross section. Sometimes a "minimum" value is used, such as the value exceeded 99, 95, or 90 percent of the time. (The reader might note that the author did not have the courage to state how the single-value cross sections listed in Table 2.1 were defined.) In any case, the variable nature of the radar cross section of real targets must be taken into account when predicting radar performance using the radar range equation.

Table 2.1 Examples of radar cross sections at microwave frequencies*

	Square meters
Conventional winged missile	0.1
Small, single engine aircraft	1
Small fighter, or four-passenger jet	2
Large fighter	6
Medium bomber or medium jet airliner	20
Large bomber or large jet airliner	40
Jumbo jet	100
Helicopter	3
Small open boat	0.02
Small pleasure boat (20–30 ft)	2
Cabin cruiser (40–50 ft)	10
Ship at zero grazing angle	See Eq. (2.38)
Ship at higher grazing angles	Displacement tonnage in m^2
Automobile	100
Pickup truck	200
Bicycle	2
Man	1
Large bird	10^{-2}
Medium bird	10^{-3}
Large insect (locust)	10^{-4}
Small insect (fly)	10^{-5}

* Although the radar cross section is given here by a single number, it is not usual that the target echo can be adequately described by a single number.

2.8 RADAR CROSS-SECTION FLUCTUATIONS

A small change in viewing aspect of a radar target such as an aircraft or ship can result in major changes in the radar cross section, as was illustrated by the cross section of an aircraft shown in Fig. 2.15. Complex targets are made up of a number of individual scattering centers, or *scatterers*. The scatterers for an aircraft might be the engines, cockpit, nose, wings, tail, and external stores. The echo from each scattering center has an amplitude and phase that usually is independent of the amplitude and phase of the echoes from other scattering centers. The phase of each scatterer is determined primarily by the distance of the individual scattering center from the radar. At the radar, the echoes from all the individual scatterers add vectorially to form a resultant amplitude and phase. If the target can be represented as a collection of independent point scatterers, the form of the echo signal $s_r(t)$ can be written as

$$s_r(t) = \sum_{i=1}^{N} a_i \sin(2\pi f t + \phi_i) = A \sin(2\pi f t + \Phi) \qquad [2.39]$$

where

$$A = \left[\left(\sum_i a_i \sin \phi_i\right)^2 + \left(\sum_i a_i \cos \phi_i\right)^2\right]^{1/2} \quad \text{and} \quad \Phi = \arctan \frac{\sum_i a_i \sin \phi_i}{\sum_i a_i \cos \phi_i}$$

In the above a_i = amplitude of the ith point scatterer, $\phi_i = 2\pi f T_i$, T_i is the round-trip time to the ith scatterer, and f is the radar frequency. A point scatterer is assumed to be one whose a_i and ϕ_i are independent of the viewing aspect. Equation (2.39) is a relatively simple model for scattering from a complex target, and it has limitations. It does not take account of multiple reflections, the shadowing of one scatterer by another, or that the target might not always be able to be represented as a collection of point scatterers. Also, the distance to the radar is assumed to be very large compared to the extent of the target so that the R^{-4} variation of the echo signal power with range R need not be taken into account for the individual scatterers. Nevertheless, it is an adequate target representation for many purposes.

If the target aspect changes relative to the radar, there will be changes in the distances to the scattering centers and the times T_i. These can cause a change in the relative phases of the echo signals from the various scatterers that make up the target. A relative phase shift greater than 2π radians can yield a significant change in the resultant phase and amplitude of the composite echo signal, which results in target cross-section fluctuations. (Sometimes the term *fading* is used in the literature for what here is called *fluctuations*.)

One straightforward method to account for a fluctuating radar cross section in the radar equation is to select a small value of cross section that has a high probability of being exceeded almost all of the time. This procedure has the advantage of being simple. It is not precise, but neither are the more widely used analytical methods, mentioned later in this section, that require knowledge of the actual statistics of the target fluctuations.

The method often employed for finding the minimum detectable signal-to-noise ratio when the target cross section is not constant is based on the *probability density*

function that describes the cross-section fluctuations. The probability density function, or pdf, gives the probability of finding a particular value of the target cross section between the values of σ and $\sigma + d\sigma$. In addition to the pdf, the variation or *correlation* of the cross section with time, or pulse to pulse, must also be known. The time variation of cross-section fluctuations differs from that of receiver noise since receiver noise is statistically independent, or uncorrelated, from pulse to pulse.

Swerling Target Models A popular method for representing the fluctuations of targets are the four statistical models described by Peter Swerling.[40] For each of these he calculated the signal-to-noise ratio required as a function of the probability of detection, probability of false alarm, and the number of pulses integrated. The four Swerling fluctuating target models are:

Case 1. The echo pulses received from a target on any one scan are of constant amplitude throughout the entire scan, but are independent (uncorrelated) from scan to scan. A target echo fluctuation of this type is called *scan-to-scan fluctuation.* It is also known as *slow fluctuations.* The probability density function for the cross section σ is

$$p(\sigma) = \frac{1}{\sigma_{av}} \exp\left(-\frac{\sigma}{\sigma_{av}}\right) \qquad \sigma \geq 0 \qquad [2.40]$$

where σ_{av} is the average over all values of target cross section. This probability density function, or pdf, applies to a target consisting of many independent scatterers of comparable echo areas; that is, no scatterer is large compared to the others. Although the pdf assumes a large number of scatterers, it has been said that as few as four or five produce a reasonably close approximation for many purposes.[40,41] The target model in Case 1 is sometimes called a *Rayleigh scatterer.* The pdf of Eq. (2.40), however, is that of the exponential [Eq. (2.18)] rather than the Rayleigh [Eq. (2.17)]. It might be recalled that the exponential pdf represents the statistics of the square of a voltage that is described by a Rayleigh pdf.

Case 2. The probability-density function is the same as that of Case 1, but the fluctuations are independent from pulse to pulse rather than from scan to scan. This is sometimes called *fast fluctuations.*

Case 3. As in Case 1, the radar cross section is assumed to be constant within a scan and independent from scan to scan; but the probability density function is given by

$$p(\sigma) = \frac{4\sigma}{\sigma_{av}^2} \exp\left(-\frac{2\sigma}{\sigma_{av}}\right) \qquad \sigma \geq 0 \qquad [2.41]$$

Swerling states that this probability density function is representative of targets that can be modeled as one large scatterer together with a number of small scatterers.

Case 4. The fluctuation is pulse to pulse, but with the same pdf as Case 3. The cross section to be substituted in the radar equation for these four cases is the average value σ_{av}.

A comparison of the four Swerling target fluctuation models and the nonfluctuating case, here called Case 0, is illustrated in Fig. 2.22 for $n = 10$ hits integrated

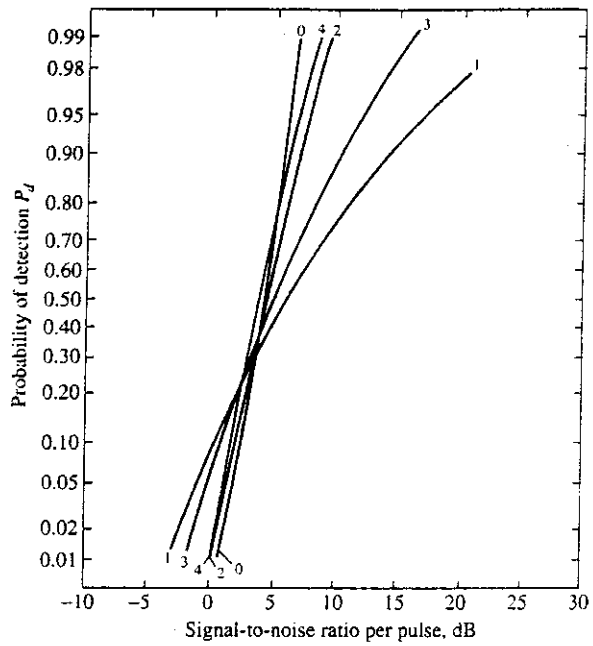

Figure 2.22 Comparison of the detection probabilities for the four Swerling models and the nonfluctuating model, for $n = 10$ pulses integrated and a false-alarm number $n_f = 10^8$. (Adopted from Swerling.[40])

postdetection and false-alarm number of 10^8 (inverse of the false-alarm probability). In general, fluctuating targets require a larger signal-to-noise ratio than nonfluctuating targets. For example, Fig. 2.22 shows that if the probability of detection is required to be 0.95, a signal-to-noise ratio of 6.2 dB per pulse is necessary when the radar cross section is constant (Case 0); but a 16.8 dB per pulse signal-to-noise ratio is required if the target fluctuates according to Case 1. Thus if the radar had been designed on the basis of a constant cross section equal to σ_{av}, but in reality the cross section fluctuated according to the model of Case 1, there would be a reduction in range by a factor of 1.84 because of the 10.6 dB difference between the two cases.

Case 1 puts more demand on the radar than do the other cases. Figure 2.22 also indicates that for probabilities of detection greater than about 0.3 (which is always true in practical situations), a greater signal-to-noise ratio is required when the fluctuations are independent scan to scan (Cases 1 and 3) than when the fluctuations are independent pulse to pulse (Cases 2 and 4). The pulse-to-pulse fluctuations of Cases 2 and 4 tend to average to that of the constant cross-section case (Case 0) as the number of independent pulses integrated increases.

The statistical theory of detection can be applied to find for each Swerling case the signal-to-noise per pulse required for a given probability of detection, probability of false alarm (or false-alarm number), and number of pulses integrated. Curves similar to those of Fig. 2.6 for the constant cross section are available for the four fluctuating models.[40,42,43] They are also included in commercially available computer programs for the radar equation.[68]

The required signal-to-noise ratio $(S/N)_1$ for Swerling Cases 1 and 3 when $n = 1$ (single-pulse detection) can be obtained by adding the value found from Fig 2.23 (dB) to

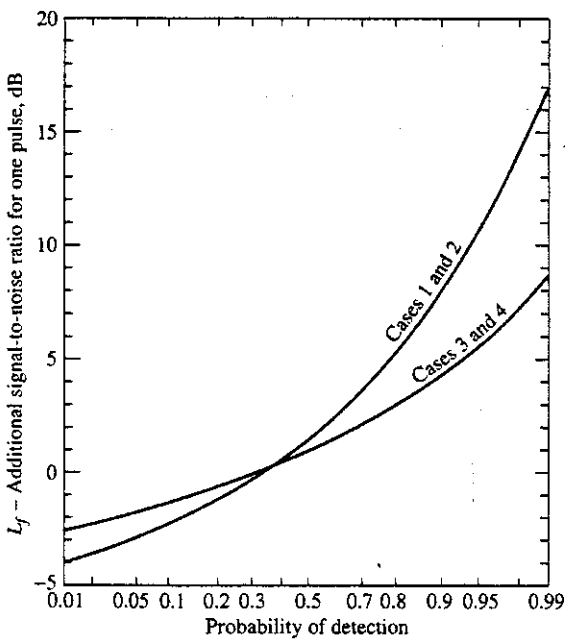

Figure 2.23 Additional signal-to-noise ratio required to achieve a particular probability of detection when the target fluctuates according to a Swerling model. The ordinate is sometimes called the *fluctuation loss*, L_f.

the signal-to-noise ratio (dB) for the nonfluctuating single-pulse signal-to-noise ratio of Fig. 2.6.

Barton[44,45] calls the ordinate of Fig. 2.23 the *fluctuation loss*, which is denoted as L_f. With scan-to-scan target fluctuations (Cases 1 and 3), the integration improvement factor $nE_i(n)$ is the same as that given by Eq. (2.7) for a constant (nonfluctuating) cross section.

To account for a fluctuating target in the radar range equation when the target is Swerling Cases 1 and 3, $(S/N)_1$ is replaced with $(S/N)_1 L_f$ and the same integration improvement factor is used as for a constant cross section. In practice, Swerling Case 1 is used more than the other three cases to describe target cross-section statistics since it requires a larger (more conservative) value of signal-to-noise ratio than the others. When the number of pulses integrated is greater than about 10 to 20, Case 2 approaches Case 1, and Case 4 approaches Case 3. Therefore, they do not have to be treated separately. The procedures for using the Swerling Cases in the radar equation are summarized later, after the discussion of partial correlation.

Partial Correlation of Target Cross Section The Swerling Cases assume that the pulses received as the antenna scans by the target are either completely correlated pulse to pulse (correlation coefficient $\rho = 1$) or completely uncorrelated pulse to pulse ($\rho = 0$). When the correlation of the pulses is some value of ρ other than 0 or 1, Barton[46] provides an empirical relationship for the required signal-to-noise ratio which compares favorably with an exact analysis by Kanter.[47] Barton states that the fluctuation loss when n_e independent samples are integrated is approximately

$$L_f(n_e) = (L_f)^{1/n_e} \qquad [2.42]$$

where L_f is the fluctuation loss as was given by Fig. 2.23 for detection with a single pulse for either Case 1 or 3. (Note that L_f in Fig. 2.23 is in dB; so that $L_f(n_e)_{dB}$ is equal to $L_f(1)_{dB}/n_e$.) The number of independent samples received from a target and integrated during the observation time t_0 is the smaller of n and n_e, where n_e is given as

$$n_e = 1 + \frac{t_0}{t_c} \leq n \qquad [2.43]$$

where t_c is the correlation time of the target echo signal and n is the total number of pulses available. Barton states that the correlation time is the inverse of the effective noise bandwidth of the two-sided fluctuation spectrum of the echo signal. It is the time required for the target cross section to change to a new value. It is not easy to specify and is highly dependent on the particular scenario.

Kanter[47] provides exact curves for the signal-to-noise ratio when expressed in terms of the correlation coefficient ρ rather than n_e. He gives the relationship between the two as

$$n_e = 1 + (n - 1)\, ln\left(\frac{1}{\rho}\right) \leq n \qquad [2.44]$$

The values of n_e in the above cannot be greater than the number of pulses n available for integration.

Radar Equation for Swerling Cases The radar equation for partially correlated Swerling Cases can be written

$$R_{max}^4 = \frac{P_t G A_e \sigma n E_i(n)}{(4\pi)^2 k T_0 B F_n (S/N)_1 (L_f)^{1/n_e}} \qquad [2.45]$$

where L_f is the fluctuation loss, or the additional signal-to-noise ratio for one pulse for a fluctuating target (given by Fig. 2.23); and n_e is the equivalent number of independent samples integrated [given by Eq. (2.43) or (2.44)]. The curve in Fig. 2.23 labeled "Cases 1 and 2" is used when the radar cross section fluctuates according to the Rayleigh pdf of Eq. (2.40). The curve labeled "Cases 3 and 4" is used when the target cross-section pdf is described by Eq. (2.41). Equation (2.45) applies to the partially correlated Swerling Cases 1 and 3 when the partial correlation is represented by the effective number of pulses integrated $n_e < n$. It also applies to the Swerling cases when the target echo is not partially correlated; i.e., $\rho = 0$ or $\rho = 1$, as summarized below:

Case 1. Completely correlated: $\rho = 1$, $n_e = 1$, L_f is that labeled for Cases 1 and 2 in Fig. 2.23.

Case 2. Completely uncorrelated: $\rho = 0$, $n_e = n$, and L_f is that labeled for Cases 1 and 2 in Fig. 2.23. When n is large ($n > 20$, $P_d \leq 0.9$), Case 2 can be replaced by Case 0 (nonfluctuating target).

Case 3. Completely correlated: $\rho = 1$, $n_e = 1$, and L_f is that labeled for Cases 3 and 4 in Fig. 2.23.

Case 4. Completely uncorrelated: $\rho = 0$, $n_e = n$, and L_f is that labeled Cases 3 and 4 in Fig. 2.23. When n is large ($n > 10$, $P_d \leq 0.9$), Case 4 can be replaced by Case 0.

Case 0. Set $L_f = 1$.

In all cases, including partial correlation, $(S/N)_1$ is given by Fig. 2.6 and the integration improvement factor $nE_i(n)$ is given by Fig. 2.7. The above procedures give results that are suitable for many engineering purposes. When more exact values are required, one should use the procedures given in the previously cited references or a suitable radar equation computer software package.

Decorrelation by Frequency Diversity or Frequency Agility A change in the radar cross section of a complex target can be obtained by a change in radar frequency, even when the target aspect is fixed. In other words, the target echo can be decorrelated by a sufficient change in frequency. If a target can be considered as made up of only two major scatterers separated in the range (radial) coordinate by a distance D, the phase difference of the echo signals from the two is $4\pi(f/c)D$. A change in frequency Δf produces a change in phase $\Delta\phi = 4\pi(\Delta f/c)D$. If the phase change is greater than 2π radians, the resultant signal is considered independent of the previous signal. Thus a change in frequency $\Delta f \geq c/2D$ decorrelates the echo. (The separation D in an actual target may be some characteristic target dimension projected along the radial coordinate. It might be the projected separation between two major scatterers that are near the extremes of the target. It is not necessarily the projected physical length of the target since the echoes from the target extremes might be small compared to those from other scatterers that make up the target.)

Decorrelation of the echo signal can be obtained by either frequency diversity or frequency agility. *Frequency diversity* means that more than one transmitter, each at a different frequency, is utilized in parallel with each transmitter channel operating as a separate radar. (The separate frequencies can also be obtained from one wideband transmitter, but that is not what is envisioned in this particular discussion.) Most air-traffic-control radars usually employ two transmitters in order to achieve the redundancy necessary for reliable civil air-traffic control. Rather than have each transmitter operate at the same frequency, they generally operate at two different frequencies in order to obtain two independent echo signals. If the echo is very small on one frequency, it will likely be larger on the other if the second frequency is widely separated from the first. The improvement that might be gained in using frequency diversity can be found from Fig. 2.23 for the fluctuation loss. For example, if the target cross section is described by Case 1 (scan-to-scan independence), the fluctuation loss for a 0.8 probability of detection (the value usually specified by the U.S. Federal Aviation Agency for its air-traffic-control radars) is 5.4 dB. When two independent frequencies are used, the fluctuation loss (in dB) is one-half this value; so that there is a gain due to frequency diversity of 2.7 dB, in addition to the 3 dB provided by the second transmitter.

Although there is a gain in using frequency diversity, it is more difficult to accurately quantify than indicated by the simple example above. It depends on the probability of detection. If the probability of detection were $P_d = 0.9$, the improvement due to frequency diversity is 4 dB when two independent frequencies are used, rather than the 2.7 dB when $P_d = 0.8$. With $P_d = 0.5$, the diversity improvement is only 0.8 dB, so that use of two

frequencies in this case offers little value. On the other hand, when the P_d is required to be 0.99, two independent frequencies provide a diversity improvement of 8.6 dB. Thus frequency diversity can be of value when a high probability of detection is required and the pulses are very highly correlated.

There is not much to gain, however, in continuing to add transmitters beyond two or three. If the fluctuation loss is 5.4 dB (as for $P_d = 0.8$ in the above example) two transmitters give a diversity improvement of 2.7 dB, three give a diversity improvement of 3.6 dB, and four give an improvement of 4.1 dB. Most applications of frequency diversity radar are satisfied with the gain offered by just two transmitters.

Pulse-to-pulse change in frequency is called *frequency agility*. The target cross section is decorrelated if the change in radar frequency is greater than $\Delta f = c/2D$, where D is the effective radial size of the target. The total number of independent samples available within a total bandwidth B is

$$n_e = 1 + \frac{B}{\Delta f} \qquad [2.46]$$

Frequency agility can be accomplished with a single wideband transmitter. It is mentioned here as a method for increasing the detectability of a target. It is also a tactic available to combat narrowband hostile jamming. Pulse-to-pulse frequency agility, however, is not suitable for radars that require doppler processing to detect moving targets in clutter (as in the MTI and pulse doppler radars discussed in Chap. 3) since these radars must utilize multiple pulses at the same frequency in order to extract the doppler frequency shift. Doppler processing, on the other hand, is compatible with frequency diversity.

Chi-Square Target Model The two probability density functions of Eqs. (2.41) and (2.42) that are used in the four Swerling models are special cases of the chi-square probability density function of degree $2m$.[41,48] The chi-square pdf is

$$p(\sigma) = \frac{m}{(m-1)!\,\sigma_{\text{av}}} \left(\frac{m\sigma}{\sigma_{\text{av}}}\right)^{m-1} \exp\left(-\frac{m\sigma}{\sigma_{\text{av}}}\right) \qquad \sigma > 0 \qquad [2.47]$$

where σ_{av} is the average, or mean, value of the cross section σ. The chi-square prf is also known as the *gamma probability density function*. In statistics texts, $2m$ is an integer equal to the number of degrees of freedom. When applied to target cross-section models, however, $2m$ is not restricted to integer values. It can be any positive, real number. When $m = 1$, the chi-square reduces to the exponential, or Rayleigh-power, pdf that applies to Swerling Cases 1 and 2. Cases 3 and 4 are equivalent to the chi-square with $m = 2$. The ratio of the standard deviation to the mean value of the chi-square pdf is equal to $m^{-1/2}$. The larger the value of m, the less will be the fluctuations; that is, the fluctuations are more constrained. The limit as $m \to \infty$ corresponds to the nonfluctuating target.

The chi-square pdf with parameter m between 0.3 and 2 has been found to approximate the statistics of certain simple shapes, such as cylinders or cylinders with fins.[49]

Other Target Models The Rice probability density function that was encountered in Sec. 2.5 has also been suggested as a target cross-section model when the target can be

represented as one dominant scatterer together with a collection of small independent scatterers.[50] The Rice pdf is

$$p(\sigma) = \frac{1+s}{\sigma_{av}} \exp\left[-s - \frac{\sigma}{\sigma_{av}}\left(1+s^2\right)\right] I_0\left(2\sqrt{\frac{\sigma}{\sigma_{av}} s(1+s)}\right) \qquad \sigma > 0 \quad [2.48]$$

where s is the ratio of the radar cross section of the single dominant scatterer to the total cross section of the small scatterers, and $I_0(\cdot)$ is the modified Bessel function of zero order. Its description appears similar to the description of the chi-square with $m = 2$ (Swerling Cases 3 and 4), but it is not the same.

The log-normal pdf has also been considered for representing some types of target echo fluctuations. It is given by

$$p(\sigma) = \frac{1}{\sqrt{2\pi} s_d \sigma} \exp\left\{-\frac{1}{2s_d^2}\left[ln\left(\frac{\sigma}{\sigma_m}\right)\right]^2\right\} \qquad \sigma > 0 \quad [2.49]$$

where s_d = standard deviation of $ln\,(\sigma/\sigma_m)$, and σ_m = median value of σ. The ratio of the mean to the median value of σ is exp $(s_d^2/2)$. There is no theoretical target model that leads to the log-normal pdf, but it has been suggested that it can approximate cross-section statistics from some satellite bodies, ships, cylinders, plates, and arrays.[51,52] The log-normal pdf usually has higher values of mean-to-median than other pdfs. It also has a higher probability of obtaining abnormally high values than other pdfs (usually expressed as its distribution having "high tails").

There are a number of other statistical models that might be used. Shlyakin[53] provides a comprehensive review of many of the statistical representations that have been considered for modeling radar signals. Although most of these are two-parameter pdfs, he includes three- and four-parameter statistical models as well. The more parameters, the closer it might fit experimental data. Only a few of these statistical pdfs, however, can be derived from some basic physical model. It seems that the only justification for using most of the available analytical statistical models is that they can be made to "curve fit" some particular set of experimental data.

Which Target Model to Use A valid concern is how to model real target behavior so that radar performance can be predicted from the radar range equation. If the statistics of the target's cross section can be determined or assumed, application of the classical theory of detection of signals in noise can provide the required signal-to-noise ratio as a function of the probabilities of detection and false alarm, and the number of pulses integrated. As has been indicated, however, this is not practical except in special cases. It is made difficult because the cross-section statistics can vary with aspect, duration of observation, and frequency.

Although few real targets uniquely fit a mathematical model with any precision, it has been said that measurements[54] of aircraft targets indicate that in many cases the Rayleigh model (chi-square with $m = 1$) provides a closer fit than other models. On the other hand, experimentally measured values of the parameter m in the chi-square pdf were found to change with aspect and could vary from about 0.5 to almost 20. There were even examples when no value of m could fit the data. Thus it is difficult to reliably fit a target with a statistical model that is applicable over a variety of conditions.

Another concern when using statistical target models, such as the chi-square, is what average value of target cross section σ_{av} to insert in the radar equation. If the cross section is averaged over the entire 4π steradians of viewing aspect, the average will be dominated by the very high values that occur at and near the broadside aspect as well as the top and bottom aspects. One can argue that these should be eliminated from the average since targets such as aircraft, missiles, or ships are seldom viewed from these aspects. If the average is to be taken only over the aspects that occur in a given scenario, then the scenario (the nature of the trajectories that determine the range of viewing aspects) needs to be specified (something not always easy to do). To make the situation worse, the average value of cross section is rarely reported. (Note that the average cross section is not the average of its values given in decibels, but the average of its numerical values.)

It can be said that there may be no analytical statistical target model or models that can reliably represent the statistics of complex target cross sections, except in special situations. This may be true, but the radar engineer has to make predictions of radar performance using the radar equation whether or not there is perfection. Engineers often have to work with compromise solutions that give usable results, if not absolute accuracy. There are at least three approaches that have been used for dealing with the radar cross section of practical targets:

1. Use the best guess for a statistical target model based as much as possible on (successful) past experience.
2. Use a constant cross-section model, but select a value of cross section that is exceeded a large fraction of the time, say 90 or 95 percent or higher. This is the simplest method.
3. Use the Swerling Case 1 model (chi-square with $m = 1$ and scan-to-scan fluctuations). It produces a conservative estimate (large signal-to-noise ratio). This model is often used by radar procurement agencies when specifying the contractual performance required of a new radar. Its large values of signal-to-noise ratios when the probability of detection is high provide a bit of a cushion to the radar design.

Because of its simplicity, the author prefers using the constant cross section (no. 2 above). The Swerling Case 1, however, is probably the most widely employed. It is a good approach if a large probability of detection is used, such as $P_d = 0.9$ or higher. Sometimes a lower P_d has been used with Case 1, but this defeats its advantage as a conservative estimate. There is little difference among the Swerling models and the constant cross-section model with a P_d of 0.5. There is no point, therefore, in specifying a sophisticated target model for low values of P_d.

Sellers of radars like to quote the range performance of their products with P_d of 0.5; buyers of radars want to see the performance based on a P_d of 0.9 or higher. The author's preference is that radar performance be based on a high P_d, such as 0.9.

2.9 TRANSMITTER POWER

The power P_t in the simple radar equation derived in Sec. 1.2 was not actually specified but is usually *peak power* of the pulse. (It is not the *instantaneous* peak power of a pulse of sinewave, but one-half the instantaneous peak value.) The *average power* P_{av} of a radar

is also of interest since it is a more important measure of radar performance than the peak power. It is defined as the average transmitter power over the duration of the total transmission. If the transmitter waveform is a train of rectangular pulses of width τ and constant pulse-repetition period $T_p = 1/f_p$ (f_p = pulse repetition frequency), the average power is related to the peak power by

$$P_{av} = \frac{P_t \tau}{T_p} = P_t \tau f_p \qquad [2.50]$$

The radar *duty cycle* (sometimes called *duty factor*) can be expressed as P_{av}/P_t, or τ/T_p, or τf_p. Pulse radars might typically have duty cycles of from 0.001 to 0.5, more or less. A CW radar has a duty cycle of unity. The duty cycle depends on the type of waveform, the pulse width, whether or not pulse compression is used, the problems associated with range and doppler ambiguities, and the type of transmitter employed.

Writing the range equation of Eq. (2.45) in terms of average power by substituting Eq. (2.50) for P_t gives

$$R_{max}^4 = \frac{P_{av} G A_e \sigma n E_i(n)}{(4\pi)^2 k T_0 F_n (B\tau)(S/N)_1 f_p} \qquad [2.51]$$

For simplicity, the fluctuation loss L_f, as included in Eq. (2.45), has been set equal to unity. It should be reinserted, of course, when needed to account for Swerling target models. The symbols in this equation have been defined previously, but the reader can find them listed under Eq. (2.61) in Sec. 2.13. The bandwidth and the pulse width are grouped together since the product of the two is approximately unity in a well-designed radar.

From the definition of duty cycle given above, the energy per pulse, $E_p = P_t \tau$, is also equal to P_{av}/f_p. Substituting the latter into Eq. (2.51) gives the radar equation in terms of energy, or

$$R_{max}^4 = \frac{E_p G A_e \sigma n E_i(n)}{(4\pi)^2 k T_0 F_n (B\tau)(S/N)_1} = \frac{E_T G A_e \sigma E_i(n)}{(4\pi)^2 k T_0 F_n (B\tau)(S/N)_1} \qquad [2.52]$$

where E_T is the total energy of the n pulses, which equals nE_p.

2.10 PULSE REPETITION FREQUENCY

The pulse repetition frequency (prf) is often determined by the maximum unambiguous range beyond which targets are not expected. As in Sec. 1.1, the prf corresponding to a maximum unambiguous range, R_{un}, is given by $f_p = 2R_{un}/c$, where c is the velocity of propagation. There are times, however, when echoes might appear from beyond the maximum unambiguous range, especially for some unusually large target or clutter source (such as a mountain), or when anomalous propagation conditions (Sec. 8.5) occur to extend the normal range of the radar beyond the horizon. Echo signals that arrive at a time later than the pulse-repetition period are called *second-time-around echoes*. They are also called *multiple-time-around echoes*, particularly when they arrive from ranges greater than $2R_{un}$. The apparent range of these ambiguous echoes can result in error and confusion.

Another problem with multiple-time-around echoes is that clutter echoes from ranges greater than R_{un} can mask unambiguous target echoes at the shorter ranges.

Some types of radars, such as pulse doppler radars, always operate with a prf that can result in range ambiguities. As described in Sec. 3.9, range ambiguities are tolerated in a pulse doppler radar in order to achieve the benefits of a high prf when detecting moving targets in the midst of clutter. Resolving the range ambiguities is an important part of the operation of pulse doppler radars.

The existence of multiple-time-around echoes cannot be readily recognized with a constant prf waveform. Consider the three targets labeled *A*, *B*, and *C* in Fig. 2.24a. Target *A* is within the unambiguous range interval R_{un}, target *B* is at a distance greater than R_{un} but less than $2R_{un}$, while target *C* is greater than $2R_{un}$ but less than $3R_{un}$. Target *B* is a second-time-around echo; target *C* is a multiple-time-around echo. When these three pulse repetition intervals, or sweeps, are superimposed on a radar display such as the A-scope of Fig. 2.24b or a PPI, the ambiguous echoes (*B* and *C*) look no different from the unambiguous-range echo of *A*. Only the range of *A* is correct, but it cannot be determined from this display that the other two are not at their apparent range.

Ambiguous-range echoes can be recognized by changing the prf of the radar. When the prf is changed, the unambiguous echo (at a range less than R_{un}) remains at its true range. Ambiguous-range echoes, however, appear at different apparent ranges for each

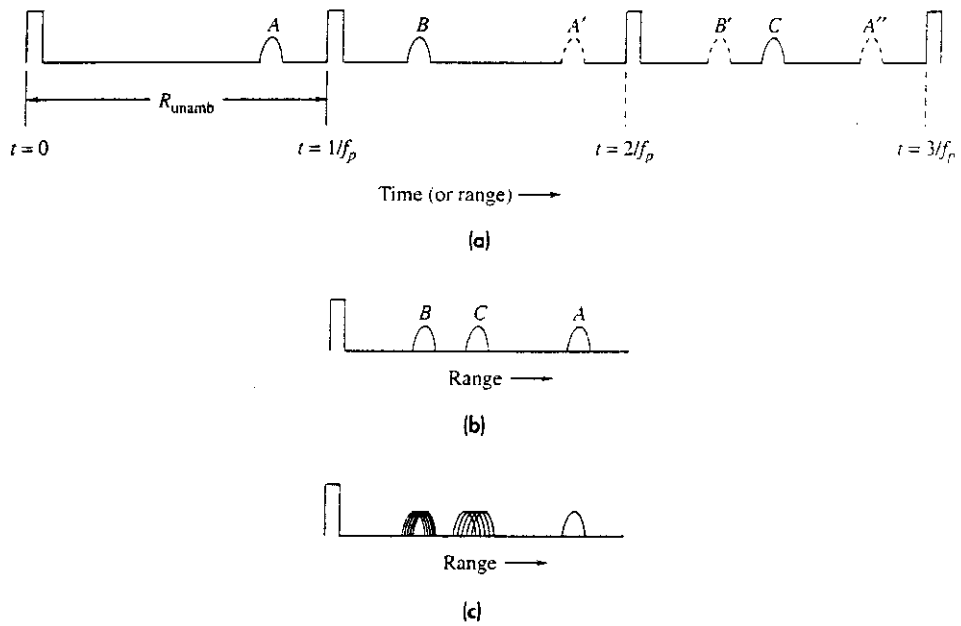

Figure 2.24 Multiple-time-around radar echoes that give rise to ambiguities in range. (a) Three targets *A*, *B*, and *C*, where *A* is within the unambiguous range R_{un}, *B* is a second-time-around echo, and *C* is a multiple-time-around echo; (b) the appearance of the three echoes on an A-scope; (c) appearance of the three echoes on the A-scope with a changing prf.

prf. An example of how these three echoes might appear on an A-scope is shown in Fig. 2.24c. A similar effect would be seen on the PPI. Thus the ambiguous target ranges can be readily identified.

If the first pulse repetition frequency f_1 has an unambiguous range R_{un1}, and if the apparent range measured with prf f_1 is denoted R_1, then the true range is one of the following

$$R_{true} = R_1, \text{ or } (R_1 + R_{un1}), \text{ or } (R_1 + 2R_{un1}), \text{ or } \ldots$$

Anyone of these might be the true range. To find which is correct, the prf is changed to f_2 with an unambiguous range R_{un2}, and if the apparent measured range is R_2, the true range is one of the following

$$R_{true} = R_2, \text{ or } (R_2 + R_{un2}), \text{ or } (R_2 + 2R_{un2}), \text{ or } \ldots$$

The correct range is that value which is the same with the two prfs. In theory, two prfs can resolve the range ambiguity; but in practice, three prfs are often used for increased accuracy and avoiding false values.

The pulse repetition frequency may be changed pulse to pulse, every half beamwidth (with a scanning antenna), or on every rotation of the antenna. Each method has been used, and there are benefits as well as limitations of each.

2.11 ANTENNA PARAMETERS

Almost all radars use *directive antennas* with relatively narrow beamwidths that direct the energy in a particular direction. The antenna is an important part of a radar. As was found from the derivation of the radar equation in Sec. 1.2, it serves to place energy on target during transmission, collect the received echo energy reflected from the target, and determine the angular location of the target. There is always a trade between antenna size and transmitter size when long-range performance is required. If one is small the other must be large to make up for it. This is one reason why large antennas are generally desirable in most radar applications when practical considerations do not limit their physical size. Thus far, the antenna has been thought of as a mechanically steered reflector. Radar antennas can also be electronically steered or mechanically steered phased arrays, as described in Chap. 9.

Antenna Gain The antenna gain $G(\theta,\phi)$ is a measure of the power per unit solid angle radiated in a particular direction by a directive antenna compared to the power per unit solid angle which would have radiated by an omnidirectional antenna with 100 percent efficiency. The gain of an antenna is

$$G(\theta,\phi) = \frac{\text{power radiated per unit solid angle at an azimuth } \theta \text{ and an elevation } \phi}{\text{(power accepted by the antenna from the transmitter)}/4\pi} \quad [2.53]$$

This is the *power gain* and is a function of direction. If it is greater than unity in some directions, it must be less than unity in other directions. There is also the *directive gain*,

which has a similar definition except that the denominator is the power *radiated* by the antenna per 4π steradians rather than the power *accepted* from the transmitter. The difference between the two is that the power gain accounts for losses within the antenna. The power gain is more appropriate for the radar equation than the directive gain, although there is usually little difference between the two in practical radar antennas, except for the phased array. The power gain and the directive gain of a radar antenna are usually considered to be the same in this text. When they are significantly different, then the distinction between the two must be made. In the radar equation, it is the maximum power gain that is meant by the parameter G.

Effective Area and Beamwidth It was mentioned in Sec 1.2 that the directive gain G and the effective area A_e (sometimes called *effective aperture*) of a lossless antenna are related by[55]

$$G = \frac{4\pi A_e}{\lambda^2} = \frac{4\pi \rho_a A}{\lambda^2} \qquad [2.54]$$

where λ = wavelength, ρ_a = antenna aperture efficiency, and A = physical area of the antenna. The gain of an antenna is approximately equal to

$$G \approx \frac{26{,}000}{\theta_B \phi_B} \qquad [2.55]$$

where θ_B and ϕ_B are the azimuth and elevation half-power beam widths, respectively, in degrees. This results in a gain of 44 dB for a one-degree pencil beam. [The justification for this equation is given in Sec. 9.2 after Eq. (9.5c).]

The half-power beamwidth of an antenna also depends on the nature of the aperture illumination and, therefore, the sidelobe level. When no specific information is available regarding the nature of the antenna, the following relation between beamwidth and antenna dimension D is sometimes used

$$\theta_B = 65\,\lambda/D \qquad \text{degrees} \qquad [2.56]$$

where the wavelength λ has the same units as the aperture dimension D. When D is the horizontal dimension of the antenna, the beamwidth θ_B is the azimuth beamwidth; when D is the vertical dimension, θ_B is the elevation beamwidth. Equation (2.56) might apply for an antenna with 25 to 28 dB peak sidelobe level.

The half-power beamwidth of an antenna can be measured somewhat accurately, but the antenna gain "is probably one of the least accurate measurements made on an antenna system."[56] It has been questioned whether "many gain estimates are more accurate than $\pm$ 0.5 dB.[57] Therefore, it is not necessary to give the gain of the usual radar antenna (in dB) to more than one decimal place.

Revisit Time The *revisit time* is the time that an antenna takes to return to view the same region of space. It usually represents a compromise between (1) the need to collect sufficient energy (a sufficient number of pulses) for the detection of weak targets and (2) the need to have a rapid re-measurement of the location of a moving target so as to quickly determine its trajectory. The revisit time is also called the *scan time;* and both are

inversely related to the *rotation rate* (rpm) of a scanning antenna. The revisit times of long-range civil air-traffic-control radars are generally in the vicinity of 10 to 12 s, corresponding to an antenna rotation rate of 6 to 5 rpm. Military air-surveillance radars, unlike civil radars, have to detect and track high-speed maneuvering targets. A revisit time of 10 to 12 seconds is too long. Revisit times for long-range military radars are more like 4 seconds (15 rpm). Short-range military radars that must detect and quickly respond to low-flying high-speed targets that pop up over the near horizon generally require revisit times of 1 or 2 seconds (60 or 30 rpm), depending on the radar type and design. A small civil marine radar commonly found on boats and ships might have a rotation rate of about 20 rpm (3-s revisit time). High-resolution radars which monitor the ground traffic at major airports, as the ASDE shown in Fig. 1.6, generally have rotation rates of 60 rpm.

Beam Shape Radars employ either *fan beams* or *pencil beams*. The beam width of the pencil beam, Fig. 2.25a, in the horizontal plane is equal or almost equal to the beamwidth in the vertical plane. Its beamwidth is generally less than a few degrees; one degree might be typical. It is found in radars that must have accurate location measurements and resolution in both azimuth and elevation. The pencil beam is popular for tracking radars, 3-D radars (rotating air-surveillance radars that obtain elevation angle measurement as well as azimuth and range), and many phased array radars.

The fan-beam antenna, Fig. 2.25b, has one angle small compared to the other. In air-surveillance radars that use fan beams, the azimuth beamwidth might typically be one or a few degrees, while the elevation beamwidth might be from perhaps four to ten times the azimuth beamwidth. Fan beams are found with 2-D (range and azimuth) air-surveillance radars that have to search out a large volume of space. The narrow beamwidth is in the horizontal coordinate so as to obtain a good azimuth angle measurement. The elevation beamwidth is broad in order to obtain good elevation coverage, but at the sacrifice of an elevation angle measurement.

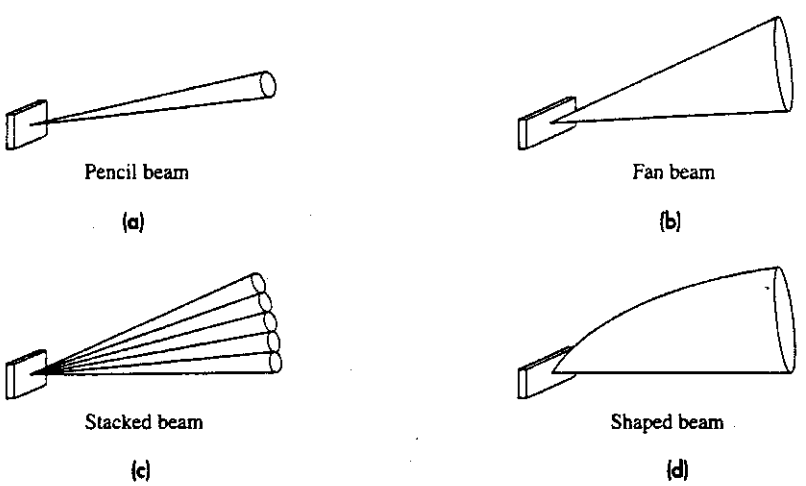

Figure 2.25 Typical radar antenna pattern types: (a) pencil beam; (b) fan beam; (c) stacked beams, or 3-D; and (d) shaped beam, such as cosecant-squared shaping.

A single pencil beam has difficulty searching out a large angular volume. Employing a number of scanning pencil beams (3 to 9 have been used) can solve this problem, as is found in some 3-D radars.[58] Sometimes in a 3-D radar a *stacked-beam* coverage is used in the vertical dimension. This consists of a number of contiguous fixed pencil beams, as in Fig. 2.25c. Six to sixteen contiguous beams have been typical in the past.

Usually the shape of a fan beam has to be modified to obtain more complete coverage. An example is the cosecant-squared shaped beam, indicated by Fig. 2.25d.

Cosecant-Squared Antenna Pattern The coverage of a simple fan beam is not adequate for the detection of aircraft targets at high altitudes close to the radar. The detection of such targets requires a very broad fan beam and therefore an undesirable low gain. In addition, a fan beam radiates more energy at the higher elevation angles than is needed since aircraft are not at long ranges when viewed at high elevation angles. To obtain better illumination of close-in targets at high elevation angles, the fan-beam pattern is modified so that its gain in the elevation-angle coordinate is proportional to the square of the cosecant of the elevation angle, Fig. 2.25d. In other words, a *cosecant-squared antenna* is one whose elevation gain as a function of elevation angle ϕ is

$$G(\phi) = G(\phi_0) \frac{\csc^2 \phi}{\csc^2 \phi_0} \qquad \text{for } \phi_0 \le \phi \le \phi_m \qquad [2.57]$$

where $G(\phi)$ is the gain at the elevation angle ϕ, and ϕ_0 and ϕ_m are the angular limits between which the beam follows a cosecant-squared shape. Section 9.7 discusses this type of antenna and gives an approximate expression for the reduction in gain and effective area that occurs because of the cosecant-squared beam shape. The loss in gain or effective area can be as much as 3 dB. Also discussed in Sec. 9.7 are other forms of beam shaping that can have an effect on the gain and radar coverage.

In designing a cosecant-squared antenna for a surface-based air-surveillance radar, an elevation beamwidth ϕ_B is selected, based on the elevation coverage required at the longest range. The elevation beamwidth should be as narrow as conditions will allow (so as to obtain as high a gain as practical). One method for selecting the basic beamwidth ϕ_B is to place the maximum of the antenna beam at an elevation $\phi_B/2$, so that the direction corresponding to the lower half-power point of the radiation pattern is directed towards the horizon ($\phi = 0$ degrees). The upper half-power direction is set so that it passes through the point defined by the maximum range and the maximum target altitude. This elevation angle is $\phi_0 = \phi_B$. Then the antenna gain is made to vary as cosecant-squared from ϕ_0 to the maximum elevation angle ϕ_m. This assumes the earth is flat. With long-range radars, the round earth must be considered and the above characterization of cosecant-squared coverage must be further modified. (It will not be as simple.)

Most surface-based 2-D air-surveillance radars use some form of shaped beam, such as the cosecant-squared, to provide the desired coverage. Some airborne ground-surveillance radars also use the cosecant-squared beam shape, but inverted compared to the surface-based air-surveillance radar.

The cosecant-squared antenna for an air-surveillance radar has the property that the echo power P_r received from a target of constant cross section flying at constant altitude h is independent of the target's range R from the radar. This assumes a flat earth and that

the surface-reflection multipath which causes lobing is ignored. (The effect of lobing due to multipath is discussed in Sec. 8.2). Substituting the gain of the cosecant-squared antenna [Eq. (2.57)] into a variation of the simple form of the radar equation [Eq. (1.6) with $A_e = G\lambda^2/4\pi$] gives

$$P_r = \frac{P_t G^2 \lambda^2 \sigma}{(4\pi)^3 R^4} = \frac{P_t G^2(\phi_0) \csc^4\phi\, \lambda^2 \sigma}{(4\pi)^3 \csc^4\phi_0\, R^4} = K_1 \frac{\csc^4\phi}{R^4} \qquad [2.58]$$

where K_1 is a constant. The height h of the target is assumed constant, and since $\csc \phi = R/h$, the received power becomes $P_r = K_1/h^4 =$ constant. The echo signal is therefore independent of range when the antenna elevation pattern is proportional to the cosecant-squared of the elevation angle ϕ, with the assumptions stated.

2.12 SYSTEM LOSSES

At the beginning of this chapter it was said that one of the important factors omitted from the simple radar equation was the loss that occurs throughout the radar system. The loss due to the integration of pulses and the loss due to a target with a fluctuating cross section have been already encountered in this chapter. Propagation losses in the atmosphere are considered later, in Chap. 8. This section considers the various *system losses*, denoted L_s, not included elsewhere in the radar equation. Some system losses can be predicted beforehand (such as losses in the transmission line); but others cannot (such as degradation when operating in the field). The latter must be estimated based on experience and experimental observations. They are subject to considerable variation and uncertainty. Although the loss associated with any one factor may be small, there can be many small effects that add up and result in significant total loss. The radar designer, of course, should reduce known losses as much as possible in the design and development of the radar. Even with diligent efforts to reduce losses, it is not unusual for the system loss to vary from perhaps 10 dB to more than 20 dB. (A 12-dB loss reduces the range by one-half.)

All numerical values of loss mentioned in this section, including the above values of system loss, are meant to be illustrative. They can vary considerably depending on the radar design and how the radar is maintained.

System loss, L_s (a number greater than one), is inserted in the denominator of the radar equation. It is the reciprocal of efficiency (number less than one). The two terms (loss and efficiency) are sometimes used interchangeably.

Microwave Plumbing Losses There is always loss in the transmission line that connects the antenna to the transmitter and receiver. In addition, there can be loss in the various microwave components, such as the duplexer, receiver protector, rotary joint, directional couplers, transmission line connectors, bends in the transmission lines, and mismatch at the antenna.

Transmission Line Loss The theoretical one-way loss in decibels per 100 ft for standard waveguide transmission lines is shown in Table 2.2.[59] Since the same transmission line

Table 2.2 Attenuation of Rectangular Waveguides*

Frequency Band	EIA *Waveguide* Designation†	Frequency Range (GHz) for Dominant TE_{10} Mode	Outer Dimensions and Wall Thickness, inches	Theoretical Attenuation, Lowest to Highest Frequency, dB/100 ft (one-way)
UHF	WR-2100	0.35–0.53	21.25 × 10.75 × 0.125	0.054–0.034
L band	WR-770	0.96–1.45	7.95 × 4.1 × 0.125	0.201–0.136
S band	WR-284	2.6–3.95	3.0 × 1.5 × 0.08	1.102–0.752
C band	WR-187	3.95–5.85	2.0 × 1.0 × 0.064	2.08–1.44
X band	WR-90	8.2–12.40	1.0 × 0.5 × 0.05	6.45–4.48
K_u band	WR-62	12.4–18.0	0.702 × 0.391 × 0.04	9.51–8.31
Ka band	WR-28	26.5–40.0	0.36 × 0.22 × 0.04	21.9–15.0

*After "Reference Data for Engineers," 8th ed., M. E. Van Valkenburg, editor-in-chief, Chap. 30, *Waveguides and Resonators*, by T. Itoh, SAMS Prentice Hall Computer Publishing, Carmel, Indiana, 1993.

†UHF and *L*-band guides are made of aluminum, K_a band is silver, the rest are copper-zinc alloy.

generally is used for both transmission and reception, the loss to be inserted in the radar equation is twice the one-way loss. Flexible waveguides and coaxial lines can have higher losses than conventional waveguides. At the lower radar frequencies, the transmission line introduces little loss unless its length is exceptionally long. At the higher frequencies, attenuation may not always be small and may have to be taken into account. When practical, the transmitter and receiver should be placed close to the antenna to keep the transmission-line loss small. Additional loss can occur at each connection or bend in the line. Connector losses are normally negligible, but if the connection is poorly made, it can contribute measurable attenuation.*

Duplexer Loss The loss due to a gas duplexer that protects the receiver from the high power of the transmitter is generally different on transmission and reception. It also depends, of course, on the type of duplexer used. Manufacturers' catalogs give values for a duplexer's *insertion loss* and (for a gas duplexer) the *arc loss* when in the fired condition. The radar might also have a waveguide shutter, with some insertion loss, that closes when the radar is shut down so as to protect the receiver from extraneous high-power signals when its duplexer is not activated. A solid-state receiver protector is often used as well as a solid-state attenuator in the receiver transmission line for applying sensitivity time control (STC). The duplexer and other related devices that might be used could, in some cases, contribute more than 2 dB of two-way loss.

*At a particular radar laboratory many years ago, an old *L*-band air-surveillance radar was used as an experimental test-bed system. Its range was poor, and the engineers attributed this to its "age"—whatever that meant. Its poor performance was tolerated for many years. One day, a technician working near the transmission line to the antenna happened to find, accidentally, that one of the transmission-line connectors had not been properly secured. He tightened a few bolts and the radar "miraculously" achieved a significant increase in performance. Sometimes, it's the little things that count!

Example Although each radar can have different losses, an *S*-band (3-GHz) radar might have, by way of illustration, two-way microwave plumbing losses as follows:

100 ft of RG-113/U aluminum waveguide line	1.0 dB
Duplexer and related devices	2.0 dB
Rotary joint	0.8 dB
Connectors and bends (estimate)	0.3 dB
Other RF devices	0.4 dB
Total "example" microwave plumbing loss	4.5 dB

Antenna Losses The antenna efficiency, discussed in Chap. 9, is not included as a system loss. It should be accounted for in the antenna gain. Shaping of the antenna pattern, for example, to provide a $\csc^2$ pattern (Sec. 2.11), results in a loss that is included as an additional lowering of the antenna gain (Sec. 9.11) rather than as a system loss. The beam-shape loss of a surveillance radar, however, is usually included as part of the system losses.

Beam-Shape Loss The antenna gain that appears in the radar equation is assumed to be a constant equal to the maximum value. But in reality the train of pulses returned from a target by a scanning antenna is modulated in amplitude by the shape of the antenna beam, Fig. 2.26. Only one out of n pulses has the maximum antenna gain G, that which occurs when the peak of the antenna beam is in the direction of the target. Thus the computations of probability of detection (as given earlier in this chapter) have to take account of an amplitude-modulated train of pulses rather than constant-amplitude pulses. Some published probability of detection computations and computer programs for the radar equation account for the beam-shape loss. Others do not. When using published values of detection probability one needs to determine whether the beam-shape effect has been included or whether it must be accounted for separately. In this text, the approach is to

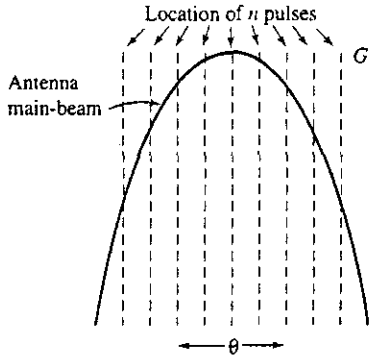

Figure 2.26 Nature of the beam-shape loss. The simple radar equation assumes n pulses are integrated, all with maximum antenna gain G. The dashed lines represent n pulses with maximum gain, and the solid curve is the antenna main-beam pattern $G(\theta)$. Except for the pulse at the center of the beam, the actual pulses illuminate the target with a gain less than the maximum.

assume a constant-amplitude pulse train as determined by the maximum antenna gain, and then add a beam-shape loss to the total system losses in the radar equation. This is a simpler, albeit less accurate, method. It is based on calculating the reduction in total signal energy received from a modulated train of pulses compared to what would have been received from a constant-amplitude pulse train. As defined, it does not depend on the probability of detection.

To obtain the beam-shape loss, the one-way-power antenna pattern is approximated by a gaussian shape given by $\exp[-2.78\ \theta^2/\theta_B^2]$, where θ is the angle measured from the center of the beam and θ_B is the half-power beamwidth. If n_B is the number of pulses received within the one-way half-power beamwidth θ_B, and n the total number of pulses integrated (n does not necessarily equal n_B), the beam-shape loss is

$$\text{Beam-shape loss} = \frac{n}{1 + 2\sum_{k=1}^{(n-1)/2} \exp[-5.55k^2/(n_B - 1)^2]} \qquad [2.59]$$

This expression applies for an odd number of pulses with the middle pulse appearing at the beam maximum. For example, if $n = 11$ pulses are integrated, all lying uniformly between the 3-dB beamwidth ($n = n_B$), the beam-shape loss is about 2 dB.

The above applies to a fan beam. It also applies to a pencil beam if the target passes directly through the center of the beam. If the target passes through any other part of the pencil beam, the maximum signal will be reduced. The beam-shape loss is increased, therefore, by the square of the maximum antenna gain seen (if the antenna were to pass through the beam center) to the square of the maximum gain actually seen (when the antenna passes through other than the beam maximum). The ratio is the square because of the two-way radar propagation.

When a large number of pulses are integrated, the scanning loss was found by Blake[60] to be 1.6 dB for a fan beam scanning in one coordinate and 3.2 dB for a pencil beam scanning in two coordinates. Blake's values are commonly used as the beam-shape loss in the radar equation, unless the number of pulses integrated is small.

A similar loss must be taken into account when searching a volume with a step-scanning pencil beam antenna (as with a phased array) since not all regions of space are illuminated with the same value of antenna gain. (In *step scanning*, the antenna beam is stationary and dwells in a fixed direction until all n pulses are collected, and then rapidly switches to dwell in a new direction.) Some tracking radars, such as conical scan, also have a loss due to the antenna beam not illuminating the target with maximum gain.

Scanning Loss When the antenna scans rapidly enough, relative to the round-trip time of the echo signal, the antenna gain in the direction of the target on transmit might not be the same as that on receive. This results in an additional loss called the *scanning loss*. It can be important for some long-range scanning radars such as those designed for space surveillance or ballistic missile defense, rather than for most air-surveillance radars.

Radome Loss introduced by a radome (Sec. 9.17) will depend on the type and the radar frequency. A "typical" ground-based metal space-frame radome might have a two-way

transmission loss of 1.2 dB at frequencies ranging from L to X band.[61] Air-supported radomes can have lower loss; the loss with dielectric space-frame radomes can be higher.

Phased Array Losses Some phased array radars have additional transmission-line losses due to the distribution network that connects the receiver and transmitter to each of the many elements of the array. These losses are more correctly included as a reduction in the antenna power gain, but they seldom are. When not included as a loss in antenna gain, they should be included under the system losses.

Signal Processing Losses Sophisticated signal processing is prevalent in modern radars and is very important for detecting targets in clutter and in extracting information from radar echo signals. Unfortunately, signal processing can introduce loss that has to be tolerated. The factors described below can introduce significant loss that has to be accounted for; doppler processing radars might have even greater loss.

Nonmatched Filter There can be from 0.5 to 1.0 dB of loss due to a practical, rather than ideal, matched filter (Sec. 5.2) A similar loss can occur with a pulse-compression filter (which is an example of a matched filter).

Constant False-Alarm Rate (CFAR) Receiver As mentioned in Sec. 5.7, this loss can be more than 2.0 dB depending on the type of CFAR.

Automatic Integrators The binary moving-window detector, for example, can have a theoretical loss of 1.5 to 2.0 dB (Sec. 5.6). Other automatic integrators might have more or less loss.

Threshold Level A threshold is established at the output of the radar receiver to achieve some specified probability of false alarm or average false-alarm time (Sec. 2.5). Because of the exponential relationship between false-alarm time and the threshold level, the threshold might be set at a slightly higher level as a safety factor to prevent excessive false alarms. Depending on how accurately the threshold can be set and maintained, the loss might be only a small fraction of a dB.

Limiting Loss Some radars might use a limiter in the radar receiver. An example is pulse-compression processing to remove amplitude fluctuations in the signal. The so-called Dicke-fix, an electronic counter-countermeasure to reduce the effects of impulsive noise, employs a hard limiter. Early MTI radars used hard limiters, but this is now considered poor practice and is almost never used since they reduce the clutter attenuation that can be obtained (Sec. 3.7). Analysis of an ideal bandpass hard limiter shows that, for small signal-to-noise ratio, the reduction in the signal-to-noise ratio of a sinewave imbedded in narrowband gaussian noise is theoretically $\pi/4$, which is about 1 dB.[62] Hard limiting with some forms of pulse compression can introduce greater loss (Table 6.6).

Straddling Loss A loss, called the *range straddling loss*, occurs when range gates are not centered on the pulse or when, for practical reasons, they are wider than optimum.

Likewise in a doppler filter bank (Sec. 3.4) there can be a *filter straddling loss* when the signal spectral line is not centered on the filter. These occur in both analog and digital processing.

Sampling Loss When digital processing is employed, a related loss to the straddling loss can occur when the video signal after the matched filter is sampled prior to digitizing by the analog-to-digital (A/D) converter. If there is only one sample per pulse width, sampling might not occur at the maximum amplitude of the pulse. The difference between the sampled value and the maximum pulse amplitude represents a *sampling loss*. The loss is about 2 dB when the sampling is at a rate of once per pulse width (applies for a probability of detection of 0.90 and probability of false alarm of 10^{-6}).[63] The larger values occur with higher probability of detection. Decreasing the sampling interval rapidly decreases the loss. When two samples per pulse are taken, the loss is approximately 0.5 dB; and with three samples per pulse, it is under 0.2 dB.

Losses in Doppler-Processing Radar* When range and/or doppler ambiguities exist (as discussed in Sec. 2.10 and Chap. 3 for MTI and pulse doppler radars), multiple redundant waveforms may be used to resolve the ambiguities or to prevent "blind speeds." Compared to a radar that has no ambiguities the redundant waveforms can represent a significant loss. The use of redundant waveforms is seldom considered as a system loss; but it can certainly affect the range of a radar. For example, in some medium prf pulse doppler radars (Sec. 3.9), eight different waveforms, each with a different prf, might need to be transmitted so as to obtain at least three dwells (with no missed targets due to blind speeds) in order to resolve the range ambiguities. The represents a loss of signal of 8/3, or 4.3 dB.

There can be an eclipsing loss in pulse doppler radars when echoes from (ambiguous) multiple-time-around targets arrive back at the radar at the same time that a pulse is being transmitted. MTI doppler processing also introduces loss due to the shape of the doppler (velocity) filters if the target velocity does not correspond to the maximum response of the doppler filter. Fill pulses in MTI and pulse doppler radar sometimes are necessary, but they represent wasted pulses from the point of view of detection of signals in noise.

Losses due to doppler processing are not always included as part of the system losses. This is justified in an MTI radar by noting that the clutter that the doppler processing is designed to remove generally does not occur at the maximum range of a radar, which is where the range performance of a radar usually is determined. Nevertheless, it should be recognized that MTI radars that employ the doppler frequency shift to detect moving targets in the presence of large clutter echoes (as discussed in Chap. 3) can seriously reduce the ability of a radar to detect a target when no clutter is present. This is why MTI processing is disconnected at ranges beyond where clutter is not expected.

Fill pulses are sometimes used in an MTI radar when the pulses are processed in batches, as in the MTD radar of Sec. 3.6. They are also sometimes used with high prf

*Doppler processing is described in Chap. 3. The reader not familiar with MTI and pulse doppler radar can skip this subsection.

doppler radar to avoid the effects of multiple-time-around clutter echoes. They are necessary for performing some types of doppler processing, but they are wasted pulses when signal-to-noise, and not signal-to-clutter, is important. They have not usually been considered as introducing a system loss, but they could if the fill pulses affect the detection of signals in noise.

Collapsing Loss If the radar were to integrate additional noise samples along with signal-plus-noise pulses, the added noise would result in a degradation called the *collapsing loss*. An example is in a 3-D radar that has a "stack" of multiple independent pencil beams in elevation. If the outputs from the N beams are superimposed on a single PPI display, at a given range resolution cell that contains the target echo the display will add $N - 1$ noise samples along with the single target echo. A collapsing loss can also occur when the output of a high-resolution radar is shown on a display whose resolution is coarser than that inherent in the radar. If the radar receiver output is automatically processed and thresholded rather than rely on an operator viewing a display to make the detection decision, there need not be a collapsing loss in the above two examples.

The mathematical derivation of the collapsing loss, assuming a square-law detector, may be carried out as suggested by Marcum.[64] He has shown that the integration of m noise pulses along with n signal-to-noise pulses with signal-to-noise ratio per pulse $(S/N)_n$ is equivalent to the integration of $m + n$ signal-to-noise pulses each with signal-to-noise ratio $n(S/N)_n/(m + n)$. Thus the collapsing loss, $L_c(m,n)$, is equal to the ratio of the integration loss L_i (Sec. 2.6) for $m + n$ pulses to the integration loss for n pulses, or

$$L_c(m,n) = \frac{L_i(m + n)}{L_i(n)} \qquad [2.60]$$

For example, assume there are 10 signal-plus-noise pulses integrated along with 30 noise-only pulses, and that $P_d = 0.90$ and $P_{fa} = 1/n_f = 10^{-8}$. From Fig. 2.8a, $L_i(40) = 3.5$ dB and $L_i(10) = 1.7$ dB, so that the collapsing loss according to Eq. (2.60) is 1.8 dB.

The above applies for a square-law detector. Trunk[65] has shown that the collapsing loss for a linear detector can be much greater than that for the square-law detector when the number of pulses integrated is small and the collapsing ratio is large, where collapsing ratio is defined as $(m + n)/n$. As the number of pulses becomes large, the difference between the two detectors becomes less, especially for low values of collapsing loss.

Operator Loss Most modern high-performance radars provide the detection decision automatically without intervention of a human operator. Processed information is presented directly to an operator or to a computer for some other action. In the early days of radar, operators were depended upon to find targets on a display. Sometimes, when the radar range performance was less than predicted, the degradation of performance was attributed to an operator loss. As engineers began to learn more about radar and the performance of the operator, it was found that an alert, motivated, well-trained operator can perform as well as indicated by theory for electronic detection. For this reason, an operator loss factor is seldom included even if the operator makes the detection decision. (When an operator is used to make detection decisions from the output of a radar display, he or she

should be replaced with a rested, alert operator every 20 to 30 min, or else performance can seriously degrade.)

Equipment Degradation It is not uncommon for radars operated under field conditions to have lower performance than when they left the factory. This loss of performance can be recognized and corrected by regularly testing the radar, especially with built-in test equipment that automatically indicates when equipment deviates from specifications. It is not possible to be precise about the amount of loss to be assigned to field degradation. From one to three dB might be used when no other information is available.

Propagation Effects The effect of the environment on the propagation of radar waves can be significant and can make the actual range considerably different from that predicted as if the radar were operated in free space. Propagation effects can increase the free-space range as well as decrease it. The major effects of propagation on radar performance are: (1) reflections from the earth's surface, which cause the breakup of the antenna elevation pattern into lobes; (2) refraction, or bending, of the propagating wave by the variation of the atmosphere's index of refraction as a function of altitude, which usually increases the radar's range; (3) propagation in atmospheric ducts, which can significantly increase the range at low altitudes; and (4) attenuation in the clear atmosphere or in precipitation, which usually is negligible at most radar frequencies.* Propagation effects are not considered part of the system losses. They are accounted for separately by a *propagation factor,* usually denoted as F^4 and, when appropriate, by an *attenuation factor* $\exp[-2\alpha R]$, where α is the attenuation coefficient (nepers per unit distance†), and R is the range. (This assumes the attenuation coefficient is independent of range.) The factor F^4 mainly includes the effects of lobing of the elevation antenna pattern due to reflection from the earth's surface (Sec. 8.2), but it can include all other propagation effects except attenuation. Both the propagation and the attenuation factors, as written, are in the numerator of the radar equation.

The effect of the environment on radar propagation and performance is the subject of Chap. 8.

Radar System Losses—the Seller and the Buyer There is no universally agreed upon procedure for determining system losses or what losses should be considered when predicting radar performance. It is natural for a person selling a radar to be optimistic about the total system loss and claim a lower loss than might a potential buyer of the radar or an independent evaluator of a radar's performance. The advertised performance predicted by a radar manufacturer cannot be adequately verified or compared to the advertised predictions for similar radars by other manufacturers without complete knowledge of the losses that each radar designer has included.

*Although attenuation in rain is usually not a factor in radar performance, the reflection from rain that competes with the target echo can seriously degrade the performance of a radar at the higher microwave frequencies, as discussed in Sec. 7.6.

†Neper is a dimensionless unit for expressing the ratio of two values of amplitude, and thus is used to express attenuation. The number of nepers is the natural logarithm of the amplitude ratio $\ln(A_2/A_1)$. Radar engineers more usually describe attenuation in decibels. One decibel equals 8.686 nepers.

2.13 OTHER RADAR EQUATION CONSIDERATIONS

Prediction of Radar Range This chapter discussed many, but not all, of the factors that might enter into the radar equation for the prediction of range, when limited by receiver noise. The simple form of the radar equation we started with as Eq. (2.1), with the modifications indicated in this chapter, now becomes

$$R_{\max}^4 = \frac{P_{\text{av}} G A \rho_a \sigma n E_i(n) F^4 e^{-2\alpha R_{\max}}}{(4\pi)^2 k T_0 F_n (B\tau) f_p (S/N)_1 L_f L_s} \qquad [2.61]$$

where

$R_{\max}$ = Maximum radar range, m
P_{av} = Average transmitter power, W
G = Antenna gain
A = Antenna area, m^2
ρ_a = Antenna aperture efficiency
σ = Radar cross section of the target, m^2
n = Number of pulses integrated
$E_i(n)$ = Integration efficiency
F^4 = Propagation factor
α = Attenuation coefficient, nepers per unit distance
k = Boltzmann's constant = 1.38×10^{-23} J/deg
T_0 = Standard temperature = 290 K
F_n = Receiver noise figure
B = Receiver bandwidth, Hz
τ = Pulse width, s
f_p = Pulse repetition frequency, Hz
$(S/N)_1$ = Signal-to-noise ratio required as if detection were based on only a single pulse
L_f = Fluctuation loss (for a Swerling target model)
L_s = System loss

The product $kT_0 = 4 \times 10^{-21}$ w/Hz. In most radar designs the product $B\tau \approx 1$. The average power can be expressed as $P_{\text{av}} = P_t \tau f_p = E_p f_p$, where E_p is the energy in a transmitted pulse. The total energy transmitted in n pulses is $E_T = nE_p$. The signal-to-noise ratio for a rectangular pulse can be expressed as an energy ratio since $S/N = (E/\tau)/N_0 B = E/(N_0 B\tau)$, where E is the energy of the received pulse, and N_0 is the receiver noise power per unit bandwidth. When $B\tau = 1$, then $(S/N)_1 = (E/N_0)_1$. Omitting the propagation factors, atmospheric attenuation, and the fluctuation loss, the radar equation can be written

$$R_{\max}^4 = \frac{E_T G A \rho_a \sigma E_i(n)}{(4\pi)^2 k T_0 (E/N_0)_1 L_s} \qquad [2.62]$$

This radar equation can be applied to any waveform, not just a rectangular pulse, so long as a matched filter is used on reception and the energy parameters are properly defined.

The radar equation, Eq. (2.61), developed in this chapter for a pulse waveform can be modified for other radars, such as CW, FM-CW, pulse doppler, and MTI. It also can be adapted to specialized radar applications such as the surveillance-radar equation, derived next. Tracking radars, synthetic aperture radars, HF over-the-horizon radars, and other specialized radars require modification of the classical radar equation to account for the special attributes of different radar systems.

When radar performance is limited by clutter echoes rather than receiver noise, the radar equation takes on a completely different form from the equations presented here, as discussed in Chap. 7. When assessing radar performance when hostile ECM noise jamming dominates, receiver noise in the denominator of the radar equation is replaced by the jamming noise that enters the radar receiver.

Surveillance-Radar Range Equation The radar equation described so far applies to a radar that dwells on the target for n pulses. The radar equation for a surveillance radar, however, is slightly different since it must account for the defining characteristic of a surveillance radar which is that it search a specified angular region in a given time. The *scan time*, or *revisit time*, is t_s, in seconds. The angular region to be searched is denoted by Ω, in steradians. (A steradian is the area subtended by a solid angle Ω on the surface of a sphere of unit radius. The total solid angle about a point is therefore 4π steradians. If the region Ω, for instance, represents 360° in azimuth and 30° in elevation, the solid angle in steradians is $2\pi \sin 30° = \pi$ steradians.)

The scan time, t_s, is equal to $t_0\Omega/\Omega_0$, where $t_0 = n/f_p$ is the time that the radar beam dwells on the target, n is the number of pulses received as the antenna scans past the target, f_p = prf, and Ω_0 is the solid angular beamwidth that is approximately equal, for small beamwidths, to the product of the azimuth beamwidth θ_a times the elevation beamwidth θ_e in radians. (This assumes θ_A/θ_a and θ_E/θ_e are integers, where θ_A is the total azimuth coverage and θ_E the total elevation coverage.) The antenna gain is approximately $G = 4\pi/\Omega_0$. With the above substitutions into a slightly simplified Eq. (2.61), the surveillance-radar equation becomes

$$R_{\max}^4 = \frac{P_{av} A_e \sigma E_i(n)}{4\pi k T_0 F_n (S/N)_1 L_s} \frac{t_s}{\Omega} \qquad [2.63]$$

This equation shows that the important parameters of a surveillance radar under the control of the radar designer are the *average power* and the *effective aperture*. The *power-aperture product*, therefore, is an important measure of the capability of a radar to perform long-range surveillance. The frequency does not appear explicitly. In practice, however, it is easier to achieve high power and large antennas at lower rather than higher frequencies. Furthermore, weather effects are less of a bother at the lower frequencies, which is something not indicated by this form of the surveillance-radar equation.

Although Eq. (2.63) illustrates the basic radar characteristics that affect the range of a surveillance radar, it is not a good equation on which to base a radar design. Too many factors are not explicitly stated. It is better to use Eq. (2.61) and the several auxiliary equations that relate to the surveillance application, such as the number of pulses received

per scan [Eq. (2.31)], and the relationship between the scan time and the coverage volume.

The surveillance radar equation does not explicitly contain the number of pulses per dwell. There should, of course, be at least one pulse; but in most cases there need to be more than one pulse. If only one or two pulses are obtained from a target, the beam-shape loss is large. In an MTI or pulse doppler radar for the detection of moving targets in clutter, the greater the time on target, the larger the number of pulses processed, and the greater will be the reduction in clutter (as discussed in Sec. 3.7 on antenna scanning modulation in MTI radar.) The surveillance radar equation given above, therefore, might need to be modified when doppler processing requires a fixed dwell time or minimum number of pulses.

M-out-of-N Criterion What has been discussed thus far is the probability of detection based on a single scan, or single observation, as the radar antenna scans by the target. A surveillance radar, however, seldom makes a detection decision that a target is present based on only a single observation. One criterion for announcing that a target is present is based on requiring M detections on N scans, where $1 < M \leq N$. For instance, the criterion for detection might be to require a detection (threshold crossing) on each of 2 successive scans, or 2 detections over 3 scans, or 3 out of 4, or 3 out of 5. Denoting the probability of detection on a single trial (scan) by P, the probability of detecting a target on M out of N trials, is given by the classical expression

$$\text{prob}\,[M \text{ out of } N] = \sum_{k=M}^{N} \frac{N!}{k!(N-k)!} P^k (1-P)^{N-k} \qquad [2.64]$$

From this expression the probability of detecting a target on $M = 2$ out of $N = 3$ scans is $3P^2 - 2P^3$. With a 2-out-of-3 criterion, the detection probability is larger than that of a single scan when the single-scan probability is greater than 0.5.

The probability of false alarm with the M-out-of-N criterion also can be found from Eq. (2.64). It will be much lower than the single-scan probability of false alarm. This means that a higher false-alarm probability per scan can be tolerated in order to achieve a specified overall false-alarm probability. For example, if the single-scan false-alarm probability were 10^{-8}, Eq. (2.64) shows that the probability of obtaining a false report of a target, when the detection criterion is 2 out of 3, would be 3×10^{-16}, which is a very low number. If the false-report probability is to be 10^{-8} when the detection criterion is 2 out of 3, the single-scan false-alarm probability can be set equal to 0.6×10^{-4}, which results in a lowering of the required detection threshold with a concurrent savings in transmitter power (or its equivalent).

Track Establishment as a Detection Criterion Many modern air-surveillance radars declare that a target is present when a track is established rather than when a single detection decision is made. As discussed in Sec. 4.9, establishment of a track requires multiple observations of a target. Since the likelihood is very small that noise alone can establish a logical track, the single-observation probability of false alarm can be relaxed. Thus the false-alarm probability of a threshold-crossing with noise alone might be as high as 10^{-3} without excessive false track-reports. One criterion used to establish a track is that there

be target echoes detected on at least 3 out of 5 scans. This is similar to the M-out-of-N criterion, except for the added constraint that the track should be within an expected speed range and not exhibit unusual changes in its trajectory. When the establishment of a valid track is taken as the criterion for the report of a target's presence, a false alarm can be made an exceedingly rare event with a well-designed radar and well-designed tracking algorithms.

Cumulative Probability of Detection If a target is observed over multiple scans, the cumulative probability of detection can be large even though the single-scan probability is small. Cumulative probability is the probability that the target is detected *at least* once on N scans. Consider a radar that can observe a target on N successive scans of the rotating antenna. It is assumed, for convenience of discussion, that the range does not change significantly over the N scans so that the change in received signal power with range need not be taken into account. The probability of detecting a target at least once during the N scans is called the *cumulative probability of detection*, P_c, and is written

$$P_c = 1 - (1 - P_d)^N \qquad [2.65]$$

where P_d = single-scan probability of detection. (The maximum radar range based on the cumulative probability of detection has been said to vary as the third power rather than the more usual fourth power variation based on the single-scan probability.[66,67]) The cumulative probability of detection, however, is *not* a good measure of radar performance since a target-detection decision can seldom be made on the basis of a single threshold crossing. Generally, more than one observation of a detection is needed before a reliable report of the presence of a target can be announced.

Verification of Predicted Range This chapter has shown that there are many factors affecting the range of a radar, and they are not always known accurately. The prediction of the maximum range is not something that can always be done as well as might be desired. Even if one could make an accurate prediction of range, there is the problem of trying to verify the prediction experimentally. Suppose, for example, an air-surveillance radar is required to have a 0.90 probability of detecting a one square meter target at a range of 200 nmi, with a false-alarm probability of 10^{-8}. A large number of observations are needed to insure that the probability of detection is actually 0.90 and not 0.80 or 0.95. It is often difficult to account for the varying target cross section not being exactly one square meter (or whatever other value the radar is designed to detect), especially when the cross section varies with viewing aspect. The effect of atmospheric refraction and multipath lobing of the elevation pattern must be known. One can, and should, experimentally determine the range performance of a radar, but one should not expect highly precise measurements.

Radar range performance of a ground-based air-surveillance radar is sometimes determined experimentally by measuring the *blip-scan ratio* as a function of range. The blip-scan ratio is an experimental approximation to the single-scan probability of detection. It is typically found by having a radar fly back and forth at constant altitude on a radial course relative to the radar, and on each scan of the antenna it is recorded whether or not a target blip is detected. This process is repeated many times until sufficient data are

obtained to compute, as a function of range, the number of scans (blips) on which the target was detected, divided by the number of times it could have been detected (scans). It provides a measure of performance for a particular aircraft flying at a particular altitude when viewed from the head-on and tail-on aspects. Ducting and other anomalous propagation effects that might occur during testing can make for difficulty, and ought to be avoided if possible.

Just as in tossing a coin many times to determine the fraction of events that it is heads, the blip-scan ratio is a statistical quantity whose accuracy depends on how many times the measurement is attempted. This is a classical statistical problem in Bernoulli trials. It is related to Eq. (2.64), which describes the probability of obtaining at least M successes out of N trials. In the experimental verification of a radar's performance, however, the problem is: given M successes out of N trials, what is the underlying probability of detection. When the number of trials is large, the probability of detection approaches M/N. Figure 2.27, provided to the author by Fred Staudaher, shows pairs of curves that statistically bound the correct values, with a confidence level of 90 percent, when the number of trials N equals 10, 100, and 1000. The abscissa is the experimentally measured blip-scan ratio of M/N. The ordinate is the range of values within which the true value of blip-scan ratio might be, with a specified probability of confidence. For example, assume that

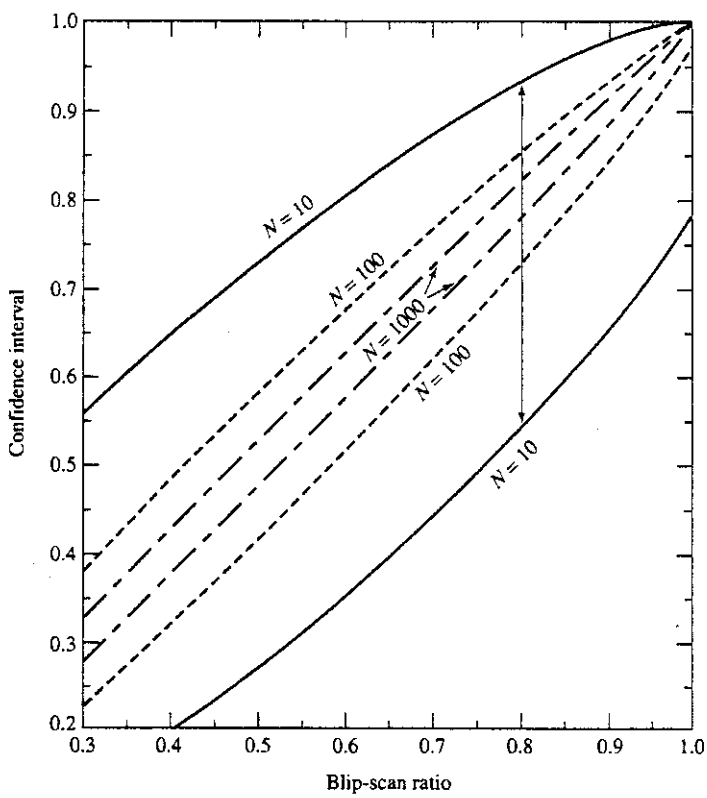

Figure 2.27 The ordinate of each pair of similarly labeled curves gives the range of confidence that the abscissa (measured blip-scan ratio) represents the true value of the blip-scan ratio (or single-scan probability of detection) with a confidence coefficient of 90 percent. N is the number of trials. See text for example. (Courtesy of Fred Staudaher.)

the measured blip-scan ratio M/N is 0.80 after 10 trials. Figure 2.27 states that there is 90 percent confidence that the true value lies between 0.54 and 0.93 (see the vertical line in Fig. 2.27). If there were only 10 trials, one would not have a good idea of the true value of the blip-scan ratio. If the measured blip-scan ratio were again 0.80 after 100 trials, its true value has 90 percent confidence of lying between 0.73 and 0.86. With 1000 trials, the true value lies within 0.78 and 0.82 with 90 percent confidence. Thus a relatively large number of trials might be required to be sure the radar meets its performance specifications.

The prediction of the range of a radar is not as exact as might be desired, and the accurate experimental measurement of its range performance is not easy. For this reason, the acceptance of a new radar system by a buyer is not usually based on the costly experimental measurement of performance. One might make a limited number of trials to insure that radar performance is not far out of line. However, for contracting purposes when buying a radar, the performance of the individual subsystems is specified (such as transmitter power, antenna gain, receiver noise figure, receiver dynamic range, and so forth) since these can be measured and used in calculations to predict what the actual performance might be when the radar is operated as a system. If each of the subsystem specifications are met, and if the specifications are properly devised, the buyer can be confident that the radar will perform as predicted.

Accuracy of the Radar Range Computation There are those who believe that each parameter that enters into the computation of range should be determined with the highest accuracy possible. The author, however, is of the opinion that the limited accuracy of many of the values that enter the radar equation, as well as the difficulty in experimentally verifying the predicted radar performance, do not justify a precision approach to radar prediction. One can't be sloppy, of course, but in engineering one cannot always be overly precise. In spite of difficulties, the engineer has to be able to guarantee that the radar can perform as required.

Calculation of the Radar Equation The range of a radar can be obtained with nothing more complicated than a simple calculator and a set of tables or graphs similar to what has been presented in this chapter. There exist, however, computer programs on the market for calculation of the radar equation.[68] They make the calculation of range easy; but they are not necessary except when it is required to plot coverage diagrams that take into account the effect of the earth's surface and other propagation factors mentioned in Chap. 8.

This chapter has been concerned with radar detection when receiver noise is the dominant factor hindering detection. The prediction of radar range when clutter echoes from the land, sea, or rain are larger than receiver noise requires a different formulation of the radar range equation, as well as a different design of the radar. Detection of targets in clutter is the subject of Chap. 7. It has been suggested[69] that computer simulation on a computer can be employed when clutter echoes, jamming noise, and receiver noise have to be considered and cannot be faithfully represented by gaussian statistics. The success of simulation depends on how well the clutter and other interfering effects can be modeled. They need to be accurate, which is not always easy to achieve in the "real world."

Radar Equation in Design In this chapter the radar equation has been discussed mainly as a means for predicting the range of a radar. It also serves the important role of being the basis for radar system design. Some parameters that enter into the radar equation are given by the customer based on the nature of the task the radar is to perform. Examples are the required range, coverage, and target characteristics. Generally there might be trade-offs and compromises required in selecting values of the other parameters that are under the control of the radar designer. It is the radar equation that is used to examine the effect of the trade-offs among the various parameters, such as the trade between a large antenna or a large transmitter power. The decision as to the radar frequency is also something that should come from examining the radar equation. Thus almost all radar design starts with the radar equation.

Conservative Design Because of the lack of precision in knowing many of the parameters that enter into the radar equation, it is advisable to design a radar as conservatively as possible. This means taking full account of all the factors affecting performance that are knowable—and then adding a safety factor to increase the signal-to-noise ratio. (One method for doing this is to specify the Swerling Case 1 target model with a probability of detection of 0.9 or greater.) Such practice has produced excellent radars that do the job required. In a few cases the radar signal-to-noise ratio was 20 dB greater than actually needed. This may be high, however, by today's standards. Only a few radars have been built with a large safety factor, but they have verified the validity of this approach. Unfortunately, the procurement practices of most agencies that buy radars, as well as the competitive nature of the marketplace, usually do not permit this degree of conservative design to occur very often.

REFERENCES

1. Ridenour, L. N. *Radar System Engineering,* MIT Radiation Laboratory Series, vol. 1, p. 592. New York: McGraw-Hill, 1947.
2. Blake, L. V. "Prediction of Radar Range." In *Radar Handbook,* 2nd ed., ed. by M. Skolnik. New York: McGraw-Hill, 1990, Chap. 2.
3. Blake, L. V. *Radar Range-Performance Analysis.* 2nd ed. Norwood, MA: Artech House, 1986.
4. Johnson, J. B. "Thermal Agitation of Electricity in Conductors." *Phys. Rev.* 32 (July 1928), pp. 97–109.
5. Lawson, J. L., and G. E. Uhlenbeck, eds. *Threshold Signals,* MIT Radiation Laboratory Series, vol. 24, p. 17. New York: McGraw-Hill, 1950.
6. Dixon, R. C. *Radio Receiver Design.* Sec. 5.5. New York: Marcel Dekker, 1998.
7. Van Vleck, J. H., and D. Middleton. "A Theoretical Comparison of the Visual, Aural, and Meter Reception of Pulsed Signals in the Presence of Noise," *J. Appl. Phys.* (November 1946), pp. 940–971.
8. Bennett, W. R. "Methods of Solving Noise Problems," *Proc. IRE* 44, (May 1956), pp. 609–638.

9. Rice, S. O. "Mathematical Analysis of Random Noise." *Bell System Tech. J.*, vol. 23, pp. 282–332, 1944; and vol. 24, pp. 46–156, 1945.
10. Davenport, W. B., and W. L. Root. *Introduction to the Theory of Random Signals and Noise.* New York: IEEE Press, 1987.
11. Albersheim, W. J. "A Closed-Form Approximation to Robertson's Detection Characteristics," *Proc. IEEE* 69 (July 1981), p. 839.
12. Tufts, D. W., and A. J. Cann. "On Albersheim's Detection Equation," *IEEE Trans.* AES-19, (July 1983), pp. 643–646.
13. Scott, A. W. *Understanding Microwaves.* New York: John Wiley, 1993.
14. Marcum, J. I. "A Statistical Theory of Target Detection by Pulse Radar, Mathematical Appendix," *IRE Trans.* IT-6 (April 1960) pp. 145–267.
15. Skolnik, M. I., and D. G. Tucker. "Discussion on 'Detection of Pulse Signals in Noise: Trace-to-Trace Correlation in Visual Displays.'" *J. Brit. IRE* 17 (December 1957), pp. 705–706.
16. Meyer, D. P., and H. A. Mayer. *Radar Target Detection.* New York: Academic, 1973.
17. Rheinstein, J. "Scattering of Short Pulses of Electromagnetic Waves." *Proc. IEEE* 53, (August 1965), pp. 1069–1070.
18. Crispin, J. W., and K. M. Siegel. *Methods of Radar Cross-Section Analysis.* New York: Academic, 1968.
19. Ruck, G. T., D. E. Barrick, W. D. Stuart, and C. K. Krichbaum. *Radar Cross Section Handbook* (2 vols.). New York: Plenum, 1970.
20. Knott, E. F., J. F. Shaeffer, and M. T. Tuley. *Radar Cross Section.* 2d ed. Norwood, MA: Artech House, 1993.
21. Shamansky, H. T., A. K. Dominek, and L. Peters, Jr. "Electromagnetic Scattering by a Straight Thin Wire," *IEEE Trans.* AP-37 (August 1989), pp. 1019–1025.
22. Peters, L., Jr. "End-fire Echo Area of Long, Thin Bodies." *IRE Trans.* AP-6 (January 1958), pp. 133–139.
23. Knott, E. F. et al. Ref. 20, Sec. 1.4, p. 228, and Sec. 6.3.
24. Ross, R. A. "Radar Cross Section of Rectangular Flat Plates." *IEEE Trans.* AP-14 (May 1966), pp. 329–335. Also discussed in Ref. 20, Sec. 6.3.
25. Knott, E. F. "Radar Cross Section." In *Radar Handbook* (ed. M. Skolnik), New York: McGraw-Hill, 1990, Chap. 11.
26. Kennaugh, E. M., and D. L. Moffatt. "On the Axial Echo Area of the Cone-Sphere Shape," *IRE Trans.* AP-10 (February 1962), pp. 199–200. See also Moffatt. D. L. "Low Radar Cross Sections, The Cone-Sphere," Ohio State University Dept. of Elect. *Eng. Rept.* 1223-5, Contract No. AF 33(616)-8039, Columbus, Ohio, May 15, 1962.
27. Pannell, J. H., J. Rheinstein, and A. F. Smith. "Radar Scattering from a Conducting Cone-Sphere," MIT Lincoln Laborataory Tech. Rept. no. 349, Mar. 2, 1964.
28. Ridenour, L. N. *Radar System Engineering.* MIT Radiation Laboratory Series, vol. 1. New York: McGraw-Hill, 1947, Fig. 3.8.
29. Knott, E. F., et al. Ref. 20, Sec. 6.5.

30. J. W. Crispin, Jr., and K. M. Siegel. *Methods of Radar Cross Section Analysis.* New York: Academic, 1962, Chap. 10.

31. Howell, N. A. "Design of Pulse Gated Compact Radar Cross Section Range," *1970 IEEE G-AP Int. Prog & Dig.,* IEEE Publ. 70c 36-AP, pp. 187–195, Sept. 1970. (Also available in refs. 20 and 25.)

32. Olin, I. D., and F. D. Queen. "Dynamic Measurement of Radar Cross Sections." *Proc. IEEE* 53 (August 1965), pp. 954–961.

33. Harris, R., R. Redman, B. Freburger, and J. Hollis. "Dynamic Air-to-Air Imaging Measurement System." *Conf. Proc. of the 14th Annual Meeting of the Antenna Measurements Techniques Assoc.* October 19–23, 1992, pp. 6-11–6-16.

34. Jain, A., and I. Patel. "Dynamic Imaging and RCS Measurements of Aircraft." *IEEE Trans.* AES-31 (January 1995), pp. 211–226.

35. Skolnik, M. I. "An Empirical Formula for the Radar Cross Section of Ships at Grazing Incidence." *IEEE Trans.* AES-10 (March 1972), p. 292.

36. Mensa, D. L. *High Resolution Radar Cross-Section Imaging.* Norwood, MA: Artech House, 1991, Sec. 4.1.

37. Chandler, R. A., and L. E. Wood. "System Considerations for the Design of Radar Braking Sensors." *IEEE Trans.* VT-26 (May 1977), pp. 151–160.

38. Williams, P. D. L., H. D. Cramp, and K. Curtis. "Experimental Study of the Radar Cross-Sections of Maritime Targets." *IEE (London) J. Electronic Circuits and Systems* 2, no. 4 (July 1978), pp. 121–136.

39. Schultz, F. V., R. C. Burgener, and S. King. "Measurement of the Radar Cross Section of a Man." *Proc. IRE* 46 (February 1958), pp. 476–481.

40. Swerling, P. "Probability of Detection for Fluctuating Targets." *IRE Trans.* IT-6 (April 1960), pp. 269–308.

41. Nathanson, F. E. *Radar Design Principles,* 2nd ed. New York: McGraw-Hill, 1991, Sec. 5.3.

42. Meyer, D. P., and H. A. Mayer. *Radar Target Detection.* New York: Academic, 1973.

43. DiFranco, J. V., and W. L. Rubin. *Radar Detection.* Englewood Cliffs, NJ: Prentice-Hall, 1968, Chap. 11.

44. Barton, D. K. *Modern Radar System Analysis.* Norwood, MA: Artech House, 1988, Sec. 2.4.

45. Barton, D. K., C. E. Cook, and P. Hamilton. *Radar Evaluation Handbook.* Norwood, MA: Artech House, 1991, Sec. 4.5.

46. Barton, D. K. "Simple Procedures for Radar Detection Calculations." *IEEE Trans.* AES-5 (September 1969), pp. 837–846.

47. Kanter, I. "Exact Detection Probability for Partially Correlated Rayleigh Targets." *IEEE Trans.* AES-22 (March 1986), pp. 184–196.

48. Swerling. P. "Radar Probability of Detection for Some Additional Fluctuating Target Cases." *IEEE Trans* AES-33 (April 1997), pp. 698–709.

49. Weinstock, W. "Target Cross Section Models for Radar Systems Analysis," doctoral dissertation, Univ. of Pennsylvania, Philadelphia, 1964.
50. Jao, J. K., and M. Elbaum. "First-Order Statistics of a Non-Rayleigh Fading Signal and Its Detection." *Proc. IEEE* 66 (July 1978), pp. 781–789.
51. Heidbreder, G. R., and R. L. Mitchell. "Detection Probabilities for Log-Normally Distributed Signals." *IEEE Trans.* AES-3 (January 1967), pp. 5–13.
52. Pollon, G. E. "Statistical Parameters for Scattering from Randomly Oriented Arrays, Cylinders, and Plates." *IEEE Trans.* AP-18 (January 1970), pp. 68–75.
53. Shlyakhin, V. M. "Probability Models of Non-Rayleigh Fluctuations of Radar Signals (A Review)." *Soviet J. Communications Technology and Electronics* 33, no. 1 (January 1988), pp. 1–16.
54. Nathanson, F. E. Ref. 41, Sec. 5.4.
55. Kraus, J. D. *Antennas,* 2nd ed. New York: McGraw-Hill, 1988, Sec. 2–22.
56. Stegen, R. J. "The Gain-Beamwidth Product of an Antenna." *IEEE Trans.* AP-12 (July 1964), pp. 505–506.
57. Evans, G. E. *Antenna Measurement Techniques.* Norwood, MA: Artech House, 1990.
58. Murrow, D. J. "Height Finding and 3D Radar." In *Radar Handbook,* 2nd ed., ed. M. Skolnik. New York: McGraw-Hill, 1990, Chap. 20.
59. Van Valkenburg, M. E., ed. *Reference Data for Engineers.* 8th ed. SAMS, Carmel, IN: Prentice-Hall Computer Publishing, 1993, Chap. 30.
60. Blake, L.V. "Prediction of Radar Range." In *Radar Handbook,* ed. M. Skolnik. New York: McGraw-Hill, 1990, Sec. 2.7.
61. Information obtained from Electronic Space Systems Corporation (Essco), Concord, MA. See also Dicaudo, V. J. "Radomes." In *Radar Handbook,* 1st ed., ed. M. Skolnik. New York: McGraw-Hill, 1970, Chap. 14.
62. Davenport, W. B., Jr. "Signal-to-Noise Ratios in Band-Pass Limiters." *J. Appl. Phys.* 24 (June 1953), pp. 720–727.
63. D'Aloisi, D., A. DiVito, and G. Galati. "Sampling Losses in Radar Signal Detection." *J. IERE* 56 (June/July 1986), pp. 237–242.
64. Marcum, J. I. Ref. 14, pp. 213–215.
65. Trunk. G. V. "Comparison of the Collapsing Losses in Linear and Square-Law Detectors." *Proc. IEEE* 80 (June 1972), pp. 743–744.
66. Mallett, J. D., and L. E. Brennan. "Cumulative Probability of Detection for Targets Approaching a Uniformly Scanning Search Radar." *Proc. IEEE* 51 (April 1963), pp. 596–601, and 52 (June 1964), pp. 708–709.
67. Brookner, E. *Radar Technology.* Dedham, MA: Artech House, 1977, Chap. 3.
68. Barton, D. K., and W. F. Barton. *Modern Radar System Analysis Software and User's Manual.* Boston, MA: Artech House, 1993.
69. Schleher, D. C. "Solving Radar Detection Problems using Simulation." *IEEE AESS Systems Magazine* 10 (April 1995), pp. 36–39.

PROBLEMS

2.1 If the noise figure of a receiver is 2.5 dB, what reduction (measured in dB) occurs in the signal-to-noise ratio at the output compared to the signal-to-noise ratio at the input?

2.2 What is the noise bandwidth B_n of a low-pass RC filter whose frequency-response function is $H(f) = \dfrac{1}{1 + j\,(f/B_v)}$, where B_v is the half-power bandwidth? That is, find the ratio B_n/B_v.

2.3 The random variable x has an exponential probability density function:

$$p(x) = a \exp\,[-bx] \qquad x > 0$$

where a and b are constants.

a. Determine the relation between a and b required for normalization.
b. Determine the mean m_1 and the variance σ^2 for the normalized $p(x)$.
c. Sketch $p(x)$ for $a = 1$.
d. Find the probability distribution function $P(x)$, and sketch the result for a = 1.

2.4 Show that the standard deviation of the Rayleigh probability density function [Eq. (2.17)] is proportional to the mean value. You should use integral tables when integration cannot be performed in a simple manner. (This result is used in deriving the form of the log-FTC clutter suppression circuit described in Sec. 7.8.)

2.5 The average time between false alarms is specified as 30 min and the receiver bandwidth is 0.4 MHz.

a. What is the probability of false alarm?
b. What is the threshold-to-noise power ratio (V_T^2/Ψ_0)?
c. Repeat (*a*) and (*b*) for an average false alarm time of one year (8760 h).
d. Assume the threshold-to-noise power ratio is to be set to achieve a 30-min false-alarm time [value as in part (*b*)]; but, for some reason, the threshold is actually set lower by 0.3 dB than the value found in part (*b*). What is the resulting average time between false alarms with the lower threshold?
e. What would be the average time between false alarms if the threshold were to increase by 0.3 dB?
f. Examine the two values of threshold-to-noise ratio you have calculated in (*d*) and (*e*) and comment on the practicability of precisely achieving a specified value of false-alarm time.

2.6 A radar has a bandwidth $B = 50$ kHz and an average time between false alarms of 10 min.

a. What is the probability of false alarm?
b. If the pulse repetition frequency (prf) were 1000 Hz and if the first 15 nmi of range were gated out (receiver is turned off) because of the use of a long pulse, what would be the new probability of false alarm? (Assume the false-alarm time has to remain constant.
c. Is the difference between (*a*) and (*b*) significant?
d. What is the pulse width that results in a minimum range of 15 nmi?

2.7 A transmission line with loss L is connected to the input of a receiver whose noise figure is F_r. What is the overall noise figure of the combination?

2.8 A radar at a frequency of 1.35 GHz has an antenna of width $D = 32$ ft, a maximum unambiguous range of 220 nmi, and an antenna scan time (time to make one rotation of the antenna) of 10 s.

a. What is the number of echo pulses per scan received by the radar from a point target? [Use the relationship that the antenna half-power beamwidth in radians is $\theta_B = 1.2\lambda/D$ (λ = wavelength).]

b. What is the integration loss and the integration-improvement factor when the probability of detection is 0.9 and the probability of false alarm is 10^{-4}?

2.9 Show that the far right-hand side of Eq. (2.36), a definition of the radar cross section, is the same as the simple radar equation, Eq. (1.6). [It easier to start with Eq. (2.36) and obtain Eq. (1.6), than vice versa.]

2.10 *a.* What frequency will result in the maximum radar cross section of a metallic sphere whose diameter is 1 m?

b. At what frequency will the radar cross section of a ball bearing one millimeter in diameter be maximum?

2.11 *a.* What is the maximum radar cross section (square meters) of an automobile license plate that is 12 inches wide by 6 inches high, at a frequency of 10.525 GHz (the frequency of an X-band speed radar)?

b. How many degrees in the vertical plane should the plate be tilted in order to reduce its cross section by 10 dB? For purposes of this problem you may assume the license plate is perfectly flat. The radar cross section of a flat plate as a function of the incidence angle ϕ may be written, for ϕ not too large, as:

$$\sigma(\phi) \approx \sigma_{\max} \frac{\sin^2 [2\pi(H/\lambda) \sin \phi]}{[2\pi(H/\lambda) \sin \phi]^2}$$

where $\sigma_{\max}$ = maximum radar cross section of a flat plate = $4\pi A^2/\lambda^2$, A = area of plate, λ = radar wavelength, and H = height of the plate. (Be careful of units. You will have to sketch a portion of the cross section pattern as a function of ϕ to find the value of ϕ corresponding to -10 dB.)

c. What other parts of an automobile might contribute to its radar cross section when viewed directly from the front?

2.12 Describe briefly the behavior of the radar cross section (in the microwave region) of a raindrop and a large aircraft with respect to its dependence on (*a*) frequency and (*b*) viewing aspect.

2.13 Describe the chief characteristic of the radar echo from a target when its radar cross section is in the (*a*) Rayleigh region, (*b*) resonance region, and (*c*) optical region.

2.14 A typical value of an individual "sea spike" echo at X band (wavelength = 3.2 cm), as discussed in Sec. 7.4, might be 1 m^2. What is the dimension of the side of a square flat plate that produces the same radar echo when the plate is viewed at normal incidence?

2.15 A radar noncoherently integrates 18 pulses, each of uniform amplitude (the nonfluctuating case). The IF bandwidth is 100 kHz.

a. If the average time between false alarms is 20 min, what must be the signal-to-noise ratio per pulse $(S/N)_n$ in order to achieve a probability of detection of 0.80? (Suggest the use of Albersheim's equation.)
b. What is the corresponding value of $(S/N)_1$?
c. What would $(S/N)_1$ be if the target cross section fluctuated according to a Swerling Case 1 model?

2.16 Why does the cross section of a complex target, such as that in Fig. 2.15, fluctuate so rapidly with a small change in aspect angle when the radar wavelength is small compared to the target's dimensions?

2.17 Show that the probability density function for the Swerling Case 1 model is the same as the chi-square of degree 2 [Eq. (2.47)].

2.18 *a.* What signal-to-noise ratio is required for a radar that makes a detection on the basis of a single pulse, when the probability of detection is 0.50 and the probability of false alarm is 10^{-6}? Assume a nonfluctuating target echo.
b. Repeat for a 0.99 probability of detection and the same probability of false alarm.
c. Repeat parts (*a*) and (*b*), but for a Swerling Case 1 fluctuating target.
d. Compare your results in a table. What conclusions can you obtain from this?

2.19 A radar measures an apparent range of 7 nmi when the prf is 4000 Hz, but it measures an apparent range of about 18.6 nmi when the prf is 3500 Hz. What is the true range (nmi)?

2.20 *a.* Show that the echo signal power P_r received from an aircraft flying at a constant height h over a perfectly conducting flat earth is independent of the range R, when the antenna elevation gain varies as the cosecant-squared of the elevation angle ϕ (that is; $G = G_0 \csc^2 \phi$).
b. In addition to having a received signal that is independent of the range (requiring less dynamic range in the receiver), what is another reason for employing an antenna with a $\csc^2 \phi$ elevation pattern for an air-surveillance radar when compared to a conventional unshaped fan-beam elevation pattern?
c. What are the limitations in applying the simple result of (*a*) to a radar in the real world?

2.21 A surface-based air-surveillance radar with a fan-beam antenna that rotates 360° in azimuth has a maximum range of 150 nmi and height coverage to 60,000 ft. Its maximum elevation-angle coverage is 30°. What percentage of the total available volume coverage is lost because of the overhead "hole" compared to a radar with complete angular coverage up to 90° (no hole in the coverage)? Assume, for simplicity, a flat earth.

2.22 A radar receives five pulses within its half-power (3 dB) beamwidth as the antenna beam scans past a point target. The middle of the five pulses is transmitted when the maximum of the antenna pattern points in the direction of the target. The first and the fifth pulses are transmitted when the leading and trailing half-power points are, respectively, directed at the target. What is the two-way beam-shape loss (dB) in this case?

2.23 Five identical radars, each with a receiver having a square-law detector, have partial overlap in their radar coverages so that not all radars are guaranteed to see each target. The outputs of all five radars are combined before a detection decision is made. If a target is

seen on only one of the five radars and the other four radars see only receiver noise, what is the collapsing loss when the detection probability is 0.5 and the false-alarm probability is 10^{-4}?

2.24 A civil marine radar is employed on boats and ships for observing navigation buoys, detecting land-sea boundaries, piloting, and avoiding collisions. Consider the following civil-marine radar:

frequency: 9400 MHz (X band)
antenna: horizontal beamwidth = 0.8°
vertical beamwidth = 15°
gain = 33 dB
azimuth rotation rate = 20 rpm
peak power: 25 kW
pulse width: 0.15 μs
pulse repetition rate: 4000 Hz
receiver noise figure: 5 dB
receiver bandwidth: 15 MHz
system losses: 12 dB
average time between false alarms: 4 hours

a. Plot the single-scan probability of detection as function of range (nmi), assuming a constant cross-section target of 10 m^2 (a navigation buoy) and free-space propagation. [You will find it easier to select the probability of detection and find the corresponding signal-to-noise ratio, rather than the reverse. You need only consider probabilities of detection from 0.30 to 0.99. You may, for purposes of this problem, select a single (average) value of the integration improvement factor rather than try to find it as a function of P_d (since the curve in the text does not permit otherwise).]
b. Repeat (*a*) for a Swerling Case 1 target fluctuation model with average cross section of 10 m^2. Plot on the same diagram as (*a*).
c. Comment on whether the average power of this radar is too low, just right, or too high for the job it has to perform here.
d. Why do you think this ship-mounted radar antenna has a 15° elevation beamwidth when all the targets are located on the surface of the sea?

2.25 Consider the following air-surveillance radar:

frequency: 2.8 GHz (S band)
peak power: 1.4 MW
pulse width: 0.6 μs
pulse repetition frequency: 1040 Hz
receiver noise figure: 4 dB
antenna rotation rate: 12.8 rpm

antenna gain: 33 dB
antenna azimuth beamwidth: 1.35 deg
system losses : 12 dB
average false-alarm time: 20 min
target cross section: 2 m^2

Plot each of the following on the same coordinates (with range as the abscissa):

a. The free-space single-scan probability of detection as a function of range (in nautical miles) for a constant cross-section target. [You will find it easier to select the probability of detection and find the corresponding signal-to-noise ratio, rather than the reverse. You need only consider probabilities of detection from 0.30 to 0.99. You may, for purposes of this problem, select a single (average) value of the integration improvement factor rather than try to find it as a function of P_d (since the curve in the text does not permit otherwise).]

b. The probability of detection as a function of range for the same situation as part (a) but with the detection criterion that the target must be found on at least 2 out of 3 scans of the rotating antenna. [You may assume that the range and the received signal power do not change appreciably over the three scans. For convenience of this calculation, you may assume that the single-scan false-alarm probability is the same as used in part (*a*).]

c. Repeat (*a*) for a Swerling Case 1 with average target cross section of 2 m^2.

d. Repeat (*b*) for a Swerling Case 1 with average target cross section of 2 m^2.

e. Is the prf adequate for avoiding range ambiguities?

(The radar in this problem is similar to the airport surveillance radar known as the ASR.)

2.26 Starting with Eq. (2.51) derive the surveillance radar equation [Eq. (2.63)]. You may omit the propagation factor, attenuation, and fluctuation loss.

2.27 What is the effect of receiver bandwidth on the maximum range of a well-designed radar, assuming the average power remains constant? Explain your answer.

2.28 *a.* What is the probability of detecting a target on at least 2 out of 4 scans when the single-scan probability of detection is 0.8?

b. What is the corresponding probability of false alarm in this case when the single-scan false-alarm probability is 10^{-8}?

c. What should be the single-scan false-alarm probability if the overall false-alarm probability with a detection criterion of 2 out of 4 scans is 10^{-8}?

d. When the higher single-scan probability of false alarm of part (*c*) is employed rather than a 10^{-8} single-scan probability of false alarm, what reduction in the signal-to-noise ratio can be obtained?

2.29 In this problem, it is assumed that the targets for an air-surveillance radar are characterized by a Swerling Case 1 model. There are n pulses received from a target. Half of the n pulses are at one frequency and the other half are at a second frequency that is far enough removed from the first to completely decorrelate the second set of $n/2$ pulses relative to

the first set of $n/2$ pulses. What is the improvement in signal-to-noise ratio obtained from this use of frequency diversity when (*a*) $P_d = 0.95$ and (*b*) $P_d = 0.6$? (*c*) If the radial extent (in range) of a target is 30 m, what must the difference in the two frequencies be to decorrelate the target echo?

2.30 *a*. Make a list of the system losses that might occur in a long-range air-surveillance radar, and estimate an approximate value for the loss due to each factor. You need not include losses due to doppler processing. (There is, of course, no unique answer for this question.)

b. Using the total system loss you have estimated, what is the reduction in radar range that occurs due to the system losses if the radar range without losses is 200 nmi?

2.31 Question 1.8 of Chapter 1 asked "How does radar range depend on the wavelength?" Based on Chapter 2, how would you now answer this question for an air-surveillance radar? (Please justify your answer.)

2.32 An experimental measurement of the blip-scan ratio (single-scan probability of detection) of a particular target at a particular range gives a value of 0.5 after 10 trails (antenna scans).

a. What is the confidence interval of this measurement if the confidence level has to be 90 percent?

b. What is the confidence interval (with the same confidence level of 90 percent) after 100 scans, assuming the measured blip-scan ratio is still 0.5?

chapter

3

MTI and Pulse Doppler Radar

3.1 INTRODUCTION TO DOPPLER AND MTI RADAR

The radars discussed in the previous chapter were required to detect targets in the presence of noise. In the real world, radars have to deal with more than receiver noise when detecting targets since they can also receive echoes from the natural environment such as land, sea, and weather. These echoes are called *clutter* since they can "clutter" the radar display. Clutter echoes can be many orders of magnitude larger than aircraft echoes. When an aircraft echo and a clutter echo appear in the same radar resolution cell, the aircraft might not be detectable. Chapter 7 describes the characteristics of clutter and discusses methods for reducing these unwanted echoes in order to detect the desired target echoes. However, the most powerful method for detecting moving targets in the midst of large clutter is by taking advantage of the doppler effect, which is the change of frequency of the radar echo signal due to the relative velocity between the radar and the moving target. The use of the doppler frequency shift with a pulse radar for the detection of moving targets in clutter is the subject of this chapter.

Radar deserves much credit for enabling the Allies (chiefly the United Kingdom and the United States) in the first half of World War II to prevail in the crucial air battles and night naval engagements against the Axis powers. Almost all of the radars used in World War II, however, were by today's standards relatively simple pulse systems that did not employ the doppler effect. Fortunately, these pulse radars were able to accomplish their mission without the use of doppler. This would not be possible today. All high-performance military air-defense radars and all civil air-traffic control radars for the detection and tracking of aircraft depend on the doppler frequency shift to separate the large

clutter echoes from the much smaller echoes from moving targets. Clutter echoes can be greater than the desired target echoes by as much as 60 or 70 dB, or more, depending on the type of radar and the environment.

MTI Radar and Pulse Doppler Radar A pulse radar that employs the doppler shift for detecting moving targets is either an MTI (moving target indication) radar[1] or a pulse doppler radar.[2] The MTI radar has a pulse repetition frequency (prf) low enough to not have any range ambiguities as defined by Eq. (1.2), $R_{un} = c/f_p$. It does, however, have many ambiguities in the doppler domain. The pulse doppler radar, on the other hand, is just the opposite. As we shall see later in this chapter, it has a prf large enough to avoid doppler ambiguities, but it can have numerous range ambiguities. There is also a medium-prf pulse doppler that accepts both range and doppler ambiguities, as discussed in Sec. 3.9.

In addition to detecting moving targets in the midst of large clutter echoes, the doppler frequency shift has other important applications in radar; such as allowing CW (continuous wave) radar to detect moving targets and to measure radial velocity, synthetic aperture radar and inverse synthetic aperture radar for producing images of targets, and meteorological radars concerned with measuring wind shear. These other uses of the doppler frequency shift are not discussed in this chapter.

Doppler Frequency Shift The doppler effect used in radar is the same phenomenon that was introduced in high school physics courses to describe the changing pitch of an audible siren from an emergency vehicle as it travels toward or away from the listener. In this chapter we are interested in the doppler effect that changes the frequency of the electromagnetic signal that propagates from the radar to a moving target and back to the radar. If the range to the target is R, then the total number of wavelengths λ in the two-way path from radar to target and return is $2R/\lambda$. Each wavelength corresponds to a phase change of 2π radians. The total phase change in the two-way propagation path is then

$$\phi = 2\pi \times \frac{2R}{\lambda} = 4\pi R/\lambda \qquad [3.1]$$

If the target is in motion relative to the radar, R is changing and so will the phase. Differentiating Eq. (3.1) with respect to time gives the rate of change of phase, which is the angular frequency

$$\omega_d = \frac{d\phi}{dt} = \frac{4\pi}{\lambda}\frac{dR}{dt} = \frac{4\pi v_r}{\lambda} = 2\pi f_d \qquad [3.2]$$

where $v_r = dR/dt$ is the radial velocity (meters/second), or rate of change of range with time. If, as in Fig. 3.1, the angle between the target's velocity vector and the radar line of sight to the target is θ, then $v_r = v \cos\theta$, where v is the speed, or magnitude of the vector velocity. The rate of change of ϕ with time is the angular frequency $\omega_d = 2\pi f_d$, where f_d is the *doppler frequency shift*. Thus from Eq. (3.2),

$$f_d = \frac{2v_r}{\lambda} = \frac{2f_r v_r}{c} \qquad [3.3]$$

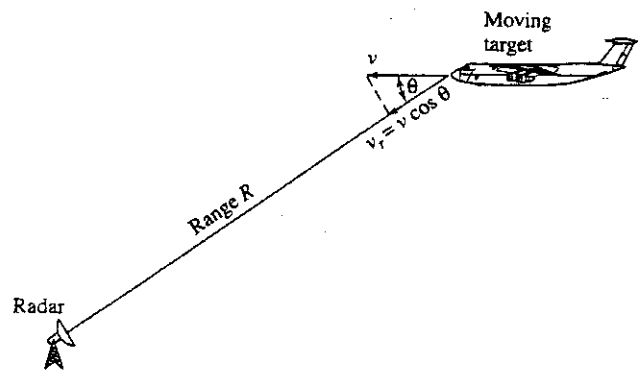

Figure 3.1 Geometry of radar and target in deriving the doppler frequency shift. Radar, target, and direction of target travel all lie in the same plane in this illustration.

The radar frequency is $f_t = c/\lambda$, and the velocity of propagation $c = 3 \times 10^8$ m/s. If the doppler frequency is in hertz, the radial velocity in knots (abbreviated kt), and the radar wavelength in meters, we can write

$$f_d \text{ (Hz)} = \frac{1.03 v_r \text{ (kt)}}{\lambda \text{ (m)}} \approx \frac{v_r \text{ (kt)}}{\lambda \text{ (m)}} \qquad [3.4]$$

The doppler frequency in hertz can also be approximately expressed as $3.43 v_r f_t$, where f_t is the radar frequency in GHz and v_r is in knots. A plot of the doppler frequency shift is shown in Fig. 3.2 as a function of the radial velocity and the various radar frequency bands.

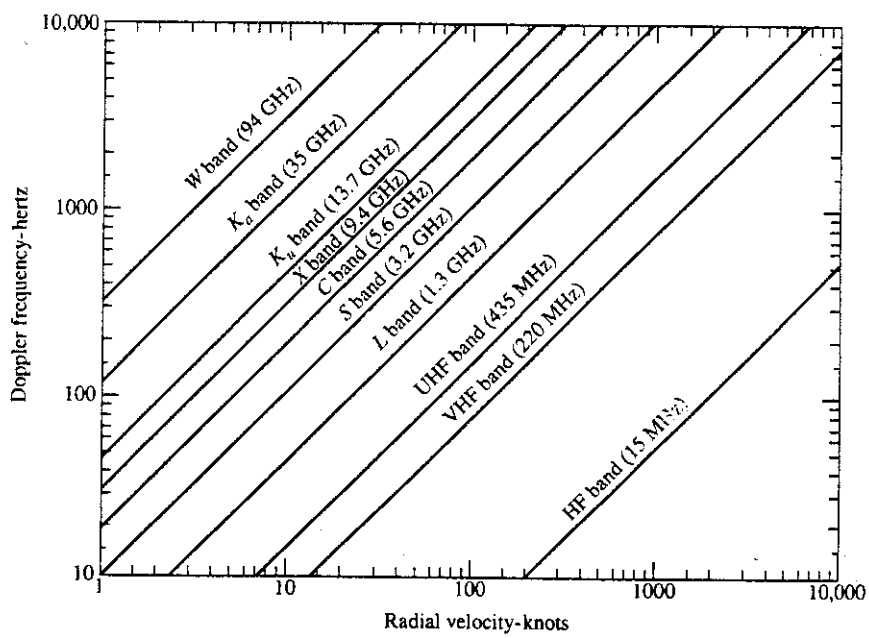

Figure 3.2 Doppler frequency shift from a moving target as a function of the target's radial velocity and the radar frequency band.

Simple CW Doppler Radar Before discussing the use of doppler in pulse radar, it is instructive to begin by considering the doppler frequency shift experienced with a CW radar. The block diagram of a very simple CW radar that utilizes the doppler frequency shift to detect moving targets is shown in Fig. 3.3a. Unlike a pulse radar, a CW radar transmits while it receives. Without the doppler shift produced by the movement of the target, the weak CW echo signal would not be detected in the presence of the much stronger signal from the transmitter. Filtering in the frequency domain is used to separate the weak doppler-shifted echo signal from the strong transmitter signal in a CW radar.

The transmitter generates a continuous (unmodulated) sinusoidal oscillation at frequency f_t, which is then radiated by the antenna. On reflection by a moving target, the transmitted signal is shifted by the doppler effect by an amount $\pm f_d$, as was given by Eq. (3.3). The plus sign applies when the distance between radar and target is decreasing (a closing target); thus, the echo signal from a closing target has a larger frequency than that which was transmitted. The minus sign applies when the distance is increasing (a receding target). To utilize the doppler frequency shift a radar must be able to recognize that the received echo signal has a frequency different from that which was transmitted. This is the function of that portion of the transmitter signal that finds its way (or leaks) into the receiver, as indicated in Fig. 3.3a. The transmitter leakage signal acts as a reference to determine that a frequency change has taken place. The detector, or mixer, multiplies the echo signal at a frequency $f_t \pm f_d$ with the transmitter leakage signal f_t. The doppler filter allows the difference frequency from the detector to pass and rejects the higher frequencies. The filter characteristic is shown in Fig. 3.3a just below the doppler-filter block. It has a lower frequency cutoff to remove from the receiver output the transmitter leakage signal and clutter echoes. The upper frequency cutoff is determined by the maximum

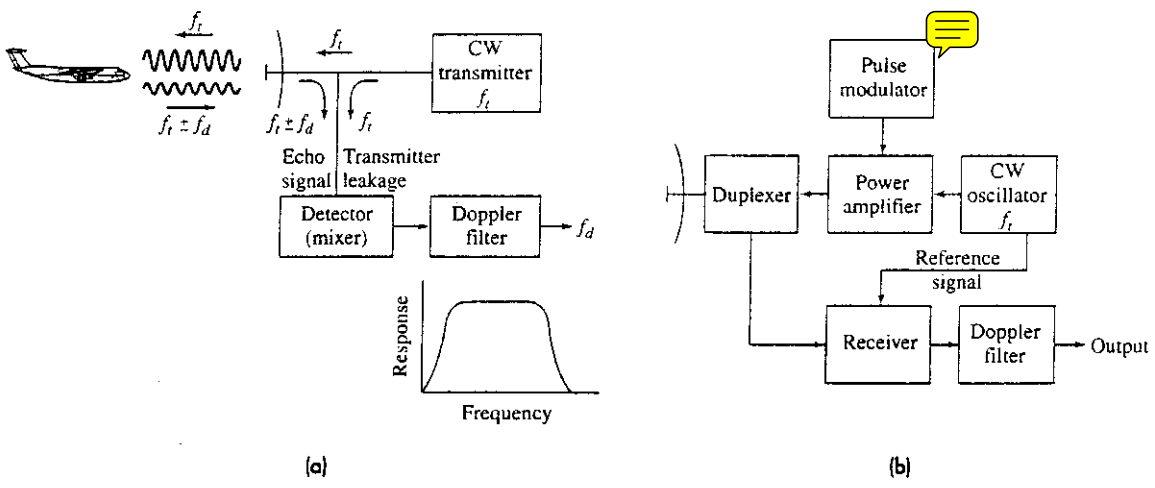

Figure 3.3 (a) Simple CW radar block diagram that extracts the doppler frequency shift from a moving target and rejects stationary clutter echoes. The frequency response of the doppler filter is shown at the lower right. (b) Block diagram of a simple pulse radar that extracts the doppler frequency shift of the echo signal from a moving target.

radial velocity expected of moving targets. The doppler filter passes signals with a doppler frequency f_d located within its pass band, but the sign of the doppler is lost along with the direction of the target motion. CW radars can be much more complicated than this simple example, but it is adequate as an introduction to a pulse radar that utilizes the doppler to detect moving targets in clutter.

Pulse Radar That Extracts the Doppler Frequency-Shifted Echo Signal One cannot simply convert the CW radar of Fig. 3.3a to a pulse radar by turning the CW oscillator on and off to generate pluses. Generating pulses in this manner also removes the reference signal at the receiver, which is needed to recognize that a doppler frequency shift has occurred. One way to introduce the reference signal is illustrated in Fig. 3.3b. The output of a stable CW oscillator is amplified by a high-power amplifier. The amplifier is turned on and off (modulated) to generate a series of high-power pulses. The received echo signal is mixed with the output of the CW oscillator which acts as a *coherent reference* to allow recognition of any change in the received echo-signal frequency. By *coherent* is meant that the phase of the transmitted pulse is preserved in the reference signal. The change in frequency is detected (recognized) by the doppler filter.

The doppler frequency shift is derived next in a slightly different manner than was done earlier in this section. If the transmitted signal of frequency f_t is represented as $A_t \sin(2\pi f_t t)$, the received signal is $A_r \sin[2\pi f_t(t - T_R)]$, where A_t = amplitude of transmitted signal and A_r = amplitude of the received echo signal. The round-trip time T_R is equal to $2R/c$, where R = range and c = velocity of propagation. If the target is moving toward the radar, the range is changing and is represented as $R = R_0 - v_r t$, where v_r = radial velocity (assumed constant). The geometry is the same as was shown in Fig. 3.1. With the above substitutions, the received signal is

$$V_{\text{rec}} = A_r \sin\left[2\pi f_t\left(1 + \frac{2v_r}{c}\right)t - \frac{4\pi f_t R_0}{c}\right] \qquad [3.5]$$

The received frequency changes by the factor $2f_t v_r/c = 2v_r/\lambda$, which is the doppler frequency shift f_d.* If the target had been moving away from the radar, the sign of the doppler frequency would be minus, and the received frequency would be less than that transmitted.

The received signal is heterodyned (mixed) with the reference signal $A_{\text{ref}} \sin 2\pi f_t t$ and the difference frequency is extracted, which is given as

$$V_d = A_d \cos(2\pi f_d t - 4\pi R_0/\lambda) \qquad [3.6]$$

where A_d = amplitude, $f_d = 2v_r/\lambda$ = doppler frequency, and the relation $f_t\lambda = c$ was used. (The cosine replaces the sine in the trigonometry of the heterodyning process.) For stationary targets $f_d = 0$ and the output signal is constant. Since the sine takes on values from $+1$ to -1, the sign of the clutter echo amplitude can be minus as well as plus. On the other hand, the echo signal from a moving target results in a time-varying output (due to the doppler shift) which is the basis for rejecting stationary clutter echoes (with zero doppler frequency) but allowing moving-target echoes to pass.

*The terms *doppler frequency shift*, *doppler frequency*, and *doppler shift* are used interchangeably in this chapter.

If the radar pulse width is long enough and if the target's doppler frequency is large enough, it may be possible to detect the doppler frequency shift on the basis of the frequency change within a single pulse. If Fig. 3.4a represents the RF (or IF) echo pulse train, Fig. 3.4b is the pulse train when there is a recognizable doppler frequency shift. To detect a doppler shift on the basis of a single pulse of width τ generally requires that there be at least one cycle of the doppler frequency f_d within the pulse; or that $f_d\tau > 1$. This condition, however, is not usually met when detecting aircraft since the doppler frequency f_d is generally much smaller than $1/\tau$. Thus the doppler effect cannot be utilized with a *single* short pulse in this case. Figure 3.4c is more representative of the doppler frequency for aircraft-detection radars. The doppler is shown sampled at the pulse repetition frequency (prf). More than one pulse is needed to recognize a change in the echo frequency due to the doppler effect. (Figure 3.4c is exaggerated in that the pulse width is usually small compared to the pulse repetition period. For example, τ might be of the order of 1 μs, and the pulse repetition period might be of the order of 1 ms.)

Sweep-to-Sweep Subtraction and the Delay-Line Canceler Figures 3.5a and b represent (in a very approximate manner) the bipolar video (both positive and negative amplitudes) from two successive sweeps* of an MTI (moving target indication) radar defined at the beginning of this chapter. The fixed clutter echoes in this figure remain the same from sweep to sweep. The output of the MTI radar is called *bipolar video*, since the signal has negative as well as positive values. (*Unipolar video* is rectified bipolar video with

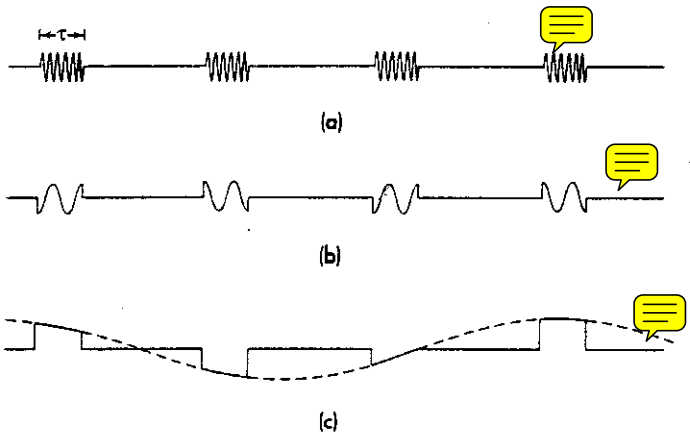

Figure 3.4 (a) Representation of the echo pulse train at either the RF or IF portion of the receiver; (b) video pulse train after the phase detector when the doppler frequency $f_d > 1/\tau$; (c) video pulse train for the doppler frequency $f_d < 1/\tau$, which is usually the case for aircraft-surveillance radar. The doppler frequency signal is shown dashed in (c), as if it were CW. Note that the pulses in (c) have an exaggerated width compared to the period of the doppler frequency.

*Sweep as used here is what occurs in the time between two transmitted pulses, or the pulse repetition interval. It is a more convenient term to use than is *pulse repetition period*, but the latter is more descriptive. The term *sweep* originally signified the action of moving the electron beam of a cathode ray tube display across the face of the tube during the time of a pulse repetition.

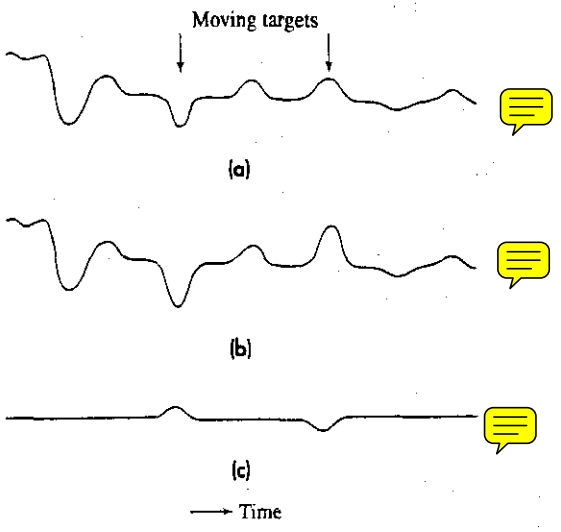

Figure 3.5 Two successive sweeps, (a) and (b), of an MTI radar A-scope display (amplitude as a function of time, or range). Arrows indicate the positions of moving targets. When (b) is subtracted from (a), the result is (c) and echoes from stationary targets are canceled, leaving only moving targets.

only positive values.) If one sweep is subtracted from the previous sweep, fixed clutter echoes will cancel and will not be detected or displayed. On the other hand, moving targets change in amplitude from sweep to sweep because of their doppler frequency shift. If one sweep is subtracted from the other, the result will be an uncancelled residue, as shown in Fig. 3.5c.

Subtraction of the echoes from two successive sweeps is accomplished in a *delay-line canceler*, as indicated by the diagram of Fig. 3.6. The output of the MTI receiver is digitized and is the input to the delay-line canceler (which performs the role of a doppler filter). The delay T is achieved by storing the radar output from one pulse transmission, or sweep, in a digital memory for a time equal to the pulse repetition period so that $T = T_p = 1/f_p$. The output obtained after subtraction of two successive sweeps is *bipolar (digital) video* since the clutter echoes in the output contain both positive and negative amplitudes [as can be seen from Eq. (3.6) when $f_d = 0$]. It is usually called *video*, even though it is a series of digital words rather than an analog video signal. The absolute value

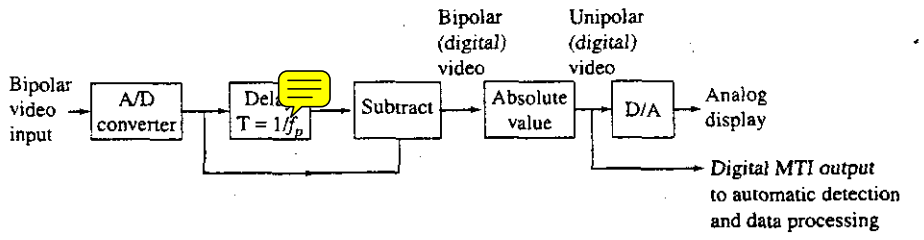

Figure 3.6 Block diagram of a single delay-line canceler.

of the bipolar video is taken, which is then *unipolar video*. Unipolar video is needed if an analog display is used that requires positive signals only. The unipolar digital video is then converted to an analog signal by the digital-to-analog (D/A) converter if the processed signal is to be displayed on a PPI (plan position indicator). Alternatively, the digital signals may be used for automatically making the detection decision and for further data processing, such as automatic tracking and/or target recognition. The name *delay-line canceler* was originally applied when analog delay lines (usually acoustic) were used in the early MTI radars. Even though analog delay lines have been replaced by digital memories, the name delay-line canceler is still used to describe the operation of Fig. 3.6.

MTI Radar Block Diagram The block diagram of Fig. 3.3 illustrated the reference signal necessary for an MTI radar, but it is oversimplified. A slightly more elaborate block diagram of an MTI radar employing a power amplifier as the transmitter is shown in Fig. 3.7. The local oscillator of an MTI radar's superheterodyne receiver must be more stable than the local oscillator for a radar that does not employ doppler. If the phase of the local oscillator were to change significantly between pulses, an uncancelled clutter residue can result at the output of the delay-line canceler which might be mistaken for a moving target even though only clutter were present. To recognize the need for high stability, the local oscillator of an MTI receiver is called the *stalo*, which stands for *stable local oscillator*. The IF stage is designed as a matched filter, as is usually the case in radar. Instead of an amplitude detector, there is a *phase detector* following the IF stage. This is a mixer-like device that combines the received signal (at IF) and the reference signal from the *coho* so as to produce the difference between the received signal and the reference signal frequencies.[3] This difference is the doppler frequency. The name *coho* stands for

Figure 3.7 Block diagram of an MTI radar that uses a power amplifier as the transmitter.

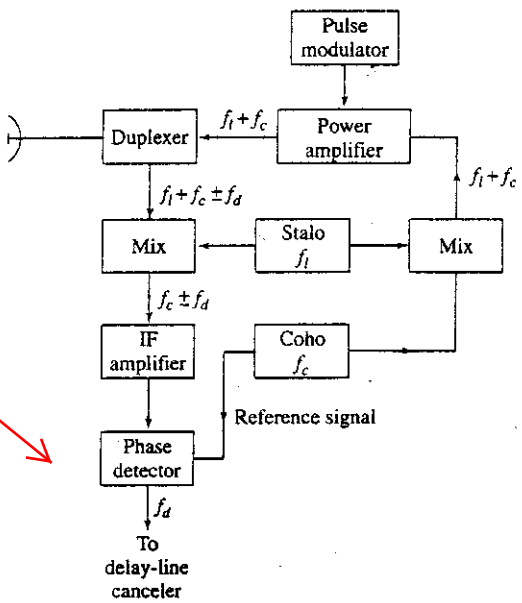

استفاده از يك كانال پردازشي براي فيلتر MTI باعث ايجاد فاز كور مي شود. براي حل اين مشكل بايد از دو كانال پردازشي I و Q استفاده كرد.

coherent oscillator to signify that it is the reference signal that has the phase of the transmitter signal. Coherency with the transmitted signal is obtained by using the sum of the coho and the stalo signals as the input signal to the power amplifier. Thus the transmitter frequency is the sum of the stalo frequency f_l and the coho frequency f_c. This is accomplished in the mixer shown on the upper right side of Fig. 3.7. The combination of the stalo and coho sometimes is called the *receiver-exciter* portion of the MTI radar. Using the receiver stalo and coho to also generate the transmitter signal insures better stability than if the functions were performed with two different sets of oscillators. The output of the phase detector is the input to the delay-line canceler, as in Fig. 3.6. The delay-line canceler acts as a high-pass filter to separate the doppler-shifted echo signals of moving targets from the unwanted echoes of stationary clutter. The doppler filter might be a single delay-line canceler as in Fig. 3.6; but it is more likely to be one of several other more elaborate filters with greater capability, as described later in this chapter.

The power amplifier is a good transmitter for MTI radar since it can have high stability and is capable of high power. The pulse modulator turns the amplifier on and off to generate the radar pulses. The klystron and the traveling wave tube have usually been the preferred type of vacuum-tube amplifier for MTI radar. The crossed-field amplifier has also been used, but it is generally noisier (less stable) than other devices; hence, it might not be capable of canceling large clutter echoes. Triode and tetrode vacuum tubes have also been used with success for radars that operate at UHF and lower frequencies, but they have been largely replaced at these lower radar frequencies by the solid-state transistor. The transistor has the advantage of good stability and it does not need a pulse modulator.

Before the development of the high-power klystron amplifier for radar application in the 1950s, the only suitable RF power generator at microwave frequencies was the magnetron oscillator. In an oscillator, the phase at the start of each pulse is random so that the receiver-exciter concept of Fig. 3.7 cannot be used. To obtain a coherent reference in this case, a sample of each transmitter pulse is used to lock the phase of the coho to that of the transmitted pulse until the next pulse is generated. The phase-locking procedure is repeated with each pulse. The RF locking-pulse is converted to IF in a mixer that also uses the stalo as the local oscillator. This method of establishing coherence at the receiver sometimes is called *coherent on receive.* Further information on the MTI using an oscillator may be found in previous editions of this text or in the chapter on MTI in the *Radar Handbook.*[1]

3.2 DELAY-LINE CANCELERS

The simple MTI delay-line canceler (DLC) of Fig. 3.6 is an example of a *time-domain filter* that rejects stationary clutter at zero frequency. It has a frequency response function $H(f)$ that can be derived from the time-domain representation of the signals.

Frequency Response of the Single Delay-Line Canceler The signal from a target at range R_0 at the output of the phase detector can be written

$$V_1 = k \sin (2\pi f_d t - \phi_0) \qquad [3.7]$$

where f_d = doppler frequency shift, ϕ_0 = a constant phase equal to $4\pi R_0/\lambda$, R_0 = range at time equal to zero, λ = wavelength, and k = amplitude of the signal. [For convenience, the cosine of Eq. (3.6) has been replaced by the sine.] The signal from the previous radar transmission is similar, except it is delayed by a time T_p = pulse repetition interval, and is

$$V_2 = k \sin [2\pi f_d(t - T_p) - \phi_0] \qquad [3.8]$$

The amplitude k is assumed to be the same for both pulses. The delay-line canceler subtracts these two signals. Using the trigonometric identity $\sin A - \sin B = 2 \sin[(A - B)/2] \cos [(A + B)/2]$, we get

$$V = V_1 - V_2 = 2k \sin (\pi f_d T_p) \cos \left[2\pi f_d\left(t - \frac{T_p}{2}\right) - \phi_0\right] \qquad [3.9]$$

The output from the delay-line canceler is seen to consist of a cosine wave with the same frequency f_d as the input, but with an amplitude $2k \sin (\pi f_d T_p)$. Thus the amplitude of the canceled video output depends on the doppler frequency shift and the pulse repetition period. The frequency response function of the single delay-line canceler (output amplitude divided by the input amplitude k) is then

$$H(f) = 2 \sin (\pi f_d T_p) \qquad [3.10]$$

Its magnitude $|H(f)|$ is sketched in Fig. 3.8.

دو عیب استفاده از فیلتر MTI

The single delay-line canceler is a filter that does the job asked of it: it eliminates fixed clutter that is of zero doppler frequency. Unfortunately, it has two other properties that can seriously limit the utility of this simple doppler filter: (1) the frequency response function also has zero response when moving targets have doppler frequencies at the prf and its harmonics, and (2) the clutter spectrum at zero frequency is not a delta function of zero width, but has a finite width so that clutter will appear in the pass band of the delay-line canceler. The result is there will be target speeds, called *blind speeds*, where the target will not be detected and there will be an uncanceled clutter residue that can interfere with the detection of moving targets. These limitations will be discussed next.

Blind Speeds The response of the single delay-line canceler will be zero whenever the magnitude of $\sin (\pi f_d T_p)$ in Eq. (3.10) is zero, which occurs when $\pi f_d T_p = 0, \pm\pi, \pm 2\pi, \pm 3\pi, \ldots$. Therefore,

فرکانس داپلر برای سرعت کور

$$f_d = \frac{2v_r}{\lambda} = \frac{n}{T_p} = nf_p \qquad n = 0,1,2,\ldots \qquad [3.11]$$

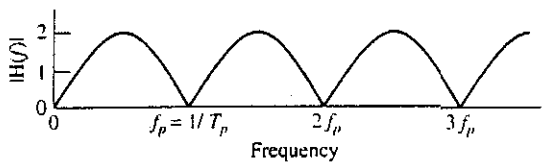

Figure 3.8 Magnitude of the frequency response $|H(f)|$ of a single delay-line canceler as given by Eq. (3.10), where f_p = pulse repetition frequency and $T_p = 1/f_p$.

This states that in addition to the zero response at zero frequency, there will also be zero response of the delay-line canceler whenever the doppler frequency $f_d = 2v_r/\lambda$ is a multiple of the pulse repetition frequency f_p. (The doppler shift can be negative or positive depending on whether the target is receding or approaching. When considering the blind speed and its effects, the sign of the doppler can be ignored—which is what is done here.) The radial velocities that produce blind speeds are found by equating Eqs. (3.11) and (3.3), and solving for the radial velocity, which gives

سرعت کور

$$v_n = \frac{n\lambda}{2T_p} = \frac{n\lambda f_p}{2} \qquad n = 1,2,3\ldots \tag{3.12}$$

where v_r has been replaced by v_n, the nth blind speed. Usually only the first blind speed v_1 is considered, since the others are integer multiples of v_1. If λ is measured in meters, f_p in hertz, and the radial velocity in knots, the first blind speed can be written

$$v_1 \text{ (kt)} = 0.97\ \lambda \text{ (m)}\ f_p \text{ (Hz)} \approx \lambda \text{ (m)}\ f_p \text{ (Hz)} \tag{3.13}$$

A plot of the first blind speed as a function of the pulse repetition frequency and the various radar frequency bands is shown in Fig. 3.9.

Blind speeds can be a serious limitation in MTI radar since they cause some desired moving targets to be canceled along with the undesired clutter at zero frequency. Based on Eq. (3.13) there are four methods for reducing the detrimental effects of blind speeds:

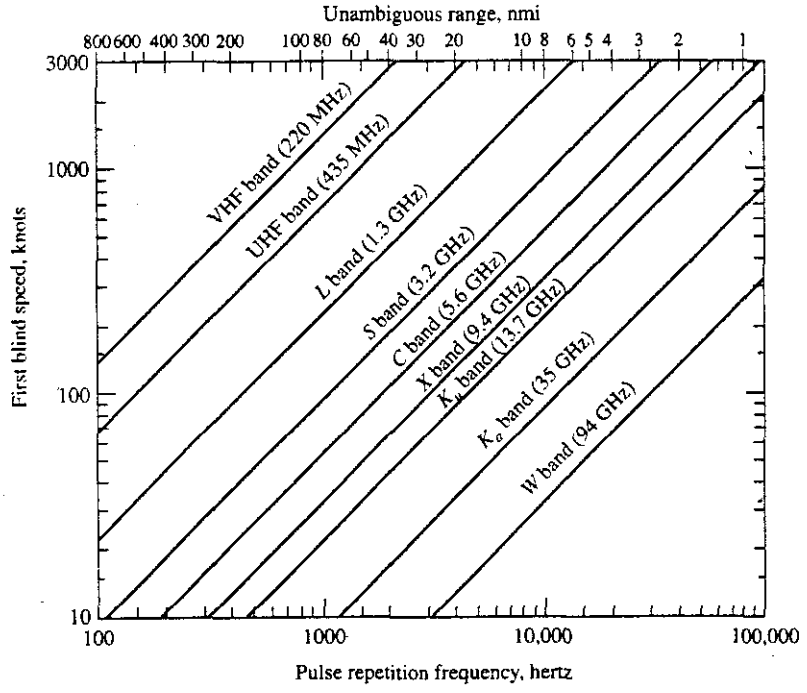

Figure 3.9 Plot of the first blind speed, Eq. (3.13), as a function of the pulse repetition frequency for the various radar frequency bands.

راه کارهاي مقابله با سرعت کور

1. Operate the radar at long wavelengths (low frequencies).
2. Operate with a high pulse repetition frequency.
3. Operate with more than one pulse repetition frequency.
4. Operate with more than one RF frequency (wavelength).

Combinations of two or more of the above are also possible to further alleviate the effect of blind speeds. Each of these four methods has particular advantages as well as limitations, so there is not always a clear choice as to which to use in any particular application.

استفاده از فرکانس حامل VHF داراي معايبي است که عبارتنداز

Consider the case where a low RF frequency is chosen to avoid blind speeds. If, for example, the first blind speed is to be no lower than 640 kt (approximately Mach 1) and the prf is selected as 330 Hz (which gives an unambiguous range of 245 nmi), then the radar wavelength from Eq. (3.13) is 2 m. This corresponds to a frequency of 150 MHz (the VHF region of the spectrum). Although there were many radars at VHF built in the 1930s and early 1940s and there are still advantages to operating a radar at these frequencies, VHF is not usually considered a desirable frequency choice for a long-range air-surveillance radar for a number of reasons: (1) resolution in range and angle are poor due to narrow bandwidths and large beamwidths, (2) this portion of the electromagnetic spectrum is crowded with other than radar services (such as broadcast FM and TV), and (3) low-altitude coverage generally is poor. Thus attempting to use low frequencies to avoid the blind speed problem is not usually a desirable option for many radar applications.

On the other hand, if we choose to operate at a high RF frequency and increase the prf to avoid blind speeds, we would then have to tolerate the many range ambiguities that result. For example, if the first blind speed was again chosen to be 640 kt and the wavelength were 0.1 m (an *S*-band frequency of 3000 MHz), the prf would have to be 6600 Hz. This results in a maximum unambiguous range of 12.3 nmi, which is small for many radar applications. (Such an approach, however, is used successfully in pulse doppler radars, as discussed later in this chapter.)

When two or more prfs are used in a radar, the blind speeds at one prf generally are different from the blind speeds at the other prfs. Thus targets that are highly attenuated with one prf might be readily seen with another prf. This technique is widely used with air-surveillance radars, especially those for civil air-traffic control. A disadvantage of a multiple-prf waveform is that multiple-time-around clutter echoes (from regions beyond the maximum unambiguous range) are not canceled.

A radar that can operate at two or more RF frequencies can also unmask blind speeds, but the required frequency change is often larger than might be possible within the usual frequency bands allocated for radar use. A limitation of multiple frequencies is the need for greater system bandwidth.

In some circumstances, it might be desirable to tolerate the blind speeds rather than accept the limitations of the above methods. As in many aspects of engineering, there is no one single solution best for all cases. The engineer has to decide which of the above limitations can be accepted in any particular application.

Blind speeds occur because of the sampled nature of the pulse radar waveform. Thus it is sampling that is the cause of ambiguities, or aliasing, in the measurement of the doppler frequency, just as sampling in a pulse radar (at the prf) can give rise to ambiguities in the range measurement.

Clutter Attenuation The other limitation of the single delay-line canceler is insufficient attenuation of clutter that results from the finite width of the clutter spectrum. The single delay-line canceler whose frequency response was shown in Fig. 3.8 does what it is supposed to do, which is to cancel stationary clutter with zero doppler shift. In the "real world," however, the clutter spectrum has a finite width due to such things as the internal motions of the clutter, instabilities of the stalo and coho oscillators, other imperfections of the radar and its signal processor, and the finite signal duration. (The factors that widen the clutter spectrum will be discussed later in Sec. 3.7.) For present purposes we will assume the clutter power spectral density is represented by a gaussian function, and is written as

$$W(f) = W_0 \exp\left(-\frac{f^2}{2\sigma_c^2}\right) = W_0 \exp\left(-\frac{f^2\lambda^2}{8\sigma_v^2}\right) \qquad f \geq 0 \qquad [3.14]$$

where W_0 = peak value of the clutter power spectral density, at $f = 0$, σ_c = standard deviation of the clutter spectrum in hertz, and σ_v = standard deviation of the clutter spectrum in meters/second. The relation between the two forms of the clutter-spectrum standard deviation is based on applying the doppler frequency expression of Eq. (3.3) such that $\sigma_c = 2\sigma_v/\lambda$. The advantage of using the standard deviation σ_v is that it is often independent of the frequency; whereas σ_c is in hertz and depends on the radar frequency. Nevertheless, we will generally use σ_c in this chapter for the clutter spectrum.

The consequences of a finite-width clutter spectrum can be seen from Fig. 3.10. The frequency response of the single delay-line canceler shown by the solid curve encompasses a portion of the clutter spectrum; therefore, clutter will appear in the output. The greater the standard deviation σ_c, the greater the amount of clutter that will be passed by the filter to interfere with moving target detection. The clutter attenuation (CA) produced by a single delay-line canceler is

طيف فركانسي كلاتر گوسي است.

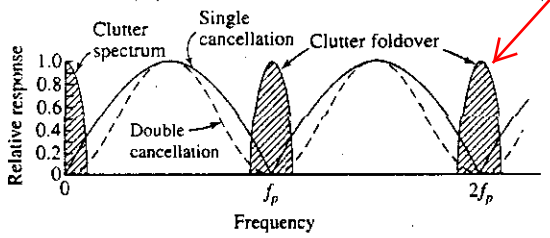

Figure 3.10 Relative frequency response of a single delay-line canceler (solid curve) and the double delay-line canceler (dashed curve), along with the frequency spectrum of the clutter (shaded area). Note the clutter spectrum is folded over at the prf and its harmonics because of the sampled nature of a pulse radar waveform.

CA=C_{in}/C_{out}

$$\text{CA} = \frac{\int_0^\infty W(f)\, df}{\int_0^\infty W(f)|H(f)^2|\, df} \qquad [3.15]$$

where $H(f)$ is the frequency response of the delay-line canceler. Substituting for $H(f)$ [Eq. (3.10)], the clutter attenuation becomes

$$\text{CA} = \frac{\int_0^\infty W_0 \exp\left[-f^2/2\sigma_c^2\right] df}{\int_0^\infty W_0 \exp\left[-f^2/2\sigma_c^2\right] 4 \sin^2(\pi f T_p)\, df} = \frac{0.5}{1 - \exp\left(-2\pi^2 T_p^2 \sigma_c^2\right)} \qquad [3.16]$$

If the exponent in the denominator at the right-hand part of this equation is small, the exponential term exp $[-x]$ can be replaced by $1 - x$, so that

$$\text{CA} \approx \frac{f_p^2}{4\pi^2\sigma_c^2} = \frac{f_p^2\lambda^2}{16\pi^2\sigma_v^2}$$

single- ميزان تضعيف كلاتر براي delay line canceller

In this equation the pulse repetition period T_p has been replaced by $1/f_p$. The clutter attenuation provided by a single delay-line canceler is not sufficient for most MTI radar applications.

If a second delay-line canceler is placed in cascade, the frequency response of the two filters is the square of the single delay-line canceler, or

Double delay line canceller

$$H(f) = 4 \sin^2(\pi f T_p) \qquad [3.18]$$

This is indicated in Fig. 3. 10 by the dashed curve (except that we have plotted the relative response rather than the absolute response). Less of the clutter spectrum is included within the frequency response of the double delay-line canceler; hence, it attenuates more of the clutter. The clutter attenuation for the double delay-line canceler is

$$\text{CA} \approx \frac{f_p^4}{48\pi^4\sigma_c^4} = \frac{f_p^4\lambda^4}{768\pi^4\sigma_v^4}$$

double- ميزان تضعيف كلاتر براي delay line canceller

Additional delay-line cancelers can be cascaded to obtain a frequency response $H(f)$ which is the nth power of the single delay-line canceler given by Eq. (3.10), where n is the number of delay-line cancelers.

MTI Improvement Factor The clutter attenuation is a useful measure of the performance of an MTI radar in canceling clutter, but it has an inherent weakness if one is not careful. The clutter attenuation can be made infinite by turning off the radar receiver! This, of course, would not be done knowingly since it also eliminates the desired moving-target echo signals. To avoid the problem of increasing clutter attenuation at the expense of desired signals, the IEEE defined[4] a measure of performance known as the *MTI improvement factor* which includes the signal gain as well as the clutter attenuation. It is defined as "The signal-to-clutter ratio at the output of the clutter filter divided by the

signal-to-clutter ratio at the input of the clutter filter, averaged uniformly over all target radial velocities of interest." It is expressed as

$$\text{improvement factor} = I_f = \frac{(\text{single/clutter})_{\text{out}}}{(\text{single/clutter})_{\text{in}}}\bigg|_{f_d} = \frac{C_{\text{in}}}{C_{\text{out}}} \times \frac{S_{\text{out}}}{S_{\text{in}}}\bigg|_{f_d} =$$

$$= \text{CA} \times \text{average gain} \qquad [3.20]$$

The vertical line on the right in the above equation indicates that the average is taken with respect to doppler frequency f_d. The improvement factor can be expressed as the clutter attenuation CA = $(C_{\text{in}}/C_{\text{out}})$ times the average filter gain. The average gain is determined from the filter response $H(f)$ and is usually small compared to the clutter attenuation. The average gain for a single delay-line canceler is 2 and for a double delay-line canceler is 6. The improvement factors for single and double delay-line cancelers are

$$I_f(\text{single DLC}) \approx \frac{1}{2\pi^2(\sigma_c/f_p)^2} = \frac{\lambda^2}{8\pi^2(\sigma_v/f_p)^2} \qquad [3.21]$$

$$I_f(\text{double DLC}) \approx \frac{1}{8\pi^4(\sigma_c/f_p)^4} = \frac{\lambda^4}{128\pi^4(\sigma_v/f_p)^4} \qquad [3.22]$$

The general expression for the improvement factor for a canceler with n delay-line cancelers in cascade is[5]

$$I_f\ (n \text{ cascaded DLCs}) \approx \frac{2^n}{n!}\left(\frac{1}{2\pi(\sigma_c/f_p)}\right)^{2n} \qquad [3.23]$$

As with the previous expressions, this applies when σ_c/f_p is small. A plot of the improvement factor as a function of σ_c/f_p is provided later in Fig. 3.13. The ratio σ_c/f_p is a measure of the amount of "doppler space" occupied by clutter. Equation (3.23) also applies for the so-called *N-pulse canceler* with $N = n + 1$, to be discussed next.

N-Pulse Delay-Line Canceler A double delay-line canceler is shown in Fig. 3.11a. A canceler with two delay lines that has the same frequency response as the double delay-line canceler, but which is arranged differently, is shown in Fig. 3.11b. This is known as a *three-pulse canceler* since three pulses are added, with appropriate weights as shown. To obtain a $\sin^2(\pi f T_p)$ response, the weights of the three pulses are +1, −2, +1. When the input is $s(t)$, the output of the three-pulse canceler is then

$$s(t) - 2s(t + T_p) + s(t + 2T_p)$$

which is the same as the output from the double delay-line canceler

$$s(t) - s(t + T_p) - [s(t + T_p) - s(t + 2T_p)].$$

Thus the double delay-line canceler and the three-pulse canceler have the same frequency response function.

A four-pulse canceler with weights +1, −3, +3, −1 has a frequency response proportional to $\sin^3(\pi f T_p)$. A five-pulse canceler has weights +1, −4, +6, −4, +1. If n is

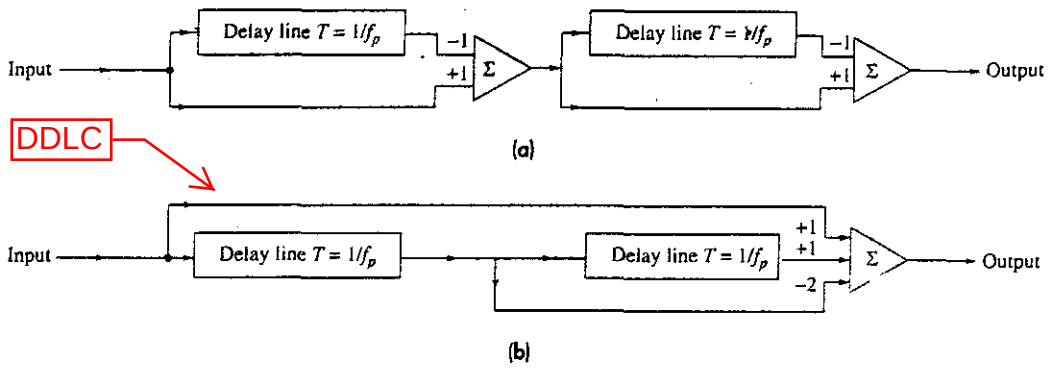

Figure 3.11 (a) Double delay-line canceler; (b) three-pulse canceler. The two configurations have the same frequency response. The three-pulse canceler of (b) is an example of a transversal filter.

the number of delay lines, there are $n + 1 = N$ pulses available to produce a frequency response function proportional to $\sin^n(\pi f T_p)$ when the weights are the coefficients of the expansion of the binomial series $(1 - x)^n$ with alternating signs. The binomial weights with alternating sign are given by

$$w_i = (-1)^{i-1} \frac{n!}{(n - i + 1)!(i - 1)!} \qquad i = 1,2,\cdots, n + 1 \qquad [3.24]$$

The N-pulse canceler has the same frequency response as n single delay-line cancelers in cascade, where $n = N - 1$. The greater the value of N, the greater will be the clutter attenuation.

Transversal (Nonrecursive) Filter The three-pulse canceler of Fig. 3.11b is an example of a *transversal filter.* Its general form with n delay lines is shown in Fig. 3.12. The weights w_i are applied to the $N = n + 1$ pulses and then combined in the summer, or adder. The transversal filter is a time-domain filter with feed-forward lines and taps with weights w_i.

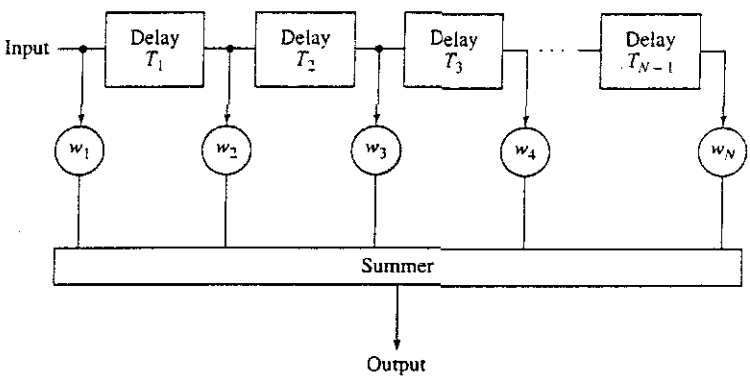

Figure 3.12 Transversal, or nonrecursive, filter for MTI signal processing.

The delays T_i are usually equal, but they need not be (Sec. 3.3). The configuration of Fig. 3.12 is also known as a *nonrecursive filter, feed-forward filter, finite impulse-response (FIR) filter,* or *finite memory filter.*

"Optimum" MTI Filter Transversal filters can have other than a $\sin^n(\pi f T_p)$ frequency response by choosing other than binomial weights. It is logical to ask what might be an optimum MTI filter. If one speaks of an optimum, there must be some criterion on which it is based. In the case of the so-called *optimum MTI filter*[6] the criterion is that it maximize the *improvement factor,* Eq. (3.20). It can also be considered as one which maximizes the clutter attenuation. It happens that a close approximation to the "optimum" MTI filter is a transversal filter with binomial weights of alternating sign that has a frequency response function proportional to $\sin^n(\pi f T_p)$, where n is the number of delay lines, as was discussed above. The optimum weights $(1, -1)$ of a transversal filter with a single delay line are the same as that of the single delay-line canceler, if the clutter spectrum can be modeled as a gaussian probability density function.[7] The difference between the three-pulse canceler and the "optimum" three-pulse MTI filter is less than 2 dB.[8] The difference is also small for higher values of n. Figure 3.13 is a plot of the improvement factor as a function of σ_c/f_p, where σ_c = the standard deviation of the clutter spectrum assuming it is of gaussian shape, and f_p = the pulse repetition frequency.[9] The solid curves apply for optimum weights and the dashed curves apply for binomial weights. There are two things to be noted from this plot. First, the differences between the two sets of curves are small so that we will take the optimum MTI filter to be adequately approximated by the filter with binomial weights whose response is proportional to $\sin^n(\pi f T_p)$. Second, sufficient improvement factor for many applications might be obtained with no more than two

فیلتر MTI بهینه را به خوبي مي توان با فیلتر با وزنهاي دوجمله اي تقریب زد.

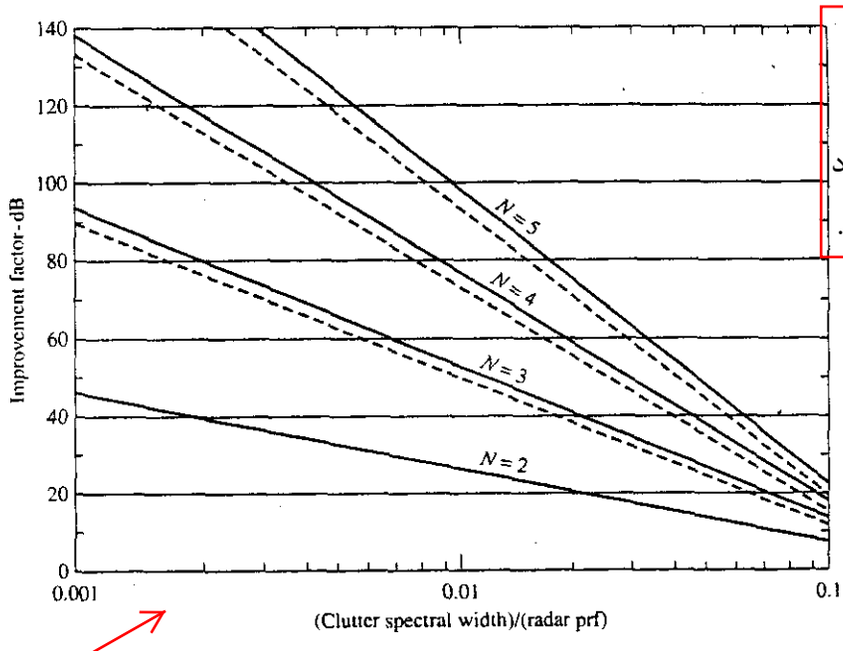

Figure 3.13 MTI improvement factor for an N-pulse delay-line canceler with binomial weights (dashed curves) and optimum weights (solid curves) as a function of the clutter spectral width σ_c. (After Andrews.[9])

معمولا با فیلتر MTI با N=2 or 3 (خط تاخیر) می توان به ضریب بهبود MTI بهینه دست یافت.

هرچه طیف کلاتر داراي گستردگي فرکانسي کمتري باشد حذف کلاتر بیشتر و بهتر انجام مي شود چون بیشتر توان کلاتر در اطراف فرکانس صفر است.

or three delay lines, if the improvement factor is the major criterion for the design of the MTI filter.

The term *optimum* is sometimes mistaken for the *best* that can be achieved. Optimum, however, is defined as the best under some implied or specified conditions. A so-called optimum solution might not be desired if the conditions for which it is defined are not suitable. This happens to be the case for the "optimum" MTI filter mentioned above. It is optimum if one wishes to have a filter that maximizes the improvement factor or the clutter attenuation. This may seem to be a suitable criterion, but it is not necessarily what one wants to achieve in a MTI filter. As the number n of delay lines increases in a filter with $H(f) \sim \sin^n(\pi f T_p)$, the response of $H(f)$ narrows and more and more clutter is rejected. The narrower bandwidth of the filter also means that fewer moving targets will be detected. If, for example, the -10 dB width of $H(f)$ is taken as the threshold for detection, and if all targets are uniformly distributed across the doppler frequency band, the following reductions in performance occur:

هرچه پهناي باند فيلتر MTI كمتر شود به اين معني است كه تعداد اهداف متحرك كمتري آشكارسازي خواهند شد.

- 20 percent of all targets will be rejected by a two-pulse canceler
- 38 percent of all targets will be rejected by a three-pulse canceler
- 48 percent of all targets will be rejected by a four-pulse canceler

Thus if the "optimum" clutter filter is used, the loss of desired target detections is another reason it should not employ a large value of n.

از يك transversal filter مي توان به عنوان يك rectangular-like filter استفاده كرد به شرط اينكه وزن هاي w_i به طور مناسبي انتخاب شوند.

"Rectangular-like" Transversal Filter Response If one examines the clutter spectrum, such as the shaded region in Fig. 3.10, it can be seen that a desirable filter should approximate a rectangular passband that attenuates the clutter but has uniform response over as much of the doppler space as practical. It would not have as much clutter attenuation as an "optimum" filter of the same number of delay lines; but as we have seen from Fig. 3.13, the clutter attenuation of the "optimum" generally is far greater than can be used in practice when the number of delay lines n is large. A transversal filter, as in Fig. 3.12, can be designed to approximate a rectangular passband if it contains a sufficient number of delay lines and if the weights w_i are chosen appropriately.

Some examples of transversal, or nonrecursive, filters for MTI applications that have appeared in the literature have been summarized by Y. H. Mao.[10] Procedures for nonrecursive filter design can be found in classical text books on digital filters. An early example due to Houts and Burlage,[11] based on a Chebyshev filter response that employs 15 pulses, is in Fig. 3.14. Also shown for comparison is the response of a three-pulse canceler with binomial weights and the response of a five-pulse canceler with "optimum" weights. Generally, the goal in such filter design is to achieve the necessary improvement factor by choosing the attenuation in the stopband of a bandpass filter, the extent of the stopband, the extent of the passband, and the ripple that can be tolerated in the passband.

The large improvement factor that results with the "optimum" MTI filter when n is large can be traded for increased doppler-frequency passband. For example, when $\sigma_c/f_p = 0.001$, Eq. (3.22) indicates that the three-pulse-canceler, or double delay-line canceler, (which is close to the "optimum") has a theoretical improvement factor of 91 dB. This is a large improvement factor and is usually more than is required for

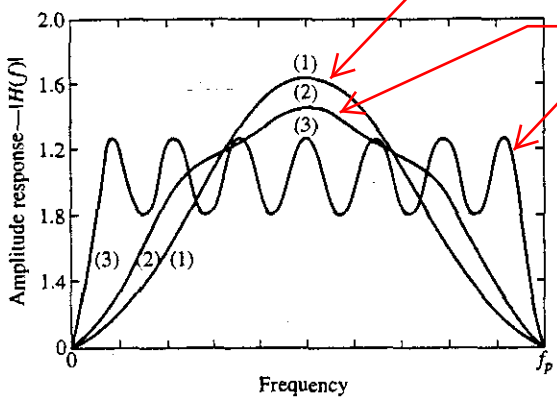

Figure 3.14 Amplitude response for three MTI delay-line cancelers. (1) Classical three-pulse canceler, (2) five-pulse delay-line canceler with optimum weights, and (3) 15-pulse Chebyshev design.
| (After Houts and Burlage.[11])

ناپايداري تجهيزات و عوامل ديگر مي توانند روي I.F تاثيرگذار باشند.

routine MTI radar applications. Furthermore, it might be difficult to achieve such high values in practice considering the problems of equipment instability and other factors that can limit the improvement factor. The five-pulse "optimum" of Fig. 3.14 is indicated by Houts and Barlage[11] as having an improvement factor of 85 dB for this clutter spread and the 15-pulse Chebyshev design has an improvement factor of 52 dB. If there are many pulses available for MTI processing, an approximately rectangular filter response may be preferred over the "optimum" since increased doppler-frequency passband is more important than extremely large theoretical values of improvement factor which are not needed or cannot be achieved in practice. It has been said[11] that even with only five pulses available, a five-pulse Chebyshev design provides significantly wider doppler space than the five-pulse "optimum" design.

تخصيص باند گذر بيشتر براى

When only a few pulses are available for processing, there is probably little that can be done to control the shape of the nonrecursive filter characteristic, and there might not be much gained by using other than a filter with binomial weights that has a $\sin^n(\pi f T_p)$ response.

Recursive Filters The N-pulse nonrecursive canceler discussed above allows the designer N zeros for synthesizing the frequency response using the classical z-plane procedure for filter design. Each feedforward line and its weight w_i correspond to a zero in classical filter design on the z-plane. Filter design using only zeros does not have the flexibility of filter design based on poles as well as zeros. Poles can be obtained with delay-line cancelers by employing feedback. With both feedback and feedforward lines providing both poles and zeros, arbitrary filter frequency-response functions can be synthesized from cascaded delay lines, within the limits of realizability.[12] These are known as *recursive filters* or *infinite impulse response (IIR) filters*. Significantly fewer delay lines (and fewer pulses) are needed to achieve desirable frequency-response functions than with nonrecursive filters that only have zeros available for design in the z-plane.

طراحي فيلتر با بكاربردن تنها صفرها داراي انعطاف پذيري كمتري نسبت به طراحي بر اساس صفرها و قطب ها است.

فيلترهاي IIR نسبت به FIR خطوط تاخير كمتر (و پالس هاي كمتر) را نياز دارند تا به توابع پاسخ فركانسي مطلوب دست يابند.

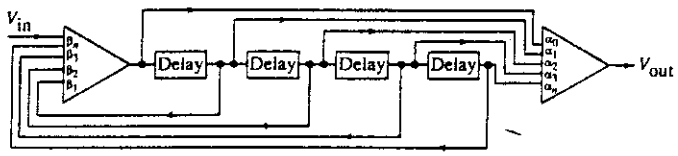

Figure 3.15 Canonical configuration of a recursive delay-line filter with both feedforward and feedback.
[After White and Ruvin, *IRE Natl. Conv. Rec.*, vol. 5, pt. 2, 1957.]

پاسخ فرکانسي فيلتر بازگشتي نسبت به فيلتر غيربازگشتي، با تعداد پالس هاي کمتر، شباهت بيشتري به شکل rectangular ايجاد مي کند

The canonical configuration of a time-domain filter with both feedback and feedforward is shown in Fig. 3.15. More usually, the canonical configuration is broken into sections with feedback and feedforward around individual delay lines. An example is the three-pole Chebyshev filter of Fig. 3.16a. The frequency response of this recursive filter is shown in Fig. 3.16b, with 0.5 dB ripple in the passband.[13] The width of the passband can be changed with different sets of weights. Figure 3.17, due to J. S. Shreve,[14] compares the response of a nonrecursive and recursive filter. It is seen that the recursive filter provides a frequency response that better resembles the rectangular shape than the nonrecursive, and does so with only two delay lines rather than the four of the nonrecursive filter.

کاربري فيلتر بازگشتي به دليل پاسخ گذراي فقيرتر محدود مي شود.

The recursive filter provides more flexibility in shaping the frequency response to produce better response than the nonrecursive filter, and it does it with fewer delay lines. Unfortunately, its utility is limited by poor transient response because of the feedback. Large discrete clutter echoes, interference pulses from a nearby radar, deliberate pulse jamming, or the beginning of a dwell by a step-scan radar (a phased array radar, for example) can all produce transient ringing that can mask the target signal until the transient dies out. A frequency response with steep sides might allow 15 to 30 or more pulses to be generated at the filter output from a single input pulse because of the feedback.[15] It

عواملي که مي توانند transient ringing ايجاد کنند:

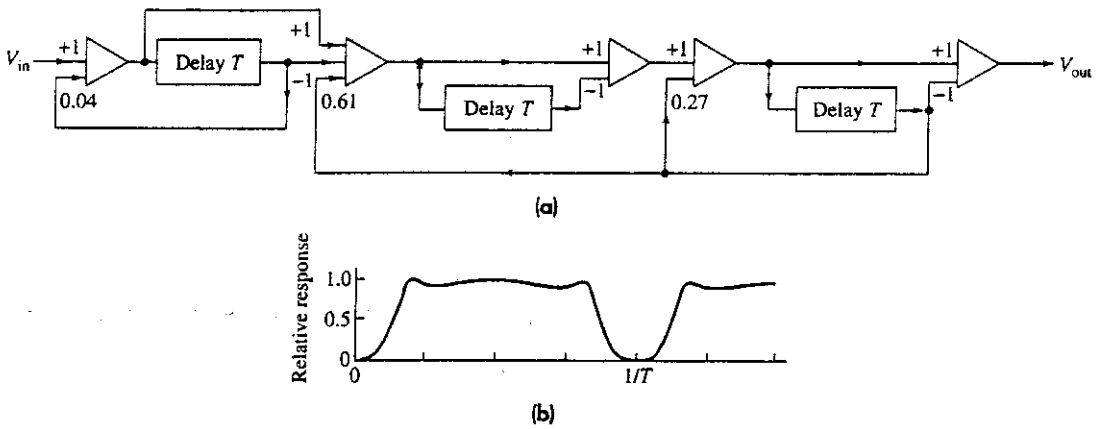

Figure 3.16 Shown in (a) is a recursive delay-line filter whose frequency response in (b) is based on a three-pole Chebyshev design with 0.5-dB ripple in the passband.
[After W. D. White.[13]]

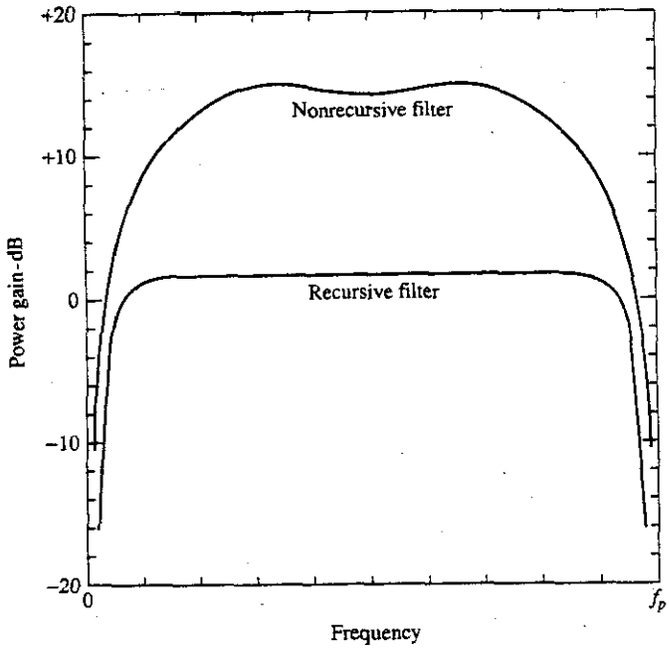

Figure 3.17 Example of the frequency response of a recursive filter with two delay lines and a nonrecursive filter with four delay lines. For the recursive filter the feedforward weights are 1, −2, and 1 and its feedback weights are 1, 1.561, and −0.641. The feedforward weights for the nonrecursive filter are 1, 1.25, −4.75, 1.75, and 0.75.
(After J. S. Shreve.[14])

has been suggested[16] that the undesirable transient in a stepped-scan radar can be mitigated by using the first return from each new beam position to apply initial conditions to the MTI recursive filter to cancel or reduce the transient effects. The clutter returns can be approximated by a step-input equal in magnitude to the first return for each beam position. The steady-state values that would normally appear in the (digital) filter are calculated and loaded into the filter to suppress the transient response.

از فیلترهای IIR با پاسخ گذرای ضعیف در رادارهای نظامی استفاده نمی شود.

Because of the poor transient response of recursive filters (infinite impulse response), they are usually avoided in military radars that might be subject to deliberate electronic countermeasures. They have been widely used, however, to eliminate clutter in civilian doppler weather radars. The Nexrad radar, for example, uses a five-pole (fifth-order) elliptic filter with its notch width under software control, and the Terminal Doppler Weather Radar uses a four-pole elliptic filter.[17] Recursive filters are used in this application because of the requirements for sharp filter notch widths around zero doppler and a flat response within the passband so that accurate estimates can be made of weather reflectivity and precipitation regardless of the doppler frequency. The elliptic filter is said to have the advantage of narrower notch widths than any other filter of the same order.

فیلتر elliptic دارای پهنای notch باریکتر نسبت به فیلترهای دیگر با مرتبه یکسان است.

Although the recursive filter seems attractive for MTI, its transient response makes it of limited application. There are several other approaches to achieving an MTI filter.

The use of multiple staggered prfs will be discussed next, which increases the first blind speed as well as provide limited filter shaping. This will be followed by the doppler filter bank that provides capabilities not available with the filters discussed previously.

The multiple delay-line canceler, the *N*-pulse canceler, the transversal (nonrecursive) filter, and the recursive filter are all examples of time-domain filters rather than frequency-domain filters. The doppler filter bank in Sec. 3.4 is also considered as a time-domain filter.

3.3 STAGGERED PULSE REPETITION FREQUENCIES

The use of multiple waveforms with different pulse repetition frequencies allows the detection of moving targets that would otherwise be eliminated with a constant-prf waveform if their radial velocities were at, or in the vicinity of, a blind speed [as defined by Eq. (3.12)]. A simple illustration is shown in Fig. 3.18 which graphs the frequency response of a single delay-line canceler with two different pulse repetition frequencies (prfs). At prf f_1, blind speeds (nulls) occur when the doppler frequency is f_1 or $2f_1$ (and other integer multiples, which are not shown). With prf $f_2 = 2f_1/3$, blind speeds occur when the doppler frequency equals f_2, $2f_2$, or $3f_2$. It can be seen in Fig. 3.18 that targets not detectable because of a blind speed in the frequency response of one prf will be detectable with the other prf. A target is lost on both prfs, however, when the blind speeds occur simultaneously, as when $2f_1 = 3f_2$. Thus the first blind speed at prf f_1 has been doubled in this simple example. The above illustrates the benefit of using more than one prf to reduce the effects of blind speeds; but it might be cautioned that it is not usual to use prfs with the relatively large ratio of 3/2.

There are several methods for employing multiple prfs to avoid losing target echoes due to blind speeds. The prfs can be changed (1) scan to scan, (2) dwell to dwell, or (3) pulse to pulse (usually called a staggered prf). A *dwell* is the *time on target*, and is

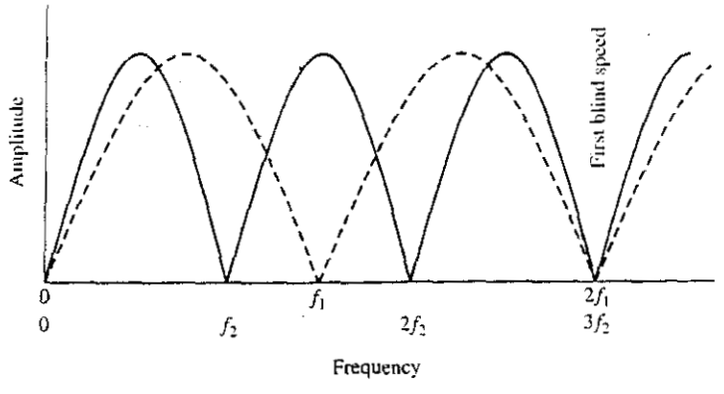

Figure 3.18 Frequency response of two prfs f_1 (dash curve) and f_2 (solid curve), where $f_1 = 3f_2/2$. The blind speeds of the first prf are shown at f_1 and $2f_1$, and the blind speeds of the second prf are shown at f_2, $2f_2$, and $3f_2$. A target at the blind speeds of one prf are "covered" by the response of the other prf, except when $2f_1 = 3f_2$, where both prfs have the same blind speed.

usually the time it takes to scan the antenna beam over a beamwidth or some fraction of a beamwidth. A dwell can be the time to scan one half-beamwidth, if there are only two prfs (as in the MTD discussed in Sec. 3.6). Staggered prfs have been popular for air-traffic control radars. An example of the four intervals of a staggered prf waveform is given in Fig. 3.19. The four-interval sequence is then repeated.

Each of the three strategies for applying the prfs for relieving the problem of blind speeds has its particular advantages as well as limitations, and each has been used in operational radars systems.

Staggered prfs In pulse-to-pulse staggered prfs, as in Fig. 3.19, the time between pulses is an interval or a period. The term *interval* is more appropriate, but the term *period* arose historically and its use remains even though it might not always be used precisely. In this discussion, the term *period* will be used for the interval between pulses of a staggered waveform. Multiple staggered prfs can be processed with a transversal filter, as was shown in Fig. 3.12. The filter samples the doppler frequency at nonuniform times rather than the uniformly spaced time-samples when the prf is constant. The frequency response of this filter is

$$H(f) = w_0 + w_1 e^{j2\pi f T_1} + w_2 e^{j2\pi f(T_1+T_2)} + \cdots + w_n e^{j2\pi f(T_1+T_2+\cdots+T_n)} \qquad [3.25]$$

The selection of the $n + 1$ weights w_i and the n pulse repetition periods T_i is generally constrained by several design factors:

1. The minimum period should not result in range ambiguities.
2. The sequence of the periods should be selected so as not to stress the transmitter by employing a widely varying duty cycle or a duty cycle for which the transmitter is not designed.
3. The maximum period should not be too long since any range beyond the maximum unambiguous range represents "dead time" to a radar.
4. The response in the filter stopband should produce the required MTI improvement factor for detection of targets in clutter.
5. The deepest null in the passband should not be excessive. Usually the deepest null occurs at a frequency equal to the inverse of the average period.
6. The variation (or ripple) of the response over the passband should be minimized and relatively uniform.

Not all of these conditions can be satisfied simultaneously. Design of a staggered prf and its processing is often a compromise.

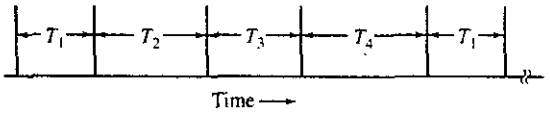

Figure 3.19 Staggered pulse-train with four different pulse periods, or intervals.

An example of the frequency response with a four-period (five-pulse) stagger with dual-canceler weighting is shown in Fig. 3.20. This is due to W. W. Shrader[18] and might be typical for a long-range en-route civil air-traffic control radar. The ratios of the pulse repetition periods are 25:30:27:31. These were found by computer search. Shrader states that with four periods, the stagger ratios can be obtained by adding the numbers -3, 2, -1, and 3 to the desired first blind speed expressed as v_1/v_B, where v_1 is the first blind speed and v_B is the blind speed that would have been obtained if a waveform with a constant prf had been used whose pulse repetition period was the average of the four staggered periods. This ratio is given by Eq. (3.26). If v_1/v_B were 28, adding the four numbers given above by Shrader results in the particular stagger ratios used in Fig. 3.20. [Substituting these four period-ratios into Eq. (3.26), however, gives $v_1/v_B = 28.25$ (instead of 28).]

Although the staggered prfs remove the blind speeds that would have been obtained with a constant prf, there will eventually be a new blind speed that occurs when the n prfs have the following relationship $\eta_1 f_1 = \eta_2 f_2 = \cdots = \eta_n f_n$, where $\eta_1, \eta_2, \ldots, \eta_n$ are relatively prime integers (with no common divisor other than 1). The ratio of the first blind speed v_1 with a staggered prf waveform to the first blind speed v_B of a waveform with constant prf equal to the average period is

$$\frac{v_1}{v_B} = \frac{\eta_1 + \eta_2 + \cdots + \eta_n}{n} \qquad [3.26]$$

In deriving the above, the average period is $T_{av} = (T_1 + T_2 + \cdots + T_n)/n$ where $T_i = 1/f_i$, and the new first blind speed is given by $v_1 = \lambda\eta_1 f_1/2 = \lambda\eta_1/2T_1$. A slightly different expression is obtained if the average prf were used instead of the average period.

Another example of the frequency response is that for a medium-range civil air-traffic control airport surveillance radar shown in Fig. 3.21. Note that there is a change in scale of the abscissa. The amplitude weighting is based on a dual canceler. The solid curve of Fig. 3.22 shows the response of a four-period canceler with weightings of $\frac{7}{8}$, 1, $-3\frac{3}{4}$, 1, $\frac{7}{8}$, and four interpulse periods of -15 percent, -5 percent, $+5$ percent, and $+15$ percent of the fixed period equal to the average period.[19] The deepest null is 6.6 dB. The dashed curve is the frequency response for the same amplitude weights, but with a fixed period.

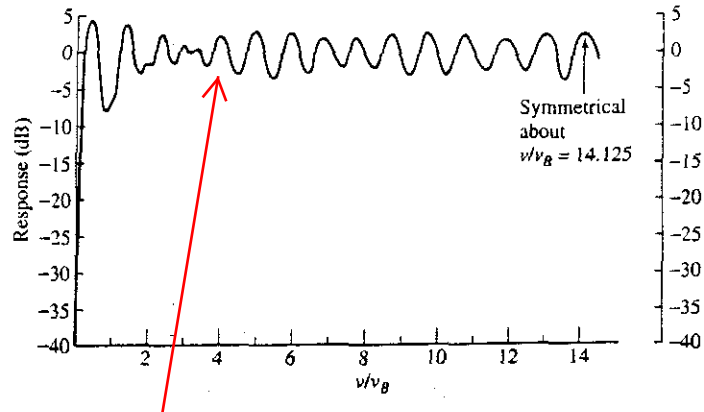

Figure 3.20 Frequency response of a *five-pulse (four-period) stagger.* (From Shrader and Gregers-Hansen,[1] courtesy McGraw-Hill Book Co.)

آیا در زمان استخراج زاویه تغییر دامنه سیگنال هدف با تغییر داپلر هدف منجر به خراب شدن دقت زاویه اي نمي شود؟

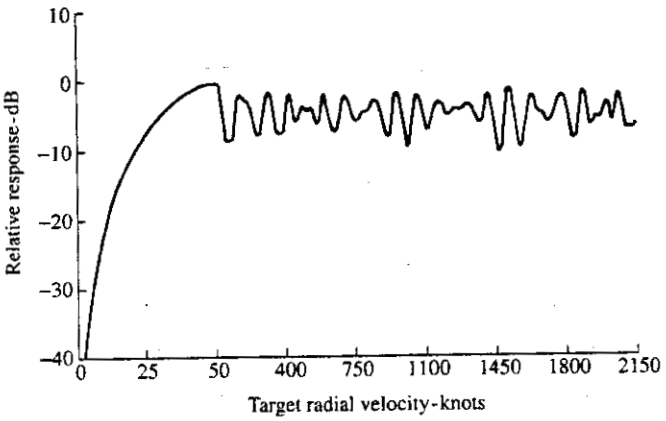

Figure 3.21 Example of the frequency response of a staggered MTI with four periods for an S-band ASR air-traffic control radar as a function of the target's radial velocity. The four periods are 876, 961, 830, and 1177 μs, with amplitude weighting based on a dual-canceler response. (Note change of scale of the abscisso.)

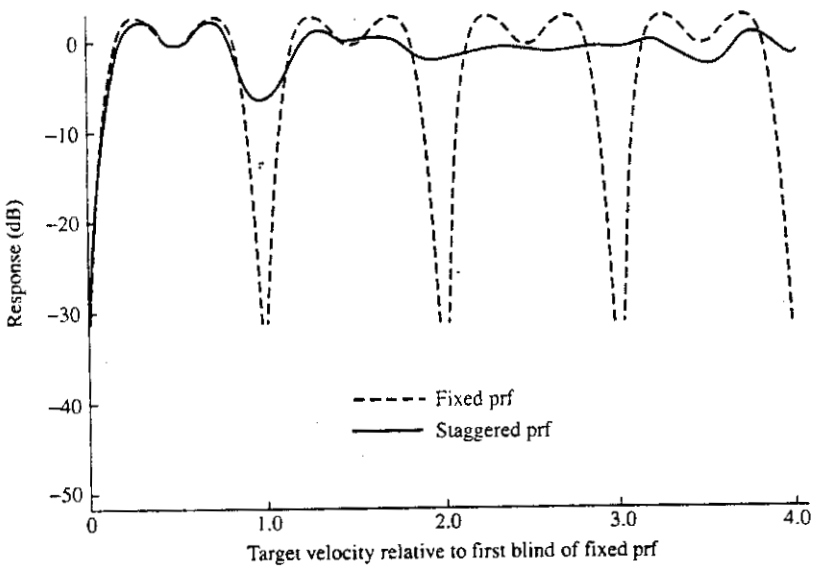

Figure 3.22 Frequency response of a weighted four-period staggered waveform compared with the frequency response using a constant prf waveform. Dashed curve, constant prf; solid curve, staggered prf.
(From Zverev,[19] Courtesy IEEE.)

عمق نول به نسبت ماکزیمم پریود به مي نیمم پریود وابسته است اما به نوع کنسلر (تك پالس، دوپالسه یا سه پالسه) ربطي ندارد.

Null Depth and Improvement Factor There have been two methods proposed for finding the effect of the stagger periods on the depth of the null and the MTI improvement factor. One is based on computer search, the other on an analytic formulation.

Computer Search The depth of the deepest null within the MTI filter passband when using a staggered waveform is shown in Fig. 3.23, as found by Shrader based on computer search for the best sets of pulse periods.[18] He found that the null was relatively independent of the type of canceler (whether single, double, or triple) or the number of hits per beamwidth. The null depth depended mainly on the ratio of the maximum-to-minimum period, which is the abscissa of Fig. 3.23.

There have been other methods proposed for finding in a logical manner the values of the weights w_i and the periods T_i.[20–23] Some of these are concerned mainly with minimizing the extent of the deepest null and do not examine the effect on the improvement factor. Computer search on a trial-and-error basis, such as that of Shrader, has probably produced as good a result as any.

Analytic Formulation Using the rms value σ_n of the periods of a staggered-prf waveform, Cleetus[24] extended earlier work of McAulay[25] and Wardrop[26] to arrive at an estimate of the maximum improvement factor as

$$I_{\max} = \frac{1}{4\pi^2\sigma_c^2\sigma_n^2} \qquad [3.27]$$

where σ_c^2 = total variance of a gaussian clutter spectrum as defined by Eq. (3.14), σ_n^2 = mean square value of $\epsilon_n = T_i - T_{av}$, T_i = period of the ith stagger, and T_{av} = average value of the n periods. This is called the maximum improvement factor since it assumes an ideal rectangular MTI filter. It depends only on the spread of the T_i's and not

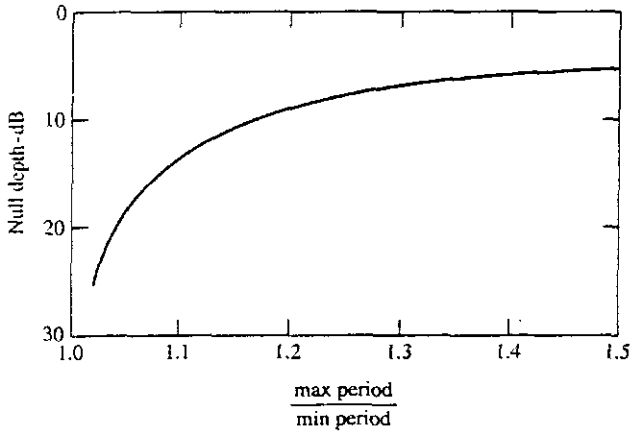

Figure 3.23 Approximate depth of the first null in the frequency response of a pulse-to-pulse staggered prf MTI as a function of the ratio of the maximum period to the minimum period. (After W. W. Shrader and V. Gregers-Hansen.[1] Courtesy McGraw-Hill Publishing Co.)

on the number of stagger pulses. The depth of the deepest null was also explored by Cleetus. From the graph presented in his paper (his Fig. 3) the following expression can be obtained for the depth of the first null

$$\text{null depth} = 40\left(\frac{\sigma_n}{T_{av}}\right)^2 \qquad [3.28]$$

This applies for values of σ_n/T_{av} less than approximately 0.09 (which produces a null depth of 5 dB). At higher values of σ_n/T_{av} the null depth rises slowly and approaches zero at $\sigma_n/T \approx 0.3$. Comparing Eqs. (3.27) and (3.28) shows that the null depth and improvement factor cannot be selected independently since they both depend on the variance σ_n^2 of the stagger periods. The computer-derived null depth given in Fig. 3.23 depends only on the ratio T_{max}/T_{min}, whereas Eq. (3.28) depends on the variance of the periods.

Shrader also presents a computer-derived expression for the improvement factor, which is

$$I = \left[\frac{2.5n_B}{(T_{max}/T_{min}) - 1}\right]^2 \qquad [3.29]$$

where n_B = number of pulses per beamwidth. This is based on the width of the clutter spectrum being determined mainly by the antenna scan modulation. It may seem quite different from the improvement factor of Eq. (3.27), but the two can be shown to be somewhat similar. If we make the following very gross assumptions, this equation can be put in almost the same form as Eq. (3.27): (1) the number of pulses $n_B \approx t_0/T_{av}$, where t_0 = time on target and T_{av} = average stagger period; (2) the value of t_0 is replaced by ($\sigma_s = 1/3.77t_0$) [Eq. (3.45)], the standard deviation for antenna scan modulation; (3) the antenna scan modulation σ_s is replaced by the more general σ_c, the symbol for the standard deviation of the clutter spectrum, whatever its cause; and (4) the distribution of stagger periods is assumed uniform between T_{max} and T_{min} so that its standard deviation σ_n can be written (Sec. 2.4) as $\sigma_f = (T_{max} - T_{min})/2\sqrt{3}$. With these assumptions,

$$I = \left(\frac{1}{5.22\sigma_c\sigma_n}\frac{T_{min}}{T_{av}}\right)^2 \qquad [3.30]$$

This resembles Eq. (3.27), and would be identical if $(T_{av}/T_{min}) = 2\pi/5.22 = 1.2$.

Comparison of Multiple-prf Methods It was said earlier that there are three methods for applying multiple prfs to reduce the effects of blind speeds. These were (1) staggering a number of periods pulse to pulse, (2) alternating between two periods every half-beamwidth, and (3) changing periods (prfs) from one antenna scan to the other. Each has advantages and limitations.[27] Pulse-to-pulse stagger with several pulse periods can significantly increase the blind speed compared to a constant prf waveform and it doesn't have large regions of doppler space where moving targets are not detected as, for example, when a double or triple delay-line canceler is used. Also, compared to recursive filters, staggered-prf filter design is simplified since it does not require the feedback found in recursive filters nor does it experience poor transient response. Staggering the prfs degrades slightly the improvement factor by transferring clutter energy to the

يعني كلاتري كه فراتر از multiple time around clutter
برد نامبهم پريود پالس شروع مي شوند

doppler-frequency space and it is more difficult to stabilize a transmitter that doesn't have a constant prf. Also, it does not cancel multiple-time-around clutter (clutter that originates beyond the maximum unambiguous range of the pulse period). In many radar systems that employ pulse-to-pulse stagger there is usually a constant prf waveform available that can be selected when the radar looks in those directions where multiple-time-around clutter is encountered.

The radar that changes its prf from scan to scan is easier to implement and it can cancel multiple-time-around clutter. It takes a longer time (more than one scan time) to unmask doppler blind speeds compared to pulse-to-pulse stagger. Seldom would more than two different prfs be used to unmask blind speeds in a scan-to-scan staggered system. With only two prfs, the reduction in blind speeds is not as effective as when many periods are employed, as in a staggered waveform. Dwell-to-dwell stagger has similar advantages as scan-to-scan changes, and unmasking of blind speeds is done quicker. Half-beamwidth dwells have been used effectively with filter-bank processing, as in the MTD radar discussed later in Sec. 3.6.

3.4 DOPPLER FILTER BANKS

چند هدف متحرك را مي توان در يك بانك فيلتر داپلر از يكديگر جدا كرد.

A doppler filter bank is a set of contiguous filters for detecting targets as shown in Fig. 3.24. A filter bank has several advantages over the single filters that have been considered previously in this chapter:

1. Multiple moving targets can be separated from one another in a filter bank. This can be particularly important when one of the echo signals is from undesired moving clutter; such as a rain storm or birds with a nonzero doppler shift. When the clutter and target echo signal appear in different doppler filters, the clutter echo need not interfere with the detection of the desired moving target.

مي توان سرعت شعاعي هدف را اندازه گيري كرد. حتي در صورت ابهام داپلر با تغيير PRF مي توان اين ابهام را برطرف كرد.

2. A measure of the target's radial velocity can be obtained. It might be ambiguous, but a change in the prf can resolve the ambiguity in the radial velocity,[28] just as changing the prf can resolve range ambiguities.

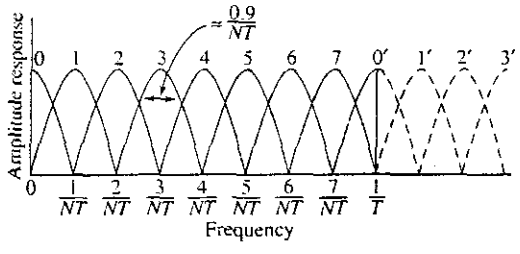

Figure 3.24 MTI doppler filter bank resulting from the processing of $N = 8$ pulses with the phase weights of Eq. (3.31), yielding the response of Eq. (3.34). N is the number of pulses processed and the number of filters generated; T is the pulse repetition period. The sidelobe structure of the filters is not shown.

فيلترهاي داپلر باندباريك نويز بيشتري را نسبت به فيلتر MTI حذف مي كنند و امكان جمع بندي همدوس را فراهم مي كنند.

3. The narrowband doppler filters exclude more noise than do the MTI delay-line cancelers described previously, and provide coherent integration. In general, this improvement in signal-to-noise ratio by means of coherent integration is seldom the major reason for using filter banks in MTI radar. The gain due to the coherent integration of n pulses is not that much greater than the gain due to the noncoherent integration of n pulses when n is not too large.

The price paid for these advantages is greater complexity, difficulty in achieving filters with low enough sidelobes to reduce clutter, and the need for a significant number of pulses to produce desirable filter characteristics. The basic method for achieving a doppler filter bank is to employ the transversal filter with complex weights rather than real (amplitude) weights as in the transversal filters discussed before. Complex weights mean that phase shifts as well as amplitude weights are employed.

Consider the transversal filter of Fig. 3.12, with N pulses (N taps) and $N - 1$ delay lines. With proper phase weights this will form N contiguous filters covering the frequency range from 0 to f_p (or from $-f_p/2$ to $+f_p/2$), where f_p is the pulse repetition frequency. The time delay between each tap of the transversal filter is $T = 1/f_p$. Not shown in this simple depiction of a transversal filter are the N parallel outputs at each of the N taps, one for each filter. The weights $w_{i,k}$ for each of N taps, with k outputs at each tap can be expressed as

این وزن ها براي transversal filter با n-tap است كه با داشتن N خروجي، N فيلتر را در يك بانك فيلتر شبيه سازي مي كند.

$$w_{i,k} = e^{j[2\pi(i-1)k/N]} \tag{3.31}$$

where $i = 1, 2, \ldots, N$ represents the N taps and k is an index from 0 to $N - 1$ that corresponds to a different set of N weights, each for a different filter. In this example, the amplitude is the same at each tap, only the phases are different. The N filters generated by the index k constitute the filter bank. If there were eight pulses available to generate eight filters, the phase weights $w_{i,0}$ for the filter $k = 0$ [found from Eq. (3.31)] are all of zero phase. For the next filter, $k = 1$, Eq. (3.31) gives the phase weights $w_{i,1}$ as 0, 45, 90, 135, 180, 225, 270, and 315 degrees, respectively. The phase weights for the higher filters (k from 2 to 7) are the same as those for $k = 1$, but multiplied by k, modulo 360.

We next obtain the frequency response of the N filters of the filter bank. The impulse response of the transversal filter of Fig. 3.12 with the weights given by Eq. (3.31) can be formulated (almost) by inspection as

$$h_k(t) = \sum_{i=1}^{N} \delta[t - (i-1)T] e^{j2\pi(i-1)k/N} \tag{3.32}$$

where $\delta(t)$ is the delta function. The Fourier transform of the impulse response is the frequency response function, so that

$$H_k(f) = \sum_{i=1}^{N} e^{-j2\pi(i-1)[fT - k/N]} \tag{3.33}$$

The magnitude of the frequency response function is the amplitude passband characteristic of the filter, which is

$$|H_k(f)| = \left| \sum_{i=1}^{N} e^{-j2\pi(i-1)[fT - k/N]} \right| = \left| \frac{\sin[\pi N(fT - k/N)]}{\sin[\pi(fT - k/N)]} \right| \tag{3.34}$$

This is sketched in Fig. 3.24. The peak response occurs whenever the denominator is zero, or when $\pi(fT - k/N) = 0, \pi, 2\pi, \ldots$. The numerator also will be zero when the denominator is zero. The value of 0/0 is indeterminate; but by using L'Hopitals rule, the peak value of Eq. (3.34) is found to be N when both numerator and denominator are zero. Nulls in the frequency response function occur when the numerator is zero and the denominator is not zero. The width of the main response as defined by the spacing between the first pair of zeros is $2/NT$. The half-power width is approximately $0.9/NT$. When the doppler filter bank is shown, as in Fig. 3.24, the sidelobes are not usually included. This is done for clarity; but they are there and can limit the amount of clutter attenuation obtained. The shape of an individual filter is as sketched in Fig. 3.25.

When $k = 0$, the peak response occurs at $f = 0, 1/T, 2/T, \ldots$. This defines a filter with peak response at zero frequency, at the prf ($f_p = 1/T$), and at harmonics of the prf. Thus the $k = 0$ filter corresponds to the clutter spectrum and does not reject clutter as do the other $N - 1$ filters. When $k = 1$, the peak response occurs at $f = 1/NT$, as well as $1/T + 1/NT$, $2/T + 1/NT$, and so forth. For $k = 2$, the peaks occur at $f = 2/NT$, $1/N + 2/NT$, $2/N + 2/NT$, etc. Thus each value of k corresponds to one of N separate doppler filters, as in Fig. 3.24. Together the N filters cover the frequency region from 0 to $f_p = 1/T$ (or, equivalently, from $-f_p/2$ to $+f_p/2$). In this particular case where the amplitude weights at each tap are all the same, the first nulls of each filter are at the peaks of the adjacent filters. Being a periodic signal, the remainder of the frequency domain is covered by similar filters, but with ambiguity and aliasing.

ابهام و aliasing دو مشكل مهم در بانك فيلتر داپلر هستند.

The generation of N filters from the output of N taps of a transversal filter requires a total of $(N - 1)^2$ digital multiplications. The process is equivalent to that of a discrete Fourier transform. In many cases, the fast Fourier transform (FFT) can be used to speed computations if the value of N is some power of 2; which is why the above example was for $N = 8 = 2^3$.

فرايند توليد بانك فيلتر داپلر بسياز شبيه به گرفتن تبديل فوريه گسسته يا FFT در زماني كه N تواني از 2 مي باشد است.

The improvement factor for each of the eight filters of an eight-pulse filter bank with uniform amplitude weights is shown in Fig. 3.26 as a function of σ_c/f_p, where σ_c is the standard deviation of the clutter spectrum, which is assumed to be gaussian.[29] The average improvement factor for all filters is indicated by the dotted line. This might be compared to the improvement factor for an N-pulse canceler with response $\sin^N \pi f T_p$, which was shown in Fig. 3.13. Note that the improvement factor for a two-pulse canceler is about the same as the average of the eight-pulse doppler filter bank. The three-pulse canceler is even better. Thus lower sidelobes are needed if large values of the improvement factor are to be obtained with a doppler filter bank.

8 فيلتر در يك بانك فيلتر داپلر يعني بانك فيلتر 8 پالسه

Figure 3.25 Sketch of an individual filter of the doppler filter bank of Fig. 3.24, including the sidelobes.

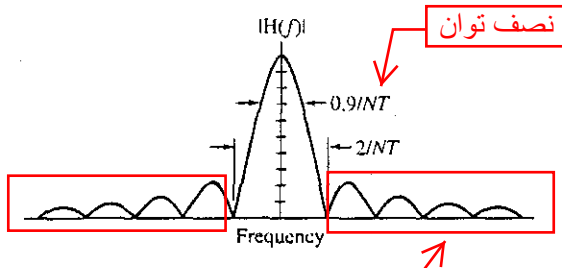

فركانس نصف توان

وقتيكه بانك فيلتر داپلر را نشان مي دهند اين سايدلوب ها را نشان نمي دهند.

وجود اين سايدلوب ها ميزان حذف كلاتر را محدود مي كنند.

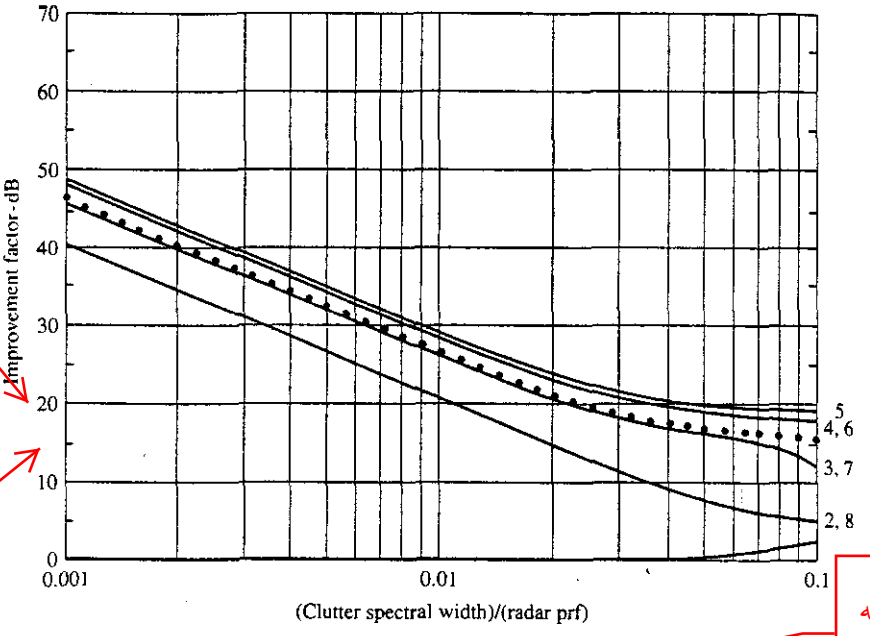

Figure 3.26 Improvement factor for each filter of an eight-pulse doppler filter bank, with uniform amplitude weighting, as a function of the clutter spectral width (standard deviation). The average improvement factor is indicated by the dotted curve. (From Andrews.[29])

در این شکل طیف کلاتر گوسي در نظر گرفته شده است.

يعني به ازاي FFT گرفتن از 8 پالس ورودي به بانك فيلتر داپلر نيز ضريب بهبود MTI تعريف مي شود و تنها به ازاي K=0 حذف كلاتري انجام نمي شود.

3/3/88

31/3/88

Reducing the Filter Sidelobes The frequency-response function of each filter of the filter bank derived above is of the form $(\sin NX)/\sin X$; thus the highest sidelobes are 13.2 dB below the peak response. These are relatively high and are not good at rejecting clutter, especially for those filters near zero frequency or near a blind speed. The sidelobes can be reduced by employing amplitude weights in addition to phase weights. Shrader and Gregers-Hansen[30] indicate that when only a few pulses are available (about six or so) in a coherent processing interval (CPI), empirical design procedures can be used since there is little flexibility for more sophisticated design. With a larger number of pulses available a more systematic approach can be employed based on Chebyshev filter design.[31] The frequency response of the Chebyshev filter has all its sidelobes equal and the width between the nulls of the main response is a minimum for a given sidelobe level.[32] (This is similar to the Dolph-Chebyshev array antenna pattern synthesis technique known to antenna engineers.) When the sidelobes are lowered, however, the main response is widened, the peak gain is reduced, but the straddling loss at filter crossover is less. For example, with 68-dB sidelobe level the null width is 3.5 times the half-power bandwidth, and the peak is 2.1 dB lower than that of a filter with uniform weighting.[30]

در بانك فيلتر داپلر تابع پاسخ فركانسي هر فيلتر به صورت SIN(NX)/SIN(X) است. بنابراين بزرگترين سايدلوب 13.2 dB نسبت به پيك پاسخ پايين تر است. و اين سايدلوب براي حذف كلاتر يا سرعت كور مناسب نيست. اما با وزن دهي دامنه مي توان سايدلوب را كاهش داد.

To further reduce the clutter, especially in those filters close to zero frequency or the clutter spectral lines at the harmonics of the prf, a relatively simple delay-line canceler such as a three-pulse canceler with $\sin^2 \pi f T_p$ response can be placed ahead of the filter bank. It is an expedient to compensate for the inability to reduce the sidelobes of the filter bank as much as might be desired. Figure 3.27a shows the improvement factor for a three-pulse canceler cascaded with an eight-pulse filter bank with uniform amplitude weights; Fig. 3.27b is the same but for 25-dB Chebyshev weights.[29] The average improvement for all filters is shown by the dotted curves.

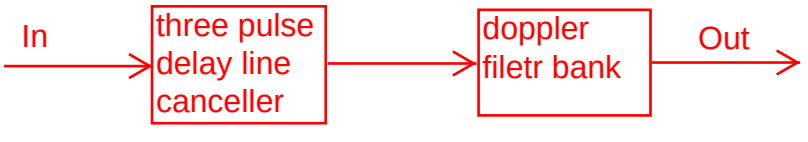

بانك فيلتر داپلر با وزن دهي
دامنه يكسان بعد از فيلتر 3
پالسه

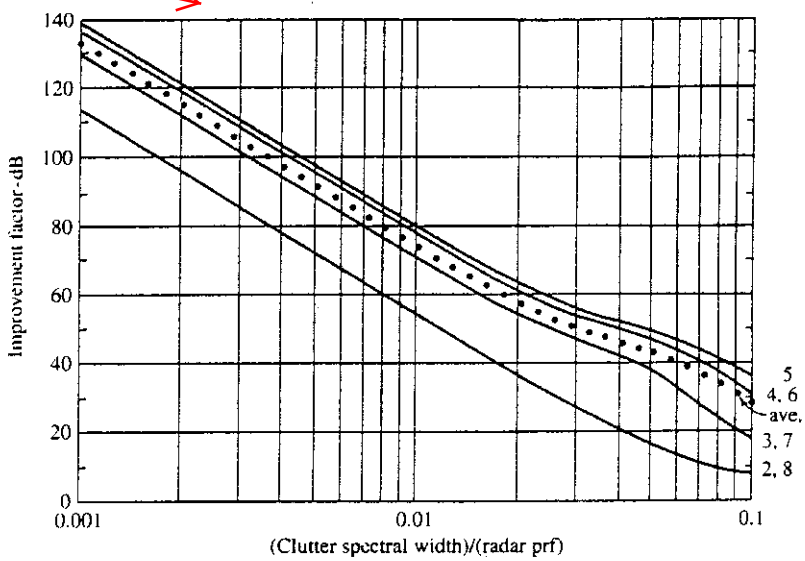

(a)

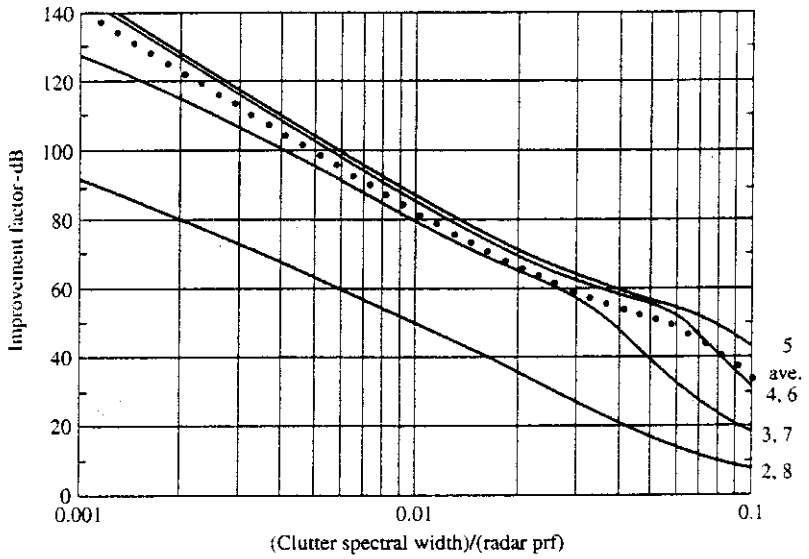

(b)

Figure 3.27 Improvement factor for a three-pulse canceler followed by an eight-pulse doppler filter bank. (a) Uniform amplitude weights and (b) 25-dB Chebyshev weights. The average improvement factor for all filters is indicated by the dotted curve. (From Andrews.[29])

Other Limitations . In addition to the difficulty in obtaining low filter sidelobes and large improvement factors, the doppler filter bank is more complex than the simpler delay-line cancelers discussed previously in this chapter, it generally requires more pulses for good performance, and it requires a larger signal-to-noise ratio if the true radial velocity is to

تلف straddling به معني كاهش نسبت SNR در محل گذر دوفيلتر جانبي نسبت به پيك فيلتر است.

be extracted when two or more prfs are employed. There will also be a reduction in the signal-to-noise ratio at the crossover of adjacent filters, relative to the peak response at the center of the filter This is called a *straddling loss.* The doppler filter bank is used, however, since it has capabilities not available with delay-line cancelers, as was enumerated at the beginning of this section.

3.5 DIGITAL MTI PROCESSING

Most of the basic theoretical aspects of MTI filter design were formulated when the delay lines were analog acoustic devices. Sophisticated MTI doppler filters were difficult to implement with analog methods, so it was rare for an MTI radar to employ more than two analog delay lines in a delay-line canceler. The rapid development of digital technology beginning in the early 1970s, however, allowed the delays to be obtained by storing digital words in a memory for whatever length of time was required. This greatly increased the options open to the radar signal-processing engineer. Digital doppler filters with many delay lines are now practical so that sophisticated filters can be readily obtained when a large number of pulses are available for processing. Thus the theoretical aspects of MTI doppler filters, which were only of academic curiosity when analog delay lines were all that was available, now can be implemented using digital methods. In addition to making practical the design of more sophisticated filters, the advantages offered by digital MTI processing include:

مزاياي ديجيتالي شدن فيلترهاي MTI

- Compensation for "blind phases," which cause a loss due to the difference in phase between the echo signal and the MTI reference signal. This is achieved by use of *I* and *Q* processing (in-phase and quadrature), something that was always known to be of value for MTI processing, but which was not convenient to implement with analog methods.

1. از بين بردن اثر فاز كور با استفاده از روش I و Q

- Greater dynamic range can be obtained than was possible with acoustic delay lines.
- Unwanted changes in the delay times of acoustic delay lines due to temperature changes are eliminated by the accurate timing of digital methods.

تغييرات ناخواسته در زمان هاي تاخير خطوط تاخير صوتي به خاطر تغييرات دمايي بوسيله زمانبندي دقيق روش هاي ديجيتال حذف مي شوند.

- There is no problem in making the delay time in the digital memory synchronous with the radar's prf, something difficult to do with acoustic delay lines.

زمان هاي تاخير در حافظه ديجيتال را مي توان با PRF رادار سنكرون كرد در حاليكه در خطوط تاخير صوتي مشكل مي شد.

- The flexibility offered by digital methods allows signal processors to be readily obtained with many different filter characteristics. Digital processors can be made reprogrammable.
- Digital MTI is more stable and reliable than analog MTI, and requires less adjustments during operation in the field.

Although digital processing does not have the serious weaknesses associated with analog delay lines, it has other characteristics that have to be understood if full advantage is to be taken of its capabilities for significantly improving doppler processing in an MTI radar.

31/3/88

2/4/88

Blind Phases, *I* and *Q* Channels The block diagram of an MTI radar that was shown in Fig. 3.7 had a single phase detector and filter channel. With a single phase detector and single processing channel, there is a loss when the doppler-shifted signal is not sampled at the peak positive and negative values of the sinewave. When the phase between the doppler signal and the sampling at the prf results in a loss, it is called a *blind phase.* A blind phase is different from the blind speed discussed previously. It will be recalled that a blind speed occurs when the sampling pulse appears at the same point in the doppler cycle at each sampling time, as in Fig. 3.28a. Figure 3.28b illustrates the loss due to a

زمانيكه فاز ميان سيگنال داپلر و نمونه برداري در prf يك تلف را نتيجه دهد، اين مساله را فاز كور مي نامند.

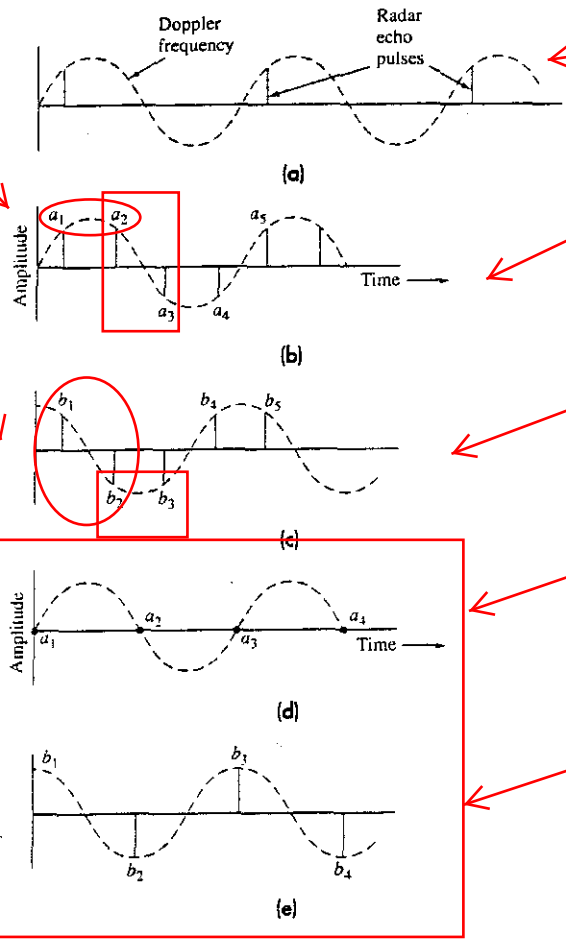

blind speed

دامنه يكسان دارند بنابراين $a_2-a_1=0$ بنابراين در اين حالت نصف انرژي سيگنال به هدر مي رود.

تلف به خاطر فاز كور در كانال I

دامنه يكسان با فازهاي مختلف دارند بنابراين $b_2-b_1=2b_2$

تلف به خاطر فاز كور در كانال Q

هيچ سيگنالي را در خروجي نداريم (كانال I)

براي مثال d، با نمونه برداري در كانال Q سيگنال كامل را داريم.

Figure 3.28 (a) Example of a blind speed in an MTI radar. The target's doppler frequency is equal to the prf. (b) Example of the effect of a blind phase in the *I* channel, and (c) in the *Q* channel. (d) The *I* channel of another special example of a blind speed. The prf is twice the doppler frequency and the phase of the sampling is such that there is no response at all since the sampling is at the zeros of the doppler frequency. Nothing is detected. (e) The *Q* channel for the example of (d) in which the sampling is at the positive and negative peaks of the doppler frequency so that there is complete recovery of the signal.

در اين حالت خاص، نصف انرژي سيگنال به هدر مي رود. اگر كانال پردازشي دومي وجود داشته باشد و سيگنال COHO با 90 درجه اختلاف فاز اعمال شود مي توان نصف ديگر انرژي سيگنال بازيابي كرد.

blind phase. The sampled signals in this particular example are all of the same amplitude and with a spacing such that when pulse a_2 is subtracted from pulse a_1, the result is zero. When pulse a_3 is subtracted from a_2, however, there is a finite output; but when a_4 is subtracted from a_3 the result is zero, and so on. Thus in this particular case, half of the signal energy is lost. The other half of the signal energy can be recovered if a second identical processing channel is used and there is a 90° phase change of the coho (reference) signal that is applied to its phase detector. This second channel is called the Q, or *quadrature*, channel. The original channel is called the I or in-phase channel. If the coho signal in the I channel is $\sin 2\pi f_{if}t$, the coho in the Q channel is $\cos 2\pi f_{if}t$. The result of the 90° phase change in the Q channel is shown in Fig. 3.28c. Those pulse pairs that had zero output in the I channel now have a finite residue in the Q channel. Likewise those pulse pairs which had a finite residue in the I channel now have zero output in the Q channel. What was lost in the I channel is recovered in the Q channel, and vice versa. The combination of the I and Q channels results in a uniform output with no loss.

The example of Fig. 3.28b and c is a special case. Another very special case of a blind phase is when the prf is twice the doppler frequency (this is not a blind speed) and the phase of the prf is such that the samples occur whenever the doppler signal in the I channel passes through a zero crossing, Fig. 3.28d. There is no output in this case. In the Q channel, Fig. 3.28e, where the phase of the prf is shifted 90°, the doppler signal is sampled whenever it is at a positive or a negative peak. The maximum signal is obtained. Again, what was lost in one channel is recovered in the other channel.

2/4/88

Block Diagram The block diagram of a digital MTI signal processor with I and Q channels is shown in Fig. 3.29. The signal from the IF amplifier is split into two channels. The phase detectors in each channel extract the doppler-shifted signal. In the I channel the doppler signal is represented as $A_d \cos(2\pi f_d t + \phi_0)$ and in the Q channel it is the same except that sine replaces the cosine. The signals are then digitized by the analog-to-digital (A/D) converter. A sample-and-hold circuit usually is needed ahead of the A/D converter for more effective digitizing. Sample and hold is often on the same chip as the A/D converter. (Some A/D converters, such as the flash type, do not require a sample and hold.[33]) The digital words are stored in a digital memory for the required delay time(s) and are processed with a suitable algorithm to provide the desired doppler filtering. The magnitude of the doppler signal is obtained by taking the square root of $I^2 + Q^2$. Sometimes, for simplicity, the sum of the magnitudes of the two channels, $|I| + |Q|$, is taken;

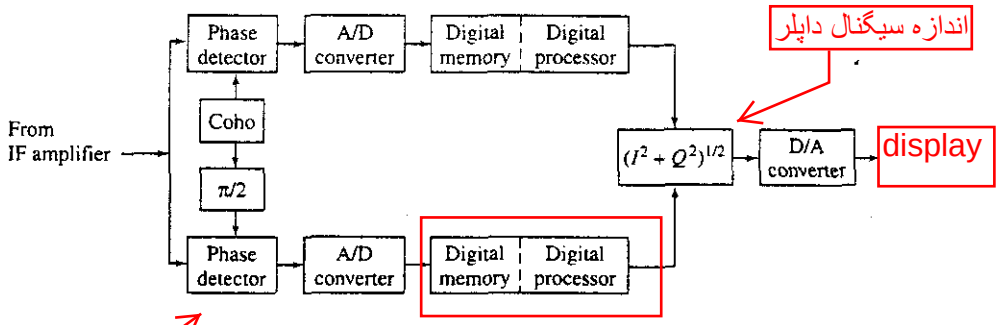

Figure 3.29 Block diagram of a digital MTI doppler signal processor.

اندازه سيگنال داپلر

اين phase detector شامل يك ميكسر و يك LPF است.

در اين بلوك فيلتر MTI در كانال Q انجام مي شود.

or the "greater of" of the two channels might be used instead.[34] The I and Q processor of Fig. 3.29 has a square-law detector characteristic. A linear-law detector can be approximated by the greater of $|I| + |Q|/2$ or $|Q| + |I|/2$.

If required, the combined unipolar output can be converted to an analog signal by a digital-to-analog (D/A) converter for display. Otherwise the digital output might be subject to further processing.

There are several methods for implementing an A/D converter, depending on the speed and number of bits required. Since there are two channels (the I and the Q), sampling in each can be at one-half the Nyquist rate, which generally makes the implementation of the A/D converters simpler. (The Nyquist rate is twice the signal bandwidth.) The number of quantization levels in the A/D is generally given as 2^N. D/A converters are usually easier to achieve than A/D converters of the same resolution.

يك ADC، ب 10 بيتي داراي 2^{10} سطح كوانتيزاسيون مي باشد.

با افزايش تعداد بيت هاي مبدل ADC فركانس كلاك آن كاهش مي يابد.

The available technology of A/D converters has sometimes been a serious limitation to MTI performance, but there have been continual advances in this technology. A 16-bit A/D, for example, might have a sampling rate of several MHz; a 14-bit A/D, a 50-MHz sampling rate; a 12-bit AD, a 100-MHz sampling rate; and an 8-bit A/D, a 1-GH_3 sampling rate.

The output of the IF amplifier is usually made to limit at a level consistent with the MTI improvement factor (as in Sec. 3.7) and the full-scale range of the A/D converter. The IF portion of the receiver is then a linear-limiting amplifier. The limiting action means that the peak excursion of the signal that the A/D converter must handle is known, and the A/D can be designed to cover this excursion. The signal should not be allowed to exceed the full-scale range of the A/D converter, since the output would then be degraded and severe harmonics generated. [35]

معمولا يكي دو بيت آخر خروجي ADC به دليل وجود نويز همراه سيگنال، معتبر نيستند.

Limitation on the Improvement Factor Due to the A/D Converter All analog signals that lie within the same quantization step of the A/D converter are represented by the same digital word. Since the rms value of the noise accompanying the signal is usually greater than the quantization step of the A/D converter, the digital word can change slightly from pulse to pulse in a noiselike manner. Thus the quantization of the analog signal results in noise or uncertainty, called *quantization noise*, which can limit the MTI improvement factor.

نويز كوانتيزاسيون ضريب بهبود MTI را محدود مي كند.

Shrader and Gregers-Hansen[36] give the limitation to the improvement factor due to quantization noise as

$$I_q = 20 \log [(2^N - 1)\sqrt{0.75}] \quad \text{(dB)} \tag{3.35}$$

اين فرمول محدوديت ضريب بهبود به خاطر نويز كوانتيزاسيون را نشان مي دهد. كه تقريبا برابر با dB/bit ب 6 است.

where N = number of bits. This is approximately 6 dB per bit. (Each bit represents a factor of two in amplitude resolution.) Thus a 10-bit A/D theoretically limits the improvement factor to about 60 dB. In practice, the A/D converter generally requires one or more additional bits to achieve the desired performance.

The limitation on the improvement factor based on Eq. (3.35) assumed that the quantization error was independent from pulse to pulse. This happens when the rms noise is greater than a quantization step. It was suggested by Glen Preston that there will be a quieting effect that reduces the quantization noise if the pulse-to-pulse clutter samples are correlated rather than independent. Brennan and Reed[37] derived an expression for the

quieting that is a function of the correlation, and they found quieting to be small. When it occurs, the quantization step is large compared to the rms noise, a condition that is not preferred for best performance in a practical radar system.

6/4/88

Dynamic Range The dynamic range is the maximum signal-to-noise ratio that can be handled by an A/D converter without saturation. The noise level relative to the quantization step affects the dynamic range. The available dynamic range (power ratio) is given as[35]

این مقدار برابر است با:
D.R=6.02*N+1.76
برابر توان $N_q=Q^2/12$
نویز کوانتیزاسیون است.

$$\text{dynamic range} = 2^{2N-3}/k^2 \qquad [3.36]$$

where N = number of bits in the A/D converter (the sign bit is included), and k = rms noise level divided by the quantization level. The larger k is, the less the dynamic range. A value of k less than one means that the receiver noise at the input to the A/D converter is less than the quantization noise, which results in a loss of detectability. Generally k equals 1 or 2. With $k = 2$ (a value recommended by Shrader and Gregers-Hansen), the dynamic range for a 10 bit A/D according to Eq. (3.36) is 45.2 dB, which is considerably less than the 60 dB improvement factor based on a value of 6 dB per bit. If the limitation on the improvement factor is taken as 2^{2N} (6 dB per bit), the dynamic range given by Eq. (3.36) when $k = 2$ is seen to be about 15 dB less than the improvement factor. Thus the limitation on the improvement factor might be determined by the dynamic range of Eq. (3.36) rather than by the quantization noise limitation usually given as 6 dB per bit. (This could be the reason why, in practice, one or more bits are added to the A/D converter when the improvement factor limitation is taken as 6 dB per bit.)

Other Limitations The above has, for the most part, assumed ideal A/D converters and ideal I and Q detection. There are several practical conditions that need to be considered when good MTI performance is required. Errors and reduced performance can be due to:[35,38] (1) other than a 90° phase difference between the I and Q reference signals,[39] (2) gain and phase imbalance in the two channels, (3) timing jitter in the sample-and-hold circuits, (4) nonlinearity in the A/D,[40] and (5) range straddling loss due to the sampling not being at the peak of the output of the matched filter.

مدار sample and hold
ممکن است
jitterزماني داشته باشد.

The degradation in performance caused by the inability to precisely match the I and Q channels in phase, amplitude, and frequency spectrum can be significantly reduced by employing a single channel whose signal is down converted (from IF or RF, by mixing) to obtain the in-phase and quadrature channels. There have been several methods proposed in the past to perform this form of *bandpass sampling*, also sometimes called *digital down conversion*. A technique described by Rader[41] for a band-limited signal of bandwidth B down-converts (mixes) the IF or RF signal to a center frequency of B. The signal is sampled at a rate of $4B$. Two filters are realized as a pair of 90° phase splitting networks with several symmetries which are used to reduce the computations. The in-phase and quadrature samples are obtained at an output rate of B. It has been said[42] that the oversampling by a factor of 2 from the Nyquist rate ($2B$) results in a simple and efficient implementation of the filters. Only one mixer and one A/D converter are needed, but the sampling is four times faster.

In another method for baseband sampling,[43] IF samples taken near the Nyquist rate are interpolated, based on a number of stored samples, to provide the in-phase and

7/4/88

quadrature channels. Experimentally it was found that the phase errors could be reduced by an order of magnitude compared with conventional baseband I,Q processing.

Fast Fourier Transform (FFT) Digital filtering involves the use of the Fourier transform. The fast Fourier transform requires less computational effort, and it has been popular for many applications. It has some limitations, however, compared to the classic Fourier transform. The number of samples used has to be expressed as 2^N. If a filter bank is being generated, all filters have identical responses, they will be uniformly spaced in frequency, and the weighting coefficients are not optimum since they cannot be chosen independently for each filter. The filters possible with a non-FFT filter bank also can achieve greater attenuation of moving clutter (such as rain or chaff) because of the greater flexibility available in their design. There are times, therefore, when the classical Fourier transform may be more advantageous than the FFT even though the FFT might be quicker and require less complexity.[44]

Loss Due to Blind Phases in Using a Single Channel[45] *With only a single channel, the effect of a blind phase can be anything from complete loss of the signal to no loss at all, as was indicated by the special cases mentioned earlier in this section in the discussion of the I,Q processor. With a nonfluctuating target and only a single channel there is a loss of 2.8 dB and 13.7 dB for a probability of detection of 0.5 and 0.9, respectively, and a probability of false alarm of 10^{-6}.*[34] When the target fluctuates pulse to pulse with a Rayleigh probability density function (Swerling Case 2) and with postdetection integration of from 2 to 8 pulses, the loss in using only a single channel is about 2.4 dB when $0.5 < P_d < 0.9$ and $10^{-6} < P_{fa} < 10^{-10}$. For a very large number of pulses integrated (greater than 1000), the loss approaches 1.5 dB. When the target fluctuations are described by Swerling Case 1, there is a loss of 3.2 dB in using a single channel with postdetection integration of only two pulses.[46] The loss is about 2 dB when more than 20 pulses are integrated.

It might be concluded that these losses are moderate, so that a single channel might be acceptable when it is important to reduce hardware complexity. This was the conclusion reached in the early days of MTI radar (the 1950s and 1960s) when the delay lines were analog. Hardware complexity, however, is seldom a consideration with digital MTI processing, so that both the I and Q channels are always employed. A block diagram of a digital processor, therefore, almost always shows I and Q processing.

3.6 MOVING TARGET DETECTOR

The Moving Target Detector (MTD) is an example of an MTI processing system that takes advantage of the various capabilities offered by digital techniques to produce improved detection of moving targets in clutter. It was originally developed by the MIT Lincoln Laboratory for the airport-surveillance radar (ASR), a 60-nmi radar found at major airports for control of local air traffic. The introduction of the MTD represented an innovative and significant advance in radar detection of aircraft in the presence of clutter.

9/4/88

Original MTD[47–49] The original MTD concept was designed for a radar similar to the FAA's ASR-8, which operated at *S* band (2.7–2.9 GHz) with a pulse width of 0.6 μs, 1.35° azimuth beamwidth, antenna rotation rate of 12.8 rpm, average prf of 1040 Hz, and an average power of 875 W. The ASR-8 employed four staggered prfs; but staggering of the prfs was not used with the MTD. The original MTD included the following:

- An *eight-pulse FFT digital filter bank* with eight filters, preceded by a three-pulse delay-line canceler. The three-pulse canceler reduced the dynamic range of the signals which the doppler filter bank had to handle, and it compensated for the lack of adequate cancellation of stationary clutter in the doppler filters. The doppler filter bank separated moving targets from moving weather clutter if they appeared in different doppler filters.
- *Frequency-domain weighting* to reduce the doppler-filter sidelobes for better clutter attenuation.
- *Alternate prfs* to eliminate blind speeds and to unmask aircraft echoes from weather clutter.
- *Adaptive thresholds* to take advantage of the nonuniform nature of clutter.
- *Clutter map* to detect crossing targets with zero radial velocity that would otherwise be canceled by an ordinary MTI.
- *Centroiding* of multiple reports from the same target for more accurate location measurements.

The range coverage of this processor totaled 47.5 nmi.

The MTI processor was preceded by a large dynamic range receiver to avoid the reduction in improvement factor caused by limiting (Sec. 3.7). The output of the receiver IF amplifier was fed to *I* and *Q* phase detectors. From there the A/D converters changed the analog signals to 10-bit digital words. Figure 3.30 is a block diagram of the MTD, but further explanation is probably required before the block diagram becomes clear.

Coherent Processing Interval (CPI) The range was quantized into $\frac{1}{16}$-nmi intervals, which were approximately equal to the range resolution of the pulse. The azimuth angle

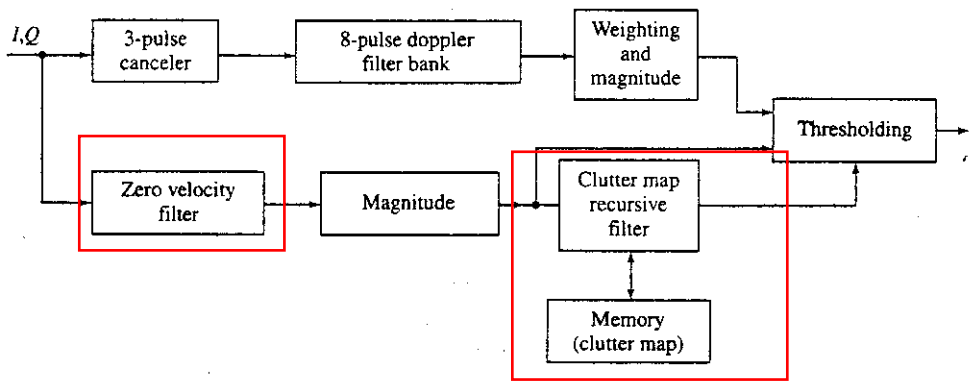

Figure 3.30 Block diagram of the original Moving Target Detector (MTD) signal processor.

آيا منظور از بانك فيلتر داپلر همان فيلترهاي FFT است؟

MTI-3pulse → FFT

FFT مي تواند هدف متحرك را از كلاتر آب و هواي در حال حركت جدا كند.

20/4/88

ظاهرا منظور تقسيم بندي برد براي پردازش هم دوس است. اما با توجه به توضيح صفحه بعد منظور از CPI تعداد پالس هاي هم دوس برگشتي در يك سلول زاويه اي سمت است.

was quantized into $\frac{3}{4}$-degree intervals, which were about one-half-beamwidth. Thus there were a total of 365,000 range-azimuth resolution cells within the 47.5-nmi range coverage. In each $\frac{3}{4}$-degree azimuth cell there were 10 pulses transmitted at a constant prf. On receive, these ten pulses were called a *coherent processing interval* (*CPI*). The ten pulses of the CPI were processed by an eight-pulse filter bank that was preceded by a three-pulse delay-line canceler. The filter bank produced eight contiguous filters. There were then 2,920,000 range-azimuth-doppler resolution cells. Each of these cells had its own adaptive threshold (described later) which was controlled by the amount of clutter echo seen in the vicinity of the target. In the next $\frac{3}{4}$-degree azimuth cell, the prf of the 10-pulse CPI was changed to eliminate blind speeds and to unmask moving targets hidden by moving weather clutter (as will be described later). Changing the prf every 10 pulses (every half-beamwidth) eliminated second-time-around clutter echoes that would normally degrade a conventional MTI using pulse-to-pulse stagger of the prf.

Filter Bank The filter bank was implemented by a FFT. Although there were 10 pulses in the CPI, there are only eight doppler filters. Since the three-pulse canceler requires all three pulses before it can cancel clutter, the first two output pulses were discarded. The discarded pulses are called *fill pulses* since they are needed to "fill" the canceler before cancellation of the clutter can begin.

The frequency response of each filter of the FFT filter bank had a $(\sin x)/x$ shape with the first sidelobes 13.2 dB down from the peak. These sidelobes were high and generally did not have sufficient rejection of nearby targets or clutter. The sidelobes were reduced in this MTD by subtracting from the output of each filter $\frac{1}{4}$ the sum of the two adjacent filters.[50] [If A, B, and C represent the unweighted outputs of three contiguous filters, the weighted output applied to filter B is $B - (A/4 + C/4)$.]

Ideally the three-pulse canceler is not needed if the filter bank can be designed to obtain the necessary clutter attenuation for both stationary and moving clutter. It was not possible, however, to eliminate the three-pulse canceler in the original MTD. In the block diagram of Fig. 3.30, the *magnitude* is the operation $(I^2 + Q^2)^{1/2}$, or an approximation thereto.

Clutter Map A conventional MTI processor eliminates stationary clutter, but it also eliminates aircraft moving on a crossing trajectory (one perpendicular to the radar line of sight) which causes the aircraft's radial velocity to be zero. This is unfortunate since the radar cross section of an aircraft is relatively large when viewed at the broadside aspect presented by a crossing trajectory. The MTD took advantage of this large cross section to detect targets that normally would be lost to a simple MTI radar. It did this with the aid of a clutter map that stored the magnitude of the clutter echoes in a digital memory. The clutter map established the thresholds used for detecting those aircraft targets which produced zero radial velocity.

Since the three-pulse canceler removed all echoes with zero velocity, the zero-velocity filter had to be re-established in order to produce the clutter map, as indicated in Fig. 3.30. Each of the 365,000 range-azimuth resolution cells of the clutter map stored the average value of the output of the zero-velocity filter received during the last eight scans (32 s). On each scan, one-eighth of the output of the zero-velocity filter was added

FFT مورد استفاده در این رادار با وزن دهي خاص مي باشد و با FFT معمولي متفاوت است!

زمانيكه هدف به صورت عمود بر خط ديد رادار حركت مي كند، RCS آن نسبتا بزرگ است. اين اهداف در رادار MTI ساده گم مي شوند.

از روش MTD با استفاده از clutter map بيشتر در فرودگاهها استفاده مي شود.

to seven-eighths of the value stored in the map. The map, therefore, was built up in a recursive manner. About 10 to 20 scans were required to establish steady-state values. This number of scans was necessary so that aircraft echoes would not affect the threshold. (They didn't stay in one cell too long.) As rain moved into the area or as propagation conditions changed, the clutter map changed accordingly. The values in the clutter map were multiplied by an appropriate constant to establish the threshold which allowed the detection of moving targets with zero radial velocity. The MTD proved highly successful in using this technique to detect crossing targets that would have been rejected by a simpler MTI processor.

Adaptive Thresholds As mentioned, each of the 2,920,000 range-azimuth-doppler resolution cells had an adaptive threshold to allow detection of moving targets in either stationary or moving clutter. Consider the eight doppler filters diagrammed at the top of Fig. 3.31 (indicated as prf-1). (For the moment concentrate only on this one prf and its set of filters and ignore the rest of the figure which will be discussed in the next subsection.) There are three different criteria for selecting the thresholds, depending on the location of the filter with respect to zero velocity.

The adaptive threshold setting for filter no. 1 (which was the filter centered at zero radial velocity) was determined by what was stored in the clutter map. The adaptive thresholds for filters nos. 3 through 7 were set by a clutter CFAR similar to what is described in Sec. 5.7 and shown in Fig. 5.7. Briefly, the clutter CFAR in the MTD established a threshold based on the mean level of the signals received in the 16 range cells centered around the range cell of interest. The 16 range cells correspond to a distance one-half mile behind and one-half mile ahead of the range cell of interest. The mean value of the signals in these 16 cells, when multiplied by an appropriate constant, established a threshold at each of the nonzero-velocity filters 3 through 7. Thus the threshold continually adapted to the local environment as the radar pulse traveled in time through space. For the remaining two filters, 2 and 8, which lie adjacent to the zero-velocity filter, the threshold was selected as the larger of that given by the clutter map and the clutter CFAR. Large echoes from moving clutter, which might be confused as real target echoes by a conventional MTI with a single filter covering the doppler space, are not detected in the MTD.

Unmasking Moving Targets in Moving Clutter An advantage of a filter bank is that it allows moving targets to be separated from moving clutter (such as rain) so that detection can take place. Since the doppler-shifted radar echo from a moving target usually (but not always) has a radial velocity greater than the maximum unambiguous velocity (or first blind speed), its doppler frequency can fold over into one of the eight filters of the filter bank. This is shown happening with prf-2 of Fig. 3.31. The true target velocity is represented by the solid vertical arrow lying to the right of the maximum unambiguous velocity. In this case it folds over into filter no. 8, as indicated by the dashed arrow. The rain echo is also in filter no. 8; hence, it masks the echo of the aircraft on the CPI with prf-2. On prf-1, however, the aircraft echo folds into a different filter, in this case filter no. 7. The rain echo remains in filter no. 8 since its radial velocity is less than the maximum unambiguous velocity. In this manner the change in prf and the use of a doppler filter bank allow moving aircraft echoes to appear in at least one CPI that is free from

با تغییر RF مي توان محل داپلر هدف را
با توجه به پديده fold over جابجا كرد.

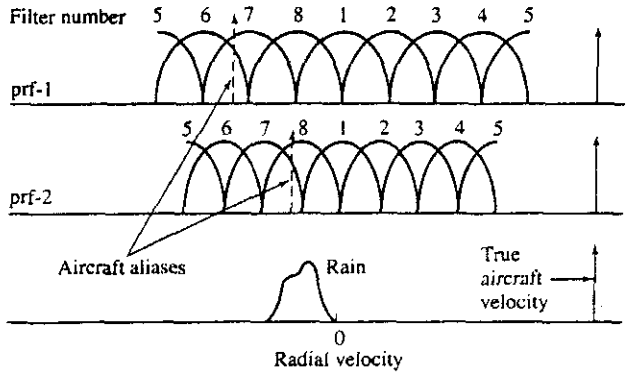

Figure 3.31 Detection of an aircraft in rain by use of two prfs and a doppler filter bank, illustrating the unmasking of the aircraft's echo on prf-1 due to doppler foldover when it is masked by rain on prf-2.
(From Muehe,[52] Copyright 1974 IEEE.)

rain echoes. A change in prf of about 20 percent was used in the MTD to allow this unmasking of the aircraft echo. (The echo at *S* band from precipitation might typically have a spectral width of about 25 to 30 kt; and might be centered anywhere from -60 to $+60$ kt, depending on the wind conditions and the antenna pointing direction.[51])

Interference and Saturation Pulses from a nearby radar might be received by the radar and appear as a large signal among the 10 pulses normally processed as a CPI. In the MTD an *interference eliminator* compares the magnitude of each of the 10 pulses against the average of the 10. If any pulse is greater than five times the average, all information from that range-azimuth cell is discarded. A *saturation detector* detects whether any of the 10 pulses within a processing interval saturates the A/D converter and, if it does, the entire 10 pulses of that particular CPI are discarded.

Post-processor Centroiding The output of the MTD processor was a *hit report* which contained the azimuth, range, and amplitude of the target echo as well as the filter number and prf. On a particular scan, a large aircraft echo might be reported from more than one doppler filter, from several coherent processing intervals, and from adjacent range cells. As many as 20 hit reports might be generated by a single large target.[52] A *post-processor* grouped together all reports that appear to originate from the same target and interpolated to estimate the target's azimuth, range, amplitude, and radial velocity. The target amplitude and doppler were used as the basis to eliminate small cross-section and low-speed echoes (such as birds and insects) before the target reports were delivered to the automatic tracking computer. The automatic tracker also eliminated false reports that did not form logical tracks. The output of the automatic tracker is what is displayed to the operator. Since the MTD processor eliminated a large amount of the clutter and had a low false-detection rate, its output could be reliably transmitted to a different location, if desired, by narrow-bandwidth telephone lines.

Performance The improvement factor of the original MTD measured on an airport-surveillance radar (ASR) was about 45 dB, which was said to be a 20-dB increase over the ASR's conventional three-pulse MTI processor with a limiting IF amplifier. In addition, the MTD achieved a narrower clutter rejection notch at zero velocity and at the blind speeds. The MTD has proven to be an important model for the design of radars for detecting moving targets in stationary as well as moving clutter.

Second Generation MTD[53] The original MTD, as does any electronic development, used the technology that was available when it was first developed. Advances in digital hardware occurred rapidly, however, and an improved version soon appeared. The original hard-wired processor was replaced by a parallel microprogrammed processor (PMP) which operated out to the full instrumented 60 nmi range of the radar. The characteristics of the second generation MTD are summarized as follows:

بانك فيلتر به جاي اينكه با يك FFT پياده سازي شود با يك transversal filter پياده سازي شد تا انعطاف پذيري بيشتري را در طراحي ايجاد كند و سايدلوب هاي فيلترهاي داپلر را كاهش دهد.

- The filter bank was implemented as a *generalized transversal (FIR) filter* rather than as an FFT so as to provide more flexibility in design and reduce the doppler-filter sidelobes.
- A *two-pulse delay-line canceler* (rather than the three-pulse canceler of the original) preceded the filter bank.
- The *zero radial-velocity filter* was also designed as a transversal filter. It utilized the Chebyshev criterion to produce relatively uniform filter gain across the portion of the doppler space not covered by the nonzero-doppler filters.
- The *clutter map* had one cell for each range-azimuth cell rather than one cell for each range-CPI.
- The *nonzero-doppler filters* were based on the method of DeLong and Hoffstetter (mentioned in ref. 53). They provided sidelobe levels 10 dB lower than the original MTD, and thus gave better performance in rain. When the two-pulse delay line preceded the filter bank, the number of bits required in the transversal filter decreased, so that the filter weights only had to be 3 or 4 bits plus sign.
- The *CPI* consisted of eight pulses. One CPI had a 900-μs period, and the other had a period of 1100 μs. The prfs were 1111 Hz and 909 Hz.
- *Correlation and interpolation algorithms* clustered the threshold crossings in range, azimuth, and doppler to provide in a single report the best values of the radar observables of a single target, whether it be aircraft, automobile, or bird. Target signal strength was one of the observables as well as range, angle, and doppler. The doppler interpolation was one part in 64 across the band of eight doppler cells.

بعد از گذر سيگنال از MTD بايد از CFAR بگذرد.

- An *area CFAR* was used after the MTD thresholding to eliminate single CPI false alarms due to birds, interference, and weather clutter that were not removed by the signal processing algorithms.
- The *scan-to-scan correlator* was an automatic tracker that deleted those targets whose scan-to-scan behavior was not what would be expected of an aircraft. This removed low-speed targets as well as echoes that lacked spatial correlation from scan to scan. The scan-to-scan correlator determined when a track was of a quality sufficient to allow the data associated with it to be displayed.

Experimental demonstration of the second-generation MTD installed on an ASR-7 at MIT Lincoln Laboratory showed that the PMP processor produced approximately 500 to 600 range-azimuth-doppler threshold crossings per scan out of a total of about 3,000,000 cells within the radar coverage. There were typically 5 to 15 threshold crossings per aircraft target.

The FFT of the original MTD constrained the type of filter characteristic that could be obtained. Performance was sacrificed for reduced cost. By employing FIR filters in the second generation MTD, the frequency response of each filter of the filter bank could be shaped as desired. Less power was wasted by using the eight-pulse FIR filters since only one fill pulse was required rather than the two fill pulses of the 10-pulse FFT. The reduced number of pulses allowed better performance with a shorter observation time.

Both the first and second generation MTDs were developed by the MIT Lincoln Laboratory. The MTD concept further evolved into a third configuration used in the ASR-9 airport-surveillance radar developed for the FAA by Westinghouse (later known as Northrop-Grumman) at Baltimore, MD.

Third Generation MTD for the ASR-9[54,55] The first operational air-traffic control implementation of the MTD concept was for the ASR-9, a radar employed at the major airports of the United States and elsewhere in the world. It utilized the basic philosophy of the second generation Lincoln Laboratory MTD and significant extensions by Westinghouse.

The pulse periods of the two CPIs in the ASR-9 were not equal, but were in the ratio of 9/7. The longer-pulse-period CPI processed 8 pulses and the shorter-period CPI processed 10 pulses, for a total of 18 pulses. The different number of pulses allowed the doppler space covered by the two CPIs to be more equal than the unequal coverage of the two CPIs of the original MTD (whose filters were sketched in Fig. 3.31). There were approximately 21 pulses received over the radar's half-power beamwidth, but only 18 of these were used for establishing the clutter map that helped to control the false-alarm rate. Twelve-bit filter weights were used rather than the five-bit weights of the Lincoln MTD. This enabled the filter to be designed to achieve 40-dB doppler sidelobes for rain rejection and 44-dB ground-clutter rejection (relative to noise) for the heavy clutter filters. In mountain clutter, an alternate filter design was used that provided 52 dB of attenuation at the expense of less rain-clutter rejection. Sensitivity time control (STC) was employed to reduce the large clutter echoes that exceeded the available dynamic range of the system.

The range and azimuth resolutions of this radar were improved compared to the original MTD. In a simple CFAR, the threshold increases when there are two nearby targets, thus reducing the probability of resolving them in range. The ASR-9 CFAR algorithm, however, omitted the strongest cluster of samples from the estimate of interference (that determined the threshold) so that a neighboring target of comparable echo strength didn't cause the threshold to be raised. Without this cluster editing, the two targets would not be resolved and only the larger target would be detected.

When detections were obtained that extended for more than two beamwidths in azimuth, the shape of the response in azimuth was compared to what would be expected from a single target. A significant deviation from the expected response indicated that the extended azimuth signature was caused by two targets, thus increasing the probability of resolution.

22/4/88

دقت رادار MTD اوليه خوب نبود

Accuracy with the MTD[56] The accuracy of the original MTD was not as good as might be obtained with a conventional scanning radar. The angle in the original MTD was determined on the basis of the two CPIs rather than as is usually done in a scanning radar that uses all the pulses received from a target to estimate its center by beam splitting.

در رادار جستجوي MTD الگوريتم هايي توسعه يافت تا اهداف غيرهمسايز با يكديگر را با فاصله زاويه اي كمتر از 2 پهناي بيم (كه باراي رادار FM-80 معادل با 1 درجه است) و با فاصله در برد كمتر از 2 سلول برد از يكديگر جدا كنند.

In the Westinghouse, or third generation, version a typical aircraft might give rise to 35 individual threshold crossings (which were called *primitive reports*) in range, azimuth, doppler, and amplitude. A large aircraft might produce 100 such reports. These have to be centroided to produce a single report of range, azimuth, doppler, and amplitude. The radar must also provide an accurate measurement of angle and be able to resolve two nearby targets. Algorithms were developed to resolve unequal-size targets separated in azimuth by less than two beamwidths and separated in range by less than two range cells, which was $\frac{1}{8}$ nmi.* Since a large target might affect up to five range cells, range resolution in the MTD had to be obtained by using a simplified form of pulse-shape matching. For azimuth resolution and estimate of angle, one of four algorithms was used, depending on the extent of the data in angle. The most elaborate of the four employed beamshape matching when target primitive reports were obtained on three or more CPIs with the same prf. The typical number of primitive reports with this algorithm was greater than 30. The rms angle accuracy was said to be about 0.04 beamwidth.

چرا داده در زاويه توسعه پيدا مي كند؟

When the received signal was so strong that it saturated the A/D converter, the accuracy of centroiding and the ability to resolve two targets were degraded. In the first two versions of the MTD, any CPI that experienced saturation by a large target or interference signal was eliminated. It was found, however, that eliminating the CPI caused splitting of the target due to premature termination of a report. The Westinghouse MTD avoided this problem by providing information about its *presence* (rather than nothing) when the data saturated.

Hit, or Primitive, Reports In the above discussion of the various evolutions of the MTD, there were various values given for the number of hit reports, or primitive reports, generated by a single aircraft target. According to the references cited in this section, these varied from 15 to 100. Apparently the number depends on the type of MTD, the radar with which it was used, and the nature of the trials that were conducted.

Extension to Other Radars The three generations of MTD systems described above were well suited for use in an *S*-band medium-range airport-surveillance radar. The MTD has also been adapted for use with a solid-state transmitter, as in the ASR-12 air-traffic control radar.[57] Although the individual techniques that constitute the MTD have applicability to other types of air-surveillance radars, it is more difficult to apply in its entirely the MTD systems as described above to long-range radars or those at other frequencies. Some features of the MTD concept described here might not be suitable for military air-surveillance radar applications since they might make the radar more vulnerable to countermeasures.

استفاده از روش MTD براي رادارهاي با برد بلند يا رادارها در فركانس هاي ديگر، سخت تر است.

*It is generally accepted that a good radar can resolve two targets of equal size if the targets are separated in angle by at least 0.8 beamwidth. Similarly, two targets can be separated in range, in the absence of CFAR, if they are at least 0.8 pulse width apart.

استفاده از بعضي ويژگي هاي رادار MTD براي كاربردهاي نظامي مناسب نيست چون آنها را نسبت به مباحث جنگ الكترونيك آسيب پذيرتر هستند.

27/4/88

3.7 LIMITATIONS TO MTI PERFORMANCE

محدوديت هاي اعمالي به عملكرد MTI باعث مي شود طيف كلاتر پهن شود.

In this section we consider the degradation in performance of MTI radars caused by (1) antenna scanning modulation, (2) internal fluctuations of clutter, (3) equipment instabilities, and (4) limiting. The adverse effects of the A/D converter and other aspects of digital processing on MTI performance were considered in Sec. 3.5.

The limitations to MTI performance to be discussed cause the clutter spectrum to widen. More clutter energy is then passed by the doppler filter, which lowers the improvement factor. If the clutter power spectral density can be expressed as a gaussian function with a standard deviation σ_c in Hz, it can be represented as

$$W(f) = W_0 \exp\left(-\frac{f^2}{2\sigma_c^2}\right) \qquad [3.37]$$

where W_0 is the peak value of the clutter power spectral density at $f = 0$. This equation was given previously as Eq. (3.14). The clutter standard deviation is sometimes written in terms of the radial velocity, in units of meters/second, and denoted σ_v. The two may be related by $\sigma_c = 2\,\sigma_v/\lambda$, where λ = wavelength in meters. (The standard deviation expressed in velocity, σ_v, is sometimes, but not always, independent of frequency for wind-blown clutter.) If the MTI filter has a frequency response $H(f)$, the clutter attenuation is [a repeat of Eq. (3.15)]

$$\text{CA} = \frac{\int_0^\infty W(f)\,df}{\int_0^\infty W(f)\,|\mathrm{H}(f)|^2\,df} \qquad [3.38]$$

The improvement factor, Eq. (3.20), is found by multiplying the clutter attenuation by the average gain of the filter.

The improvement factors for a single delay-line canceler and a double delay-line canceler were derived in Sec. 3.2 when the clutter spectrum is represented by a gaussian spectrum. The general expression for the improvement factor with n delay-line cancelers in cascade was given by Eq. (3.23) as

$$I_f \approx \frac{2^n}{n!}\left(\frac{f_p}{2\pi\sigma_c}\right)^{2n} \qquad [3.39]$$

where f_p is the pulse repetition frequency, or prf. We shall use this expression to determine the improvement factor when the clutter spectrum is gaussian.

If there are N different effects that contribute to the widening of the clutter spectrum, and if each is gaussian and independent of one another, the overall standard deviation is

$$\sigma_c = (\sigma_1^2 + \sigma_2^2 + \sigma_3^2 + \cdots + \sigma_N^2)^{1/2} \qquad (3.40)$$

where the subscripts indicate the various effects, such as oscillator stability, quantization of the A/D converter, antenna scanning modulation, and so forth. The overall

improvement factor is given by the following expression when multiple effects contribute to the total (whether or not their clutter spectra are gaussian)

$$\frac{1}{I_f} = \frac{1}{I_1} + \frac{1}{I_2} + \frac{1}{I_3} + \cdots + \frac{1}{I_N} \qquad [3.41]$$

where I_i represents the limit on the improvement factors due to each effect.

Antenna Scanning Modulation The duration of the echo signal received from a target or a clutter scatterer as the antenna of a pulse radar scans past is given by $t_0 = n_B/f_p = \theta_B/\dot{\theta}_s$, where n_B = number of pulses received, f_p = pulse repetition frequency, θ_B = antenna beamwidth, degrees, and $\dot{\theta}_s$ = antenna scanning rate in degrees per second. The frequency spectrum has a bandwidth inversely proportional to the time duration t_0. Consequently, even if the clutter scatterers were perfectly stationary and there were no instabilities in the radar equipment, there would still be a finite spectral spread due to the finite duration of the echo signal. This limitation has been called *antenna scanning modulation,* but it is basically due to the finite time on target. The longer the time on target, the less will be the spread in the clutter spectrum.

The pulse-to-pulse difference in echo amplitude due to the antenna pattern shape also contributes to the clutter residue that is part of the antenna scanning modulation. In many MTI radars, the finite duration of the signal is what sets the limit on the clutter attenuation that can be obtained. It is also the reason why a long signal duration is needed for good clutter rejection. Short duration signals, therefore, usually are not consistent with good MTI performance.

The two-way voltage waveform of the received echo signal from clutter will be modified in amplitude by the square of the one-way antenna electric-field-strength pattern. The two-way voltage is equal to the one-way antenna power pattern, which can often be approximated by a gaussian function such as

رابطه پترن آنتن تك راه

$$G(\theta) = G_0 \exp\left(-\frac{2.776\theta^2}{\theta_B^2}\right) \qquad [3.42]$$

where G_0 = maximum antenna gain, θ = angle coordinate, and θ_B = beamwidth. The scanning antenna beam modulates the amplitude of the received pulse-train. If the antenna scans at a rate of $\dot{\theta}_s$ deg/s, the modulation with time of the echo pulse-train is found by dividing both the numerator and denominator of the exponent of Eq. (3.42) by $\dot{\theta}_s$. Then we let $\theta/\dot{\theta}_s = t$, which is the time variable, and we let $\theta_B/\dot{\theta}_s = t_0$, the time duration of the signal (or time on target). The modulation of the received echo signal from an individual clutter scatterer due to the antenna pattern is then

$$s_a(t) = k \exp\left(-\frac{2.776t^2}{t_0^2}\right) \qquad [3.43]$$

where k = constant. The power spectrum of $s_a(t)$ is given by the square of the Fourier transform of the above equation, which is

$$|S(f)|^2 = K \exp\left(-\frac{\pi^2 f^2 t_0^2}{1.388}\right) \qquad [3.44]$$

where K = constant. Since this is a gaussian function with exponent of the form $f^2/2\sigma_a^2$ the standard deviation σ_a of the clutter spectrum caused by antenna scanning modulation is

$$\sigma_a = \frac{1}{3.77 t_0} = \frac{0.265 f_p}{n_B} \qquad [3.45]$$

When this is substituted into Eq. (3.39), the limitation on the improvement factor due to antenna scanning, assuming n delay-line cancelers in cascade, is

تغییر ضریب بهبود به خاطر اثر مدولاسیون آنتن

$$I_f = \frac{2^n}{n!}(0.6 n_B)^{2n} \qquad [3.46]$$

where $n_B = f_p t_0$ is the total number of pulses received from a scatterer during the time the antenna scans past it. For a single delay-line canceler, $I_f = 0.72\, n_B^2$, and for a double delay-line canceler, $I_f = 0.26\, n_B^4$. A plot of the limitation to the improvement factor due to antenna scanning modulation is shown in Fig. 3.32.

A broadening of the clutter spectrum can be obtained even with a nonscanning antenna beam, such as happens with a phased array radar whose antenna beam dwells in one direction for a finite number of pulses before it jumps to another direction to again dwell for a fixed number of pulses. (This is called *step scan.*) The batch of N_T pulses obtained in this manner will have a frequency spectrum with a bandwidth of approximately the inverse of the time on target or $(N_T T_p)^{-1}$. If processed by a conventional filter, there will be incomplete attenuation of the clutter and there will be a limitation on the improvement factor. This limitation does not occur with digital processing if sufficient fill pulses are used to initialize the filter before canceled outputs are obtained.[58] For

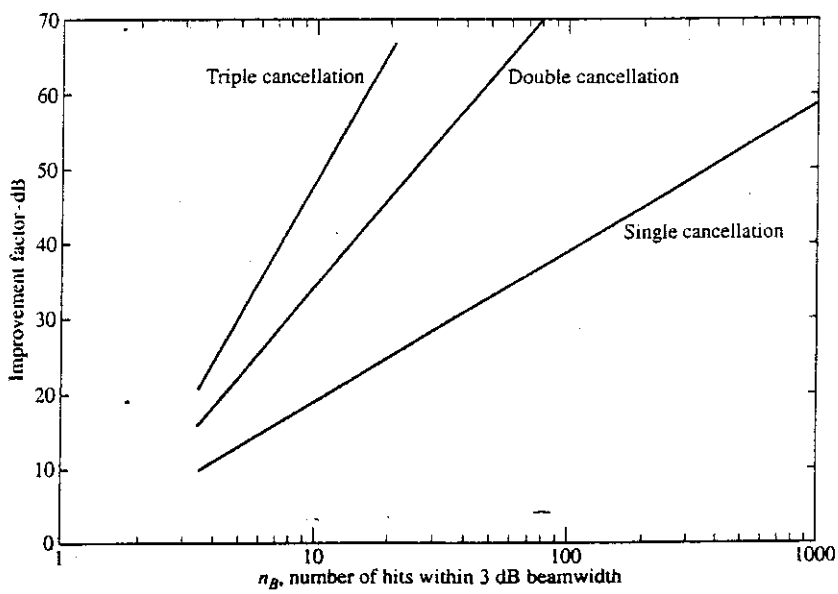

Figure 3.32 Limitation to the improvement factor due to antenna scanning or a finite time on target, as a function of the number of pulses received over the half-power beamwidth. The antenna pattern is assumed to have a gaussian shape.

example, with a three-pulse binomial canceler (as was used in the original MTD), there are two fill pulses and a useful output doesn't occur until the third pulse is processed. The energy associated with these two fill pulses is not utilized for detection in noise.

3/5/88

Internal Modulation of Clutter Previously in this section, we have assumed that clutter was perfectly stationary. Echoes from mountains, rocks, buildings, water towers, fences, thick tree trunks, and bare hills usually can be considered stationary. Many other sources of clutter echoes, however, can be in motion. These include echoes from the sea, rain, and chaff, as well as trees, large vegetation, and structures blowing in the wind. The amplitude and phase fluctuations of windblown trees and vegetation can result in a widened frequency spectrum of the clutter echo that can be a limitation on the achievable MTI improvement factor, which is this subject of this section.

اولین مدل طیف کلاتر، تابع گوسی در نظر گرفته شد.

The first model of clutter spectrum suggested in World War II was based on the *gaussian* function.[59] A gaussian spectrum was, and still is, popular since it fit the early experimental clutter measurements and it is relatively easier to manipulate mathematically. Later, when more sensitive radars were employed, it was found that experimentally measured clutter spectra did not decrease with increasing frequency as rapidly as predicted by the gaussian function. Overly optimistic predictions of radar performance were therefore obtained. This began to occur for clutter spectral values in the vicinity of 15 to 20 dB below the peak of the clutter spectrum at zero doppler frequency. A *power-law* spectrum, which did not fall off as fast as the gaussian, was then proposed to account for the available measured spectral data. It improved on the gaussian, but when even more sensitive modern radars became available with capability to measure clutter spectra 60 to 80 dB below the peak at zero doppler, it was found that the power-law spectrum did not adequately describe the measurements much beyond 35 to 40 dB below the peak. Experimental windblown clutter measurements were found to decrease faster with frequency than predicted by the power law. Thus the power law resulted in overly pessimistic predictions of radar performance and could be excessively demanding when designing high-performance MTI radars. It was then found that the *exponential* model could adequately represent measured clutter spectra over a wide dynamic range down to 80 dB below the peak. Although no single model fits all data over a wide dynamic range, the exponential seems to be the best of those proposed to account for experimental measurements of windblown clutter over a wide variety of conditions and a large dynamic range of values. These three clutter spectral models are described in turn.

Gaussian Spectrum The gaussian model was widely used in the past to describe the frequency spectrum of clutter, especially windblown land clutter. It is a convenient representation and easy to work with. It fits reasonably well to measured clutter data so long as the required MTI improvement factor is not large. The gaussian spectrum of Eq. (3.37) is described by its variance or standard deviation. It is generally assumed that the standard deviation of windblown clutter echo fluctuations when measured in meters/second is independent of frequency. Here the standard deviation in meters/second is denoted σ_v, and the standard deviation in hertz is denoted σ_f. Substituting the standard deviation in Eq. (3.39) gives the limitation on the MTI improvement factor due to windblown clutter for n delay-line cancelers in cascade.

The often-quoted "representative values" of the gaussian model standard deviation of clutter spectra, based on experimental measurements as first reported by Barlow[60] at a frequency of 1 GHz, were:

- Heavily wooded hills, 20-mph wind: 1.5 Hz (0.22 m/s)
- Sparsely wooded hills, calm day: 0.11 Hz (0.02 m/s)
- Sea echo, windy day: 6.0 Hz (0.9 m/s)
- Rain clouds: 13.4 Hz (2.0 m/s)
- Chaff: 7.1 Hz (1.1 m/s)

The nature of the clutter examined by Barlow was not precisely defined. Barton[61] gives the following range of values of σ_v for clutter spectra:

- Wooded hills: 0.01–0.32 m/s
- Sea echo: $v_w/8$, where v_w is the wind speed in meters/second
- Rain and chaff: 1 to 2 m/s

Based on a composite of many sources of data, Nathanson[62] provides for wooded terrain a plot of the standard deviation of a gaussian clutter spectrum as a function of wind speed. The mean and 90th percentile values of the standard deviation, both in meters/second, can be approximated by the following expressions

انحراف استاندارد طیف کلاتر به سرعت باد وابسته است.

$$\sigma_v(\text{mean}) = 0.0115w^{1.12} \qquad [3.47a]$$

$$\sigma_v(90\%) = 0.021w^{1.10} \qquad [3.47b]$$

where w = wind speed in meters/second. This was said to apply over a frequency range from about 3 GHz to 24 GHz and wind speeds from 1 to 25 m/s. Polarization did not seem to be a significant factor. Values of the ratio of the d-c to the a-c components of land clutter spectra were also given by Nathanson.

The use of a gaussian spectrum may be convenient, but as mentioned above, it falls off more rapidly with frequency than experimental measurements indicate. Its application is limited, therefore, to situations when the clutter attenuation or the improvement factor are not large.

Power-Law Model The normalized power-law spectrum is given by

$$P(f) = \frac{1}{1 + (f/f_c)^n} \qquad [3.48]$$

This was first suggested by Fishbein et al.[63] as being a better description of measured clutter spectra than the gaussian. At X band, they found the value of the exponent n to be equal to 3. The clutter spectrum *characteristic frequency*, denoted f_c, is the value of the spectral density when it is reduced by one-half its zero-frequency value. It was said to equal $k_1 \exp[k_2 w]$ (in hertz), where $k_1 = 1.33$ Hz, $k_2 = 0.1356$ kt^{-1}, and w = wind speed in knots. Their work was extended by Li Neng-jing[64] who stated that experimental measurements at X, S, and L bands suggested that the characteristic frequency f_c increased with increasing wind and the exponent n varied with radar frequency and wind speed.

Based on measurements at L band by the Chinese Airforce Radar Institute, Li states that as the wind speed increased from low values (0 to 3 m/s) to high values (13 to 15 m/s), the exponent n decreased from 3.3 to 2.2, and f_c increased from 0.8 to 1.9. Experiments by Georgia Institute of Technology indicate that the power-law expression also can be applied for frequencies from 35 to 95 GHz with appropriate selection of the two parameters f_c and n.[65]

As the clutter spectrum decreases below about 40 dB from its peak zero doppler-frequency value, it is found that the power-law spectrum does not decrease as fast as indicated by experimental measurements. (Note that with $n = 3$, the falloff is 30 dB per decade of frequency.) Consequently, the power-law model will give erroneous results by predicting less clutter attenuation than actual. A modified exponential law provides a better representation of the windblown land clutter faced by high-performance doppler radars, as discussed next.

5/5/88

Exponential Law The information in this subsection is taken from an excellent examination of low grazing angle land-clutter spectra as reported by J. B. Billingsley of the MIT Lincoln Laboratory.[66] His work was based on extensive, well-calibrated clutter measurements made over a long period of time at many different sites at frequencies from VHF to X band, with equipment sensitive enough to measure clutter spectral levels 60 to 80 dB below the zero-doppler clutter level. (These clutter measurements are discussed further in Sec. 7.3.) The measurements were accurately made to the very low spectral power-density levels important for the design of high-performance radars that must see small moving targets in clutter. The Lincoln Laboratory clutter spectral model from windblown vegetation and trees (forest) is given by the next three equations, the first of which is

$$\text{total power spectral density: } P_{\text{tot}}(v) = \frac{r}{r+1}\delta(v) + \frac{1}{r+1}P_{\text{ac}}(v) \qquad [3.49]$$

where v = doppler velocity in meters/second, $-\infty < v < \infty$, r = ratio of the d-c power in the spectrum to the a-c power, $\delta(v)$ = delta function that represents the shape of the d-c component of the spectrum, and $P_{\text{ac}}(v)$ is the shape of the a-c component of the spectrum. Note that this is written in terms of velocity v rather than frequency f. (Billingsley actually takes the near zero doppler, or quasi d-c power region, to be $0 < |v| < 0.25$ m/s.) $P_{\text{ac}}(v)$ is normalized such that its integral over all frequencies equals unity, and is the quantity usually represented by analytical expressions of the spectral shape. P_{tot} represents the measured clutter spectra.

The a-c portion of the spectrum is given by the two-sided exponential

$$P_{\text{ac}}(v) = \frac{\beta}{2}\exp\left[-\beta|v|\right] \qquad -\infty < v < \infty \qquad [3.50]$$

where β is the *exponential shape parameter*, and is given in Table 3.1. Billingsley[66] also gives an empirical relation for β as

$$\beta^{-1} = 0.105\,[\log_{10} w + 0.476]$$

Table 3.1 Exponential a-c shape-parameter β versus wind speed*

Wind Conditions	Wind Speed (knots)	β typical $(m/s)^{-1}$	β worst case $(m/s)^{-1}$
Light air	1–6	12	—
Breezy	6–12	8	—
Windy	12–25	5.7	5.2
Gale force (est.)	25–45	4.3	3.8

*After J. B. Billingsley, ref. no. 66

with w the wind speed in knots. Measurements made from VHF to X band indicate that the values in this table are largely independent of frequency. It follows that the doppler velocity is relatively independent of frequency for windblown vegetation and trees. Equations (3.49) and (3.50) can be expressed in hertz rather than velocity by use of the equation $f = 2v/\lambda$.

The value of r, the d-c/a-c ratio, is dependent on both wind speed and radar frequency. It is given by

$$r = 394\, w^{-1.55} f_0^{-1.21} \qquad [3.51]$$

where the wind speed is in knots and f_0 is the carrier frequency in gigahertz.

Equations (3.49), (3.50), and (3.51) and Table 3.1 as given by Billingsley describe the exponential clutter spectral model for windblown vegetation and trees over spectral dynamic ranges down to 60 to 80 dB below the zero-doppler peak. At these low levels, the observed clutter doppler velocities are limited to 3 to 4 m/s.

The shape of the a-c component is invariant with frequency from VHF to X band. It is independent of polarization, but strongly depends on the wind speed. The d-c component, however, is much larger at VHF than at X band. Within the limits of the experimental situations covered by these measurements, there is little noticeable dependence on (1) the type of trees (species, density, growth stage), (2) the season of the year (whether the leaves are on or off), (3) resolution cell size, (4) polarization, (5) grazing angle, (6) wind direction, and (7) angle of illumination.*

The exponential clutter model was derived to describe the spectrum of windblown trees, but Billingsley states that it seems to apply as well to the clutter spectra from scrub desert, range land, and cropland vegetation by suitably adjusting the d-c/a-c term. He also estimates that the correlation time for windblown trees might be about 4 s for light wind and about 1 s for windy days.

Figure 3.33 is an example of a windblown X-band clutter spectrum for a forested area showing the effect of wind speed.[67] The radar cell contained mixed deciduous and

*This, and the related land-clutter measurements mentioned in Sec 7.3, tend to question the utility of radar for the remote sensing of the land-surface environment. It might explain why there has been so little success for radar remote sensing in such applications. It also seems to indicate that explanations for radar echoes from trees might be in doubt if the scattering models assume that significant scattering is obtained from the leaves.

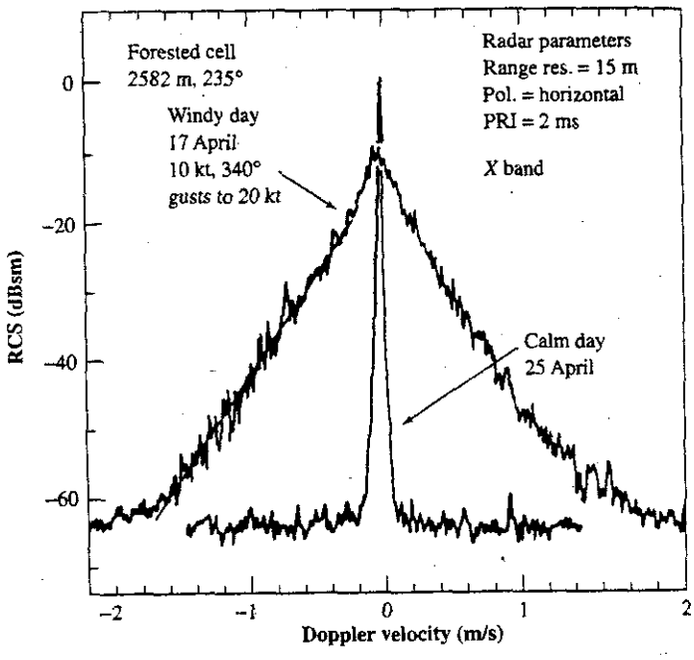

Figure 3.33 Power spectra of X-band radar echoes showing the effect of the wind.
[From J. B. Billingsley,[67] reprinted with permission of *MIT Lincoln Laboratory*, Lexington, MA.]

evergreen trees to an approximate height of 60 to 70 ft. On the windy day, the wind speed was recorded as 10 kt with gusts to 20 kt. An example of the frequency dependence of clutter spectra is shown in Fig. 3.34. This is cropland (wheat) in North Dakota. The delta-function-like component at d-c is clearly indicated.

The three different models of clutter spectra that have been discussed (gaussian, power law, and exponential) are compared in Fig. 3.35. The three are normalized so that they each have $\int_{-\infty}^{\infty} P_{ac}(v)\, dv = 1$, which allows the comparison to be made on equivalent total a-c spectral power. (This type of normalization is seldom found in the past literature of clutter spectra, but Billingsley recommends it should be done. The value at zero frequency, when normalized in this manner, is not necessarily unity.) The gaussian spectrum may be appropriate for low clutter doppler velocities, the power law for moderate velocities, but the exponential is best for covering the largest clutter velocities as well as representing the entire range of clutter spectral values.

11/5/88

Improvement Factor for Exponential Clutter Billingsley gives the MTI improvement factor for an exponential clutter spectrum with a single delay-line canceler as[66]

ضريب بهبود (IF) براي كلاتر نمايي

$$I_\beta = (r+1)\left(\frac{\lambda f_p \beta}{4\pi}\right)^2 = (r+1)\left(\frac{v_1}{\pi}\right)^2\left(\frac{1}{2\sigma_\beta^2}\right) \qquad [3.52]$$

where the standard deviation of the exponential spectrum is $\sigma_\beta = \sqrt{2}/\beta$ (σ_β is in units of meters/second) and $v_1 = \lambda f_p/2$ is the first blind speed as was given by Eq. (3.12). The other symbols have been defined previously. If in the right hand portion of this equation

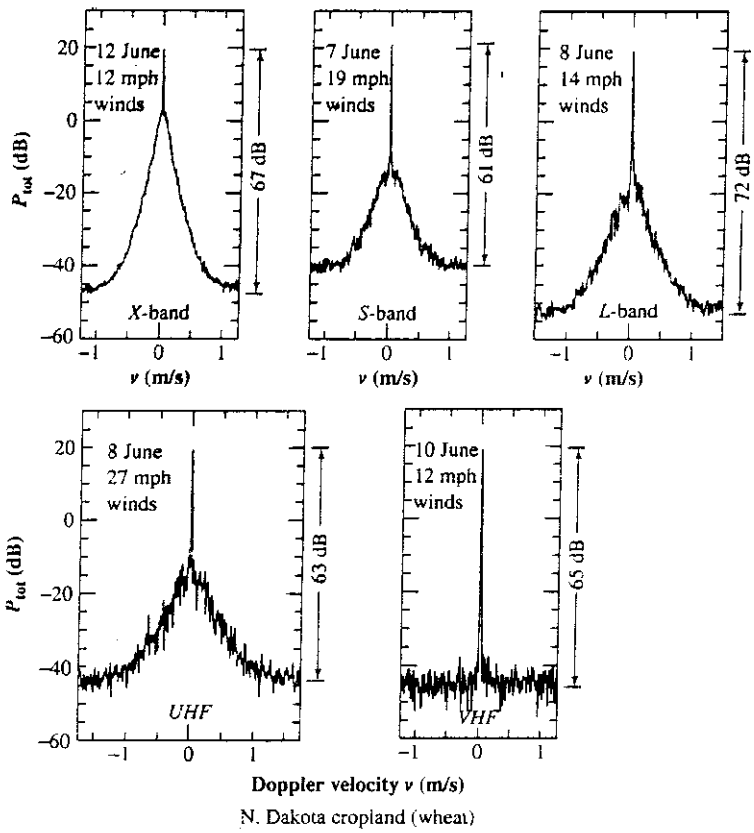

Figure 3.34 Power spectra of North Dakota wheatland measured on four different days under various windy conditions. (From J. B. Billingsley,[66] reprinted with permission of MIT Lincoln Laboratory, Lexington, MA.)

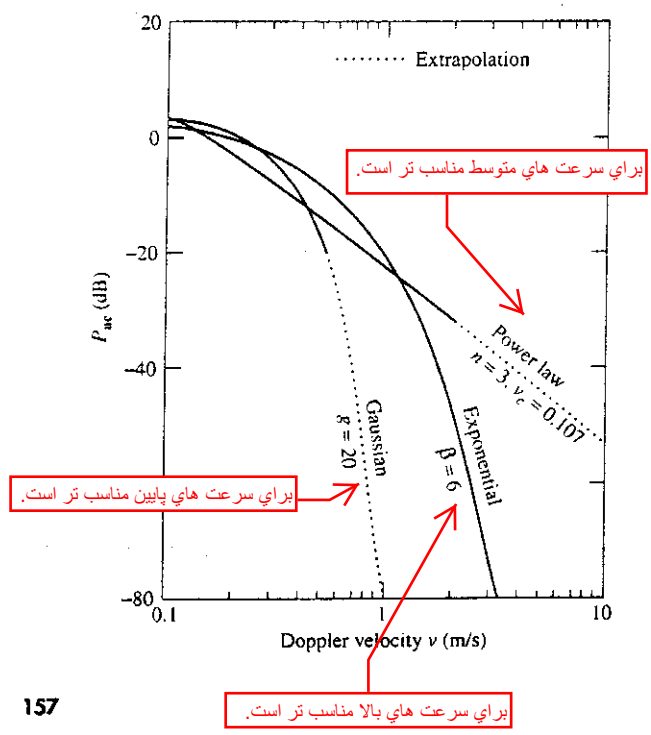

Figure 3.35 Three analytic spectral shapes, each normalized to unit spectral power. The parameter g in the gaussian spectrum is called the gaussian shape parameter and is equal to $1/(2\sigma_v^2)$, where σ_v is the standard deviation in meters/second. (From J. B. Billingsley,[66] reprinted with permission of MIT Lincoln Laboratory, Lexington, MA.)

we were to identify σ_β as the standard deviation of a gaussian distribution and if we take $r = 0$, this equation is identical to Eq. (3.21), the improvement factor for a single delay-line canceler with a gaussian spectrum.

The improvement factor for an exponential clutter spectrum with n delay-line cancelers in cascade [$(n + 1)$ delay-line canceler], is

$$I_\beta(n) = (r + 1)\left(\frac{\lambda f_p \beta}{2\pi}\right)^{2n} \frac{1 \times 3 \times 5 \times \cdots \times (2n - 1)}{2^n n!\,(2n)!} \qquad [3.53]$$

System Instabilities Changes in amplitude, frequency, or phase of the stalo or coho oscillators as well as changes in the pulse-to-pulse characteristics of the transmitted signal or errors in the timing can result in uncanceled clutter echoes and cause a limit to the improvement factor that can be achieved.[68] In this subsection we briefly review some of the major system instabilities that limit MTI radar performance.

Amplitude Changes If in a single delay-line canceler, the amplitude of the first pulse received from a stationary clutter scatterer is A and that of the second pulse is $A + \Delta A$, the voltage output of the delay-line canceler is ΔA. The clutter attenuation is therefore $(\Delta A)^2/A^2$, and the improvement factor is twice this.

Nathanson[69] presents a slightly different way of looking at the limitation on the improvement factor that results from amplitude pulse-to-pulse changes. Let ΔV_1 and ΔV_2 represent the voltage variation of each of the two pulses about the mean value V_m. The clutter attenuation for a single delay-line canceler is then

$$\text{CA} = \frac{V_m^2}{(\Delta V_1 - \Delta V_2)^2} = \frac{V_m^2}{\Delta V_1^2 + \Delta V_2^2} = \frac{V_m^2}{2\sigma_v^2} \qquad [3.54]$$

where σ_v^2 is the variance of ΔV. The clutter attenuation for a double delay-line canceler is $V_m^2/6\sigma_v^2$. When the average gain is included, the limitation to the improvement factor for both the single and the double delay-line canceler due to amplitude changes is

$$I_1 = I_2 = V_m^2/\sigma_v^2 \qquad [3.55]$$

Phase Changes If the echo received from the first pulse from stationary clutter is represented as $A \sin(\omega t + \phi)$, and if the echo from the second pulse is $A \sin(\omega t + \phi + \Delta\phi)$, there will be an uncanceled residue from a single delay-line canceler equal to the difference, $2A \sin(\Delta\phi/2)$, where $\Delta\phi$ is the phase change between pulses. For small phase changes, the output voltage is $A\Delta\phi$. The clutter attenuation is then $(1/\Delta\phi)^2$ and the improvement factor is twice this.

For the double delay-line canceler, Nathanson describes two different cases. In the first case, the phase errors from one pulse to the next are assumed equal ($\Delta\phi_1 = \Delta\phi_2$), as in an oscillator with a constant drift in phase. In the second case, the phase errors from pulse to pulse are assumed to be statistically independent. The limitations in improvement factor for a double delay-line canceler in these two cases are given by Nathanson as

$$I_2 = \frac{6}{(\Delta\phi)^4} \qquad \text{for } \Delta\phi_1 = \Delta\phi_2 \qquad [3.56]$$

تغییرات در دامنه، فرکانس یا فاز نوسانسازهاي stalo و coho به همراه تغییرات در مشخصات پالس به پالس سیگنال فرستاده شده یا خطاها در زمانبندي مي تواند اکوهاي کلاتر حذف نشده را نتیجه دهد و باعث محدود شدن ضریب بهبود MTI گردد.

آیا این تغییر دامنه در اثر fading است؟

تغییرات دامنه باعث کاهش IF مي شود.

if=(s/c)out/(s/c)in

26/7/88

$$I_2 = \frac{3}{(\Delta\phi)^2} \qquad \text{for } \Delta\phi \text{ statistically independent} \qquad [3.57]$$

Phase Noise Noise due to phase fluctuations associated with the stalo and coho oscillators can be a major limitation to the improvement factor of high-performance MTI radars. Generally, phase noise has a much larger effect than noise caused by amplitude instabilities. The phase noise from oscillators in the exciter of a power amplifier affect the transmitted signal as well as the signal in the receiver. The spectrum of a CW oscillator is not a classical delta function; but has a finite spectrum, as in Fig. 3.36a.[70] The ordinate is dBc/Hz, which is the noise power within a one-hertz bandwidth relative to the noise at the carrier frequency (at $f = 0$) given in decibels. Phase noise decreases as the frequency increases from the carrier and then levels off to a constant value when thermal noise dominates. Significant spectral energy can appear in the doppler space of the echo signal. This can limit the minimum velocity with which a moving target can be detected. The nature

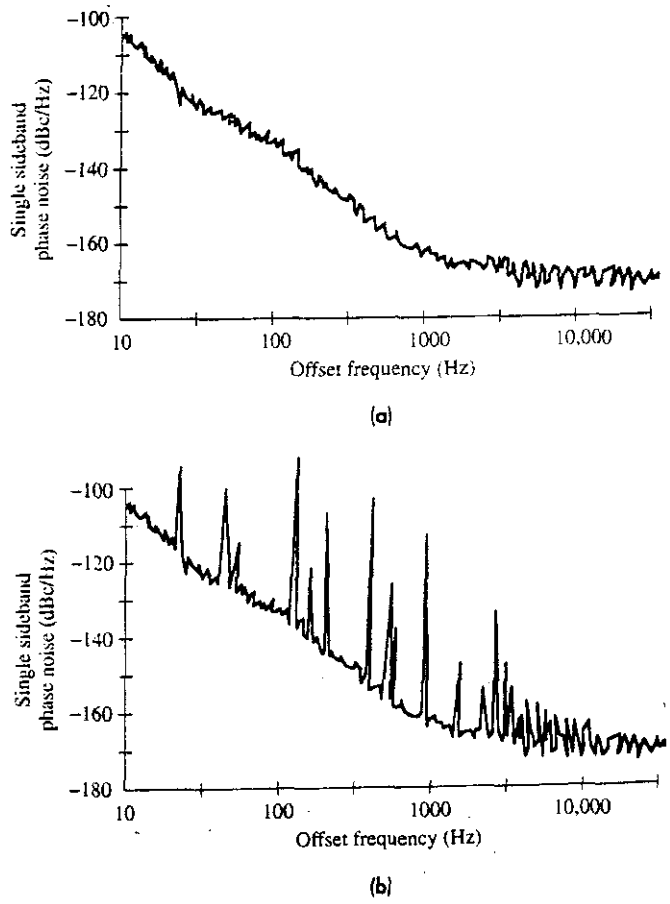

Figure 3.36 (a) An example of an oscillator phase noise spectrum. (b) Example of large spurious signals (spurs) resulting from the power supply.
(From C. L. Everett,[70] Courtesy of Bell Helicopter TEXTRON and the *Microwave Journal*.)

of the noise spectrum depends on the type of oscillator, whether it is a transistor, a crystal oscillator in a temperature-controlled oven, SAW oscillator, dielectric resonator oscillator, or whatever.[71] The shape of the noise spectrum is influenced by the Q of the resonator or resonant circuit associated with the oscillator. Sometimes there are discrete frequency spikes appearing in the spectrum, as in Fig. 3.36b. These are called *spurious*, or *spurs*, and are often associated with the power supply or mechanical vibrations. Phase noise can be introduced by mixers, by the high-power amplifier, and it can ride on the echo signals from clutter.

Stable, low-noise oscillators are usually easier to achieve at the lower frequencies (10 MHz, for instance). They can be multiplied to a higher frequency by using a diode or varactor to generate harmonics. A filter selects the desired harmonic. When oscillators are multiplied in frequency, their phase noise increases as the square of the frequency multiplication, or 20 dB per decade of multiplication. (For example, a 10-MHz oscillator multiplied in frequency to 10 GHz would have its sideband noise levels increased by 60 dB.)

It has been said[72] that if a 1-GHz doppler radar, with a doppler bandwidth of 10 kHz, is to detect a 1-m^2 target at a range of 100 km with a minimum detectable radial velocity of at least 40 m/s (about 80 kt) in clutter with a cross section per unit area $\sigma^0 = 0.02$, the subclutter visibility has to be 80 dB and the transmitter noise sidebands must be better than -120 dB/Hz at sideband frequencies greater than 200 Hz from the carrier.

The phase noise of an oscillator can be reduced by utilizing superconductive resonators to increase its Q.[72] This technique becomes more attractive with advances in high-temperature superconductors that can operate with liquid nitrogen cooling at 77 K rather than the 4 K of liquid helium.[73] The use of dielectric resonator oscillators and high-temperature superconducting films is said to provide at 10 GHz a phase noise lower than -140 dBc/Hz offset 1 kHz from the carrier.[74]

Phase noise can significantly increase due to mechanical vibrations and acceleration as experienced in airborne platforms. Quartz crystal resonators are particularly sensitive to vibrations. Filler and Vig[75] state that mechanical vibrations might increase the phase noise of a crystal oscillator almost 50 dB at a frequency 100 Hz from the carrier under a 0.1 g^2 random vibration (assuming 10^{-9} per g acceleration sensitivity). The dielectric resonator oscillator is less sensitive to shock and vibration than others since it is small and has a high degree of rigidity.[71] Reduced sensitivity to acceleration and vibration (3×10^{-10} per g) has been claimed for oscillators based on "surface transverse waves" (STW), which is a surface-skimming bulk wave with most of the energy confined near the surface but not as tightly confined as in the case of SAW propagation.[76]

The calculation of the limitation on the MTI improvement factor due to the oscillator phase-noise spectrum is described by Shrader and Gregers-Hansen (pp. 15.48 to 15.50 of Ref. 1) and by R. Kerr.[77]

Other limitations due to system instabilities can be found in the discussion of Table 15.4 in Ref. 1.

Limiting in MTI Radar[78,79] Clutter echoes often can be large enough to saturate the radar receiver, obscure target echoes on a display, and cause false alarms. Saturation of the receiver by clutter echoes also results in a spreading of the clutter spectrum that reduces the improvement factor. If the receiver is of large enough dynamic range, and there are

sufficient bits in the A/D converter, and if the improvement factor is large enough to make the uncanceled clutter residue smaller than receiver noise, there will be no problem since there will be no limiting. Large dynamic range and cancellation of all the large clutter, however, are not the usual situation.

A limiter in the MTI receiver has sometimes been used to reduce the clutter to the level of receiver noise. The radar literature of World War II recommended that a hard limiter be used for an MTI radar,[80] but we now know this can cause quite serious degradation of the MTI performance. Instead, the limiter should be set above receiver noise by an amount equal to the improvement factor. If it is less than this amount, the improvement factor will not be as predicted when it is assumed that the receiver is linear.

Shrader and Gregers-Hansen[79] provide the following example for a particular air-surveillance radar which receives 16.4 pulses per scan from a target. When the receiver is designed so that a point clutter echo doesn't exceed the limit level, the improvement factor for a two-pulse, three-pulse, and four-pulse canceler is 22.4, 42.2, and 59.9 dB, respectively. If, on the other hand, the limit level is lowered so that the point clutter echo exceeds the limit level by 20 dB, these numbers reduce to 20.4, 29.4, and 33.3 dB, respectively. In this situation with the 20 dB limit level, a four-pulse canceler has very little advantage over a three-pulse canceler. Thus it is important to have the limiter set correctly if the expected MTI performance is to be achieved.

Clutter Map[81] Sensitivity time control, small radar resolution cells, reduced antenna gain near the horizon, and CFAR are also used to keep clutter from saturating the receiver. In spite of efforts to reduce the amount of clutter viewed by a radar, uncancelled clutter residue might exist which must be surpressed to avoid saturation of the display and/or excessive false alarms in an automatic detection and tracking system. With improvements in digital memories, it became practical to employ digital clutter maps to establish thresholds based on the clutter echo in each radar resolution cell (or combinations of cells). This acts as a type of CFAR, and is superior to conventional cell-averaging CFAR (Sec. 5.7) especially when the clutter is not spatially homogeneous, as with typical land clutter. The use of a clutter map avoids the problems of a limiter in an MTI radar, but introduces some limitations of its own. As with other forms of CFAR, there is a loss in sensitivity with the clutter map, which could be two dB, more or less. The loss increases as fewer past scans are used to establish the clutter map.[82]

3.8 MTI FROM A MOVING PLATFORM (AMTI)

When the radar is on a moving platform such as a ship, aircraft, or spacecraft, the doppler frequency shift from clutter is no longer at zero frequency. The doppler frequency of the clutter echo depends on the relative velocity with respect to the moving radar platform so it will vary with the speed of the radar platform as well as the azimuth and elevation of the clutter cell with respect to the radar. The doppler shift from the clutter can seriously degrade the MTI improvement factor if it is not taken into account.

If the radar were on a moving ship and the antenna is not scanning too fast, it might be practical to compensate for the change in clutter doppler frequency by changing the

frequency of the coherent reference oscillator (coho) in an open-loop manner if the speed of the platform and the direction of antenna pointing are known. Compensation for the clutter doppler frequency can be achieved by mixing the output of the coho with a signal from a tunable oscillator whose frequency is made equal to the clutter doppler. It might also be possible in some cases to widen the doppler filter rejection notch so as to exclude the nonzero doppler from clutter if it doesn't remove too much of the available doppler space. With airborne radar, however, the clutter doppler frequency shift can be too large and too rapidly varying with time to compensate open loop. A form of closed-loop compensation must be used.

There is another problem associated with a moving radar platform that can degrade the performance of a moving MTI radar. Not only does the center frequency of the clutter spectrum vary, but so does the clutter spectral width. The widening of the clutter spectrum is due to the finite beamwidth of the antenna which makes the doppler frequency shift from the clutter scatterers within the radar resolution cell differ depending on their location within the antenna beam. For example, the doppler from a scatterer at the center of the beam will differ from that of a scatterer located a half-beamwidth away. These two effects, a nonzero clutter doppler shift and a widening of the clutter spectrum, can seriously degrade the performance of a radar on a moving platform. They are compensated by two different techniques: the change in center frequency of the clutter spectrum by what is known as TACCAR, and the widening of the clutter spectrum by DPCA. These are discussed in this section.

An MTI radar on a moving platform that uses these two methods (TACCAR and DPCA) for compensating for *platform motion* is known as an *AMTI radar.*[83] Although the *A* originally stood for airborne, the term is now almost universally applied to MTI radar on any moving platform that uses these two methods of platform motion compensation.

Compensation for Clutter Doppler Shift (TACCAR)[84] The doppler frequency shift from clutter can be compensated by using the clutter echo signal itself to set the frequency of the reference oscillator, or coho, so that the rejection notch of the MTI doppler filter attenuates the clutter echo. This has been called *clutter-lock MTI* in the past, but it is more usually known as *TACCAR,* which stands for *time-averaged-clutter coherent airborne radar.* TACCAR was originally developed by MIT Lincoln Laboratory for a particular airborne MTI system, but it now refers to the clutter-lock technique that was the special feature of that system. The chief feature of the original TACCAR was the use of a voltage-controlled oscillator arranged in a phase-lock loop that averaged the measurement of the clutter doppler frequency within a sampled range interval. It also compensates for drift in various system components. Further information on TACCAR can be found in Ref. 84, by Fred Staudaher.

Moving Clutter A similar problem occurs in a stationary radar when the clutter has a velocity of its own, as might occur for ocean currents, weather, and windblown chaff. TACCAR can also be applied for reducing the effects of moving clutter as seen by a stationary radar. Generally, such techniques do not adequately eliminate both stationary and moving clutter simultaneously when they appear within the same radar resolution cell. A TACCAR, for example, might be designed to reject ground clutter close-in or to reject

moving weather clutter at a different doppler at ranges beyond the ground clutter; but not to cancel both simultaneously.[85] A doppler filter bank in the MTD, however, can detect moving targets in the presence of both moving clutter as well as stationary clutter if their doppler frequency shifts are different. When the clutter spectrum consists of both stationary and moving components (a bimodal clutter spectrum), the doppler filter of an MTI radar might be made adaptive to reject the moving clutter as well as have a rejection notch at zero frequency to remove stationary clutter.[86]

Compensation for Clutter Doppler Spread (DPCA)[87] The doppler frequency shift of the echo from a stationary clutter scatterer when viewed by a moving radar is given as $f_c = 2(v/\lambda) \cos \theta$, where v = velocity of the platform carrying the radar, λ = wavelength, and θ = angle between the velocity vector of the vehicle carrying the radar and the line of sight to the clutter scatterer. The angle θ includes both a horizontal (azimuth) and a vertical (elevation) component; but for simplicity in the discussion here, we will consider only the azimuth component. The doppler frequency from those scatterers located along the center of the antenna beam, Fig. 3.37, will be compensated by TACCAR so that it appears at zero frequency. The echoes from all other scatterers that do not lie along the center of the main beam will not be compensated by TACCAR. Thus there will be a spread in the clutter doppler frequency spectrum due to the finite antenna beamwidth of Fig. 3.37. The clutter spectral spread due to the many clutter scatterers within the finite beamwidth can be found by taking the differential of the doppler frequency, which is

$$\Delta f_c = \frac{2v}{\lambda} \sin \theta \, \Delta\theta = \frac{2v}{\lambda} \theta_B \sin \theta \qquad [3.58]$$

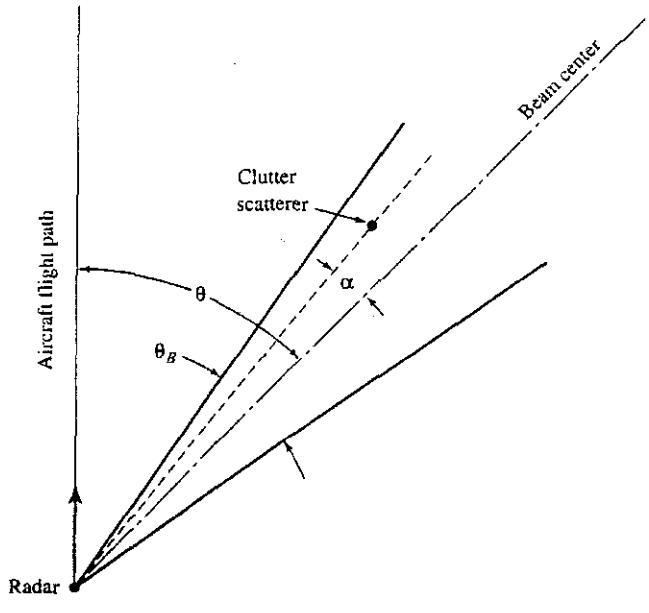

Figure 3.37 Geometry of scattering from a single clutter scatterer located at an angle α from the beam center. Antenna beamwidth = θ_B.

where the antenna beamwidth θ_B is taken to be the same as $\Delta\theta$. (The negative sign introduced by differentiating the cosine is ignored.) The spectral spread Δf_c varies with the angle θ. When the antenna points in the direction of the platform velocity vector ($\theta = 0$), the doppler shift of the clutter echo is maximum, but the width Δf_c of the spectrum is theoretically zero. On the other hand, when the antenna is directed perpendicular to the direction of the platform velocity ($\theta = 90°$, or broadside), the clutter doppler center frequency is zero, but the spread is maximum. The widening of the clutter spectral spread as a function of the azimuth angle can set a limit on the improvement factor.

Figure 3.38 is an example of the spread of the clutter spectrum caused by motion of the radar platform. It assumes a UHF airborne radar at a speed of 400 kt, with an antenna beamwidth of 7 degrees. The width of the clutter spectrum and its center frequency both depend on the angle θ that the radar beam makes with the platform vector velocity. In Fig. 3.38a, the clutter spectra are shown as a function of angle θ. The prf is assumed to be high enough to not include any foldover of the clutter. (At $\theta = 0$ degrees, the clutter spectrum is shown as an infinitesimal line, but in reality there will be effects other than platform motion that contribute to its widening.) In Fig. 3.38b, the foldover of the clutter spectrum at $\theta = 90°$ is shown when the prf is 360 Hz, which corresponds to a maximum unambiguous range of 225 nmi. This figure illustrates the relatively large portion of the frequency domain (doppler space) occupied by the clutter spectrum because of the travel of the aircraft carrying the radar, or platform motion. The widening of the clutter spectrum needs to be reduced in order for AMTI radar to be effective.

There would be no spreading of the clutter spectrum ($\Delta f_c = 0$) if the antenna could be made to think that it is stationary. It is possible to do this with two separate antennas. Consider the case where the two antennas are separated in line with the platform's velocity vector, and with their beams pointing broadside at $\theta = 90°$. The spacing between the phase centers of the two antennas is made equal to vT_p, where v is the velocity of the aircraft and T_p is the pulse repetition period. One is the forward antenna, the other is the trailing antenna. The first pulse is transmitted and received by the forward antenna. When the trailing antenna arrives at the spot where the forward antenna was when it transmitted its pulse, the trailing antenna transmits its pulse. Thus the two pulses from the two

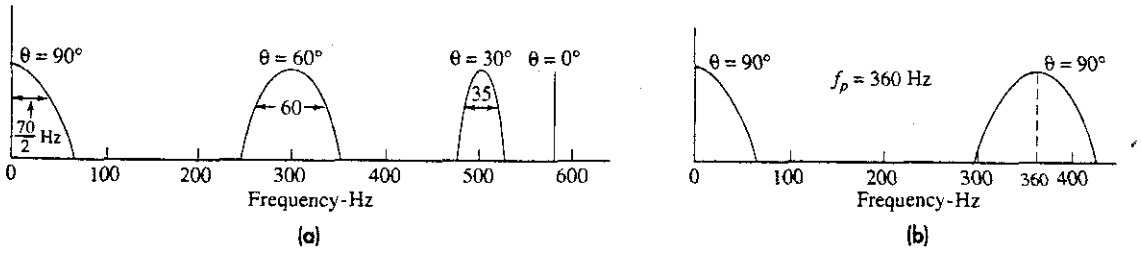

Figure 3.38 Change in shape and location of the clutter spectrum due to platform motion as a function of azimuth angle. (a) Case for a very high prf or CW. (b) $\theta = 90°$, with spectrum folded about the prf at 360 Hz.

antennas are transmitted (and received) at the same point in space. To the radar, it is as if there were a single stationary antenna. The two pulses are then processed in a delay-line canceler and there is no effect of platform motion.

There are some problems, however, with this solution. The prf must be synchronized with the aircraft speed and the spacing between the two antennas has to vary with the cosine of the angle θ if the antenna scans in azimuth. The antennas are coincident when looking in the direction of the aircraft's velocity vector at $\theta = 0$ and furthest apart at $\theta = 90°$. In fact, the antennas always overlap, even at 90°. A single sidelooking phased array can be used with a fraction of its columns operating on the first pulse and an overlapping fraction of its columns operating on the second pulse, so that the phase center is shifted in the horizontal plane. On the first pulse, the phase center might be slightly ahead of the physical center of the array antenna and on the second pulse the phase center might be slightly behind the physical center, with the locations of the phase center in space being the same on each of the two pulses. This is an example of a *displaced phase center antenna* (DPCA). Phased arrays for this purpose have been built and flown, but there is another, usually simpler, method to obtain the same effect using a single antenna with two squinted beams.

Consider a mechanically rotating antenna that generates two overlapping (squinted) beams, Fig. 3.39. This can act as a DPCA when the outputs of the two squinted beams are properly combined. The sum (Σ) and the difference (Δ) of the two squinted beams are taken (similar to the sum and difference beams of a monopulse tracking radar as described in Sec. 4.2). The sum beam is used for transmit, and both the sum and difference beams are used on receive. The received signal from the first pulse is processed to form $\Sigma_r + jK\Delta_r$, where $+j$ represents a 90° phase advance applied to the difference signal, K is a constant that determines the amount of the phase center shift, and the subscript r denotes the received signals in the sum and difference channels (as will be described later).

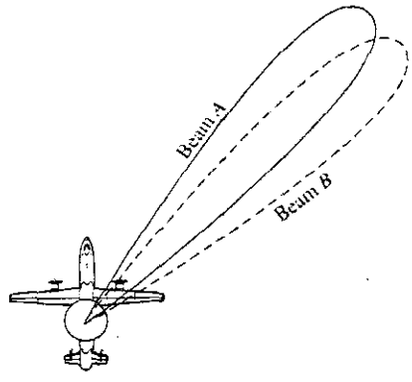

Figure 3.39 *Mechanically rotating airborne antenna (within a rotodome) with two squinted beams. The sum of these two beams is used for transmitting, and the echo signal is received on both the sum and the difference of the two beams.*

The constant K depends on the aircraft velocity, the prf, and the angle θ. This process applies an apparent forward displacement to the phase center on the first pulse. From the second pulse is formed $\Sigma_r - jk\Delta_r$, where $-j$ is a 90° phase lag. This applies an apparent rearward displacement to the phase center. The two signals are then subtracted from one another, resulting in the cancellation of the doppler spread in the clutter. It is not obvious from the above explanation why this works. A bit of mathematical analysis, however, will show why the doppler spread does not occur.

In Fig. 3.40a, the phasor E_1 represents the clutter amplitude and phase of the echo from the first pulse. Phasor E_2 represents the clutter amplitude and phase from the second pulse. The single clutter scatterer is shown in Fig. 3.37 at an angle α with respect to the beam center at θ. If both the radar and the clutter were stationary, the phase difference 2η between the two echoes would be zero and the two echoes would cancel when subtracted in a delay-line canceler. Thus there would be no clutter residue. The movement of the platform carrying the radar, however, will result in the clutter echo having a doppler frequency shift δf_c relative to the echoes from the TACCAR-compensated beam center. In the time T_p between two pulses, the phase shift resulting from the clutter doppler frequency is

$$\Delta\phi_c = 2\eta \approx 2\pi(\delta f_c)T_p \qquad [3.59]$$

From Fig. 3.37, the doppler frequency shift from a clutter scatterer at an angle α is

$$\delta f_c = \frac{2v}{\lambda}\cos(\theta - \alpha) - \frac{2v}{\lambda}\cos\theta \approx \frac{2\alpha}{\lambda}v\sin\theta \qquad [3.60]$$

The far-right expression assumes α is small. Substituting the above into Eq. (3.59) gives

$$2\eta = \frac{4\pi T_p \alpha}{\lambda}(v\sin\theta) \qquad [3.61]$$

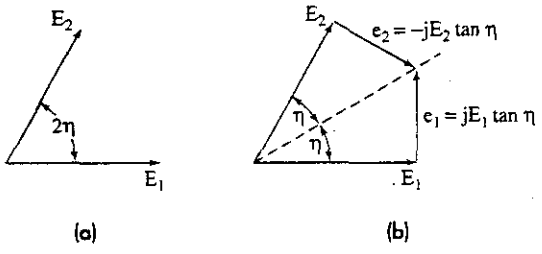

Figure 3.40 *Phasor diagrams illustrating the nature of the DPCA action to compensate for platform motion using the sum and difference patterns of two squinted beams formed from a single antenna. (a) Phasors representing the clutter echo signals received on two successive pulse transmissions. The angle 2η represents the phase change due to the travel (platform motion) of the radar antenna between pulses. (b) Corrections applied to each pulse so that a cancellation of the clutter echoes occurs on two successive pulses.*

This phase shift gives rise to the angular separation of the two phasors of Fig. 3.40a so that when the two are subtracted in a delay-line canceler, there will be an uncanceled, unwanted clutter residue.

If correction signals e_1 and e_2 are applied to each pulse as indicated in Fig. 3.40b, the two resultant signals cancel after passing through a delay-line canceler and (theoretically) there would be no clutter residue. Thus there is no effect of the clutter spread due to platform motion. From the geometry of Fig. 3.40b, the correction to the clutter echo from the first pulse needs to be $e_1 = +jE_1 \tan \eta$, and the correction to the second pulse is $e_2 = -jE_2 \tan \eta$. The $+j$ in e_1 means that the phase of the correction signal is advanced 90°, and the $-j$ in e_2 means that its phase is delayed 90°. These corrections can be obtained from the signals received in the sum and difference beams from the two squinted beams of Fig. 3.39.

The DPCA radar transmits on the sum Σ of the two squinted beams and receives on both the sum Σ and difference Δ of the two squinted beams. Because of the two-way path of radar signals, the received sum and difference signals may be represented as

$$\Sigma_r(\alpha) = k_1 \Sigma^2(\alpha) \qquad [3.62a]$$

$$\Delta_r(\alpha) = k_2 \Sigma(\alpha) \Delta(\alpha) \qquad [3.62b]$$

where the constants k_1 and k_2 account for the parameters of the radar equation. The amplitudes of the two pulses are assumed equal so that

$$|E_1| = |E_2| = |\Sigma_r(\alpha)| = k_1 |\Sigma^2(\alpha)| \qquad [3.63]$$

From a uniformly illuminated aperture of dimension D, the sum pattern is proportional to

$$\Sigma(\alpha) = \frac{\sin [\pi(D/\lambda) \sin \alpha]}{\pi(D/\lambda) \sin \alpha} \qquad [3.64]$$

and the difference pattern is

$$\Delta(\alpha) = \frac{1 - \cos [\pi(D/\lambda) \sin \alpha]}{\pi(D/\lambda) \sin \alpha} \qquad [3.65]$$

Using Eqs. (3.61) and (3.64), the correction signals e_1 and e_2 are

$$e_{1,2} = \pm jk_1 \frac{\sin^2 [\pi(D/\lambda) \sin \alpha]}{[\pi(D/\lambda) \sin \alpha]^2} \tan \left[\frac{2\pi T_p \alpha}{\lambda} (v \sin \theta) \right] \qquad [3.66]$$

For small α and small values of the arguments

$$e_{1,2} = \pm jk_1 \frac{2\pi T_p \alpha}{\lambda} (v \sin \theta) \qquad [3.67]$$

On substituting Eqs. (3.64) and (3.65) into the received difference signal of Eq. (3.62b), and when the arguments are small, the signal in the difference channel can be approximated as

$$\Delta_r(\alpha) \approx k_2 \frac{\pi}{2} \frac{D}{\lambda} \alpha \qquad [3.68]$$

Substituting the above into Eq. (3.67) gives the correction signals as

$$e_{1,2} = j\frac{k_1}{k_2}\frac{4\ v \sin\theta}{D} T_p \Delta_r(\alpha) = \pm jk'\ v \sin\theta\ \Delta_r(\alpha) \qquad [3.69]$$

Thus the above are applied to the received signals so that the input to the delay-line canceler is

$$\text{Pulse No. 1} = \Sigma_r(\alpha) + jk\ (v \sin\theta)\ \Delta_r(\alpha) \qquad [3.70a]$$

$$\text{Pulse No. 2} = \Sigma_r(\alpha) - jk\ (v \sin\theta)\ \Delta_r(\alpha) \qquad [3.70b]$$

The constant k accounts for the difference in gains between the sum and difference channels, as well as the factor $4T_p/D$.

Thus one takes the received difference signal, multiplies it by $k(v \sin\theta)$, shifts its phase forward or back by 90° (depending on which pulse), and adds it to the received sum signals. Note that the multiplier $k(v \sin\theta)$ is bipolar in that it must be capable of changing sign when the antenna pointing direction changes from one side of the platform to the other.

Compensation for Antenna Scan Modulation.[88–90] In Sec. 3.7, the limitation on the MTI improvement factor due to antenna scan modulation was discussed, and Eq. (3.46) gave the limitation when the MTI processor consisted of n delay-line cancelers in cascade. Antenna scan modulation is affected by the change in amplitude from pulse to pulse caused by the shape of the antenna pattern. It is possible in an AMTI radar to compensate for this change in amplitude by adding half of the needed correction to one pulse and subtracting half from the other pulse. The mechanization for this form of scan-motion compensation is similar to the DPCA compensation described previously except that the difference signal is applied in phase with the sum signal and is amplified by an amount determined by the antenna rotation between pulses. It is also possible to combine the DPCA and antenna scan-motion compensation by properly scaling and applying the difference pattern both in phase and quadrature.

Antenna Sidelobes.[91] If the antenna sidelobes of an AMTI radar are not sufficiently low, the clutter that enters the receiver via the sidelobes can set a limit to the improvement factor equal to

$$I_{SL} = \frac{K\int_{-\pi}^{+\pi} G^2(\theta)\, d\theta}{\int_{SL} G^2(\theta)\, d\theta} \qquad [3.71]$$

where K is the average gain of the delay-line canceler, and $G^2(\theta)$ is the one-way power gain of the antenna in the plane of the ground surface. The integral in the denominator is taken outside the main-beam region, and it assumed the sidelobes are well distributed in azimuth. This limitation to the improvement factor would be one of the many inserted into Eq. (3.41) to find the overall MTI improvement factor for the radar.

Space-Time Adaptive Processing (STAP) When greater clutter attenuation is required of an AMTI radar than can be achieved with conventional DPCA, adaptivity in both the

antenna pattern and the doppler processing can be considered. Both forms of adaptivity, spatial and temporal, are used together in what is known as *STAP*. Spatial and temporal adaptivity will be briefly discussed individually before discussing their combination as STAP.

Adaptive Antennas The adaptive antenna is a phased array that automatically adjusts the phase and amplitude at each element to place one or more antenna-pattern nulls in the direction of external noise, jamming, or interference for the purpose of reducing or eliminating unwanted signals that enter the receiver via the antenna.[92–94] It is also possible to employ an adaptive antenna to place nulls in the direction of large clutter echoes so as to act as a *spatial* filter, something that can be of importance for AMTI.[95] On the basis of the signals received at the individual elements of the array antenna, algorithms in the adaptive processor determine the phase and amplitude weights that should be applied at each element of the receiving array to maximize the signal-to-noise ratio. *Noise* in this case can be considered as all unwanted signals that arrive at the antenna. It can include clutter echoes, jamming, and interference. Adaptive antennas can automatically compensate for mechanical or electrical errors in an antenna by sensing the errors and applying corrective signals. They can also compensate for failed elements, radome effects, and blockage of the aperture from nearby structures. Any adaptive system must be able to distinguish desired from undesired signals. Thus an adaptive antenna requires some *a priori* knowledge of the desired signal, such as it direction, waveform, doppler, or statistical properties.

Adaptive MTI The adaptive antenna places its nulls so as to minimize the clutter (or other interference) that enters via the antenna sidelobes. A transversal filter, such as was shown in Fig. 3.12, is similar in some respects to an array antenna in that there are a number of equally spaced taps whose outputs can be weighted to provide the doppler-filter response to select moving targets and reject clutter. Analogous to the adaptive antenna, it is possible to have an *adaptive MTI* (an adaptive doppler filter) which selects the necessary weights for the taps of the transversal filter to adaptively maximize the signal-to-clutter ratio on the basis of its doppler frequency spectrum.[96,97] If there were only a single point-clutter echo, the adaptive MTI filter would place the nulls it has available at the frequency that corresponds to its doppler frequency. If the clutter were distributed over a range of doppler frequencies (as might be the echoes from rain in an atmosphere with wind shear), the nulls of the adaptive MTI filter would be automatically placed over the doppler region occupied by the clutter. A three-pulse adaptive canceler, for example, with three zeros to place, can adaptively locate three nulls at three different frequencies, or it can place the three nulls so as to make a single wide notch depending on the nature of the clutter spectrum, or it can place its three nulls at the same doppler frequency for greater attenuation. Also, if the clutter spectrum varies with range, the filter can automatically adapt and change its weights so as to continue to maximize the signal-to-clutter ratio. Adaptive MTI can also handle bimodal clutter, as when surface clutter and weather clutter occur in the same range resolution cell.

STAP[98–100] The benefits of adaptive antenna (spatial) processing and adaptive doppler (temporal) processing can be combined in a synergistic manner to achieve improved

performance of AMTI radar. The combination of the two is called *space-time adaptive processing*, (STAP). A highly simplified block diagram of STAP is shown in Fig. 3.41. The antenna is a linear phased array of N elements. At each element of the array there is a tapped delay line that processes K pulses. The $K - 1$ time delays between the taps are each equal to the pulse repetition interval. The K pulses constitute a coherent processing interval (CPI). At each range resolution cell there are $N \times K$ outputs that are processed by a suitable algorithm to obtain W_{nk}, the $N \times K$ adaptive weights that are necessary for maximizing the signal-to-noise ratio. At the output of each tap there is an adaptive processor (not shown) that compares the received signal, V_{nk}, with the output of the summer, V_Σ, to develop the proper weight. The signal V_{kn} is the output of the kth pulse from the nth element of the array. The system output is

$$V_\Sigma = \sum_{k=1}^{K} \sum_{n=1}^{N} W_{nk} V_{nk} \qquad [3.72]$$

These quantities are complex in that both phase and amplitude are employed in the adaptive process. The signal processing is linear and simultaneously controls the antenna pattern and the doppler filter response. The direction of the receiving antenna beam is determined by steering signals injected into the adaptive array control circuits at each element. Being a phased array with control of the amplitude and phase weights, the antenna can be made to perform DPCA to compensate for the broadening of the clutter spectrum caused by platform motion. Adaptive processing reduces the response in the spatial or the temporal domains only when there is clutter or other interference that is to be eliminated.

When nulls are placed in the sidelobe region, the shape of the main beam can be distorted. If this occurs within the CPI, the main-beam clutter will not be fully canceled. In an adaptive antenna such as STAP, some of the available spatial degrees of freedom can be used to maintain the shape of the main beam when nulls are placed in the sidelobe region.

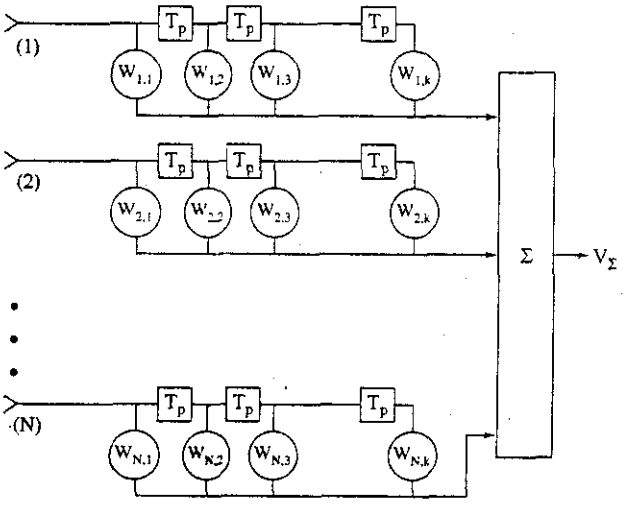

Figure 3.41 A highly simplified block diagram of space-time adaptive processing, consisting of an array antenna of N elements and a doppler processor with K weights.

In brief, STAP can provide the following capabilities for an AMTI radar:

- Reduction in clutter by adaptively locating the nulls of the doppler filter response to attenuate the clutter spectrum.
- Reduction of clutter, jamming, and interference that enters the receiver via the antenna sidelobes by adaptively placing the antenna nulls in the direction of the unwanted clutter echoes and interfering signals. This takes some of the burden off the doppler processor, especially when the clutter is not at zero doppler (as would be the echoes from rain or chaff).
- When clutter echo that enters the antenna sidelobes has the same doppler frequency as an aircraft target echo in the main beam, doppler filtering alone might not be able to separate the clutter echo from the target echo, but the antenna pattern nulls introduced by STAP will.
- Adaptive selection of antenna weights to provide platform motion compensation.
- Ability to compensate for radar scattering from aircraft structures near the antenna, failed antenna elements, or errors in the antenna array.

The more elements in the array and the more pulses processed during each CPI, the greater will be the degrees of freedom that can be used in placing spatial and temporal nulls. That flexibility, however, comes with a price—sometimes a severe price. The greater the number of antenna elements and the greater the number of pulses to be processed, the greater the demand placed on the digital processing and the longer it might take for the adaptive weights to be computed. In practice, therefore, there will be a limit on the number of adaptive elements that can be employed and the number of pulses to be processed. For this reason, it is unusual to have a fully adaptive array (an adaptive processor at each element) when the number of elements in the array antenna is large.

3.9 PULSE DOPPLER RADAR

In an MTI radar the prf is chosen so that there are no range ambiguities, but there are usually many doppler ambiguities, or blind speeds. The MTI radar has proven to be a fine method for the detection of moving targets in clutter if the effect of the blind speeds can be tolerated. There are important situations, however, where the proliferation of blind speeds can eliminate a large portion of the available *doppler space* (the doppler region where desired moving targets can be detected). A reduction in the available doppler space causes loss in the detection of moving targets. Blind speeds become troublesome when the radar frequency is increased. An increase in frequency, when the prf remains constant, means a decrease in the first blind speed [according to Eq. (3.12)] and more of them will appear within the desired doppler space. The degradation of performance caused by blind speeds can be especially difficult in an airborne radar that has to operate at a high microwave frequency in order to have a narrow beamwidth with the relatively small antenna size that can be tolerated in an aircraft. Also, as described in the previous section, airborne radars suffer a widening of the clutter spectral width due to platform motion, further aggravating the reduction in the doppler space available for detection of targets. The

result is that at the higher microwave frequencies, the MTI technique needs to be replaced since it cannot perform satisfactorily. The luxury of having no range ambiguities in a low-prf MTI radar has to be sacrificed in order to eliminate the serious consequences of the ambiguous doppler and its accompanying blind speeds. Increasing the prf increases the first blind speed [Eq. (3.12)] and reduces the number of nulls found within the doppler space. A high prf, however, can increase the problem of range ambiguities. Thus the trading of doppler ambiguities (blind speeds) for range ambiguities is something that has to be tolerated in order to obtain good detection of moving targets at the high microwave frequencies.

A radar that increases its prf high enough to avoid the problems of blind speeds is a called a *pulse doppler radar.* More precisely, a *high-prf pulse doppler radar* is one with no blind speeds within the doppler space. In some situations, however, it may be beneficial to operate at a slightly lower prf and accept both range and doppler ambiguities. Such a radar is called a *medium-prf pulse doppler radar.* Thus there are three different types of pulse radars that use doppler. They differ in their prfs and the type of ambiguities they are willing to tolerate. These are:

1. The *MTI* with no range ambiguities and many doppler ambiguities.
2. The *high-prf pulse doppler* with just the opposite: many range ambiguities and no doppler ambiguities.
3. The *medium-prf pulse doppler radar* with some of each.

At one time there was a significant difference in the type of transmitter and the signal processing techniques used for MTI and pulse doppler radar. In the early days of MTI radar, a magnetron oscillator was commonly used as the transmitter. A pulse doppler radar, on the other hand, usually used a high-power amplifier transmitter such as the klystron. Both MTI and pulse doppler radars now use a high-power amplifier of some sort. The MTI radar originally used analog delay-line cancelers and the pulse doppler radar used analog filter banks. Both now use digital processing and an MTI radar can use a filter bank (as did the MTD described in Sec. 3.6). Thus the equipment differences between the two are no longer significant enough to distinguish one from the other. The basic difference between an MTI and a pulse doppler radar is the prf and duty cycle that each employ. Another significant difference is that the pulse doppler radar generally receives much more clutter than an MTI radar (because of the foldover in range of clutter echoes when ambiguous prfs are employed), so that the pulse doppler radar requires a much greater improvement factor than does an MTI radar of comparable performance.

High-prf Pulse Doppler Radar The pulse doppler radar will be described here in terms of an airborne radar[101,102] such as AWACS (Airborne Warning and Control System).* Figure 3.42 is a sketch of the airborne geometry showing the *main beam* of the antenna, the *antenna sidelobes* which illuminate clutter over a wide range of viewing angles, and the *altitude return* which is reflected from the ground directly below the radar. It will be recalled that a train of pulses, like that of a pulse doppler radar, produces a line spectrum,

*The terms AEW, AWACS, and AEW&C have all been used to indicate an *airborne air-surveillance radar.*

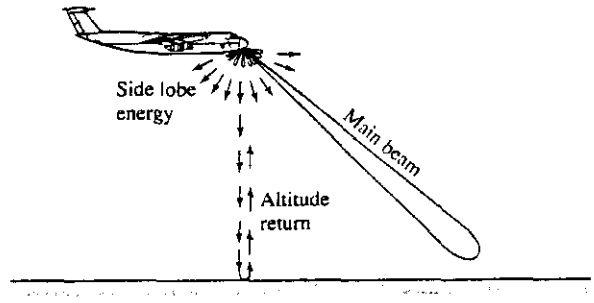

Figure 3.42 Sketch of the geometry of an airborne pulse doppler radar illustrating the scanning main beam, the antenna sidelobes illuminating ground clutter, and the strong altitude return from directly below the radar.

Fig. 3.43a, with the separation between spectral lines equal to the prf. Figure 3.43b illustrates the carrier frequency f_0 and the two adjacent spectral lines at $f_0 + f_p$ and $f_0 - f_p$, where f_p is the prf. The spectrum of the received echo signal is not a pure line spectrum because of the finite time on target and other factors such as modulations introduced by the clutter echoes. At the carrier frequency f_0 there will be a large return due to echoes received from directly below the radar. Such echoes can be relatively large. This altitude

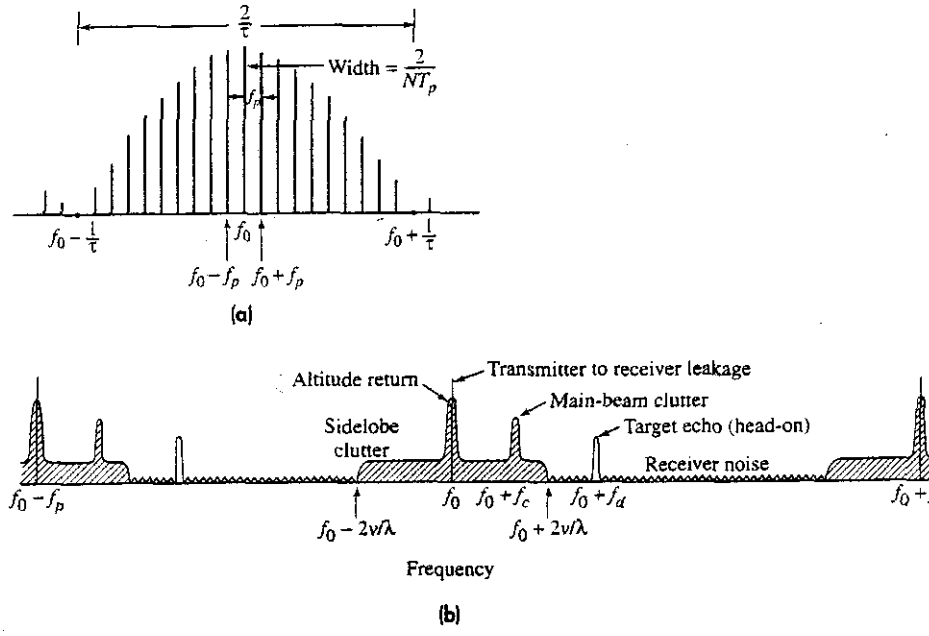

Figure 3.43 (a) Transmitted spectrum of a train of N rectangular sinewave pulses of carrier frequency f_0, width τ, pulse repetition frequency $f_p = 1/T_p$, and total duration NT_p. Null width of the spectral lines (not indicated in the figure) is $2/NT_p$. (b) Portion of the received signal spectrum in the vicinity of the RF carrier frequency f_0, for a high-prf pulse doppler radar.

return has no doppler frequency shift since its relative velocity is zero. Because of fold-over, or aliasing, the altitude line (and the rest of the spectrum) is repeated at frequencies $f_0 \pm nf_p$, where n is an integer. There can also be leakage of the transmitter signal into the receiver. The altitude line and the transmitter leakage can be removed with a notch filter centered at f_0.

The antenna sidelobes will illuminate clutter over a large range of incidence angles (from 0 to almost 90°). Thus there can be clutter echoes extending almost $\pm 2v/\lambda$ about the carrier frequency and the other spectral lines, where v is the radar's absolute velocity. For convenience, the shape of the sidelobe clutter spectral region is shown in Fig. 3.43b as uniform. In practice, however, the shape will not be uniform as shown. Sidelobe clutter echoes usually decrease in amplitude the farther their doppler-shifted echo frequency is from the carrier.

The antenna sidelobe clutter is large in a high-prf pulse doppler radar since there are many range-ambiguous pulses simultaneously illuminating the clutter. With a duty cycle of 50 percent, the antenna sidelobes are simultaneously illuminating half the total clutter within the radar's coverage, much more than would be seen by a low-prf AMTI radar. The large sidelobe clutter viewed by a pulse doppler radar is a reason why it requires a higher improvement factor than an AMTI radar of equivalent performance. The greater improvement factor required of a pulse doppler radar does not necessarily mean it can detect targets in clutter better than the AMTI. (It just means the pulse doppler radar designer has a tougher task to accomplish than does the AMTI radar designer.) One must look further to determine the relative capability of the two radars and not rely only on the improvement factor as the measure of relative merit.

The sidelobe clutter region is seen to extend over a relatively large portion of the doppler space. To detect aircraft targets within the sidelobe clutter region, a bank of narrowband doppler filters with adaptive thresholds can be used. To keep the sidelobe clutter from swamping the detection of small targets, the antenna must have exceptionally low sidelobes compared to conventional antennas. The success of the *S*-band AWACS high-prf pulse doppler radar depended on achieving, for the first time, antennas with ultralow sidelobes (Sec. 9.13).[103]

The clutter echo seen by the main beam can be relatively large in amplitude, and is shown in Fig. 3.43b. It lies somewhere within the sidelobe clutter region. As the antenna beam scans in angle, the doppler frequency of the main-beam clutter varies, so its location within the echo-signal spectrum will also vary. Main-beam clutter can be removed by a tunable filter that tracks the doppler-shifted frequency of the clutter echo. Platform motion can also affect the width of the main-beam clutter just as it does with an AMTI. The broadening of the main-beam clutter spectrum in this type of pulse doppler radar, however, usually is not a problem since the spectral width, even when broadened, is small compared to the high prf that is employed.

In Fig. 3.43b it can be seen that there is a region of the clutter spectrum where only receiver noise is present. This is the *clutter-free* or *receiver-noise region*, and it corresponds to viewing nose-on approaching targets with high closing velocities that result in high doppler shifts. The presence of a clutter-free region is an important advantage of a high-prf pulse doppler radar, especially if detecting high-speed closing targets at long range is required. On the other hand, if the relative velocity of the target is low, as when

targets are viewed tail-on or when the target is on a crossing trajectory, the echo can fall within the sidelobe clutter region and its detectability is much less than a high-speed target in the clutter-free region. Such targets with low doppler frequency shifts are detected by a high-prf pulse doppler radar at significantly shorter ranges than high-speed targets that are in the clutter-free region.

The prf of an X-band high-prf pulse doppler radar designed for use with a military airborne fighter/interceptor might be from 100 to 300 kHz. With such a high prf, there is not much room for long pulses. It is not unusual for the duty cycles of high-prf pulse doppler radars to have values from 0.3 to 0.5. Such radars might operate with only one range gate. Only one set of doppler filters is needed, rather than one set for each of the many range gates of radars that employ lower duty cycles.

As mentioned, the prf is chosen high enough so that there are no doppler ambiguities and no foldover of the clutter spectrum. The prf required can be determined from an examination of the spectrum of Fig. 3.43b. It has been shown[104,105] that if the center of the doppler filter bank is always maintained at the frequency of the main-beam clutter, the minimum prf that can be used is $4v_T/\lambda$, where v_T is the maximum ground speed of the target. For this to occur, the main-beam clutter frequency must be known and a tracking device used to keep the filter bank centered at the main-beam clutter frequency. If, on the other hand, the doppler filter bank is fixed with its center always at the radar transmitted frequency, f_0, the prf might be as large as $4v_T/\lambda + 2v_R/\lambda$, depending on the maximum angle scan in azimuth, where v_R = radar platform velocity. When the doppler filter bank is centered on the radar frequency, more filters are required than when it is centered on the doppler of the main-beam clutter.

Eclipsing Loss Since the pulse doppler radar cannot receive when it is transmitting, the high duty cycle can result in a loss if the echo signal arrives when a pulse is being radiated and the receiver is gated (turned) off. This is called *eclipsing loss*, and can be anything between zero and a large value depending on the exact location of the received echo pulse within the timing of the transmission.[106] There are some things that might be considered, however, to reduce the effects of eclipsing loss. The degree of eclipsing varies as the target range changes with time so eclipsing can cause periodic holes in the coverage. A rapidly approaching target, on the other hand, will not remain eclipsed for long, so that detections will occur at a slightly shorter range when eclipsing is present. With low relative-velocity targets, the time during which eclipsing occurs may be reduced by using more than one prf. If a single target is being tracked, a change in prf at the appropriate time can keep the target echo from arriving when the receiver is gated off. A reduction of the duty cycle and an increase in the number of range gates will reduce the effect of eclipsing, but if the prf is too low, one no longer has a high-prf pulse doppler radar.[107]

Resolution of Range Ambiguities The high-prf pulse doppler radar results in many range ambiguities. These can be resolved by use of multiple prfs, although other methods that involve modulating the RF frequency or the pulse characteristics are possible.[108] From the measurement of the ambiguous ranges on two prfs, the true range can be determined similar to what was outlined in Sec. 2.10. Three different prfs are usually used rather than two, in order to increase the unambiguous range that can be achieved and to reduce the

possibility of "ghosting." (A "ghost" can occur if there is more than one target present and if an ambiguous range of one target is the same as one of the ambiguous ranges of another target. The false coincidence of the two will result in a decision being made that this is the true range of a target, which it is not.) The ratios of the prfs are usually related by relatively prime integers (that is, they do not have a common factor among them). If, for example, the prfs were in the ratio 7, 8, and 9, the unambiguous range from these three prfs would be $7 \times 9 = 63$ times that of the middle prf. The Chinese remainder theorem has been used to calculate the true range from the unambiguous measurements,[108] but there are other algorithms available for the same purpose.[109]

Other Considerations A high-prf pulse doppler radar that uses three different prfs to obtain the true range measurement of a target requires that a target detection and range measurement be made on each of the three prfs. This results in a power-aperture product (or whatever other appropriate figure of merit is used) three times greater than a radar that doesn't require redundant transmissions. For a given range performance, the high-prf pulse doppler radar will therefore require much larger transmitter average power than an AMTI radar, if everything else remains unchanged. The high prf and high duty cycle also result in poor resolution of multiple targets and may make it difficult to determine the number of military aircraft that might be flying in close formation. A high-prf pulse doppler radar is more complex and more costly than an AMTI. On the other hand, because of the absence of doppler ambiguities and good doppler processing, this radar produces a good measurement of the target's radial velocity. Detection of aircraft targets based only on extracting the doppler without attempting to resolve range ambiguities can produce large detection ranges. This is called the *velocity search mode* and is often employed for the initial detection of targets at long range with a multimode airborne radar.

The airborne air-surveillance radar application can be accomplished equally well with the AMTI approach (the U.S. Navy's E2 aircraft radar at UHF) or the pulse doppler approach (the U.S. Air Force E3 AWACS aircraft radar at *S* band). The performance of these two surveillance radars can be said to be comparable;[110] but in the past, the cost of the E2 AMTI system has been considerably less than that of the high-prf pulse doppler AWACS E3 system. The AMTI method, however, cannot be used at the higher microwave frequencies that are necessary for military fighter/attack aircraft.

Medium-prf Pulse Doppler Radar A medium-prf pulse doppler radar is one whose prf is between that of the high-prf pulse doppler and the MTI radar. It therefore has both range and doppler ambiguities. The medium prf results in less clutter being seen by the antenna sidelobes than the high-prf radar since there are fewer pulses viewing ambiguous range cells. The lower clutter level in the sidelobe region of the echo signal spectrum allows better detection of moving targets with low doppler velocity (such as those viewed at tail-aspect as well as those with near-crossing trajectories), and will detect slow targets at longer ranges than can the high-prf pulse doppler. The reduced prf, however, causes the prf lines to become much closer, the sidelobe clutter regions will overlap, and there is no clutter-free region as in the high-prf pulse doppler. Although the lower prfs cause the sidelobe clutter from higher prf lines in the spectrum to fold over and increase the sidelobe

clutter, it does not completely eliminate the benefit obtained by lowering the clutter when fewer pulses are received with the medium prf.

In engineering, few things are ever perfect. Compromises are often necessary. This is true when trying to select which of the two types of pulse doppler radars should be used. The high-prf pulse doppler radar has good performance against high-speed closing targets; but poorer performance against targets with low relative velocity. The opposite is true for the medium-prf pulse doppler. It does much better against slower targets than does the high prf, but it is much poorer against high-speed targets. According to Morris,[111] the high-prf pulse doppler radar can typically provide 50 percent greater detection range against high-speed, head-on targets than can a medium-prf pulse doppler radar with the same average transmitter power. On the other hand, the medium-prf pulse doppler radar is superior for receding (low relative velocity) targets at altitudes less than 10,000 ft. In the original *S*-band AWACS procurement, one major bidder proposed high-prf pulse doppler, the other major bidder proposed medium prf. The high-prf radar was selected, but either probably could have done the job.

In the *X*-band airborne radar designed for fighter/interceptor aircraft, it is not unusual to employ both high-prf and medium-prf modes interleaved so as to obtain the advantages of each. Such airborne radars operate with a number of modes, including a low-prf radar mode used when the antenna beam is looking up where it doesn't see clutter and doesn't need doppler processing. When high-prf and medium-prf pulse doppler waveforms are interleaved, more time is required to do both (if nothing else is done to maintain constant the time to make a detection). The transmitter power and antenna scanning must be increased to allow a detection decision in shorter time or there must be a sacrifice in the detection range and/or the time to make a decision.

The altitude line in the medium-prf pulse doppler can be removed by range gating or by filtering, whereas in the high-prf pulse doppler it can only be removed by filtering. Range gating permits the detection of low relative-velocity targets near the radar transmitted frequency that might be rejected in a high-prf system where the altitude return is rejected by filtering.

Because of the lower duty cycle of the medium-prf pulse doppler radar, its range accuracy and ability to resolve multiple targets in range are better than those of a high-prf system. The medium-prf pulse doppler, just as with the high-prf, cannot employ sensitivity time control (STC) to reduce the effects of clutter at short ranges as can a low-prf radar.

It is important in the medium-prf pulse doppler, just as with the high-prf pulse doppler, to have antennas with reduced sidelobe levels in order to minimize the clutter that enters the radar via the sidelobes.

Resolution of Range Ambiguities[112] As with the high-prf pulse doppler radar, range ambiguities that occur in the medium-prf system are resolved by using transmissions on three different prfs. In the medium-prf pulse doppler radar, however, there are regions of doppler space where the main-beam clutter might be so strong that detection of targets is not practical. In order to insure that a target will be detected outside of these *blind zones* on at least three prfs, a medium-prf pulse doppler has to transmit on seven or eight different prfs. An example is shown in Fig. 3.44. The upper part of the figure depicts the

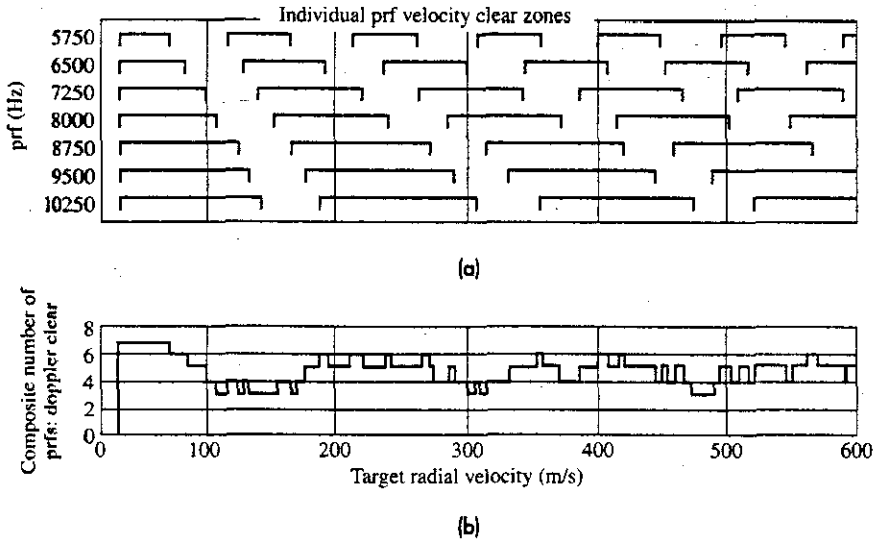

Figure 3.44 (Upper) The clear zones available with seven different medium prfs in which target detection can take place. (Lower) The number of prfs in which a target can be seen in a clear zone, as a function of the target's radial velocity.
[This illustration was originally provided the author by the late Frederick C. Williams.]

clear zones of seven prfs. The lower part of the figure shows the number of clear zones available as a function of the target's radial velocity. The minimum number of clear zones is three in this case, as required for resolving range ambiguities. The fact that seven or eight different transmissions have to be used means that the radar's power-aperture product has to be much larger than that of a high-prf pulse doppler radar if equivalent range performance is to be had, and even higher than that of an AMTI radar with equivalent detection range. Each time the prf is changed there needs to be a settling time before processing begins, which can reduce the range of detection. If the processor requires *fill pulses* for each prf to increase the doppler filter performance, this can also reduce the range performance.

The prfs used in a medium-prf pulse doppler radar might extend over a range of values of almost two-to-one. If the pulse width remains constant, the range of the radar will vary as the prf is changed since the transmitter duty cycle and total energy of the radiated signal will depend on the prf (assuming the peak power is constant, which it usually is). This variability in the radar range with prf is undesirable. Furthermore, high-power radar transmitters generally like to operate with a constant duty cycle in order to minimize the changes in operating conditions and heating cycles. It is important, therefore, to maintain the duty-cycle constant. This can be done in the medium-prf pulse doppler radar by changing the pulse width as the prf is changed. The change in pulse width requires that the bandwidth of the receiver's matched filter be altered accordingly.

The Three prfs[113] Throughout this section, there have been comparisons made among the high-prf, medium-prf, and low-prf radars. Table 3.2 summarizes "typical" values that characterize these three prf regimes for airborne radar. The values of prf and duty cycle

Table 3.2 Comparison of the three prfs

Radar	prf*	Duty Cycle*
X-band high-prf pulse doppler	100–300 kHz	< 0.5
X-band medium-prf pulse doppler	10–30 kHz	0.05
X-band low-prf pulse radar	1–3 kHz	0.005
UHF low-prf AMTI	300 Hz	Low

*These are illustrative values only. Actual radars can have values that extend to either side of what is shown.

listed in this table are illustrative only (especially the duty cycles). Airborne radars can be, and often are, found outside these values. The three entries for *X*-band apply to radars used for fighter/interceptor applications. The low-prf *X* band airborne pulse radar does not have doppler processing to detect moving aircraft in clutter. It is mainly used in a *look-up* mode where no clutter is seen rather than in a *look-down* mode that sees clutter. For pulse doppler radars at frequencies other than *X* band, the prfs would be in proportion to the RF frequency. For comparison, a UHF AMTI wide-area surveillance radar with low prf is included in the table. Not included are the wide-area surveillance radars at *S* band with either medium or high-prf waveforms. The characteristics of airborne doppler radars at each of the three prf regimes are summarized below:

High-prf pulse doppler:

- No ambiguities in doppler frequency, no blind speeds, but many range ambiguities.
- Range ambiguities can be resolved by transmitting three redundant waveforms, each at a different prf.
- Transmitter leakage and altitude return are removed by filtering.
- Main-beam clutter is removed by a tunable filter.
- High closing-speed aircraft are detected at long range in the clutter-free region.
- There is poor detection of low radial-speed targets that are masked in the frequency domain by short-range sidelobe clutter folded over in range.
- Often only a single range gate is employed, but with a large doppler filter bank.
- For comparable performance, a much larger improvement factor is required than lower prf systems since the high prf results in more clutter being viewed by the antenna sidelobes.
- The antenna sidelobes must be quite low in order to minimize the sidelobe clutter.
- Range accuracy and the ability to resolve multiple targets in range are poorer than with other radars.

Medium-prf pulse doppler:

- Has both range and doppler ambiguities.
- There is no clutter-free region as in the high-prf system, so detection of high-speed targets will not be as good as with the high-prf system.

- Fewer range ambiguities mean that there will be less clutter seen in the antenna sidelobes so that targets with low relative speeds will be detected at longer range than with a high-prf system.
- The trade-off of detectability of high-speed targets for better detection of low-speed targets often makes the medium-prf system preferred over the high-prf system for airborne fighter/interceptor radar applications, if only a single system is used.
- The altitude return can be eliminated by range gating.
- More range gates are required than in the high-prf system, but the number of doppler filters at each range gate is less.
- Seven or eight different prfs must be used to insure that a target will have the proper doppler frequency to be detected on at least three prfs in order to resolve range ambiguities.
- For comparable range performance the large number of redundant waveforms means that the transmitter must be larger.
- Better range accuracy and range resolution are available than with high-prf systems.
- The antenna must also have low sidelobes to reduce the sidelobe clutter.

Low-prf AMTI:

- No range ambiguities, but many doppler ambiguities (blind speeds).
- Requires TACCAR and DPCA to remove effects of platform motion.
- Operates clutter free at long range where no clutter is seen due to curvature of the earth.
- Sidelobe clutter is usually not as important as it is in pulse doppler systems.
- Best employed at UHF or perhaps *L* band. Increased blind speeds and the lower effectiveness of platform motion compensation prevent its use at the higher microwave frequencies.
- The lower RF frequency (UHF) of the AMTI radar results in wider antenna beamwidths than a higher frequency (*S* band) pulse doppler radar whose mission is wide-area air-surveillance.
- Because there are no range ambiguities to be resolved, redundant waveforms with multiple prfs are not needed.
- For comparable performance the required product of average power and antenna aperture is less than for pulse doppler radars.
- Usually simpler than pulse doppler radars.
- Cost is generally much less than pulse doppler radars of comparable performance.
- AMTI cannot be used in fighter/interceptor *X*-band radars for look-down detection of targets in clutter. The low-prf mode without doppler processing, however, is used to advantage when there is no clutter present, as when the antenna is looking up or the target is at a range less than the height of the radar over the ground so that near-in ground clutter that enters via the sidelobes can be gated out.

Airborne Air-Surveillance Radar Antennas Airborne air-surveillance radars such as the U.S. Navy's E2 AEW (AMTI) radar at UHF (Fig. 3.45a) and the U.S. Air Force's E3 AWACS (high-prf pulse doppler) radar at S band (Fig. 3.45b) both employ a large externally mounted rotodome antenna. (The *rotodome* is a radome-enclosed antenna in which

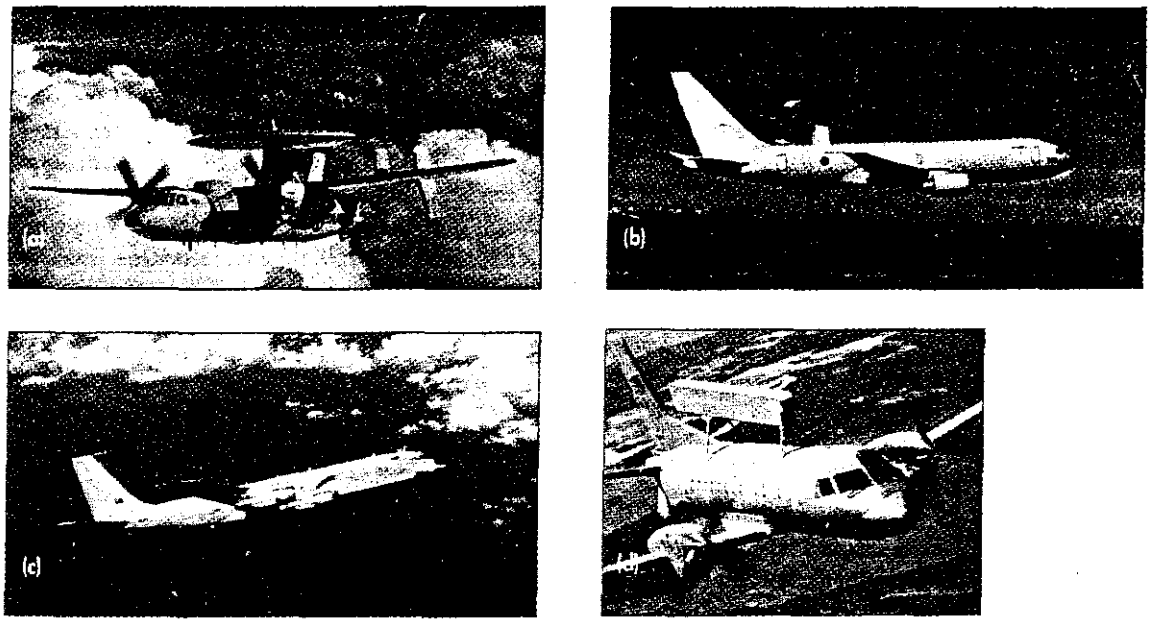

Figure 3.45 Photos of four different types of airborne air-surveillance radars. (a) U.S. Navy aircraft-carrier-based E2C Hawkeye Airborne Early Warning (AEW) radar operating at UHF. A rotating array of Yagi end-fire antenna elements is enclosed within a 24-ft by 2.5-ft rotodome. The small cone-shaped addition on top of the rotodome is a satellite communications (SATCOM) antenna.
(Courtesy of Northrop Grumman Corp.)

(b) U.S. Air Force E3 AWACS S-band pulse doppler radar with a rotating 24-ft by 5-ft ultralow-sidelobe planar array in a rotodome. This particular example is that of the Japan Air Self-Defense Force mounted in a 767 aircraft. The original AWACS was in a 707 aircraft.
(Courtesy of Northrop Grumman Corporation.)

(c) Phalcon L-band Airborne Early Warning System that employs "conformally" mounted electronically scanned phased array radars mounted on the left and right side of the forward part of the fuselage. This example is on a 707 aircraft. The arrays are 12 by 2 m (39 by 6.6 ft), and extend 1.5 ft out from the side of the fuselage. Each side array contains 600 solid-state T/R (transmit/receive) modules. The 3-m (9.8-ft) diameter radome in the nose of the aircraft provides coverage of the forward sector. A total of 280° of azimuth coverage is obtained. Provision was made for installing smaller 4-m by 2-m (13-ft by 6.6-ft) phased arrays along the sides of the rear fuselage to extend the coverage to 360°.
(Courtesy IAI ELTA Electronics Industries, Ltd., Israel.)

(d) Erieye S-band AEW&C pulse doppler radar with back-to-back electronically scanned phased array antennas mounted in a dorsal unit on top of a Saab 340B aircraft. There are 192 solid-state T/R modules in the 8-m-long array. Each side of the array covers an azimuth sector of 120°.
(Courtesy of Ericsson Microwave Systems AB, Molndal, Sweden.)

the antenna and radome rotate together.) The UHF radar antenna is an array of Yagi endfire radiators that provide the equivalent of vertical aperture even though it has a low physical profile. The antenna for the *S*-band AWACS is an ultralow-sidelobe array of slotted waveguides. Both the E2 and E3 antennas have comparable effective aperture areas, even though their antenna gains are different. Russian (formerly Soviet Union) AEW radars also have used rotodomes. Phased arrays mounted conformally around the aircraft are employed in the Israeli Phalcon *L*-band AEW radar (Fig. 3.45c). The Swedish *S*-band Eyrieye AEW radar (Fig. 3.45d) uses a phased array mounted along the top of the aircraft's fuselage to view on either side of the aircraft. The Eyrieye was designed for a small aircraft and had a shorter range for the same size target than larger systems. An electronically steerable phased array antenna, as in the Phalcon, can be mounted to conform to the aircraft's structure or externally along the fuselage. It is difficult with either fixed phased array method to achieve 360° azimuth coverage or to obtain as large an antenna as can be placed in a rotodome. The rotodome can be mounted relatively high above the aircraft's fuselage so as to minimize blockage from the wings and engines that might result in unwanted sidelobes. It can be more difficult to avoid antenna blockage from the aircraft's structure with flush-mounted phased arrays. The mechanical disadvantages of a rotodome have not been a limitation for past AEW radars. The rotodome can have aerodynamic lift to compensate in part for its weight. In spite of its limitations and the aesthetic desire to replace it with conformal antennas, the rotodome has proven to be an excellent choice for long-range AEW aircraft that must have 360° coverage. Another method for using an electronically scanned phased array is the Wedgetail system shown in Fig. 1.14.

Surface-Based Pulse Doppler Radars Most of the discussion in this section on pulse doppler radar has been concerned with airborne applications. Pulse doppler radars have also been used with land-based and shipborne radar to detect small targets in clutter, especially high-speed hostile targets rapidly approaching a military air-defense system. Pulse doppler surface-based radars have been used at *L* band for both short and long-range detection of aircraft and missiles, and at *X* band for detection of low altitude antiship missiles as they appear at short range just as they come within the horizon. A *C*-band shipborne radar for detection of missiles at ranges of 10 km has been described[114] as using a prf of 4 kHz and a 45-rpm antenna, with unambiguous range of 37.5 km and unambiguous velocity of 110 m/s.

3.10 OTHER DOPPLER RADAR TOPICS

Noncoherent MTI In an MTI radar there must be a reference signal to recognize that the echo signal of a moving target is shifted in frequency by the doppler effect. In the type of MTI radars discussed thus far, often called *coherent MTI* radars, the reference signal is an oscillator whose phase is referenced to the transmitter signal. The echo signal from clutter also has the characteristics of the transmitted signal and can be used as a reference to extract the doppler frequency shift of the target echo signal. Since the clutter echo and

the moving target echo appear together at the input to the receiver, an internal reference signal is not needed. A radar that uses the clutter echo as the reference signal to extract the doppler-shifted target echo is known as a *noncoherent MTI* radar. It might also be called an *externally coherent MTI.*

A simple block diagram of a noncoherent MTI with a power oscillator as the transmitter is shown in Fig. 3.46. It is similar to the block diagram of a conventional pulse radar, except for the MTI filter, which is usually a delay-line canceler. The detector following the IF amplifier is a more or less conventional amplitude detector rather than a phase detector that requires a coho as reference. It is a nonlinear device which acts to multiply the clutter signal and the doppler-shifted moving target signal to produce the doppler (difference frequency) that is then extracted by the MTI filter.

The advantage of the noncoherent MTI is its relative simplicity. It was used in the past for both land-based and airborne MTI applications. A limitation is that it requires that clutter echo be present along with the target echo. This seems, at first glance, to be a reasonable requirement to achieve since an MTI radar would not be needed if there were no clutter. Clutter, however, is seldom spatially uniform. Since the target will be canceled by the delay-line canceler if there were no clutter present, the delay-line canceler must be switched out when there is no clutter within the radar resolution cell that contains the target. Some method is required to recognize the presence or absence of clutter and to rapidly switch the delay-line canceler in and out. Because of the patchy nature of clutter, the delay-line canceler might have to be switched in and out multiple times as the pulse travels out in range.

The improvement factor of a noncoherent MTI will usually be much poorer than that of a coherent MTI.[115] Since the clutter "reference signal" is not separately available, a Q channel cannot be employed. Significant loss, therefore, can occur due to blind phases (Sec. 3.3). Furthermore, the clutter echo as the reference signal is likely to be noisier than the internal reference oscillator (coho) of a coherent MTI. The combined effect of all these less than desirable features of a noncoherent MTI does not make this radar an attractive candidate for most MTI applications that require large improvement factors. Noncoherent radar has been successfully used, however, to detect moving ground vehicles with a side-looking airborne radar (SLAR) described in the next subsection.

Airborne Radar Detection of Ground Moving Targets[116,117] AMTI radar and airborne pulse doppler radars for the detection of aircraft can also detect moving ground vehicles when

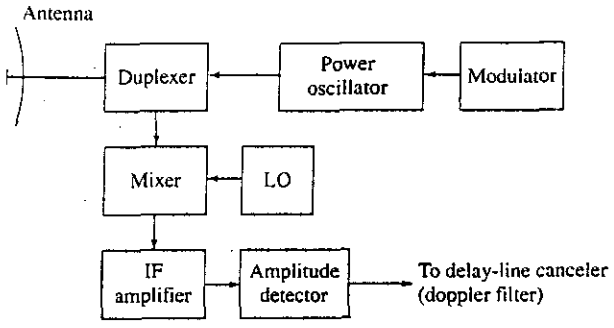

Figure 3.46 Block diagram of a noncoherent MTI radar.

operating over land. Truck and auto traffic on major highways can be present in large numbers, are of large cross section, and travel at speeds that are within the doppler passbands of these radars. The result can be large numbers of unwanted echoes that can overload the radar's tracking computer.

On the other hand, ground vehicles are of interest for military purposes. The mission of airborne battlefield surveillance radars is to detect and track such targets. There are at least four different airborne radar methods for detection of ground moving targets:

- A variant of AMTI called GMTI (ground moving target indication).
- Side-looking airborne radar (SLAR) with noncoherent MTI.
- Synthetic aperture radar (SAR) with doppler filtering.
- Interferometric SAR (InSAR)

Each will be briefly discussed.

GMTI The modern airborne strike/fighter aircraft has as one of its many air-to-surface radar modes the detection of ground moving targets, usually called *ground moving target indication* (GMTI). When the targets of interest are ground vehicles, radar echoes from aircraft are the nuisance targets.

The GMTI mode uses a low or a medium prf, chosen to be unambiguous over the range and doppler frequency coverage of interest. A goal in the design of such radars is to have a low minimum detectable velocity. For a fixed minimum detectable doppler frequency, the minimum detectable velocity will be lower the higher the frequency. Thus K_u or K_a band air-to-surface radars might be more capable of detecting slow-speed targets than X band or lower frequency radars.

The AN/APG-67, a small low-cost X-band airborne radar (weighing only 270 lb) for the F-20 aircraft used a medium-prf waveform to detect ground vehicles within a $\pm 45°$ sector when the vehicle velocity was greater than 5 kt.[118] The maximum range in the GMTI mode was 50 nmi. Tank-type targets could be detected out to 20 nmi range.

A low-prf MTI mode, similar to the GMTI mode, can be used to detect moving ships. The AWACS radar employs a special "maritime mode" specifically designed to detect ships. (Since ships are relatively large targets and sea clutter is much smaller than land clutter, ships can be readily detected with a modest radar with modest resolution, usually without the need for doppler processing.)

SLAR[119, 120] A side-looking airborne radar (SLAR) employs a relatively conventional high-resolution radar in an unconventional manner to obtain a maplike image of a surface scene as well as detect moving targets using noncoherent MTI. An example is the Motorola SLAMMR which is an X-band airborne imaging radar with a 16-ft fixed side-looking antenna, 0.2-μs pulse width, and a magnetron transmitter with 60-W average power. Noncoherent MTI processing uses the clutter echo signal as the reference to extract the doppler-shifted moving target echo. An attenuated version of the SLAR image of the ground usually is superimposed on the moving target detections to aid in geographically locating targets. At each range cell, SLAMMR digitally generates a filter bank with 32 contiguous filters. A form of adaptive threshold is employed at the lower frequency

filters to reduce the effect of the spread of the clutter spectrum due to platform motion. This dynamic biasing of the low-frequency filters allows the filters to adapt to the requirements imposed by the ground clutter in each range cell.[119] It has been said that such a SLAR with noncoherent MTI can extract small moving targets with speeds down to five miles per hour at a range of 50 nmi. Larger, faster targets can be detected out to 80 nmi.

SAR with MTI[121] A synthetic aperture radar (SAR) produces a high-resolution image, or map, of a scene by synthesizing in its processor the equivalent of a large antenna to obtain good resolution in the cross-range direction. High resolution in the range direction is obtained by either a short pulse or pulse compression. A good SAR might have a resolution in range and cross-range of one meter, but it can be much less if desired. A SAR is more complex than the SLAR, but it produces much higher resolution images.

A conventional SAR is normally designed to image stationary objects. Moving targets are smeared, distorted, and misplaced when seen by a SAR. Moving targets can be detected with a SAR if they have a doppler frequency shift greater than the spectral bandwidth of the stationary ground clutter echo. (Clutter in this case *is* the desired signal for a SAR.) This technique has been limited, however, because it needs a prf high enough to avoid doppler foldover of echo signals. A high prf, on the other hand, might give rise to range ambiguities. This method for extracting moving targets with a SAR might not be able to detect moving targets that have a low radial velocity.

Interferometric SAR The resolution cells, or pixels, of a SAR image usually are described by the amplitude of the signal within the pixel. In addition to the amplitude, there is also a phase that can be associated with each pixel. An interferometric SAR is one that takes advantage of the phase information to detect moving targets. The phase information can also be used to obtain a measurement of the height of the object within a pixel,[122,123] but this is not the subject of this subsection.

The original interferometric SAR employed two identical sidelooking antennas mounted longitudinally along the line of travel of the aircraft or space vehicle. They were separated in the horizontal dimension and looked 90° (broadside) to the line of travel. A SAR image of the same scene was formed by each antenna, but at a slightly different time because of the forward travel of the aircraft. Thus the information at a particular pixel obtained by the forward antenna was at a slightly earlier time than the information at the corresponding pixel obtained by the aft (trailing) antenna. If there were a moving target in a particular pixel, the phase would be different in the two images. The phase of a stationary object, however, would be unchanged. Moving targets could then be detected by examining corresponding pairs of pixels in the two images to determine if there were a phase change. (A change in phase with time means there was a doppler frequency shift.) The amount of phase change depended on the separation between the forward and aft antennas, the speed of the aircraft carrying the radar, as well as the speed of the target within the pixel. This technique was capable of detecting slowly moving targets and was a good method for detecting moving targets that appear on SAR images. One of the first applications for the interferometric SAR was the detection and measurement of the radial velocity of ocean currents.[124]

A more sophisticated form of interferometric SAR has been employed for the detection of ground vehicles along with imaging the ground and fixed surface targets, as in the X-band Joint STARS (Joint Surveillance Target Attack Radar System) AN/APY-3 developed by Northrop Grumman. This is a U.S. Air Force/Army airborne battle-management system that detects both moving and fixed targets by an interferometric SAR that uses a side-looking antenna operating in a Boeing 707 aircraft designated E-8C. According to Northrop-Grumman,[125] Joint STARS is supposed "to detect, locate, identify, classify, and track trucks, tanks, and a variety of other military targets." "In its Wide Area Surveillance/Moving Target Indicator (MTI) mode, the radar covers a nearly 50,000-square kilometer area . . . [and] can even differentiate tracked and wheeled vehicles." "It can see vehicles at ranges in excess of 200 kilometers, moving at walking speeds. And, it can accurately locate them within meters of their actual position."

The Joint STARS slotted-array antenna is 24 ft wide by 2 ft high with 456 by 28 horizontally polarized elements.[126] The beam can be electronically scanned $\pm 60°$ in azimuth and is rotated mechanically in elevation. The antenna is divided into three independent apertures, but the entire antenna can be fed to act as a single aperture with a narrow beamwidth. This is called the *sum mode* and is for transmitting and SAR mapping. The three independent apertures are each 8 ft in width and have three times the beamwidth of the sum mode. They provide the *interferometer mode* for moving target detection and tracking. Although two separated apertures are sufficient for detecting and accurately locating targets, at least three apertures are needed when spatially correlated ground clutter appears at the same range and with the same doppler as the target.

Moving target echoes detected by the three antenna apertures are distinguished from surface clutter echoes by taking advantage of the different angles of arrival associated with targets and clutter that have the same range and doppler frequency. This is accomplished by adding the signals from adjacent antenna apertures (left and center as one pair, and center and right as the other pair) and applying a relative weighting that depends on the doppler. This is designed to generate a null in the receiving antenna pattern in the direction of clutter while retaining, as much as possible, the target signals that arrive from a slightly different direction. This interferometric clutter cancellation results in two separate clutter-canceled channels which, through the application of classical detection and angle measurement methods, allow the residual signals from the surface moving target to be readily detected and located.[127]

The left and center apertures as well as the center and right apertures of the Joint STARS antenna act as displaced phase center antenna (DPCA) to cancel main-beam clutter and produce two clutter-free channels containing moving target information.[128,129]

The interferometric SAR with three beams as used on Joint STARS can detect targets moving with smaller relative velocities than can a conventional airborne MTI with only a single beam. To be detected by a conventional airborne MTI system, a moving ground target located near the center of the illuminated clutter area would have to have a radial speed that produced a doppler frequency shift that was outside the doppler clutter spectrum. For example, a side-looking antenna with 2° beamwidth, centered at broadside, located on an airborne platform traveling at 240 m/s (about 470 kt), produces a ground-clutter velocity spectrum that subtends approximately ± 4 m/s (about 8 kt). A target located near the center of the illuminated area would have to have a radial component of

velocity greater than ±4 m/s before it could be detected. A target approaching the radar platform from a direction located near the trailing edge of the antenna beam would need a ground speed greater than 8 m/s before it was sufficiently separated from the background clutter spectrum. An interferometric SAR, on the other hand, that was able to detect and measure the angle of arrival of the target and the angle of arrival of the clutter to an accuracy of 0.1 beamwidth (±0.1°) would theoretically be capable of detecting targets with one-tenth the radial speed, or in this case ±0.4 m/s (about 0.8 kt).[127]

The two modes for detecting stationary targets and moving targets are time shared (interleaved). The detection of parked tanks and other vehicles is determined by the SAR mode, and slowly moving targets are found with the interferometer doppler mode.

Joint STARS is a long-range wide-area surveillance system that uses a relatively large antenna in a large aircraft. The same basic technology has been employed in a much smaller radar, the Northrup Grumman AN/APG-76 K_u-band system, which is small enough to fit in a pod or in the nose of a fighter/attack aircraft.[130] Such an interferometric SAR uses more than two antennas, the antennas do not have to be identical, and they need not be side-looking or mounted longitudinally along the line of travel of the aircraft. The AN/APG-76 uses forward-looking bulkhead-mounted mechanically gimbaled antennas with a set of fixed interferometric arrays whose mechanical boresights are physically steered toward the target. It provides a SAR image and moving target detection with an interferometer antenna. It also has apertures displaced in the vertical dimension to provide on a pixel-to-pixel basis altitude information of scattering objects, to produce a 3-D SAR image. The APG-76 has 10-ft resolution with 20 ft elevation sensitivity per pixel.[131]

Effect of MTI on Signal-to-Noise Ratio An MTI delay-line canceler generally attempts to cancel clutter with fewer pulses than are available from the target. Therefore, coherent integration of the available pulses following the MTI processor is usually performed to increase the output signal-to-noise ratio. It has been shown, however, that there will be a degradation in detection performance because the MTI processing correlates the independent input noise when the MTI pulses are integrated.[132,133] This results in an MTI noise integration loss that is approximately 1.0, 1.8, and 2.2 dB for single, double, and triple delay-line cancelers, respectively.[134] The loss can be reduced by applying amplitude weights to the pulses to be integrated.[135]

The loss in signal-to-noise ratio, however, is generally not of major concern in many applications of MTI radar. MTI is needed at the shorter radar ranges where clutter is a serious limitation to the detectability of targets, and receiver noise is not an issue. This is why MTI processing is usually turned off after the pulse travels beyond the maximum range at which clutter appears. If MTI processing were to remain in the radar signal-processing channel at long range where there is no clutter, other losses in signal to noise could occur because of the attenuation by the doppler processor of targets with radial velocities at or in the vicinity of the blind speeds.

The lesser concern for the detectability of signals when clutter is much larger than noise is evidenced by the willingness of the radar designer (and the radar buyer) of high-performance pulse doppler radars to tolerate the use of redundant waveforms for resolving range ambiguities and the use of fill pulses for sophisticated doppler processors in order to successfully detect moving targets in heavy clutter.

Pulse-Burst Radar[136–138] This is a waveform that attempts to obtain the benefits of a pulse doppler waveform without some of its disadvantages. It consists of a burst of pulses at a high or medium prf, which are repeated at a prf low enough for the burst to be unambiguous in range. The *pulse burst* has also been called a *burst pulse* or *pulse train.* Nathanson[137] states that the number of pulses within a burst might be from 8 to 32; but, of course, these are not meant to be firm limits and depend on the nature of the radar application. Sometimes amplitude and phase weightings are employed across the burst to further reduce the sidelobes of the waveform (and increase the clutter attenuation), especially in clutter that extends in range further than the range extent of the burst waveform. Amplitude weighting of the radiated signal, however, can present demands on the radar transmitter that might not be easily met.

Single-Pulse Doppler Radar Ambiguities in the doppler and range measurement occur when the radar waveform is not continuous, and such ambiguities cause problems in MTI and pulse doppler radars, as has been described previously in this chapter. There are some limited situations, however, when a single pulse might be used for detection of the doppler frequency shift. In order to detect a doppler shift on the basis of a single pulse, there must be at least one cycle of doppler frequency during the pulse duration. This requires that the pulse duration τ be greater than the period T_d of the doppler frequency $f_d = 2v_r/\lambda = 1/T_d$, which means that $f_d\tau > 1$. Thus $\tau > \lambda/2v_r$, where λ = wavelength and v_r = radial velocity. If the minimum detectable velocity is $v_{\min}$, then $v_{\min} = \lambda/2\tau$. (If the clutter is strong, the minimum detectable velocity might be greater than this value.) A low $v_{\min}$ requires either long pulses and/or very short wavelengths. If moving targets are to be detected in clutter, however, the expression for the minimum detectable velocity as given above is too simplistic, and more precise methods are needed to assess MTI performance. Longer pulses might be required for good doppler discrimination than is indicated by the above expression for $v_{\min}$.

The single-pulse doppler method was used in early space surveillance radars for the detection of ballistic missiles and satellites. However, such radars did not have to detect targets in ground or weather clutter. The single-pulse doppler measurement was employed in these radars to extract the radial velocity to aid in establishing the track of the target. Such radars operated at UHF with unusually long pulses. If the pulse width were 2 ms and the wavelength were 70 cm (UHF), the minimum detectable velocity is 175 m/s, or about 350 kt. This is high for detection of aircraft, but is suitable for detection of extraterrestrial targets with their much higher speeds.

At the other extreme, that of short wavelength, a millimeter-wave radar operating at a frequency of 94 GHz would require a pulse duration of 32 μs in order to have a minimum detectable velocity of 100 kt, based on the above criterion for $v_{\min}$. The possible advantage of a single-pulse doppler waveform for millimeter-wave radar is that it would not experience the many blind speeds that occur with a conventional pulse doppler waveform. In order to obtain range resolution with a long single pulse, pulse compression can be employed. For detection of moving targets in clutter, a single pulse waveform, with or without pulse compression, would have to be designed with good spectral characteristics and doppler filtering so as to have an acceptable minimum detectable velocity.

Area MTI Originally an *area MTI* radar was one that stored the amplitude of the echoes received at each range-azimuth resolution cell over an entire scan of the radar, and subtracted these stored signals from similar data received from the next scan. This results in cancellation of echoes from stationary clutter, but echoes from moving targets that appear in a different resolution cell from scan to scan (because of their movement) are not canceled. Area MTI does not depend on the doppler frequency shift to discriminate moving targets from stationary clutter; hence, a coherent radar is not needed. It does not have the limitations of blind speeds or doppler and range ambiguities that are experienced by doppler moving target detection methods. This form of area MTI is a video detection method that requires clutter to be stationary from scan to scan. Early forms of area MTI used analog storage tubes to record the video data. The poor analog storage technology and the limitation of other early radar equipment restricted the ability of this form of area MTI to extract small targets in clutter. A digital clutter map would be better for this application than the analog storage tube.

A more suitable area MTI is one that uses very short pulses and subtracts them pulse to pulse rather than scan to scan.[139] The subtraction can be done in the video rather than coherently. It can require less memory than scan-to-scan subtraction and avoids many of the problems found with doppler forms of MTI. For detection of aircraft, however, pulse widths need to be of the order of nanoseconds. It is more attractive at the higher microwave frequencies where the available bandwidths are large and the usual doppler MTI suffers from the detrimental effects of excessive blind speeds.

Area MTI has also been examined for detection of moving targets using ultrawideband (UWB) radar. The concept of doppler is quite different with UWB radar than with the narrow relative bandwidths usually employed in radar. In conventional-bandwidth radar, the bandwidth is narrow enough that the doppler frequency shift can be considered constant over the entire spectral width of the signal. With UWB systems, this assumption is no longer true. The variation of the doppler frequency over the signal's frequency spectrum has to be taken into account. For this reason, the time domain is more useful for UWB than is the frequency domain. The potential for extremely high resolution and its independence of doppler make area MTI attractive for UWB application. A particular UWB radar concept examined was a 30 percent bandwidth radar centered on X band. Its purpose was to detect sea-skimmer missiles flying at high speed, low over water, at ranges where they just came over the local radar horizon.[140] The minimum detectable velocity of this conceptual radar was 100 kt and its prf was 8 kHz. With the high resolution (5 cm) of a 3-GHz bandwidth pulse, the sea echo is from "sea spikes" which are nonstationary in both time and space, as discussed in Sec. 7.4. The ultrahigh resolution and the nonstationarity of the sea spikes allows detection of targets in the region where there is no clutter. (This is sometimes called *interclutter visibility*). When the target happens to coincide with a clutter spike, the area MTI cancels the clutter, but preserves moving target echoes. A serious limitation of an UWB area MTI radar, however, is its need for large allocations of the electromagnetic frequency spectrum.

Coherent on Receive The term *coherent on receive MTI* is sometimes used to describe an MTI radar that uses a power oscillator, such as the magnetron, as the transmitter rather than a power amplifier. Each time a power oscillator is pulsed, the phase of the pulse is

random from pulse to pulse. To provide a coherent reference at the receiver so that the doppler signal may be detected, the phase of the coho (coherent oscillator) is set equal to the phase of the power oscillator each time the pulse is transmitted. That is, the phase of the coho is "locked" to the phase of the transmitter on each pulse, as was mentioned at the end of Sec. 3.1. This method of operation is sometimes called *coherent on receive* to distinguish it from an MTI that uses a power amplifier.

The amplifier MTI has been called *fully coherent* by some radar engineers to distinguish it from coherent on receive, but this is unnecessary nomenclature. Almost all modern high-performance MTI radars are "fully coherent" in the sense that they employ I and Q processing and a power amplifier transmitter, so the use of the term "fully coherent" is often superfluous.

The power oscillator MTI that employs a magnetron as the transmitter was the original form of MTI used for many years until the much more capable high-power amplifier became available. The power oscillator, however, is seldom used for high-performance radars. It finds application in those radars where high clutter attenuation is not required and where low cost is more important than high performance.

Adaptive MTI[141] In this chapter adaptive processing in MTI, AMTI, and pulse doppler radar has already been mentioned. Each of the filters of the MTD doppler filter bank, for example, had an adaptive threshold that was set by the amount of clutter seen in each filter. Similarly, the filters of a pulse doppler radar also have individual thresholds whose level is determined by the clutter. In an AMTI radar, TACCAR adaptively adjusts the frequency of the reference oscillator (coho) to compensate for clutter whose doppler frequency is other than zero. STAP is also a form of adaptive processing that employs both the spatial (antenna) and temporal (doppler) domains.

The technique usually known as *adaptive MTI*, however, is different from these. It can be considered as an n-pulse delay-line canceler whose filter weights, and therefore its frequency response, are determined by the clutter seen by the radar. It is analogous to what is known as coherent sidelobe cancellation which places nulls in the radiation pattern of an antenna in the direction of unwanted noise sources such as jamming.[142] For example, if a four-pulse canceler is used, three nulls can be adaptively placed at three different frequencies depending on the nature of the clutter spectrum. If the clutter were concentrated at d-c, all three nulls would be placed at d-c. If the clutter were narrowband and in motion, the nulls would be placed at the doppler frequency of the clutter. When the clutter is rain or chaff, the spectrum can be broad and the nulls would be staggered in frequency to cover the spectral width of the clutter. The wider the clutter spectral width, the wider will be the adaptive filter notch, but it would not be as deep. If the clutter is bimodal in that both stationary surface clutter and moving weather clutter were present in the same resolution cell, the adaptive filter would place its nulls to cancel both as best it can. Adaptive MTI has been said to be potentially desirable when there is bimodal clutter or when the clutter characteristics change with range, angle, or time.

Although the adaptive MTI appears to have some attractive features, it has not seen much use. This might be due to the success of other methods, such as the MTD, for dealing with bimodal clutter. It might also be due in part to the difficulty in assuring that the adaptive MTI doesn't cancel the target echo along with the clutter.

Frequency Agility and MTI Pulse-to-pulse frequency agility has the important benefit of increasing detectability of some targets, as when the pulse-to-pulse correlated echoes of a Swerling Case 1 target are decorrelated by frequency agility to produce a Swerling Case 2 fluctuating target echo. As mentioned in Sec. 2.8, a Swerling pulse-to-pulse fluctuating echo allows a lower detection threshold than one that is not. Frequency agility can also reduce the harmful effects of glint in a tracking radar and makes for more accurate target tracking (Sec. 4.4). In military radars, pulse-to-pulse frequency agility is important in causing a hostile jammer to spread its power over a wide bandwidth and not concentrate all its energy within the narrow bandwidth of a fixed-frequency radar receiver.

Unfortunately, frequency agility is not compatible with doppler processing. If the frequency is changed by an amount Δf, the phase of the echo return from a stationary point target at a range R is changed by $4\pi\Delta fR/c$. The change in phase with a change in frequency means there will be an uncanceled residue from the clutter if each pulse of the doppler processor is not of the same frequency. The effect is even worse when there are multiple clutter scatterers within the radar resolution cell. Thus frequency agility and doppler processing are not compatible.

One possible compromise that allows different frequencies to be used is to transmit multiple frequencies in close sequence (or pulse to pulse) over a relatively wide band.[143] For MTI purposes, however, the radar has to eventually retransmit these same frequencies. The order of transmission of the multiple frequencies can be varied so as to make fixed narrowband jamming difficult. If narrowband jamming takes out one or more of the radar frequencies, those frequencies can be blanked at the receiver.

An interesting method for using multiple frequencies with MTI radar was demonstrated with the Senrad experimental long-range air-surveillance radar by the Radar Division of the Naval Research Laboratory.[144] This radar operated in two frequency bands simultaneously: the normal L band from 1215 to 1400 MHz and the band from 850 to 942 MHz, sometimes called L_u. There were various waveforms used for this radar, but the clear-sky MTI waveform was a three-pulse MTI. The three MTI pulses have to be at the same frequency in order to perform MTI, which makes them vulnerable to narrowband electronic countermeasures if only a single MTI frequency is used. In Senrad, however, the three MTI waveforms are radiated on multiple frequencies in both sub-bands as the antenna scans by the target. Thus a three-pulse MTI waveform is simultaneously transmitted in both the lower and the upper sub-bands. As the antenna scans by the target there are six sets of three MTI pulses radiated in the lower sub-band and four sets of three MTI pulses in the upper sub-band, with each set of three pulses at a different frequency. (The lower sub-band provided more opportunities for putting pulses on the target because its beamwidth was wider than that of the upper sub-band.) The same antenna was used for both sub-bands, but a separate transmitter was used for each sub-band. A jammer would have to spread (dilute) its power to completely cover both sub-bands simultaneously. This can significantly reduce the amount of noise jamming that the radar encounters.

Clutter Decorrelation with Frequency Agility Sometimes it has been claimed that frequency agility can improve the detection of stationary or slowly moving targets in clutter by decorrelating the clutter echoes by changing the radar frequency pulse to pulse. This is supposed to make the clutter echo look more like receiver noise rather than

correlated clutter. Doppler processing is not employed. Integration of the signal and the pulse-to-pulse decorrelated clutter echoes can increase the signal-to-clutter ratio compared to when clutter is correlated pulse to pulse. This may be correct, but it is usually not a good method for detecting targets in clutter. Random or pseudorandom frequency hopping does not decorrelate the clutter effectively when the clutter statistics are not described by the Rayleigh probability density function (which it often isn't). Degradation can also occur if the frequency change is large enough to decorrelate the target echo as well as the clutter echo.

If one is given a fixed wide bandwidth to use to improve detectability of stationary targets in clutter, it is usually much better to use that bandwidth in a coherent fashion to radiate a narrow pulse or the equivalent pulse compression waveform rather than employ frequency agility. High range resolution increases the signal-to-clutter ratio by excluding clutter echoes outside the vicinity of the target. In this manner, one uses the available bandwidth to reduce clutter, rather than depend on the less efficient clutter-rejection method of a random-like hopping of a narrowband transmission over the same bandwidth. If the target is moving, however, doppler processing can provide greater detectability in clutter than can high range resolution.

Two-Frequency MTI It has been proposed in the past that an MTI radar transmit two different frequencies and on receive operate with the difference frequency rather than either of the RF frequencies. The difference frequency, being much lower than either of the two RF frequencies, was thought to have higher blind speeds than if the radar operated on only one of the RF frequencies. If, for example, the two frequencies of the MTI radar were 9.3 and 9.4 GHz, the difference frequency would be 100 MHz and would have blind speeds 93 times that of the lower RF frequency. This possibility has attracted the attention of radar engineers more than once.

It is true that when two or more RF frequencies are used, the first blind speed can be increased just as it can when two or more prfs (pulse repetition frequencies) are used, as mentioned later in this subsection. There are some serious limitations, however, that negate the supposed advantages of two-frequency MTI when the difference frequency is used. One doesn't obtain the target scattering characteristics of a low-frequency radar by operating with the difference frequency. Also, the width of the clutter spectrum seen at the difference frequency is not that of a 100 MHz radar (in the above example), but is greater than the clutter spectrum seen with either RF frequency.[145] The potential blind speed advantage of a two-frequency MTI and its claimed ability to see slower targets are largely nullified by the increased clutter spectral width caused by the mixing process. Furthermore, there can be potential problems with spurious signals generated whenever nonlinear operations of multiple signals are performed as they are in this system to extract the difference frequency.

Meyer and Muehe[146] characterize the problem nicely when they say that ideas like the two-frequency MTI (and others) are nonsolutions that "crop up again and again, and for some reason, continue to attract attention. Much labor and money is used re-examining these ideas with the result that attention is diverted from the principal job." These nonsolutions are often reinvented by those not familiar with the past.

Delta-k Radar This was another two-frequency radar with nonlinear processing that extracted the difference frequency, but for different purposes than the two-frequency MTI. It was promoted by remote sensing scientists, rather than by radar engineers, as providing information about the environment just as would a radar that radiated only the difference frequency. If, for example, an X-band radar radiated at 9.3 and 9.4 GHz and the 100-MHz difference signal was extracted at the receiver (by mixing the two X-band signals), the result was said to be the same as obtained by a 100-MHz radar. Assuming that the target dimensions were such that scattering was in the resonance region (Fig. 2.8) at 100 MHz (and thus had a large radar cross section), it was suggested that similar behavior would be obtained by extracting the 100 MHz difference frequency when two microwave frequencies were used. This does not happen.

The delta-k concept has also been proposed for investigation of sea clutter based on the Bragg scatter model. (It is mentioned in Sec. 7.4 that the Bragg model for sea clutter applies at HF and VHF, but not at the higher microwave frequencies.) The limited information obtained about the sea that is provided by the nonlinear processing of a delta-k radar with two (or a few) frequencies is suspect, and is overshadowed by the information that can be obtained by a radar with a short pulse.

Sometimes the delta-k radar used more than two frequencies. The ultimate would be to have many frequencies so as to obtain a filled spectrum, as with a single short pulse that does not use nonlinear processing. Nonlinear processing, as used in the delta-k, can degrade the information contained in a signal and generate spurious responses, especially when multiple signals are present or when signal-to-noise ratios are modest. Furthermore, the technology of short pulse radar is such that there does not seem to be any hardware advantages in using a delta-k radar, even if it did perform as its proponents hope. One should be very cautious, therefore, when considering using the delta-k or any other radar-like method that uses similar nonlinear processing.

Blind Speeds with Multiple Frequencies There is a potentially useful application of two or more frequencies in MTI radar, but for a different purpose than the two-frequency MTI radar or delta-k radar discussed above. Just as two or more pulse repetition frequencies can be used to resolve doppler ambiguities or to increase the first blind speed in an MTI radar, two or more frequencies can be used instead of two or more prfs to achieve this purpose.[144] This follows from Eq. (3.12) which gives the first blind speed as $v_1 = \lambda f_p/2$. Instead of employing different f_p's, one can employ different λ's.

CW Radar An entire chapter was devoted to CW radar in the earlier two editions of this text. It was omitted in this edition since, over time, the role of CW radar has changed. Although the use of CW radar to detect targets in clutter has been replaced by pulse doppler radar, there are still important applications of CW radar, as will be briefly discussed in this subsection.

Simple CW Radar The block diagram of a simple CW radar that extracts the doppler frequency shift of a moving target was shown in Fig. 3.3a. This represents such CW radar applications as the familiar police speed meter,[147] the speed gun used in baseball and other

sports, the artillery proximity fuze of World War II, artillery-projectile muzzle velocity measurement radar, radars for the docking of large ships, the airborne doppler navigator, and many other CW radars whose purpose is the simple noncontact measurement of velocity.[148] The relatively short-range CW radar has also been employed for vibration measurement, intruder detection, monitoring the respiration rate of humans and animals, miss-distance indication, gunfire detector, as a sensor for vehicle braking, and for the precision measurement of the ground speed[149] for both railway and automotive applications.

All of the above are short-range applications. When a CW radar is needed for long range, as for air defense, space surveillance, or ballistic missile detection, the simple CW configuration of Fig. 3.3a has several serious limitations. These include: (1) lack of isolation between the transmitter and receiver, which can cause receiver burnout if the transmitter power is large enough and/or introduce transmitter noise in the receiver which masks the detection of wanted targets, (2) introduction of flicker-effect noise because the receiver is a homodyne (zero IF frequency), (3) lack of a matched filter in the receiver, (4) lack of knowledge as to whether the target is approaching or receding, (5) increased clutter compared to pulse radars, and (6) no measurement of the range to the target.

Each of these limitations can be mitigated or sometimes eliminated. The long-range high-performance CW radar, however, even with improvements, usually is no longer competitive with a modern pulse doppler radar.

CW, however, has been and still is used with success for semiactive missile guidance because of its ability to discriminate against clutter on the basis of the doppler frequency shift, which makes it capable of operation at low altitudes.[150]

Isolation of Transmitter and Receiver Reducing the leakage of the transmitter signal from the receiver can be achieved by using two antennas, one for receive and the other for transmit. They are physically separated so as to minimize their mutual coupling. Absorbing material and/or baffles between the two antennas further prevent the transmitter signal from entering the receiver. Also, a small sample of the transmitter signal can be directed to the receiver to adaptively cancel the portion of the transmitter signal that leaks into the receiving system via the inevitable coupling between the two antennas. Even if there were perfect isolation between transmitter and receiver, the transmitted signal can also enter the receiver via scattering from nearby clutter or other obstructions. Since the transmitter signal cannot be prevented from completely entering the receiver, it is important that it be as clean a signal as practicable (i.e., one with little accompanying noise).

Significant isolation for some CW radar applications can be obtained using only a single antenna by modulating the CW carrier with sinewave frequency modulation.[151] On reception, the difference signal (between the received signal and the transmitted signal) may be mathematically expressed in terms of Bessel functions. A harmonic of the modulation frequency is selected by filtering. Usually this has been the third harmonic ($3f_m$), which has an amplitude given by the Bessel function of third order, $J_3(D)$, where D is a function of the range. Since the higher order Bessel functions are zero at $D = 0$ (range = 0), the leakage signal is attenuated and isolation is achieved.

Reduction of Flicker-Effect Noise The simple CW receiver of Fig. 3.3a is called a homodyne, or a superheterodyne with zero IF frequency. Semiconductor devices, including

diodes and transistors, and vacuum tubes with oxide cathodes generate noise whose power is inversely proportional to frequency. It is known as $1/f$ noise or flicker-effect noise. It can be a concern at frequencies below about 100 kHz; hence, it will limit the sensitivity of a simple CW radar. Flicker-effect noise can be avoided by replacing the homodyne receiver with a superheterodyne whose IF frequency is large enough to make the flicker-effect noise negligible.

Matched Filter The doppler filter in Fig. 3.3a uses a wide passband and is not a matched filter (one that maximizes the output signal-to-noise ratio). If T_d is the time duration of the CW signal processing, then an approximation to the matched filter is one whose bandwidth is $1/T_d$. A single tunable filter might be used in the doppler amplifier to search the entire frequency range over which the signal might appear. Time sharing a single tunable filter in this way can lead to missed targets simply because the filter is being time shared to operate over a wide frequency range. A filter bank doesn't have such limitations and is preferred. It approximates a matched filter implementation and simultaneously covers the entire expected doppler space so it will not miss targets as would a single scanning filter.

Direction of Target Motion The simple CW radar loses the sign of the doppler in the mixing process shown in Fig. 3.3a so that one cannot tell whether the target is approaching or receding. The sign of the doppler, which gives the direction of target motion, can be obtained with a second processing channel whose reference signal is shifted by 90°, similar to the I,Q processing discussed in Sec. 3.5. The sign of the doppler may be determined by noting whether the output of the second channel leads or lags the output of the first by 90°.

Clutter in a CW Radar The clutter seen by an MTI radar with a low prf is only that cutter within the range-angle resolution cell of the radar. A CW radar, on the other hand, sees clutter everywhere. Since the CW radar encounters more clutter than most other radars, it must have wider dynamic range receivers (compared to a low-prf MTI radar) and larger MTI improvement factors.

FM-CW Radar for the Measurement of Range The determination of range requires that the CW waveform be marked in some manner so that the transit time out to the target and back can be measured. A popular method in CW radar is to linearly frequency modulate the waveform, as in Fig. 3.47a. The modulation is triangular (since what goes up eventually has to come down). The transmitted signal is shown by the solid triangular waveform. The frequency excursion Δf corresponds to the bandwidth of a pulse radar, and the frequency modulation at a rate f_m is the equivalent of the pulse repetition frequency of a pulse radar. The dashed curve represents the frequency of the received echo signal from a stationary target. It arrives back at the radar at a time $T = 2R/c$, where R = range to the target. The time-delayed received signal and the transmitted signal are multiplied in a mixer to produce a difference frequency f_r (in Fig. 3.47b). From the geometry of Fig. 3.47a, f_r can be shown to be $4Rf_m\Delta f/c$. If there is a doppler frequency shift f_d from the target, during half the modulation period the difference frequency is $f_r + f_d$ and during the

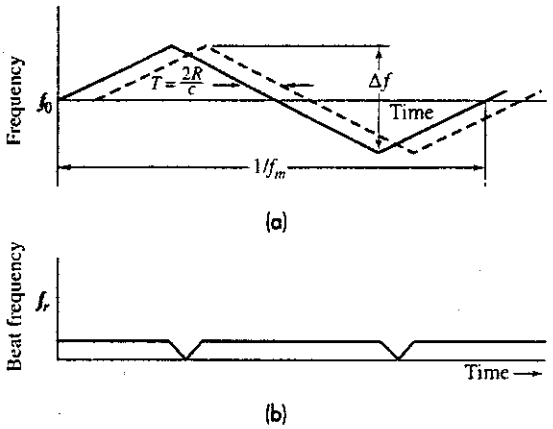

Figure 3.47 (a) Frequency-time relation in a FM-CW radar with linear triangular frequency modulation. Solid lines represent the transmitted signal, dash lines represent the receive signal delayed a time $T = 2R/c$. Δf = frequency excursion, f_m = modulation frequency. (b) Difference frequency between the transmitted and received signals.

other half of the modulation period it is $f_r - f_d$. By averaging these two difference frequencies over the period $1/f_m$ the target range can be obtained.

The FM-CW radar has been widely used in the past as an altimeter. In an altimeter there is only a single large target (the earth) and the range is not large so the radar can be relatively modest. (There is no clutter since the clutter is the target.) A similar application is the determination of distances for industrial purposes, such as the measurement of the distance to molten pig-iron in a blast furnace.

The FM-CW radar that uses the beat frequency between the transmitted and received signals to determine range does not work well when there are multiple targets. If the mixing process is not perfectly linear when multiple targets appear, there can be spurious signals generated. This may be all right for an altimeter when there is only one target, but it is not satisfactory for an air-defense radar. A better method for detecting signals and extracting range is to think of the FM-CW radar as a linear-FM pulse compression radar (discussed in Sec. 6.5) but with a unity duty cycle. The processing is with a matched filter in a superheterodyne receiver.

The U.S. Air Force, U.S. Navy (ROTHR), and the Australian (Jindalee) HF over-the-horizon radars employ FM-CW waveforms with extraction of the doppler frequency shift to separate clutter echoes from moving aircraft echoes. FM-CW radar works for this application, but with some serious penalties compared to a pulse radar. The FM-CW radar requires a greater receiver dynamic range, greater improvement factor, and two widely separated sites (to obtain isolation).

The FM-CW radar has been suggested for naval navigation radars. The chief advantage in that application is that its CW signal has lower peak power than does an equivalent pulse radar, thus making it more difficult (but not impossible) for a hostile electronic warfare receiver to intercept.[152]

Hawk Air-Defense System The CW radar has also been used in the past for the detection of moving aircraft targets in clutter. The U.S. Army's Hawk air-defense system, whose concept dates back to the 1950s, was an example that was employed operationally by many countries of the world for many years. CW radar was the basis for the Hawk since the development of pulse doppler radar at the time of its development was not sufficiently advanced. This has changed. With the development of the high-prf pulse doppler radar, the long-range, high-power CW radar has been much less attractive. CW radar has the disadvantage that it requires two separate antennas for transmit and receive that have to be well isolated from one another. The pulse doppler radar needs only one antenna. The CW radar requires some method for measuring target range; the pulse doppler radar requires some method for resolving the ambiguities of the range it measures. The CW radar sees more clutter than a pulse doppler radar. A pulse doppler radar avoids seeing unwanted echoes from nearby clutter or reflections from other nearby objects since, unlike the CW radar, its receiver is turned off when the pulse is being radiated. The doppler processing employed in a high-prf pulse doppler radar signal after range gating is similar to the doppler processing of a CW radar. The pulse doppler radar is generally superior to the CW radar in several ways and has replaced it for the detection of aircraft in clutter.

Further information on CW radars can be found in either of the two previous editions of this text or in the *Radar Handbook*, published by McGraw-Hill.

REFERENCES

1. Shrader, W. W., and V. Gregers-Hansen. "MTI Radar." In *Radar Handbook*, 2nd ed., M. Skolnik, Ed. New York: McGraw-Hill, 1990, Chap. 15.
2. Long, W. H., D. H. Mooney, and W. A. Skillman. "Pulse Doppler Radar." In *Radar Handbook*, 2nd ed., M. Skolnik, Ed. New York: McGraw-Hill, 1990, Chap. 17.
3. Taylor, J. W., Jr. "Receivers." In *Radar Handbook*, 2nd ed., M. Skolnik, Ed. New York: McGraw-Hill, 1990, Chap. 3, Sec. 3.10.
4. IEEE Standard Radar Definitions, IEEE Std. 686-1997.
5. Andrews, G. A. "Airborne Radar Motion Compensation Techniques, Evaluation of TACCAR," Naval Research Laboratory Report 7407, Washington, D.C., Apr. 12, 1972.
6. Capon, J. "Optimum Weighting Functions for the Detection of Sampled Signals in Noise." *IEEE Trans.* IT-10 (April 1964), pp. 152–159.
7. Kretschmer, F. F. "MTI Weightings." *IEEE Trans.* AES-10 (January 1974), pp. 153–155.
8. Murakami, T., and R. S. Johnson. "Clutter Suppression by Use of Weighted Pulse Trains." *RCA Rev.* (September 1971), pp. 402–428.
9. Andrews, G. A., Jr. "Optimal Radar Doppler Processors." Naval Research Laboratory Report 7727, Washington, D.C., May 29, 1974.

10. Mao, Y. H. "MTI, MTD, and Adaptive Clutter Cancellation." In *Advanced Radar Techniques and Systems,* G. Galati, Ed. London: Peter Peregrinus, 1993, Sec. 6.6.2.
11. Houts, Y. C., and D. W. Burlage. "Maximizing the Usable Bandwidth of MTI Signal Processors." *IEEE Trans.* AES-13 (January 1977), pp. 48–55.
12. Rabiner, L. R., and C. M. Rader. *Digital Signal Processing.* New York: IEEE Press, 1972.
13. White, W. D. "Synthesis of Comb Filters." *Proc. Natl. Conf. on Aeronaut. Electronics,* 1958, pp. 279–285.
14. Shreve, J. S. "Digital Signal Processing." In *Radar Handbook,* 1st ed., M. Skolnik, Ed. New York: McGraw-Hill, 1970.
15. Ellis, J. G. "Digital MTI, A New Tool for the Radar User." *Marconi Rev.* 36 (1973), pp. 237–248, 4th qtr.
16. Fletcher, R. H., Jr., and D. W. Burlage. "An Initiation Technique for Improved MTI Performance in Phased Array Radars." *Proc. IEEE* 60 (December 1972) pp. 1551–1552. See also by the same authors: "Improved MTI Performance for Phased Array Radars in Severe Clutter Environments." *IEE Conference on Radar—Present and Future.* IEE Conference Publication No. 105, London, pp. 280–285, 1973.
17. Aalfs, D. D., E. G. Baxa, Jr., and E. M. Bracalente. "Signal Processing Aspects of Windshear Detection." *Microwave J.* 36 (September 1993), pp. 76–96.
18. Shrader, W. W., and V. Gregers-Hansen. Ref. 1, Sec. 15.9.
19. Zverev, A. I. "Digital MTI Radar Filters." *IEEE Trans.* AU-16 (September 1968), pp. 422–432.
20. Thomas, H. W., and T. M. Abram. "Stagger Period Selection for Moving Target Radars." *Proc. IEE* 123 (March 1976), pp. 195–199.
21. Hsiao, J. K., and F. F. Kretschmer, Jr. "Design of a Staggered-PRF Moving Target Indication Filter." *The Radio and Electronic Engineer* 43 (November 1973), pp. 689–693.
22. Thomas, H. W., and T. M. Abram. "Stagger Period Selection for Moving-Target Radars." *Proc. IEE* 123 (March 1976) pp. 195–199.
23. Ewell, G. W., and A. M. Bush. "Constrained Improvement MTI Radar Processors." *IEEE Trans.* AES-11 (September 1975), pp. 768–780.
24. Cleetus, G. M. "Properties of Staggered PRF Radar Spectral Components." *IEEE Trans.* AES-12 (November 1976), pp. 800–803.
25. McAulay, R. J. "The Effect of Staggered PRF's on MTI Signal Detection." *IEEE Trans.* AES-9 (July 1973), pp. 615–618.
26. Wardrop, B. "The Performance of MTI Systems When Used with P.R.F. Stagger." *The Marconi Review* 4th quarter, 1974, pp. 217–231.
27. Shrader, W. W., and V. Gregers-Hansen. Ref. 1, pp. 15–34 to 15–35.
28. Ludloff, A., and M. Minker. "Reliability of Velocity Measurement by MTD Radar." *IEEE Trans.* AES-21 (July 1985), pp. 522–528.

29. Andrews, G. A., Jr. "Performance of Cascaded MTI and Coherent Integration Filters in a Clutter Environment." *Naval Research Laboratory Report* 7533, Washington. D.C., March 27, 1973.

30. Shrader, W. W., and V. Gregers-Hansen. Ref. 1, Sec. 15.8.

31. Ward, H. R. "Properties of Dolph-Chebyshev Weighting Functions." *IEEE Trans.* AES-9 (September 1973), pp. 785–786.

32. Gregers-Hansen, V. "Optimum Pulse Doppler Search Radar Processing and Practical Approximations." *International Conference Radar—82* IEE Conference Publication No. 216 (October 1982), pp. 138–143, 18–28.

33. Mao, Y. H. "Architectures and Implementation of Radar Signal Processor." In *Advanced Radar Techniques and Systems.* G. Galati, Ed. London: Peter Peregrinus, 1993, Chap. 8.

34. Nathanson, F. E., and P. J. Luke. "Loss from Approximations to Square-law Detectors in Quadrature Systems with Postdetection Integration." *IEEE Trans.* AES-8 (January 1972), pp. 75–77.

35. Shrader, W. W., and V. Gregers-Hansen. Ref. 1, Sec. 15.12.

36. Shrader, W. W., and V. Gregers-Hansen. Ref. 1, Sec. 15.11.

37. Brennan, L. E., and I. S. Reed. "Quantization Noise in Digital Moving Target Indication Systems," *IEEE Trans.* AES-2 (November 1966), pp. 655–658.

38. Taylor, J. W., Jr. Ref. 3, Sec. 3.12.

39. Churchill, F. E., G. W. Gar, and B. J. Thompson. "The Correction of I and Q Errors in a Coherent Processor." *IEEE Trans.* AES-17 (January 1981) pp. 131–137.

40. Suresh Babu, B. N., and C. M. Sorrentino. "Analogue-to-Digital Convertor Effects on Airborne Radar Performance." *IEE Proc.-F* 139 (February 1992), pp. 73–78.

41. Rader, C. M. "A Simple Method for Sampling in-Phase and Quadrature Components," *IEEE Trans.*, vol. AES-20 (November, 1984), pp. 821–824.

42. Mitchell, R. L. "Creating Complex Signal Samples From a Band-Limited Real Signal," *IEEE Trans.*, vol. AES-25 (May, 1989), pp. 425–427.

43. Waters, W. M., and B. R. Jarrett. "Bandpass Sampling and Coherent Detection," *IEEE Trans.*, vol. AES-18 (November 1982), pp. 731–736.

44. Taylor, J. W., Jr. "Sacrifices in Radar Clutter Suppression Due to Compromises in Implementation of Digital Doppler Filters." *International Conference Radar—82*, Institution of Electrical Engineers (London), pp. 46–50, 1982.

45. Nathanson, F. E. *Radar Design Principles*, 2nd ed. New York: McGraw-Hill, 1991, Sec. 9.1.

46. Weiss, M., and I. Gertner. "Loss in Single-Channel MTI with Post-Detection Integration." *IEEE Trans.* AES-18 (March 1982), pp. 205–208.

47. Muehe, C. E. "Digital Signal Processor for Air Traffic Control Radars." *IEEE NEREM 74 Record*, Part 4: Radar Systems and Components. (October 28–31, 1974), pp. 73–82.

48. Drury, W. H. "Improved MTI Radar Signal Processor." Report no. FAA-RD-74-185, MIT Lincoln Laboratory, April 3, 1975.

49. O'Donnell, R. M., et al. "Advanced Signal Processing for Airport Surveillance Radars." *IEEE EASCON 77,* Washington, D.C. (October 1974), pp. 71A–71F.

50. Drury, W. H. "Improved MTI Radar Signal Processor." Federal Aviation Agency Report No. FAA-RD-74-185, 3 April 1975.

51. Muehe, C. E. "Digital Signal Processors for Air Traffic Control Radars." *IEEE NEREM 74 Record,* Part 4: Radar Systems and Components. IEEE Catalog no. 74 CHO 934-0 (1974), pp. 73–82.

52. Muehe, C. E. "Advances in Radar Signal Processing." *IEEE Electro '76,* Boston, MA, May 11–14, 1976.

53. O'Donnell, R. M., and C. E. Muehe. "Automated Tracking for Aircraft Surveillance Radar Systems." *IEEE Trans.* AES-15 (July 1979), pp. 508–517.

54. Taylor, J. W., Jr. "Sacrifices in Radar Clutter Suppression Due to Compromises in Implementation of Digital Doppler Filters." *International Conference Radar-82,* IEEE Conference Publication No. 216 (October 18–20, 1982), pp. 46–50.

55. Taylor, J. W., Jr., and G. Brunins. "Design of a New Airport Surveillance Radar (ASR-9)." *Proc. IEEE* 73, (February 1985), pp. 284–289.

56. Cole, E. L., M. J. Hodges, R. G. Oliver, and A. C. Sullivan. "Novel Accuracy and Resolution Algorithms for the Third Generation MTD." *IEEE 1986 National Radar Conference Proceedings,* pp. 44–47, IEEE Catalog no. 86CH2270-7.

57. Cole, E. L., et al. "ASR-12: A Next Generation Solid State Air Traffic Control Radar." *Proc. 1998 IEEE Radar Conference,* Dallas, Texas, May 11–14, 1998, pp. 9–14.

58. Shrader, W. W., and V. Gregers-Hansen. Ref. 1, Sec. 15.5.

59. Goldstein, H. "The Fluctuations of Clutter Echoes." *Propagation of Short Radio Waves,* D. E. Kerr, Ed. MIT Radiation Lab Series, vol. 13, New York: McGraw-Hill, 1951, pp. 550–587.

60. Barlow, E. J. "Doppler Radar." *Proc. IRE* 37 (April 1949), pp. 340–355.

61. Barton, D. K. *Modern Radar Analysis.* Norwood, MA: Artech House, 1988, p. 246.

62. Nathanson, F. E. Ref. 45, Fig. 7.32.

63. Fishbein, W., S. Graveline, and O. R. Rittenbach. "Clutter Attenuation Analysis." *Technical Report ECOM-2808, U. S. Army Electronics Command, Ft. Monmouth, NJ,* March, 1967. Reprinted in Schleher, D. C. *MTI Radar.* Dedham, MA: Artech House, 1978.

64. Li Neng-jing. "A Study of Land Clutter Spectrum." *Proc. Second International Symposium on Noise and Clutter Rejection in Radars and Imaging Sensors.* T. Suzuki, H. Ogura, and S. Fujimura, Eds. IEICE, Elsevier, North Holland, 1990, pp. 48–53.

65. Currie, N. C., and C. E. Brown. *Principles and Applications of Millimeter Wave Radar.* Norwood, MA: Artech House, 1987, Table 5.4.

66. Billingsley, J. B. "Exponential Decay in Windblown Radar Ground Clutter Doppler Spectra: Multifrequency Measurements and Model." *MIT Lincoln Laboratory Technical Report 997* July 29, 1996.

67. Billingsley, J. B. "Ground Clutter Measurements for Surface-Sited Radar." *MIT Lincoln Laboratory Technical Report* 786 (Revision 1), February 1, 1993.

68. Shrader, W. W., and V. Gregers-Hansen. Ref. 1, Sec. 15.11.

69. Nathanson, F. E. Ref. 45, Sec. 9.7.

70. Everett, C. L. "Phase Noise Contamination to Doppler Spectra." *Microwave J.* 39 (September 1996), pp. 105–122.

71. Ewell, G. W. "Stability and Stable Sources." In *Coherent Radar Performance Estimation.* J. A. Scheer and J. L. Kurtz, Eds. Norwood, MA: Artech House, 1993, Chap. 2.

72. Bloomfield, D. L. H. "Low-Noise Microwave Sources." *IEE International Conference on Radar—Present and Future,* London, IEE Conference Publication No. 105, pp. 178–183, October 23–25, 1973.

73. Khanna, A. P. S., M. Schmidt, and R. B. Hammond. "A Superconducting Resonator Stablized Low Phase Noise Oscillator." *Microwave J.* 34, (February 1991), pp. 127–130.

74. Mage, J. C., B. Marcilhac, P. Hartemann, and J. P. Castera. "Low Phase Noise Oscillator for Stealth Target Detection." *International Conference on Radar,* Paris, May 3–6, 1994, pp. 202–206.

75. Filler, R. L., and J. R. Vig. "Low-Noise Oscillators for Airborne Radar Applications." *Army Research Laboratory, Ft Monmouth, Research and Development Technical Report* SLCET-TR-91-26 (Rev. 1), August 1993. DTIC AD-A269 372.

76. Almar, R. C, and M. S. Cavin. "Low g-Sensitivity Fixed-Frequency Oscillators." *Microwave J.* 38 (February 1995), pp. 88–98.

77. Kerr, R. R. "MTI Systems." In *Coherent Radar Performance Estimation.* J. A. Scheer and J. L. Kurtz, Eds. Norwood, MA: Artech House, 1993, Chap. 8. Sec. 8.5.

78. Ward, H. R., and W. W. Shrader. "MTI Performance Caused by Limiting," *EASCON '68 Record.* Supplement to *IEEE Trans.* AES-4, pp. 168–194, November 1968.

79. Shrader, W. W., and V. Gregers-Hansen. Ref. 1, Sec. 15.10.

80. Ridenour, L. N. *Radar System Engineering.* MIT Radiation Laboratory Series 1, New York: McGraw-Hill, 1947, Sec. 16.8.

81. Shrader, W. W., and V. Gregers-Hansen. Ref. 1, Sec. 15.14.

82. Nitzberg, R. "Clutter Map CFAR Analysis." *IEEE Trans.* AES-22 (July 1986), pp. 419–421.

83. Dickey, F. R., Jr., M. Labitt, and F. M. Staudaher. "Development of Airborne Moving Target Radar for Long Range Surveillance." *IEEE Trans.* AES-27 (November 1991), pp. 959–972.

84. Staudaher, F. M. "Airborne MTI." In *Radar Handbook.* 2nd ed. M. I. Skolnik, Ed. New York: McGraw-Hill, 1990, Chap. 16, Sec. 16.3.

85. Shrader, W. W., "MTI Radar." In *Radar Handbook,* 1st ed., M. I. Skolnik, Ed. New York: McGraw-Hill, 1970, Chap. 17, Sec. 17.9.

86. Shrader, W. W. and V. Gregers-Hansen. Ref. 1, Sec. 15.13.

87. Staudaher, F. M. Ref. 81, Sec. 16.4.

88. Grisetti, R. S., M. M. Santa, and G. M. Kirkpatrick. "Effect of Internal Fluctuations and Scanning on Clutter Attenuation in MTI Radar." *IRE Trans.* ANE-2 (March 1955), pp. 37–42.

89. Anderson, D. B. "A Microwave Technique to Reduce Platform Motion and Scanning Noise in Airborne Moving-Target Radar." *IRE Wescon Conv. Rec.* 2 (1958), pt. 1, pp. 202–211.

90. Staudaher, F. M. Ref. 84, Secs. 16.6 and 16.6.

91. Staudaher, F. M. Ref. 84, p. 16–13.

92. Farina, A. *Antenna-Based Signal Processing Techniques for Radar Systems.* Boston, MA: Artech House, 1992.

93. Ghose, R. N. *Interference Mitigation.* New York: IEEE Press, 1996.

94. Gabriel, W. F. "Adaptive Arrays—An Introduction." *Proc. IEEE* 64 (February 1976), pp. 239–272.

95. Brennan, L. E., and I. S. Reed. "Theory of Adapative Radar." *IEEE Trans.* AES-9 (March 1973), pp. 237–252.

96. Kretschmer, F. F., Jr., B. L. Lewis, and F-L C. Lin. "Adaptive MTI and Doppler Filter Bank Clutter Processing." *Proc. 1984 IEEE National Radar Conf.* IEEE Cat. No. 84CH1963-8, pp. 69–73.

97. Shrader, W. W., and V. Gregers-Hansen. Ref. 1, Sec. 15.13.

98. Brennan, L. E., J. D. Mallett, and I. S. Reed. "Adaptive Arrays in Airborne MTI Radar." *IEEE Trans.* AP-24 (September 1976), pp. 607–615.

99. Staudaher, F. M. Ref. 84, Sec. 16.8.

100. Ward, J. "Space-Time Adaptive Processing for Airborne Radar." MIT Lincoln Laboratory, Lexington, MA, Technical Report 1015, December 13, 1994.

101. Perkins, L. C., D. H. Mooney, and H. B. Smith. "The Development of Airborne Pulse Doppler Radar." *IEEE Trans.* AES-20 (May 1984), pp. 292–303.

102. Cowdery, R. E., and W. A. Skillman. "Development of the Airborne Warning and Control System (AWACS) Radar." *IEEE Trans.* AES-31, (October 1995), pp. 1357–1356.

103. Shrank, H. E. "Low Sidelobe Phased Array Antennas." *IEEE Antennas and Propagation Society Newsletter* 25, no. 2 (April 1983), pp. 5–9.

104. Goetz, L. P., and J. D. Albright. "Airborne Pulse Doppler Radar." *IRE Trans. MIL-5* (April 1961) pp. 116–126. Reprinted in *Radars,* Vol. 7, *CW and Doppler Radar.* Dedham, MA: Artech House, 1978.

105. Mooney, D. H., and W. A. Skillman. "Pulse-doppler Radar." In *Radar Handbook,* 1st ed. M. Skolnik, Ed. New York: McGraw-Hill, 1970, Chap. 19 p. 19–5.

106. Long, W. H., D. H. Mooney, and W. A. Skillman. "Pulse-Doppler Radar." In *Radar Handbook,* M. Skolnik, Ed. New York: McGraw-Hill, 1990, Chap. 17, p. 17.34

107. Stimson, G. W. *Introduction to Airborne Radar,* 2nd ed., Medham, NJ: Scitech Publishing, 1998, pp. 376–378.

108. Long, W. H., et al. Ref. 106, Sec. 17.4.

109. Hovanessian, S. A. "An Algorithm for Calculation of Range in Multiple PRF Radar." *IEEE Trans.* AES-12 (March 1976), pp. 287–289.

110. Anonymous. "AWACS vs. E2C Battle a Standoff." *EW Magazine* (May/June 1976), p. 31.

111. Morris, G. V. *Airborne Pulsed Doppler Radar.* Norwood, MA: Artech House, 1988, Sec. 6.3.

112. Morris, G. V. Ref. 108, Chaps. 10 and 11.

113. Skolnik, M. I. *Radar Applications.* New York: IEEE Press, 1988, Part 4. Airborne radar.

114. Carpentier, M. H. "Pulse Doppler Radars." In *Advanced Radar Techniques and Systems,* G. Galati, Ed. London: Peter Peregrinus, 1993, Chap. 5, Sec. 5.3.

115. Bath, W. G., and F. R. Castella. "Detection Performance of a Noncoherent MTI." *Proc. 1984 IEEE National Radar Conference,* Atlanta, GA, pp. 74–78.

116. Staudaher, F. E. Ref. 84, Sec. 16.11.

117. Skolnik, M. I. Ref. 113, p. 244.

118. Nevin, R. L., and F. W. Schatz. "AN/APG-67 Multimode Radar Development." Presented at *IEEE 1985 International Radar Conf.* (but not in the convention record). May be found as paper 4.6 in M. Skolnik, *Radar Applications,* Ref. 113.

119. Kennedy, P. D. "FFT Signal Processing for Non-Coherent Airborne Radars." *Proc. 1984 IEEE National Radar Conference,* pp. 79–83.

120. Strickland, P. C. "Multiprocessor Architecture Gives SLAR New Features." *Defense Electronics* (February 1987), pp. 92–101.

121. Raney, R. K. "Synthetic Aperture Imaging Radar and Moving Targets." *IEEE Trans.* AES-7 (May 1971) pp. 499–505.

122. Zebker, H. A., T. G. Farr, R. P. Salazar, and T. H. Dixon. "Mapping the World's Topography Using Radar Interferometry. The TOPSAT Mission." *Proc. IEEE* 82 (December 1994), pp. 1774–1786.

123. Bamler, R., and P. Hartl. "Synthetic Aperture Radar Interferometry." *Inverse Problems* 14 (August 1998), pp. R1–R54.

124. Goldstein, R. M., T. P. Barnett, and H. A Zebker. "Remote Sensing of Ocean Currents." *Science* 246 (December 8, 1989), pp. 1282–1285.

125. Anonymous. Joint Stars, Advertising Supplement to *Jane's Defense Weekly* (September 5, 1992).

126. Shnitkin, H. "Joint Stars Phased Array Radar Antenna." *IEEE AES Systems Magazine* 9 (October 1994), pp. 34–41.

127. The information in this paragraph and its wording were graciously supplied by Marshall Greenspan and his colleagues at Northrop Grumman Norden Systems. It is used here with only minor modification.

128. Tang, C. H. "Engineering Analyses Associated with the Development of an Airborne Phased Array Radar Antenna." *Antenna Applications Symposium.* Allerton Park, Monticello, IL, September 25–27, 1991.

129. DiDomizio, R., et al. "Dual Cancellation Interferometric AMTI Radar," U. S. Patent 5,559,516, September 24, 1996.

130. Tobin, M. E., and M. Greenspan. "Adaptation of AN/APG-76 Multimode Radar to the Smuggling Interdiction Mission." *Proc. 1996 IEEE National Radar Conference* (May 13–16, 1996), pp. 13–18. Reprinted in *IEEE AES Systems Magazine* (November 1996).

131. Anonymous. "Norden Offering 3-D SAR System for Moving Target Detection." *Defense Electronics* (November 1993), p. 18.

132. Hall, W. M., and H. R. Ward. "Signal-to-Noise Loss in Moving Target Indicator." *Proc. IEEE* 56 (February 1968), pp. 233–234.

133. Kretschmer, F. K., Jr. "Correlation Effects of MTI Filters." *IEEE Trans.* AES-13 (May 1977), pp. 321–322.

134. Trunk, G. V. "MTI Noise Integration Loss." *Proc. IEEE* 65 (November 1977), pp. 1620–1621.

135. Muller, B. "MTI Loss with Coherent Integration of Weighted Pulses." *IEEE Trans.* AES-17 (July 1981), pp. 549–552.

136. Schleher, D. C. *MTI Radar.* Dedham, MA: Artech House, 1978, Sec. 3, Pulse-Burst MTI Radars.

137. Nathanson, F. E. Ref. 45, Chap. 11.

138. Zeoli, G. W. "Some Results on Pulse-Burst Radar Design." *IEEE Trans.* AES-7 (May 1971), pp. 486–498.

139. Cantrell, B. H. "A Short-Pulse Area MTI." *Naval Research Laboratory Report* 8162 (September 22, 1977).

140. Skolnik, M. I., G. Andrews, and J. P. Hansen. "An Ultrawideband Microwave-Radar Conceptual Design." *Record of the IEEE 1995 International Radar Conference* (May 8–11, 1995), pp. 16–21. IEEE Catalog No. 95-CH-3571-0.

141. Lewis, B. L., F. F. Kretschmer, Jr., and W. W. Shelton. *Aspects of Radar Signal Processing.* Norwood, MA: Artech House, 1986.

142. Howells, P. W. "Explorations in Fixed and Adaptive Resolution at GE and SURC." *IEEE Trans.* AP-24 (September 1976) pp. 575–584, Sec. 4.3.

143. Xiaojun, Y., L. Yongtan, and D. Fengzeng. "A Compatible Method for Frequency Agility and MTI Operation." *Proc. 1989 International Symposium on Noise and Clutter Rejection in Radars and Imaging Sensors,* IEICE, pp. 543–547, 1989.

144. Skolnik, M. "Improvements for Air-Surveillance Radar." *Proc. 1999 IEEE Radar Conference,* Waltham, MA, April 20–22, 1999, pp. 18–21.

145. Hsiao, J. K. "Analysis of a Dual Frequency Moving Target Indication System." *The Radio and Electronic Engineeer* 45 (July 1975), pp. 351–356.

146. Meyer, J. W., and C. E. Muehe. "Report of a Survey of Airborne Moving Target Indicator Radar Systems," *MIT Lincoln Laboratory Technical Note* 1970–14, 28 April 1970, AD 509740, p. 20.

147. Nichols, R. E., Jr. *Police Radar.* published by Springfield, IL: C. C. Thomas, 1982.

148. Heide, P., R. Schubert, V. Magori, and R. Schwarte. "A High Performance Multisensor System for Precise Vehicle Ground Speed Measurement." *Microwave J.* 39 (July 1996), pp. 22–34.

149. Skolnik, M. *Radar Applications.* New York: IEEE Press, 1988, Sec. 7.1.

150. Ivanov, A. "Radar Guidance of Missiles." In *Radar Handbook.* M. Skolnik, Ed. New York: McGraw-Hill, 1990, Chap. 19, Sec. 19.2.

151. Saunders, W. K. "Post-War Developments in Continuous-Wave and Frequency-Modulated Radar." *IRE Trans.* ANE-8 (March 1961), pp. 7–19.

152. Stove, A. G. "Linear FMCW Radar Techniques." *IEE Proc.-F* 139 (October 1992), pp. 343–350.

PROBLEMS

3.1 A satellite orbiting the earth in a circular orbit at an altitude of 5000 nmi has a speed of 2.7 nmi/s. (a) What is the doppler frequency shift if the satellite is observed by a UHF radar (450 MHz) lying in the plane of orbit, just as the satellite appears over the horizon? (The radius of the earth is 3440 nmi. You may ignore the effects of refraction by the earth's atmosphere and reflection from the earth's surface.) (b) What is the doppler frequency shift when the satellite is observed at the zenith?

3.2 A VHF radar at 220 MHz has a maximum unambiguous range of 180 nmi. (a) What is its first blind speed (in knots)? (b) Repeat, but for an *L*-band radar at 1250 MHz. (c) Repeat, but for an *X*-band radar at 9375 MHz. (d) What would be the unambiguous range (nmi) of the *X*-band radar of part (c) in order to give the same blind speed you found in part (a) for the VHF radar? (e) If you needed to have a radar with the first blind speed of the VHF radar of part (a), would you rather have the VHF radar of part (a) or the *X*-band radar of part (d)? Please explain your answer (There might not be a unique answer.)

3.3 An *L*-band radar (1250 MHz) has a prf of 340 Hz. It detects a rainstorm moving at a radial velocity of 12 kt. Assume that the width of the thunderstorm's doppler spectrum is very small (a narrow spectral line; which is not, of course, reality but it makes the problem easier). The radar employs a single delay-line canceler. (a) How much does the single delay-line canceler attenuate (in dB) the storm echo compared to the response if the storm were moving with a radial velocity corresponding to the velocity which gives the

maximum filter response? (b) What would be the attenuation of the storm compared to the maximum response, if a double delay-line canceler were used?

3.4 (a) Show that the product of the maximum unambiguous range R_{un} and the first blind speed v_1 is equal to $c\lambda/4$, where c = velocity of propagation and λ = radar wavelength. (b) What guidance, if any, does this relation give for avoiding ambiguities?

3.5 What is the highest frequency that a radar can be operated if it is required to have a maximum unambiguous range of 200 nmi and no blind speeds less than 600 kt.

3.6 Show that a triple delay-line canceler is equivalent to a four-pulse delay-line canceler with weights equal to the coefficients of the binomial expansion with alternating sign.

3.7 (a) Derive the expression for the ratio v_1/v_B, where v_1 is the first blind speed of a staggered prf with N different prfs, and v_B is the first blind speed obtained with a constant prf waveform equal to the average of the N staggered prfs. (b) What is the ratio v_1/v_B when $N = 4$ and the prfs are related as 30:35:32:36?

3.8 (a) How can the transmission of N constant-prf radar waveforms, each at a different RF frequency, be used to avoid blind speeds? (b) Derive an expression for v_1/v_{cf}, where v_1 is the first blind speed when N different RF frequencies are transmitted, all at the same prf, and v_{cf} is the blind speed when only a single RF frequency is transmitted equal to the average of the N RF-frequencies. (c) Is there any advantage in changing both the prf and the RF frequency to avoid blind speeds?

3.9 An S-band (3.1 GHz) air-surveillance radar utilizes a staggered waveform with four different prfs, which are 1222, 1031, 1138, and 1000 Hz.

a. What is the first blind speed (knots) if a constant prf is used which has a pulse repetition period equal to the average of the four periods of the staggered waveform?

b. What is the first blind speed (knots) of the staggered prf waveform? Note that the n_i for these four frequencies are 27, 32, 29, 33 respectively.

c. What is the maximum unambiguous range of the staggered prf waveform?

d. What is the depth (dB) of the first null of the staggered prf waveform?

e. What is the maximum MTI improvement factor for the staggered prf waveform, assuming a gaussian clutter spectrum with a standard deviation of 10 Hz?

3.10 (a) What is the first blind speed (knots) of an L-band radar (1250 MHz) when the prf has a maximum unambiguous range of 240 nmi? (b) Determine the periods of a pulse-to-pulse staggered MTI waveform with three different periods, for the purpose of increasing the radar's first blind speed found in (a) to a value no less than 1200 kt. The maximum unambiguous range of the three periods is to be no less than 240 nmi. (Note: There is no unique answer for this part. In practice the choice of the three periods also should be selected to achieve an acceptable null depth and a desired improvement factor, something beyond the scope of this particular problem.)

3.11 (a) In a digital filter bank with 16 filters, what phase increment (degrees) is required for the phase shifts at each of the 16 taps of the delay line so as to generate the filter that is adjacent to the zero doppler filter? (b) What is the null-width (the distance between the two nulls that define the main response) of the filters if the pulse repetition frequency of

the radar is 2560 Hz? (c) If a four-pulse canceler precedes the 16-tap delay line of the filter bank, how many pulses are there in a coherent processing interval?

3.12 Consider an MTD processor with a bank of eight contiguous doppler filters installed in an airport surveillance radar operating at *S* band (2.8 GHz). The MTD uses two different pulse repetition frequencies to unmask a moving target whose echo signal might be in the same doppler filter as moving weather clutter. Let one of the two prfs be 1100 Hz. Weather clutter is assumed to have a spectrum of radial velocities extending from 0 to 25 kt. An aircraft flying at a radial velocity of 250 kt is aliased in doppler and falls into the same doppler filter (near the middle of filter no. 2—please verify this) as the weather clutter. It is masked by the clutter and not detected. (Note that filter no. 1 is designated as the filter centered at zero frequency.) (a) What should be the second prf (smaller than the first, so as not to decrease the maximum unambiguous range) in order to move the aliased aircraft velocity completely outside of the main response of filter no. 2 and into the middle of filter no. 4? (b) What percent change has been made in the first prf to arrive at the second prf? (c) Instead of changing the prf to unmask the target, how much should the RF frequency be changed in order to unmask the target (by shifting it to the middle of the fourth filter) when the prf is kept at 1100 Hz?

3.13 An MTI radar with a single delay-line canceler has the following characteristics:

frequency = 3000 MHz

azimuth beamwidth = 1.2 degrees

antenna rotation rate = 10 rpm

prf = 1000 Hz

A/D converter with 8 bits quantization

stalo phase stability = 0.6 degree

clutter standard deviation, σ_v = 0.3 m/s

a. Determine which of the following is the major limitation to the overall MTI improvement factor for this radar:

- stability of the stalo (due to phase changes)
- clutter internal motion
- antenna scanning modulation
- A/D converter noise

b. What is the overall improvement factor (dB) for this radar?

3.14 A radar is to have a total improvement factor of 45 dB. Its frequency is 3.0 GHz, the prf is 340 Hz, and it uses a single delay-line canceler. Assume that the four factors asked for below in (a) through (d) are independent of one another and that their contributions to the overall improvement factor are allocated equally.

a. What must be the overall phase stability (degrees)?

b. What must be the relative amplitude stability (percent)?

c. What is the minimum number of bits required for the A/D converter?

d. What is the maximum permissible rms velocity spread (m/s) of the clutter fluctuations?
e. What should be the limit level of the receiver?

3.15 (a) What is the limitation to the improvement factor due to antenna scanning modulation (finite time on target) with a radar that has a beamwidth of 1.5 degrees, prf of 340 Hz, and antenna scan rate of 6 rpm when a single delay-line canceler is used? (b) What two *basic* things can the radar systems designer consider to increase to at least 40 dB the limitation to the improvement factor caused by antenna scanning? (c) Which of your two methods in part (b) do you think is the better option?

3.16 In a rotating reflector antenna with dimension D, what is the relationship between the spread in doppler frequency due to the finite time on target and the doppler frequency shift from the tip (end) of the rotating antenna? (Assume that the beamwidth of the antenna is $\theta_B = \lambda/D$ radians.)

3.17 (a) Assume the MTI improvement factor is determined only by the internal motion of the clutter. How much will the improvement factor be decreased (in dB) if the frequency of a radar using a three-pulse canceler were changed from 430 MHz (UHF) to 3.3 GHz (*S* band)? (b) How much should the prf of the *S*-band radar be increased to make its improvement factor equal that of the UHF radar?

3.18 If internal motion of the clutter caused by the wind were the only factor affecting the clutter spectrum, what would be the improvement factor at a frequency of 10 GHz for a breezy wind (9 kt), prf of 1000 Hz, and a double delay-line canceler, when the clutter spectrum is modeled by an exponential clutter spectrum? (Be careful of units.)

3.19 Show that the spread in the AMTI radar clutter spectrum due to movement of the radar (platform motion), which is given by Eq. (3.58) as $\Delta f_c = \dfrac{2v}{\lambda}\,\theta_B \sin\theta$, is independent of frequency, assuming both the velocity v and the antenna dimension D are constant.

3.20 Assuming an airborne air-surveillance (AMTI) radar flying at a speed of 300 kt with a rotating fan-beam antenna whose horizontal dimension $D = 24$ ft, plot the doppler shift f_c of the ground clutter echo and the spread in doppler shift Δf_c as a function of the azimuth angle (from 0 to 180 degrees) for frequencies of 420 MHz and 3.5 GHz. (OK to assume the elevation angle is zero in this problem and that the azimuth beamwidth in degrees is $\theta_B = 65\lambda/D$, where λ is the wavelength.)

3.21 Consider an AMTI radar with a frequency of 440 MHz flying in an aircraft at a speed of 320 kt. Its azimuth beamwidth is 6 degrees and its prf is 330 Hz. (a) What is the doppler frequency of the clutter echo and the spread in the clutter doppler at azimuth angles of 0, 45, and 90 degrees, where 0 is head-on and 90 is broadside? (You may assume that the elevation angle is zero, which is unrealistic of course, but it makes the problem simpler.) (b) Assume that TACCAR is applied so that the doppler clutter frequency is fully compensated along the center of the main beam (that is, the center frequency of the clutter doppler spectrum is at zero doppler frequency). DPCA is not applied. Sketch the doppler space (the resulting clutter spectrum as a function of doppler frequency) for the case where the radar antenna is pointing broadside at 90 degrees azimuth angle. For this problem you may assume that σ_c is the same as $\Delta f_c/2$. (Draw approximately to scale along the frequency axis.) (c) What is the value of σ_c/f_p when the antenna is pointing broadside as it

is in part (b), where f_p = prf and σ_c = standard deviation of the clutter spectrum which can be approximated here by $\Delta f_c/2$? (d) How well do you think a radar of this type detects moving aircraft targets in clutter?

3.22 (a) Why does a high-prf pulse doppler radar require a much larger improvement factor than a low-prf MTI radar, assuming comparable performance in detecting moving targets in clutter? (b) Why does a high-prf pulse doppler radar (such as AWACS) generally need more average power than an AMTI radar of comparable performance? (c) Why does a high-prf pulse doppler radar not need DPCA as does an AMTI radar?

3.23 (a) What does a medium-prf pulse doppler radar do better than a high-prf pulse doppler radar? (b) What does a high-prf radar do better than a medium-prf pulse doppler radar?

3.24 Why can't the altitude line in a high-prf pulse doppler radar be eliminated by range gating rather than by filtering?

3.25 An HF over-the-horizon radar for detection of commercial aircraft targets out to a range of 2000 nmi might, for example, operate at a frequency of 15 MHz and a prf of 30 Hz. It employs doppler processing to separate moving targets from clutter. Is it an MTI radar, a pulse doppler radar, or what? Explain your answer.

chapter

4

Tracking Radar

4.1 TRACKING WITH RADAR

Types of Tracking Radar Systems Thus far we have considered radar mainly as a surveillance sensor that detects targets over a region of space. A radar not only recognizes the presence of a target, but it determines the target's location in range and in one or two angle coordinates. As it continues to observe a target over time, the radar can provide the target's trajectory, or *track*, and predict where it will be in the future. There are at least four types of radars that can provide the tracks of targets:

- *Single-target tracker* (STT). This tracker is designed to continuously track a single target at a relatively rapid data rate. The data rate, of course, depends on the application, but 10 observations per second might be "typical" of a military guided-missile weapon-control radar. The antenna beam of a single-target tracker follows the target by obtaining an angle-error signal and employing a closed-loop servo system to keep the error signal small. (A small angle-error signal means that the radar is accurately tracking the target.) Most of this chapter will be concerned with this type of tracker. The *C*-band AN/FPQ-6, shown in Fig. 4.1a is an example of a long-range precision tracking radar that was used at missile instrumentation ranges. The major application for continuous tracking radars has been for the tracking of aircraft and/or missile targets in support of a military weapon-control system.

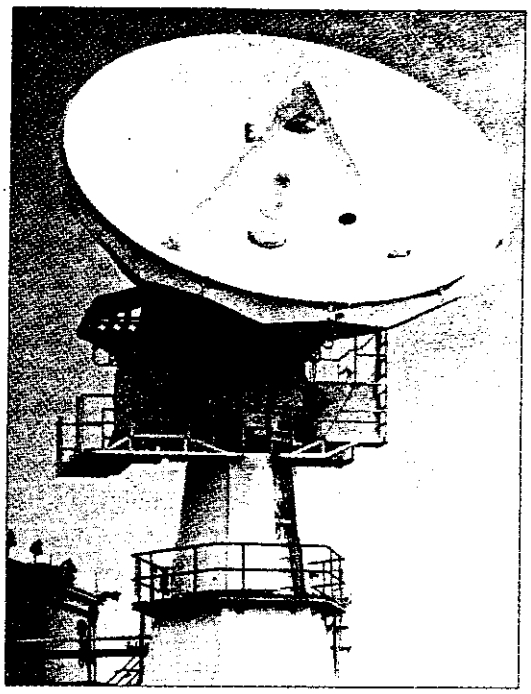

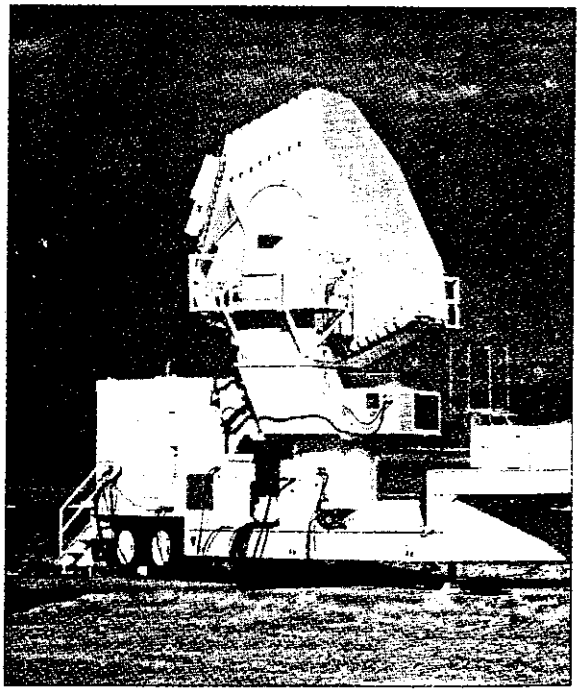

Figure 4.1 Two examples of missile-range precision instrumentation radars that use monopulse angle-tracking. Both operate at C band. (Top) Fixed-site AN/FPQ-6 Precision Tracking Radar with a 29-ft diameter Cassegrain reflector antenna capable of 0.1 mil tracking accuracy. (Bottom) Mobile AN/MPS-39 Multiple Object Tracking Radar (MOTR), a trainable space-fed 12-ft diameter electronically steerable lens array radar for simultaneously tracking up to 10 objects to a range accuracy of several feet and 0.2 mil angle accuracy.

(Courtesy of U.S. Army White Sands Missile Range). Both radars were manufactured by Lockheed-Martin Government Electronic Systems, Moorestown, New Jersey (formerly known as RCA Moorestown).

- *Automatic detection and track* (ADT). This performs tracking as part of an air-surveillance radar. It is found in almost all modern civil air-traffic control radars as well as military air-surveillance radars. The rate at which observations are made depends on the time for the antenna to make one rotation (which might vary from a few seconds to as much as 12 seconds). The ADT, therefore, has a lower data rate than that of the STT, but its advantage is that it can simultaneously track a large number of targets (which might be many hundreds or a few thousands of aircraft). Tracking is done open loop in that the antenna position is not controlled by the processed tracking data as it is in the STT. This type of tracking is discussed in Sec. 4.9.
- *Phased array radar tracking.* A large number of targets can be held in track with a high data rate by an electronically steered phased array radar. Multiple targets are tracked on a time-shared basis under computer control since the beam of an electronically scanned array can be rapidly switched from one angular direction to another, sometimes in a few microseconds. It combines the rapid update rate of a single-target tracker with the ability of the ADT to hold many targets in track. This is the basis for such air-defense weapon systems as Aegis and Patriot. An example of a phased array for multiple-target tracking is the *C*-band multiple-target tracking range instrumentation radar called MOTR which is shown in Fig. 4.1b.
- *Track while scan* (TWS). This radar rapidly scans a limited angular sector to maintain tracks, with a moderate data rate, on more than one target within the coverage of the antenna. It has been used in the past for air-defense radars, aircraft landing radars, and in some airborne intercept radars to hold multiple targets in track. It is briefly mentioned in Sec. 4.7. Unfortunately, the same name *track while scan* was also applied in the past to what is now usually called ADT.

A radar can track targets in range as well as angle. Sometimes tracking of the doppler frequency shift, or the radial velocity, is also performed. Most of the discussion in this chapter, however, will be on angle tracking.

Angle-Tracking In a simple pencil-beam radar the detection of a target provides its location in angle as being somewhere within the antenna beamwidth; but more information is needed to determine the direction the antenna should be moved to maintain the target within its beam. Consider the angle measurement in a single angular coordinate. In order to determine the direction in which the antenna beam needs to be moved, a measurement has to be made at two different beam positions. Figure 4.2 shows two beam positions A and B at two different angles. The two beams are said to be *squinted*, with a squint angle $\pm\theta_q$ relative to the boresight direction. These may be two simultaneous beams, or one beam that is rapidly switched between the two angular positions. The crossover of the two beams determines the *boresight* direction. The tracking radar has to position the two beams so that the boresight is always maintained in the direction of the target; that is, the angle θ_0 is in the direction of the target angle θ_T. In this example, the relative amplitudes a_A and a_B of the echo signals received from a target measured in the two positions determine how far the target is from boresight and in what direction the two beams have to be repositioned to maintain the target on boresight. This applies for one angle coordinate. Two additional beam positions are needed in the orthogonal plane to obtain angle

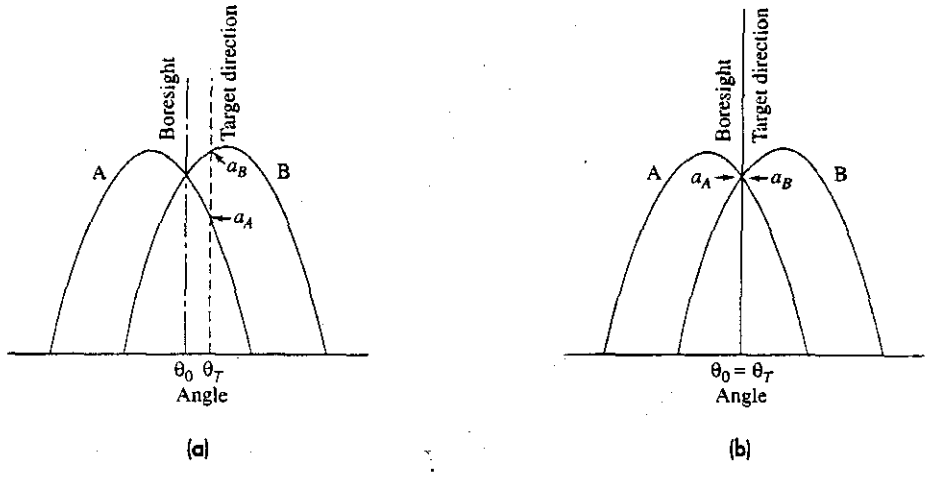

Figure 4.2 Basic principle of continuous angle tracking. (a) Two overlapping antenna patterns that cross over at the boresight direction θ_0. A target is located in this example to the right of the boresight at the angle θ_T. The amplitude a_B of the target echo in beam B is larger than the amplitude a_A in beam A, which indicates that the two beams should be moved to the right to bring the target to the boresight position. (b) Boresight position θ_0 is shown located in the direction of the target θ_T when $a_A = a_B$.

tracking in the orthogonal angle coordinate. Three beam positions are the minimum needed to obtain an angle measurement in two coordinates; but, almost always, four beams have to be used.

Early tracking radars used a single time-shared beam to track in two angles. These trackers which time share a single beam are known as either *conical scan* or *sequential lobing* trackers. (Both will be discussed later in this chapter.) Modern, high-precision tracking radars, however, use the equivalent of four simultaneous beams to perform two-dimensional tracking. They are called *simultaneous lobing* trackers, of which the most popular is *monopulse*, which is described next.

4.2 MONOPULSE TRACKING[1,2]

A monopulse tracker is defined as one in which information concerning the angular location of a target is obtained by comparison of signals received in two or more simultaneous beams.[3] A measurement of angle may be made on the basis of a single pulse; hence, the name *monopulse*. In practice, however, multiple pulses are usually employed to increase the probability of detection, improve the accuracy of the angle estimate, and provide resolution in doppler when necessary. By making an angle measurement based on the signals that appear simultaneously in more than one antenna beam, the accuracy is improved compared to time-shared single-beam tracking systems (such as conical scan or sequential lobing) which suffer degradation when the echo signal amplitude changes with time. Thus the accuracy of monopulse is not affected by amplitude fluctuations of

the target echo. It is the preferred tracking technique when accurate angle measurements are required.

The monopulse angle method may be used in a tracking radar to develop an angle error signal in two orthogonal angle coordinates that mechanically drive the boresight of the tracking antenna using a closed-loop servo system to keep the boresight positioned in the direction of the moving target. In radars such as the phased array, angle measurements can be obtained in an open-loop fashion by calibrating the error-signal voltage in terms of angle.

There are several methods by which a monopulse angle measurement can be made. The most popular by far has been the *amplitude-comparison monopulse* which compares the amplitudes of the signals simultaneously received in multiple squinted beams to determine the angle. When the term *monopulse* is used by itself with no other descriptors, it generally refers to the amplitude-comparison version.

Amplitude-Comparison Monopulse For simplicity, this form of monopulse is first described for the measurement of only one angle coordinate. Two overlapping antenna patterns with their main beams pointed in slightly different directions are used, as in Fig. 4.3a. The two beams in this figure are said to be *squinted,* or *offset.* They might be generated by using two feeds slightly displaced in opposite directions from the focus of a parabolic reflector. The essence of the amplitude-comparison monopulse method is in

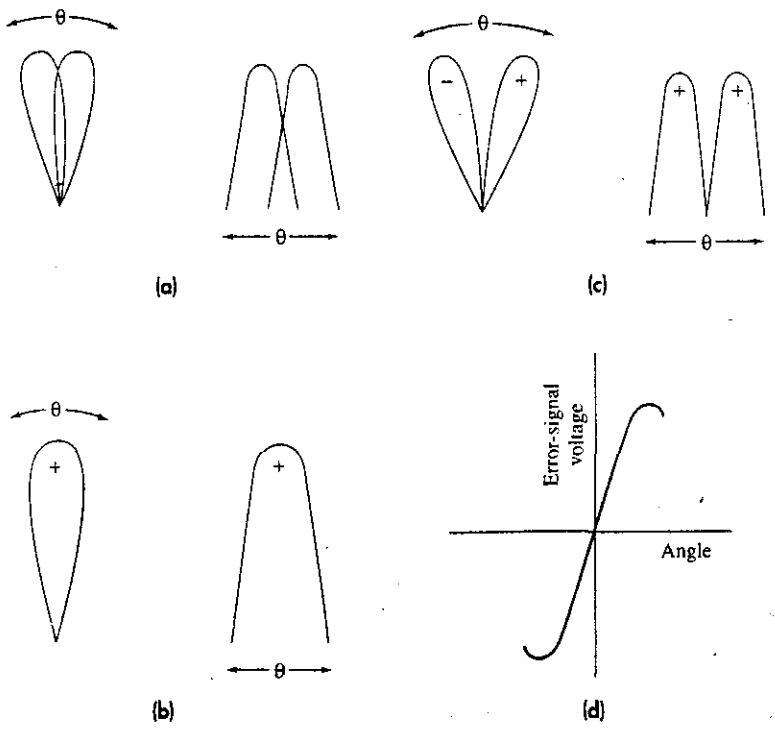

Figure 4.3 Monopulse antenna patterns and error signal. The left-hand sketches in (a) to (c) are in polar coordinates; right-hand sketches are in rectangular coordinates. (a) Two squinted antenna beams; (b) sum pattern of two squinted beams shown in (a); (c) difference pattern; (d) error signal as a function of the angle from boresight.

taking both the sum and the difference* of the two squinted antenna patterns, which are shown in Figs. 4.3b and 4.3c. The sum pattern is employed on transmission, while both the sum and the difference patterns are used on reception. The signal received with the difference pattern provides the magnitude of the angle error. The direction of the angle error is found by comparing the phase of the difference signal with the phase of the sum signal, as explained below. Signals received from the sum and difference patterns are amplified separately and combined in a phase-sensitive detector to produce the angle-error signal, Fig. 4.3d. The sum signal also provides target detection and range measurement, as well as act as a reference for determining the sign of the angle measurement.

Block Diagram A simple block diagram of the amplitude-comparison monopulse tracking radar for a single angular coordinate is shown in Fig. 4.4. The two adjacent antenna feeds are connected to the two input arms of a *hybrid junction,* which is a four-port microwave device with two input and two output ports. When two signals (such as the signals from the two squinted beams) are inserted at the two input ports, the sum and difference of the two are found at the two output ports. (There are several methods for obtaining a hybrid junction, as indicated later.) On reception, the output of the sum and difference ports are each heterodyned to an intermediate frequency and amplified in the superheterodyne receiver. It is important that the sum and difference channels have the same phase and amplitude characteristics. For this reason, a single local oscillator (LO) is shared by the two channels. The transmitter is connected to the sum port of the hybrid junction. A duplexer (TR) is included in the sum channel for the protection of the sum-channel receiver. Although it might not be needed for protection of the difference-channel receiver, a duplexer is often inserted in the difference channel so as to maintain the phase and amplitude balance of the two channels. Automatic gain control, not shown, is also used to help maintain balance.

The outputs of the sum and difference channels are the inputs to the *phase-sensitive detector,* which is a nonlinear device that compares two signals of the same frequency.

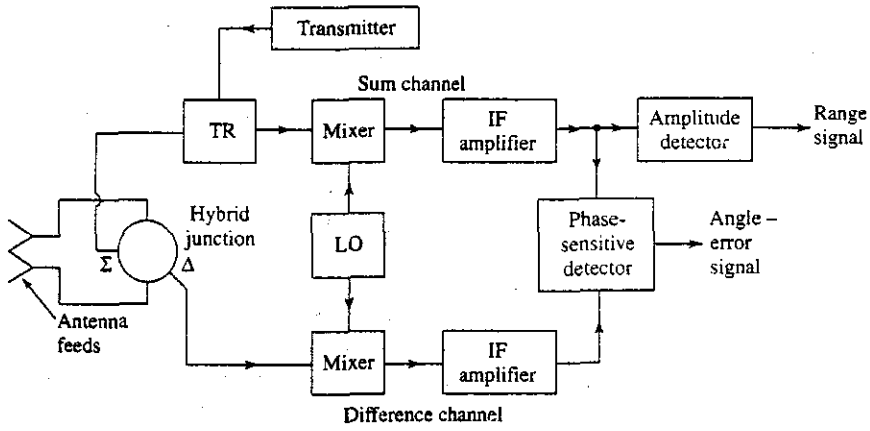

Figure 4.4 Simple block diagram of the amplitude-comparison monopulse in one angle coordinate. Σ denotes the sum channel. Δ denotes the difference channel.

*It is sometimes said that a simultaneous-lobing tracking radar should not be called monopulse unless it employs the sum and difference patterns.

In this case, the two signals are those of the sum and difference channels. The output of a phase-sensitive detector is the angle-error signal. Its magnitude is proportional to $|\theta_T - \theta_0|$, where θ_T = target angle and θ_0 = boresight, or crossover, angle. The sign of the output of the phase-sensitive detector indicates the direction of the angle error relative to the boresight. If the sum signal in the IF portion of the receiver is $A_s \cos \omega_{IF} t$, the difference signal will be either $+A_d \cos \omega_{IF} t$ or $-A_d \cos \omega_{IF} t$, depending on which side of boresight is the target. (In the above, $A_s > 0$ and $A_d > 0$.) Since $-A_d \cos \omega_{IF} t = A_d \cos \omega_{IF}(t + \pi)$, the sign of the difference signal may be found with the phase-sensitive detector by determining whether the difference signal is in phase with the sum signal or 180° out of phase; that is, whether the output phase is 0 or π radians.

Although a phase comparison is part of the amplitude-comparison monopulse radar, the magnitude of the angle-error signal is determined by comparing the echo-signal amplitudes received with simultaneous squinted beams. The separation of the two antenna feeds is small so that the phases of the signals in the two beams are almost equal when the target angle is not far from boresight.

Hybrid Junctions[4] As mentioned, the hybrid junction is a four-port device that provides at its two output ports the sum and difference of the signals that are at its two input ports. For monopulse radar, they are usually constructed from waveguide; but they can also be in coax or stripline. The hybrid junction known as the *magic-T*, sketched in Fig. 4.5a, consists of an E-plane T-junction (shown vertical) and an H-plane T-junction (shown horizontal) arranged as indicated. A signal, whose E-field (electric field) is indicated by the solid arrow, is shown as the input at port 1. It is divided equally in power and appears with the same phase at both ports 3 and 4. Nothing will appear at port 2. A signal whose E-field is indicated by the dashed arrow is the input at port 2. It is divided equally between ports 3 and 4, and no energy appears at port 1. The nature of the E-plane junction is such as to make the two signals at ports 2 and 3 out of phase by 180°, as is indicated by the dashed arrows being reversed in direction. Thus the output of port 4 is the *difference* of the signals at ports 1 and 2; and the output of port 3 is the *sum* of ports 1 and 2. The magic-T is inherently a broadband device. As shown, it is bulky, but its arms can be folded to make it more compact without changing its electrical characteristics. Folding means making arms 3 and 4 to be parallel to arm 2 (by folding either up or down) or they may be folded forward to be parallel to arm 1.

The *rat-race*, or *hybrid-ring junction*, is shown sketched in Fig. 4.5b. Ports 1 and 2 are the two inputs. A signal at port 1 can reach port 4 by two separate paths, one clockwise and the other counterclockwise. The two paths are of the same length (3/4 wavelength), so they reinforce and a signal will appear at this output port. The signal input at port 1 also reaches port 3 by two paths—one which travels 5/4 wavelength and the other 1/4 wavelength. They are also in phase, so a signal will appear at port 3 from port 1. At port 2, however, the two signals from port 1 are 180° out of phase (the clockwise signal travels one wavelength and the counterclockwise signal travels one-half wavelength). Thus a signal that is input at port 1 will be divided equally and appear at ports 3 and 4, but not appear at 2. Similarly, a signal input at port 2 will appear at ports 3 and 4 and not at port 1. At port 4, however, the signal from port 2 can be seen to be 180° out of phase with the signal that arrives there from port 1. Thus the output of port 4 is the *difference* of the

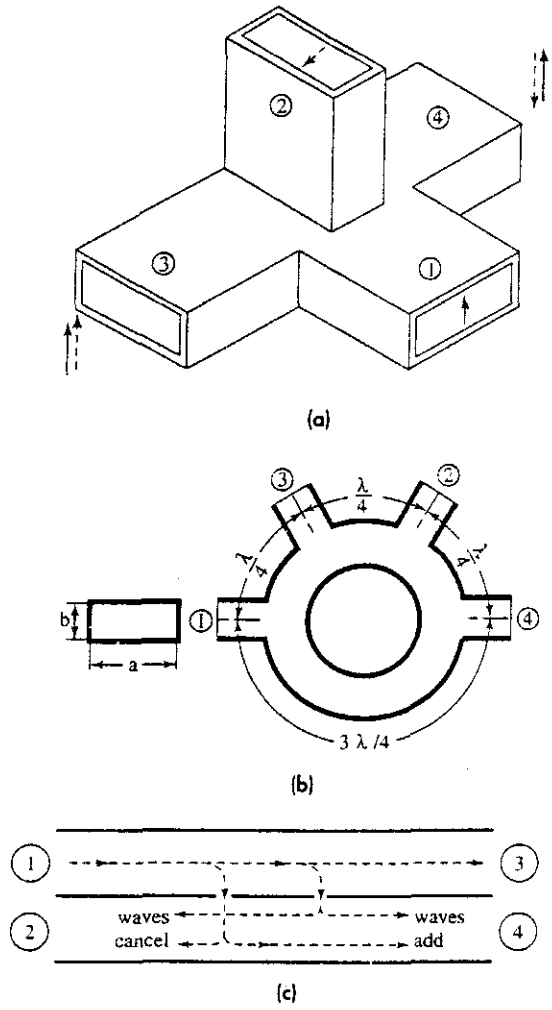

Figure 4.5 Examples of hybrid junctions as might be used in monopulse radar. (a) Magic-T; (b) rat-race, or hybrid-ring junction; (c) 3-dB directional coupler obtained by use of two rectangular waveguides with narrow walls touching and with quarter-wavelength spacing between the two coupling holes.

input signals at ports 1 and 2; and port 3 is the *sum* of the signals at ports 1 and 2. Since the operation of this device depends on the lengths between ports being some fraction of a wavelength, it will be frequency sensitive and not as broadband as the magic-T.

The *3-dB directional coupler* is a relatively compact form of hybrid junction that can also be used to obtain the sum and difference signals for monopulse. One method of obtaining a 3-dB directional coupler is to align two rectangular waveguides with their narrow walls touching, as in Fig, 4.5c. Microwave energy from one of the waveguides is coupled to the other by means of appropriate holes or slots between the two waveguides. Because of the quarter-wave spacing between the two coupling holes shown in the figure, this configuration is a frequency-sensitive device, but by employing more than two coupling holes or by using slots instead of holes, it can be made to operate over a useful

frequency band.[5] (In the configuration of Fig. 4.5c, a 90° phase shift has to be inserted in either port 1 or 2 in order to provide the sum and difference at the other two.)

Monopulse in Two Angle Coordinates A block diagram of a monopulse radar for extracting angle-error signals in both azimuth and elevation is shown in Fig. 4.6. The cluster of four feed horns generate four partially overlapping (squinted) beams. The four feeds might be used to illuminate a parabolic reflector, Cassegrain reflector, or a space-fed phased array antenna. The arrangement of the four feeds is shown in the upper left-hand portion of the figure. All four feeds are used to generate the sum pattern on transmission and reception. The difference pattern in one plane is formed by taking the sum of two adjacent feeds and subtracting them from the sum of the other two adjacent feeds. The difference pattern in the orthogonal plane is obtained similarly. For example, based on the arrangement of the feeds shown in Fig. 4.6, the sum pattern is found from $A + B + C + D$; the azimuth difference pattern is obtained from $(A + B) - (C + D)$; and the elevation difference pattern is $(B + D) - (A + C)$. Note that the upper feeds form the lower beams when radiated by a reflector antenna. A total of four hybrid junctions are needed to obtain the sum pattern and the two difference patterns. The three mixers for the sum, elevation difference, and azimuth difference channels use a common local oscillator to better maintain the phase relationships among the three channels. Two phase-sensitive detectors extract the angle-error information; one for azimuth and the other for elevation. Range information is extracted from the output of the sum channel after envelope detection.

Since a phase comparison is made between the output of the sum channel and each of the difference channels, it is important that large relative phase differences not occur among the three channels. The phase difference between channels should be maintained to within 25° or better for reasonably proper performance.[6]

Automatic Gain Control (AGC) AGC is required in the receiving system in order to maintain a stable closed-loop servo system for angle tracking and to insure that the

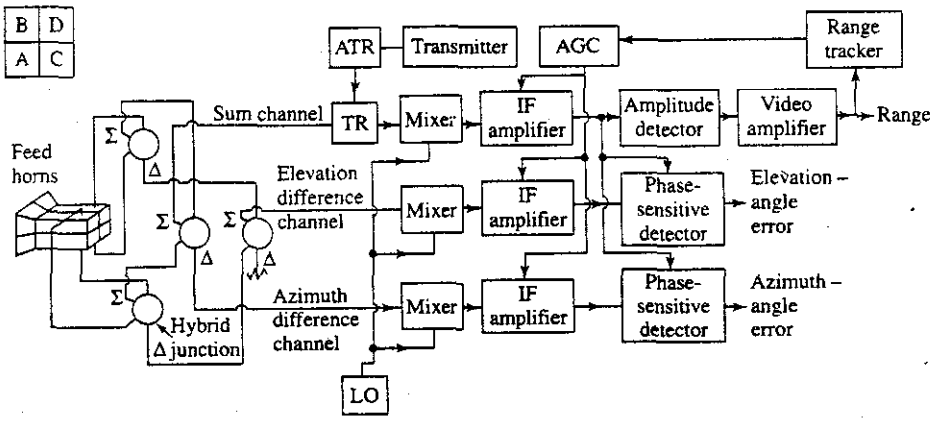

Figure 4.6 Block diagram of two-coordinate (azimuth and elevation) amplitude-comparison monopulse tracking radar. Diagram in the upper left corner represents the four-horn feed. (After Fig. 18.9, Ref. 1.)

angle-error signal is not affected by changes in the received signal amplitude. As indicated in the block diagram of Fig. 4.6, the AGC signal is obtained from the peak voltage of the sum channel and generates a negative dc voltage proportional to the peak signal voltage. The AGC signal from the sum channel is fed back to control the gain of all three channels so as to provide a constant angle sensitivity independent of changes in target cross-section fluctuations or changes in range.

Antennas for Monopulse The assemblage of hybrid junctions, waveguides, and other microwave components needed to extract the sum and difference signals in a monopulse radar is called a *comparator.* The comparator circuitry of the early monopulse radars was quite large and bulky. If it were placed at the feed of a parabolic reflector antenna, it would cause considerable blockage of the antenna radiation and result in high sidelobes and reduced angle accuracy. For this reason, the original amplitude-comparison monopulse radar that was developed by the Naval Research Laboratory employed a metal-plate lens antenna. A lens does not cause aperture blocking, but it experiences greater loss than does a reflector antenna because there will be unwanted reflections from both the input surface and the output surface of the lens. With advances in microwave hardware technology, the size of the comparator circuitry was reduced and the AN/FPS-16 precision tracking radar (introduced in the late 1950s) was able to use a reflector antenna with the microwave circuitry at the focus of the parabolic reflector. The four waveguide transmission lines to the four feeds at the focus were made of Invar to reduce the adverse effects of temperature differences that might be experienced by the waveguides. The introduction of the Cassegrain reflector antenna (also in the late 1950s) allowed the microwave circuitry to be placed behind the parabolic reflector at its apex without aggravating the antenna blockage problem. Also, the feed system at the apex is easier to support mechanically than if it had to be placed in front of the reflector at the focus. Almost all continuous tracking precision monopulse radars employ the Cassegrain antenna. The monopulse principle can also be used with phased array antennas.

Optimum Squint Angle The greater the squint angle, the greater will be the slope of the angle-error signal at boresight and the better will be the accuracy of the angle measurement. As the squint angle increases, however, the on-axis gain of the sum pattern decreases. Thus there will be an optimum value of the squint angle. Figure 4.7 plots the slope of the error signal as a function of the squint angle θ_q, assuming the shape of the squinted beams can be modeled by a gaussian function and that mutual coupling between the feeds can be ignored. (The basis for this curve was described in the first edition of this text.[7]) The signal received in the sum channel is proportional to the square of the sum pattern (the sum pattern on transmit times the sum pattern on receive), and the signal in the difference channel is proportional to the product of the sum and the difference patterns. The error signal is the output of the phase-sensitive detector. The optimum squint angle is found to be $\theta_q = 0.31\theta_B$, where θ_B is the half-power beamwidth of the squinted beams. This corresponds to a crossover 1.2 dB down from the peak. A different optimum squint angle, based on a different criterion, is given by both Rhodes[8] and Sherman[9] as $0.46\theta_B$, which corresponds to a crossover 2.6 dB down from the peak. Berger[10] has pointed out that the analysis of Rhodes (as well as Sherman) which gives a greater optimum squint

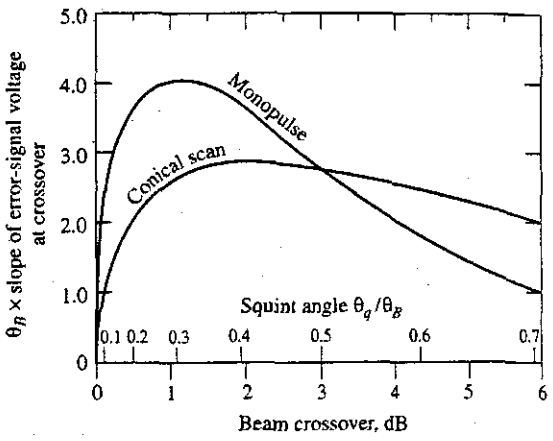

Figure 4.7 Slope of the angle-error signal at crossover for monopulse and conical-scan tracking radars. θ_B = *half-power beamwidth*, θ_q = *squint angle*.

angle applies for one-way beacon tracking (instead of two-way radar tracking) since it assumes a one-way signal is being tracked, but the curve in Fig. 4.7 is based on two-way radar tracking.

Monopulse Antenna Feed Systems[11] The question of optimum sum and difference patterns also can be examined on the basis of optimum antenna aperture illuminations rather than the concept of optimum squint angle. The desired illumination of the antenna has to be convenient to implement and produce low antenna sidelobes. The sum and difference patterns for a reflector or lens antenna are determined by the system of feeds that are used. The original four-horn feed system is the simplest to consider, but it cannot provide a difference pattern and a sum pattern that are independently optimized. The sum pattern should have maximum gain on axis, which requires a uniform aperture illumination. The difference pattern should have an aperture illumination that results in a large slope of the error signal at the beam crossover. Also, the antenna patterns should have low sidelobes and be able to maintain their favorable characteristics over a wide bandwidth. If circular polarization is needed, the demands on the feed system are further increased and often some compromise in performance must be accepted.

An improvement over the original four-horn monopulse system is shown in Fig. 4.8. This has been approximated in some precision tracking radars with a five-horn feed consisting of one horn generating the sum pattern surrounded by four horns generating the difference patterns. What makes the arrangement of Fig. 4.8 more suitable for monopulse tracking than the original four-horn feed is that analysis indicates that the size of the feed system generating the difference pattern should be about twice that of the feed generating the sum pattern.[12] This is approximately true of the feed of Fig. 4.8. Another approximation to the ideal is a 12-horn feed, but it is relatively large and complex.[13] Simpler and more compact feed systems can be obtained by using higher-order waveguide modes to obtain independent control of the sum and difference patterns. These are called *multimode feeds*.

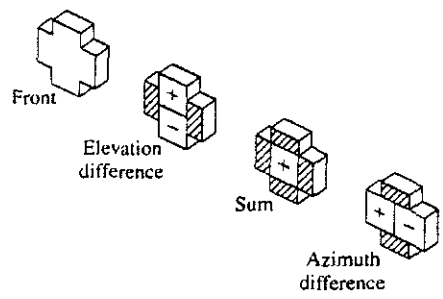

Figure 4.8 Approximately "ideal" feed illumination for monopulse sum and difference channels.[1]

For circular polarization, a five-horn feed system can be obtained so that the antenna can be switched to operate with either horizontal, vertical, or circular polarization. This feed does not provide optimum sum and difference patterns; but it is a practical compromise between complexity and efficiency in obtaining circular polarization for monopulse trackers. In a radar with dual-polarization monopulse tracking, insufficient isolation between the polarizations can degrade the angle accuracy due to crosstalk from cross-polarized target scattering.

Phased Array Monopulse Difference Patterns If monopulse angle measurement is required with a phased array antenna, it is possible to independently control the sum and the difference patterns by means of separate beam-forming systems for the phased array. The sum pattern may be chosen for maximum gain and low sidelobes, and the difference pattern for good angle accuracy and low sidelobes. In Sec. 9.11, the synthesis of good antenna patterns based on the Taylor aperture illumination is discussed. The Taylor illumination[14] is widely used to design a pattern with predetermined peak sidelobes for radar antennas, such as the sum beam of a monopulse tracking antenna. An extension of the Taylor method, due to Bayliss,[15] is also widely used to obtain good monopulse difference patterns, which are known as Bayliss patterns.

Two-Channel and One-Channel Monopulse[16–20] Three channels, or three receivers, are required to obtain monopulse angle tracking in two orthogonal angle coordinates. Good phase and amplitude balance must be maintained among the three receivers. To simplify this problem, monopulse radars that need only two or even one receiver were considered in the past. Systems with less than three receivers that process two or even three of the monopulse channels on a shared basis were conceived when receiver hardware was large and its technology was based on vacuum tubes. Over the years, improved technology has allowed better and smaller receivers so that the need for compromising the performance of a monopulse radar by employing fewer than three receiving channels has become less important.

Conopulse[21] This is another attempt to obtain the benefits of monopulse, but with only two channels rather than three. Conopulse, also called *scan with compensation* by the Russians,[22] employs two simultaneous beams that are squinted in opposite directions from the antenna axis. The pair are mechanically rotated around the boresight axis. The two beams are similar to those of a single angle-coordinate amplitude-comparison

monopulse; but their rotation allows the angle measurement in the two orthogonal coordinates to be obtained by time sharing a single channel. The sum and difference of the two squinted beams are processed similar to a conventional monopulse radar.

Since it provides a measurement of angle with simultaneous beams, the accuracy of conopulse is not degraded by amplitude fluctuations of the target as happens with conventional conical scan radars. A single-pulse measurement is not obtained as in a true monopulse, so it has a lower angular data rate than can be obtained with a three-receiver system. Although two receivers are used in conopulse rather than three, it has the disadvantage of requiring the two beams to be rotated mechanically. This can be difficult especially when the polarization has to be maintained constant on rotation. As with other one- and two-receiver monopulse systems, time and the advancement of technology have made conopulse almost obsolete.

Phase-Comparison Monopulse In a *phase-comparison monopulse*, two antenna beams are used to obtain an angle measurement in one coordinate, just as in amplitude-comparison monopulse. The two beams, however, look in the same direction and cover the same region of space rather than be squinted to look in two slightly different directions. In order for the two beams to look in the same direction, two antennas have to be used in the phase-comparison monopulse, Fig. 4.9a, rather than using two feeds at the focus of a

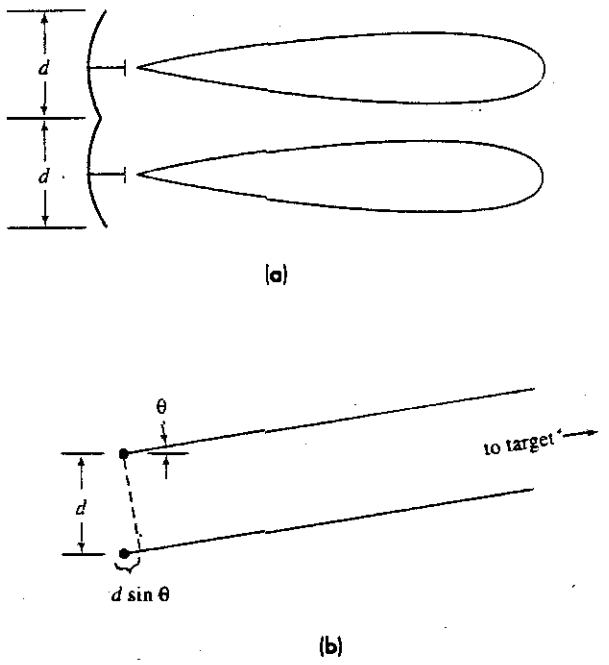

Figure 4.9 Phase-comparison monopulse in one angle coordinate. (a) Two antennas radiating identical beams in the same direction; (b) geometry of the signals at the two antennas of (a) when received from a target at an angle θ, measured with respect to the perpendicular to the baseline of the two radiators.

single antenna as is the case for an amplitude-comparison monopulse. The amplitudes of the signals are the same, but their phases are different. This is just the opposite of the amplitude-comparison monopulse. Consider two antennas spaced a distance d apart, as in Fig. 4.9b. If the signal arrives from a direction θ with respect to the normal to the baseline, the phase difference in the signals received in the two antennas is

$$\Delta\phi = 2\pi\frac{d}{\lambda}\sin\theta \qquad [4.1]$$

where λ = wavelength. A measurement of the phase difference of the signals received in the two antennas can provide the angle θ to the target. The phase-comparison monopulse is sometimes known as an *interferometer radar*.

The phase-comparison monopulse was invented during World War II about the same time as amplitude-comparison monopulse. Its early implementation was less efficient than that of amplitude-comparison monopulse. Four reflector antennas were used arranged in two rows of two columns. One of the antennas might be used as the transmitter (for purposes of this discussion, assume it is the aperture at the upper left of the two-by-two set of apertures). It also provides range information on reception. The other three antennas are used as receivers to obtain the azimuth and elevation angles. The upper right and the lower right antennas might obtain the phase difference in elevation which gives the elevation angle. The lower left and the lower right might obtain the azimuth angle. (The lower right antenna in this case is used for both the elevation and azimuth measurements.) A disadvantage of this method of obtaining the two angle coordinates is that only one-fourth of the available antenna area is used for transmitting and only one-half the area is used on receive to obtain each angle coordinate. Thus, the gain and effective area of a phase-comparison monopulse operating in this manner is less efficient than if the same total antenna area had been used for amplitude-comparison monopulse that generates sum and difference beams.

Angle information can also be extracted in a phase-comparison monopulse by employing sum and difference patterns and processing the signals similar to that described for the amplitude-comparison method. The full antenna aperture area can then be utilized, which is an advantage over the phase-measurement method described above. An analysis of the sum and difference patterns for phase-comparison monopulse shows that a 90° phase shift has to be introduced in the difference signal so that the output of the phase-sensitive detector is an error signal whose amplitude is a function of the sine of the angle of arrival from the target measured with respect to the perpendicular to the two antennas. (The phase-sensitive detector in this case performs a multiplication of the sum and difference signals.)

One of the limitations of phase-comparison monopulse is the effect of grating lobes due to the separation d of the two antennas each of dimension d. Grating lobes in phased array antennas are discussed in Sec. 9.5, but they apply to this situation as well. If the spacing d between the phase centers of the antenna is greater than that of the antenna diameter, high sidelobes are produced in the sum pattern and ambiguities can occur in the angle measurement. Even when the spacing is the same as the antenna diameter, a poor antenna pattern can result. In practice, the separation between the two antennas should be less than the antenna diameter d if good radiation patterns are to be obtained on transmit

and angle ambiguities are to be avoided on receive. In the past when parabolic reflectors were used, a portion of the right-hand side of one antenna was sliced off (truncated), and a portion of the left-hand side of the other antenna was also sliced off so that when the two sliced-off edges were butted together, the separation between the two truncated reflector antennas could be made less than the original diameter d.

There has been little application of the phase-comparison monopulse as compared to the more popular amplitude-comparison method.

4.3 CONICAL SCAN AND SEQUENTIAL LOBING

The monopulse tracker described in the previous section utilized multiple fixed beams to obtain the angle measurement. It is also possible to time share a single antenna beam to obtain the angle measurement in a sequential manner, as was done in early tracking radars. Time sharing a single antenna beam is simpler and uses less equipment than simultaneous beams, but it is not as accurate.

Sequential Lobing The first U.S. Army angle-tracking air-defense radar in the 1930s (SCR-268) switched a single beam between two squinted angular positions to obtain an angle measurement. This is called *lobe switching, sequential switching,* or *sequential lobing*. Figure 4.10a is a polar representation of the antenna beam in the two switched positions. The same in rectangular coordinates is in Fig. 4.10b. The error signal obtained

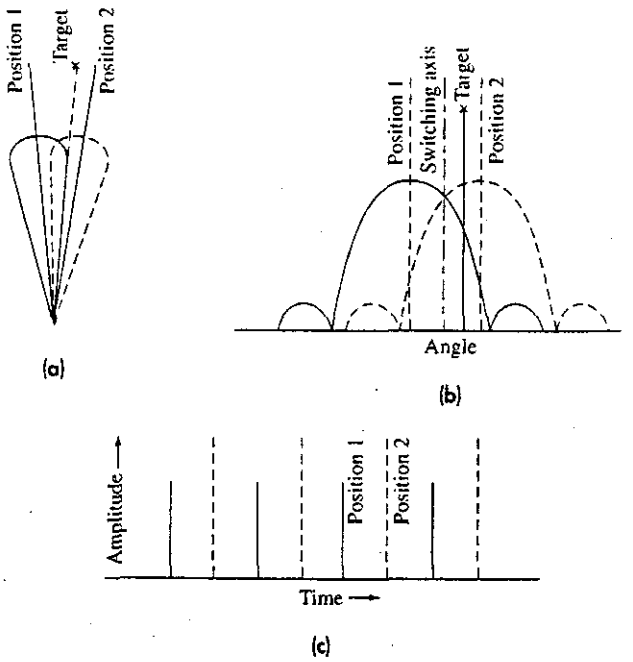

Figure 4.10 Lobe-switching antenna patterns and the error signal (for one angle coordinate). (a) Polar representation of the switched antenna pattern; (b) rectangular representation; (c) error signal.

from a target not located on the switching axis (boresight) is shown in Fig. 4.10c. The difference in amplitude between the voltages obtained in the two switched positions is a *measure of the angular displacement of the target from the switching axis.* The direction in which to move the beam to bring the target on boresight is found by observing which beam position has the larger signal. When the echo signals in the two beam positions are equal, the target is on axis and its direction is that of the switching axis.

Two additional switching positions are needed to obtain the angle measurement in the orthogonal coordinate. Thus a two-dimensional sequentially lobing radar might consist of a cluster of four feed horns illuminating a single reflector antenna, arranged so that the right–left, up–down sectors are covered by successive antenna positions. A cluster of five feed horns might also be used, with a central feed used for transmission and four outer feeds used for reception on a sequential basis.

In a sequential lobing system, a pulse might be transmitted and received when the beam is squinted to the right, again when the beam is squinted up, when the beam is squinted to the left, and when the beam is squinted down. Thus the beam might be switched right, up, left, down, right, and so forth. After living with this type of scanning for a while, it must have become obvious that the four horns and RF switches could be replaced by a single feed that radiated a single beam squinted off axis. The squinted feed could then be continuously rotated to obtain angle measurements in two coordinates. This is a *conical-scan* radar.

Conical Scan The basic concept of conical scan, or *con-scan,* is shown in Fig. 4.11. The angle between the axis of rotation and the axis of the antenna beam is the squint angle. Consider a target located at position *A*. Because of the rotation of the squinted beam and the target's offset from the rotation axis, the amplitude of the echo signal will be modulated at a frequency equal to the beam rotation frequency (also called the conical-scan frequency). The amplitude of the modulation depends on the angular distance between the target direction and the rotation axis. The location of the target in two angle coordinates determines the phase of the conical-scan modulation relative to the conical-scan beam rotation. The conical-scan modulation is extracted from the echo signal and applied

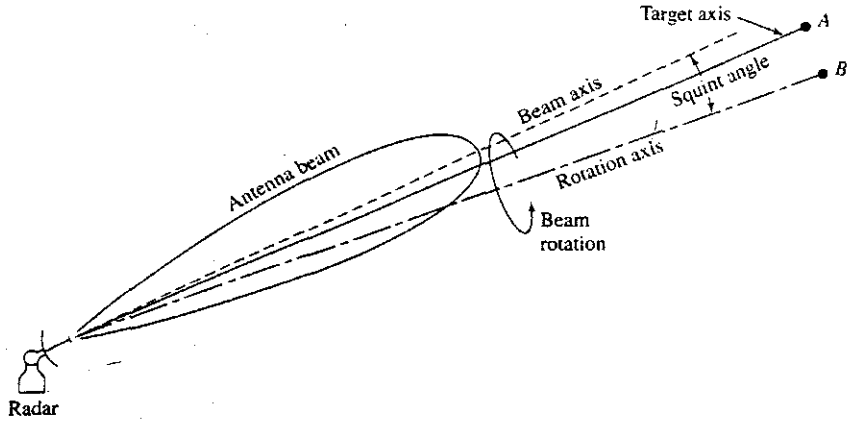

Figure 4.11 Conical-scan tracking.

to a servo control system that continually positions the antenna rotation axis in the direction of the target. It does this by moving the antenna so that the target line of sight lies along the beam rotation axis, as at position B in Fig. 4.11. Two servos are required, one for azimuth and the other for elevation. When the antenna is "on target," the conical-scan modulation is of zero amplitude.

Block Diagram A block diagram of the angle-tracking portion of a conical-scan tracking radar is shown in Fig. 4.12. The antenna is mounted so that it can be mechanically positioned in both azimuth and elevation by separate motors. The antenna beam is squinted by displacing the feed slightly off the focus of the parabola.

The parabolic-antenna feed can be a rear-feed design for mechanical convenience. When the feed is designed to maintain the plane of polarization as it rotates about the axis, it is called a *nutating* feed. A *rotating* feed is one which causes the plane of polarization to rotate. The nutating feed is preferred over the rotating feed since a rotating polarization can cause the amplitude of the target echo signal to change with time even for a stationary target on-axis. A change in amplitude caused by a modulated echo signal can result in degraded angle-tracking accuracy. The nutating feed is usually more complicated, however, than the rotating feed. If the antenna is small enough (as in a missile guidance system), it might be easier to mechanically rotate the tilted reflector rather than the feed, thus avoiding the problems of either a rotary joint or a flexible RF joint for the nutating feed.

A typical conical-scan rotation speed might be in the vicinity of 30 rev/s. The same motor that provides the conical-scan rotation of the antenna beam also drives a two-phase reference generator with electrical outputs at the conical-scan frequency that are 90° apart in phase. These two outputs serve as reference signals to extract the elevation and azimuth errors as indicated in Fig. 4.12. The received echo signal is fed to the receiver from the antenna via two rotary joints (not shown in the block diagram). One rotary joint permits motion in azimuth; the other, in elevation.

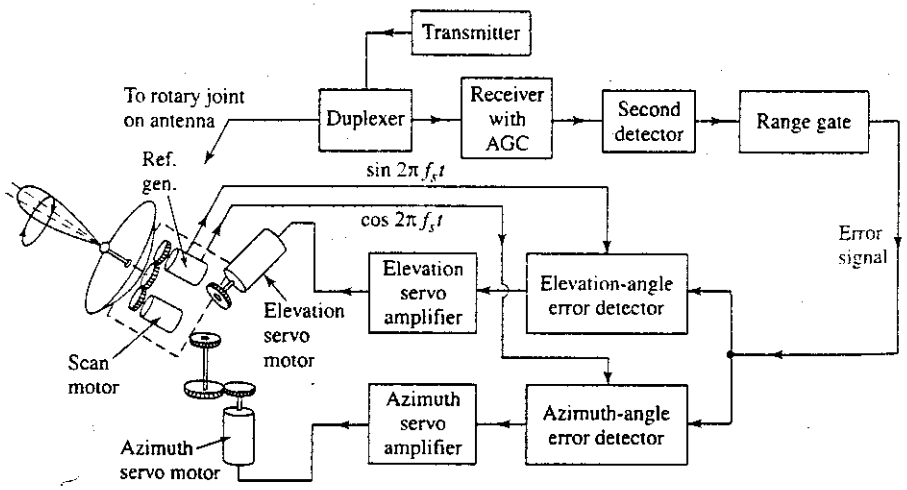

Figure 4.12 Block diagram of conical-scan tracking radar.

The receiver is a superheterodyne except for features related to the conical-scan tracking. The error signal is extracted in the video after the second detector. A single target is put into track by having the receiver scan a range gate to search for the target and lock on to it and then continually track it in range (as described later in the chapter). Range gating eliminates noise and excludes all targets other than the desired target. The error signal from the range gate is compared with both the elevation and azimuth reference signals in the angle-error detectors, which are phase-sensitive detectors. As described previously, the phase-sensitive detector is a nonlinear device in which the input signal is mixed with a reference signal. The magnitude of the d-c output from the angle-error detector is proportional to the angle error, and its sign (polarity) indicates the direction of the error. The angle error outputs are amplified and used to drive the antenna elevation and azimuth servo motors. The angular position of the target may be determined from the elevation and azimuth of the antenna axis.

The video signal is a pulse-train modulated by the conical-scan frequency, as in Fig. 4.13a. It is usually convenient to stretch the pulses before low-pass filtering so as to increase the energy at the conical-scan frequency and to perform analog-to-digital conversion. Pulse stretching, Fig. 4.13b, is accomplished by a *sample-and-hold* circuit; which has also been known in the past as a *boxcar* generator.

The pulse repetition frequency must be sufficiently large compared with the conical-scan frequency for proper filtering and avoiding inaccuracy of the angle measurement. There must be at least four pulses during each revolution of the conical scanning beam (so as to obtain up–down and right–left comparisons). The prf, therefore, must be at least four times that of the conical-scan frequency; but it is preferable that it be more than 10 times greater.

Automatic Gain Control As with monopulse radar, AGC is employed in the conical-scan radar. It has the purpose of maintaining constant angle-error sensitivity in spite of

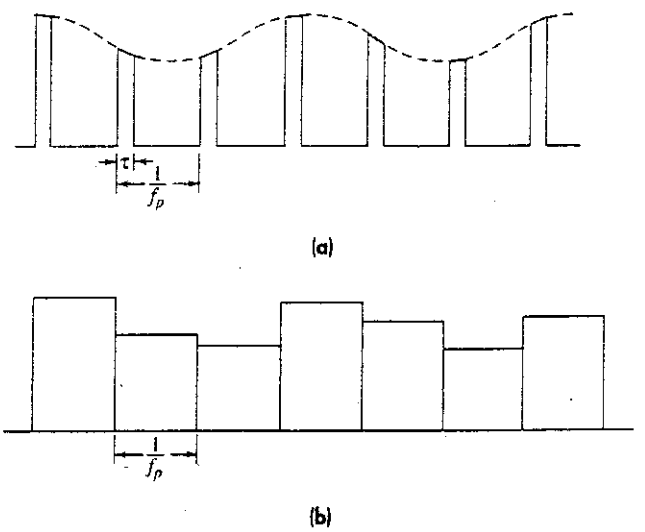

Figure 4.13 (a) Pulse-train with conical-scan modulation; (b) same pulse-train after stretching by a sample-and-hold circuit.

amplitude fluctuations or changes of the echo signal due to changes in range. Constant angle-error sensitivity is required to provide stable tracking. AGC is also important for avoiding saturation by large signals which could cause the loss of the scanning modulation and the accompanying error signal. It also attempts to smooth or eliminate as much of the noiselike amplitude of the target echo signal as is practical without disturbing the extraction of the desired echo signal at the conical-scan frequency. The gain of the AGC loop at the conical-scan frequency should be low so that the error signal will not be suppressed by the AGC action.

The required dynamic range* for the AGC will depend on the variation in range over which targets are tracked and the variation expected in the target cross section. If, for example, the range variation were 10 to 1, its contribution to the required dynamic range would be 40 dB. The target cross section might contribute another 40-dB variation. Another 10 dB might be allowed to account for other variations in the parameters of the radar equation. Hence, the dynamic range in this example that is required for operation of the receiver AGC might be of the order of 90 dB. In practice, a large dynamic range cannot be obtained with only one stage of AGC.[23]

Optimum Squint Angle The greater the squint angle in the conical-scan tracker the greater will be the slope of the error signal around boresight and the more accurate will be the angle measurement. In Fig. 4.7 is shown the theoretical slope of the error signal for a conical-scan radar when the target is on boresight, or crossover, computed for an antenna pattern with a gaussian shape. The maximum slope occurs at a squint angle equal to 0.41 of the half-power beamwidth. The maximum is seen to be not too sensitive to squint angle in this case. A squint angle of $0.41\theta_B$ corresponds to a point on the antenna pattern of about 2 dB down from the peak. This means that when a conical-scan radar has a target in track, the echo signal is 4 dB less than if the target were viewed at the peak of the antenna beam. (This is sometimes called the *crossover loss.*) A monopulse radar, it will be recalled, tracks the target with the peak of the sum beam so that it does not incur such a loss. Thus the monopulse tracker will have a larger signal-to-noise ratio which provides more accurate tracking in both angle and range than that of the conical-scan tracker.

In a conical-scan tracker a compromise is often made between the range and angle accuracy by selecting a smaller squint angle than that which produces maximum angle-error-signal slope. A compromise value might be $\theta_q/\theta_B = 0.28$, which corresponds to a point on the antenna pattern about 1.0 dB below the peak. The two-way loss in antenna gain is 2.0 dB instead of 4.0 dB, which makes more accurate range tracking but lower accuracy angle tracking. If the radar is used to track a beacon on a one-way path rather than the two-way path of the radar "skin echo," the optimum squint angles are larger.[24]

Scan on Receive Only[25] Military conical-scan and lobe-switching tracking radars are especially vulnerable to electronic countermeasures (ECM) since it is easy for a hostile intercept receiver to detect and determine the conical-scanning frequency. With such

*Dynamic range is the ratio, usually expressed in decibels, of the maximum to the minimum signal power over which a device (in this case, the AGC) can operate within some specified level of performance.

knowledge, a hostile ECM jammer can cause a conical-scan radar to cease tracking a target (called *break-lock*) by retransmitting the received radar signal with an amplitude modulation that is the inverse of the conical-scan frequency. This produces a return signal that is out of phase with the signal which would have been received from the skin-echo of the target, and break-lock might occur. This type of countermeasure is called *inverse gain*, and can degrade conical-scan or lobe-switching tracking systems.

To prevent the hostile ECM jammer from detecting a conical-scan frequency, a tracking radar can operate with a nonscanning transmitting beam to illuminate the target and apply conical scanning or lobe switching only on receive. This is called COSRO, which stands for *conical scan on receive only*. The analogous operation with sequential lobing is called LORO, or *lobe on receive only*.

4.4 LIMITATIONS TO TRACKING ACCURACY

In this section several of the major effects that determine the accuracy of a tracking radar will be discussed, including:

- Glint, or angle noise, which affects all tracking radars, especially at short range.
- Receiver noise, which also affects all radars, and mainly determines tracking accuracy at long range.
- Amplitude fluctuations of the target echo that bother conical-scan and sequential-lobing trackers, but not monopulse.

Other factors that influence the overall accuracy of a tracking radar include the mechanical properties of the antenna and pedestal, the servo system, the method by which the pointing of the antenna boresight is determined, the antenna beamwidth, atmospheric effects, and multipath.[26]

Glint This has also been called *angle noise, target noise, angle fluctuations*, and *angle scintillation;* but *glint* is the term commonly used. It occurs with complex targets that have more than one scattering center within the resolution cell of the radar. A single "point" scatterer, such as a sphere, does not show the phenomenon of glint. Complex targets with multiple scattering centers, such as aircraft, can cause glint and degrade tracking. The echo from a single scatterer generally arrives at the radar antenna with a uniform planar waveform that has a tilt which depends on the angle of arrival, Fig. 4.14a. The usual method for measuring angle almost always assumes that the arriving wavefront is planar and uniform. If, however, the target consists of multiple scatterers, each at a different angle, their individual echo signals arrive at the antenna with slightly different wave tilts, as sketched in Fig. 14.14b (exaggerated to show the principle). These tilted wavefronts add vectorially across the aperture to give a composite wavefront whose amplitude and phase are not uniform across the aperture. Glint from a complex target is sometimes thought of as a distortion of the echo wavefront.

The result of having a nonuniform wavefront from a complex target, when the radar is designed to process the echo wavefront that is planar, is an error in the measurement

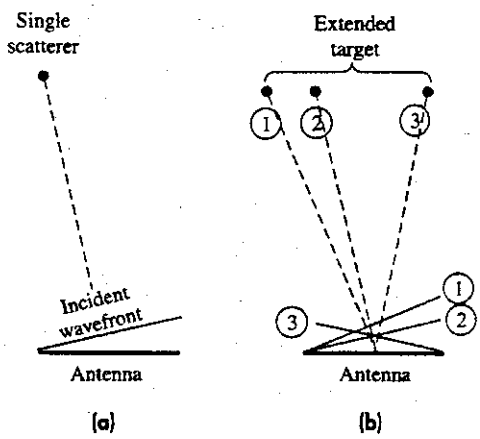

Figure 4.14 (a) Plane wave from one scatterer incident on the antenna. (b) Plane waves from three scatterers incident on the antenna. Resultant aperture illumination is the vector sum of the three plane waves.

of the angle of arrival. The measured angle does not bear a simple relationship to some distinctive property of the target, such as its center, leading edge, or its largest scatterer. Furthermore, the measured angle of arrival can sometimes cause the boresight of the tracking antenna to point *outside* the angular extent of the target, which can cause the radar to break track. The greater the extent of the target in angle as seen by the radar, the worse will be the angle measurement, as we shall see. Glint, therefore, can be a major source of error when making angle measurements, especially at short range where the angular extent of the target can be relatively large. It bothers all continuous tracking radars that employ closed-loop angle tracking, whether conical-scan, sequential lobing, amplitude-comparison monopulse, or phase-comparison monopulse.

theta $_D$ < theta$_{3dB}$

Example of Glint from a Simple Target Model Consider a target model consisting of two independent, isotropic scatterers separated by an angular distance θ_D as measured from the radar, Fig. 4.15a. (Sometimes this is called a *dumbbell target*.) The two scatterers are assumed to be located symmetrically to each side of the perpendicular from the antenna at $\pm\theta_D/2$. Although it may be a fictitious target model chosen for reasons of simplicity, it illustrates the effects that a complex (multiple-scatterer) target has on the accuracy of a tracking radar. The relative amplitude of the echo signals from the two isotropic scatterers is taken to be a (a number less than unity) and the relative phase difference is α. Differences in the phase might be due to differences in range between the two scatterers or to differences in the reflecting characteristics of the two scatterers. The angular error $\Delta\theta$ as measured from the larger of the two isotropic scatterers is given by J. E. Meade as[27]

$$\frac{\Delta\theta}{\theta_D} = \frac{a^2 + a\cos\alpha}{1 + a^2 + 2a\cos\alpha}$$

از این فرمول نمي توان براي اندازه گيري خطاي multipath استفاده كرد.

This is shown plotted in Fig. 4.15b. The larger of the two scatterers is at $\Delta\theta/\theta_D = 0$, and the smaller is at $\Delta\theta/\theta_D = +1$. Positive values of $\Delta\theta$ correspond to the angular region to the left of the larger of the two scatterers; negative values lie outside the target, at angles to the right of the larger target. When the echo signals from both scatterers are in phase

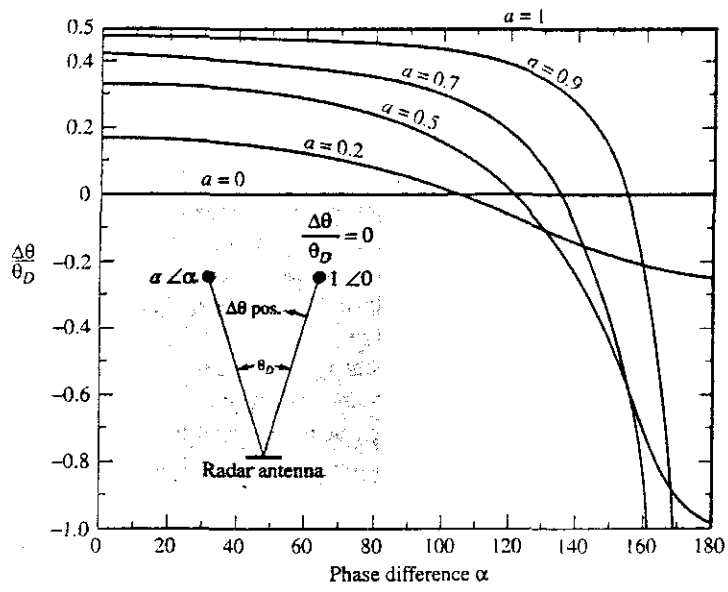

Figure 4.15 Plot of Eq. (4.2) of the error $\Delta\theta/\theta_D$ as a function of a and α. Insert shows two isotropic scatterers of relative amplitude a and relative phase shift α, separated by an angular extent θ_D as viewed from the radar. The angle $\Delta\theta$ is measured with respect to the larger of the two scatterers.

($\alpha = 0$), $\Delta\theta/\theta_D$ reduces to $a/(a + 1)$, sometimes called the "center of gravity" of the two scatterers. When the signals are of equal amplitude ($a = 1$) and the phase difference $\alpha = \pi$ radians, Eq. (4.2) indicates the antenna points to $\Delta\theta/\theta_D = -\infty$; that is, the antenna is driven well outside the bounds of the target. It should be cautioned that an assumption made in deriving Eq. (4.2) is that the voltage of the angle-error signal is directly proportional to the angle error; that is, the angle-error signal is linear. This implies that angle errors are small; but when $\Delta\theta/\theta_D \to -\infty$, the angle error is not small. As was indicated in Fig. 4.3d, as the angle error increases, the angle-error signal voltage will no longer be linear and its slope can even change sign. Equation (4.2) no longer applies when $\Delta\theta/\theta_D$ becomes large. Nevertheless, the simple model of Eq. (4.2) describes the general nature of the behavior to be expected by a radar tracker subjected to glint from a complex target.

The relative phase, α, changes if the relative ranges to the two scatterers change. This can occur, for example if the aspect angle of an aircraft changes due to its flight path or atmospheric turbulence. Thus the value of α can vary with time. The radar tracker theoretically can point outside the target region a significant fraction of the time.

Equation (4.2) indicates that the tracking error $\Delta\theta$ for the two-scatterer target is proportional to the angular extent of the target θ_D, which is why the tracking error due to glint varies inversely with range. The error becomes larger as the range becomes shorter. Although this statement is based on the simple two-scatterer target, it is a reasonable approximation to a real target provided the angular extent is not greater than the antenna beamwidth. When the angular extent of the target is greater than the antenna beamwidth, the two scatterers can be resolved and there is no glint.

A slightly more complex model than the two-scatterer target considered above is one consisting of many individual scatterers, each of the same cross section, arranged

uniformly along a line of length L perpendicular to the line of sight from the radar. The resultant cross section from such a target is assumed to behave according to the Rayleigh probability density function. It was found that the probability is 13.4 percent that the apparent direction of the target measured by the radar will be outside of the target region.[28] Similar results for a two-dimensional model consisting of equal cross-section scatterers uniformly spaced over a circular area indicate that the probability the apparent direction lies outside the target is 20 percent. Howard[29] states that measurements made on actual aircraft of the rms value of angle noise, expressed in the same length units as the target extent L in cross-range, are between $0.15L$ and $0.2L$. A small single-engine aircraft viewed nose-on might have a value near $0.1L$, and larger aircraft and aircraft viewed from the side approach $0.2L$.

Although glint is a deterministic phenomenon if the target configuration and its scattering properties are known, it has sometimes been analyzed in statistical terms.[30,31] The deterministic approach, however, helps in understanding what is taking place with the target and the radar, something that statistical models cannot do as well. Glint is usually thought of as a target effect; but to some extent, the radar enters also. Glint occurs when the radar cannot resolve the individual scatterers of a complex target; so that some radars might not be affected by glint that would seriously bother others.

Methods for reducing the effects of glint on radar tracking performance are discussed later in this section. The phenomenon of glint also occurs in the range dimension, as will be discussed in Sec. 4.6. A brief survey of radar glint, along with an extensive bibliography of the early work in this field, has been given by Wright.[31]

In addition to tracking radars, it has been said in the literature that glint also occurs with scanning surveillance radars.[32] This might not be completely accurate. Surveillance radars estimate the target direction as the antenna pointing angle where the echo signal is a maximum. The estimate of angle in scanning surveillance radars is often made by *beam splitting*, or something equivalent. Closed-loop angle tracking is not employed. A complex target might cause an error in the beam-splitting angle estimate because of the nonuniform response of the target with angle, but the error does not seem to produce an angle measurement that extends beyond the angular confines of the target as does the glint that occurs in a radar with closed-loop tracking. Thus, glint does not occur with a scanning radar, only one with closed-loop tracking.

Receiver Noise The noise at the input of a radar receiver affects the accuracy of radar tracking just as it does the detection capability of a radar. In Sec. 6.3, the accuracy of radar measurements is discussed, based on a noise model described by the gaussian probability density function. All theoretical expressions for the rms value of the error of a radar measurement (such as angle) are inversely proportional to the square root of the signal-to-noise ratio. From our previous discussion of the radar range equation in Chap. 2, we know that the range of a radar is inversely proportional to the fourth root of the signal-to-noise ratio. The rms value of a radar measurement error is, therefore, directly proportional to the square of the range. Receiver noise is a major factor limiting the accuracy of a radar at long range where signal-to-noise ratios are small. Section 6.2 also indicates that the rms error in the radar measurement of angle is directly proportional to the antenna beamwidth.

The theoretical accuracy of a tracking radar, given as the rms error in the angle measurement, has been given by Barton[33] and can be found in Howard,[34] It is

$$\delta_{\text{ang}} = \frac{k\theta_B}{k_s\sqrt{B\tau(\text{S/N})(f_p/\beta_n)}} \tag{4.3}$$

where the constant $k = 1$ for a monopulse radar and 1.4 for a conical-scan radar, θ_B = half-power beamwidth, k_s = slope of the angle-error signal at boresight (which is different for monopulse and conical-scan radars), B = bandwidth, τ = pulse width, (S/N) = signal-to-noise ratio per pulse (assumed in the derivation of this expression to be greater than 6 dB), f_p = pulse repetition frequency, and β_n = servo bandwidth. Generally, $B\tau \approx 1$, and $f_p/2\beta_n$ = number of pulses integrated. According to Howard,[34] the value of the slope k_s for a good four-horn monopulse feed is 1.57. Its value for a conical-scan radar is 1.5 when the offset angle is chosen to optimize overall radar performance. Since the conical-scan radar does not track a target with its maximum antenna gain, the signal-to-noise ratio is lower than that of a monopulse radar. Earlier in this chapter, we have said that the conical-scan tracker might suffer a two-way loss of 2.0 dB More elaborate expressions for the angle error for the conical-scan tracker[35] and the monopulse tracker[36] can be found in the literature, but the above expression is often suitable for many purposes.

Amplitude Fluctuations The amplitude of the radar echo from a complex target with multiple scattering centers will fluctuate as the aspect of the target changes with respect to the radar. (Changes in aspect may be due to the motion of the target in yaw, roll, or pitch. Aspect changes also occur even if the target moves in a straight line.) Conical-scan and sequential-lobing radars interpret any change in amplitude of the target echo signal as being due to the target not being on boresight. They then direct the antenna to move in a direction to make the "error signal" zero. Thus a change in amplitude due to fluctuations in the target echo during the time interval of the sequential measurement can degrade the accuracy of the measurement. Amplitude fluctuations in the target echo signal, which are also known as *target fading*, do not affect the angle-error measurement accuracy of simultaneous lobing or monopulse systems that extract an angle-error voltage with each pulse.

Since the percentage modulation of the echo signal due to fluctuations in the target cross section is independent of range if AGC is used, the angle error as a result of amplitude fluctuations will be independent of range.

Amplitude fluctuations from aircraft targets are classified as either low frequency or high frequency. According to Howard,[29] the low-frequency pulse-to-pulse amplitude fluctuations might be concentrated mainly below 10 Hz at X band. These are due to variations in the target cross section caused by changes in the relative distances of the individual scattering centers. The amplitude spectrum does not seem to depend strongly on the size of the target. An aircraft with a large wingspan has its scattering centers (the engines, for example) spaced wider than would an aircraft with a small wingspan so that a higher fluctuation frequency would be expected if the rate of change of yaw were the same in the two cases. The large aircraft, however, has slower rates of yaw than a small aircraft so that the frequency extent of the spectra might be expected to be similar. The spectral width of the amplitude fluctuations is closely proportional to the radar frequency,

since a change in the relative distances of the scatterers will result in a larger change in wavelengths if the frequency is high than if it is low.

High-frequency amplitude fluctuations can be caused by reflections from propellers and jet engines. The frequency of propeller modulation depends on the number of blades and the rotation rate. The modulation is not sinusoidal and has harmonics of the fundamental frequency. The fundamental frequency of the propeller modulation and its harmonics do not depend on the radar frequency.

The effect of amplitude fluctuations on the accuracy of conical-scan tracking can be reduced by choosing a conical-scan frequency that corresponds to a low value of the target's amplitude fluctuation spectrum. If the amplitude fluctuation noise power were large at the conical-scan or lobing frequency, it could not be readily eliminated by AGC or filtering. A typical conical-scan frequency, for example, might be 30 Hz. Generally the higher the scan frequency, the less the noise due to amplitude fluctuations. At the higher scan frequencies, however, propeller modulation might be present and needs to be avoided. A sufficiently high scanning frequency, however, will have little degradation in tracking because of amplitude fluctuations. It has been reported that experimental measurements with radars operating with pulse repetition frequencies from 1000 to 4000 Hz and a lobing or scan rate one-quarter of the prf are not limited by amplitude fluctuations of the target.[37]

Servo Noise This is the hunting action of the tracking servomechanism which results from backlash and compliance in the gears, shafts, and structures of the antenna mount. The magnitude of the noise is independent of the target echo and will therefore be independent of range.

Summary of Errors The contributions of glint, receiver noise, and amplitude fluctuations to the accuracy of a tracking radar as a function of range is illustrated in Fig. 4.16. The error due to glint varies inversely with range; receiver noise causes the error to vary as the square of the range; and both amplitude fluctuations and servo noise are independent of range. This is a very qualitative plot showing the general nature of each of these factors. Two resultant curves are shown. Curve A might be representative of conical-scan and sequential-lobing trackers. It assumes that the error due to servo noise is less than that due to amplitude fluctuations. Curve B might represent monopulse trackers since it does not include the effect of amplitude fluctuations. Tracking accuracy deteriorates at both long and short range with the best angular accuracy occurring at the intermediate ranges.

The best tracking radars have been able to achieve an angle accuracy of about 0.1 milliradian. Such accuracy does not come easy. It can only be achieved by full attention to the many internal and external factors affecting tracking accuracy and by timely, accurate calibration.[38]

Methods for Reducing Angle Errors Due to Target Glint Glint can be debilitating to a military tracking radar or a radar guided missile. It is important, therefore, to reduce its adverse effects when highly accurate tracking is required. There have been a number of methods proposed to reduce glint. Some can provide significant improvement but may require operating the radar in a manner that is not always best for achieving the radar mission. Other methods might not degrade the major task of the radar, but they do not always

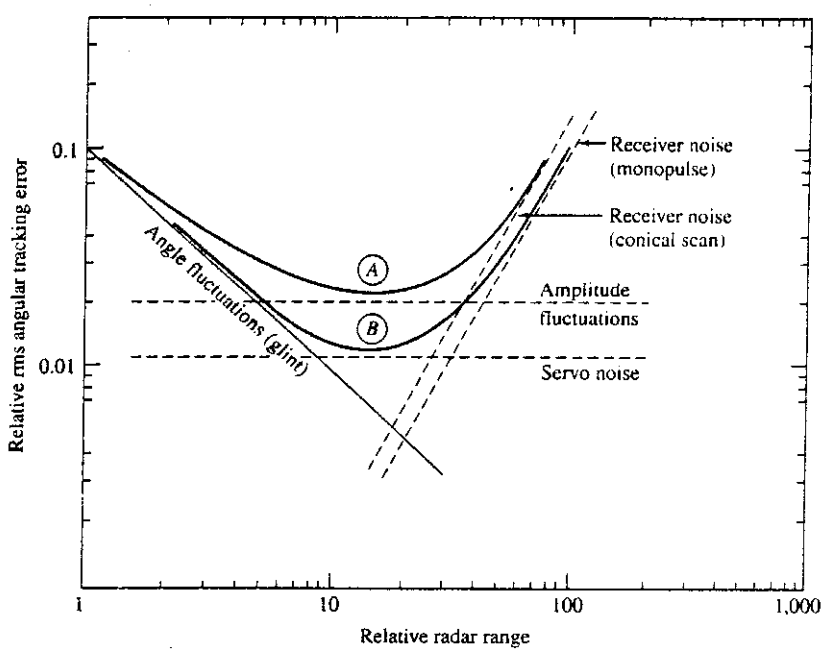

Figure 4.16 Relative contributions to the angle tracking error due to glint, amplitude fluctuations, receiver noise, and servo noise. Curve A represents the composite error for a conical-scan or sequential-lobing radar; curve B represents the composite error for monopulse.

have sufficient effect on reducing glint effects. As with many things, compromises usually have to be made.

Frequency Agility The angle error due to glint depends on the radar frequency since the relative phase α in the simple two-scatterer model depends on frequency. A change in the relative phase α can change the glint error (Fig. 4.15); it can be smaller or it can be larger. If the relative phase α is due primarily to the difference in range ΔR between the two scatterers, then the phase difference $\alpha = 4\pi(\Delta R)f/c$, where f = radar frequency, c = velocity of propagation, and $f/c = \lambda$ = radar wavelength. A change in radar frequency results in a change in the relative phase α and a change in the angle error $\Delta\theta$. There must be a sufficient change in frequency to decorrelate the phase measurement and make the measurements independent. Decorrelation occurs when the phase α changes by more than 2π radians. With this criterion, the frequency should be changed by an amount[39]

$$\Delta f \text{ (Hz)} = \frac{c \text{ (m/s)}}{2D \text{ (m)}} \quad \text{or} \quad \Delta f \text{ (MHz)} = \frac{150}{D \text{ (m)}} \qquad [4.4]$$

where D = the depth of the target. (In the two-scatterer case, D is the same as ΔR.) The depth D of an aircraft target as seen by radar usually is not the same as the projected physical size of the target since the extremities of the target might be too small to be detected by the radar or they might be masked by other scatterers.

There are several methods that have been proposed to use the frequency dependence of glint to reduce its effect on tracking accuracy. One method is based on the observation

that a large glint error is accompanied by a low echo-signal power. This inverse relationship between glint error and receiver signal power was apparently recognized as early as the mid-1950s.[40] This can be seen qualitatively with the two-scatterer model. When the amplitudes of the two signals are almost equal and their relative phase is almost 180°, Fig. 4.15 indicates that glint errors will be large. But when the two signals are almost equal in amplitude and almost 180° out of phase, they will destructively interfere at the antenna and result in a low echo-signal amplitude. Thus when the signal received by the radar is found to be low, when it is not normally expected to be low, it is likely that the angle measurement is in error. To take advantage of this effect, several different frequencies are radiated with frequency separation greater than that given by Eq. (4.4). The angle estimates of the received echo signals are weighted according to some criterion (such as proportional to their signal-to-noise ratios), and the average is taken. Several other weightings were analyzed by Loomis and Graf.[41] It was found that simply using the angle measurement associated with the largest signal amplitude provides the most accurate estimate of angle. The reduction in rms tracking error by processing only that signal whose frequency results in the largest echo amplitude is approximately

$$\delta_{\text{rms}} \approx \frac{\delta_g}{N} \qquad 1 \le N \le 4 \qquad [4.5]$$

where δ_g is the single-frequency (no agility) glint error and N is the number of independent frequencies. More than four frequencies were found to offer no significant improvement in accuracy.

Although pulse-to-pulse frequency agility can reduce the effects of glint, it has some drawbacks. Detection of moving targets in clutter using MTI or pulse doppler methods is not compatible with pulse-to-pulse frequency agility. To employ doppler processing, the frequency must remain constant for a significant number of pulses. Frequency diversity is possible by transmitting either simultaneously or in sequence a number of constant-frequency pulses at each of several frequencies that are separated by more than the Δf of Eq. (4.4).

Pulse-to-pulse frequency agility reduces the glint found in conical-scan and sequential-lobing radars, but it can increase the amplitude fluctuations in such radars because of the dependence of radar cross section on frequency. It might result in a net increase in the angle error, and is not always appropriate to use with such radars.

In some crowded radar bands, it might not be easy to achieve the required range of frequencies needed to obtain a reduction in the glint error. If, for example, the effective depth D of a target were 10 m, Eq. (4.4) indicates that the change in frequency must be at least 15 MHz to decorrelate the glint error. If four different frequencies were required, there must be at least 45 MHz of bandwidth available.

Range Resolution It was mentioned that glint occurs when there are multiple scatterers within the radar resolution cell. Range resolution can be quite good in a microwave radar, far better than the angle resolution. Therefore, if the radar has sufficiently high range-resolution to be able to resolve the multiple scatterers that constitute a target, angle glint (as well as range glint) will not occur and the tracking accuracy in angle as well as range will be improved compared to that of a low-resolution system. If, for example, the radar has to have a range resolution of one meter to resolve the various target

scatterers, the required spectral width must be 150 MHz. The higher microwave frequencies are therefore more suitable for this method of glint reduction than are lower frequencies.

In some respects the use of high range-resolution for reduction of angle glint is related to the use of frequency agility for the same purpose. Both take advantage of wide bandwidth. The frequency agility method uses a finite number of discrete narrowband frequencies within a wide frequency band rather than a continuous spectrum as is required for high range-resolution. If both methods use the same extent of spectral bandwidth, it is suspected that the high-resolution method should produce more accurate tracking than the use of frequency agility. High range-resolution can be used in conjunction with MTI or pulse doppler radar if digital signal-processing technology is not limited by the wide bandwidth required for high resolution.

Servo Bandwidth and AGC Bandwidth[31] Angular error due to glint may be reduced by keeping the servo bandwidth small. This might not be a good idea in practice since the servo bandwidth usually is determined by the requirement that the tracker be able to follow a maneuvering target. Too narrow a servo bandwidth might cause the track of the maneuvering target to be broken and the target lost.

The effects of glint also may be reduced by reducing the bandwidth (increasing the time constant) of the AGC system.[42] A narrowband AGC does not respond to rapid fluctuations in signal amplitude with the result that the echo-signal amplitude might not maintain constant signal level. This can cause a reduction in the angle-error sensitivity during large angle-noise peaks, and smaller rms tracking noise can result. This reduction in angle noise, however, is accompanied by a new component of noise due to amplitude fluctuations associated with the echo signal. Narrowing of the AGC bandwidth generates additional noise in the vicinity of zero frequency that can result in poor tracking. In spite of the potential benefits of a narrowband AGC, a wideband (fast) AGC is usually preferred especially at short and medium ranges where target maneuvers result in high angular rates and the lag in the tracking can be large if a narrowband AGC were used.

Thus narrow servo and/or AGC bandwidth as a means for reducing glint produce other undesirable effects. Bandwidths should be selected so as to be consistent with the various factors that can affect the tactical requirements that determine the acceptable tracking error and probability of breaking lock on a target.

Filtering of Angle Noise One of the first methods for dealing with the angle error due to glint was to consider it as a noise that could be filtered if its characteristics were known.[43] This is one reason glint is sometimes called angle noise. The noise model has not been too successful, however, since the statistical description of glint is considered to be nongaussian and nonstationary.[44] Glint can often be better modeled as deterministic or nonstatistical[45] rather than statistical. Another problem in modeling glint as noise to be filtered is that glint errors are "spiky." They tend to be of large value only when the phase difference α in the two-scatterer model is near π radians. Filtering to smooth the relatively large spikes in the glint can result in a bandwidth too narrow to maintain the track of a maneuvering target, as mentioned above when discussing the servo and AGC bandwidth. It has continued to be fashionable to consider glint as a noise problem, but there has not been the success that one might desire.

Excising of Measurements Associated with Fades It has been mentioned previously that when the glint error is large, the received signal amplitude is small. If the signal level is properly monitored so as to recognize a low signal amplitude, the corresponding angle measurement can be removed (censored) and the tracking error improved. It has been suggested[46] that when a Kalman tracking filter is used in conjunction with a rank detector preprocessor to detect fades and remove the accompanying angle measurement an improvement of 15 percent in the angle tracking accuracy can be obtained.

Polarization[47] It has been suggested that polarization agility can reduce the glint error based on the expectation that the scattering centers will be different with different polarizations. The assumption is that the target echo will be produced by scatterers with widely different polarization response characteristics so that glint will be decorrelated when there is a change in polarization. In practice, however, it might not be expected that polarization agility can decorrelate the glint errors as well as can frequency agility. It has been said[44] that with polarization agility "the improvements are often modest (at best)."

Spatial and Aspect Diversity It also has been suggested that glint can be reduced with either spatial or aspect diversity.[48] By spatial diversity is meant viewing of a target from a different location. The required separation of the antennas for spatial diversity need not be large. Aspect diversity requires that the target rotate with respect to the radar so as to change its aspect with respect to the radar. Not all targets cooperate by changing their aspects sufficiently to obtain the necessaray diversity. Furthermore, a change in aspect takes time, which is usually not available with weapon control radars subject to glint. Both spatial and aspect diversity, therefore, have operational limitations that tend to restrict their practical application for glint reduction.

Avoiding Closed-Loop Tracking As mentioned previously in this section, a radar that extracts the angle of a target without performing closed-loop tracking is not susceptible to the large errors caused by glint. There have been many solutions proposed for reducing the adverse effects of glint. No one method solves all problems, each has its advantages and disadvantages, and no one solution is universally applicable. As with so many other things, compromises might have to be made in order to deal with the potential effects of glint.

4.5 LOW-ANGLE TRACKING

A radar that tracks at low elevation angles illuminates the target via two paths, as shown in Fig. 4.17. One is the direct path from radar to target. The other is the path that includes a reflection from the earth's surface. It is as though the radar were illuminating two targets, one above the surface and the other its image below the surface. This is an example of the classic two-scatterer model mentioned in the previous section on glint. An error in the measured elevation angle of the target occurs because of the effect of glint. The error can be large enough to seriously degrade the quality of the tracking. At low grazing

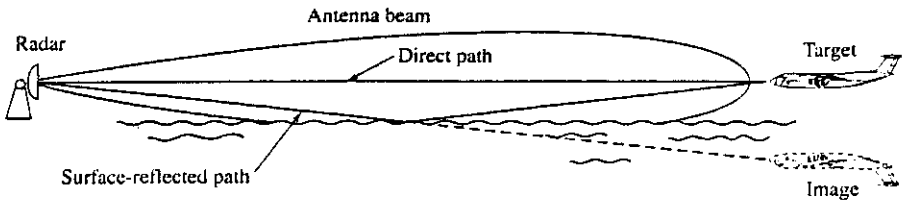

Figure 4.17 Low-angle tracking illustrating the surface-reflected path and the target's image below the surface.

angles over a perfectly smooth reflecting surface, the reflection coefficient from the surface is approximately -1 (Sec. 8.2). That is, its phase is in the vicinity of 180° and its magnitude is approximately unity so that the signal amplitude reflected from the surface is almost equal to the signal amplitude incident on the surface. This is, unfortunately, close to the worse condition for the angle error due to glint, as can be seen from the plot for the two-scatterer target model of Fig. 4.15. For this reason, the tracking of targets at low elevation angles can produce significant errors in the elevation angle and can cause loss of target track. The surface-reflected signal is sometimes called the *multipath signal* and the glint error due to the geometry of Fig. 4.17, a *multipath error.* Multipath errors can be a serious limitation to the radar guidance of missiles to targets low on the water as well as to surface or shipborne radars used for defense against low-altitude cruise missiles or sea-skimmer missile attack.

The effects of multipath depend on what part of the antenna pattern strikes the surface. Three regions can be identified,[49] according to elevation angle:

1. *Sidelobe region.* Elevation angles are such that the near-in sidelobes, rather than the main beam, illuminate the surface. The accuracy of a precision tracking radar (such as the AN/FPQ-6) begins to be degraded when the elevation angle is less than six beamwidths above the horizon.[50]
2. *Main-beam region.* The effects of multipath can begin to be severe when the elevation angle is less than about 0.8 beamwidth.
3. *Horizon region.* At grazing angles approaching zero degrees when there is specular reflection from the surface, the echo signal from the target and its image are approximately equal and out of phase so that combined direct and surface-reflected signal is very low. This reduction in signal-to-noise ratio further aggravates the accuracy problem.

Figure 4.18 shows an experimental measurement of the elevation-angle error obtained with an *S*-band radar as a function of range for an aircraft flying at low altitude.[51,52] The antenna beamwidth in this case was 2.7°. The aircraft flew out in range at a nearly constant altitude of 3300 ft. The start of the track is at about 4° elevation. At this angle the antenna sidelobes, rather than the main beam, illuminate the surface and the effect of multipath on angle accuracy is relatively small. At the center of Fig. 4.18 where the elevation angle is less than 2°, the main beam illuminates the surface and the effect of the surface-reflected wave becomes significant. Large elevation errors occur, which cause the antenna

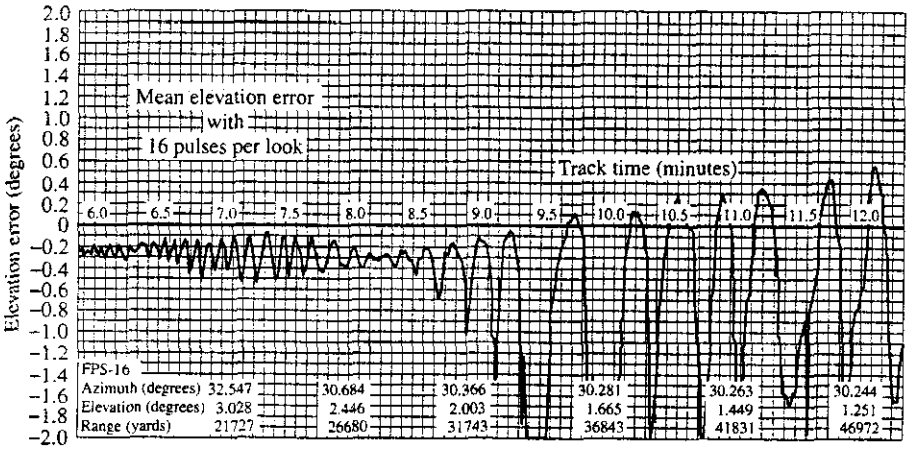

Figure 4.18 Example of the measured elevation tracking error using a phased array radar with 2.7° beamwidth. The aircraft target flew out in range at a nearly constant altitude. The numbers along the zero-error line indicate the track time in minutes.
[From Linde.[51]]

to look at the image below the ground rather than at the target. The errors are cyclic because a phase greater than 2π radians appears to the radar as if it where within 0 and 2π radians. It is seen in the example of Fig. 4.18 that there are times the antenna can point at an angle greater than 2° below the target. The tracking has been described as "wild" and great enough to cause the radar to lose track. The effect is most pronounced over a smooth water surface where the surface-reflected signal is strong. It can be so great that it becomes impossible to maintain a track at low altitudes with conventional tracking radars. According to Barton,[49] in the horizon region when the magnitude of the reflection coefficient exceeds 0.7 and the target is below 0.7 beamwidth, "there will be a strong tendency for the radar to track a centroid of reflection at or near the horizon." (This did not appear to occur for the data shown in Fig. 4.18.)

The multipath problem is similar to the glint error that results from tracking a classical two-scatterer target. Careful examination, however, of the theoretical glint error given in Fig. 4.15 and the experimental data of Fig. 4.18 show a significant difference. The two-scatterer model indicates there will be large errors when the surface reflection coefficient approaches -1. The large tracking errors appear to the side of the larger scatterer of the pair rather than the smaller scatterer. Generally, it is expected that in the multipath situation, the larger scatterer will be the target and the image will be the smaller (because the reflection coefficient is not greater than 1). The data of Fig. 4.18 show, however, that the large elevation angle errors are in the direction of the image rather than the true target. Thus the antenna is more likely to look into the ground than in the direction of the sky. Howard et al.[50] state that this difference can be explained by the failure to account for the amplitude distortion across the aperture, in addition to the phase distortion.

Although it has been easy to accept the two-scatterer target model as applied to low-angle tracking multipath case, there is a difference between the two. In the two-scatterer

model there are two propagation paths: the two two-way paths from the radar to each scatterer and back. In the multipath case, there are actually four propagation paths.[53] These are: (1) the path from radar to target and return by the same path; (2) the path from radar to target via reflection from the surface and return by the same path (this is the image path); (3) the path from radar directly to target and return via reflection from the surface; and (4) the inverse of path no. 3 which is the path from radar to target via the surface reflection, or image, and return directly to the radar. Thus paths no. 3 and 4 are the same except for direction of travel. (These four paths are made use of in multipath time-delay height finding to obtain the height of a target using high-range resolution with a fan-beam antenna pattern rather than a pencil-beam pattern.) The echoes from the four paths in the multipath geometry will provide a different composite echo signal at the radar than that obtained from the two-scatterer model. It should be expected, therefore, that the nature of the glint error in the multipath situation will be different from that predicted by the two-scatterer model, as has been demonstrated by experiment.

Another complication with surface multipath not modeled by the two-scatterer target is the effect of surface roughness which results in two components of the surface reflected signal; one is specular scatter and the other is diffuse scatter.[49]

With a rough surface, the angle error due to multipath is reduced because the surface-reflected wave is of lower magnitude (the reflection coefficient is less). Note that the roughness of a surface depends on its physical variations in height relative to the radar wavelength. The higher the radar frequency, the greater will be the "electrical" roughness of the surface (in wavelengths) for a given physical roughness, so that the effect of multipath on the elevation-angle accuracy might be less at the higher frequencies. At millimeter-wave frequencies, the surface reflection is more likely to be diffuse scatter rather than specular scatter.[54]

In addition to causing errors in elevation-angle tracking, it is also possible for multipath to introduce errors in the azimuth-angle tracking channel. This can be caused by *cross talk* where a portion of the elevation-angle channel signal enters in some manner the azimuth-angle channel. It might also be caused by the target-image plane departing from the vertical as when over sloping land or when the radar is on a rolling or pitching ship.

Methods for Reducing Multipath Effects at Low Angles There have been a number of methods demonstrated or proposed for reducing the large elevation angle errors that can occur due to the multipath experienced at low elevation angles.[49,55,56] There is not, however, a single method suitable for all applications where low-angle tracking is required. Each has its limitations. They are mainly for eliminating the large errors that occur when the main beam, rather than the sidelobes, illuminate the surface. Many of the methods mentioned below assume the use of a monopulse tracker. Only the first three seem to have had application. The others are mentioned because of some particular technical interest, and can be skipped if desired.

Narrow Beamwidth The surest method for reducing or eliminating tracking errors due to multipath is to have a narrow antenna beam that does not illuminate the surface. The beamwidth of an antenna is approximately $\theta_B \approx \lambda/D$ radians, where λ = radar wavelength

and D = antenna dimension, both in the same units. Thus a narrow beamwidth requires a large antenna, a high radar frequency, or both. Although a narrow beamwidth can eliminate the multipath problem, it is not always possible to do so in practice since there may be compelling reasons for not using a large antenna or for operating the radar at high frequency.

A method that has been successfully used operationally to obtain low-angle tracking capability is to employ two radars, one at X band (9 GHz) and the other at K_a band (35 GHz), using a single antenna system to provide operation at the two frequencies.[57,58] The lower frequency radar generally has a longer range. Target acquisition can be initiated with the lower-frequency tracker and then precision low-altitude tracking can be obtained by switching to the higher-frequency tracker. It has been said that with the dual-frequency tracker "targets at 100-ft altitude were successfully tracked over water with less than 0.4 mils multipath error to ranges in excess of 30,000 yds." Another advantage of a dual-frequency radar for military applications is that it makes hostile electronic countermeasures more difficult since both frequencies have to be jammed.

Illogical Target Trajectory Prior knowledge of potential target behavior can be used to reduce the effects of low-angle multipath without overly complicating the radar. Since aircraft or missile targets will not likely go below the surface of the earth and are limited in their ability to accelerate upward and downward, radar tracking data indicative of unreasonable target behavior can be recognized and rejected. In some situations, the target might be flying fast enough and the inertia of the antenna might be great enough to dampen the angle-error excursions caused by multipath.

Off-Axis, or Off-Boresight, Monopulse Tracking Advantage can be taken of the fact that large angle errors are usually limited to a region of low elevation angle predictable from the antenna pattern and the terrain. It should be possible, therefore, to determine when the target is in the low-angle region by sensing large elevation-angle errors. The antenna is then locked at a small positive elevation angle (usually about 0.7 to 0.8 beamwidth) while continuing closed-loop azimuth-angle tracking. With the beam fixed at a positive elevation angle, the target's elevation angle may be determined open-loop from the error-signal voltage. Alternatively, the elevation angle may simply be assumed to be halfway between the horizon and the antenna boresight. In the extreme, the peak-to-peak tracking error would not exceed 0.7 to 0.8 beamwidth, and the rms error would be typically about 0.3 beamwidth. The tracking accuracy is only slightly improved, but wide swings of the antenna and loss of track are avoided.

Double-Null Elevation-Difference Pattern[59,60] A monopulse radar when tracking a single target attempts to have the null of its difference pattern pointing in the direction of the target. When this occurs at low elevation angles the echo signal that arrives in the lower beam of the difference pattern via the surface reflection can result in a glint error. By using a more complicated antenna pattern than that of the usual four-horn monopulse antenna, a second null can be independently steered to the direction of the surface-reflected echo signal (the image echo) so as to cancel it before it reaches the radar receiver. The second null can be obtained by employing a third pair of feeds in the vertical

plane. The signals in elevation from the three pairs of vertical feeds are combined to produce two nulls, one in the direction of the target and the other in the direction of its image, as has been described by White in the cited references. The second null is maintained in the direction of the image, as computed by Snell's law for the measured target range.

A conventional four-element feed in a monopulse tracker has only one degree of freedom in the vertical plane (as well in the horizontal plane). It is designed to track only a single target. When multipath occurs, there are two target signals present (the actual target and its image). A conventional monopulse radar cannot cope since it is designed on the assumption that there is only a single target present. When a third pair of feed-elements is employed in the vertical, two degrees of freedom result so that there are now two nulls that can be positioned in the direction of the target and its image. This can be extended to even more feeds in the elevation plane (providing additional degrees of freedom and nulls) which enables better control of the nulling of the unwanted image.

Experiments over water have demonstrated good tracking (0.05 to 0.1 beamwidth rms) with the double-null technique to elevations as low as 0.25 beamwidth.[50]

There have been several other variants of this approach. The signal incident on the antenna aperture can be sampled at multiple points across the aperture (especially if an array antenna is used) and the maximum likelihood decision criterion employed to determine the location of the target and its image. Barton[55] states that these methods degrade in the presence of diffuse surface reflection. They also require more complicated feed structures and processing than a conventional monopulse.

High Range-Resolution The surface-reflected signal travels a longer path than the direct signal so it may be possible in some cases to separate them by use of high range-resolution waveforms. By tracking only the direct signal, the angle errors introduced by multipath are avoided. The range resolution ΔR required to separate the direct from the ground-reflected signal is approximately

$$\Delta R = \frac{2h_a h_t}{R} \qquad [4.6]$$

where h_a = antenna height, h_t = target height, and R = range. For a radar antenna height of 20 m, target height of 30 m, and a range of 4 km, the range resolution ΔR must be 0.3 m. This requires a pulse width of 2 ns and a bandwidth of 500 MHz, which is a shorter pulse and a greater bandwidth than usually found in operational radars. If the target were a sea-skimmer antiship missile at an altitude as low as 2 m above the sea, the bandwidth required to eliminate the multipath effect is too great to be practical for most applications. Thus range resolution has not usually been a satisfactory solution to the multipath problem.

Frequency Agility It was stated in Sec. 4.4 in the discussion of the two-scatterer model that use of more than one frequency each sufficiently separated from one other could smooth the angle error due to glint and produce an average result that was less likely to have large errors. The frequencies had to be separated by the amount given by Eq. (4.4) in order to obtain independent values of the glint error. The same can occur with the elevation-angle measurement when multipath is present if D in Eq. (4.4) is taken as the

difference in the path lengths; but there are two reservations. First, the average measurement of angle is more likely to be somewhere near the horizon rather than indicate the elevation angle of the target. Second, the bandwidth within which the various frequencies must occur is likely to be large. It is likely to be comparable to the bandwidth, discussed in the above, that is required of a short pulse for resolving the direct target echo from the image target echo. If a sufficiently large bandwidth were available to the radar designer, it might be better to employ that bandwidth for high range-resolution rather than for frequency agility. We have indicated previously, however, that this bandwidth is often larger than can be conveniently obtained in practice, especially when the target is at a very low altitude.

Doppler Resolution Since the target and its image are at different elevation angles, their doppler frequency shifts are slightly different. With sufficient doppler resolution, the target can be separated from its image. In practice, however, the difference in the doppler frequencies generally is too small to be used for isolating the target from its image, unless exceptionally long observation times are employed.

Clutter Fence A fence surrounding the radar can mask the echo from the image, especially when the near-in sidelobes are a factor in creating a multipath error. Fences can be expensive and are only of value when the radar is at a fixed site. Since the main beam illuminates the top edge of the fence, diffracted energy might illuminate the image.

Polarization Vertical polarization, which is often used in tracking radars, reduces the surface-reflected signal from the image when the image elevation angle is in the vicinity of the Brewster angle (Sec. 8.2). It has no special advantage, however, at low grazing angles when the angle to the image is much less than the Brewster angle.

Complex Angle (CA)[49,61] The normal monopulse receiver uses only the in-phase (or the out-of-phase) component of the difference signal. When a multipath signal is present along with the direct signal, the difference signal has a quadrature component. The in-phase and quadrature components of the error signal define a *complex angle* error signal. In the complex plane, with the in-phase and quadrature components as the two axes, the locus of the complex angle as a function of elevation angle is a spiral path. By measuring the complex angle, the target elevation can, in principle, be inferred. In using the complex-angle technique, the radar antenna is fixed at some angle above the horizon and an open-loop measurement of the complex angle is compared with a predicted set of values for the particular radar installation, antenna elevation-pointing angle, and terrain properties. A given in-phase and quadrature measurement does not give a unique value of the elevation angle since the plot of the complex angle shows multiple, overlapping turns of a spiral with increasing elevation angle of the target. The ambiguity can be resolved with frequency diversity or by continuous tracking over a long enough interval to recognize the ambiguous spirals.

This technique is limited by the need to resolve ambiguities, by the echoes from the real surface being different from theoretical when the surface is rough and the reflection is diffuse, and by random variations in the measurements which are difficult to remove by calibration because they vary rapidly with time and depend on target position.

Superresolution In general, two equal-amplitude signals can be resolved in angle if they are separated by at least 0.8 beamwidth. Sometimes it can be better than this since resolution depends on the phase between the two signals as well as the signal-to-noise ratio. Many attempts have been made in the past to improve angular resolution beyond 0.8 beamwidth, but without the desired success. *Superresolution*[62] is an example that is based on *spectral estimation* or *spectral analysis* to provide resolution in angle. It has been of interest for low-altitude tracking because of the claim that it can produce improved resolution compared to conventional linear methods, but it does not work for radar signals. Such methods do provide enhanced resolution of uncorrelated signals (such as independent noise), as occur with multiple jamming signals or the radio astronomy observation of cosmic sources. They are not applicable, however, for the resolution of correlated signals—and radar echo signals are correlated since they originate from the same transmitter. W. D. White[63] has shown the limitation of superresolution for coherent echo signals and that it has little, if any, value in solving the radar low-angle tracking problem.

Superresolution methods produce impressive-looking plots with sharp responses indicating the target locations. Depending on the algorithm used, however, the amplitude and position of the responses might not always be related to the features of the target. Spurious responses can be obtained when the algorithm used is nonlinear. Of importance, but of lesser concern compared to its other limitations, is that the signal-to-noise ratio must be high to use these methods and many of the algorithms are computationally complex. Superresolution is a technique whose name implies more than has been delivered and whose promises have not materialized as advertised.

Maximum Likelihood Estimation There have been many papers in the literature that describe the application of maximum likelihood estimation (MLE) to obtain the target's elevation angle in a multipath situation. Only a few are referenced here.[64–66] MLE also has been applied in conjunction with multiple frequencies[67] and with three-aperture antennas.[68,69] There have been some interesting results, but the technique has had limitations.

Electro-Optical and Infrared Optical and IR sensors offer the advantage of far better angular resolution than can be obtained with radar. They have the important advantage of not suffering from the multipath problem. Both optical and IR have been used to supplement radar coverage at low angles. At low angles, they are of short range since they are seriously limited by high attenuation in the clear atmosphere as well as in rain. Furthermore, they do not provide range or doppler velocity measurements. If reliable all-weather capability is necessary, radar is the sensor that has to be seriously considered.

Other Comments In addition to the above there have been several other methods proposed or investigated for mitigating the effects of glint when tracking a target at low angle. These include height diversity,[70] the use of neural nets,[71] the use of maximum likelihood estimation based on deterministic modeling that requires finding only four unknowns and which doesn't need to know the range,[72] the use of a threshold in the sum channel that must be exceeded in order to accept an elevation-angle measurement (this eliminates the large errors that can occur when the direct and the image signals are

almost out of phase—the condition for a large glint error and for a small signal in the sum channel),[73] and the use of bias compensation to reduce the glint error along with a threshold on the sum signal that eliminates measurements made with small signal-to-noise ratio.[74] The large number of publications on this subject is an indication of the importance of low-angle tracking and that there has been a lack of a good all-purpose solution.

When conditions permit, the use of a narrow beamwidth is the best method to ensure accurate tracking at low angle. Off-axis tracking with the antenna at a fixed elevation, and with the elevation angle measurement made open-loop, is simple and can provide relief from the wild swings of the antenna caused by multipath glint.

The low-angle tracking problem as discussed here concentrated on the effect of multipath. Radars concerned with low-angle tracking also have to be able to detect targets in the presence of clutter echoes that can be many orders of magnitude larger than the target, so that doppler methods, as discussed in Chap. 3, need to be considered.

In this section, the radar was usually considered to be located on or near the surface and tracking a target at low altitude. The problem of low-angle multipath is also important for missile guidance at low altitudes.[75]

4.6 TRACKING IN RANGE[76,77]

In the early days of radar, tracking of a target in range was usually done manually by an operator who watched an A-scope or similar presentation and positioned a handwheel to maintain a marker on the display over the desired target pip. The setting of the handwheel was a measure of the target range and was converted to an electrical signal and supplied to a data processor. Manual tracking has many limitations and it cannot be used in systems such as missiles where there is no operator present. It was soon replaced by closed-loop automatic tracking, such as the *split-gate tracker.*

Split-Gate Tracker The technique for automatically tracking in range is based on the split range gate. Two range gates, as indicated in Fig. 4.19, are generated. One is the *early gate* and the other is the *late gate.* The video echo pulse is shown in Fig. 4.19a, the relative position of the two gates at a particular instant is in Fig. 4.19b, and the difference signal is in Fig. 4.19c. In this example the portion of the signal in the early gate is less than that of the late gate. The signals in the two gates are integrated and subtracted to produce the difference error signal. The sign of the difference indicates the direction the two range gates have to be moved in order to have the pair straddle the echo pulse. The amplitude of the difference determines how far the pair of gates are from the "center" of the pulse, sometimes called the centroid. When the error signal is zero, the range gates are centered on the pulse and the position of the two gates gives the target's range. Deviation of the pair of gates from the center of the echo pulse increases the signal energy in one of the gates and decreases it in the other. This produces an error signal that causes the two pulses to be moved so as to reestablish equilibrium.

Range gating allows a single target to be isolated. The gate rejects unwanted signals and improves the signal-to-noise ratio by eliminating noise from other ranges. The AGC

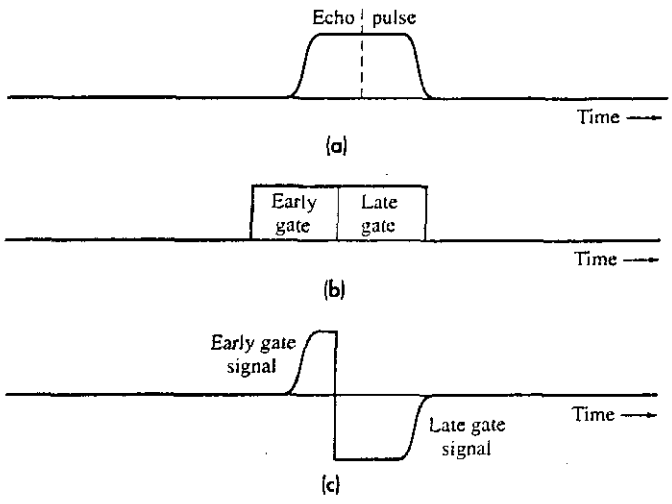

Figure 4.19 Split-gate range tracking: (a) Echo pulse; (b) early–late range gates; (c) difference signal between early and late range gates.

circuits respond only to the short time interval of the range gate where the echo from the target is expected. The range-gate width should be sufficiently narrow so as to minimize extraneous noise, but not so narrow that an appreciable fraction of the signal energy is excluded. Generally, the gate width is approximately equal to the pulse width. If tracking of the leading edge of the echo pulse is desired rather than its center, a bias can be inserted to move the gates forward. With leading-edge track, the gates should be "considerably narrower than with normal radar tracking."[78]

Range Glint A target with multiple scatterers distributed in range can cause tracking errors because of glint similar to the glint error experienced in angle tracking that was discussed in Sec. 4.4.[79]

Assume a two-scatterer model, similar to that considered for angle glint, but with the scatterers separated in range rather than angle. One scatterer is at a range $R_1 = cT_1/2$ and the other is at $R_2 = cT_2/2$, where c = velocity of propagation and T_1 and T_2 are the respective two-way time delays to the two scatterers. The two scatterers are assumed to be unresolved. The error ΔT_R due to range glint in the measurement of the time delay, relative to the center of the two scatterers, is found to be[79]

$$\Delta T_R = \frac{\Delta T}{2} \cdot \frac{1 - a^2}{1 + a^2 + 2a \cos (2\pi f_0 \, \Delta T} \qquad [4.7]$$

where $\Delta T = 2(R_2 - R_1)/c$ = time extent of the target; a = ratio of the amplitudes of the signals from the two scatterers ($a \leq 1$); and f_0 is the radar carrier frequency. This expression is equivalent to the angle-glint expression of Eq. (4.2) if the error in Eq. (4.2) is referred to the center of the two scatterers as it is here rather than referred to the larger scatterer. The range measurement error can be larger than the extent of the target.

Some reservations need to be mentioned about the use of this expression for range-glint error. It is based on the time delay (or range) of a target being given as the rate of

change of the echo signal phase with respect to frequency, or $\delta\phi/\delta f$. This can be seen by differentiating Eq. (3.1) as a function of frequency. Cross and Evans state[79] that the split-gate range tracker makes a measurement equivalent to finding range from the derivative of phase with respect to frequency. When the target consists of multiple scatterers, a glint error is introduced when using this criterion for extracting time delay.[80]

If, however, range is determined without a closed-loop tracker, a glint error does not occur. There can be range errors in this case due to the effect of noise, but they do not generate the type of effects that can happen when glint is possible. A glint error does not appear, for example, when the measurement is made manually by viewing the output signal on an A-scope display (amplitude versus range). A complex target with multiple scatterers within the radar resolution cell can cause inaccuracy in the measurement of the exact center of the target, but an operator would not be misled as would an automatic closed-loop tracker to position the range gate well outside of the target extent or the resolution of the pulse. Thus Eq. (4.7) does not apply to manual tracking or its electronic equivalent that doesn't used closed-loop tracking.

If range glint is a problem, some of the methods previously described for reducing angle glint might offer relief. The best approach, when sufficient bandwidth is available, is to employ high range-resolution. If the individual scatterers of a target can be resolved in range, both angle glint and range glint are not a problem. Tracking in range is generally much more accurate than tracking in angle (as measured by cross-range distance) so that any effects of range glint, if it occurs at all, is less of a concern than errors in angle, or cross-range.

4.7 OTHER TRACKING RADAR TOPICS

Target Acquisition A tracking radar must first find and acquire (lock on to) its target before it can operate as a tracker. Most tracking radars employ a narrow pencil beam for accurate tracking in angle; but it can be difficult to search a large volume for targets when using a narrow antenna beamwidth. Some other radar, therefore, must first find the target to be tracked and then designate the target's coordinates to the tracker. These radars have been called *acquisition radars* or *designation radars* and are surveillance radars that search a large volume.

The tracker is slewed to the direction of the target based on the target coordinates supplied by the acquisition radar. These coordinates are not always accurate enough to bring the tracker directly onto the target. Some searching in both azimuth and elevation angle might have to be done by the tracker in order to find the target. There have been several different types of patterns employed to search a limited angular region, as was described in Sec. 5.7 of the 2d edition of this book; but the raster scan has been one of the most popular. The *raster,* or *TV, scan* paints a rectangular search area in a uniform manner. An airborne intercept radar, for example, might acquire its target by scanning a 3° pencil beam over a target space 60° in azimuth by 15.5° in elevation by scanning six elevation steps, or bars.[81] The search space is relatively large in this example; but it can be much smaller if the target location information provided to the tracker is more accurate.

Raster scan is a simple and convenient means for searching a limited sector. It is also known as N-bar scan, where N is the number of azimuth scans, or bars.

If a 2D air-surveillance radar (range and azimuth) is used for designating a target to a surface-based mechanical tracking radar, the tracker might acquire its target with a nodding-beam scan in elevation, which is a raster scan in the vertical rather than the horizontal. Surface-based mechanical tracking radars can be designed to slew ±80° in one second and perhaps take another second to bring the target into track, so that acquisition can take place in under two seconds from the time of designation.

The target must be found in range as well as in angle. During the acquisition process, the tracking radar receiver range gate is scanned in range as the pulse propagates outwards in space. As has been mentioned, narrow range gates are important for restricting the noise the receiver must handle and to have only one target within the gate. The range gate is scanned from minimum to maximum range and is usually set to acquire the first target echo signal it detects. In some trackers there might be several contiguous range gates to shorten the acquisition time.[76]

A multifunction phased array radar for air defense usually performs as both the acquisition radar and the tracking radar. There is usually not much time that can be allocated for target acquisition in a multifunction radar that must maintain track on many targets and perform surveillance with adequate revisit times. The target-designation information obtained by a phased array needs to be accurate enough so that the tracking beam can be placed directly on the target without having to perform a search in angle. For this reason the target designation data from the surveillance portion of the multifunction phased array radar must be much more accurate than in air-defense systems that employ separate tracking and surveillance radars.

Servo System The automatic tracking of a target in angle employs a servo system that utilizes the angle-error signals to maintain the pointing of the antenna in the direction of the target. The servo system introduces a lag in the tracking that results in an error. The lag error will depend on the nature of the target trajectory (whether it is a straight line, a gradual turn, or a rapid maneuver). The error also depends on the ability of the servo system to accommodate to changes in speed, velocity, or acceleration. A so-called *Type II servo system*, which has often been used in tracking radar, theoretically has no steady-state error when the target velocity is constant. For this reason, it is also known as a *zero velocity-error system*. A steady-state error will exist, however, for a step-acceleration input. The operation of the Type II servo is similar to the alpha-beta tracker discussed in Sec. 4.9 for automatic tracking in a scanning surveillance radar. There are other types of servo systems depending on the required tracking accuracy and the expected target characteristics.[82] The effect of velocity and acceleration on a servo system can be described by the frequency response of the tracking loop.[83]

Servo Bandwidth The tracking bandwidth of a servo system is that of a low-pass filter. There are conflicting requirements on the choice of tracking bandwidth. On the one hand, the bandwidth should be narrow to minimize the effects of noise or jitter, reject unwanted signal components (such as the conical-scan frequency or aircraft-engine modulation), and to provide a smoothed output of the desired measurement parameters. A wide

tracking bandwidth, on the other hand, is desired for following rapid changes in the target trajectory or the changes in the vehicle carrying the radar. Thus a wide bandwidth is needed so as not to lose track of a maneuvering target, but a narrow bandwidth is needed for sensitivity. The choice of servo bandwidth, therefore, usually must be a compromise.

A target at long range will have low angular rates of change and a low signal-to-noise ratio. The bandwidth can then be narrow to increase sensitivity and yet follow the target with minimum tracking lag. At short range, on the other hand, angular rates are likely to be large so that a wide bandwidth tracking filter is needed in order to follow the target without loss of track. Thus the loss in sensitivity because of the wider bandwidth is offset by the greater target signal at the shorter ranges. At shorter ranges, errors due to target glint can become a problem; hence, the bandwidth should be no wider than necessary in order to keep glint errors from becoming excessive. The tracking bandwidth can be made variable or even adaptive to conform automatically to the target conditions.

Lowest Servo Resonant Frequency Another restriction on the tracking bandwidth of a mechanical tracker is that it should be small compared to the lowest natural resonant frequency of the antenna and its structural foundation in order to prevent the antenna system from oscillating at its resonant frequency. Figure 4.20 illustrates the bounds of measured data on the lowest resonant frequency as a function of antenna size. This figure is based on a compilation by the Aerospace Corporation of the lowest servo resonant frequencies for 190 individual radar, radio-telescope, and communications parabolic-

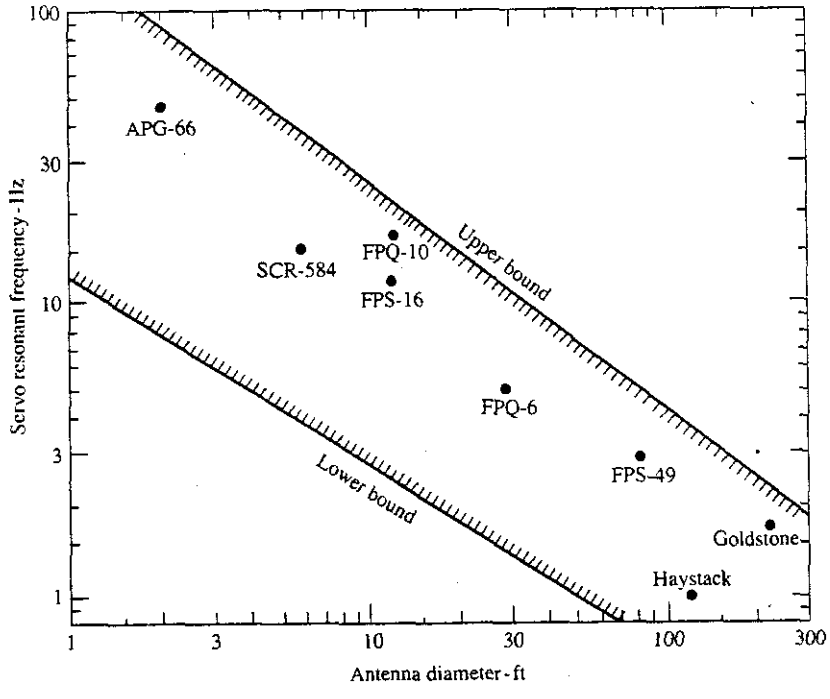

Figure 4.20 Bounds of the servo resonant frequency as a function of antenna diameter for actual tracking radars using parabolic-reflector antennas. (Based on extensive data compiled January 1994 by D. D. Pidhayny and Alan R. Lewis of the Aerospace Corporation.)

reflector antenna systems. Also shown are the resonant frequencies for several tracking radars. Howard[83] states that it is desired that the lowest resonant frequency be at least 10 times the servo bandwidth. This might be difficult to do with large antennas, and is not always practical. He mentions that the highly accurate AN/FPQ-6 radar tracker with a 29-ft diameter Cassegrain reflector antenna (Fig. 4.1a) has a resonant frequency only three times its servo bandwidth of 3.5 Hz. He also states that the smaller 12-ft antenna (such as for the AN/FPS-16) can provide a servo bandwidth up to 7 or 8 Hz.

Precision "On-Axis" Tracking[84,85] Some of the most precise tracking radars are those associated with the instrumentation used at missile test-ranges.[86] One such class of highly precise tracking radar that achieves better than usual performance is known as *on-axis tracking.*

The output of a conventional servo system lags its input, which results in a tracking error. The on-axis tracker accounts for this lag and keeps the target being tracked in the center of the beam or on the null axis of the difference pattern. This improves tracking accuracy by reducing coupling between the azimuth and elevation angle-track channels, by minimizing the generation of cross polarization, and by reducing the effects of any system nonlinearities.

On-axis tracking includes (1) the use of adaptive tracking whose output updates a stored prediction of the target trajectory rather than control the antenna servo directly, (2) removal of the static and dynamic system biases and errors by prior calibration, and (3) use of appropriate coordinates for filtering (smoothing) the target data.

The radar's angle-error signals are smoothed and compared to a predicted measurement based on a target-trajectory model updated by the results of previous measurements. This is especially useful for situations where prior knowledge of the target trajectory is approximately known, as when tracking ballistic missiles or satellites. If the measurement is the same as the prediction, no adjustment is made and the antenna beam is pointed according to the stored prediction. If they do not agree, the target trajectory prediction is changed until they do. Thus the pointing of the antenna is performed open-loop based on the stored target-trajectory prediction which is updated by the radar measurements. The servo loop that points the antenna is made relatively wideband (a high data rate) to permit fast response when tracking targets have high acceleration. The adjustment of the predicted position based on the measured position, however, is performed with a narrow bandwidth. This error-signal bandwidth is adaptive and can be made very narrow, yet the system will continue to point open-loop based on the stored target-trajectory prediction and the wide bandwidth of the antenna-pointing servos. The radar makes its measurements of the target in the polar coordinates of range, azimuth, and elevation (r, θ, ϕ). A target on a straight-line trajectory has a curvilinear track in polar radar coordinates which can generate apparent accelerations and can complicate the processing. These can be avoided by converting the polar coordinates to rectilinear coordinates (x, y, z) for data smoothing and comparison with prediction. After updating the target prediction, the rectilinear coordinates are converted back to radar polar coordinates to drive the antenna.

Systematic tracking errors include (1) error in the zero reference of the encoders used to indicate the orientation of the antenna axis, (2) misalignment of the elevation axis with respect to the azimuth axis (nonothogonality), (3) droop or flexing of the antenna and

mount caused by gravity, (4) misalignment of the antenna with respect to the elevation axis (skew), (5) noncoincidence of the azimuth plane of the mount to the local reference plane (mislevel), (6) insufficient dynamic range in the servo system, (7) finite transit time that results in the target being in a different position by the time the echo is received by the radar (which could be important for tracking of space objects), and (8) bending and additional time delay of the propagation path due to atmospheric refraction. Systematic errors are determined by prior measurement. They are then used to adjust the encoded position of the antenna to provide the correct target position.

A boresight telescope mounted on the radar antenna permits calibration of the mechanical axis of the antenna with respect to a star field. This calibration accounts for bias in azimuth and elevation, mislevel, skew, droop, and nonorthogonality. Tracking a visible satellite with the radar permits the position of the RF axis to be determined relative to the mechanical (optical) axis. The difference between the position measured by the optics and that measured by the radar is obtained after correction is made for the difference in atmospheric refraction for optical and RF propagation. This type of dynamic calibration requires that the radar be large enough to track satellites.

The calibration and compensation procedures to insure the tracking radar is of the highest accuracy might take several hours before the radar is ready for use. Such calibration might have to be repeated regularly. This is something that can be tolerated in precision instrumentation radars where time might not be important, but such times are less likely to be available for operational military radars. Also the performance of on-axis tracking can be degraded when the target performs unanticipated maneuvers.

There is nothing unique about any of the individual processes that enter into on-axis tracking. They can each be applied individually, if desired, to any tracking radar to improve the accuracy of track.[87]

Tracking in Doppler Coherent radars can also track the doppler frequency shift of the moving target echo. This is especially important for airborne pulse doppler radars and missile-guidance radars. The tracking doppler filter not only provides a measure of relative velocity, but also improves the ability of the radar to isolate the moving target echo from much larger clutter echoes. The doppler tracking filter is sometimes called a *speed gate*. Modulations of the target echo due to moving parts such as the propellers of piston engines or the compressor stages of jet engines extend the doppler spectrum and can degrade tracking accuracy.

Track While Scan (Limited Sector Scan) It was said at the beginning of this chapter that in the past the term *track while scan* has been applied to two different types of tracking radars. The name has been used to denote the tracking performed by a rotating-antenna air-surveillance radar which obtains target location updates each time the antenna beam rotates past the target, which might be from about 1 to 12 seconds. The name track while scan for this type of radar is now seldom used since almost all modern air-surveillance radars provide the equivalent with what is called *automatic detection and track (ADT)*, which is discussed in Sec. 4.9. Here we will briefly discuss the type of track-while-scan (TWS) radar used to rapidly scan a relatively narrow angular sector, usually in both

azimuth and elevation. It combines the search function and the track function. Scanning may be performed with a single narrow-beamwidth pencil beam (or a monopulse cluster of beams) that might cover a rectangular sector in a raster fashion. Scanning can also be performed with two orthogonal fan beams, one that scans in azimuth and the other in elevation. TWS radars have been used in airport landing radars, airborne interceptors, and air-defense systems.

A difference between a continuous tracker and the TWS radar is that the angle-error signal in a continuous tracker is used in a closed-loop servo system to control the pointing of the antenna beam. In the TWS radar, however, there is no closed-loop positioning of the antenna. Its angle output is sent directly to a data processor. Another significant difference is that the TWS radar can provide simultaneous tracks on a number of targets within its sector of coverage, while the continuous tracker observes only a single target, which is why it is sometimes called a *single-target tracker* (STT). With comparable transmitters and antennas, the energy available to perform tracking is less in a TWS radar than a STT since the TWS shares its radiated energy over an angular sector rather than concentrate it in the direction of a single target. In airborne-interceptor applications, the TWS radar might be preferred when multiple targets have to be maintained in track and the tracking accuracy only has to be good enough to launch missiles which contain their own guidance systems to home on the target. On the other hand, if highly accurate tracking is needed, a single-target tracker might be preferred.[81]

Limited sector-scan TWS radars have been used in *Precision Approach Radars* (PAR) or *Ground-Controlled Approach* (GCA) systems that guide aircraft to a landing.[88] These radars allow a ground controller to direct an aircraft to a safe landing in bad weather by tracking it as it lands. The ground controller communicates to the pilot directions to change his or her heading up, down, right, or left. In the control of aircraft landing, fan beams have been used which are electromechanically scanned over a narrow sector at a rate of twice per second. The azimuth sector that is scanned might be 20° and the elevation sector 6 or 7°. Landing radars using limited-scan phased array antennas, such as the AN/TPS-19, operate differently than scanning fan beams since they electronically scan a pencil beam over a region 20° in azimuth and 15° in elevation at a rate of twice per second. The AN/TPN-19 used multiple receive beams to obtain a monopulse angle measurement. Being a phased array, the AN/TPN-19 could simultaneously track up to six aircraft at a 20-Hz data rate. In the past, radars for the control of landing aircraft have been mainly used by the military. Civilian pilots prefer to use landing systems in which the control of landing is in the aircraft's cockpit rather than from a voice originating from the ground.

Track-while-scan radars have also been used successfully for the control of weapons in surface-to-air missile systems for both land and ship-based air defense, especially by the former Soviet Union.

Generally, TWS systems using fan beams have some limitations compared to systems that operate with one or more pencil beams. The fan-beam system can see more rain and surface clutter, it is more vulnerable to electronic countermeasures, and there might be problems with associating multiple targets that appear in the two beams.

The advantage of TWS compared to a continuous tracker is that multiple targets can be tracked. Because it shares its energy over a region of space, the TWS radar needs to

have a larger transmitter to obtain the same detection and tracking capabilities of a STT that dwells continuously on a single target. If the target's angle is found from the centroid of the angle measurements obtained as the TWS antenna beam scans past the target, inaccuracies can occur if the target signal fluctuates in amplitude. TWS radars are also more vulnerable to angle jamming than are continuous trackers.[89] TWS radars can use monopulse angle measurements in an open-loop manner, similar to a phased array. Since the monopulse measurement is not made with closed-loop tracking, a TWS radar should not experience the wild fluctuations in angle caused by glint when there are multiple scatterers within the resolution cell or when there is multipath at low elevation angles.

Tracking with Phased Array Radar Tracking with a phased array radar is more like that of a track-while-scan radar or automatic tracking with a surveillance radar than the continuous single-target tracker that has been the subject of most of this chapter thus far. The advantage of a phased array is that it can have a much higher data rate than radars with mechanically scanned antennas and it can simultaneously track multiple targets by time sharing a single antenna beam. This is possible because of the rapid inertialess beam positioning that, in some systems, can switch the antenna beam from one direction to another within microseconds. There is no closed-loop feedback to control the positioning of the beam as in a STT. When it is time to update a track, the computer controlling the radar directs the beam in an open-loop fashion to the expected present position of the target to either transmit or to receive the expected echo signal. Many targets can be tracked simultaneously in this manner.

An example of a phased-array instrumentation radar used for multiple target tracking on missile ranges is the AN/MPS-39 that was shown in Fig. 4.1b. It is also known as MOTR (Multiple Object Tracking Radar). This is a transportable C-band radar capable of tracking up to 10 targets simultaneously with an angle accuracy of 0.2 mrad. Its space-fed lens array is mounted on an elevation-over-azimuth tracking pedestal so that its 60° cone-angle coverage can be positioned anywhere in the hemisphere. A 1° (at broadside) beamwidth is obtained with a 12-ft diameter aperture. The monopulse tracking capability is achieved with a four-horn triple-mode feed. The manufacturer's literature states it is able to can acquire a target in less than 1 s. The advantage of a phased array for range instrumentation is that a single system simultaneously can track a drone target or targets, the aircraft that launches a weapon, multiple parts of a destroyed target, and other aircraft that might be observing the test or be in the vicinity. Without the phased array, a separate single-target tracker, such as the AN/FPS-16 or equivalent, would have to be used for each target that is to be tracked.

An excellent review of tracking with phased arrays and multifunction phased array radar has been given by Barton.[90]

Signal-to-Noise Ratio In Chapter 2, we found that reliable detection of a target required an integrated or single-pulse signal-to-noise ratio of the order of 12 to 15 dB. The tracking accuracy of the best radars is about 0.1 mrad. Such highly accurate tracking in angle requires much higher signal-to-noise ratios than required for detection. As indicated by Eq. (4.3) or the discussion of angle accuracy in Sec. 6.3, integrated or single-pulse

signal-to-noise ratios need to be more than 40 dB to achieve the inherent accuracy available in the best of the precision trackers.

Distinguishing Feature of Monopulse There are other types of simultaneous tracking methods, in addition to amplitude-comparison monopulse, that can obtain an angle measurement based on a single pulse. One might, for example determine the angle-error signal in one angular coordinate by taking the difference of the signals produced by two squinted beams at the video outputs of two separate receivers. Obtaining an accurate difference signal in this manner requires that the total gains of the two receiver channels be equal and remain that way. The high stability required to maintain balance of the two channels is not practical considering the total amount of gain there is in a receiver from the input antenna to the output difference circuit. The ineffectiveness of such a method was the reason why amplitude-comparison monopulse was invented during World War II by Robert Page of the U.S. Naval Research Laboratory.[91] By taking the sum and the difference of the two squinted beams right at the antenna, there is no need for ultrastable receivers as would be required to make an accurate measurement of angle in the video. It is the sum and difference networks at the antenna that distinguish monopulse from other simultaneous angle-measurement methods.

4.8 COMPARISON OF TRACKERS

In this chapter we have concentrated on two major tracking systems: the amplitude-comparison monopulse and the conical scan. There are several other types of trackers that were mentioned and others that could have been mentioned, but these two are the only ones that will be considered in the comparison in this section since they are quite representative of simultaneous tracking and sequential scanning.

Signal-to-Noise Ratio When the target is being tracked, the signal-to-noise ratio from a monopulse radar is greater than that from a conical-scan radar since the monopulse antenna views the target at the peak of its sum pattern. The conical-scan radar views the target at some angle off the peak of the antenna beam. Thus the signal-to-noise ratio of monopulse might be from 2 to 4 dB greater than with conical scan.

Accuracy The monopulse radar will have greater angle accuracy since its signal-to-noise ratio is higher (important when accuracy is limited by thermal noise). Also its angle accuracy is not affected by fluctuations in the amplitude of the echo signal as are sequential scanning systems. Both monopulse and conical-scan systems are degraded by the wandering of the apparent position of the target caused by glint. Monopulse, because of its better signal-to-noise ratio, has a better range accuracy than conical scan.

Complexity The monopulse radar is the more complex of the two since it requires RF combining circuitry at the antenna and three receiving channels. Conical scan has only one receiving channel and uses a single feed, but it has to rotate or nutate the

antenna beam at a high speed. In the early days of tracking radar, the relative complexity of monopulse was more pronounced. Receivers were big since they were based on vacuum-tube technology, and the combining circuitry was also large. Many a tracking radar development started out with monopulse, but had to switch to conical scan when its size or cost became too large. This is no longer a major consideration. Receivers are now solid state and small, and the combining circuitry has been made small by specially designed devices and the use of multimode feed systems. Thus complexity seldom need be a reason for not choosing monopulse. The Cassegrain is a popular antenna for monopulse since the combining circuitry and low-noise receiver front-ends can be placed behind the reflector where they can be better supported mechanically and not encounter the loss that can occur with long transmission lines.

A space-fed phased array radar can implement monopulse by using a multiple feed system similar to that used in a Cassegrain reflector antenna or a paraboloid reflector. With a corporate or constrained feed system in a phased array, the generation of multiple squinted beams requires a more complicated beam-forming network.

Minimum Number of Pulses As the name implies, a monopulse radar can perform an angle measurement in two coordinates on the basis of a single pulse. A phased array radar might make such a single-pulse angle measurement if the signal-to-noise ratio received on a single pulse is large enough. Usually, a number of pulses are integrated in a monopulse single-target tracker to increase the signal-to-noise ratio and the measurement accuracy. The conical-scan tracker requires a minimum of four pulses per revolution of the beam to extract an angle measurement in two coordinates. Ten pulses per revolution is more likely than four. Generally the pulse repetition frequency (prf) is at least 10 times the conical-scan frequency. (There have been exceptions to this, however.)

The monopulse radar first makes its angle measurement and then integrates a number of measurements to obtain the required signal-to-noise ratio and to smooth (reduce) the error. The conical-scan radar, on the other hand, integrates a number of pulses first (in its narrowband filter) and then extracts the angle measurement. The two tracking radars would have to integrate the same approximate number of pulses to achieve the same signal-to-noise ratio (assuming comparable radar systems), except that the conical-scan tracker has to process more pulses than the monopulse because of its 2 to 4 dB lower signal-to-noise ratio compared to the monopulse tracker, as mentioned above.

Susceptibility to Electronic Countermeasures The military conical-scan tracker is more vulnerable to spoofing countermeasures that take advantage of its conical-scan frequency. It can also suffer from deliberate amplitude fluctuations. A well-designed monopulse tracker is much harder to deceive.

Application Monopulse trackers should be used when good angle accuracy is wanted and/or when susceptibility to electronic countermeasures is to be minimized. When high-performance tracking is not necessary, the conical-scan tracker might be used because of its lower cost and reduced complexity.

4.9 AUTOMATIC TRACKING WITH SURVEILLANCE RADARS

This section is concerned with tracking performed by an air-surveillance radar rather than a single target tracker, or STT. Tracking with air-surveillance radars is done at a much longer revisit time (lower data rate) between observations than STTs. STTs have revisit times of the order of a tenth of a second; air-surveillance radars have revisit times of a few to many seconds. The STT tracks only a single target; the air-surveillance radar may have many hundreds, or even thousands, of targets in track.

A long-range or a medium-range air-surveillance radar can have within its coverage a large number of aircraft targets as well as many individual clutter echoes. In the busy parts of the continental United States, a long-range radar might have more than 600 aircraft within view during the heavy air-traffic part of the day. Military radars might have to deal with many more than that number. In the early days of air-surveillance radars, when there were fewer aircraft in the sky and they didn't fly as fast as modern jets, target tracking was done manually by operators using grease pencils to mark the position of a target on each antenna scan, calculate its speed, and determine its direction. An alert, trained operator can update a target track manually at a rate of about once per two seconds.[92,93] With a civil air-traffic control radar antenna rotating at the relatively slow rate of 5 rpm, a good operator might be able to hold in track 5 or 6 aircraft. Such a rate cannot be sustained, however, for more than about 20 to 30 minutes before the operator's performance is reduced. With the higher antenna rotation rates of military radars, manual tracking of aircraft is even more limited. When there are more aircraft than can be tracked manually, automatic methods must be used for target detection, coordinate extraction, and tracking. This is called *automatic detection and track* (ADT).

ADT requires a good radar that eliminates clutter echoes and other undesired signals. This might sound like an obvious statement that can be said for many things; but when ADT was first introduced it was mistakenly applied to the then existing radars which had poor or no MTI, or any other means for reducing clutter. Its performance was a disaster when used with poor radars. A tracking system can be designed to recognize and eventually eliminate clutter echoes that do not form logical tracks; but it takes time and computer capacity which might not be available when a large number of targets must be maintained in track. Thus good tracking starts with a good radar that eliminates unwanted clutter echoes and other extraneous signals.

When clutter targets cannot be completely eliminated by doppler processing, the ADT radar has to employ CFAR to maintain a *constant false-alarm rate.* (CFAR techniques are discussed in Sec. 5.7.) A CFAR senses the local clutter and noise environment in the vicinity of the radar echo signal, and automatically adjusts the receiver decision-threshold to maintain a constant false-alarm rate. When the environment consists of range-extensive clutter such as from land, sea, or rain, the clutter signal is used to change the threshold whenever the target echo competes with clutter. The required change in threshold due to a change in the clutter environment occurs almost instantaneously as the clutter seen by the radar changes. CFAR works fine to keep the ADT from being overloaded by echoes that are not from aircraft; but it comes at a price. An increase in the detection threshold

to maintain a constant false-alarm rate reduces the detection probability, thus some targets might not be detected. As discussed in Sec. 5.7, CFAR can introduce a loss of one or more dB, it can suppress desired echoes from targets in the vicinity of the target which is benefiting from the CFAR action, and it degrades the ability of the radar to resolve two closely spaced targets. CFAR may be needed in many radar systems; but one would like to have a radar that can accurately track a large number of targets without the accompanying limitations of CFAR.

Functions of an ADT[94–96] The functions performed by an ADT system include target detection, track initiation, track association, track update, track smoothing (filtering), and track termination. Each will be briefly discussed, assuming a ground-based 2D (range and azimuth) air-surveillance radar with mechanically rotating antenna.

Automatic Detection (This is reviewed in Sec. 5.5.) One approach is to first quantize the range and sometimes the azimuth angle (similar to what was done in the MTD discussed in Sec. 3.6). The quantization increment in range might be the pulse width and that in angle might be the azimuth beamwidth. At each range-azimuth quantization cell, the pulses received during the time the antenna scans past the target are integrated and a detection decision is made. CFAR generally is incorporated before the decision process in order to prevent excessive false alarms due to clutter echoes. Pulse integration is performed in some form of automatic detector, or integrator, such as discussed in Sec. 5.6. Another approach to automatic detection is the *moving window detector* which examines continuously the last n pulses and announces the presence of a target if at least m out of n of the pulses exceed a preset threshold.

A by-product of the automatic detection decision with a moving window detector or something similar, is an angle measurement made by *beam splitting.*[97] If n pulses are expected to be received from a target, beam splitting involves recognizing the beginning and end of the n pulses and locating their center. Angle accuracy depends on how well the beginning and end of the train of n pulses can be determined, as well as the number of pulses available and their signal-to-noise ratio. The beam splitting decision logic usually has no prior knowledge of a target's beginning. The logic must be sufficiently sensitive to quickly recognize the increased density region that signifies the start of an echo-signal pulse train, yet it must not be so sensitive that it generates false starts due to noise alone. Once a target's beginning is recognized, the device must sense the end of the increased density region. If the decision logic is too sensitive to change, it could cause a single target to split into two. A rough rule of thumb often quoted is that the accuracy of beam splitting is about one-tenth of a beamwidth when the signal-to-noise ratio is high enough to provide a good probability of detection.

Track Initiation In principle, a track can be initiated from the target-location information obtained on two successive scans of the radar antenna. In practice, however, target information from three or more scans is usually needed to initiate a track. Two scans would be adequate when there is only one or a few aircraft within view; but when the radar has in view a large number of echoes, one or more additional scans may be needed to

prevent false tracks from being initiated. Thus it is more usual to require three or more scans before establishing a track.

A *clutter map* is used to store the locations of fixed clutter echoes and prevent tracks from being initiated based on a clutter echo combined with a real target detection. Such tracks can eventually be recognized as false and can be dropped, but it takes time and computer capacity to do so when there are a large number of them. Clutter echoes for inclusion in the clutter map are those echoes that do not change their location with time or that change location too slowly to be targets of interest.

The process of initiating a track in a dense environment of targets and clutter not eliminated by the radar can be quite demanding in both computer software and hardware. Initiation of a new track may take more computer time and capability than any other aspect of ADT.

Requiring three scans for a civil air-traffic control radar to establish a track is usually not a burden. Waiting three scans for track establishment, however, may be an excessively long time for a military air-defense radar that has to direct weapon-control radars to defend against high-speed attackers that "pop up" at short range over the horizon. It is possible to quickly acquire the target on the basis of a single scan past the target if the radar can obtain a quick second look. This might be done with a *look-back beam* directed to the angle of the original detection. The quick look-back can provide confirmation of detection and an estimate of target's radial velocity. A phased array radar is well suited for this purpose, but mechanical rotating radars can also be outfitted with a fixed look-back beam. (One approach is shown in the antenna of Fig. 9.54.) Look-back might also be accomplished with a 3D radar whose electronically scanning beam in elevation is returned to the elevation angle of initial detection, before the radar beam entirely scans past the target.

Track Association When a new detection is received that is not at the location of a clutter echo stored in the clutter map, an attempt is made to associate it with an existing track. Association with an existing track is aided by establishing for each track a small search window, or gate, within which the detection of the target on the next scan of the radar antenna is predicted to appear. The gate should be as small as possible in order to avoid having more than one echo fall within it when the traffic density is high or when two tracks are close to one another. On the other hand, a large gate region is needed if the tracker is to follow target turns or maneuvers. More than one gate size is used to overcome this dilemma. Figure 4.21 shows a small nonmaneuvering gate situated around the predicted position of the target in track. The size of the gate is determined by the estimated errors in the predicted position and the estimated errors in speed and direction of the track. The detection threshold might be lowered in the gate region to increase the probability of detection. When an echo is not found within the nonmaneuvering gate, the larger region encompassing the maneuvering gate is then searched. The size of the maneuvering gate is determined by the estimate of the maneuvering capability of the target under track.

One reason the target might not appear in the nonmaneuvering gate is that its radar cross section might decrease, or fade, so that it is not detected. When this is the case, it

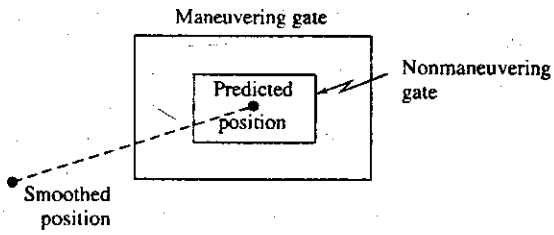

Figure 4.21 Maneuvering and nonmaneuvering gates centered at the target's predicted position. (From G. V. Trunk[110])

is possible for a false track to occur when a noise spike or an echo from another target is found in the maneuvering gate. To avoid the problem caused by a target fade and a false indication appearing in the larger maneuvering gate, the track can be divided into two tracks. (This is know as *bifurcation* of the track.) One is the original track with no new detection in the nonmaneuvering gate. The other is a new track based on the signal found in the maneuvering gate. After receiving the target position on the next scan of the radar (or sometimes after two scans), a decision is made as to which of the two tracks should be dropped.

Tracking is usually done in Cartesian coordinates, but the correlation gates are defined in polar (r, θ) coordinates.

Track Smoothing (α-β Tracker) On the basis of a series of past target detections, the automatic tracker makes a smoothed (filtered) estimate of the target's present position and velocity, as well as its predicted position and velocity. One method for accomplishing this is with the α-β (alpha-beta) tracker that computes the present smoothed target-position $\bar{x}_n$ and smoothed velocity $\dot{\bar{x}}_n$with the following equations

$$\text{smoothed position} = \bar{x}_n = x_{pn} + \alpha(x_n - x_{pn}) \qquad [4.8a]$$

$$\text{smoothed velocity} = \dot{\bar{x}}_n = \dot{\bar{x}}_{n-1} + \frac{\beta}{T_s}(x_n - x_{pn}) \qquad [4.8b]$$

The predicted position on the next scan (the n + 1st) is then

$$x_{p(n+1)} = \bar{x}_n + \dot{\bar{x}}_n T_s \qquad [4.8c]$$

where x_{pn} = predicted position of the target on the nth scan, x_n = measured position on the nth scan, α = position smoothing parameter, β = velocity smoothing parameter, and T_s = time between observations. If $\alpha = \beta = 0$, the tracker uses no current target information, only the smoothed data from prior observations. When $\alpha = \beta = 1$, no smoothing of the data is included at all. Thus the closer α and β are to zero, the more important is the smoothed track in determining the predicted track. The closer they are to 1, the more important is the currently measured data. If target acceleration is significant, a third equation can be added to describe an α-β-γ tracker, where γ = acceleration smoothing parameter.

Benedict and Bordner[98] show that if the transient response to a maneuvering target can be modeled by a ramp function, the output noise variance at steady state is minimized

in an α-β tracker when $\beta = \alpha^2/(2 - \alpha)$. It was stated that the analysis does not, and cannot, specify the optimum value of α. The value of α is determined by the bandwidth and will depend on the system application. In selecting α, a compromise usually must be made between good smoothing of the random measurement errors (requiring a narrow bandwidth) and a rapid response to maneuvering targets (wide bandwidth). Trunk[99] states that an α and a β satisfying the above relation can be chosen so that the tracking filter will follow a specified g turn.

Another criterion for selecting the α-β values is based on the best linear track fitted to the radar data in a least squares sense:[100]

$$\alpha = \frac{2(2n - 1)}{n(n + 1)} \qquad \beta = \frac{6}{n(n + 1)} \qquad [4.9]$$

where n is the number of the scan or target observation ($n > 2$). The above equations for α and β are also called the Kalman gain components.[101]

The classical α-β tracker is designed to minimize the mean-square error in the smoothed position and velocity. This type of tracker is said to be relatively easy to implement, but it does not handle the maneuvering target. Some means has to be included to detect maneuvers and change the values of α and β accordingly.

The two tracking gates described in connection with Fig. 4.21 is one example of how to deal with a large maneuver. Another example is an adaptive α-β tracker which varies the smoothing parameters to achieve a variable bandwidth that allows the radar to follow target maneuvers.[102] When the target is not maneuvering the adaptive tracking algorithm provides heavy smoothing. If the target maneuvers or makes a turn, the filter bandwidth is widened so as to allow the track filter to follow. As the selection of the values of α and β become more sophisticated and requires knowledge of the statistics of the measurement errors and the prediction errors, the α-β tracker approaches the Kalman filter.

Track Smoothing (Kalman Filter) The Kalman filter is similar to the α-β tracker except it can inherently provide for the maneuvering target.[103] A model for the measurement error has to be assumed, as well as a model for the target trajectory and the disturbance or uncertainty of the trajectory.[104] Such disturbances might be due to neglect of higher order derivatives in the model for the dynamics, random motions due to atmospheric turbulence, and deliberate target maneuvers. The Kalman filter can utilize a wide variety of models for measurement of noise and disturbance; but it is often assumed that these are described by white noise with zero mean.[105] A maneuvering target does not always fit such a model since its measurements are likely to be correlated. The proper inclusion of realistic models increases the complexity of the calculations. Furthermore, it may be difficult to describe ahead of time the precise nature of the trajectory disturbances.

When the Kalman filter is modeled with the target trajectory as a straight line, and the measurement noise and the trajectory disturbance are modeled as white, gaussian noise with zero mean, the Kalman filter equations reduce to the α-β tracker equations with α and β computed sequentially by the Kalman filter procedure.

Blackman[106] states that "Experience with airborne radars has shown the versatility of Kalman filters to be almost indispensable when dealing with problems presented by missing data, variable measurement noise statistics, and maneuvering targets with dynamic

capabilities." The Kalman filter has better performance than the α-β tracker since it utilizes more information. The α-β tracker, however, might be considered when the target's maneuver statistics are not known or in a dense target environment where computational simplicity is important.

The Kalman filter[107] and the α-β tracker also can be applied to control digitally the feedback loop in the single-target tracker.

Track Termination If the radar does not receive target information on a particular scan, the smoothing and prediction operation can be continued by properly accounting for the missing data.[108] (This is sometimes called *coasting.*) When data from a target is missing for a number of consecutive scans, the track is terminated. Although the criterion to be used for determining when to terminate a track depends on the application, it has been suggested that when three target reports are used to establish a track, five consecutive misses is a suitable criterion for termination.[109]

Tracking Performed on a Sector Basis To avoid having to correlate all new detections with all existing tracks, the correlation and track updating process can be done on a sector basis. The 360° of azimuth coverage might be divided, for example, into 64 sectors. Figure 4.22 shows sectors 4 through 12. As given by Trunk,[110] the following actions occur:

- Radar has reported all its detections found in Sector 11 and is now obtaining detections from Sector 12.
- Detections from Sectors 9, 10, and 11 are examined to see if they correlate with clutter cells from Sector 10 in the stored clutter map. Any detections associated with clutter cells are deleted from the detection file.
- Detections from Sectors 7, 8, and 9 are examined for possible association with the firm tracks in Sector 8. At this point, all detections from clutter cells have been removed from Sector 9 and below. Detections that are found to be associated with firm tracks are deleted from the detection file and are used to update the appropriate track, as with an α-β tracker.
- Preference is given to firm tracks. Thus tentative tracks are examined two sectors behind the firm tracks.
- Remaining detections not associated with either clutter cells or tracks are used to initiate new tentative tracks. Both a tentative track and a clutter cell are established until enough information is obtained to determine which of the two can be deleted.

Maneuvering Targets Target maneuvers and crossing trajectories can cause problems in tracking systems unprepared to cope with them. Some of the methods for handling maneuvering targets have been mentioned. Bar-Shalom[111] points out that a commercial aircraft that can turn at rates up to 3°/s completes a 90° turn in 30 s, so that a radar with a scan time of 10 s (rotation rate of 6 rpm) will obtain only three observations during the turn. He states that "very few of the existing schemes among the many in the literature (even adaptive ones with maneuver detection) can track such a target with good accuracy."

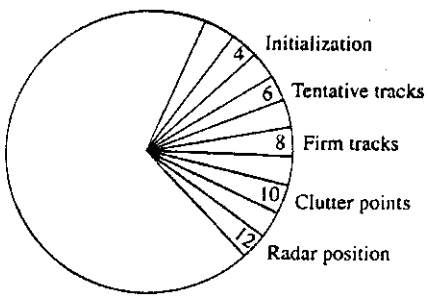

Figure 4.22 Various operations of a track-while-scan system performed on a sector basis.
(From G. V. Trunk[110])

He mentions algorithms and tracking methods to employ, but the radar must also be included. A 10-s scan time, or 6 rpm antenna rotation rate, is used for long-range civil air-traffic control radars where 90° turns are unlikely. Thus such radars are seldom exposed to a 90° turn in 30 s. Medium-range air-traffic control radars that observe traffic in the vicinity of airports, where aircraft are more likely to make a 90° turn, have shorter scan times than 10 s. The ASR-9, for example, has a scan time of 4.8 s. Military radars that have to deal with targets that maneuver more than do civil airliners, also have shorter scan times. In addition to the antenna scan time, the performance of an ADT system depends on the accuracy of the radar measurements, as well as the ability of the radar to resolve targets, reject clutter, eliminate discrete clutter echoes, and reject interference. Obtaining a good ADT is a total system problem, and should not be done in isolation by the control-system theorist without coordination with the radar systems designer.

Narrowband Data Communications Allowed by ADT One of the corollary advantages of ADT it that it allows a reduction in the bandwidth of the radar output since the information content of processed video detections or processed target tracks occupy significantly less bandwidth than the raw radar data. Narrowband telephone lines can be used for transmission rather than wideband microwave data links. Thus, if circumstances permit, when the radar has to communicate its output to a remote location, it is often better to extract the information right at the radar and transmit processed information rather than raw data.

Meaning of Target Detection When Tracking is Performed When the operators of early radars viewed the radar display, a single blip seen on the scope was taken to mean a target was detected. It was soon found that this was not sufficient, especially when clutter or noise appeared on the display. For greater reliability of detection, the operator required that echoes (blips) be seen on two consecutive scans, or two out of three (or some other combination) before the presence of a target was indicated. This is especially important when the noise or clutter has higher tails in its probability density function than the gaussian. With many modern ADT methods, the presence of a target is generally not finally confirmed until a track is formed. This criterion can employ a higher false-alarm rate per observation since multiple target observations are employed and the resulting track must be realistic. Thus the single-scan detection-threshold can be lowered and still achieve a very low probability of a false track.

Track-Before-Detect The probability of detection can be improved for weak targets, or the detection range extended for conventional-size targets, by noncoherently integrating the radar echoes received over multiple scans of the antenna. With such long-duration integration, the target can move beyond the resolution cell of the radar and may traverse many resolution cells during the integration time. In order to perform integration, knowledge is required of the speed and direction of each target in order to properly associate the echoes from scan to scan. Target trajectory information, of course, is usually not known beforehand, so scan-to-scan integration must be performed assuming all possible trajectories. A correct trajectory is one that provides a realistic speed and direction for the type of target being observed. In other words, the target must be *tracked* before it is *detected*, which is why this method was originally called *track-before-detect*. It has also been called *retrospective detection* and *long-term integration*, as well as *scan-to-scan integration*.

Track-before-detect can provide greater sensitivity because of the large number of pulses that it integrates. Also, the single-scan probability of false alarm can be much higher because of the requirement that the pulses being integrated form a logical target track from scan to scan. It can, however, be much more demanding of computer capability than conventional ADT. Track-before-detect was first examined experimentally in the 1960s, when data processing technology was still based on vacuum tubes. What it could do was quite limited at that time. As solid-state digital computer technology became available with much better capabilities, so could the performance of track-before-detect be significantly improved.

An analytical investigation[112] of a hypothetical radar with track-before-detect for detection of sea-skimming missiles by a shipborne radar when sea clutter is a problem concluded that "long-term integration [track-before-detect] provides around 10 dB increase in detection sensitivity over conventional cumulative detection . . . in 'Beaufort' sea state 4." Track-before-detect, or retrospective detection, was experimentally investigated[113] using an AN/FPS-114 shore-based sea-surveillance radar. The conclusions were that the single-scan probability of false alarm can be of the order of 10^{-3} rather than the 10^{-5} to 10^{-8} that might be typically required for conventional automatic tracking systems.

In addition to requiring increased data processing capability, track-before-detect also requires a longer observation time, which may be something that is not be available in all tracking applications. Unusual target maneuver during the scan-to-scan integration time might also limit performance.

Weak echoes on each scan are used to form the track. They will have lower signal-to-noise ratio than a radar designed to make the detection decision based on what is received with only a single scan. Thus the conventional detection philosophy as discussed in Chap. 2 has to be modified for use with track-before-detect.

The outputs of each resolution cell, whether from weak targets or from noise, are examined over N scans to determine if they form logical tracks. Tracks may be found by an exhaustive search of all possible trajectories based on the data from all N scans. The number of possible trajectories to be examined with exhaustive search can easily become impracticably large. The processing load can be narrowed by limiting the range of target speeds and placing restrictions on the type of target trajectories. Even this is usually not sufficient. Barniv,[114] however, suggests that by applying a dynamic programming algorithm the amount of computation can be significantly reduced so as to become feasible.

It can be applied with curved as well as straight-line target trajectories. When conditions permit, dynamic programming can perform the equivalent of an exhaustive search, but in a more convenient manner and with significantly less computer capability. In his example of tracking using a set of (passive) infrared mosaic-sensor images (a nonradar example), Barniv found that the use of dynamic programming typically required five or more orders of magnitude less computations than what was needed if employing an exhaustive search.

Multiple-Radar Tracking When multiple radars view a common volume, there can be improved tracking, the data rate can be greater than any of the radars acting alone, there is less vulnerability to electronic countermeasures, and less likelihood of having missed detections due to reduced echo-signal strength caused by nulls in one of the antenna patterns or changes in the target aspect. There are two related cases: one is when the radars are collocated, as on the same ship or at the same land site; the other, is when they are at separated locations and netted together.

Integrated Tracking from Collocated Radars at a Single Site When more than one radar, covering approximately the same volume in space, are located in the same vicinity, their individual outputs can be combined to form a single track. The radars might operate in different frequency bands, have different antenna characteristics, and different data rates. There is more than one way to combine the outputs of multiple radars.[115] A good approach is to combine all the detections from each radar to form a single track and to update the track rather than develop separate tracks at each radar and either select the best track or combine them in some other manner.[116] The data from the various radars do not arrive at the tracker at a uniform rate. The development of a single track file by the use of the total data available from all radars produces a better track than combining the tracks developed individually at each radar. It reduces the likelihood of a loss of data as might be caused by antenna lobing, target fading, interference, and clutter since integrated processing permits the favorable weighting of the better data and lesser weighting of the poorer data. This method of combining data from multiple radars has been known as either *Automatic Detection and Integrated Tracking* (ADIT) or *Integrated Automatic Detection and Tracking* (IADT).

Integrated Tracking from Multiple Sites When radars at multiple sites cover the same area, tracking can be combined as described above for the collocated radars; that is, the individual target data points (location and time), rather than the tracks, are transmitted to a single tracking center for processing into a single track. Farina and Studer[117] call this *centralized architecture.* They call a *distributed architecture* one in which the tracks are first formed at each radar site based only on the measurements from a single radar. These are transmitted to a tracking center which combines the tracks to establish a single track for each target. The distributed architecture allows the track information to be transmitted over telephone lines rather than wider bandwidth links, and it can employ less capable computer resources. The composite tracking accuracy it produces, however, is not as accurate as that with the centralized architecture.

To track targets over a large area as for air-traffic control or military air defense, multiple radars are located so that as a target leaves the coverage of one radar it enters the

coverage of the other and a continuous track is maintained. There needs to be some overlap in the coverages so that tracks can be properly handed over from one radar to the other. One of the problems that plagued early multisite radars was being able to associate radar detections or tracks made by one radar with data or tracks made by another radar. The absolute location of a radar site, even when fixed, was not always known accurately so that the central tracking facility might generate multiple tracks from a single target. This situation is even more serious when trying to net the radars from multiple ships or aircraft. Methods were developed for merging the data from multiple sites to provide a single track when the location or orientations of the radars was inaccurate.[118] The availability of GPS (Global Positioning System), however, readily provides the accurate location of a radar and eliminates the problem of associating data from radars located far apart.

Multiradar tracking (MRT) developed for the air-traffic control system of the Rome Flight Information Region integrates five radars sited on the west side of the center and south of Italy.[119,120] Alenia ATC radars were used with ranges up to 170 nmi. They were separated approximately 135 nmi apart. The filtering algorithm used an α-β tracker. The measured tracking accuracy of this system when the target flew a straight line course, was said to be better than 0.3 nmi. The observed accuracy with an accelerating path (acceleration was not further described) was 0.8 nmi.

Combined Tracking with Radar and Passive Direction Finding Radar provides the range and angle to a target. Passive direction finding (DF) provides angle and not range. The angle accuracy obtained by a radar is usually more accurate than the angle accuracy obtained by DF, so there is no gain in using the DF measurement in the tracking filter to produce a more accurate track. Passive DF, also called Electronic Support Measures (ESM), however, can assist in target recognition since it receives the emitted signal and can recognize the type of system that emitted it. Signals from hostile aircraft are likely to be distinctive and different from signals emitted by other aircraft, and can be used to recognize the nature of the target. This is of importance for military air-defense radars since some form of target recognition is needed to separate friendly and neutral aircraft from hostile aircraft.

Although DF systems provide target recognition and an angle measurement, they do not provide range so a track cannot be formed. If the passive angle track can be associated with a radar track, then the target being tracked by the radar can be recognized based on the information received by the passive DF system. Statistical methods for achieving this have been described.[121,122]

REFERENCES

1. Howard, D. D. "Tracking Radar." In *Radar Handbook,* M. Skolnik, Ed. New York: McGraw-Hill, 1990, Chap. 18.
2. Sherman, S. M. *Monopulse Principles and Techniques.* Norwood, MA: Artech House, 1984.
3. "IEEE Standard Radar Definitions," *IEEE Std 686–1997,* New York, 1997.

4. Sherman, S. M. Ref. 2, Sec. 4.4.
5. Sherman, S. M. Ref. 2, Sec. 4.4.2.
6. Page, R. M. "Monopulse Radar." *IRE Natl. Conv. Record* 3, pt. 8 (1955), pp. 132–134.
7. Skolnik, M. I. *Introduction to Radar Systems,* 1st ed. New York: McGraw-Hill, 1962, Sec. 5.4.
8. Rhodes, D. R. *Introduction to Monopulse.* Norwood, MA: Artech House, 1982.
9. Sherman, S. M. Ref. 2, Sec. 6.4.
10. Berger, H. "On the Optimum Squint Angles of Amplitude Monopulse Radar and Beacon Tracking Systems." *IEEE Trans.* AES-8 (July 1972), pp. 545–547.
11. Howard, D. D. Ref. 1, pp. 18.11–18.16.
12. Hannan. P. W. "Optimum Feeds for All Three Modes of a Monopulse Antenna." *IEEE Trans.* AP-9 (September 1961) pp. 444–460.
13. Barton, D. K. *Radars, Vol. 1, Monopulse Radar.* Norwood, MA: Artech House, 1974, papers nos. 11 and 12.
14. Elliott, R. S. *Antenna Theory and Design.* Englewood Cliffs, NJ: Prentice-Hall, 1981, Sec. 5.11.
15. Bayliss, E. T. "Design of Monopulse Antenna Difference Patterns with Low Side Lobes." *Bell System Tech. J.* 47 (1968), pp. 623–640.
16. Chubb, C. F., B. L. Hulland, and R. S. Noblit. Simplified Monopulse Radar Receiver, U. S. Patent 3,239,836, March 8, 1966.
17. Sherman, S. M. Ref. 2, Sec. 7.14.
18. Thomson, D. "Monopulse Design for Tactical Tracking Radar." *Microwave J.* 28 (May 1985), pp. 307–310.
19. Howard, D. D. Ref. 1, pp. 18.19–18.21.
20. Rubin, W. L., and S. K. Kamen. "SCAMP—A New Ratio Computing Technique with Application to Monopulse." *Microwave J.* 7 (December 1964) pp. 83–90.
21. Peebles, P. Z., Jr., and H. Sakamoto. "Conopulse Radar Tracking Accuracy." *IEEE Trans.* AES-16 (November 1980), pp. 870–874.
22. Bakut, P. A., and I. S. Bol'shakov. *Questions on the Statistical Theory of Radar, vol. II.* Moscow: Sovetskoye Radio, 1963, Chaps. 10 and 11. Translation available from NTIS, AD 645775, June 28, 1966.
23. Field, J. C. G. "The Design of Automatic-gain-control Systems for Auto-tracking Radar Receivers." *IEE Proc.,* Pt. C, 105 (March 1958), pp. 93–108.
24. Howard, D. D. Ref. 1, pp. 18.6–18.8.
25. Van Brunt, L. B. *Applied ECM, Vol. 2.* Dunn Loring, VA: EW Engineering, Inc., 1982, pp. 570–575.
26. Barton, D. K. *Modern Radar System Analysis.* Norwood, MA: Artech House, 1988, Chap. 11, Radar Error Analysis.

27. Meade, J. E. "Target Considerations." In *Guidance,* A. S. Locke, Ed. Princeton, NJ: D. Van Nostrand, 1955, Chap. 11, pp. 440–442.

28. Delano, R. H. "A Theory of Target Glint or Angular Scintillation in Radar Tracking." *Proc. IEEE* 41 (December 1952), pp. 1778–1784.

29. Howard, D. D. Ref. 1, Sec. 18.8.

30. Ostrovityanov, R. V., and F. A. Basalov: *Statistical Theory of Extended Radar Targets.* Norwood, MA: Artech House, 1985.

31. Wright, J. W. "Radar Glint—A Survey." *Electromagnetics* 4 (1984), pp. 205–227.

32. Howard, D. D. "Radar Target Angular Scintillation in Tracking and Guidance Systems Based on Echo Signal Phase Front Distortion." *Proc. Natl. Electronics Conf.,* vol. XV, Chicago, IL, Oct. 13–15, 1959.

33. Barton, D. K. *Radar System Analysis.* Norwood, MA: Artech House, 1977, Sec. 9.2.

34. Howard, D. D. Ref. 1, Sec. 18.10.

35. Lange, S., and A. Hammer. "Thermal Noise Analysis in Conical-Scan Radars." *IEEE Trans.* AES-14 (March 1978), pp. 400–413.

36. Peebles, P. Z., Jr., and T. K. Wang. "Noise Angle Accuracy of Several Monopulse Architectures." *IEEE Trans.* AES-18 (November 1972), pp. 712–721.

37. Dunn, J. H., D. D. Howard, and A. M. King. "Phenomena of Scintillation Noise in Radar Tracking Systems." *Proc. IRE* 47 (May 1959), pp. 855–863.

38. Howard, D. D. Ref. 1, Sec. 18.11.

39. Lind, G. "Reduction of Radar Tracking Errors with Frequency Agility." *IEEE Trans.* AES-4 (May 1968), pp. 410–416.

40. Weimer, F. C., and L. Peters, Jr. "Study of Pointing Errors in Conically Scanning and Monopulse Tracking Radars for Multipoint Targets." Antenna Lab., Ohio State University, Rept. 601-12, AD 123 476, 1956.

41. Loomis, J. M., and E. R. Graf. "Frequency Agility Processing to Reduce Radar Glint Pointing Error." *IEEE Trans.* AES-10 (November 1974), pp. 811–820.

42. Dunn, J. H., and D. D. Howard. "The Effects of Automatic Gain Control Performance on the Tracking Accuracy of Monopulse Radar Systems." *Proc. IRE* 47 (March 1959) pp. 430–435.

43. Delano, R. H. "A Theory of Target Glint or Angle Scintillation in Radar Tracking." *Proc. IRE* 41 (December 1953), pp. 1778–1784.

44. Borden, B. "What is the Radar Tracking 'Glint' Problem and can it be solved?" *Naval Air Warfare Center Weapons Division,* China Lake, CA, NAWCWPNS TP 8125, May 1993, AD-A266 509.

45. Borden, B. "Requirements for Optimal Glint Reduction by Diversity Methods." *IEEE Trans.* AES-30 (October 1994), pp. 1108–1114.

46. Guest, I. W., and C. K. Pauw. "Radar Detector Preprocessor for Glint Reduction in a Tracking Radar." *IEEE Trans.* 29 (April 1993), pp. 527–531.

47. Hatcher, J. L., and C. Cash. "Polarization Agility for Radar Glint Reduction." *IEEE Region 3 Convention,* Huntsville, Alabama, Nov. 19–21, 1969.

48. Sims, R. J., and E. R. Graf. "The Reduction of Radar Glint by Diversity Techniques." *IEEE Trans.* AES-19 (July 1971), pp. 462–468.

49. Barton, D. K. "Low-Angle Radar Tracking." *Proc. IEEE* 62 (June 1974), pp. 687–704.

50. Howard, D. D., J. T. Nessmith, and S. M. Sherman. "Monopulse Tracking Errors Due to Multipath Causes and Remedies." *IEEE EASCON '71* (1971), pp. 175–182.

51. Linde, G. J. "Improved Low-Elevation Angle Tracking with Use of Frequency Agility." Naval Research Laboratory, Washington, D.C. Report No. 7378, March 17, 1972.

52. Howard, D. D. Ref. 1, Sec. 18.9.

53. Skolnik, M. I. *Introduction to Radar Systems.* 2nd ed. New York: McGraw-Hill, 1980, p. 546.

54. Bruder, J. A., and J. A. Saffold. "Multipath Effects on Low-Angle Tracking at Millimeter-Wave Frequencies." *IEE Proc.-F* 138, No. 2 (April 1991), pp. 172–184.

55. Barton, D. K. "Low-Angle Tracking." *Microwave J.* 19 (December 1976), pp. 19–24 & 60.

56. Barton, D. K. *Modern Radar System Analysis.* Norwood, MA: Artech House, 1988, Sec. 11.2.

57. Cross, D., D. Howard, M. Lipka, A. Mays, and E. Ornstein: "TRAKX: A Dual-Frequency Tracking Radar." *Microwave J.* 19 (September 1976), pp. 39–41.

58. Klaver, L. J. "Combined X/K_a-Band Tracking Radar." *Conference Proc. Military Microwaves,* London, England, October 25–27, 1978, pp. 147–155.

59. White, W. D. "Low-Angle Radar Tracking in the Presence of Multipath." *IEEE Trans.* AES-10 (November 1974), pp. 835–852.

60. White, W. D. "Double Null Technique for Low Angle Tracking." *Microwave J.* 19 (December 1976), pp. 35–38 and 60.

61. Howard, D. D., S. M. Sherman, D. N. Thomson, and J. J. Campbell. "Experimental Results of the Complex Indicated Angle Technique for Multipath Correction." *IEEE Trans.* AES-10 (November 1974), pp. 779–787.

62. Gabriel, W. F. "Spectral Analysis and Adaptive Array Superresolution Techniques." *Proc. IEEE* 68 (June 1980), pp. 654–666.

63. White, W. D. "Angular Spectra in Radar Applications." *IEEE Trans.* AES-15 (November 1979), pp. 895–899. See also discussion in the same issue, pp. 899–904.

64. Zoltowski, M. D. "Beamspace ML Bearing Estimation Incorporating Low-Angle Geometry." *IEEE Trans.* AES-27 (May 1991), pp. 441–458.

65. Reilly, J., J. Litva, and P. Bauman. "New Angle-of-Arrival Estimator Comparative Evaluation Applied to the Low-Angle Tracking Radar Problem." *IEE Proc.* 135, Pt. F (October 1988), pp. 408–420.

66. Zoltowski, M. D. "Beamspace ML Bearing Estimation for Adaptive Phased Array Radar." In *Adaptive Radar Detection and Estimation,* S. Haykin and A. Steinhardt, Eds. New York: John Wiley, 1992, Chap. 5.

67. Bosse, E., R. M. Turner, and E. S. Riseborough. "Model-Based Multifrequency Array Signal Processing for Low-Angle Tracking." *IEEE Trans.* AES-31 (January 1995), pp. 194–209.

68. Cantrell, B. H., W. B. Gordon, and G. V. "Trunk Maximum Likelihood Elevation Angle Estimates of Radar Targets Using Subapertures." *IEEE Trans.* AES-17 (March 1981), pp. 213–221.

69. Taha, A., and J. E. Hudson. "Trigonometric High-Resolution Method to Resolve Two Close Targets." *IEE Proc.* 134, Pt. F (October 1987), pp. 597–601.

70. Giuli, D., and R. Tiberio. "A Modified Monopulse Technique for Radar Tracking with Low-Angle Multipath." *IEEE Trans.* AES-11 (September 1975), pp. 741–748.

71. Wong, T., T. Lo, H. Leung, J. Litva, and E. Bossse. "Low-Angle Radar Tracking Using Radial Basis Function Neural Network." *IEE Proc.* 140, Pt. F (October 1993), pp. 323–328.

72. Lo, T., and J. Litva. "Use of a Highly Deterministic Multipath Signal Model in Low-Angle Tracking." *IEE Proc.* 138, Pt. F (April 1991), pp. 163–171.

73. Seifer, A. D. "Monopulse-Radar Angle Tracking in Noise or Noise Jamming." *IEEE Trans.* AES-28 (July 1992), pp. 622–638.

74. Daeipour, E., W. D. Blair, and Y. Bar-Shalom. "Bias Compensation and Tracking with Monopulse Radars in the Presence of Multipath." *IEEE Trans.* AES-33 (July 1997), pp. 863–882.

75. Ivanov, A. "Radar Guidance of Missiles." In *Radar Handbook,* M. Skolnik, Ed. New York: McGraw-Hill, 1990, chap. 19, p. 19.30.

76. Howard, D. D. Ref. 1, Sec. 18.5.

77. Barton, Ref. 56, Chap. 9.

78. Van Brunt, L. B. *Applied ECM.* Dunn Loring, VA: EW Engineering, 1982, Vol. 2, pp. 309–315.

79. Cross, D. C., and J. E. Evans. Target-Generated Range Errors, Naval Research Laboratory, Washington, D.C., Memorandum Report 2719, January, 1974.

80. Skolnik, M. I. Radar Information from the Partial Derivative of the Echo Signal Phase from a Point Scatterer, Naval Research Laboratory, Washington, D.C., Memorandum Report 6148, February 17, 1988.

81. Stimson, G. E. *Introduction to Airborne Radar.* El Segundo, CA: Hughes Aircraft Co., 1983, p. 472. See also the second edition, published by Menhdam, NJ: Scitech, 1998, pp. 388–390.

82. Barton, D. K. Ref. 56, Sec. 10.2.

83. Howard, D. D. Ref. 1, Sec. 18.4.

84. Schelonka, E. P. "Adaptive Control Techniques for On-Axis Radars." *IEEE 1975 International Radar Conference*, Arlington, VA, April 21–23, 1975, pp. 396-401, IEEE Publication 75 CHO 938-1 AES.

85. Clark, B. L., and J. A. Gaston. "On-Axis Pointing and the Maneuvering Target." *IEEE NAECON '75 Record*, pp. 163–170, 1975.

86. Nessmith, J. T. "Range Instrumentation Radars. *IEEE ELECTRO '76*, Boston, MA, May 11–14, 1876. Reprinted in Skolnik, M. *Radar Applications*. New York: IEEE Press, 1988, pp. 458–468.

87. Nessmith, J. T., and Patton, W. T. "Tracking Antennas." In *Antenna Engineering Handbook*, 2d ed. R. C. Johnson and H. Jasik, Eds. New York: McGraw-Hill, 1984, Chap. 34.

88. Ward, H. R., C. A. Fowler, and H. I. Lipson. "GCA Radars: Their History and State of Development." *Proc. IEEE* 62 (June 1974), pp. 705–716.

89. Barton, D. K., and S. A. Leonov. *Radar Technology Encyclopedia*. Norwood, MA: Artech House, 1997, p. 445.

90. Barton, D. K. Ref. 56, Sec. 10.4.

91. Page, R. M. Accurate Angle Tracking by Radar, Naval Research Laboratory, Washington, D.C. Report RA 3A 222A, 28 December 1944. Reprinted in D. K. Barton, Ref. 13, paper No. 1.

92. Plowman, J. C. "Automatic Radar Data Extraction by Storage Tube and Delay Line Techniques." *J. Brit. IRE* 27 (October 1963), pp. 317–328.

93. Baker, C. H. *Man and Radar Displays*. New York: Macmillian, 1962.

94. Brookner, E. *Tracking and Kalman Filtering Made Easy*. New York: Wiley, 1998.

95. Trunk, G. V. "Automatic Detection, Tracking, and Sensor Integration." In *Radar Handbook*, 2nd ed., M. Skolnik, Ed. New York: McGraw-Hill, 1990, Chap. 8.

96. Farina, A, and F. A. Studer. *Radar Data Processing. Vol. I—Introduction and Tracking*. New York: Wiley, 1986.

97. Dinneen, G. P., and I. S. Reed. "An Analysis of Signal Detection and Location by Digital Means." *IRE Trans.* IT-2 (March 1956), pp. 29–38.

98. Benedict, T. R., and G. W. Bordner. "Synthesis of an Optimal Set of Radar Track-While-Scan Smoothing Equations." *IRE Trans.* AC-7 (July 1962) pp. 27–32.

99. Trunk. G.V. Ref. 95, Sec. 8.3.

100. Quigley, A. L. C. "Tracking and Associated Problems." *International Conf. on Radar—Present and Future*, Oct. 23–25, 1975, London, pp. 352–359, IEE Conference Publication No. 105.

101. Farina, A., and F. A. Studer. Ref. 96, Sec. 3.4.2.

102. Cantrell, B. H. "Adaptive Tracking Algorithm." Naval Research Laboratory, Washington, D.C., Memorandum Report 3037, April, 1975.

103. Kalman, R. E., and R. S. Bucy. "New Results in Linear Filtering and Prediction Theory." *J. Basic Eng.* (ASME Trans., Ser. D) 83 (March 1961), pp. 95–107.

104. Morgan, D. R. "A Target Trajectory Noise Model for Kalman Trackers." *IEEE Trans.* AES-12 (May 1986) pp. 405–408.

105. Hampton, R. L. T., and J. R. Cooke. "Unsupervised Tracking of Maneuvering Vehicles." *IEEE Trans.* AES-9 (March 1973), pp. 197–207.

106. Blackman, S. S. *Multiple-Target Tracking with Radar Applications.* Dedham, MA: Artech House, 1986, Chap. 2.

107. Biernson, G. *Optimal Radar Tracking Systems.* New York: Wiley, 1990, Chap. 8.

108. Kanyuck, A. J. "Transient Response of Tracking Filters with Randomly Interrupted Data." *IEEE Trans.* AES-6 (May 1970), pp. 313–323.

109. Leth-Espensen, L. "Evaluation of Track-While-Scan Computer Logics." In *Radar Techniques for Detection, Tracking, and Navigation,* W. T. Blackband, Ed. New York: Gordon and Breach, 1966, Chap. 29.

110. Trunk, G. V. "Survey of Radar ADT." Naval Research Laboratory, Washington, D.C., Report 8698, June 30, 1983.

111. Bar-Shalom, Y. *Multitarget-Multisensor Tracking Applications and Advances,* Vol. II, Boston, MA: Artech House, 1992, p. xiii.

112. Urkowitz, H., and M. R. Allen. Long Term Noncoherent Integration Across Resolvable Sea Clutter Areas." *Proc. 1989 IEEE National Radar Conference,* March 29–30, 1989, pp. 67–72. For more technical details, see Allen, M. R., S. L. Katz, and H. Urkowitz. "Geometric Aspects of Long-Term Noncoherent Integration." *IEEE Trans.* AES-25 (September 1989), pp. 689–700.

113. Prengaman, R. J., R. E. Thurber, and W. G. Bath. "A Retrospective Detection Algorithm for Extraction of Weak Targets in Clutter and Interference Environments." *IEE International Conference Radar-82,* October 18–20, 1982, pp. 341–345, IEE Conference Publication No. 216.

114. Barniv, Y. "Dynamic Programming Algorithm for Detecting Dim Moving Targets" In *Multitarget-Multisensor Tracking,* Vol. I. Y. Bar-Shalom, Ed. Norwood, MA: Artech House, 1990, Chap. 4.

115. Trunk, G.V. Ref. 95, Sec. 8.4.

116. Cantrell, B. H., G. V. Trunk, J. D. Wilson, and J. J. Alter. "Automatic Detection and Integrated Tracking." *IEEE 1975 International Radar Conference* pp. 391–395. Arlington, VA, Apr. 21–23, 1975.

117. Farina, A., and F. A. Studer. *Radar Data Processing. Vol. II—Advanced Topics and Applications.* New York: Wiley, 1986.

118. Bath, W. G. "Association of Multisite Radar Data in the Presence of Large Navigational and Sensor Alignment Errors." *IEE Int. Radar Conf.,* London, pp. 371–379, 1982.

119. Farina, A., and F. A. Studer. "Radar and Sensor Netting Present and Future." *Microwave J.* 29 (January 1986), pp. 97, 98, 100, 104, 106, 108, 110, 112, 114, and 124.

120. Farina, A., and F. A. Studer. Ref. No. 117, Sec. 7.2.6.

121. Trunk, G. V., and J. D. Wilson. "Association of DF Bearing Measurements with Radar Measurements." *IEEE Trans.* AES-23 (July 1987), pp. 438–447.

122. Farina, A., and B. La Scala. "Methods for the Association of Active and Passive Tracks for Airborne Sensors." *International Radar Symposium, IRS-98.* September, 15–17, 1998, Munich, Germany, pp. 735–744.

PROBLEMS

4.1 If the one-way antenna power pattern of a conical-scan tracking antenna is described by the gaussian function of Eq. (3.34), what is the loss in received signal when the target is directly at the beam crossover? The antenna half-power beamwidth is 2 degrees and the squint angle is 0.75 degree.

4.2 One reason that automatic gain control (AGC) is used in continuous-tracking radars is to prevent saturation of the receiver due to such things as the variation of the target echo signal with range and with aspect. (a) How much might a target echo vary in power (in dB) if the radar has to observe targets from a minimum range of 2 nmi to a maximum of 100 nmi? (b) How much might the echo vary because of different size aircraft targets? [See Table 2.1.] (c) How much might an aircraft echo change due to a change in aspect? [See Figs. 2.15 and 2.16.]

4.3 Compare the amplitude-comparison monopulse tracker and the conical scan tracker with respect to accuracy at long, medium, and short ranges; complexity; the number of pulses usually used for an angle measurement; and the type of application where each might be preferred.

4.4 (a) Why is the amplitude-comparison monopulse more likely to be preferred over the phase-comparison monopulse? (b) Why is the conical scan tracker more likely to be preferred over the sequential lobing, or lobe switching, tracker?

4.5 Derive the error signal in one angle coordinate for the amplitude-comparison monopulse. Show that for small angular errors, the error signal is linearly proportional to θ_T, where θ_T is the angle of the target measured from the antenna pointing direction. The angular separation between the two squinted antenna beams is $2\theta_q$. [The one-way (voltage) pattern of the two antenna beams when not squinted can be approximated by the normalized gaussian function $\exp(-a^2\theta^2/2)$; where $a^2 = 2.776/\theta_B^2$, and θ_B is the half-power beamwidth. Note that the hyperbolic cosine can be expressed as $\cosh x = (e^x + e^{-x})/2$ and the hyperbolic sine as $\sinh x = (e^x - e^{-x})/2$; and for small values of x, $\sinh x \approx x$ and $\cosh x \approx 1$. Also, $\sinh 2x = 2 \sinh x \cosh x$.].

4.6 Two echo signals from a finite size target arrive at a single-coordinate radar tracking antenna from a direction of $+\theta_D/2$ and $-\theta_D/2$, respectively, measured with respect to the antenna broadside (boresight) direction. How can one use the output of the sum channel to recognize that a serious glint error is occurring?

4.7 A tracking radar is tracking a "dumbbell" target consisting of two isotropic scatterers separated by an angular extent θ_D when seen at the location of the radar. (This is similar to the geometry shown in Fig. 4.15a in the discussion of glint.) The ratio of the echo-signal amplitudes from the two scatterers is $a = 0.5$. If the phase difference α between the two scatterers varies uniformly with time over the range of values 0 to 2π radians, what fraction of the time will the radar angle-error signal indicate an "apparent" target direction that is pointing outside the angular extent θ_D of the dumbbell target? (You may assume that the angular extent of each of the two scatterers is very small compared to θ_D.)

4.8 A monopulse radar is found to be tracking a target with an angular accuracy of 0.5 mil at a particular range. (a) What is this accuracy in degrees? (b) Assuming the accuracy is determined solely by the receiver noise, what would be the angle accuracy at this range of a similar conical scan tracker (the same frequency, beamwidth, power, noise figure, prf, number of pulses processed, and antenna effective area)? (c) If, on the other hand, the accuracy is at short range so that angle accuracy is determined solely by glint, what would be the accuracy of the conical scan tracker relative to that of the monopulse tracker?

4.9 Show that the phase of the echo from a dumbbell target (two unresolved isotropic scatterers separated by a distance D) oriented along the radial (range) direction (rather than the cross-range direction) is decorrelated if the frequency is changed by at least $c/2D$, where c is the velocity of propagation.

4.10 A target has an effective depth in the radial (range) dimension of 15 m. What must be the change in frequency in order to get a decorrelated measurement of angle glint?

4.11 This problem involves range glint. (a) A dumbbell target at a long range from the radar has its two unresolved equal cross-section isotropic scatterers located in line in the radial (range) direction and separated by 10 m. What is the phase difference between the echoes from these two scatterers when viewed by a radar at a frequency of 3 GHz? What is the range glint error in this case? (b) What change in aspect angle (such as might be caused by a rotation of the target about its center) will cause the two echoes to be 180° out of phase, resulting is a severe glint error in range? (c) What change in frequency is needed to decorrelate the echo when the target is oriented as in (b)? (d) What must be the pulse width [in (a)] in order to resolve the two scatterers (so that glint may be avoided)?

4.12 What two measures might be taken to reduce the effects of the glint error in both angle and range?

4.13 (a) Why does a tracking radar have poor accuracy at low elevation angles? (b) Summarize the two methods that may be worth considering when it is necessary to avoid poor tracking of targets at low altitudes.

4.14 One approach (mentioned in Sec. 4.5) to minimize the probability of breaking lock and the large errors that can occur in elevation angle when tracking at low-angles is to fix the antenna beam at some low elevation angle θ_e and cease closed-loop tracking until the target returns to a higher elevation angle where multipath is reduced. In such a case, all that might be said about the target's elevation angle is that it is somewhere within the half-power beamwidth θ_B of the antenna. Let $\theta_e = \theta_B/2$. (a) If it is assumed, when using this method, that the probability of the target being within the half-power elevation beamwidth

θ_B is uniform, the estimate of its location is the mean value, which is $\theta_B/2$. What is its standard deviation under these assumptions? (b) The assumption that the elevation-angle measurements are uniformly distributed within the elevation beamwidth may or may not be correct; but if it were valid, what does the result of (a) say about the use of more sophisticated methods that give rms values of the elevation that are no better than 0.1 to 0.3 beamwidths?

4.15 What might be the upper bound of the resonant frequency of the servo when the tracking antenna is 30 ft in diameter?

4.16 a. If an alert, well-trained air-surveillance radar operator can manually update an aircraft track in two seconds, how many aircraft can be held in track by a single operator when the radar antenna scans at a rate of 6 rpm?

b. If seven operators were available for performing manual tracking, how many targets do you think could be held in track with the radar of part (a) (assuming each operator had a display)? [Caution: This is a little like the question: How many engineers does it take to change a light bulb?]

4.17 (a) What is meant by beam splitting? (b) Describe briefly how is it accomplished? (c) What accuracy might it typically have?

4.18 Under what conditions does the Kalman filter perform like the α-β tracking filter?

4.19 (a) What is the chief advantage of automatic detection and tracking? (b) What are its limitations?

chapter

5

Detection of Signals in Noise

5.1 INTRODUCTION

A radar *detects the presence* of an echo signal reflected from a target and *extracts information* about the target (such as its location). One without the other has little meaning. The detection of radar signals in noise was discussed in Chap. 2, detection of moving targets in clutter was the subject of Chap. 3, and detection of stationary targets in clutter is discussed in Chap. 7. In the current chapter, additional aspects of the detection of radar signals in noise will be presented, chiefly the matched filter and related topics. The extraction of information from a target echo signal is the subject of the following chapter, Chap. 6.

Methods for the detection of desired signals and the rejection of undesired noise, clutter, and interference in radar are called *signal processing*. The matched filter, described next, is an important example of a radar signal processor.

5.2 MATCHED-FILTER RECEIVER[1,2]

Under certain conditions, usually met in practice, maximizing the output peak-signal-to-noise (power) ratio of a radar receiver maximizes the detectability of a target. A linear network that does this is called a *matched filter*. Thus a matched filter, or a close approximation to it, is the basis for the design of almost all radar receivers.

Matched Filter Frequency Response Function The matched filter that maximizes the output peak-signal-to-mean-noise ratio when the input noise spectral density is uniform (white noise) has a frequency response function[1]

$$H(f) = G_a S^*(f) \exp(-j2\pi f t_m) \tag{5.1}$$

where G_a is a constant, t_m is the time at which the output of the matched filter is a maximum (generally equal to the duration of the signal), and $S^*(f)$ is the complex conjugate of the spectrum of the (received) input signal $s(t)$, found from the Fourier transform of the received signal $s(t)$ such that

$$S(f) = \int_{-\infty}^{\infty} s(t) \exp(-j2\pi f t)\, dt$$

(The matched filter that maximizes the output signal-to-noise ratio should not be confused with the circuit-theory concept of impedance matching, which maximizes the power transfer between two networks.)

The received signal spectrum can be written as $S(f) = |S(f)| \exp[-j\phi_s(f)]$, where $|S(f)|$ is the amplitude spectrum and $\phi_s(f)$ is the phase spectrum. Similarly, the matched filter frequency-response function can be expressed in terms of an amplitude and phase as $H(f) = |H(f)| \exp[-j\phi_m(f)]$.

Letting the constant G_a equal unity, we can use these relations to write Eq. (5.1) as

$$|H(f)| \exp[-j\phi_m(f)] = |S(f)| \exp\{j[\phi_s(f) - 2\pi f t_m]\} \tag{5.2}$$

Equating the amplitudes and phases in the above gives

$$|H(f)| = |S(f)| \tag{5.3}$$

$$\phi_m(f) = -\phi_s(f) + 2\pi f t_m \tag{5.4}$$

It is seen that the magnitude of the matched-filter frequency-response function is the same as the amplitude spectrum of the input signal, and the phase of the matched-filter frequency response is the *negative* of the phase spectrum of the signal plus a phase shift proportional to frequency. The effect of the negative sign before $\phi_s(f)$ is to cancel the phase components of the received signal so that all frequency components at the output of the filter are of the same phase and add coherently to maximize the signal.

Matched Filter Impulse Response The matched filter may also be described by its *impulse response* $h(t)$, which is the inverse Fourier transform of the frequency response function $H(f)$ of Eq. (5.1), or

$$h(t) = \int_{-\infty}^{\infty} H(f) \exp(j2\pi f t)\, df = G_a \int_{-\infty}^{\infty} S^*(f) \exp[-j2\pi f(t_m - t)]\, df \tag{5.5}$$

Since $S^*(f) = S(-f)$, Eq. (5.5) becomes

$$h(t) = G_a \int_{-\infty}^{\infty} S(f) \exp[j2\pi f(t_m - t)]\, df = G_a s(t_m - t) \tag{5.6}$$

The expression on the far right comes from recognizing that the integral is an inverse Fourier transform. Equation (5.6) indicates that the impulse response of a matched filter

is the time inverse of the received signal. It is the received signal reversed in time, starting from the fixed time t_m. Figure 5.1 shows an example of the impulse response $h(t)$ of the filter matched to a signal $s(t)$.

The impulse response of a filter, if it is to be realizable, must not have any output before the input signal is applied. Therefore, we must have $(t_m - t) > 0$, or $t < t_m$. This is equivalent to the condition on the frequency response function that there be a phase $\exp(-j2\pi f t_m)$, which implies a time delay of t_m. For convenience, the impulse response is often written simply as $s(-t)$ and the frequency response function as $S^*(f)$, with the realizability conditions understood.

Receiver Bandwidth The matched filter is implemented in the IF stage of a superheterodyne receiver since the bandwidth of a superheterodyne receiver is essentially that of the IF. (The bandwidths of the RF and the mixer stages are usually large compared to that of the IF.) Thus the maximum signal-to-noise ratio occurs at the output of the IF. The second detector and the video portion of the receiver have negligible effect on the output signal-to-noise ratio if the video bandwidth is greater than one half the IF bandwidth.

Derivation of the Matched-Filter Frequency Response The frequency response function of the matched filter can be derived using the calculus of variations[1] or the Schwartz inequality.[3] In this section, the Schwartz inequality is used.

We wish to show that the frequency-response function of the linear, time-invariant filter that maximizes the output peak-signal-to-mean-noise ratio is

$$H(f) = G_a S^*(f) \exp(-j2\pi f t_m)$$

when the input noise is stationary and white (uniform spectral density). The ratio to be maximized is

$$R_f = \frac{|s_0(t)|^2_{\max}}{N} \qquad [5.7]$$

where $|s_0(t)|_{\max}$ is the maximum value of the output signal voltage and N is the mean square noise power at the receiver output. (The ratio R_f is not quite the same as the

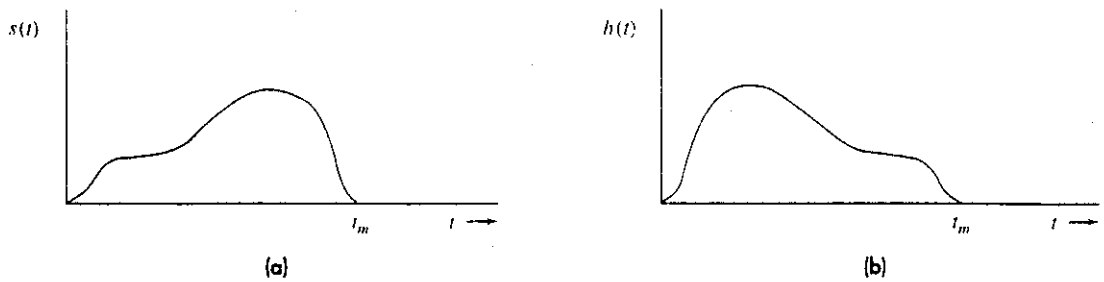

Figure 5.1 (a) Example of a received waveform $s(t)$; (b) impulse response $h(t)$ of the matched filter for the input signal $s(t)$ of (a).

signal-to-noise ratio considered previously in the radar range equation of Chap. 2. The peak power here is the peak *instantaneous* power, whereas the peak power in the discussion of the radar equation in Chap. 2 was the average value of the power over the *duration* of a pulse of sinewave. The ratio R_f is *twice* the average signal-to-noise ratio when the input signal $s(t)$ is a rectangular sinewave pulse.) The magnitude of the output voltage of a filter with frequency-response function $H(f)$ is

$$|s_0(t)| = \left| \int_{-\infty}^{\infty} S(f)H(f) \exp(j2\pi ft)\, df \right| \qquad [5.8]$$

where $S(f)$ is the Fourier transform of the input (received) signal. The mean output noise power is

$$N = \frac{N_0}{2} \int_{-\infty}^{\infty} |H(f)|^2\, df \qquad [5.9]$$

where N_0 is the input noise power per unit bandwidth. The factor 1/2 appears before the integral because the limits extend from $-\infty$ to $+\infty$, but N_0 is defined as the noise power per unit bandwidth *only* over positive values of f.

Substituting Eqs. (5.8) and (5.9) into (5.7), and letting t_m denote the time t at which the output $|s_0(t)|^2$ is a maximum, the ratio R_f becomes

$$R_f = \frac{\left| \int_{-\infty}^{\infty} S(f)H(f) \exp(j2\pi ft_m)\, df \right|^2}{\frac{N_0}{2} \int_{-\infty}^{\infty} |H(f)|^2\, df} \qquad [5.10]$$

Schwartz's inequality states that if P and Q are two complex functions, then

$$\int P^*P\, dx \int Q^*Q\, dx \geq \left| \int P^*Q\, dx \right|^2 \qquad [5.11]$$

The equality sign applies when $P = kQ$, where k is a constant. Letting

$$P^* = S(f) \exp(j2\pi ft_m) \quad \text{and} \quad Q = H(f)$$

and recalling that $\int P^*P\, dx = \int |P|^2\, dx$, application of the Schwartz inequality to the numerator of Eq. (5.10) gives

$$R_f \leq \frac{\int_{-\infty}^{\infty} |H(f)|^2\, df \int_{-\infty}^{\infty} |S(f)|^2\, df}{\frac{N_0}{2} \int_{-\infty}^{\infty} |H(f)|^2\, df} = \frac{\int_{-\infty}^{\infty} |S(f)|^2\, df}{\frac{N_0}{2}} \qquad [5.12]$$

Parseval's theorem, which relates the energy in the frequency domain and the energy in the time domain, states that

$$\int_{-\infty}^{\infty} |S(f)|^2\, df = \int_{-\infty}^{\infty} |s(t)|^2\, dt = \text{signal energy} = E \qquad [5.13]$$

Therefore,

$$R_f \leq \frac{2E}{N_0} \tag{5.14}$$

which states that the output peak-signal-to-mean-noise ratio from a matched filter depends only on the total energy of the received signal and the noise power per unit bandwidth. It does not depend explicitly on the shape of the signal, its duration, or bandwidth; hence, these characteristics of a signal can be used to achieve radar capabilities other than signal detectability.

The frequency response function which maximizes the peak-signal-to-mean-noise ratio R_f is obtained by noting that the equality sign in Eq. (5.11) applies when $P = kQ$, or

$$H(f) = G_a S^*(f) \exp(-j2\pi f t_m) \tag{5.15}$$

where the constant k has been set equal to $1/G_a$.

The matched filter has the interesting property that no matter what the shape, time duration, or bandwidth of the input-signal waveform, the maximum ratio of the output peak-signal-power-to-mean-noise power is simply twice the energy E contained in the received signal divided by the noise power per unit bandwidth N_0. The noise power per hertz of bandwidth is equal to kT_0F_n, where k in this case is the Boltzmann constant, T_0 is the standard temperature (290 K), and F_n is the receiver noise figure.

The concept of the matched filter assumes that the input signal is of the same form $s(t)$ as the transmitted signal (except for a difference in amplitude). This requires that the shape of the transmitted signal not change on reflection by the target or by propagation through the atmosphere. It also requires that the radial dimension of the target be small compared to the range resolution of the radar.

Output Signal from the Matched Filter From linear filter theory the output $y_0(t)$ of a filter is the convolution of the input $y_{in}(t) = s(t) + n(t)$ and the filter's impulse response $h(t)$, where $s(t)$ is the input signal and $n(t)$ is the input noise. It may be written as

$$y_0(t) = \int_{-\infty}^{\infty} y_{in}(\lambda) h(t - \lambda)\, d\lambda \tag{5.16}$$

It was found previously that the impulse response of a matched filter is $h(t) = s(-t)$. (Here, for convenience, $G_a = 1$ and $t_m = 0$.) Then $h(t - \lambda) = s(-t + \lambda)$ and Eq. (5.16) becomes

$$y_0(t) = \int_{-\infty}^{\infty} y_{in}(\lambda) s(\lambda - t)\, d\lambda \tag{5.17}$$

It is seen that the output of a matched filter as given by Eq. (5.17) is the cross correlation between the received signal $y_{in}(t)$ and the signal $s(t)$ that was transmitted, since the cross-correlation function between two signals $y_1(t)$ and $y_2(t)$ is defined as

$$\Phi(t) = \int_{-\infty}^{\infty} y_1(\lambda) y_2(\lambda - t)\, d\lambda \tag{5.18}$$

When the signal-to-noise ratio is large, $y_{in}(t) \approx s(t)$, and the output signal from the matched filter is approximated by the autocorrelation function of the transmitted signal $s(t)$.

Figure 5.2 illustrates, in a highly simplified manner, the nature of the matched filter for a perfectly rectangular pulse of sinewave when the signal-to-noise ratio is large. In Fig. 5.2 (a) is the input signal; (b) is the frequency response function of the matched filter; (c) is the output of the matched filter (in the IF); and (d) is the envelope of the output of the matched filter, which is what appears in the video portion of the receiver.

Correlation Receiver Since the output of the matched filter is the cross-correlation function of the received signal and the transmitted signal, it is possible to implement the matched filter as a correlation process based on Eq. (5.17). In a correlation receiver the input signal $y_{in}(t)$ is multiplied by a delayed replica of the transmitted signal $s(t - T_R)$, where T_R is an estimate of the time delay of the target echo signal. The product is passed through a low-pass filter to perform the integration. If the output of the integrator (filter) exceeds a predetermined threshold at a time T_R, a target is said to be at a range $R = cT_R/2$, where c is the velocity of propagation. The cross-correlation receiver tests for the presence of a target at only a single time delay T_R. Targets at other time delays, or ranges, are found by either varying the value of T_R on successive transmissions or employing multiple channels and simultaneously performing the correlation process at all possible values of T_R. The need to search through all possible values of T_R can seriously complicate the correlation receiver.

Since the cross-correlation receiver and the matched-filter receiver are equivalent mathematically, the choice as to which to use in a particular radar application is determined by which is more practical to implement. The matched-filter receiver has almost always been preferred over the correlation receiver.

Approximation to the Matched Filter for a Rectangular-like Pulse The early radar pioneers in the 1930s were not aware of the concept of the matched filter; yet they learned from experience how to maximize the output signal-to-noise ratio for the simple pulse waveforms that were used at that time. They found that if the receiver passband was too wide compared with the spectral bandwidth of the radar signal, extra noise was introduced (since noise power is proportional to bandwidth); and the signal-to-noise ratio was reduced. On the other hand, if the receiver bandwidth was too narrow, the noise was

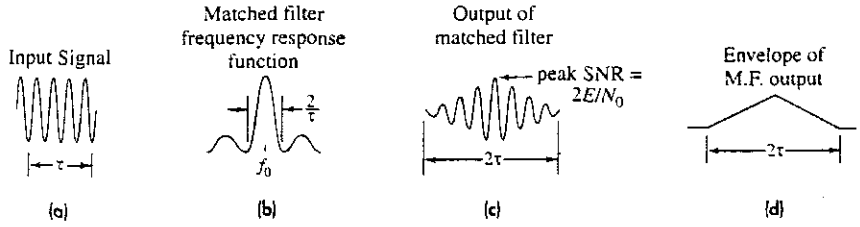

Figure 5.2 (a) Sketch of a perfectly rectangular pulse of sinewave of width τ and frequency f_0; (b) frequency-response function of the matched filter, where $H(f) = S^*(f) = S(f)$; (c) output of the matched filter; (d) envelope of matched-filter output.

reduced but so was the signal energy. Consequently, too narrow a bandwidth relative to the signal spectral width reduced the signal-to-noise ratio, and too wide a bandwidth also reduced the signal-to-noise ratio. Thus there was an optimum value of bandwidth relative to signal spectral width that maximized the signal-to-noise ratio. With rectangular-like pulses and conventional filter design, experience showed that the maximum signal-to-noise ratio occurred when the receiver bandwidth B was approximately equal to the reciprocal of the pulse width τ, or when $B\tau \approx 1$.

In practice the matched filter cannot be perfectly implemented. There will usually be some loss in signal-to-noise ratio compared to that of a theoretically perfect matched filter. The measure of efficiency is taken as the peak-signal-to-mean-noise ratio from the nonmatched filter divided by the peak-signal-to-noise ratio ($2E/N_0$) obtained from a matched filter. Table 5.1 lists values of $B\tau$ that maximize the signal-to-noise ratio (SNR) for various combinations of hypothetical filters and pulse shapes.[4,5] Note that the rectangular pulse assumed in Table 5.1 is not a realistic waveform since it has zero rise time, which implies infinite bandwidth. Radar pulses are bandwidth limited, and the rise time is approximately $1/B$. Also, several of the filters in Table 5.1 are not likely to be used in practice. Nevertheless, Table 5.1 is offered as an example of the performance of nonmatched filters. The usual "rule of thumb" when no other information is available, is to assume that a practical approximation to a matched filter has $B\tau \approx 1$ and a loss in SNR of about 0.5 dB.

Matched Filter for Nonwhite Noise In the derivation of the matched-filter characteristic [Eq. (5.15)], it was assumed that the spectrum of the input noise accompanying the signal was white; that is, it was independent of frequency. When this assumption does not

Table 5.1 Efficiency of nonmatched filters compared with matched filters

Input signal	Filter	Optimum $B\tau$	Loss in SNR, dB
Rectangular pulse	Third-order Bessel filter	0.78	0.47
Rectangular pulse	Quadruply tuned (Butterworth)	1.06	0.48
Rectangular pulse	Double tuned (Butterworth)	0.81	0.46
Rectangular pulse	5 cascaded single-tuned stages	0.67	0.51
Rectangular pulse	2 cascaded single-tuned stages	0.61	0.56
Rectangular pulse	Single tuned	0.40	0.88
Rectangular pulse	Rectangular	1.37	0.85
Rectangular pulse	Gaussian	0.74	0.51
Gaussian pulse	Rectangular	0.74	0.51
Gaussian pulse	Gaussian	0.44	0 (matched)

hold and the noise is represented by a nonwhite power spectrum $[N_i(f)]^2$, the frequency-response function that maximizes the peak-signal-to-mean-noise power has been shown to be[6,7]

$$H(f) = \frac{G_a S^*(f) \exp(-j2\pi f t_m)}{[N_i(f)]^2} \quad [5.19]$$

This is the frequency response function of the *nonwhite-noise matched (NWN) filter.* When the noise is white, $[N_i(f)]^2$ = constant, and Eq. (5.19) reduces to that of Eq. (5.15) derived assuming white noise.

Equation (5.19) for nonwhite noise can be rewritten as

$$H(f) = \frac{1}{N_i(f)} \times G_a \left(\frac{S(f)}{N_i(f)}\right)^* \exp(-2\pi f t_m) \quad [5.20]$$

From this the nonwhite-noise matched filter can be interpreted as the cascade of two filters. The first filter, with frequency-response function $1/N_i(f)$, makes the noise spectrum uniform, or white. It is sometimes called the *whitening filter.* The second is the matched filter given by Eq. (5.15) when the input noise is white and the signal spectrum is $S(f)/N_i(f)$.

It is seldom that noise is nonuniform over the bandwidth of the radar receiver. The nonwhite-noise matched filter is interesting, but it has had almost no application in radar.

Summary of the Matched Filter The characteristics of the matched filter for an input signal $s(t)$ are summarized below in short notation, omitting realizability factors and constants. The symbols have been defined previously in this section.

1. Frequency response function: $S^*(f)$
2. Maximum output signal-to-noise ratio: $2E/N_0$
3. Magnitude of the frequency response: $|H(f)| = |S(f)|$
4. Phase of the frequency response: $\phi_m(f) = -\phi_s(f)$
5. Impulse response: $s(-t)$
6. Output signal waveform for large signal-to-noise ratio: autocorrelation function of $s(t)$
7. Relation between bandwidth and pulse width for a rectangular-like pulse and conventional filter: $B\tau \approx 1$
8. Frequency response function for nonwhite noise: $S^*(f)/[N_i(f)]^2$

The matched filter makes radar-signal detection quite different from detection in conventional communication systems. The detectability of signals with a matched-filter receiver is a function only of the received signal energy E and the input noise spectral density N_0. Detection capability and the range of a radar do not depend on the shape of the signal or the receiver bandwidth. The shape of the transmitted signal and its bandwidth therefore can be selected to optimize the extraction of information without, in theory, affecting detection. Also different from communications is that the signal out of the matched filter is not the same shape as the input signal. It should be no surprise that the output

signal's shape is different from the input since the criterion for the matched filter states only that detectability is to be maximized, not that the shape of the signal is to be preserved.

5.3 DETECTION CRITERIA

Detection of signals is equivalent to deciding whether the receiver output is due to noise alone or to signal plus noise. This is the type of decision made (probably subconsciously) by a human operator from the information presented on a radar display. When the detection process is carried out automatically by electronic means without the aid of an operator, the detection criterion must be carefully specified and built into the decision-making device.

In Chap. 2, the radar detection process was described in terms of threshold detection. If the envelope of the receiver output exceeds a pre-established threshold, a signal is said to be present. The threshold level divides the output into a region of no detection and a region of detection. The radar engineer selects the threshold that divides these two regions so as to achieve a specified probability of false alarm, which in turn is related to the average time between false alarms. The engineer then determines the other parameters of the radar needed to obtain the signal-to-noise ratio for the desired probability of detection.

Neyman-Pearson Observer The usual procedure for establishing the decision threshold at the output of the radar receiver is based on the classical statistical theory of the *Neyman-Pearson observer.* This is described in terms of the two types of errors that might be made in the detection decision process.

One type of error is to mistake noise for signal when only noise is present. It occurs whenever the noise out of the receiver is large enough to exceed the decision-threshold level. In statistics this is called a Type I error. In radar it is a *false alarm.* A Type II error occurs when a signal is present, but is erroneously considered to be noise. The radar engineer would call such an error a *missed detection.* It might be desired to minimize both errors, but they both cannot be minimized independently. In the Neyman-Pearson observer, the probability of a Type I error is fixed, and the probability of a Type II error is minimized.

As discussed in Sec. 2.5, the threshold level is set by the radar engineer so that a specified false-alarm probability is not exceeded. This is equivalent to fixing the probability of a Type I error and minimizing the Type II error (or maximizing the probability of detection), which is the Neyman-Pearson test used in statistics for determining the validity of a specified statistical hypothesis.[8] In statistical terms it is claimed to be a uniformly most powerful test and an optimum one, no matter what the a priori probabilities of signal and noise. The Neyman-Pearson criterion is employed in most radars for making the detection decision, whether knowingly or not.

Likelihood-Ratio Receiver The *likelihood ratio* is a statistical concept that has been used in radar detection theory and information extraction theory to model optimum decision

procedures. It is defined as the ratio of two probability density functions, with and without signal present, or

$$L_r(v) = \frac{p_{sn}}{p_n} \qquad [5.21]$$

where p_{sn} is the probability-density function for signal plus noise and p_n is the probability-density function for noise alone. In Chap. 2 these two probability-density functions were given by Eqs. (2.27) and (2.21), respectively. The likelihood ratio is a measure of how likely it is that the envelope v of the receiver output is due to signal plus noise as compared with noise alone. If the likelihood ratio is sufficiently large, it would be reasonable to conclude that a signal is present.

The Neyman-Pearson observer is equivalent to examining the likelihood ratio and determining if $L_r(v) \geq K$, where K is a real, nonnegative number that depends on the probability of false alarm selected.

One does not find likelihood-ratio receivers in equipment catalogs. It is a statistical concept that models the basic nature of a receiver for maximizing the detectability of radar signals or a receiver that provides the most accurate measurement of radar parameter (such as range). The likelihood ratio is an analytical tool used to indicate optimum receiver and detector design. In most cases of practical interest a radar that employs a matched filter is equivalent to a likelihood-ratio receiver.[8]

Inverse Probability Receiver This is another statistical concept and is based on the relationship known as Bayes' rule for the probability of causes.[9,10] As with the likelihood ratio, inverse probability has been used as an analytical basis to model "optimum" receivers for detection and information extraction. *Inverse probability* is different from the more familiar *direct probability* that describes the chance of an event happening on a given hypothesis. If an event actually happens (such as a voltage appearing at the output of the radar receiver), the problem of forming the best estimate of its cause is a problem in inverse probability.

The operation of the inverse probability receiver will not be described here. (More detail can be found in earlier editions of this text and in the references thereto.) The inverse probability receiver, likelihood receiver, and matched-filter receiver, however, are all related to one another under certain conditions which are often met in most radar applications. The design information obtained from one can usually be obtained from the others as well. The inverse probability receiver differs from the likelihood-ratio receiver (and the matched filter) in that it requires knowledge of a priori probabilities. (An a priori probability is one that is known before the event occurs; e. g., the a priori probability that a flip of a coin results in a heads is 0.5.) It is not usually possible in radar to define quantitatively the a priori probability (for example, the probability of observing an aircraft echo signal at the output of the radar at a range of 110 nmi, azimuth of 75°, at 0630 tomorrow morning). Therefore, the inverse probability receiver has only been of academic interest. Sometimes it has been suggested that the problem of selecting the a priori probability can be satisfied by assuming it to be constant. If the a priori probability is constant, the inverse probability receiver reduces to the likelihood-ratio receiver. Thus one might as well start with the likelihood-ratio receiver in the first place.

The inverse probability receiver and the likelihood-ratio receiver are statistical models that have been used in the past to derive important relations in the theory of signal detection and information extraction. Although one does not build either type of receiver, they both have been useful since theoretical results derived from them indicate the best that can be achieved under the given assumptions.

Sequential Observer, Sequential Detection In a conventional radar based on the Neyman-Pearson observer, a fixed number of pulses, n, are obtained before a detection decision is made. When the signal-to-noise ratio is large, it might not be necessary to collect all n pulses before being able to make the decision that a target echo signal is present. Also, it might be possible to determine after only a few pulses that the receiver output is so low it is unlikely that, even with the remaining pulses, the integrated receiver output would cross the threshold. It should be possible, by taking advantage of the possibility of a quick decision, to make a detection decision with fewer pulses, on average, than would be needed for the Neyman-Pearson observer. This procedure is called the *sequential observer.*[11,12] It is an interesting detection method that, in some cases, can result in almost an order of magnitude decrease in power or revisit time when it can be applied. Unfortunately, its application in radar is limited.

After a single sample of the receiver output, the sequential observer makes one of three choices: (1) the sample is due to the presence of signal and noise; (2) it is due to noise alone; or (3) it cannot be determined whether it is due to noise alone or signal-plus-noise. If it can be decided that either No. 1 or No. 2 applies, the test is completed and the radar moves to the next resolution cell to repeat the operation. If the choice is No. 3, a decision cannot be made, and another observation is obtained and the choices examined again on the basis of the two observations. This procedure is repeated until a decision can be made as to whether noise alone or signal-plus-noise is present.

The sequential observer fixes the probability of errors beforehand and allows the number of observations (integration time) to vary. This procedure theoretically allows a significant reduction in the average number of pulses (samples) needed for making a decision. The sequential observer makes a relatively prompt decision when only noise is present. In one reported example,[13] the sequential observer can, on average, come to a decision with less than one-tenth the number of observations required for the Neyman-Pearson observer when only noise is present. When a threshold signal is present, the sequential observer requires, on average, about one-half the number of observations of the equivalent fixed-sample Neyman-Pearson observer.

A flexible phased array radar, or equivalent agile antenna, is required for the sequential observer in order to take advantage of the variable number of pulses to be integrated. Unfortunately, there is a severe limitation to its use. If there is only one range cell in each angular resolution cell, such as a "guard band," the sequential observer works as indicated above. At each angular position of a surveillance radar antenna, however, there can be a large number of range cells. The sequential observer must come to a decision in every one of these cells before moving on to the next angular position. Any savings in time to make a decision is lost when the number of cells is large, since the observation time at any angular position is determined by the time it takes for the slowest cell to make a decision.[12]

Although the sequential observer can, in principle, result in a saving in transmitter power or in revisit time, it is limited to applications such as a guard ring, the detection of border penetration,[14] or a radar with an omnidirectional transmit antenna and many contiguous fixed narrow-beam receiving antennas that look everywhere all the time.

The term *sequential detection* is sometimes used synonymously with the term sequential observer; but it is also used to describe a two-stage detection process that can be employed with a phased-array radar.[15,16] The radar transmits a pulse or a series of pulses in a particular direction, but with a lower threshold (and higher false-alarm probability) than normal. If no threshold crossings are obtained, the antenna beam moves to the next position. If a threshold crossing occurs, a second pulse or series of pulses is transmitted with higher energy, and with a higher threshold. A detection is declared if the threshold is crossed on both transmissions. It has been claimed that a second threshold is employed in about 4 percent of the beam positions and that there is a power saving of from 3 to 4 dB as compared with uniform scanning.

5.4 DETECTORS

The detector is that portion of the radar receiver that extracts the modulation from the carrier in order to decide whether or not a signal is present. It extends from the IF amplifier to the output of the video amplifier; thus, it is much more than a rectifying element. The conventional pulse radar as described in Chaps. 1 and 2 employs an *envelope detector* which extracts the amplitude modulation and rejects the carrier. By eliminating the carrier and passing only the envelope, the envelope detector destroys the phase information. There are other "detectors" in radar that are different from the above description. The MTI radar uses a *phase detector* to extract the phase of the radar echo relative to the phase of a coherent reference, as described in Chap. 3. In Chap. 4, the *phase-sensitive detector* employed in tracking radars for extracting angle information was mentioned.

Optimum Envelope Detector Law The envelope detector consists of the IF amplifier with bandpass filter characteristic, a rectifying element (such as a diode), and a video amplifier with a low-pass filter characteristic. The detector is called a *linear detector* if the relation between the input and output signal is linear for positive voltage signals, and zero for negative voltage. (The detector, of course, is a nonlinear device even though it bears the name *linear*.) When the output is the square of the input for positive voltage, the detector is called *square law*. The detector law is usually considered the combined law of the rectifying element and the video integrator that follows it, if an integrator is used. For example, if the rectifying element has a linear characteristic and the video integrator has a square-law characteristic, the combination would be considered a square-law detector. There can be, of course, many other detector laws beside the linear and the square law.

The *optimum detector* law can be found based on the use of the likelihood-ratio receiver. It can be expressed as[17–19]

$$y = \ln I_0(av) \qquad [5.22]$$

where y = output voltage of the detector

a = amplitude of the sinewave signal divided by the rms noise voltage

v = amplitude of the IF voltage envelope divided by the rms noise voltage

$I_0(x)$ = modified Bessel function of zero order

This equation specifies the form of the detector law that maximizes the likelihood ratio for a fixed probability of false alarm. A suitable approximation is[20]

$$y = ln\ I_0(av) \approx \sqrt{(av)^2 + 4} - 2 \qquad [5.23]$$

For large signal-to-noise ratios ($a \gg 1$), this is approximately

$$y \approx av$$

which is a linear law. For small signal-to-noise ratios, the approximation of Eq. (5.23) becomes

$$y \approx (av)^2/4$$

which has the characteristic of a square-law detector. Hence, for large signal-to-noise ratio, the optimum $ln\ I_0$ detector may be approximated by a linear detector, and for small signal-to-noise ratios it is approximated by a square-law detector.

The linear detector usually is preferred in practice since it results in a higher dynamic range than the square law and is less likely to introduce distortion. On the other hand, the square-law detector usually is easier to analyze than the linear, so many analyses assume a square-law characteristic. Fortunately, the theoretical difference in detection performance between the square-law and linear detectors when performing noncoherent integration often is relatively insignificant.[21,22] Marcum[23] also showed that for a single pulse (no integration) the probability of detecting a given signal is independent of the detector law.

Logarithmic Detector If the output of the receiver is proportional to the logarithm of the input envelope, it is called a *logarithmic detector,* or *logarithmic receiver.* It finds application where large variations of input signals are expected. Its purpose is to prevent receiver saturation and/or to reduce the effects of unwanted clutter echoes in certain types of non-MTI receivers (as in the discussion of the log-FTC receiver in Sec. 7.8). A logarithmic characteristic is not used with MTI receivers since a nonlinear characteristic can limit the MTI improvement factor that can be achieved.

There is a loss in detectability with a logarithmic receiver. For 10 pulses integrated the loss in signal-to-noise ratio is about 0.5 dB, and for 100 pulses integrated, the loss is about 1.0 dB.[24] As the number of pulses increase, the loss approaches a maximum value of 1.1 dB.[25]

***I*,Q Detector** The *I* and *Q*, or *in-phase* and *quadrature,* channels were mentioned in Sec. 3.5 in the discussion of the MTI radar. There it was noted that a single phase-detector fed by a coherent reference could produce a significant loss in signal depending on the relative timing (or "phase") of the pulse train and the doppler-shifted echo signal. In an MTI radar, the term *blind phase* (not a truly descriptive term) was used to describe this loss.

The loss due to blind phases was avoided if a second parallel detector channel, called the *quadrature,* or Q channel, were used with a reference signal 90° out of phase from the reference signal of the first channel, called the *in-phase,* or I channel. Most signal processing analyses now use I and Q channels as the receiver model especially when the doppler frequency is extracted.

The I,Q detector is more general than just for avoiding loss due to blind phases in an MTI radar. Figure 5.3 illustrates the I,Q detector. It is sometimes called a *synchronous detector.*[26] If the input is a narrowband signal having a carrier frequency f_0 (which could be the IF frequency) with a time-varying amplitude $a(t)$ and time-varying phase $\phi(t)$, then

$$\text{input signal: } s(t) = a(t) \sin [2\pi f_0 t + \phi(t)]$$

The output of the in-phase channel is $I(t) = a(t) \cos [\phi(t)]$ and the output of the quadrature channel is $Q(t) = a(t)\sin [\phi(t)]$. The input signal then can be represented as $s(t) = I(t) \sin 2\pi f_0 t + Q(t) \cos 2\pi f_0 t$. Thus the I and Q channels together provide the amplitude and phase modulations of the input signal.

If the outputs of the I and Q channels of Fig. 5.3 are squared and combined (summed), then the square root of the sum of the squares is the envelope $a(t)$ of the input signal. This describes an envelope detector. The phase $\phi(t)$ of the input signal is arctan (Q/I).

The I,Q representation is commonly used in digital signal processing.[27] The digitized signals are represented by complex numbers derived from the I and Q components. In each channel, the signal is digitized by an analog-to-digital (A/D) converter to produce a series of complex digital samples from the signal $I + jQ$. According to the sampling theorem, if the input signal has a bandwidth B there must be at least $2B$ samples per second (the Nyquist rate) to faithfully reproduce the signal. Because there are two channels in the I,Q detector, the A/D converter in each of the I and Q channels needs only to sample at the rate of B samples per second, thus reducing the complexity required of the A/D converters.

With a rate of B samples per second, there is a loss of about 0.6 dB compared to continuous sampling, since the sampling is not guaranteed to occur at the peak of the

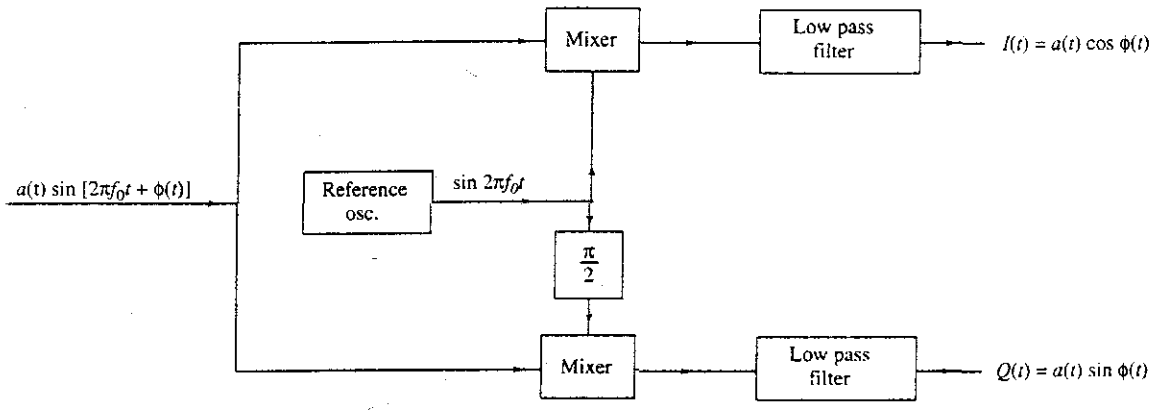

Figure 5.3 *I,Q* detector

output.[27] Much of this loss can be recovered by sampling at a rate of $2B$ samples per second. In some applications, further loss might occur due to the two channels not being precisely 90° out of phase, not being of equal gain, or if they are not perfectly linear.[28]

When I,Q channels are used for MTI processing, a doppler filter such as a delay-line canceler is included in each channel to separate moving targets from stationary clutter, as was discussed in Sec. 3.5.

Coherent Detector The so-called "coherent detector" sometimes has been described in the past literature as a single-channel detector similar to the in-phase channel of the I,Q detector, but with the reference signal at the same exact frequency and same exact phase as that of the input signal. Compared to the normal envelope detector of Chap. 2, the signal-to-noise ratio from a coherent detector might be from 1 to 3 dB greater. Unfortunately, the phase of the received radar signal is seldom known, so the single-channel coherent detector as described generally is not applicable to radar. The I,Q detector of Fig. 5.3 can also be considered as a coherent detector, but without the limitation of the coherent detector described above.

5.5 AUTOMATIC DETECTION

An operator viewing a PPI display or an A-scope "integrates" in his/her eye-brain combination the echo pulses available from the target. Although an operator in many cases can be as effective as an automatic integrator, performance is limited by operator fatigue, boredom, overload, and the integrating characteristics of the phosphor of the CRT display. With automatic detection by electronic means, the operator is not depended on to make the detection decision. *Automatic detection* is the name applied to the part of the radar that performs the operations required for the detection decision without operator intervention. The detection decision made by an automatic detector might be presented to an operator for action or to a computer for further processing.

In many respects, automatic detection requires much better receiver design than when an operator makes the detection decision. Operators can recognize and ignore clutter echoes and interference that would limit the recognition abilities of some automatic devices. An operator might have better discrimination capabilities than automatic methods for sorting clutter and interference; but the automatic, computer-based decision devices can operate with far greater number of targets than an operator can handle.

Automatic detection of radar signals involves the following:

- *Quantization* of the radar coverage into range, and maybe angle, resolution cells.
- *Sampling* of the output of the range-resolution cells with at least one sample per cell, more than one sample when practical.
- *Analog-to-digital conversion* of the analog samples.
- *Signal processing* in the receiver to remove as much noise, clutter echoes, and interference as practicable before the detection decision is attempted.
- *Integration* of the available samples at each resolution cell.

- *Constant false-alarm rate* (CFAR) circuitry to maintain the false-alarm rate when the receiver cannot remove all the clutter and interference.
- *Clutter map* to provide the location of clutter so as to ignore known clutter echoes.
- *Threshold detection* to select target echoes for further processing by an automatic tracker or other data processor.
- *Measurement of range and angle* after the detection decision is made.

The automatic detection and tracking (ADT) system, which includes the above, was discussed in Sec. 4.9. We next consider the automatic integration of signals and the application of CFAR in the automatic detection process.

5.6 INTEGRATORS

A major part of an automatic detector that operates with more than one pulse is the *integrator* which integrates, or adds, the energy from the received pulses available from a target. The subject of predetection and postdetection integration was introduced in Sec. 2.6. In this section, several integration methods will be briefly reviewed. Integration of pulses in early radars often was performed by an operator viewing a cathode-ray tube display since automatic integration of pulses was seldom practical with the then existing analog technology. Modern radars almost always implement the integration of signals digitally. (Note that in the technical literature, some integration devices are called *detectors* even though they perform *integration.*)

Moving-Window Integrator[29] The straightforward method for integrating the n pulses available from a target is to simply add them. It was not until advances in digital processing technology became available, however, that it became practical to do so. Continuous integration of the last n pulses at the output from a receiver from each range-resolution cell can be accomplished with a *moving-window integrator,* also called *moving-window detector.* The new output from the receiver is added to the previous sum, and the output received n pulses earlier is subtracted to achieve a running sum of n pulses. In a digital processor it is possible to apply weights to the outputs, based on the two-way gain of the antenna pattern, so as to provide increased signal-to-noise ratio. If uniform weighting is used instead (since it is easier to do), there is a loss in signal-to-noise ratio of about 0.5 dB compared to optimum weighting.[30]

The angular location of the target may be estimated by taking the midpoint between the first and last crossings of the detection threshold or by noting the location of the maximum value of the running sum. After correcting for the bias, the accuracy of the angular location measurement is only about 20 percent worse than theoretical.[30]

According to Trunk,[31] a disadvantage of the moving-window detector is that it is susceptible to large interference signals, a problem that can be minimized by using limiting. It also requires large storage since the last n pulses from each range cell must be put in memory. With increasing improvements in digital technology, this limitation has become less of a concern.

Binary Integration This was the first automatic method developed to integrate pulses and make the detection decision without the aid of an operator.[32] It is still an important technique. Its chief advantage is that it can be implemented without the complexity of the moving-window integrator. It is, however, less efficient than ideal postdetection integration.

As a radar antenna scans by a target it will receive n echo pulses. If m of these expected n pulses exceed a predetermined value (threshold), a target is declared to be present. The use of a detection criterion that requires m out of n echo pulses to be present is a form of integration. It is called the *binary integrator,* but it is also well-known as the *binary detector, double-threshold detector,* and *m-out-of-n detector.*

A block diagram of the binary integrator is shown in Fig. 5.4. The radar video is passed through a threshold detector, whose level is lower than the normal threshold discussed previously in Chap. 2. It is the first of two thresholds in this system, hence the name *double-threshold detector.* The output of the first threshold is sampled by the quantizer at least once per range-resolution cell. A pulse with a standard amplitude is generated if the video waveform exceeds the first threshold, and nothing is generated if it does not exceed the threshold. These outputs are designated 1 and 0, respectively. Thus the output of the quantizer is a series of 1s and 0s The 1s and 0s from the last n *pulses* at each range cell are stored and counted in the binary counter. If there are at least m 1s within the last n sweeps, a target is said to be detected at that range. The number m is the second threshold to be passed in the double-threshold detector. The two thresholds must be selected jointly for best performance.

The optimum value of m/n for a nonfluctuating echo signal is shown in Fig. 5.5.[33] This curve is only approximate since there is a slight dependence on the false alarm probability, but it is said to be independent of the signal-to-noise ratio. A fluctuating Swerling Case 1 target has the same optimum value of m/n as a nonfluctuating target, but a fluctuating Swerling Case 2 has different optimum values.[34–36] The optimum value of m is not a sensitive selection. It can be quite different from the optimum without significant penalty.

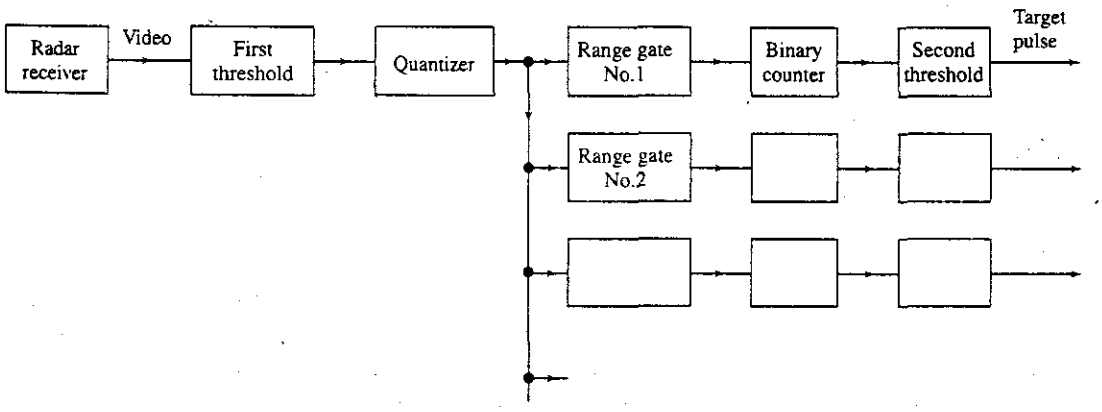

Figure 5.4 Block diagram of a binary integrator

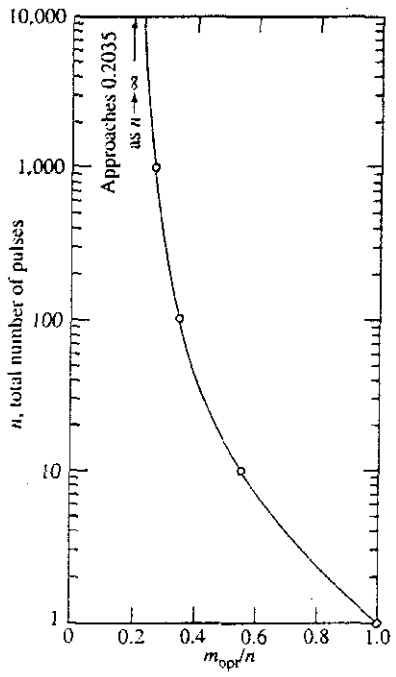

Figure 5.5 Optimum number of pulses m_{opt} (out of a maximum of n) for a binary moving window detector, assuming a constant (nonfluctuating) target echo. (After Swerling,[33] courtesy Rand Corp.)

The loss in signal-to-noise ratio due to quantizing signals into two levels (1 or 0) in the binary integrator can vary from just under 1 dB to 2.5 dB.[37] For the particular case given in ref. 37 where the probability of detection is 0.9 and the probability of false alarm is 10^{-6}, the loss can reach 1.4 dB for a nonfluctuating target and 2.2 dB for a Swerling Case 1 fluctuating target, when n is about 8 hits per target. For larger values of n (n greater than about 100) the binary integrator asymptotically approaches a loss of 0.94 dB in all cases, as compared with optimum noncoherent integration. When the amplitude is quantized into more than two levels, the loss is less. V. Gregers-Hansen[37] states that quantization into four levels (two bits) reduces the loss to about one-third that of the two-level quantization.

The binary integrator is relatively simple as an automatic detector and is less sensitive to the effects of a single large interference pulse that might exist along with the target echo pulses. In the conventional integrator, the full energy of the interference pulse is included in the sum. This could result in a false-target indication even though only one interference pulse were present. In a binary integrator, however, a large interference pulse contributes no more to the sum than would any other pulse that crosses the first threshold. No matter what the energy in the pulse, the output of the first threshold is a "1". The same advantage occurs when the background is not receiver noise, but is nongaussian (or non-Rayleigh) clutter as in high-resolution sea clutter and many forms of land clutter. If the clutter statistics have high tails (which means a higher probability of having large values than the gaussian probability density function), these high values can result in false-target reports when a detection is based on gaussian statistics. The binary integrator treats

these high values of clutter as any other first-threshold crossing, and it is not as likely to report a target when none is present as might a conventional detection criterion based on the total energy received in n pulses. The binary integrator is therefore *robust*, in that it can be used when the background noise or clutter is nongaussian.

An estimate of the target's angular position (beam splitting) also may be made by locating the center of the group of n pulses. For large n, the angular estimation error made with the binary integrator is about 25 percent greater than the theoretical lower bound.[31]

Batch Integrator[31] A *batch integrator* is used when there is a large number of pulses available. If there are kn pulses received from the target, k pulses are summed (batched) and compared to a threshold to make a binary decision (0 or 1) as to whether the threshold has been crossed. The process is repeated for each of the remaining $n - 1$ sets of k pulses. The n 0s and 1s are summed and compared to a second threshold. The batch integrator, just as the binary integrator, is simpler to implement, is less affected by interference spikes, and is robust to the noise or clutter statistics. It is said to require less storage, have better detection performance, and provide a more accurate angle estimation than the binary integrator.

Feedback Integrators[31] The advantage of the single delay-line feedback integrator is its simpler processing. As indicated in Fig. 5.6a, in this integrator the output of the delay line is recirculated so that the signals from each new sweep are added to the sum of all the previous sweeps. To prevent unwanted oscillations ("ringing") due to the positive feedback, the sum must be attenuated by an amount $k < 1$ after each pass through the delay line. The factor k is the gain of the loop formed by the delay line and the feedback path. It imparts an exponential weighting to the received pulses. The effective number of pulses integrated is equal to $(1 - k)^{-1}$.

The single delay-line feedback integrator has a loss of about 1.0 dB in signal-to-noise ratio compared to the ideal postdetection integrator that weights the received pulses in

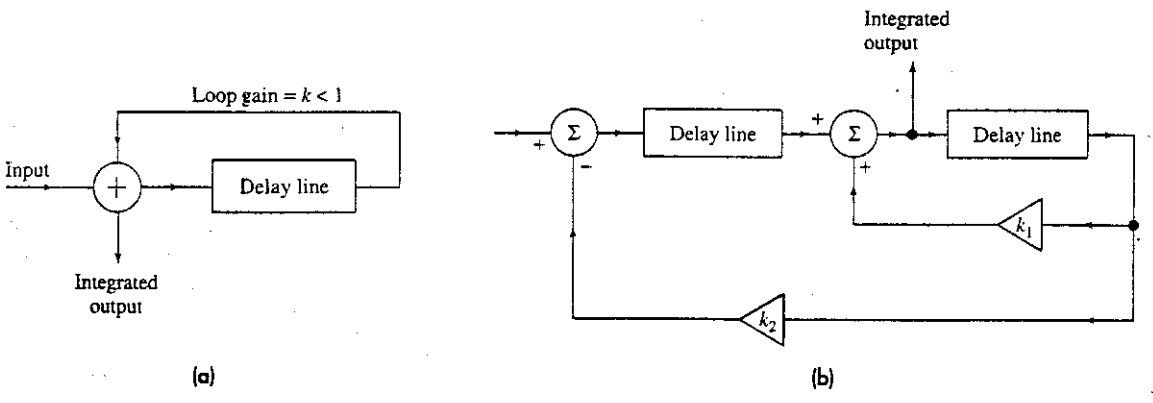

Figure 5.6 Recirculating delay-line integrator, or feedback integrator, k = loop gain < 1. (a) Single delay loop; (b) two-pole filter.

proportion to the two-way antenna gain. Estimating the angular location of the target based on threshold crossings produces a 20 percent error compared to the optimum. There is a bias, however, that must be estimated, and it can be large. The single delay-line integrator of Fig. 5.6a might have the advantage of simplicity, but its problems cause it to have only limited utility.

The two-pole filter of Fig. 5.6b requires more storage than the single delay-line feedback integrator, but its detection performance is only 0.15 dB less than the optimum. Its angular measurement accuracy has a standard deviation 15 percent greater than optimum, and the estimator based on the maximum value has a constant bias.[38] According to Trunk[31] the problems with this integrator are that it has rather high detector sidelobes (15 to 20 dB) and it is extremely sensitive to interference.

Other Types of Integrators/Detectors Some forms of integrators are also called detectors because the detection decision uses the n pulses received from a target. The *mean detector*, for example, is one that sets a threshold based on the mean, or average, of its n received pulses. It is therefore equivalent to the conventional method of setting the threshold on the basis of the addition (integration) of n pulses. The *median detector* sets a threshold based on the median value of its n expected pulses. It is more robust than a mean detector in that it is not as adversely affected by a large interference pulse that might be included among the n pulses. Also, it is not as degraded as the mean detector when the clutter or noise background is described by nongaussian statistics. There are also *censored mean detectors* in which one or more of the largest amplitude pulses of the n pulses received are eliminated from the detection decision on the assumption that they are likely to be from interference rather than from a target. The adaptive detector, nonparametric detector, and distribution-free detector are usually considered as forms of CFAR, which is discussed in the next section. Most of these detectors have been more of academic interest than candidates for application in operational radar systems.

5.7 CONSTANT-FALSE-ALARM RATE (CFAR) RECEIVER

As said before in this text, a target is detected when the output of the radar receiver crosses a predetermined fixed threshold level set to achieve a specified probability of false alarm. When noise at the receiver is due to internally generated noise of fixed level described by a gaussian probability density function, the procedure for setting the threshold is well established (Sec. 2.8). In many situations, however, clutter echoes and/or hostile noise jamming can be much larger than receiver internal noise. When this happens, the receiver threshold can be exceeded and many false alarms can occur, which cause havoc with radar detection and tracking.

A well-trained and alert operator viewing a PPI or other radar display is seldom misled into mistaking clutter or jamming for real targets, but an operator can lose effectiveness when there are many target echoes to be processed. An automatic detection and tracking (ADT) system can handle many targets, and will attempt to determine if clutter or jamming signals that cross the receiver threshold form realistic tracks. Eventually, a false alarm will not form a realistic track and will be discarded by the tracking computer. An

automatic system, however, might be of limited capability and require too much time or computer capacity to recognize and discard false alarms. Although digital computers can have a high level of capability, the task of recognizing false echoes might cause them to be overloaded when there are a large number of real targets, a large number of clutter echoes, interference, and/or high external noise levels. Therefore, if ADT is to work properly, some method is necessary to keep clutter and external noise from reaching the automatic-tracking computer. One method has been CFAR, or *constant false alarm rate* receiver. CFAR automatically raises the threshold level to keep clutter echoes and external noise from overloading the automatic tracker with extraneous information. The need for CFAR was recognized when the early automatic detection and tracking systems were installed as add-ons to existing radars with no MTI or relatively poor MTI that did not have good clutter rejection. CFAR is achieved, of course, at the expense of a lower probability of detection of desired targets. In addition, CFAR can also produce false echoes when there is nonuniform clutter, suppress nearby targets, and degrade the range resolution.

Cell Averaging CFAR, or CA CFAR The major form of CFAR has been the cell-averaging CFAR, due to Finn and Johnson,[39] and its variants. It is illustrated in Fig. 5.7. It uses an adaptive threshold whose level is determined by the clutter and/or noise in the vicinity of the radar echo. Two tapped delay-lines sample echo signals from the environment in a number of *reference cells* located on both sides of the test cell (the range cell of interest). The spacing between reference cells is equal to the radar range resolution (usually the pulse width). The output of the test cell is the radar video output, which is compared to the adaptive threshold derived from the sum of the outputs of the tapped delay lines defining the reference cells. This sum, therefore, represents the radar environment to either side of the test cell. It changes as the radar environment changes and as the pulse travels out in time. When multiplied by a predetermined constant k, the sum provides an adaptive threshold to maintain a constant false-alarm rate. Thus the threshold can adapt to the environment as the pulse travels in time.

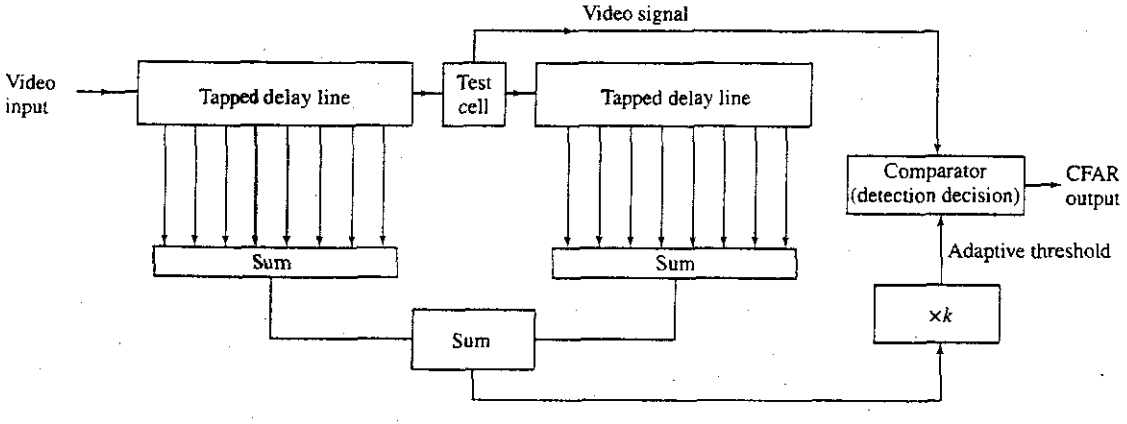

Figure 5.7 Cell averaging CFAR

If the radar output is noise or clutter described by the Rayleigh probability density function, the constant k which multiplies the sum of the tapped delay lines can be determined from classical detection theory, similar to that described in Chap. 2. When the statistics of the clutter are not known, which is often the case, the value of k can only be estimated or some form of nonparametric detector used.

CFAR Loss The greater the number of reference cells (delay-line taps) in the CA CFAR the better is the estimate of the background clutter or noise and the less will be the loss in detectability (signal-to-noise ratio). There is a limit, however, to the number of reference cells that can be used in practice since the clutter must be relatively homogeneous over the reference cells. A typical CFAR design for an aircraft-surveillance radar might have a total of 16 to 20 reference cells that sample the environment a half-mile to either side of the signal in the test cell. In a doppler processing radar, such as MTI or pulse doppler, reference cells can sometimes be taken from adjacent doppler filters as well as from adjacent range cells.

Since there are only a finite number of reference cells, the estimate of the noise or clutter is not precise and there will be a loss in detectability. Figure 5.8, derived from the publications of Mitchell and Walker[40] and from R. Nitzberg,[41] gives the theoretical CFAR loss as a function of the number of reference cells M, the probability of false alarm, and the number N of pulses integrated. (The CFAR loss is the signal-to-noise ratio required when CFAR is employed divided by the signal-to-noise ratio required for fixed-threshold

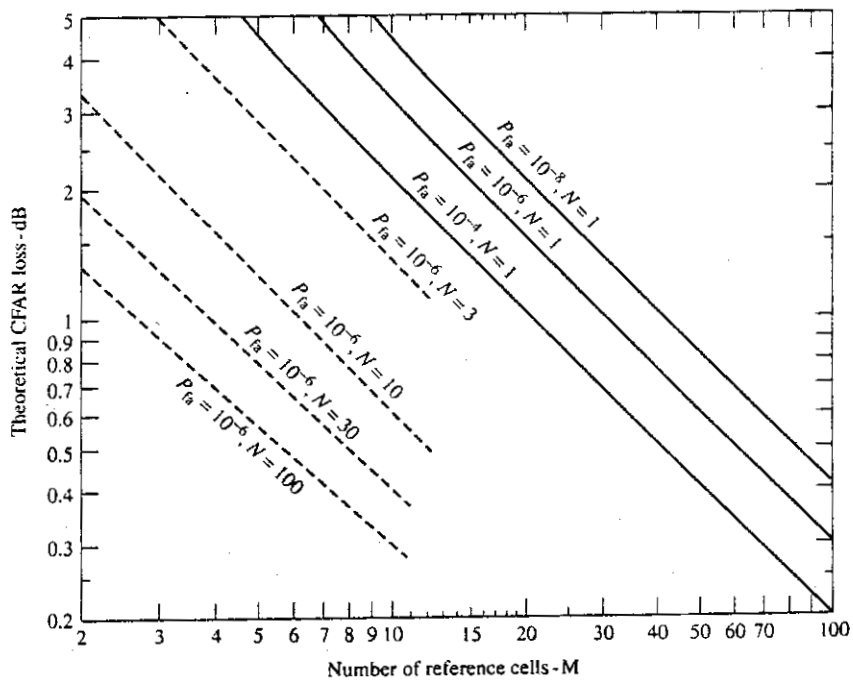

Figure 5.8 Theoretical CFAR loss.
(After R. L. Mitchell and J. F. Walker[40] and R. Nitzberg.[41])

detection.) The solid curves apply for detection using only a single pulse. The dashed curves give the loss for a probability of false alarm of 10^{-6}, when the number of pulses N is greater than one. The curves of Fig. 5.8 apply to a nonfluctuating target as well as Swerling Case 1 and Case 2. When the number of reference cells is large, the CFAR loss is small. Nitzberg shows that the CFAR loss for single-pulse detection ($N = 1$) can be approximated by

$$\text{Loss (dB)} = -\frac{5}{M} \log P_{\text{fa}} \qquad [5.25]$$

where P_{fa} is the probability of false alarm.

Clutter Edges The CA CFAR of Fig. 5.7 assumes that the statistics of the clutter or noise at each reference cell are independent, identical, and the same as the statistics at the test cell. This is not the case at the edges of clutter. As the reference cells pass over the leading and trailing edges of a patch of clutter, not all the cells contain clutter; so the threshold will be lower than when all reference cells contain clutter. False alarms (threshold crossings), therefore, can result at clutter edges. Threshold crossings from the clutter edges can be reduced by summing the leading and the lagging references cells separately, and using the greater of the two to determine the threshold.[42] The CFAR that uses the *greater of* the two sets of reference cells is known as GO-CFAR. It introduces an additional CFAR loss of from 0.1 to 0.3 dB.[43]

Effect of Multiple Targets When there are one or more targets within the reference cells along with a primary target in the test cell, the threshold is raised (even in the absence of any clutter) and the detection of the primary target in the test cell of the CA CFAR might be suppressed. One method for reducing the effect of multiple targets is to remove (censor) the outputs of those reference cells that are much larger than the rest. A predetermined number J of reference cells (those with the largest outputs) are removed and the adaptive threshold determined by the outputs of the remaining $M - J$ cells.[44] This is known as a *censored mean-level detector* (CMLD). The number of censored cells should be equal to, or at least not smaller than, the number of interfering targets. The loss associated with the CLMD has been analyzed and has been said to be small,[45] but it can be 1 dB or greater.[46]

Another approach to handling multiple nearby targets is that of *ordered statistic*, or OS, CFAR, in which the CFAR threshold is determined from one single value selected from the so-called ordered statistic.[47,48] The outputs from M reference cells are put in order from smallest to largest, and the Kth ordered value when multiplied by a scalar is used to set the threshold. For example, if $M = 16$, K might be 10. In one particular analysis of the OS CFAR, the additional loss in signal-to-noise ratio is given as about 0.5 dB for one interfering target, and about 1 dB for two interfering targets.

The problem of dealing with the effect of additional targets within the reference cells has received much attention in the literature.[49–58] Still another method for dealing with loss in detectability when multiple targets are present within the reference cells is to employ log video in which a log detector is used ahead of a CA CFAR to suppress large echoes.[59]

Range Resolution In general, two equal-amplitude targets can be resolved if they are separated in range by about 0.8 pulse width. The usual CFAR, however, considerably degrades the range resolution so that two equal-amplitude targets can be resolved only if they are spaced greater than about 2.5 pulse widths.[60] One reason for the poorer resolution is that the range cells adjacent to the test cell in Fig. 5.7 are not used as part of the reference cells since the target energy in the test cell spills over to nearby cells and affects the threshold. Another reason for degraded resolution is that in automatic detection systems, a large target can be detected in adjacent range cells, adjacent azimuth antenna beams, and adjacent elevation beams. Automatic detection systems have to merge the many detections of the same target into a single centroided detection. Trunk[61] has shown, using a generalized likelihood approach, that in theory it is possible to resolve two equal nonfluctuating targets with separations varying between 1/4 and 3/4 of a pulse width, depending on the relative phase between the two echo signals. This requires that the shape of the received echo pulse be known. (Trunk's result is a lower bound. It indicates what might be achieved, but does not necessarily apply to a specific CFAR configuration.)

Nonparametric Detectors A common assumption in most CFARs is that the statistics of the clutter or noise in the reference cells are known (usually taken to be Rayleigh), except for a scale factor. In many cases, however, the form of the clutter probability density function is not known. A *nonparametric detector,* also known as a *distribution-free detector,* has been considered as a CFAR when the clutter statistics are not known.[62] Its operation is not described here since it is seldom used. The nonparametric detector has a relatively large CFAR loss and problems with correlated samples. In addition, it is fairly susceptible to target suppression from large targets in the reference cells, its implementation might not be simple, and there is loss of amplitude information.[63]

Clutter Map[64–66] A clutter map divides the radar coverage area into range-azimuth cells on a polar or a rectangular grid. The clutter echo stored in each cell of the map then can be used to establish a threshold for that range and azimuth. It is, therefore, a form of CFAR.

The size of each clutter-map cell is equal to or greater than the radar resolution. At each of the range-azimuth cells of the clutter map, a number proportional to the amplitude of the clutter within the cell is stored in the map memory. Since clutter can change with time, the value of the clutter in each cell is updated periodically by averaging over a large number of scans (for example, 5 to 10 scans). The larger the number of scans the more accurate will be the estimate of the clutter, the lower the loss, and the less the effect of a target that moves through the cell. On the other hand, the averaging time (determined by the number of scans) should be shorter than the limited dwell time in which moving clutter (rain or chaff) is within the cell. A short averaging time also allows the threshold to recover to its proper state within a few scans after a target has passed through the cell.

A clutter map CFAR has an advantage over the CA CFAR in that it is not affected by nonhomogeneous clutter (edge effects). The response of the clutter map CFAR will be reduced when a target of slow speed remains within the cell long enough to affect the threshold. This effect can be reduced by making the map cell greater than the radar

resolution cell.[65] Increasing the size of the clutter-map cell should not be carried too far, however, since it reduces the interclutter visibility.

The loss of signal-to-noise ratio in the clutter map will depend on the averaging time. The longer the time, the less the loss. In a particular example, Khoury and Hoyle[64] state that the loss is 0.8 dB when the averaging time is approximately 2 minutes.

Another attribute of the clutter map is the elimination of those resolution cells containing slowly moving objects such as birds.[67] Each threshold crossing is checked against a clutter map before initiating an acquisition. It has been said that even with bird densities as low as 0.1 to 0.2 birds/km^2 a radar tracker can be overloaded and waste much of its time on birds.

The clutter map used in the original MTD discussed in Sec 3.6 was not a true CFAR. It could be called a *blanking clutter map* since it passes targets whose amplitude exceeds that of the clutter.[64]

Other Forms of CFAR Forms of CFAR that predate the CA CFAR include the following:

- *Siebert CFAR:* The output of a postdetection integrator (low-pass filter) provides an estimate of the average noise level which is then applied as a feedforward signal to control the threshold level to maintain the false-alarm rate constant.[68,69] This was one of the first attempts to provide a CFAR, and it was employed in the AN/FPS-23 bistatic CW radar installed by the U.S. Air Force on the DEW (Distant Early Warning) line in the middle 1960s for automatic detection of low-flying aircraft.
- *Hard limiter:* An example is the so-called *Dicke fix*, which consists of a broadband IF filter followed by a hard limiter (which is set low enough to limit receiver noise) and a narrowband matched filter.[69] The output is then unaffected by the amplitude of the noise. The Dicke fix is especially effective against impulse-like noise and broadband jamming. It would not normally be used with an MTI radar since, as mentioned in Sec 3.7, hard limiting restricts the improvement factor that can be achieved.
- *Log-FTC:* This is described in Sec. 7.8. It is a CFAR when the noise or clutter has a Rayleigh probability density function.

CFAR Use in Radar CFAR is used in radars to maintain effectiveness when there are too many extraneous crossings of a fixed threshold caused by noise or clutter. Automatic tracking of targets can be seriously degraded if excessive false alarms occur.

CFAR is to a radar as crutches are to a person with a broken foot. The crutches allow the person to be mobile, but they are something the person would rather not need. CFAR may allow a radar to continue operation, but there are limitations in performance that accompany its use. CFAR automatically adjusts the threshold to prevent threshold crossings that tie up and overload the tracking computer. Increasing the threshold to maintain a constant probability of false alarm, however, lowers the probability of detection and results in missed detections of some targets. This loss of targets has to be tolerated when CFAR is used. In addition to missed target detections, CFAR can cause a loss in the signal-to-noise ratio when the statistics of the clutter or noise are not estimated accurately. The leading and trailing edges of some CFARs can produce undesired threshold

crossings (false alarms). Target suppression can occur when one or more targets are within the reference cells. There is poor range resolution compared to a radar without CFAR. Furthermore, those CFAR designs that might be subject to spoofing by hostile electronic countermeasures have to be avoided in military radars. Thus CFAR is a "necessary evil," needed for maintaining operation of automatic detection and tracking systems that would cause excessive false alarms due to noise or clutter.

CFAR would not be required if the radar had good doppler processing to reject clutter, good ECCM (electronic counter-countermeasures) to reject hostile noise jamming, good EMC (electromagnetic compatibility) to reject interference, and a good tracking computer that recognizes (without overloading in the presence of a large number of threshold crossings) desired moving targets and rejects clutter echoes that break through the signal processing.

Doppler-Estimation False-Alarm Control A quite different method of controlling false alarms is to estimate the target amplitude and the radial velocity of the target (from a measurement of the doppler frequency shift).[70] Noise or clutter are discriminated from targets by the variation in the radial velocity and amplitude over successive measurements. Consistency tests are applied to the measurements based on the assumption that clutter and noise will fluctuate in both amplitude and estimated doppler over successive measurements; but moving targets generally will not. Also, multiple measurements at different pulse repetition intervals and/or frequencies can be used to produce an unambiguous velocity estimate from which moving targets can be separated from stationary clutter to aid in the tracking process. No reference cells are required in this method, so that the problems of nonhomogeneous environments that degrade the CA CFAR (edge effects and multiple targets) do not appear.

5.8 THE RADAR OPERATOR

The discussion in this chapter assumed automatic detection without an operator making the detection decision. Modern radars usually make the detection decision automatically. An operator viewing a display can be a good detector of targets, as has been demonstrated in the past.[71] On the other hand, operators do not have the capacity to process large quantities of information as rapidly as do electronic circuits, and they can become fatigued.

It has been demonstrated experimentally that when an operator views a display in which the pulses received from successive sweeps are presented side-by-side without saturating the display and without fading, the integration improvement achieved by an operator is equivalent to what would be expected from classical detection theory.[72,73]

To obtain the benefits of both automatic detection and the capability of an operator to interpret unusual situations, some radar designers prefer to make the raw video information available to the operator along with the automatically processed information.

5.9 SIGNAL MANAGEMENT

This chapter has been concerned with the detection of desired radar signals. To close the chapter and introduce the next one on the extraction of radar information, we briefly list below the various parts of *signal management* that occur throughout the radar system. Signal management includes everything associated with the waveforms and their processing that is required for a radar to do its job of detecting and locating targets and determining something about their nature. Signal management starts with the design of a suitable waveform and its radiation into space, the collection by the receiver of echo signals reflected from targets and other objects, the use of signal processing to extract the desired signal and reject undesired echoes, the use of data processing to extract information about the detected signals, the coordinated control of these processes throughout the radar, and keeping within the resources and constraints that affect signals and their management. Some parts of signal management listed below apply to a conventional pulse radar with an envelope detector; some apply to a radar that extracts moving targets based on their doppler frequency shift; and some to both.

Figure 5.9 indicates the various factors that enter into radar signal management.

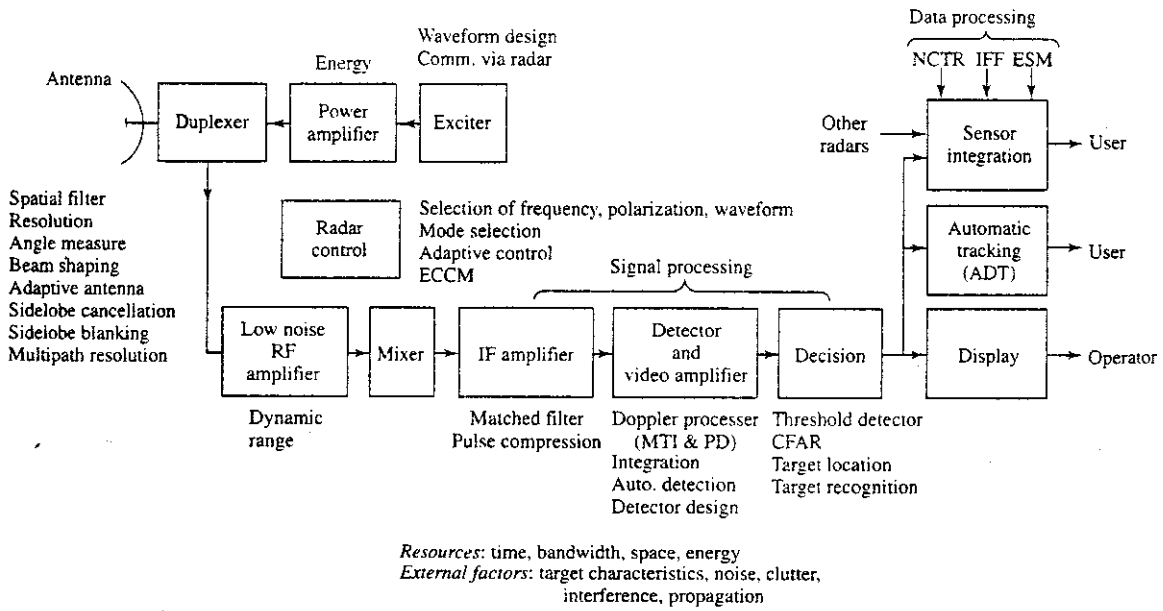

Figure 5.9 The various elements that enter into radar signal management.

Component Parts of Radar Signal Management

Signal Processing This is processing for the purpose of detecting desired echo signals and rejecting noise, interference, and undesired echoes from clutter. It includes the following:

Matched filter: to maximize the signal-to-noise ratio at the output of the radar receiver, and thus maximize detectability of echo signals.

Detector/integrator: the means for processing in a convenient and efficient manner the number of pulses received from a target so as to take full advantage of the total signal energy received from a target.

Clutter reduction: to eliminate or reduce unwanted clutter by one or more methods, of which filtering of moving targets based on the doppler frequency shift is the most important.

CFAR: used to maintain a constant false-alarm rate at the output of the threshold detector when the radar cannot eliminate unwanted echoes.

Electromagnetic compatibility (EMC): the elimination of interference from other radars and other electromagnetic radiations that can enter the radar receiver.

Electronic counter-countermeasures (ECCM): in a military radar, those methods employed to reduce or eliminate the effectiveness of jamming, deception, and other hostile electronic active and passive measures whose purpose is to degrade radar performance. ECCM can be found throughout the radar, not just as part of the signal processing.

Threshold detection: the decision as to whether the output of the radar is a desired signal.

Data Processing These are the processes that take place after the detection of the desired signals for the purpose of acquiring further information about the target.

Target location: in range, angle, and sometimes radial velocity (from the doppler shift). Location information is not generally thought of as either signal processing or data processing. It is usually obtained as part of the detection process (since detection without location is of no value).

Target trajectory: also called *target track*, which is the time history of the target's location. Usually a prediction of the target's future position is included.

Target recognition: the recognition of the type of target being viewed by the radar. It might include the recognition of aircraft from birds, one type of aircraft or ship from another, recognition of various types of weather, and information about the land and sea environment (remote sensing).

Weapon control: in military systems, the use of the radar output for the control and guidance of weapons.

Waveform Design The selection of the waveform depends on what is required of the radar for detection in noise, clutter, interference, and electronic counter-countermeasures,

as well as for the extraction of information from the radar signal. Waveform design will affect the signal and data processing. Multiple waveforms for different purposes can be an important aspect of high-performance radar. The radar signal can also be adapted to communicate with other radars.

Antenna This is not just for radiating and collecting radar signals, but is the means by which angle information is obtained and by which the radar coverage is achieved. The antenna can act as a spatial filter that can affect the spectral properties of wideband signals. It can also provide, in some cases, the angle rate and extract a *spatial* doppler shift similar to the temporal doppler shift.[74] The target's tangential velocity obtained from the spatial doppler shift, along with the radial velocity obtained from the more common temporal doppler shift, can provide the vector velocity of the target.

Automatic Radar Control A radar often employs multiple waveforms and various signal processing options to maximize performance under a variety of environmental conditions. Radar control involves the automatic selection of the proper waveform and signal processing according to the environment and interference (both natural and intentional) encountered by the radar.

Sensor Integration The outputs from other radars covering the same region may be combined to form tracks. Information from the civil aviation Air Traffic Control Radar Beacon Systems (ATCRBS) or the military identification friend or foe (IFF), or other civil or military command and control information can be used to assist in identifying the target. Noncooperative target recognition (NCTR) based on special radar waveforms and processing, as well as signals and information obtained by electronic warfare (EW) methods, such as electronic support measures (ESM), may be used as part of an integrated military target-recognition system.

Resources for Signal Management The radar engineer has available the following resources for pursuing the management of signals and extraction of information.

Energy Sufficiently large transmitted energy is important for detection of weak signals in noise at long range and for obtaining accurate radar measurements.

Bandwidth This is the classical measure of information and is especially important for accurate range measurement and the temporal resolution of targets.

Time Time is necessary for accurate measurement of the doppler frequency. Time also is a means for obtaining increased energy when peak power is a limitation. It is important for achieving multiple functions from a single-beam radar within a required time, and for handling the processing of many echo signals.

Space This applies to the physical aperture area required for an antenna. The larger the antenna aperture the greater the echo energy at the receiver and the more accurate the spatial measurements that can be obtained.

Constraints It is not always possible or practical to obtain the desired energy, bandwidth, time, and spatial extent that might be required. Furthermore, the environment might cause clutter echoes that limit a radar's performance: at high microwave and millimeter wave frequencies atmospheric attenuation can be a nuisance; atmospheric refraction can produce both good and bad effects, as discussed in Chap. 8; and the curvature of the earth limits the range of a radar to targets within the line of sight. Military radars must be able to perform their mission in spite of hostile actions designed to degrade or eliminate their effectiveness. In most applications there are constraints imposed by size, space, weight, and perhaps primary power. Spectrum availability is always a consideration and can seriously limit what the engineer might do. There is also the ever-present constraint imposed by cost.

Engineers always have constraints on what they can do and almost never have everything they need to accomplish the desired task. The essence of successful engineering, however, involves compromise so as to provide in a timely manner a new and useful capability at an acceptable cost.

REFERENCES

1. North, D. O. "An Analysis of the Factors Which Determine Signal/Noise Discrimination in Pulsed-Carrier Systems." *Proc. IEEE* 51 (July 1963), pp. 1016–1027. Originally appeared as RCA Tech. Rept. PTR-6C, June 25, 1943 (ATI 14009).
2. Introduction to Matched Filters, *Special Issue on Matched Filters of the IRE Trans. on Information Theory* IT-6, no. 3 (June 1960).
3. Van Vleck, J. H., and D. Middleton. "A Theoretical Comparison of Visual, Aural, and Meter Reception of Pulsed Signals in the Presence of Noise." *J. Appl. Phys.* 17 (November 1946), pp. 940–971.
4. D'Aloisi, D., A. DiVito, and G. Galati. "Sampling Losses in Radar Signal Detection." *J. IERE* 56, no. 6/7 (June/July 1986), pp. 237–242.
5. Taylor, J. W., Jr. "Receivers." In *Radar Handbook*, 2nd ed., M. Skolnik, Ed. New York: McGraw-Hill, 1990, Chap. 3, Sec. 3.7.
6. Dwork, B. M. "Detection of a Pulse Superimposed on Fluctuation Noise." *Proc. IRE* 38 (July 1959), pp. 771–774.
7. Urkowitz, H. "Filters for the Detection of Small Radar Signals in Clutter." *J. Appl. Phys.* 24 (October 1952), pp. 1024–1031.
8. Peterson, W. W., T. G. Birdsall, and W. C. Fox. "The Theory of Signal Detectability." *IRE Trans.* PGIT-4 (September 1954), pp. 171–212.
9. Woodward, P. M. *Probability and Information Theory with Applications to Radar.* New York: McGraw-Hill, 1953.
10. Minkoff, J. *Signals, Noise, & Active Sensors.* New York: Wiley, 1992, Chap. 5.
11. Bussgang, J. J., and D. Middleton. "Optimum Sequential Detection of Signals in Noise." *IRE Trans.* IT-1 (December 1955), pp. 5–18.

12. Bussgang, J. J. "Sequential Methods in Radar Detection." *Proc. IEEE* 58 (May 1970), pp. 731–743.

13. Preston, G. W. "The Search Efficiency of the Probability Ratio Sequential Search Radar." *IRE Intern. Conv. Record* 8, pt. 4 (1960), pp. 116–124.

14. Kazovsky, L. G. "Sequential Radar Detection of Border Penetration." *IEE Proc.* 128, Pt. F, no. 5 (October 1981), pp. 305–310.

15. Brennan, L. E., and F. S. Hill, Jr. "A Two-Step Sequential Procedure for Improving the Cumulative Probability of Detection in Radars." *IEEE Trans.* MIL-9 (July–October 1965), pp. 278–287.

16. Nathanson, F. E. *Radar Design Principles,* 2nd ed. New York: McGraw-Hill, 1991, Sec. 4.7.

17. Marcum, J. "A Statistical Theory of Target Detection by Pulsed Radar, Mathematical Appendix." *IRE Trans.* IT-6 (April 1960), pp. 209–211.

18. Woodward, P. M., See Ref. 9, Sec. 5.5.

19. Skolnik, M. *Introduction to Radar Systems,* 2nd ed. New York: McGraw-Hill, 1980, Sec. 10.5.

20. This expression was suggested by Warren D. White, who reviewed the manuscript for the second edition of this text.

21. Marcum, J. Ref. 17, p. 189 and Fig. 42.

22. Bird, J. S. "Calculating the Performance of Linear and Square-Law Detectors." *IEEE Trans.* AES-31 (January 1995), pp. 39–51.

23. Marcum, J. Ref. 17, pp. 158–159.

24. Green, B. A., Jr. "Radar Detection Probability with Logarithmic Detectors." *IRE Trans.* IT-4 (March 1958), pp. 50–52.

25. Hansen, V. G. "Radar Detection Probability with Logarithmic Detectors." *IEEE Trans.* AES-8 (May 1972), pp. 386–388. See correction, AES-10 (January 1974), p. 168.

26. Eaves, J. L. and E. K. Reedy. *Principles of Modern Radar.* New York: Van Nostrand Reinhold, 1987, pp. 254, 270–272.

27. Nathanson, F. E. Ref. 16, Sec. 8.8.

28. Taylor, J. W., Jr. "Receivers." In *Radar Handbook.* 2nd ed., M. Skolnik, Ed. New York: McGraw-Hill, Shap. 3, Sec. 3.12.

29. Hansen, V. G. "Performance of the Analog Moving Window Detector." *IEEE Trans.* AES-6 (March 1970), pp. 173–179.

30. Trunk, G. V. "Radar Signal Processing," *Advances in Electronics and Electron Physics* 45, L. Marton, Ed. New York: Academic, 1978, pp. 203–252.

31. Trunk, G. V. "Automatic Detection, Tracking, and Sensor Intgration." *Radar Handbook,* 2nd ed. M. Skolnik, Ed. New York: McGraw-Hill, 1990, Chap. 8.

32. Harrington, J. V. "An Analysis of the Detection of Repeated Signals in Noise by Binary Integration." *IRE Trans.* IT-1 (March 1955), pp. 1–9.

33. Swerling, P. "The 'Double Threshold' Method of Detection." Rand Corp. Rept. RM-1081, Dec. 17, 1952, Santa Monica, CA.

34. Weiner, M. A. "Binary Integration of Fluctuating Targets." *IEEE Trans.* AES-27 (January 1991), pp. 11–17.

35. Walker, J. F. "Performance Data for a Double-Threshold Detection Radar." *IEEE Trans.* AES-7 (January 1971), pp. 142–146. See also comment by V. G. Hansen, p. 561, May, 1971.

36. Worley, R. "Optimum Thresholds for Binary Integration." *IEEE Trans.* IT-4 (March 1968), pp. 349–353.

37. Hansen, V. G. "Optimization and Performance of Multilevel Quantization in Automatic Detectors." *IEEE Trans.* AES-10 (March 1974), pp. 274–280.

38. Cantrell, B. H., and G. V. Trunk. "Angular Accuracy of a Scanning Radar Employing a Two-Pole Filter." *IEEE Trans.* AES-9 (September 1973), pp. 649–653.

39. Finn, H. M., and R. S. Johnson. "Adaptive Detection Mode with Threshold Control as a Function of Spatially Sampled Clutter-Level Estimates." *RCA Rev.* 29 (September 1968), pp. 414–464.

40. Mitchell, R. L., and J. F. Walker. "Recursive Methods for Computing Detection Probabilities." *IEEE Trans.* AES-7 (July 1971), pp. 671–676.

41. Nitzberg, R. "Analysis of the Arithmetic Mean CFAR Normalizer for Fluctuating Targets." *IEEE Trans.* AES-14 (January 1978), pp. 44–47.

42. Hansen, V. G. "Constant False Alarm Processing in Search Radars." *International Conference on Radar—Present and Future.* Oct. 23–25, 1973, pp. 325–332, IEE Publication No. 105.

43. Gregers-Hansen, V., and J. H. Sawyers. "Detectability Loss Due to 'Greatest Of' Selection in a Cell-Averaging CFAR." *IEEE Trans.* AES-16 (January 1980), pp. 115–116.

44. Rickard, J. T., and G. M. Dillard. "Adaptive Detection Algorithms for Multiple-Target Situations." *IEEE Trans.* AES-13 (July 1977), pp. 338–343.

45. Al-Hussaini, E. K. "Performance of the Greater-Of and Censored Greater-Of Detectors in Multiple Target Environments." *IEE Proc.* 135, Pt. F (June 1988), pp. 193–198.

46. Ritcey, J. A. "Performance Analysis of the Censored Mean-Level Detector." *IEEE Trans.* AES-22 (July 1986), pp. 443–454.

47. Rohling, H. "Radar CFAR Thresholding in Clutter and Multiple Target Situations." *IEEE Trans.* AES-19 (July 1983), pp. 608–621.

48. Levanon, N. *Radar Principles.* New York: Wiley, 1988, p. 263.

49. Weiss, M. "Analysis of Some Modified Cell-Averaging CFAR Processors in Multiple-Target Situations." *IEEE Trans.* AES-18 (January 1982), pp. 102–114.

50. Barboy, B., A. Lomes, and E. Perkalski. "Cell-Averaging CFAR for Multiple-Target Situations." *IEE Proc.* 133, Pt. F (April 1986), pp. 176–186.

51. Gandhi, P. P., and S. A. Kassam. "Analysis of CFAR Processors in Nonhomogeneous Background." *IEEE Trans.* AES-24 (July 1988), pp. 427–445.

52. Levanon, N. "Detection Loss Due to Interfering Targets in Ordered Statistics CFAR." *IEEE Trans.* AES-24 (November 1988), pp. 678–681.

53. Blake, S. "OS-CFAR Theory for Multiple Targets and Nonuniform Clutter." *IEEE Trans.* AES-24 (November 1988), pp. 785–790.

54. Barket, M., S. D. Himonas, and P. K. Varshney. "CFAR Detection for Multiple Target Situations." *IEE Proc.* 136 (October 1989), pp. 193–209.

55. Ritcey, J. A., and J. L. Hines. "Performance of MAX Family of Order-Statistic CFAR Detectors." *IEEE Trans.* AES-27 (January 1991), pp. 48–57.

56. Shor, M., and N. Levanon. "Performance of Order Statistics CFAR." *IEEE Trans.* AES-27 (March 1991), pp. 214–224.

57. Goldman, H., and I. Bar-David. "Analysis and Application of the Excision CFAR Detector." *IEE Proc.* 135, Pt. F (December 1988), pp. 563–575.

58. Minkler, G., and J. Minkler. *CFAR.* Baltimore, MD: Magellan, 1990.

59. Trunk, G. V. Ref. 31, pp. 8.17–8.18.

60. Trunk, G. V. "Range Resolution of Targets Using Automatic Detectors." *IEEE Trans.* AES-14 (September 1978), pp. 750–755.

61. Trunk, G. V. "Range Resolution of Targets." *IEEE Trans.* AES-20 (November 1984), pp. 789–797.

62. Trunk, G. V., B. H. Cantrell, and F. D. Queen. "Modified Generalized Sign Test Processor for 2-D Radar." *IEEE Trans.* AES-10 (September 1974), pp. 574–582.

63. Trunk, G. V., Ref. 31, pp. 8.19–8.20.

64. Khoury, E. N., and J. S. Hoyle. "Clutter Maps: Design and Performance." *Proc. of the 1984 IEEE National Radar Conference,* pp. 1–7, 84CH1963-8.

65. Farina, A., and F. A. Studer. "A Review of CFAR Detection Techniques in Radar Systems." *Microwave J.* 29, no. 9 (September 1986), pp. 115–128.

66. Nitzberg, R. "Clutter Map CFAR Analysis." *IEEE Trans.* AES-22 (July 1986), pp. 419–421.

67. Franzen, N. I. "The Use of a Clutter Map in the Artillery Locating Radar ARTHUR." *IEEE International Radar Conference,* Arlington, VA, May 7–10, 1990, pp. 207–210, IEEE Catalog No. 90CH-2882-9.

68. Siebert, W. M. "Some Applications of Detection Theory to Radar." *IRE Natl. Conv. Record* 6, pt. 4, pp. 5–14, 1958.

69. Hansen, V. G., and A. J. Zottl. "The Detection Performance of the Siebert and Dicke-Fix CFAR Detectors." *IEEE Trans.* AES-7 (July 1971), pp. 706–709.

70. Trunk, G. V., W. B. Gordon, and B. H. Cantrell. "False Alarm Control Using Doppler Estimation." *IEEE Trans.* AES-26 (January 1990), pp. 146–153.

71. Baker, C. H. *Man and Radar Displays.* New York: Macmillan, 1962.

72. Tucker, D. G. "Detection of Pulse Signals in Noise. Trace-to-Trace Correlation in Visual Displays." *J. Brit. IRE* 17 (June 1957), pp. 319–329.

73. Skolnik, M. I., and D. G. Tucker. "Discussion on 'Detection of Pulse Signals in Noise. Trace-to-Trace Correlation in Visual Displays.'" *J. Brit. IRE* 17 (December 1957), pp. 705–706.

74. Skolnik, M. "Radar Information from the Partial Derivatives of the Echo Signal Phase from a Point Scatterer." Naval Research Laboratory, Washington. D.C., Memorandum Rep. 6148, February 17, 1988.

PROBLEMS

5.1 (a) Find the matched-filter frequency response function $H(f)$ for a perfectly rectangular (video) pulse of duration τ, and amplitude A. (Assume the pulse extends in time from $-\tau/2$ to $+\tau/2$). (b) Sketch (roughly) its magnitude $|H(f)|$ for positive frequencies. (c) Sketch (roughly) the output of the video matched filter. (This can probably be done much easier by "inspection" than calculation.) All right to take $t_m = 0$.

5.2 (a) Find the matched-filter frequency response function $H(f)$ for a perfectly rectangular pulse of sinewave of duration τ, amplitude A, and frequency f_0. (Assume the pulse extends in time from $-\tau/2$ to $+\tau/2$). (b) Sketch (roughly) its magnitude $|H(f)|$ for positive frequencies. (c) Sketch (roughly) the output of the matched filter. (A rough sketch means it does not need to be precise or "artistic".) (d) Optional—In parts (a) and (b), your expression for $H(f)$ probably contained negative frequencies. What is the meaning of negative frequencies in $H(f)$ and what does one do about them? [Note that the answer to part (d) is not obvious or readily found in textbooks, and might require a little basic thinking about a Fourier transform and what it really is.]

5.3 From problem 5.1a you found that the output of a filter matched for a single *video* rectangular pulse of width τ and amplitude A is a triangular pulse with peak amplitude $A^2\tau$ and whose base has a width 2τ. (a) Sketch and label the output of a filter matched to a train of three equal video rectangular pulses with spacing T between pulses. (This can be done by inspection rather than by calculation.) (b) The more usual way to process a number of pulses, as discussed in Chap. 2, is to pass each pulse in sequence through a filter matched to a *single* pulse and integrate (add) the total number of pulses either coherently or noncoherently. Sketch and label the integrated output of a train of three equal video pulses when processed in this manner.

5.4 Find the ratio of the peak-signal-to-mean-noise power out of a matched filter designed for an RF signal

$$s(t) = Ae^{-at} \sin 2\pi f_0 t$$

where $0 < t < \tau$, and A and a are constants. The input noise is white and of spectral density N_0. You may assume there are many cycles of f_0 within the pulse duration τ, and that $e^{-a\tau}$ is small. (You should use integral tables.)

5.5 The input signal to its matched filter is $s(t) = (A/T)(T - t)$, where $0 \leq t \leq T$. Sketch the following: (a) the input signal, (b) the impulse response of the matched filter, and (c) the output signal from the matched filter. (d) Why is this particular waveform unrealizable?

5.6 What are the units of the constant G_a in the expression for the matched filter frequency response function given by Eq. (5.1)?

5.7 This problem involves finding the matched filter for fixed clutter modeled as nonwhite noise (NWN). The clutter power is assumed to be much larger than receiver noise so that the clutter echo rather than receiver noise determines signal detectability. It is assumed that the clutter is uniformly distributed and stationary so that the power spectral density $|N_i(f)|^2$ of the clutter echo signal can be considered to be the same as the power spectrum of the transmitted radar signal which is reflected from it. (a) Starting with Eq. (5.19) find the frequency response function $H(f)$ of the NWN matched filter for detecting a stationary point target in clutter as given by the above assumptions. (b) If the radar signal $s(t)$ were a perfectly rectangular pulse of width τ, sketch $|H(f)|$ for the NWN matched filter. (c) Why is this clutter matched filter not practical? (d) Optional—If you never heard of a matched filter, what type of radar waveform might you have selected to attempt to detect a stationary point target in uniform distributed clutter much larger than receiver noise? (e) If you answered part (d), how might your solution compare (better or worse) to the NWN matched clutter filter of part (b)?

5.8 This concerns the effectiveness of a nonmatched filter. (a) Find the peak-signal-to-mean-noise ratio (SNR) out of a one-stage low-pass RC network when the input is a rectangular pulse of width τ, amplitude A = 1, and the noise is white with a noise power per unit bandwidth of N_0. The normalized frequency response function is

$$\text{frequency response function of low-pass RC network} = H(f) = \frac{1}{1 + jf/B_v}$$

where B_v = bandwidth of the low-pass filter. Note that the maximum SNR occurs at a time equal to the pulse width τ. (b) Find the peak-signal-to-mean-noise power out of a filter that is perfectly matched to the rectangular pulse. (c) What is the loss in SNR (in dB) introduced by the nonmatched filter of (a) compared to the matched filter of (b)? (d) If the efficiency of the nonmatched filter relative to that of a matched filter is defined as

$$\rho_f = \frac{|s_0(t)|^2_{\max}/N_{\text{out}}}{2E/N_0}$$

what is the value of $B_v\tau$ that maximizes the efficiency? [Note that a low-pass RC video network produces results for the above that are equivalent to what would be obtained with a single tuned RLC resonant network as might be used in the IF, assuming $B_v = B_{IF}/2$. Thus your answer to part (d) also applies to a single tuned RLC resonant network that could be in the IF portion of the receiver. A single-tuned circuit, however, is seldom found in radar receivers, so the answers you obtain in this problem might not be typical for radar.]

5.9 (a) Draw the block diagram of a correlation receiver. (b) Explain why the correlation receiver can be considered equivalent to the matched filter receiver in detection performance.

(c) Under what conditions, if any, might one choose to implement a correlation receiver rather than a matched filter receiver?

5.10 Sketch the matched-filter frequency response function when the waveform is just one RF cycle of sinewave in duration. You may start with the answer you found for problem 5.2(a). (A *single cycle sinewave* is an *ultrawideband* waveform.)

5.11 The matched filter of Eq. (5.1) assumed that the shape of the radar echo was the same as the shape of the transmitted radar signal. When a target is observed by a high-resolution radar (one with a range-resolution cell size much smaller than the target's radial extent), the target echo is not the same as that which was transmitted. It will consist of the superposition of echoes from the individual scattering centers of the target. (An example is a large ship 500 feet in length being observed head-on by a civil marine radar using a pulse width of 80 ns.) Discuss what has to be considered about the "matched filter" when attempting to detect a target that is much longer in radial size than the range-resolution cell so that the target echo is resolved into multiple scatterers. (Note that this question does not have a simple, unique answer.)

5.12 Show that the impulse response of a matched filter $[h(t) = G_a s(t_m - t)]$ is the inverse Fourier transform of its frequency response function $H(f) = G_a S^*(f) \exp(-j2\pi f t_m)$.

5.13 Why is a CFAR needed in some radars? What are the disadvantages of using CFAR?

5.14 What does one have to do in a radar system to avoid the use of a conventional CFAR?

5.15 In the VHF frequency region (30 to 300 MHz), the external noise at the receive-antenna terminals is generally higher than receiver internal noise. If one were to design an ultrawideband radar at VHF, qualitatively describe how the matched filter of Eq. (5.1), based on white noise, would have to be modified to allow for the large external noise levels that vary with frequency? (You might want to review Sec. 8.8 or other related sources on external noise.)

5.17 Show that the optimum detector law based on the criterion of the likelihood-ratio receiver is $y = \ln I_0(av)$, where y is the receiver output, a is the amplitude of the received sinewave signal normalized (divided) by the rms noise voltage, v is the amplitude of the IF voltage envelope normalized by the rms noise voltage, and $I_0(x)$ is the modified Bessel function of zero order. [The following outlines how you might work through the derivation. Start with the likelihood ratio of Eq. (5.21). Assume there are N independent pulses with normalized envelope-amplitudes $v_1, v_2, \ldots, v_N$ available from the radar receiver. The probability density function for the ith noise pulse $p_n(v_i)$ is found from Eq. (2.21), where v_i is the ratio $R/\psi_0^{1/2}$, R is the envelope amplitude of the ith output and $\psi_0^{1/2}$ is the rms noise level. The probability density function for the ith signal-plus-noise pulse $p_s(v_i)$ is found from Eq. (2.27), with a = ratio of the sinewave signal amplitude to rms noise. The likelihood ratio of the N pulses is

$$L_r(v) = \frac{\prod_{i=1}^{N} p_s(v_i)}{\prod_{i=1}^{N} p_n(v_i)} \gtrless K$$

where K is the receiver threshold level. After making the substitutions one should take the log of both sides so that the product becomes a more convenient sum. At this point, examination of the likelihood ratio will show how the signal should be processed and indicate the nature of the detector law.] How does this "optimum detector" relate to more conventional detectors?

5.18 What are the advantages and limitations of a binary integrator?

5.19 How does the performance of a radar operator making detection decisions by viewing the raw (unprocessed) video output of a radar display compare to the performance of an automatic (electronic) detector?

chapter

6

Information from Radar Signals

6.1 INTRODUCTION

This chapter includes the *basic measurements* that can be made by a radar; the *theoretical accuracy* of radar measurements; the *ambiguity diagram* that graphically illustrates the characteristics of radar waveforms in the time (range) and frequency (radial velocity) domains; *pulse compression,* which is used to achieve high range-resolution without the need for high peak power; and target *recognition* methods whereby a radar distinguishes one type of echo signal from another.

A radar obtains information about a target by comparing the received echo signal with the signal that was transmitted. It was said in Chap. 5 that the presence of a target is announced when the echo signal is strong enough to cross the receiver detection threshold. Knowing that a target is present, however, is almost never sufficient in itself. More must be known to be useful; thus a radar must provide information about the target, as discussed next.

6.2 BASIC RADAR MEASUREMENTS

A radar can obtain a target's location in range and azimuth, and sometimes elevation. After several observations of a moving target over a period of time, the target trajectory, or track, can be obtained. Radar can also do more than simply characterize the target as a

"blob." In this section, the information available from a target first will be discussed as if the target were a point scatterer and then as a distributed scatterer. For purposes of this chapter, a *point scatterer,* or *point target,* is one with dimensions small compared to the size of the radar resolution cell in range, cross-range (angle), or both. The target's individual scattering features, therefore, are not resolved. A *distributed scatterer,* or *target* is one with dimensions large compared to the resolution-cell size, allowing the individual scatterers to be discerned. The resolution capabilities of a radar usually (but not always) determine whether a target is considered as a point scatterer (unresolved) or a distributed target (resolved). A *complex scatterer* is one that contains multiple scatterers. A complex scatterer can be either a point scatterer or a distributed scatter.

Measurements of a Point Target The basic radar measurements that can be made for a point target when only a single observation is made are range, radial velocity, direction (angle), and, in some special cases, tangential velocity.

Range It was said in Chap. 1 that the measurement of distance, or range, was obtained from the round-trip time T_R required for a radar signal to travel to the target and back. The range R is given by $cT_R/2$, where c = velocity of propagation. In many radar applications the target's range is the most significant measurement that is made. No other sensor has been able to compete with radar for determining range to a distant target, especially in accuracy, ability to make a measurement over very long or very short distances, and under adverse weather conditions. A long-range air-surveillance radar might measure range to an accuracy of many tens of meters, but accuracies of a few centimeters are possible with precision systems. In the most precise systems, the accuracy of a range measurement is limited only by the accuracy with which the velocity of propagation is known. The spectral bandwidth occupied by the radar signal is the fundamental resource required for accurate range measurement. The greater the bandwidth, the more accurate can be the range measurement.

Angle Measurement Almost all radars utilize directive antennas with relatively narrow beamwidths. A directive antenna not only provides the large transmitting gain and large receiving aperture needed for detecting weak echo signals, but its narrow beamwidth allows the target's direction to be determined accurately. It can do this by noting the direction the antenna points when its received echo signal is a maximum. A typical microwave radar might have a beamwidth of one or a few degrees. The narrowest beamwidths of operational radars have been about 0.3°. This is not an absolute limit; but the narrower the beamwidth, the greater the mechanical and electrical tolerances that are required of the antenna.

Angular accuracy can be much better than the antenna beamwidth, as described later in this chapter. Angle accuracy depends on the electrical size of the antenna (size as measured in wavelengths). With signal-to-noise ratios typical of those required for reliable detection, the angular location of a target can be determined to about 1/10th of a beamwidth. The best precision monopulse tracking radars used for range instrumentation can determine angle to about 0.1 mrad rms (0.006°) if the signal-to-noise ratio is large enough and if the proper efforts are taken to minimize errors.

Radial Velocity Measurement of the radial component of velocity in many radars is obtained from the rate of change of range. This is known as the *range rate.* The classical method for finding the radial velocity is based on $v_r = (R_2 - R_1)/(T_2 - T_1)$. It is found from the range R_1 measured at time T_1 and the range R_2 at time T_2. However, this method of finding range rate (or any other derivative of a location measurement) is not considered here as a *basic* radar measurement even though it may be widely used. Instead, the doppler frequency shift is the basic method for obtaining radial velocity. It can be made on the basis of a single observation. Using the classical expression [Eq. (3.3)] for the doppler frequency shift, f_d, the radial velocity v_r is given as

$$v_r = \lambda f_d/2 \qquad [6.1]$$

where λ = wavelength. It can be shown from the theoretical accuracy expressions presented later in this chapter that the radial velocity accuracy derived from the doppler frequency shift can be much better than that found from the range rate, assuming the time between the two range measurements in the range-rate method is the same as the time duration of the doppler frequency measurement. (See Problem 6.5.)

It will be seen later that the accuracy of the doppler-frequency measurement depends on the time duration over which it is made. The longer the time, the better the frequency accuracy. Because of the relationship between radial velocity and wavelength in Eq. (6.1), the shorter the wavelength, the shorter can be the observation time to achieve a required velocity accuracy. (The shorter the wavelength, the higher the frequency.) Or, the shorter the wavelength, the better will be the velocity accuracy for a given observation time.

In spite of its good accuracy, the doppler frequency shift is not used as often as is the range-rate for obtaining the radial velocity since it can result in ambiguities in range and/or doppler when employed with a short or a medium pulse-duration radar.

Tangential (Cross-Range) Velocity Just as the temporal doppler frequency shift can provide the radial velocity, there exists in the spatial (angle) domain an analogous *spatial doppler-frequency shift* from which the tangential velocity can be determined.[1] (If the radial velocity is $v_r = v \cos \theta$, the tangential velocity is $v_t = v \sin \theta$, where v is the target's speed and θ is the angle between the target's velocity vector and the radar line of sight.) The angle-rate times the range is equal to the tangential velocity. Together, the tangential velocity and the radial velocity can give the magnitude of the target's speed v and its direction θ. The measurement of tangential velocity has not been of practical interest in radar since it requires a long-baseline antenna system.

Measurements of a Distributed Target With sufficient resolution in the appropriate dimension, the size and shape of a distributed target can be ascertained. It should be recalled that resolution and accuracy are not the same. Range *resolution* requires that the entire bandwidth be occupied continuously without gaps in the signal frequency spectrum. Range *accuracy,* however, only requires, as a minimum, that there be adequate spectral energy at the two ends of the spectral bandwidth. The spectral bandwidth need not be fully occupied. This assumes that there is only one scattering object present. Resolution requires a filled spectrum; accuracy can be achieved with a thinned, or sparse, spectrum. A similar description applies in the temporal (time) domain for frequency measurement,

and in the spatial (antenna) domain for angle measurements. Generally, good resolution will provide good accuracy; but the reverse is not necessarily true since accurate measurements can be made with waveforms that do not provide good resolution.

Radial Profile The target's profile (and size) in the range dimension can be obtained when the radar's range resolution cell is smaller in size than the target's dimensions (i.e., when the scattering centers of the target can be resolved). To obtain a radial profile of a target it is required that $c\tau/2 << D$, where D = the target's radial component and τ = pulse width. Good resolution in the range dimension requires large spectral bandwidth. The radial profile of a target sometimes can be employed to obtain limited "recognition" of one type of target from another.

Tangential (Cross-Range) Profile With sufficient resolution in the angle dimension, the tangential (cross-range) profile of a distributed target can be determined. This can provide the angular size of the target and the location in angle of the scattering centers. If the range is known, the location of scatterers in the tangential dimension can be determined since the cross-range (tangential) dimension is equal to the product of range and angle (the latter in radians). Resolution in cross-range based on conventional angle measurements is generally not as good as the resolution that can be obtained in the range dimension. Synthetic aperture radar (SAR) and inverse synthetic aperture radar (ISAR), however, can provide excellent cross-range resolution without the need for large antennas. (In SAR and ISAR, the equivalent of resolution in angle may be thought of as being obtained because of resolution in the doppler frequency domain.)

Size and Shape When the tangential profile is obtained at each range resolution cell, the target image (size and shape) is formed. Imaging radars, such as SAR, ISAR, and SLAR (side-looking airborne radar), have sufficient resolution in both range and cross-range to resolve the major scatterers of a distributed target. (SLAR achieves its tangential resolution by use of a narrow beam antenna directed perpendicular to the flight direction of the aircraft carrying the radar.)

Symmetry The response of a target to changes in the polarization of the radar signal can provide a measure of the symmetry of the target. (The polarization of a radar signal is determined by the orientation of the electric field.) If a sphere (a perfectly symmetrical target) were directly viewed by a radar with a rotating linearly polarized signal, there would be no change of the echo signal when the polarization is changed. On the other hand, if the same rotating polarization radar were to view a long narrow rod, the echo would be maximum when the electric field (polarization) is parallel to the rod and minimum when it is perpendicular to the rod. By observing the variation of the amplitude of the echo signal as a function of polarization, the orientation and shape of the rod can be determined. Measurement of target symmetry using polarization is not widely used in radar; however, it is the basis for detection of aircraft (an asymmetrical target) in the presence of rain (symmetrical target) when using circular polarization (defined as the electric field rotating at the RF frequency, Sec. 7.8).

Change of Radial and Tangential Profiles Here it is assumed that the pulse is long enough so that the individual scatterers of a complex target are not resolved. If the individual scatterers of this complex target change their relative locations in range (radial profile), the echo signal will experience a change in amplitude due to constructive and destructive interference among the echo signals from the individual scatterers. Changes in the target echo amplitude, therefore, indicate there are changes in the relative locations of the individual scatterers of the complex target.

Examples of target effects that might be recognized by the amplitude modulation of the echo signal include changes in target aspect, propeller modulation, jet engine modulation, and the time-varying separation of two closely spaced, unresolved targets (such as two aircraft or an aircraft and a missile).

Surface Characteristics The dielectric constant of a target's surface material and the roughness of its surface can, in principle, be found from radar measurements. Surface roughness may be determined by varying the radar frequency and noting where the scattering changes from specular (a smooth surface) to diffuse (rough surface). This boundary depends on the size of the surface roughness relative to the radar wavelength. Surface roughness, such as the height of ocean waves (the sea state), can be found from a direct measurement with a high range-resolution radar, as has been done from space with a precision high-resolution altimeter.

The dielectric constant of the scattering surface can be found if the reflection coefficient can be measured and if the shape and roughness of the surface are known. This is practical under laboratory conditions, but difficult to apply with radar. Radar cross section measurements over a wide range of frequencies, however, were used to estimate the dielectric properties of the moon's surface (before astronauts landed on the moon and brought back rocks for laboratory analysis).[2,3]

The surface roughness and the dielectric constant are of interest for remote sensing with radar, especially from space. The former might indicate the sea state over the oceans of the world; and the latter, if it were practical, might be used to determine soil moisture, which is of interest for agriculture and hydrology. Although the radar determination of surface characteristics might be desirable, it has proven to be difficult to achieve except under limited circumstances.

6.3 THEORETICAL ACCURACY OF RADAR MEASUREMENTS

Noise is the fundamental limitation to accurate radar measurements. The theoretical aspects of the extraction of information from radar signals have benefited greatly from the theory of *statistical parameter estimation* just as the theory of detection has benefited from the statistical theory *of hypothesis testing.*[4] In this section, expressions for the theoretical accuracies of radar measurements will be presented. It is assumed that the signal-to-noise ratio is large. This is usually the case since it was found in Sec. 2.5 that large signal-to-noise ratios are required for detection of a signal. Detection must occur before

meaningful information can be extracted about a target echo. It is further assumed that the measurement error associated with a particular parameter is independent of the errors in any of the other parameters, that accuracy is limited only by receiver noise, and that all bias errors are accounted for separately. The measure of error is the root mean square (rms) of the difference between the measured (estimated) value and the true value.

The expressions given in this chapter for the theoretical rms error δM of a radar measurement M have the following form:

$$\delta M = \frac{kM}{\sqrt{2E/N_0}} \qquad [6.2]$$

where k is a constant whose value is in the vicinity of unity, E is the received signal energy, and N_0 is the noise power per unit bandwidth. The following will be shown later in this section:

- For a time-delay (range) measurement, k depends of the shape of the frequency spectrum $S(f)$, and M is the rise time of the pulse (inversely proportional to bandwidth).
- For a measurement of radial velocity based on the doppler frequency, k depends on the shape of the time waveform $s(t)$, and M is the spectral resolution (inversely related to the time duration of the signal).
- For an angle measurement, k depends on the shape of the aperture illumination $A(x)$, and M is the beamwidth.

Theoretical radar accuracies may be derived by a variety of methods such as (1) simple geometrical relationships among the signal, noise, and the parameter to be measured;[5] (2) the likelihood ratio;[6] (3) the method of inverse probability;[7] (4) a suitably selected gating function preceded by a matched filter;[8] and (5) minimization of the mean square error.[9]

The simple method (no. 1) for finding the rms error in the measurement of time delay when the waveform is a rectangular pulse will be illustrated next. This derivation takes some liberties, but it has the advantage of being easy to understand. Fortunately, the simple method and the more involved methods give similar answers for the rectangular pulse.

Time-Delay (Range) Accuracy—Simplified Method The measurement of range R is the measurement of the round-trip time delay T_R for the radar signal (waveform) to travel out to the target and back. The rms error in range is $\delta R = (c/2)\ \delta T_R$, where c is the velocity of propagation, and δT_R is the rms error in time delay. The range, or time-delay, measurement to be described here is based on locating the leading edge of the video pulse, Fig. 6.1. The video pulse uncorrupted by noise is shown by the solid curve. Its shape is not perfectly rectangular, but has finite rise and fall times. (Zero rise or fall times require infinite bandwidth.) The effect of noise added to the pulse is to shift the time of threshold crossing as shown by the dashed curve. Since large signal-to-noise ratio is assumed, the slope of the leading edge of the noise-free pulse (solid curve) can be equated to the slope of the leading edge of the pulse with noise added (dashed curve). The slope of the leading edge of a pulse of amplitude A at the output of a video filter is A/t_r, where t_r is the rise time. From Fig. 6.1, the slope of the signal plus noise (dashed curve) can be

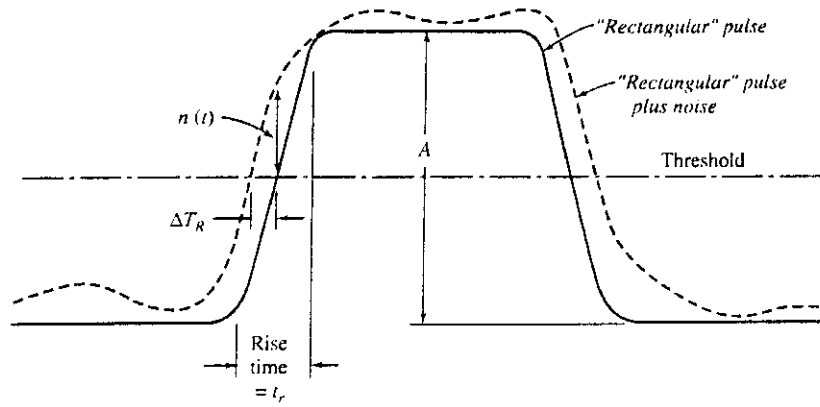

Figure 6.1 Measurement of time delay using the leading edge of the video pulse. Solid curve is the echo pulse uncorrupted by noise. Dashed curve represents signal plus noise.

written as $n(t)/\delta T_R$, where $n(t)$ is the noise voltage at the threshold crossing of the pulse, and δT_R is the error in the time-delay measurement. Equating the slope of the leading edge of the pulse without noise to the slope of the pulse with noise gives

$$A/t_r = n(t)/\Delta T_R \tag{6.3}$$

which leads to

$$[\overline{(\Delta T_R)^2}]^{1/2} = \delta T_R = \frac{t_r}{(A^2/\overline{n^2})^{1/2}} = \frac{t_r}{(2S/N)^{1/2}} \tag{6.4}$$

where $A^2/\overline{n^2}$ is the video signal-to-noise power ratio. The last part of Eq. (6.4) follows from the fact that the signal-to-noise power ratio for a rectangular video pulse is equal to $2S/N$, where S/N is the signal-to-noise power ratio of a sinewave pulse in the IF portion of the receiver. This assumes a linear detector and a large signal-to-noise ratio. Equation (6.4) indicates that accurate measurements of time delay require video pulses with short rise times and large amplitudes. The width of the pulse does not enter explicitly in this expression.

If the rise time of the video pulse is limited by the spectral bandwidth B of the rectangular-shaped IF filter, then $t_r \approx 1/B$. Letting $S = E/\tau$ and $N = N_0 B$, the error in the time delay can be written

$$\delta T_R = \left(\frac{\tau}{BE^2/N_0}\right)^{1/2} \tag{6.5}$$

where τ = pulse width, B = spectral bandwidth of the rectangular filter, E = signal energy, and N_0 = noise power per unit bandwidth. If a similar measurement of time delay is made at the trailing edge of the video pulse, and if the noise at the trailing edge is independent of the noise at the leading edge, then the two measurements can be averaged to obtain an improvement in the time-delay accuracy of $\sqrt{2}$, which gives

$$\delta T_R = \left(\frac{\tau}{4BE/N_0}\right)^{1/2} \tag{6.6}$$

The estimate of the time delay obtained by determining when either the leading edge or trailing edge of the pulse crosses a threshold, as in Fig. 6.1, will depend on the value of the threshold relative to the peak value of the pulse. The choice of threshold level is important, therefore, for consistency in accurate measurement when only the leading edge is used. It has been suggested that the bias error can be avoided by one of several methods.[10–12] One method is to use an adaptive threshold in which the level of the threshold is always a fixed fraction of the pulse amplitude. If the average of the two time delays found from both the leading and trailing edges of the pulse is used, there is no theoretical bias with change of amplitude if the pulse shape is symmetrical.

Time-Delay Accuracy and Effective Bandwidth There are several methods[6–9] based on the likelihood ratio, inverse probability, and other statistical analyses, which all lead to the following expression for the rms error in the measurement of the time delay

$$\delta T_R = \frac{1}{\beta\,(2E/N_0)^{1/2}} \qquad [6.7]$$

where E is the signal energy, N_0 is the noise power per unit bandwidth, and β is called the *effective bandwidth* and is defined as

$$\beta^2 = \frac{\int_{-\infty}^{\infty} (2\pi f)^2 |S(f)|^2\, df}{\int_{-\infty}^{\infty} |S(f)|^2\, df} = \frac{1}{E} \int_{-\infty}^{\infty} (2\pi f)^2\, |S(f)|^2\, df \qquad [6.8]$$

It has also been called the *rms bandwidth*. The effective bandwidth β is such that $(\beta/2\pi)^2$ is the normalized second moment of $|S(f)|^2$ about its mean. Equation (6.8) assumes that the mean value of $S(f)$ is at $f = 0$, where $S(f)$ is the video spectrum with negative as well as positive frequencies. The effective bandwidth β is different from other bandwidths encountered in electronic engineering. It is not related to either the half-power bandwidth or the noise bandwidth. The more the spectral energy is concentrated at the two ends of the band, the larger will be β and the more accurate will be the measurement of time delay.

The first edition (1962) of this text discussed three different methods for deriving Eq. (6.8) based on statistical concepts.[6–8] The second edition (1980) described one method to derive this equation.[8] These methods are not included in the current edition since there now appears to be less interest in the mathematical aspects of the subject. The application of Eq. (6.8), however, is important and will be discussed next.

Rectangular Pulse When the spectrum $S(f)$ of a perfectly rectangular pulse—one with zero rise time and zero fall time—is inserted in Eq. (6.8) for the effective bandwidth, the result is obtained that $\beta = \infty$. This means that $\delta T_R = 0$; hence, the measurement of the time delay can be made with zero error. It may seem strange, but it is correct for the perfectly rectangular pulse that was assumed. An infinite bandwidth implies zero rise time (infinite slope) so noise does not displace the threshold crossing in time (as it does in Fig. 6.1 for a finite rise time) and there will be no error in the delay. A perfectly rectangular

pulse, however, requires infinite bandwidth, which is not possible. Thus the bandwidth of a practical "rectangular" pulse must be finite, there will be finite rise and fall times, and the rms time-delay error will not be zero.

To obtain the effective bandwidth β for a finite-bandwidth pulse, it will be assumed that the spectrum of a perfectly rectangular IF pulse of width τ_r is limited to a finite spectral bandwidth B_s. For the time-delay measurement that uses the envelope of the IF pulse, this is equivalent to a video spectrum $S(f) = (\sin \pi f\tau_r)/\pi f\tau_r$ that is limited to a spectral width $\pm B_s/2$, as in Fig. 6.2. (The video spectrum is shown here with both negative and positive frequencies, as is required in Fourier analysis.) Although the analysis considered here is based on the video pulse of width τ_r and a low-pass filter of video bandwidth $B_s/2$, the result is the same as taking the envelope of an IF pulse of width τ_r and an IF bandpass filter of bandwidth B_s. The value of β^2 for this case is found by setting the limits of the integration in Eq. (6.8) from $-B_s/2$ to $+B_s/2$ instead of from $-\infty$ to $+\infty$, which is then

$$\beta^2 = \frac{(2\pi)^2 \int_{-B_s/2}^{B_s/2} f^2(\sin^2 \pi f\tau_r)/\pi^2 f^2 \, df}{\int_{-B_s/2}^{B_s/2} (\sin^2 \pi f\tau_r)/\pi^2 f^2 \, df} = \frac{1}{\tau_r^2} \frac{\pi B_s\tau_r - \sin \pi B_s\tau_r}{\text{Si}(\pi B_s\tau_r) + (\cos \pi B_s\tau_r - 1)/\pi B_s\tau_r} \quad [6.9]$$

where $\text{Si}(x)$ is the *sine integral* function defined by $\int_0^x (\sin u)/u \, du$. For large $B_s\tau_r$ in Eq. (6.9), the product $\beta^2\tau_r^2 \to 2B_s\tau_r$, or

$$\beta^2 \approx \frac{2B_s}{\tau_r} \approx \frac{2}{\tau_r t_r} \qquad \text{for large } B_s\tau_r \quad [6.10]$$

It was assumed in Eq. (6.10) that the rise time t_r of the pulse is approximately the inverse of the spectral bandwidth B_s (the total width of the spectrum, not the half-power bandwidth).

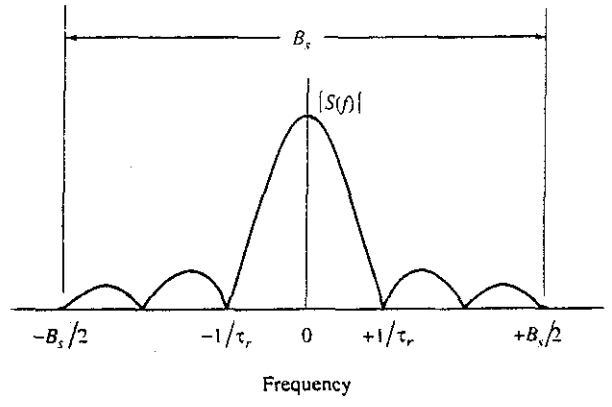

Figure 6.2 Spectrum $[(\sin \pi f\tau_r)/\pi f\tau_r]$ of a rectangular pulse of width τ_r shown limited to a spectral extent of $\pm B_s/2$.

Substituting this expression for β^2 into Eq. (6.7) gives the rms error in time delay as

$$\delta T_R = \left(\frac{\tau_r}{4B_s E/N_0}\right)^{1/2} = \left(\frac{t_r \tau_r}{4E/N_0}\right)^{1/2} \qquad \text{rectangular pulse, } B_s\tau_r >> 1 \qquad [6.11]$$

This applies for large $B_s\tau_r$, or when the rise time is small compared to the pulse width. Note that Eq. (6.11), derived in a totally different manner, is the same as Eq. (6.6) except for denoting the spectral bandwidth in Eq. (6.11) as B_s instead of B and the pulse width as τ_r instead of τ.

The value of $\beta = (2B_s/\tau_r)^{1/2}$ for a long rectangular pulse of fixed bandwidth B_s (or fixed rise time) decreases with increasing pulse width τ_r. Thus if the total energy remains the same, the time-delay accuracy decreases (becomes worse) with increasing pulse width even though the rise time remains the same.

It is not often that $B_s\tau_r >> 1$ in radar applications. Next, the more usual case is examined, where the product of half-power bandwidth and pulse width is approximately unity.

Quasi-Rectangular Pulse As before, we start with a perfectly rectangular pulse of width τ_r. The spectral extent B_s is assumed in Fig. 6.2 to be limited to the main portion of the rectangular video pulse spectrum that lies between the first nulls at $-1/\tau_r$ and $+1/\tau_r$ on either side of the spectrum peak at $f = 0$. (As mentioned, integration over negative as well as positive frequencies has to be considered in Fourier analysis). Thus the IF spectral bandwidth extent is $B_s = 2/\tau_r$. The half-power bandwidth is $B \approx B_s/2$; or $B \approx 1/\tau_r$. (The product of the half-power bandwidth B and the width τ_r of a rectangular pulse is actually equal to 0.886; but, for convenience, it is usually "rounded off" to unity. This is more like the usual case in radar where $B\tau \approx 1$.) The solid curve of Fig. 6.3 shows the pulse shape that

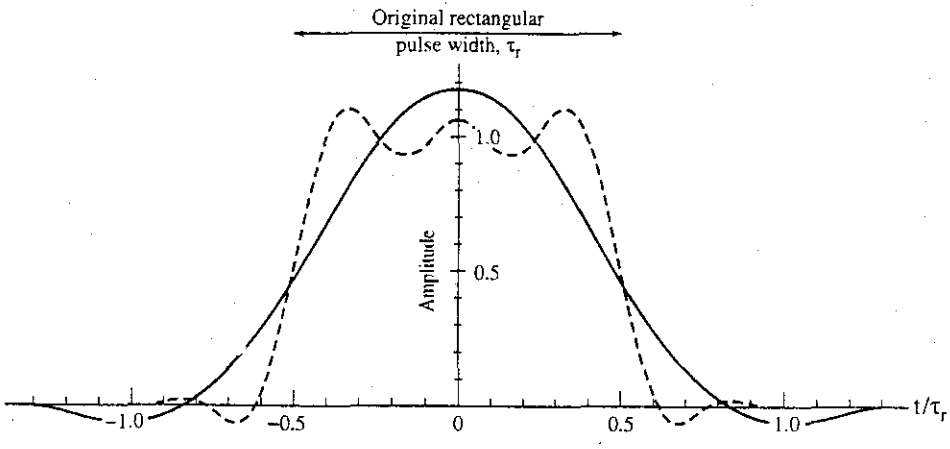

Figure 6.3 Solid curve is the theoretical waveform out of a low-pass rectangular filter of bandwidth $B_v = B_s/2 = 1/\tau_r$ when the input is a rectangular pulse of width τ_r. It is the same as the envelope out of an IF filter of bandwidth $B_s = 2/\tau_r$ when the input is a rectangular pulse of sinewave of width τ_r. In the text this is called a *quasi-rectangular pulse*. The dashed curve applies for $B_s = 6/\tau_r$.

emerges from the video low-pass filter of bandwidth $B_s/2$, which corresponds to an IF filter with bandwidth B_s. Although Fig. 6.3 doesn't resemble a perfectly rectangular pulse, it will be called the *quasi-rectangular pulse.* It is not unusual for a pulse radar to radiate a similar-looking waveform when it is thought that a "rectangular" pulse is being generated. (A rounded pulse is often used in radar since it produces less out-of-band interference to other users of the electromagnetic spectrum.) Substituting $B_s\tau_r = 2$ into Eq. (6.9), we get that $\beta\tau_r$ is very close to 2.1; which, when inserted into Eq. (6.7), gives the rms time-delay error as

$$\delta T_R = \frac{\tau_r}{2.1(2E/N_0)^{1/2}} \qquad \text{quasi-rectangular pulse, } B\tau_r \approx 1 \qquad [6.12]$$

This expression for the rms time-delay error is considered here to be representative of a conventional pulse typically used in radar. Since the rectangular IF filter is of bandwidth $B_s = 2/\tau_r$, then $\beta = 1.05B_s$. In terms of the half-power bandwidth B of the IF spectrum, $\beta = 2.4B$ when $B\tau_r = 0.886$, or $\beta \approx 2.1B$ when $B\tau \approx 1$. The dashed curve in Fig. 6.3 for $B_s\tau_r = 6$ is shown to indicate the shorter rise time of the pulse when the bandwidth B_s is much wider than the quasi-rectangular pulse.

The symbol τ_r was used for the pulse width in the above analysis instead of τ to indicate it was the width of the perfectly rectangular pulse before it is passed through a rectangular IF filter of bandwidth B_s (or video bandwidth $B_s/2$). If τ denotes the half-power pulse width that emerges from a filter of bandwidth $B_s = 2/\tau_r$, then $\tau = 0.625\tau_r$. The effective bandwidth in this case is $\beta = 1.3/\tau$.

Trapezoidal Pulse A rectangular pulse is sometimes approximated by a trapezoidal pulse with finite rise and fall times. If the width across the top of the trapezoid is τ_p and if the rise and fall times are t_r, then the rms error in time-delay measurement is

$$\delta T_R = \left(\frac{3\tau_p t_r + 2t_r^2}{12E/N_0}\right)^{1/2} \qquad \text{trapezoidal pulse} \qquad [6.13]$$

When the rise time t_r is small compared to the width τ_p of the top of the trapezoid, Eq. (6.13) becomes

$$\delta T_R = \left(\frac{\tau_p t_r}{4E/N_0}\right)^{1/2} \qquad t_r << \tau_p \qquad [6.14]$$

which is the same as Eq. (6.11) for the rectangular pulse with short rise time. Note that the larger the width τ_p, the poorer is the accuracy.

Triangular Pulse When $\tau_p = 0$ in Eq. (6.13), the pulse is triangular and its base $= 2t_r = \tau_B$. The rms error becomes

$$\delta T_R = \frac{\tau_B}{12^{1/2}(2E/N_0)^{1/2}} \qquad \text{triangular pulse} \qquad [6.15]$$

In terms of the half-power bandwidth B of the $(\sin^2 x)/x^2$ spectrum of a triangular pulse (where $x = \pi f\tau_B/2$), the effective bandwidth $\beta = 2.72\ B$.

With a triangular or rounded pulse (such as the quasi-rectangular, gaussian, or $(\sin x)/x$ time waveforms) the time delay might be found by differentiating the pulse waveform and selecting the time at which $s'(t)$ goes through zero (which is the point at which the amplitude of $s(t)$ is a max).

Gaussian Pulse Consider a pulse described by the gaussian function

$$s(t) = \exp\left(-\frac{1.38t^2}{\tau^2}\right) \qquad [6.16]$$

where τ in this case is the half-power pulse width. Its rms time-delay error is

$$\delta T_R = \frac{\tau}{1.18(2E/N_0)^{1/2}} = \frac{1.18}{\pi B(2E/N_0)^{1/2}} \qquad \text{gaussian pulse} \qquad [6.17]$$

where B is the half-power bandwidth of the gaussian-pulse spectrum.

Cosine Pulse The positive half of one cycle of a cosine also can represent practical radar pulses. Its time waveform is $\cos(\pi t/\tau_B)$, where τ_B is the width of the base. Its effective bandwidth is $\beta = \pi/\tau_B = 2.64B$, where B = half-power bandwidth. The parabolic pulse, given by $s(t) = 1 - 4t^2/\tau_B^2$, is similar in shape and has $\beta = 3.16/\tau_B$.

Pulse with Uniform Spectrum The effective bandwidth of a waveform with a uniform spectrum of width B_u is $\beta = \pi B_u/\sqrt{3}$. The time waveform is of the form $(\sin \pi B_u t)/\pi B_u t$. The rms time-delay error is

$$\delta T_R = \frac{\sqrt{3}}{\pi B_u(2E/N_0)^{1/2}} \qquad \frac{\sin \pi B_u t}{\pi B_u t} \text{ waveform} \qquad [6.18]$$

The above applies to a linear-FM pulse-compression waveform with large time-bandwidth product.

Minimum Error Examination of the integral in the numerator of the expression for β^2 in Eq. (6.8) indicates that a large value of β requires that the spectral energy be concentrated at the extremes of the spectral bandwidth [note that the origin is at the mean value of $S(f)$]. Consider, therefore, a spectrum with its entire energy concentrated in delta functions at both ends of the video spectrum, such as $S(f) = \delta(f + B_s/2) + \delta(f - B_s/2)$. Substitution of this spectrum into Eq. (6.8) yields $\beta = \pi B_s$. This is the largest value of β that can be obtained for a spectrum occupying a bandwidth B_s. The time waveform corresponds to two sinewaves, each of infinite duration, separated in frequency by B_s. (The time duration of the waveform, of course, cannot be infinite. The result is approximately the same, however, if the time duration τ is such that $1/\tau << B_s$.) This waveform, however, results in range ambiguities that have to be resolved. It does not work when multiple unresolved targets are present.

Two CW waveforms separated in frequency by B have been considered in the past for measurement of range by determining the phase difference between them.[13,14] The phase difference $\Delta\phi$ between the two frequencies separated by B gives the time delay as

$$T_R = \frac{\Delta\phi}{2\pi B} \qquad [6.19]$$

The error in time delay, δT_R, based on the theoretical error in phase $\delta\phi$ [which is $\delta\phi = (2S/N)^{-1/2}$] from each of the two sine waves (with each having one half the total energy) results in the same value of $\beta = \pi B$ as found above by substituting the two delta-function spectrum into Eq. (6.8).

The two-frequency CW waveform might have a higher effective bandwidth than the others (and better time-delay accuracy), but it is inconvenient to use because of ambiguities. In practical embodiments of this method of range measurement, four or five frequencies have been used to resolve the ambiguities and achieve good accuracy.[15]

Other Considerations In the expression for time-delay error as given by Eqs. (6.7) and (6.8), the energy E appears as a normalizing factor in the effective bandwidth β. It also appears in the signal-to-noise energy ratio ($2E/N_0$). The energy cancels, and the rms time-delay error can be written as

$$\delta T_R = \left(\frac{N_0}{2\int_{-\infty}^{\infty} (2\pi f)^2 |S(f)|^2 \, df} \right)^{1/2} \qquad [6.20]$$

The integral in the denominator also can be expressed as

$$\beta^2 E = \int_{-\infty}^{\infty} [s'(t)]^2 \, dt = -\int_{-\infty}^{\infty} s''(t) s(t) \, dt \qquad [6.21]$$

The energy E does not appear in the right-hand side of this equation for $\beta^2 E$ since $\beta^2 \sim 1/E$. When calculating β, the expressions of Eq. (6.21) sometimes are easier to compute than the integral of Eq. (6.8). Equation (6.21) implies that accurate time delay is obtained with waveforms having large first derivatives over the time duration of the signal.

Table 6.1 lists the effective bandwidths β for the various waveforms considered here. There is not much difference in β among the various waveforms in this table. One might, therefore, not be too concerned about which waveform ought to be chosen based on time-delay accuracy alone. The triangular waveform has a large theoretical accuracy, but the discontinuity of the slope at the middle of the pulse presents practical problems in its generation. The values of β for the "rounded" pulses (gaussian, cosine, and quasi-rectangular) are not much lower than the triangular, and they are better representations of the shape of practical radar pulses. Radar pulses are almost always band-limited and are, therefore, rounded rather than appear as the perfectly rectangular pulses as sometimes seen in textbooks. The cosine seems a good compromise choice as typical of these rounded waveforms. The uniform spectrum, such as that of the linear-FM pulse-compression waveform, is about 2/3d less accurate than the rounded pulse if its spectral extent B equals the half-power bandwidth of the rounded pulse, but this is not much of a difference.

Accuracy of Frequency and Radial Velocity The measurement of frequency in radar is that of the doppler frequency shift. As mentioned previously, the radial component v_r of velocity can be found from the doppler frequency shift $f_d = 2v_r/\lambda$, where λ is the radar

Table 6.1 Effective Bandwidth β for Various Waveforms

Description	Time Waveform $s(t)$	Effective Bandwidth β
Gaussian pulse	$\exp(-1.38t^2/\tau^2)$	2.66 B, or $1.18/\tau$
Cosine pulse	$\cos(\pi t/\tau_B)$	2.64 B, or $3.14/\tau_B$
Triangular pulse	$(2t/\tau_B) + 1 \quad -\tau_B/2 < t < 0$ $-(2t/\tau_B) + 1 \quad 0 < t < \tau_B/2$	2.72 B, or $3.46/\tau_B$
Quasi-rectangular* $B_s\tau_r = 2$; $B\tau_r = 0.886$	$\text{Si}[\pi(B_s t + 1)] - \text{Si}[\pi(B_s t - 1)]$	2.38 B, or $2.1/\tau_r$, or $1.3/\tau$
Uniform spectrum of width B_u	$(\sin \pi B_u t)/\pi B_u t$	1.8 B_u, or $2.04/\tau$
Band-limited, rectangular pulse; $B_s\tau_r >> 1$	$\text{Si}[\pi B_s(t + \tau_r/2)] - \text{Si}[\pi B_s(t - \tau_r/2)]$	$1.4\sqrt{B_s/\tau_r}$
2 CW sinewaves separated by B_s	video spectrum: $\delta(f + B_s/2) + \delta(f - B_s/2)$	3.14 B_s

B_s = spectral extent, B = half-power bandwidth, τ = half-power pulsewidth, τ_r = width of original rectangular pulse, τ_B = extent of pulse (at its base), Si $[X]$ = sine integral function of X.

*Considered to be typical of many pulse waveforms.

wavelength. The rms error in radial velocity is $\delta v_r = (\lambda/2)\,\delta f_d$, where δf_d is the rms error in the doppler frequency.

Using the method of inverse probability, Roger Manasse[16] showed that the rms error in the measurement of frequency is

$$\delta f = \frac{1}{\alpha\,(2E/N_0)^{1/2}} \qquad [6.22]$$

where

$$\alpha^2 = \frac{\int_{-\infty}^{\infty} (2\pi t^2) s^2(t)\,dt}{\int_{-\infty}^{\infty} s^2(t)\,dt} \qquad [6.23]$$

and $s(t)$ is the input signal as a function of time. Note the similarity of this expression for δf and that of δT_R in Eq. (6.7), as well as the similarity in the expressions for α and β. The parameter α is the *effective time duration* of the signal, and $(\alpha/2\pi)^2$ is the normalized second moment of $s^2(t)$ about the mean epoch, taken to be $t = 0$. [If the mean is not zero, but is some other value, t_0, the integrand in the numerator of Eq. (6.23) would be $(2\pi)^2(t - t_0)^2 s^2(t)$.]

Rectangular Pulse The value of α^2 for a perfectly rectangular pulse of width τ is found to be $\pi^2\tau^2/3$; thus the rms frequency error is

$$\delta f = \frac{\sqrt{3}}{\pi\tau(2E/N_0)^{1/2}} \qquad \text{rectangular pulse} \qquad [6.24]$$

The longer the pulse, the more accurate is the frequency measurement. This expression can also be applied to a frequency measurement made by a CW radar since the observation time over which the CW measurement is made is equivalent to the pulse duration τ.

Quasi-Rectangular Pulse For the bandwidth-limited rectangular pulse of Fig. (6.2), the value of α^2 is

$$\alpha^2 = \frac{\pi^2\tau_r^2}{3} \frac{\text{Si}\,(\pi B_s\tau_r) + \dfrac{\cos(\pi B_s\tau_r) - 3}{\pi B_s\tau_r} - \dfrac{2\sin\pi B_s\tau_r}{(\pi B_s\tau_r)^2} - \dfrac{8[\cos(\pi B_s\tau_r) - 1]}{(\pi B_s\tau_r)^3}}{\text{Si}\,(\pi B_s\tau_r) + [\cos(\pi B_s\tau_r) - 1]/\pi B_s\tau_r} \qquad [6.25]$$

where τ_r is the width of a rectangular pulse that is passed through a rectangular filter of bandwidth B_s, and Si (x) is the sine integral function of x. In the limit as $B_s\tau_r \to \infty$, α^2 approaches $\pi^2\tau_r^2/3$, which is the same as that obtained for the perfectly rectangular pulse.

In the discussion of the rms error in time delay given previously, a *quasi-rectangular pulse* with $B_s\tau_r = 2$ was considered. For this case, Eq. (6.25) gives $\alpha = 1.6\tau_r$, where τ_r is the width of the rectangular pulse before passing through a rectangular filter of bandwidth B_s. The half-power width τ after the pulse passes through the band-limited filter is $0.625\tau_r$, so that $\alpha = 2.6\tau$.

The value of α for a perfectly rectangular pulse is finite even though the value of β for a perfectly rectangular pulse was found to be infinite. The effective time duration α will be infinite, however, for a waveform that has a perfectly rectangular frequency spectrum of width B. Such a spectrum corresponds to a $(\sin x)/x$ time waveform of infinite duration, where $x = \pi Bt$. Any practical waveform must be limited in time, and α will therefore be finite. The frequency error for a time-limited waveform with a rectangular-like spectrum may be found in a manner similar to that which was employed for finding the time-delay error of a band-limited rectangular pulse. The $(\sin x)/x$ time waveform is limited to a duration T_s just as the $(\sin x)/x$ spectral bandwidth was limited to a bandwidth B_s. The frequency error can be found from Eq. (6.11) except the roles of bandwidth and frequency are reversed. In Eq. (6.11), replace the time-delay error δT_R with δf, replace the pulse width τ_r with the bandwidth B, and replace the bandwidth B_s with the signal duration T_s.

Trapezoidal Pulse The theoretical rms error for the measurement of frequency with a trapezoidal pulse is

$$\delta f = \frac{(3\tau_p + 2t_r)^{1/2}}{2\pi\left(\dfrac{\tau_p^3}{4} + \dfrac{\tau_p^2 t_r}{2} + \dfrac{\tau_p t_r^2}{2} + \dfrac{t_r^3}{5}\right)^{1/2}\left(\dfrac{2E}{N_0}\right)^{1/2}} \qquad \text{trapezoidal pulse} \qquad [6.26]$$

where the rise and fall time is t_r and the width across the top of the trapezoid is τ_p. Assuming, for example, that $t_r = \tau_p/2$, the value of α would be $0.81\pi\tau_p$. When t_r is small compared to τ_p, the value of α approaches $\pi\tau_p/\sqrt{3}$, which is the value found in the above for the perfectly rectangular pulse.

Triangular Pulse This is obtained from the expression for the trapezoidal pulse by setting $\tau_p = 0$ and letting $2t_r = \tau_B$, where τ_B = width of the base of the triangular waveform. This results in

$$\delta f = \frac{(10)^{1/2}}{\pi\tau_B(2E/N_0)^{1/2}} \qquad \text{triangular pulse} \qquad \textbf{[6.27]}$$

Gaussian Pulse The rms error in frequency for a gaussian pulse is

$$\delta f = \frac{1.18}{\pi\tau(2E/N_0)^{1/2}} = \frac{B}{1.18(2E/N_0)^{1/2}} \qquad \text{gaussian pulse} \qquad \textbf{[6.28]}$$

where τ = half-power pulse width and B = half-power bandwidth.

Multiple Observations The error expressions for time delay and frequency presented here apply for a single observation. When more than one independent measurement is made, the resultant error is reduced and may be found by combining errors in the usual manner for gaussian statistics: the variance (the square of δT_R or δf) of the N independent observations is equal to $1/N$ of the variance of a single observation. Alternatively, the expression for a single pulse applies to multiple pulses if the energy E is the total energy of N pulses. The above assumes that the effective bandwidth β or the effective time-duration α remains the same for each of the N measurements.

Certainty of the Uncertainty Principle The product of the effective bandwidth and the effective time-duration α must be equal to or greater than π; that is,

$$\beta\alpha \geq \pi \qquad \textbf{[6.29]}$$

This relation may be derived from the definitions of β and α given by Eqs. (6.8) and (6.23) and by applying the Schwartz inequality Eq. (5.11). It is a consequence of the Fourier-transform relationship between a time waveform and its spectrum. The longer the time duration of a waveform, the narrower will be its spectrum. The wider the spectrum, the narrower will be the time waveform. Both the time waveform and its frequency spectrum cannot be made arbitrarily small simultaneously.

Equation (6.29) has sometimes been referred to as the *radar uncertainty principle* because of its supposed analogy to the important concept in quantum physics known as the Heisenberg uncertainty principle. The physics uncertainty principle states that both the position and velocity of an object (such as a subatomic particle) cannot be measured exactly at the same time.[17] Equation (6.29) actually has the opposite interpretation for radar

signals, and it is inappropriate to refer to it as a radar uncertainty principle. It follows from this equation that there is no theoretical restriction on accuracy with which a radar can simultaneously locate the position of a target and determine its velocity. The product of the rms time-delay error, Eq. (6.7), and the rms frequency error, Eq. (6.22), is

$$\delta T_R \delta f = \frac{1}{\beta\alpha(2E/N_0)} \qquad [6.30]$$

Substituting the inequality of Eq. (6.29) into the above gives

$$\delta T_R \delta f \leq \frac{1}{\pi(2E/N_0)} \qquad [6.31]$$

This states that the time delay and the frequency may be simultaneously measured to as small a theoretical error as one desires by designing the radar to yield a sufficiently large ratio of signal energy (E) to noise power per unit bandwidth (N_0), or for fixed E/N_0, to select a waveform with a large $\beta\alpha$ product. Large $\beta\alpha$ requires waveforms with long time duration and wide spectral width. In terms of range accuracy δR and radial-velocity accuracy δv_r, the expression of Eq. (6.31) can be written

$$\delta R \delta v_r \leq \frac{c\lambda}{4\pi(2E/N_0)} \qquad [6.32]$$

where λ = radar wavelength and c = velocity of propagation. This states that the shorter the wavelength, the better will be the accuracy that can be achieved in the simultaneous measurement of range and radial velocity.

There is nothing "uncertain" about the simultaneous radar measurement of range and radial velocity. The radar "uncertainly relation" and the physics uncertainty principle that describes quantum mechanical effects should not be confused. In quantum mechanics, the observer does not have control over the waveform with which the quantum particle is being observed. The radar engineer, on the other hand, can choose the value of the $\beta\alpha$ product, the signal energy E, and to some extent the noise density N_0. Any limits to classical radar measurement accuracies are practical ones.

The use of the Schwartz inequality in deriving Eq. (6.29) shows that the poorest waveform for obtaining accurate time-delay and frequency measurements simultaneously is the one for which $\beta\alpha = \pi$ (the smallest theoretical value allowed for $\beta\alpha$). This corresponds to the gaussian-shaped pulse. The quasi-rectangular pulse has $\beta\alpha = 1.22\pi$, and the trapezoidal pulse with rise time $t_r = \tau_p/2$ has $\beta\alpha = 1.4\pi$. Thus there is not much difference in the $\beta\alpha$ products of simple-shape waveforms. Large values of $\beta\alpha$ require internal modulation of the pulse to make the bandwidth much greater than the reciprocal of the pulse width. This is what is done in pulse compression waveforms, to be discussed later in this chapter (Sec. 6.5).

Angular Accuracy The expression for the theoretical accuracy with which an antenna can measure the angle of arrival follows from the above discussion of accuracy for the time-delay measurement. This is possible because of the similarity of the mathematics in

the spatial (angle) and spectral (frequency) domains. The one-dimensional electric-field strength pattern of an antenna in one plane is given in Chap. 9 as

$$g(\theta) = \int_{-D/2}^{+D/2} A(z) \exp\left(j2\pi \frac{z}{\lambda} \sin\theta\right) dz \qquad [6.33]$$

where the antenna is of length D and lies along the z-axis, $A(z)$ is the distribution of the current across the aperture (called the *aperture illumination*), λ = radar wavelength, and θ = angle measured from broadside ($\theta = 0$ is the perpendicular to the antenna). This is an inverse Fourier transform and resembles the inverse Fourier transform between the time waveform $s(t)$ and the spectrum $S(f)$.

$$s(t) = \int_{-\infty}^{\infty} S(f) \exp(j2\pi ft)\, df \qquad [6.34]$$

The antenna pattern $g(\theta)$ can be related to the time waveform $s(t)$, the aperture illumination $A(x)$ to $S(f)$, $\sin\theta$ to the time t, and the aperture coordinate z/λ can be related to the frequency f. What is learned about signals in the frequency domain often can be applied to signals in the spatial domain—and vice versa. Using the above analogies, the rms error for an angle measurement can be obtained from Eqs. (6.7) and (6.8) as

$$\delta\theta = \frac{1}{\gamma(2E/N_0)^{1/2}} \qquad [6.35]$$

where the effective aperture width γ is defined as

$$\gamma^2 = \frac{\int_{-\infty}^{\infty} (2\pi z/\lambda)^2 |A(z)|^2\, dz}{\int_{-\infty}^{\infty} |A(z)|^2\, dz} \qquad [6.36]$$

The effective aperture width is 2π times the square root of the normalized second moment of $|A(z)|^2$ about the mean value of z. The mean is at $z = 0$.

The theoretical angle-measurement error for an antenna with a uniform (rectangular) amplitude illumination across the aperture is

$$\delta\theta = \frac{\sqrt{3}\lambda}{\pi D(2E/N_0)^{1/2}} = \frac{0.628\theta_B}{(2E/N_0)^{1/2}} \qquad [6.37]$$

where the far-right expression uses the relation that the half-power beamwidth for this aperture illumination is $\theta_B = 0.88\lambda/D$. The units of $\delta\theta$ and θ_B are radians. With a cosine illumination $A(z) = \cos(\pi z/D)$ across the aperture of dimension D (where $|z| \leq D/2$), the effective aperture width γ is $1.13D/\lambda$, or $1.37/\theta_B$. A triangular illumination has $\gamma = 0.99D/\lambda$; and for a parabolic illumination, $\gamma = 0.93D/\lambda$.

Commonality of Measurements The measurements of range, angle, and radial velocity are all carried out differently in radar, but they share the concept of locating the maximum of a time waveform similar to that in Fig. 6.4. This figure might represent the radar echo time-waveform and the measurement of time delay (range); or it might represent a

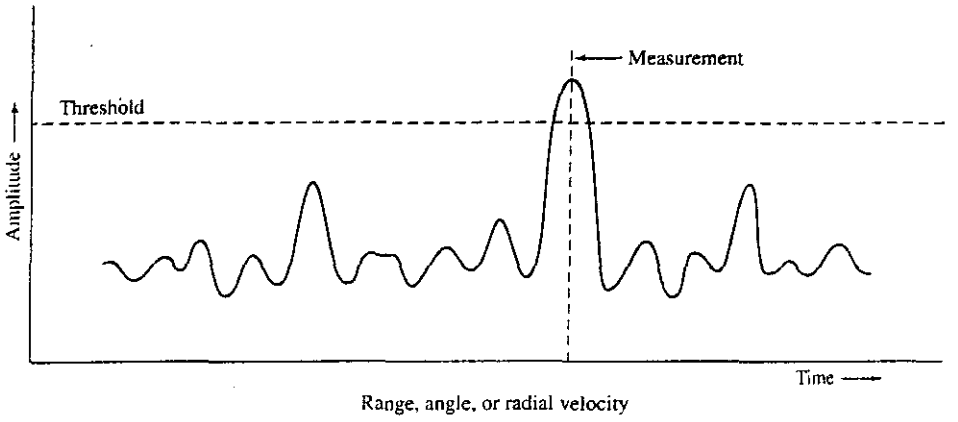

Figure 6.4 Representation of the radar measurement of range, angular location, or radial velocity by observing the waveform as a function of time, angle, or frequency.

scanning antenna pattern and the measurement of angle; or it might be the doppler frequency as observed at the output of a tunable filter that provides the radial velocity. The range, angle, or radial velocity is determined when the "signal" is a maximum.

6.4 AMBIGUITY DIAGRAM

It was mentioned in Sec. 5.2 that the output of the matched filter is the cross correlation between (1) the received signal plus noise and (2) a replica of the transmitted signal. When the signal-to-noise ratio is large (as it must be for detection), the output of the matched filter can usually be approximated by the *autocorrelation function* of the transmitted signal; that is, the noise is ignored. This assumes there is no doppler shift so that the received echo signal has the same frequency as the transmitted signal. In many radar applications, however, the target is moving so that its echo signal has a doppler frequency shift. The output of the matched filter, therefore, will not be the autocorrelation function of the transmitted signal. Instead, it must be considered as the cross correlation between the doppler-shifted received signal and the transmitted signal, with noise being ignored since the signal-to-noise ratio is assumed to be large.

The nature of the matched-filter output as a function of both time and doppler frequency is important for understanding the properties of a radar waveform, in particular its effect on measurement accuracy, target resolution, ambiguities in range and radial velocity, and the response to clutter. These aspects of the matched-filter output are examined next.

When the received echo signal is large compared to noise, the output of the matched filter [Eq. (5.17)] may be written as the following cross-correlation function:

$$\text{output of the matched filter} = \int_{-\infty}^{\infty} s_r(t)s^*(t - T_R')\,df \qquad [6.38]$$

where $s_r(t)$ is the received echo signal, $s(t)$ is the transmitted signal, $s^*(t)$ is its complex conjugate, and T'_R is the estimate of the time delay (considered a variable). Complex notation is assumed, so that the transmitted signal can be written as $u(t) \exp [j2\pi f_0 t]$, where $u(t)$ is the complex modulation function whose magnitude $|u(t)|$ is the envelope of the real signal, and f_0 is the carrier frequency. The received echo signal $s_r(t)$ is assumed to be the same as that transmitted, except for a doppler frequency shift f_d and a delay equal to the true time delay T_0. Therefore,

$$s_r(t) = u(t - T_0) \exp [j2\pi(f_0 + f_d)(t - T_0)] \qquad [6.39]$$

(The change of amplitude due to the factors in the radar equation is ignored here.) With the above definitions, the output of the matched filter is

$$\text{output} = \int_{-\infty}^{\infty} u(t - T_0)u^*(t - T'_R)e^{j2\pi(f_0+f_d)(t-T_0)}e^{-j2\pi f_0(t-T'_R)}\,dt \qquad [6.40]$$

For simplicity in understanding this equation, we take the origin to be the true time delay and the transmitted frequency; hence, $T_0 = 0$ and $f_0 = 0$. Then $T_0 - T'_R = -T'_R = T_R$. The output of the matched filter is then

$$\chi(T_R, f_d) = \int_{-\infty}^{\infty} u(t)u^*(t + T_R)e^{j2\pi f_d t}\,dt \qquad [6.41]$$

A positive time delay T_R indicates a target beyond the true target time delay T_0, and a positive doppler frequency f_0 indicates an approaching target.[18,19] The squared magnitude of Eq. (6.41), $|\chi(T_R, f_d)|^2$, is called the *ambiguity function*. Its three-dimensional plot as a function of time delay T_R and doppler frequency f_d is the *ambiguity diagram*.[20]

Properties of the Ambiguity Diagram The ambiguity function $|\chi(T_R, f_d)|^2$ has the following properties:

$$\text{maximum value: } |\chi(T_R, f_d)|_{\max}{}^2 = |\chi(0,0)|^2 = (2E)^2 \qquad [6.42]$$

$$\text{symmetry relation: } |\chi(-T_R, -f_d)|^2 = |\chi(T_R, f_d)|^2 \qquad [6.43]$$

$$\text{behavior on } T_R \text{ axis: } |\chi(T_R, 0)|^2 = \left|\int u(t)u^*(t + T_R)\,dt\right|^2 \qquad [6.44]$$

$$\text{behavior on } f_d \text{ axis: } |\chi(0, f_d)|^2 = \left|\int u^2(t)e^{j2\pi f_d t}\,dt\right|^2 \qquad [6.45]$$

$$\text{volume under surface: } \int\int |\chi(T_R, f_d)|^2\,dT_R\,df_d = (2E)^2 \qquad [6.46]$$

Equation (6.42) states that the maximum value of the ambiguity function occurs at the origin, which is the true location of the target when the doppler shift $f_d = 0$. Its maximum value is $(2E)^2$, where E is the energy contained in the echo signal. Equation (6.43) is a symmetry relation. Equation (6.44) is the form of the ambiguity function on the time-delay axis. It is the square of the autocorrelation function of $u(t)$. Equation (6.45) describes the behavior on the frequency axis and is the square of the inverse fourier transform of $[u(t)]^2$. The total volume under the ambiguity diagram is given by Eq. (6.46) and is a constant, also equal to $(2E)^2$. (All limits in the above equations go from $-\infty$ to $+\infty$.)

"Ideal" Ambiguity Diagram If there were no theoretical restrictions, the "ideal" ambiguity diagram would consist of a single peak of infinitesimal thickness at the origin and be zero everywhere else, as shown in Fig. 6.5. It would be an impulse function and have no ambiguities in range or doppler frequency (radial velocity). The infinitesimal (or very small) thickness at the origin would permit the time delay and/or frequency to be determined simultaneously to as high a degree of accuracy as desired. It would also permit the resolution of two very closely spaced targets and reject all clutter other than clutter at the origin. There would be no ambiguous responses. Such a highly desirable ambiguity diagram, however, is not theoretically allowed. It cannot be obtained because Eq. (6.42) requires that the maximum of the ambiguity diagram be equal to $(2E)^2$ and the volume under its surface as given by Eq. (6.46) also must be equal to $(2E)^2$.

The restrictions on the ambiguity diagram may be considered by imagining a box of sand.[21] The total amount of sand in the box is fixed, just as the volume under the ambiguity diagram is fixed at $(2E)^2$ by the signal energy E. The sand may be piled up in the center of the box (the origin of the ambiguity diagram), but its height can be no greater than $(2E)^2$. If one tries to pile sand at the center of the box in a very narrow pile (to obtain good accuracy and resolution), the sand that remains must be redistributed elsewhere in the box. Sand might then pile up in other parts of the box, which means ambiguities in range and/or doppler can result. Thus the nature of the ambiguity diagram indicates there have to be trade-offs made among the resolution, accuracy, and ambiguity.

An approximation to what might seem to be a good ambiguity diagram is shown in Fig. 6.6. The waveform does not result in ambiguities since there is but a single peak. In general, when a single peak is obtained, such as shown here, it might be so wide along the time-delay axis and the doppler-frequency axis that it might have poor accuracy and resolution. It appears that, in practice, waveforms generally have significant response somewhere in the ambiguity diagram outside the narrow region in the near vicinity of the origin. Practical waveforms do not approximate the ideal ambiguity diagram or even its more realistic version of Fig. 6.6.

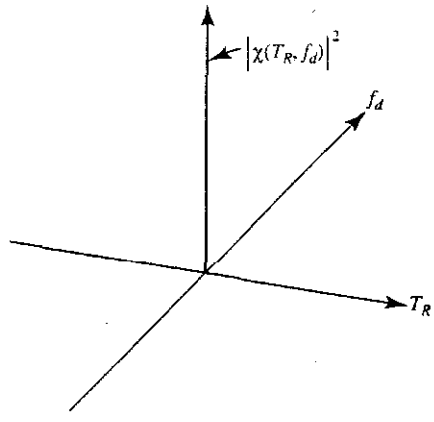

Figure 6.5 Ideal, but unattainable, ambiguity diagram.

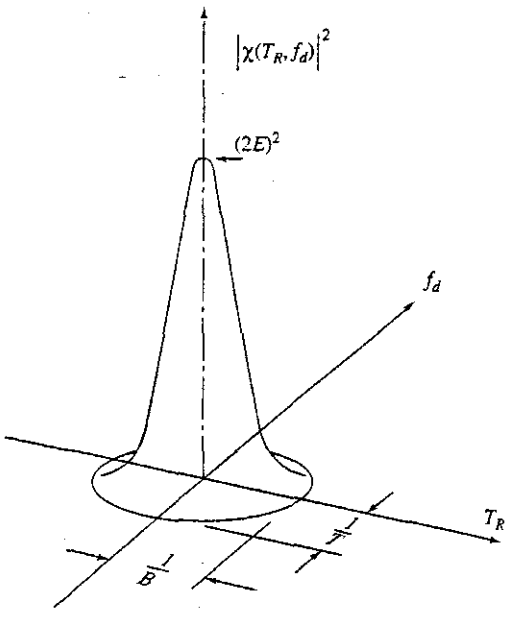

Figure 6.6 An approximation to the ideal ambiguity function with the restriction that the value at the origin is constant at $(2E)^2$ and the volume under the surface of $|\chi(T_R, f_d)|^2$ also is given by $(2E)^2$.

Single Pulse of Sinewave and the Ridge Ambiguity Diagram A computer-generated 3-D plot of $\chi|T_R, f_d|$ for a single rectangular pulse of width τ is shown in Fig. 6.7, due to A. W. Rihaczek and R. L. Mitchell. (Note that it is the magnitude of the square root of ambiguity function that is plotted here.) The triangular shape of the output of the matched filter on the time axis ($f_d = 0$) can be seen as well as the $(\sin x)/x$ shape on the frequency axis.

The essence of the information found from an ambiguity diagram can usually be obtained from simpler two-dimensional plots, as in Fig. 6.8 for (a) a long pulse of width τ and (b) for a short pulse. Shading is used to indicate the regions where $|\chi(T_R, f_d)|^2$ is

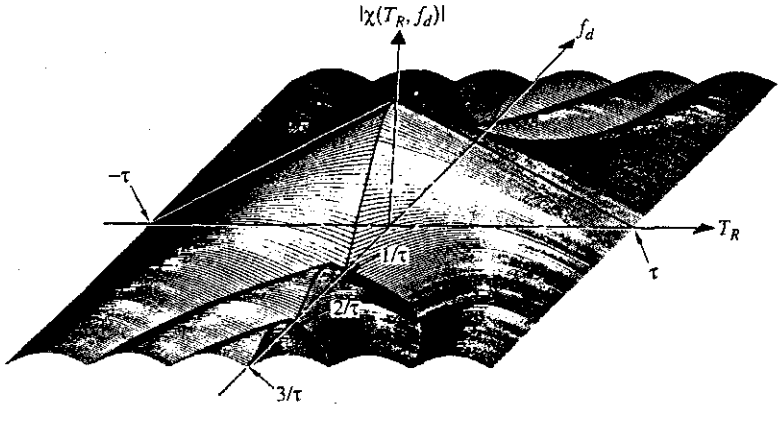

Figure 6.7 Plot of $|\chi(T_R, f_d)|$ for a simple rectangular pulse of width τ.
(Due to A. W. Rihaczek and R. L. Mitchell[22])

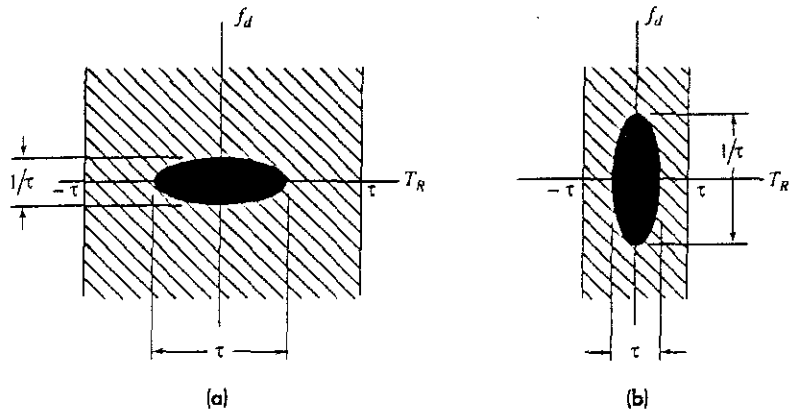

Figure 6.8 Two-dimensional representation of the ambiguity diagram for a single pulse of sinewave of width τ. (a) Long pulse; (b) short pulse.

large (completely darkened area), where it is small (lightly shaded area), and regions of zero response (no shading). The plot for a single pulse shows most of the response as a completely shaded elliptically shaped region in which $|\chi|^2$ is large. No response occurs outside the time $\pm\tau$. The time-delay measurement error is proportional to τ and the frequency measurement error is proportional to $1/\tau$. The plot of Fig. 6.8a shows the good frequency measurement accuracy and the poor time-delay accuracy of a long pulse. Figure 6.8b shows the opposite occurs for a short pulse. The ambiguity diagram indicates that as the range accuracy of a simple pulse waveform is improved, the frequency accuracy worsens and vice versa. (This follows from the box of sand analogy mentioned previously.) The short pulse is *doppler tolerant* in that a single matched filter will produce a good output if there is a significant doppler shift. That is, the output from a filter matched to a zero doppler shift will not change much when there is a doppler shift. On the other hand, a long pulse will produce greatly reduced output for a doppler-frequency shift; so it is not tolerant to changes in doppler. This is the reason why in an MTI radar a bank of doppler filters sometimes is used to cover the expected range of doppler frequencies. The ambiguity diagram of the single pulse is known as a *ridge* or *knife edge*.

Single Linear Frequency-Modulated (FM) Pulse Another example of a ridge or knife edge ambiguity diagram is that produced by linearly frequency modulating a rectangular pulse over a bandwidth B, as shown by the 2-D plot of Fig. 6.9. The pulse width T is large compared to $1/B$. The frequency modulation increases the spectral bandwidth of the pulse so that $BT >> 1$. The ridge is at an angle determined by the slope B/T. The time-delay measurement accuracy is proportional to $1/B$ and the frequency (if it can be measured) has an accuracy proportional to $1/T$. Since the pulse width T and the bandwidth B can be chosen independent of one another, the time-delay and frequency accuracies are independent of the other. This is unlike the time-delay and frequency accuracies of the simple, unmodulated rectangular pulse.

Periodic Pulse Train Consider, as shown in Fig. 6.10a, a series of five pulses, each of width τ, pulse repetition period T_p, and total duration T_d. The 2-D representation of its

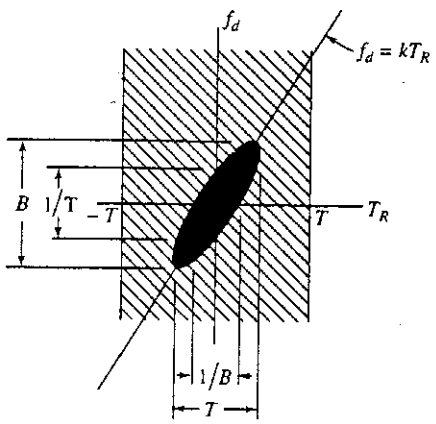

Figure 6.9 Two-dimensional representation of the ambiguity diagram for a single linear frequency-modulated pulse of width T and bandwidth B.

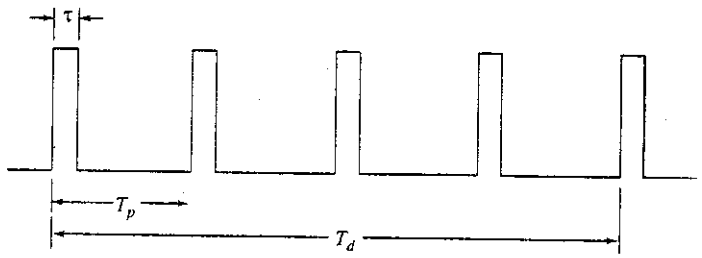

(a)

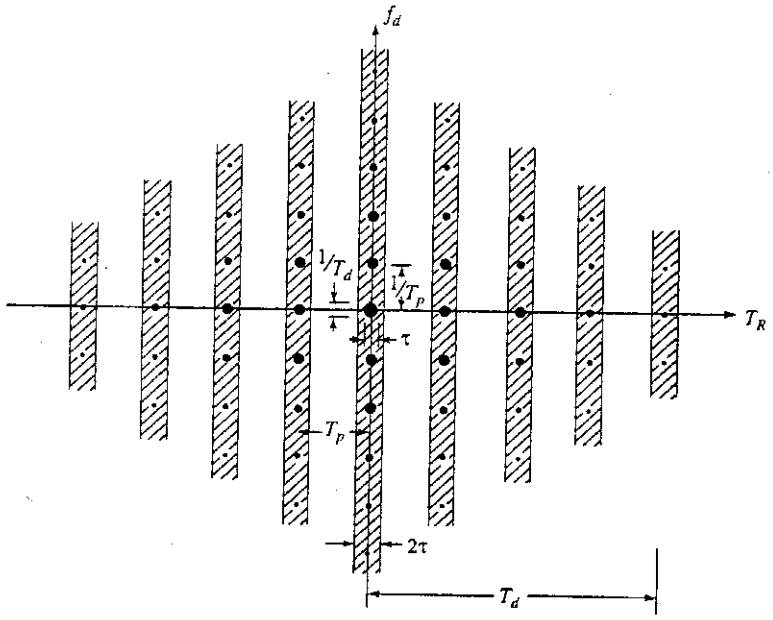

(b)

Figure 6.10 (a) Video pulse train of five pulses; (b) two-dimensional representation of the ambiguity diagram for (a).

ambiguity diagram is shown in Fig. 6.10b. This type of ambiguity function is called a *bed of spikes.* Throughout this ambiguity diagram there are many possible ambiguities in range and doppler (blind speeds) such as were encountered before in this text. Ambiguities are a consequence of discontinuous waveforms, which is why they do not appear with a single pulse. It might seem at first glance that the many ambiguities produced by a pulse train result in it being a poor radar waveform. As seen in Chap. 3, a pulse train is widely used in pulse doppler and MTI radars, and it is often possible to adequately unravel, avoid, or (sometimes) ignore the ambiguities.

Examine the center (the origin) of the ambiguity diagram shown in Fig. 6.10b. The spike at the origin is of dimension τ on the time axis and $1/T_d$ on the frequency axis. The time-delay measurement accuracy (determined by the pulse width) and the frequency accuracy (determined by the duration of the signal) can be selected independently. If the pulse repetition period T_p is such that no radar echoes are expected with a time delay greater than T_p and no doppler-frequency shifts are expected greater than $1/T_p$, then the effective ambiguity diagram reduces to just a single spike at the origin whose dimensions are determined by τ and T_d. The pulse train, therefore, can be a good radar waveform. Ambiguities that occur can be resolved with different pulse repetition frequencies (Secs. 2.10 and 3.9). The fact that many radars employ this type of waveform attests to its usefulness far better than any analysis based on its ambiguity diagram.

Although this discussion applies to a pulse train, the signal processing employed with such waveforms is almost always different from that assumed for Fig. 6.10. The ambiguity function of a pulse train is the output of a matched filter designed for the *entire* pulse train. This is why the ambiguity diagram of Fig. 6.10 for five pulses has an output (in time) consisting of nine pulses of different amplitudes when the input is five equal amplitude pulses (the autocorrelation function of five pulses). Pulse radars, however, are not usually designed with a matched filter for N pulses. Instead, a pulse radar usually uses a filter matched to a single pulse and then integrates the N pulses.

Noiselike Waveforms and the Thumbtack Ambiguity Diagram A noise waveform has an ambiguity function, called a thumbtack, similar to that of Fig. 6.11. Pure noise waveforms are seldom employed in radar; but constant-amplitude noiselike waveforms have been used to produce a thumbtack ambiguity diagram. Examples include nonmonotonic frequency modulation and pseudorandom variations of phase or frequency. These are discussed later in this chapter under the topic of pulse compression.

The thumbtack has the advantage that the time-delay and frequency measurement accuracies are independently determined, respectively, by the bandwidth of the modulation and the duration of the pulse. There are no apparent ambiguities and it resembles the approximation of the ideal ambiguity function of Fig. 6.6, except for the plateau on which the main response rests. This plateau extends over a dimension $2T$ along the time axis and $2B$ along the frequency axis. When the product BT is large, the volume under the peak response is small compared to the total volume, and almost all of the volume is in the plateau. Consequently, the average height of the plateau is approximately E^2/BT for large BT (based on Eq. 6.46).

The thumbtack ambiguity diagram, as illustrated in the sketch of Fig. 6.11, appears attractive; but it is an overly simplified sketch that can be misleading when practical

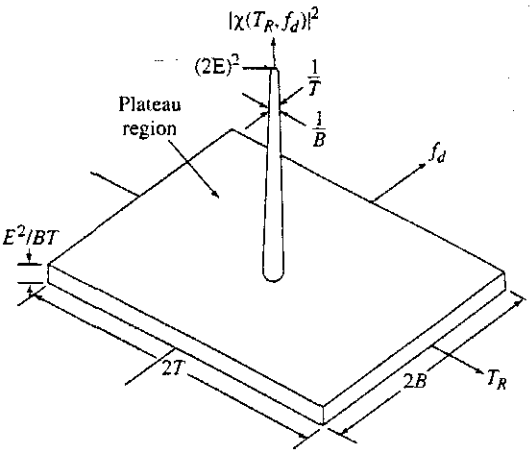

Figure 6.11 Ideal representation of the thumbtack ambiguity diagram as might be produced by a noiselike waveform or a pseudorandom coded pulse waveform (details of the sidelobe structure are not shown.)

waveforms are examined. The plateau is not uniform as shown. Most of the volume under the ambiguity function is confined to the intervals $|T_R| < T/2$ and $|f_d| < B/2$.[23] Furthermore, when there is a doppler-frequency shift, the sidelobes can be relatively high and can cause false responses. There are some waveforms, as will be mentioned later, that can produce low sidelobes when $f_d = 0$; but such waveforms should be looked at with caution when good doppler filtering is required without false responses, as for the detection of moving targets.

Waveform Design and the Ambiguity Diagram The waveform transmitted by a radar can affect (1) target detection, (2) measurement accuracy, (3) resolution, (4) ambiguities, and (5) clutter rejection. The ambiguity diagram may be used to assess qualitatively how well a particular waveform achieves these capabilities. Each of the above five capabilities will be briefly discussed.

Detection It was said in Sec. 5.2 that if the receiver is designed as a matched filter, the output peak-signal-to-mean-noise ratio (which is related to the ability to detect a target) depends only on the ratio of the received signal energy E and the receiver noise power per unit bandwidth N_0. The requirements for detection do not place any demands on the *shape* of the transmitted waveform except that (1) the waveform be practical to generate and radiate, and (2) the matched filter required for the waveform be practical to achieve. The ambiguity diagram, therefore, is seldom used to assess the detection capability of a particular waveform, except to note if the signal contains sufficient energy.

Accuracy The accuracy with which the range and radial velocity can be measured is indicated by the main response at the origin. The width along the time axis determines the range (time delay) accuracy, and the width along the frequency axis determines the radial-velocity accuracy.

Resolution The width of the central response also determines the resolution ability of a radar waveform in range and radial velocity. In order to resolve closely spaced targets, the central response must be isolated. There cannot be extraneous peaks near the main response that would mask the echo from a nearby target.

Ambiguity Ambiguities occur in radar measurements when the waveform is not continuous. For example, a pulse train is not continuous; hence, such a waveform can produce ambiguities in range (time delay) and in velocity (frequency). An ambiguous measurement is one in which there is more than one choice available, but only one is correct. Ambiguities appear in the ambiguity diagram as additional high responses similar in magnitude to the peak response at the origin. The correct response from the target cannot be readily recognized from these additional responses without taking some action to resolve the correct from the incorrect values.

The name *ambiguity function* for $|\chi(T_R, f_d)|^2$ can be misleading since this function describes more about the character of a waveform than just the ambiguities it produces. Woodward[24] coined the name for an entirely different reason than the ambiguities associated with discontinuous waveforms. The reader is advised not to be distracted by trying to understand the ambiguous use of the term "ambiguity" as the name for the function $|\chi(T_R,f_d)|^2$.

Clutter Attenuation Resolution in range and velocity can enhance the target signal echo relative to nearby distributed clutter echoes. The ambiguity diagram can indicate the ability of a waveform to reject clutter by superimposing the locations of the clutter echoes (as stored in a *clutter map*) on the T_R,f_d plane of the ambiguity diagram. If the radar is to have good clutter rejection, the ambiguity diagram should have little or no response in regions of high clutter echoes. The short-pulse waveform, for example, will reduce stationary clutter that is extensive in range since the ambiguity function for this waveform has little response on the time (range) axis.

Waveform Synthesis It is reasonable to ask if radar waveforms can be obtained by first defining a desired ambiguity diagram and then synthesizing the signal that yields this ambiguity diagram. Synthesis has not proven successful in the past. Instead, it is more usual to compute the ambiguity diagrams of various waveforms and determine which of them have suitable properties for the intended application.

6.5 PULSE COMPRESSION

High range-resolution, as might be obtained with a short pulse, is important for many radar applications, as indicated by the list of capabilities in Table 6.2. There can be limitations, however, to the use of a short pulse. Since the spectral bandwidth of a pulse is inversely proportional to its width, the bandwidth of a short pulse is large. Large bandwidth can increase system complexity, make greater demands on the signal processing, and increase the likelihood of interference to and from other users of the electromagnetic

Table 6.2 Capabilities of short-pulse, high range-resolution radar

Range resolution. Usually easier to separate (resolve) multiple targets in range than in angle.
Range accuracy. A radar capable of good range resolution is also capable of good range accuracy.
Clutter reduction. Increased target-to-clutter ratio is obtained by reducing the amount of distributed clutter with which the target echo signal must compete.
Interclutter visibility. With some types of "patchy" land and sea clutter, a high-resolution radar can detect moving targets in the clear areas between the clutter patches.
Glint reduction. Angle and range tracking errors introduced by a complex target with multiple scatterers are reduced when high range-resolution is employed to isolate (resolve) the individual scatterers that make up the target.
Multipath resolution. Range resolution permits the separation of the desired target echo from the echoes that arrive at the radar via scattering from longer propagation paths, or multipath.
Multipath height-finding. When multipath due to scattering of radar energy from the earth's surface can be separated from the direct-path signal by high range-resolution, target height can be determined without a direct measurement of elevation angle.
Target classification. The range, or radial, profile of a target in some cases can provide a measure of target size in the radial dimension. From the range profile one might be able to sort one type of target from another based on size or distinctive profile, especially if the cross-range profile is also available.
Doppler tolerance. With a short-pulse waveform, the doppler-frequency shift from a moving target will be small compared to the receiver bandwidth; hence, only a single matched filter is needed for detection, rather than a bank of matched filters each tuned for a different doppler shift.
ECCM. A short-pulse radar can negate the effects of certain electronic countermeasures such as range-gate stealers, repeater jammers, and decoys. The wide bandwidth of the short-pulse radar can, in principle, provide some reduction in the effects of broadband noise jamming and reduce the effectiveness of some electronic warfare receivers and their associated signal processing.
Minimum range. A short pulse allows the radar to operate with a short minimum range. It also allows reduction of blind zones (eclipsing) in high-prf radars.

spectrum. Another limitation is that in some high-resolution radars the limited number of resolution cells available with conventional displays might result in overlap of nearby echoes when displayed, which results in a collapsing loss (Sec. 2.12) if the detection decision is made by an operator. Wide bandwidth can also mean less dynamic range in the receiver because receiver noise power is proportional to bandwidth. Also, a short-pulse waveform provides less accurate radial velocity measurement than if obtained from the doppler-frequency shift. It spite of such limitations, the short-pulse waveform is used because of the important capabilities it provides.

A serious limitation to achieving long ranges with short-duration pulses is that a high peak power is required for a large pulse energy. The transmission line of a high peak power radar can be subject to voltage breakdown (arc discharge), especially at the higher frequencies where waveguide dimensions are small. If the peak power is limited by breakdown, the pulse might not have sufficient energy. Consider, for example, a more or less conventional radar with a pulse width of one microsecond and one megawatt peak power, as might be found in a medium-range air-surveillance radar. In this example, the energy contained in a single pulse is one joule. (The energy per pulse and the number of pulses

integrated determine the detectability of a target.) A one microsecond pulse has a range resolution of 150 m. If it were desired to have a resolution of 15 cm (one-half foot), the pulse width would have to be reduced to one nanosecond and the peak power increased to *one gigawatt* (10^9 W) in order to maintain the same pulse energy of one joule. This is an unusually large peak power that cannot be propagated without breakdown in the usual types of transmission lines employed at microwave radar frequencies.

A short pulse has a wide spectral bandwidth. A long pulse can have the same spectral bandwidth as a short pulse *if* the long pulse is modulated in frequency or phase. (Amplitude modulation can also increase the bandwidth of a long pulse, but is seldom used in radar because it can result in lower transmitter efficiency.) The modulated long pulse with its increased bandwidth B is compressed by the matched filter of the receiver to a width equal to $1/B$. This process is called *pulse compression*. It can be described as the use of a long pulse of width T to obtain the resolution of a short pulse by modulating the long pulse to achieve a bandwidth $B >> 1/T$, and processing the modulated long pulse in a matched filter to obtain a pulse width $\tau \approx 1/B$. Pulse compression allows a radar to simultaneously achieve the energy of a long pulse and the resolution of a short pulse without the high peak power required of a high-energy short-duration pulse. It is used in high-power radar applications that are limited by voltage breakdown if a short pulse were to be used. Airborne radars might experience breakdown with lower voltages than ground-based radars, and might be candidates for pulse compression. It is almost always used in high-power radars with solid-state transmitters since solid-state devices, unlike vacuum tubes, have to operate with high duty cycles, low peak power, and pulse widths much longer than normal. Pulse compression is also found in SAR and ISAR imaging systems to obtain range resolution comparable to the cross-range resolution.

The pulse compression ratio is defined as the ratio of the long pulse width T to the compressed pulse width τ, or T/τ. The bandwidth B and the compressed pulse width τ are related as $B \approx 1/\tau$. This would make the pulse compression ratio approximately BT. If amplitude weighting of the received waveform (but not the transmitted waveform) is used to reduce the time sidelobes of the linear-FM waveform (as will be discussed later in this section), the pulse compression ratio defined as BT usually is a little larger than T/τ. It is better, therefore, to define the pulse compression ratio by T/τ (the ratio of the before and after pulse widths) rather than the bandwidth-time product BT when weighting on receive is used. (In spite of this caution, the pulse compression ratio is often given as BT in this text as well as in other radar literature. The reader should be aware of which value is used, especially with linear-FM waveforms.) The pulse compression ratio in practical radar systems might be as small as 10 (although 13 is a more typical lower value) or greater than 10^5. Values from 100 to 300 might be considered typical.

There are two ways to describe the operation of a pulse compression radar. One is based on the ambiguity function of Sec. 6.4. A long pulse is modulated to increase its bandwidth. On reception the modulated long-pulse echo signal is passed through the matched filter. Its resolution in range can be found from examination of the ambiguity diagram. The constant-amplitude linear-FM pulse, whose ambiguity diagram was shown in Fig. 6.9, is an example of a widely used pulse compression waveform. Its ambiguity diagram shows that the long pulse of width T provides a compressed pulse width equal to $1/B$.

The other method for describing pulse compression is based on how linear-FM pulse compression was presented in the original patent of R. H. Dicke,[25] before the concept of the ambiguity function was known. The modulation applied to a long pulse can be considered as providing distinctive "marks" in either the frequency or the phase along the various portions of the pulse. For instance, the changing frequency of a linearly frequency-modulated pulse is distributed along the pulse so that each small segment of the pulse corresponds to a different frequency. By passing the modulated pulse through a dispersive delay line whose delay time is a function of frequency, each part of the pulse experiences a different delay, so that it is possible for the trailing edge of the pulse to be speeded up in a dispersive* delay line and the leading edge slowed down so that they "come together" to effect a compression of the long pulse.

There have been two general classes of pulse-compression waveforms used in the past. The most popular has been the *linear FM* (also known as chirp) to be discussed next. *Binary phase-coded* pulses is the other type. Also to be mentioned here are *polyphase codes* whose phase quantizations are less than π radians; *Costas codes* in which the frequencies of the subpulses are changed in a prescribed fashion; *nonlinear FM*, *nonlinear binary phase-coding*; *complimentary codes* that in principle produce zero time-sidelobes; and codes with very low or no sidelobes that require amplitude modulation of the subpulses on transmit. No one type of pulse-compression waveform can do everything that might be required; but linear FM probably has been the most widely used.

Linear Frequency Modulation (LFM) Pulse Compression The basic concept of the linear frequency-modulated pulsed compression radar was described by R. H. Dicke in a patent filed in 1945 and issued in 1953.[25] Figure 6.12, which is derived from Dicke's patent, is a block diagram of such a radar. It is similar to the block diagram of a conventional radar except that the transmitter is shown here as being frequency modulated and the receiver

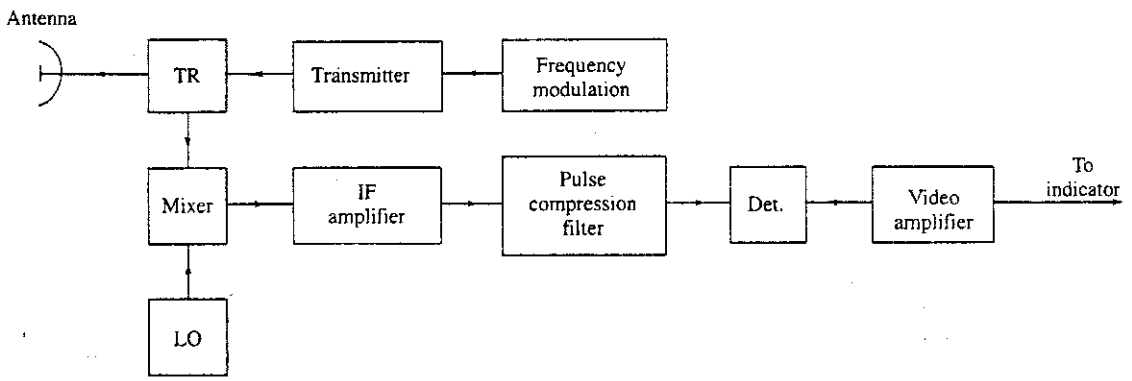

Figure 6.12 Block diagram of an FM pulse compression radar.

* "Dispersive" in this case means that the velocity of propagation is a function of frequency.

contains a pulse-compression filter (which is identical to a matched filter). More usually, however, the FM waveform is generated at low power and amplified by a power amplifier rather than by frequency modulating a power oscillator as indicated in this figure. The transmitted waveform (Fig. 6.13a) consists of a rectangular pulse of constant amplitude A and duration T. The frequency increases linearly from f_1 to f_2 over the duration of the pulse (Fig. 6.13b). This is sometimes known as an *up-chirp*. Alternatively, the frequency could just as well decrease with time, and it is then called *down-chirp*. The time waveform is represented in Fig. 6.13c. On reception, the frequency-modulated signal is passed through the pulse-compression filter, which is a delay line whose velocity of propagation is proportional to frequency. It speeds up the higher frequencies at the trailing edge of the pulse relative to the lower frequencies at the leading edge so as to compress the signal to a width $1/B$, where $B = f_2 - f_1$ (Fig. 6.13d). The pulse compression filter is a matched filter; hence, its output envelope (neglecting noise) is the autocorrelation function of the input. In this case, the output is proportional to $(\sin \pi Bt)/\pi Bt$.[26,27] The peak power of the pulse is increased by the pulse compression ratio $BT \approx T/\tau$ after passage through the filter.

The ambiguity diagram for a linear-FM pulse-compression waveform (Fig. 6.9) shows that a large doppler shift in the echo signal can result in the indicated range not being the true range. This is known as *range-doppler coupling*. In many cases, the range error due to the doppler shift is small and can be tolerated. If the range error is large, the effect of the doppler can be removed by averaging the two range indications obtained with both a rising FM (up-chirp) and a falling FM (down-chirp) similar to the manner in which the range error due to doppler is eliminated in an FM-CW radar with triangular modulation.[28]

Reduction of Time (Range) Sidelobes The $(\sin \pi Bt)/\pi Bt$ envelope out of a matched filter when the input is a linear-FM sinewave has relatively high peak time-sidelobes of -13.2 dB adjacent to the main response. This is usually not acceptable since high sidelobes can be mistaken for targets or can mask nearby weaker targets. The time sidelobes can be reduced by transmitting a pulse with nonuniform amplitude; that is, by amplitude weighting the long pulse over its duration T. (This is similar to *tapering* the aperture illumination of an antenna, Sec. 9.3, or *windowing* to reduce the spectral sidelobes of a digital filter.) Unfortunately, it is often not practical in high-power radar to have a transmitted waveform whose amplitude varies over the pulse duration. High-power transmitters such as klystrons, traveling wave tubes, and crossed-field devices should be operated saturated to obtain maximum efficiency. They don't like to be operated with amplitude modulation and they should be either full-on or full-off. Solid-state transmitters can have a linear input-output relation and be amplitude modulated if operated Class-A; but they are almost always operated Class-C because of the much higher efficiency of Class-C.[29] It is seldom that high-power microwave radar transmitters are operated with a deliberate change in amplitude over the pulse duration.

As a compromise, the time sidelobes with a linear-FM pulse-compression signal usually are reduced by applying amplitude weighting on receive (to the dispersive delay-line pulse compression filter) and not on transmit. Since the pulse compression filter is the matched filter, applying the weighting only on receive results in a mismatched filter and a loss in signal-to-noise ratio.[30] This is the price paid to reduce the time sidelobes. Table 6.3 gives examples of weightings, the peak sidelobe that results, and other properties of

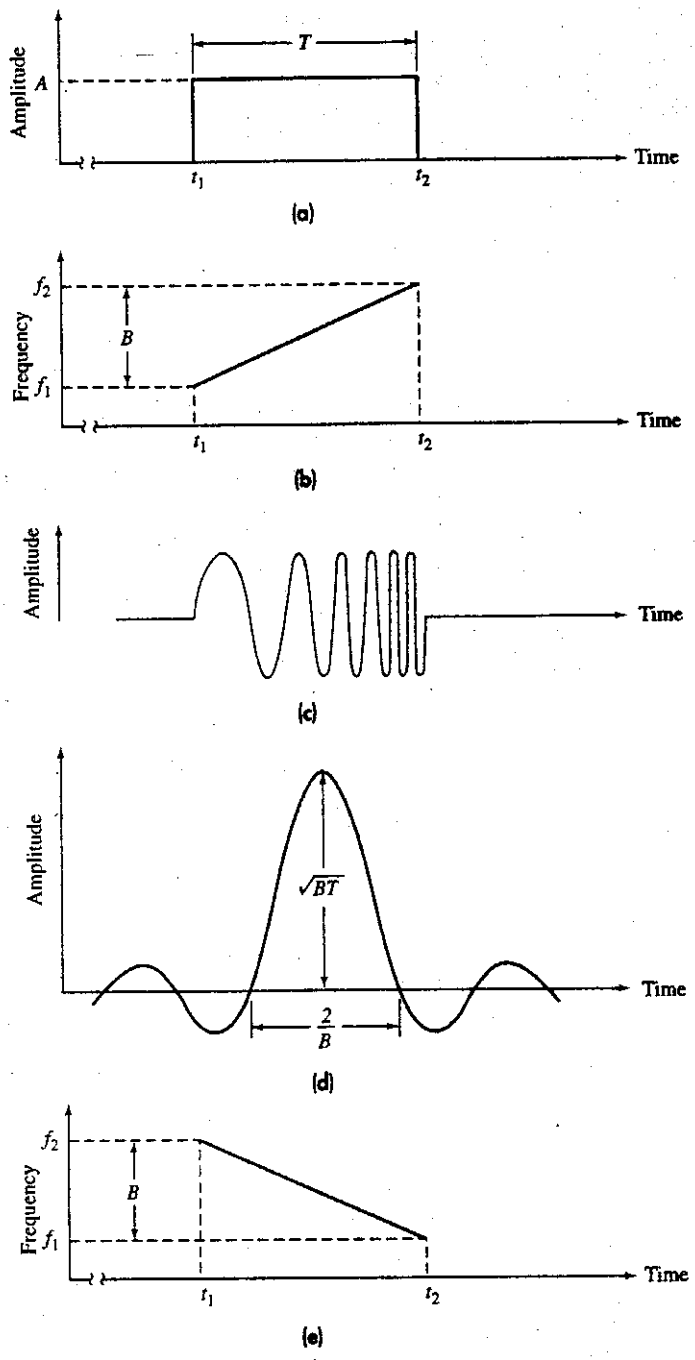

Figure 6.13 Linear FM pulse compression. (a) Transmitted waveform; (b) frequency of the transmitted waveform as a function of time; (c) representation of the linear FM waveform; (d) theoretical output from the pulse-compression filter.

Table 6.3 Properties of weighting functions to reduce time sidelobes

Weighting Function	Peak sidelobe dB	Loss dB	Mainbeam width (relative)
Uniform	−13.2	0	1.0
$0.33 + 0.66\cos^2(\pi f/B)$	−25.7	0.55	1.23
$\cos^2(\pi f/B)$	−31.7	1.76	1.65
$0.16 + 0.84\cos^2(\pi f/B)$	−34.0	1.0	1.4
Taylor ($\bar{n} = 6$)	−40.0	1.2	1.4
$0.08 + 0.92\cos^2(\pi f/B)$ (Hamming)	−42.8	1.34	1.5

the output waveform. The mismatched-filter loss can generally be kept to about 1 dB when the peak sidelobe level is reduced to 30 dB below the peak response. It is a loss that is tolerated in order to achieve lower time-sidelobe levels.

It is possible to have no theoretical loss in signal-to-noise ratio and still achieve low time-sidelobes with a uniform-amplitude transmitted waveform if a nonlinear frequency-modulated waveform is used, as discussed later in this section.

Stretch[31,32] This is a variant of linear-FM pulse compression in which narrow bandwidth processing can be employed if the extent of the range interval where high-range resolution occurs can be reduced. Stretch starts with a linear-FM waveform that is of much smaller bandwidth B_1 than required for the desired resolution. Before being transmitted, it is heterodyned (mixed) with a wideband linear FM of bandwidth B_2 to produce a signal with the desired bandwidth $B_1 + B_2$, which is radiated. On receive, the signal of bandwidth $B_1 + B_2$ is heterodyned again with the linear-FM sweep of wide bandwidth B_2. The difference signal has the narrow bandwidth B_1 and is processed as a normal (narrowband) pulse-compression signal. The heterodyne operation on receive results in a time expansion by a factor $\alpha = (B_1 + B_2)/B_1$ (time expansion means smaller bandwidth). The range resolution of a signal, however, corresponds to a signal with bandwidth $B_1 + B_2 = B$. The processing of the linear-FM signal and its generation are both done with narrow bandwidth circuitry of bandwidth $B_1 = B/\alpha$. The reduced bandwidth in waveform generation and processing is the advantage of Stretch.

Because of the "stretching" of the waveform during processing, the range interval over which high resolution is obtained is $1/\alpha$ that which would normally be obtained by a conventional linear-FM radar of bandwidth B. One trades processing bandwidth for the size of the high-resolution range interval. This capability might not be appropriate for a surveillance radar that has to look everywhere in range, but it is well suited to a tracking radar or a high range-resolution radar used for target classification.

The Stretch waveform was used in the Cobra Dane (AN/FPS-108), a large L-band phased array radar located in the Aleutian Islands of Alaska.[33] Its purpose was to gather information about Soviet/Russian intercontinental ballistic missiles (ICBM). It also has been used for space surveillance and ICBM warning. It performs high range-resolution

observation of ICBM reentry vehicles at ranges of about 1000 nmi. For this purpose it uses a 1000 μs duration linear-FM wideband waveform with 200 MHz bandwidth extending from 1175 to 1375 MHz. Its time-bandwidth product is 200,000, a relatively large value. Stretch processing examines a preselected range interval 250 ft in extent. The inherent range resolution is 2.5 ft, but the actual resolution is degraded to 3.75 ft since Taylor amplitude-weighting is employed on receive to reduce its time sidelobes to −30 dB.

Linear FM Pulse-Compression Filters In the first edition of the *Radar Handbook,* which appeared in 1970, the chapter on pulse compression[34] listed nine different devices that might be used as the pulse compression filter for linear FM. Since that time, the practice has narrowed to mainly two choices: the surface acoustic wave (SAW) dispersive delay line and digital processing. The 1970 edition briefly discussed the SAW device (then called a *surface-wave dispersive delay line*) but it didn't mention digital processing for pulse compression. Digital processing is usually preferred when the A/D converter can provide the very wide bandwidths required of high-resolution pulse-compression radar. The SAW device has been the method of choice, however, when large-bandwidth signal processing cannot be obtained digitally. Digital methods are therefore used when they are applicable and the analog SAW delay line is used for very high resolution when digital methods cannot compete.

There are two general technical areas of application for pulse compression. One is when the compressed pulse is very small, perhaps of the order of a nanosecond, but the original uncompressed pulse is of conventional width, perhaps a microsecond. High resolution might be of interest for synthetic-aperture imaging radars (SAR), radars designed to detect a person swimming in the water, or for radars required to recognize one class of ship from another based on inverse synthetic aperture radar. SAW devices have been appropriate as the pulse compression filter for such applications. The other area is when one starts with a long pulse, say a few hundred microseconds, and compresses it to a conventional width, for example, of the order of a microsecond. Digital processing can be used in such situations. An important example is when a solid-state transmitter is used that requires long pulses for efficient operation.

SAW Devices[35–37] The concept of a surface acoustic wave delay line is shown schematically in Fig. 6.14. It consists of a very smooth piezoelectric substrate, such as a thin slice of quartz, lithium niobate, or lithium tantalate. The function of the piezoelectric substrate is to support propagation of acoustical waves along the surface. The low velocity of acoustic waves (approximately 3500 m/s) compared to electromagnetic waves means that significant delay times can be achieved with a relatively small device. The input/output devices arranged on the surface are known as *interdigital transducers* (IDT). They are metallic thin films, usually aluminum, that are deposited on the substrate using photolithographic methods. The transducers are the means by which electrical signals are converted to acoustical signals, and vice versa. They determine the impulse response of the SAW delay line and the length of the IDT determines the duration of the signal. Since the IDT can launch waves in both the forward and back directions, the acoustic energy propagating in the opposite direction has to be attenuated so that it is not reflected and cause interference. One method for attenuating the unwanted signal is to use acoustic absorbers located at each end of the device, as indicated in Fig. 6.14.

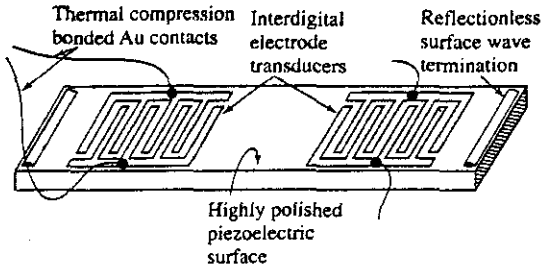

Figure 6.14 Schematic of a simple surface acoustic wave (SAW) delay line.
(From T. W. Bristol: Surface Acoustic Wave Devices—Technology and Applications, IEEE 1976 WESCON, paper 245/1. Courtesy IEEE.)

Efficient electric-to-acoustic coupling occurs when the comb fingers, or electrodes, of the IDT are spaced one-half wavelength of the acoustic signal that propagates along the substrate material. The frequency response of the delay line depends, therefore, on the spacings between the electrodes. A dispersive delay line whose delay is a function of frequency can be obtained with varying electrode spacing as illustrated in Fig. 6.15a or b. The SAW delay-line configuration in 6.15a is called an *in-line single dispersive chirp filter.* The received linear-FM signal sketched below the delay line is applied to the broadband IDT on the left. The output from the dispersive IDT structure on the right is the compressed pulse. (Either IDT can be used as the input or output since the SAW delay line is reciprocal.)

The *in-line double dispersive chirp filter* of Fig. 6.15b is capable of larger BT products (50 to 1000) than the single configuration of 6.15a.[35] The *slanted-array compressor* (SAC) sketched in Fig. 6.15c also is capable of large pulse compression ratios. An advantage the inclined IDTs have over the in-line configurations is that they avoid the distortion that occurs when the low-frequency components have to propagate under the high-frequency electrodes, and vice versa. Another advantage of the SAC configuration is that corrections in the phase characteristic of the device can be made by inserting a "phase plate" between the input and output IDTs. An example of a SAC linear-FM filter described by Cambell[37] (but attributed to S. Jen and C. F. Shaffer) operated at a center frequency of 1.4 GHz with a bandwidth of 1.1 GHz. This is a relative bandwidth of almost 80 percent, and can be called ultrawideband. The uncompressed pulse width was 0.44 μs, the compressed pulse was about 0.9 ns, and the bandwidth-time product was 484. Amplitude weighting was used to reduce the time sidelobes to 26.8 dB below the peak.

The *reflective-array compressor* (RAC) shown schematically in Fig. 6.15d is another form of SAW device. It is capable of larger pulse compression ratios (500 to 10,000) than other configurations. Shallow grooves are etched in the delay path that result in reflections to form a delay that depends on frequency. The structure is less sensitive to fabrication tolerances than conventional transducers. Compensation for phase errors can also be inserted between the oblique-angle grooves, as can attenuation for weighting the amplitude.

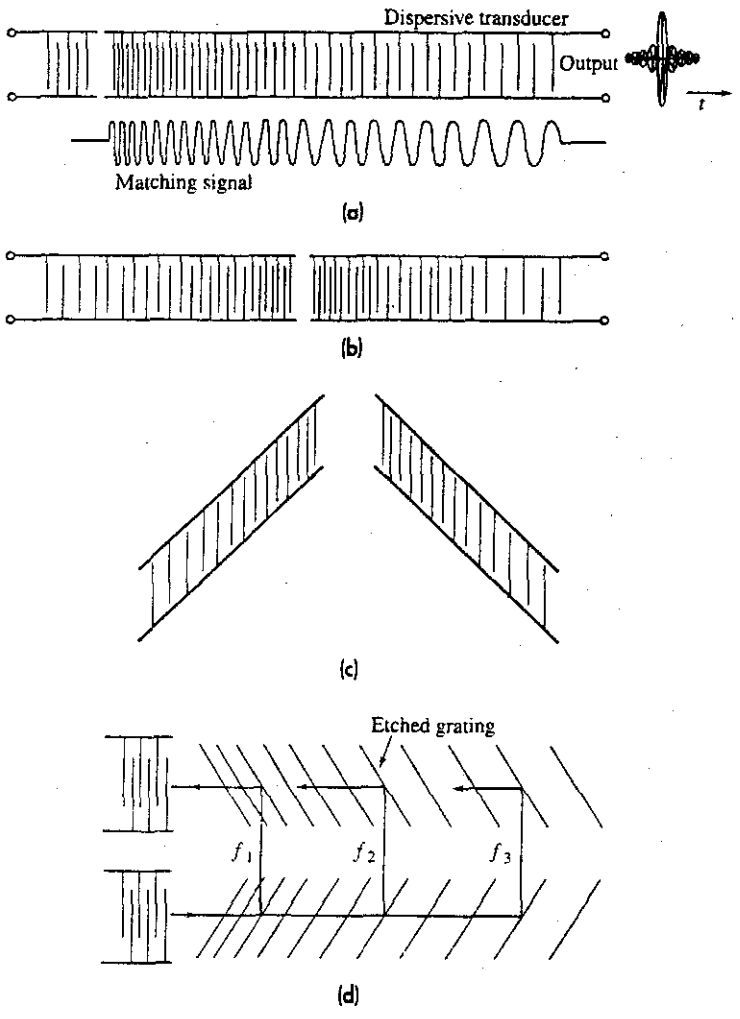

Figure 6.15 Configurations of interdigital transducers for linear-FM pulse-compression dispersive delay lines. (a) In-line single dispersive SAW delay line; (b) in-line double dispersive SAW delay line with dispersion in both transducers; (c) slanted-array compressor (SAC); and (d) reflective-array compressor (RAC). (Figs. (a), (b), and (d) are from Maines and Paige,[36] courtesy of Proc. IEEE.)

In summary, linear-FM SAW devices might have pulse compression ratios (BT) greater than 10,000, uncompressed pulse durations up to 150 μs, bandwidths greater than 1 GHz, insertion loss from 20 to 60 dB, and operate at center frequencies from 100 MHz to 1.5 GHz. They are usually found in the IF portion of the radar receiver. SAW devices provide wide bandwidth pulse-compression filters in small size packages. They are readily reproducible, easy to manufacture in large quantities, and of relatively low unit cost.

A device related to SAW devices is the IMCON, which is a reflection-mode delay line configured similar to the RAC SAW device, but fabricated on steel acoustic media. IMCONs are more suited for narrow bandwidths and low center frequencies (below 30 MHz) and when uncompressed pulse durations greater than 50 μs are desired. Bandwidths are from 0.5 to 12 MHz. Pulse durations of 600 μs are possible and units can be cascaded to obtain longer pulse durations.[38] For example, a pulse duration of 10 ms was obtained

by cascading 18 IMCONs with amplifiers. It operated at a center frequency of 7.5 MHz and bandwidth 2.5 MHz. The pulse compression ratio was 25,000 and its dimensions were 15 by 15 by 12 inches.[39]

Amplitude Weighting Amplitude shaping of the frequency response of a SAW filter can be obtained by the amount of overlap of the electrodes of the IDT, as in Fig. 6.16. This is sometimes called *apodization.*

Digital Processing for Frequency-Modulated Pulse Compression The linear-FM pulse-compression waveform, as well as most other pulse compression waveforms, can be processed and generated at low power levels by digital methods when A/D converters are available with the required bandwidth and number of bits.[40,41] Digital methods are very stable and can handle long-duration waveforms. The same basic digital system implementation can be used when one wishes to employ multiple bandwidths and pulse durations, different types of pulse compression modulations, good phase repeatability, low time-sidelobes, or when flexibility is desired in waveform selection.

Generation of the Pulse-Compression Waveform The analog and digital methods used to obtain the linear-FM pulse-compression filter can also be applied to generate the transmitted waveform. The waveforms may be generated passively or actively. An example of the former is the SAW device; an example of the latter is a voltage-controlled oscillator. Other examples of each can be found in Ref. 40.

Single Transmit-Receive Filter It will be recalled (Sec. 5.2) that the impulse response of a matched filter is the time inverse of the signal for which it is matched. If an up-chirp linear-FM is transmitted, the impulse response of its matched filter will be a down-chirp. To employ the same filter for both transmit and receive, the local oscillator frequency of the radar superheterodyne receiver should be greater than the frequency of the received signal. When the difference signal is taken from the mixing operation, the linear-FM waveform will be inverted; that is, an up-chirp becomes a down-chirp, which is the signal required for the matched filter when a transmitted up-chirp is generated using the same matched filter.

Binary Phase-Coded Pulse Compression Changes in phase can also be used to increase the signal bandwidth of a long pulse for purposes of pulse compression. A long pulse of

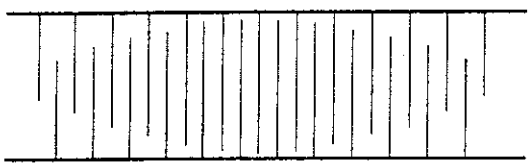

Figure 6.16 Interdigital transducer (nondispersive) showing overlap of the comb fingers to provide an amplitude weighting along the pulse.

duration T is divided into N subpulses each of width τ. An increase in bandwidth is achieved by changing the phase of each subpulse (since the rate of change of phase with time is a frequency). A common form of phase change is *binary phase coding*, in which the phase of each subpulse is selected to be either 0 or π radians according to some specified criterion. If the selections of the $0, \pi$ phases are made at random, the waveform approximates a noise-modulated signal and has a thumbtack-like ambiguity function as in Fig. 6.11. The output of the matched filter will be a compressed pulse of width τ and will have a peak N times greater than that of the long pulse. The pulse compression ratio equals the number of subpulses $N = T/\tau \approx BT$, where the bandwidth $B \approx 1/\tau$. The matched filter output extends for a time T on either side of the peak response. The unwanted, but unavoidable, portions of the output waveform other than the compressed pulse are known as *time sidelobes*. When the selection of the phases is made at random, the expected maximum (power) sidelobe is about $2/N$ below the peak of the compressed pulse.

Barker Codes Some random selections of the $0, \pi$ phases are better than others (where *better* means a lower maximum sidelobe level). Completely random selection of the phases, therefore, is not a good idea if compressed waveforms with low time-sidelobes are desired—and they usually are. One criterion for selecting the subpulse phases is that all the

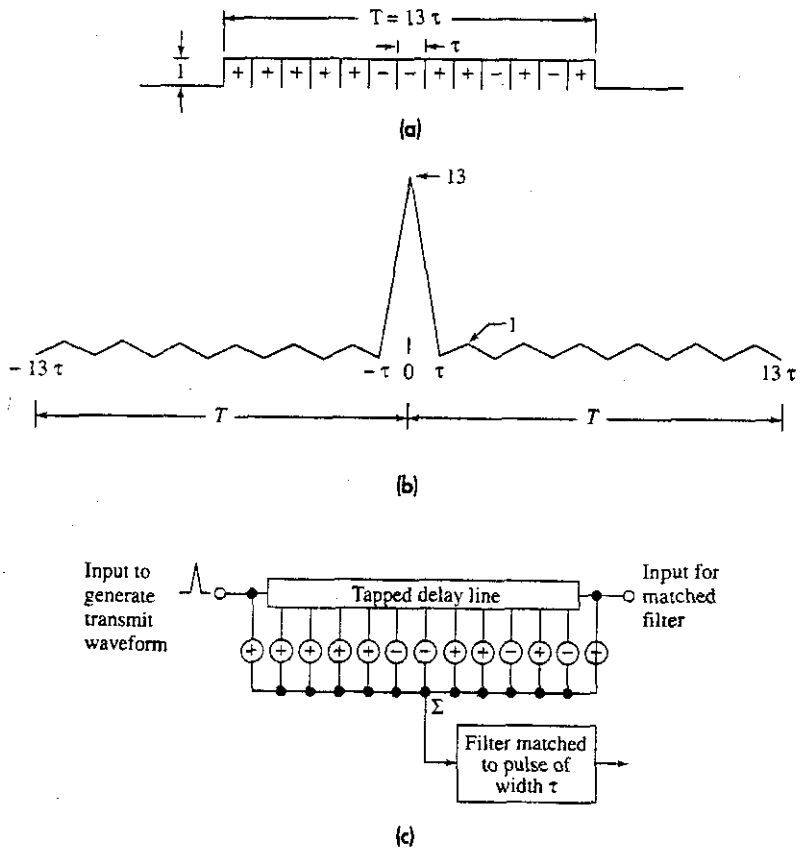

Figure 6.17 (a) Barker code of length 13; a long pulse with 13 equal subdivisions whose individual phases are either 0° (+) or 180° (−). (b) Autocorrelation function of (a), which represents the output of the matched filter. (c) Tapped delay line for generating the Barker code of length 13.

Table 6.4 Barker codes

Code length	Code elements	Sidelobe level, dB
2	+−, ++	−6.0
3	++−	−9.5
4	++−+, +++−	−12.0
5	+++−+	−14.0
7	+++−−+−	−16.9
11	+++−−−+−−+−	−20.8
13	+++++−−++−+−+	−22.3

time-sidelobes of the compressed pulse should be equal. (The reasoning here is that one can allow the small sidelobes to increase if it results in a lowering of the high sidelobes, and having all sidelobes equal is an indication that this has happened.) The $0,\pi$ binary phase-codes that result in equal time-sidelobes are called *Barker codes*. The Barker code of length $N = 13$ is shown in Fig. 6.17a. The (+) indicates 0 phase and (−) indicates π radian phase. Its autocorrelation function, which is the output of the matched filter, is shown in (b). There are six equal time-sidelobes to either side of the peak, each at a level 22.3 dB below the peak. (The sidelobe level of the Barker codes is $1/N^2$ that of the peak signal.) In (c) is shown schematically a tapped delay line that generates the Barker code of length 13 when the input is from the left. The same tapped delay-line filter can be used as the receiver matched filter if the received signal is applied from the right. The Barker codes are listed in Table 6.4. There are none greater than length 13; hence, the greatest pulse-compression ratio for a Barker code is 13. This is a relatively low value for pulse-compression applications.

Linear Recursive Sequences, or Shift-Register Codes When a pulse compression ratio larger than 13 is required, some other criterion for selecting the $0,\pi$ phases is needed. One method for obtaining a set of random-like phase codes is to employ a shift register with feedback and modulo 2 addition that generates a pseudorandom sequence of zeros and ones of length $2^n - 1$, where n is the number of stages in the shift register.[42–44] An n-stage shift register consists of n consecutive two-state memory units controlled by a single clock. The two states considered here are 0 and 1. At each clock pulse, the state of each stage is shifted to the next stage in line. Figure 6.18 shows a seven-stage shift register used to generate a pseudorandom sequence of zeros and ones of length 127. In this particular case, feedback is obtained by combining the output of the 6th and 7th stages

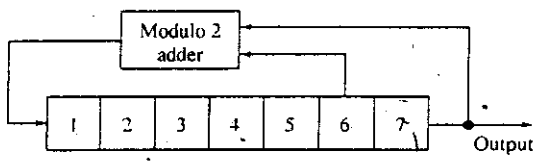

Figure 6.18 Seven-bit shift register for generating a pseudorandom linear recursive sequence of length 127

in a modulo-2 adder. (In a modulo-two adder the output is *zero* when both inputs are the same [(0,0) or (1,1)] and the output is *one* when they are not the same. It is equivalent to base-two addition with only the least-significant bit carried forward.) An n-stage binary device has a total of 2^n different possible states. The shift register cannot, however, employ the state in which all stages are zero since it would produce all zeros thereafter. Thus an n-stage shift register can generate a binary sequence of length no greater than $2^n - 1$ before repeating. The actual sequence obtained depends on both the feedback connection and the initial loading of the shift register. When the output sequence of an n-stage shift register is of period $2^n - 1$, it is called a *maximal length sequence*, or *m-sequence*.

This type of waveform is also known as a *linear recursive sequence* (LRS), *pseudorandom sequence*, *pseudonoise* (PN) sequence, or *binary shift-register sequence*. They are linear since they obey the superposition theorem. When applied to phase-coded pulse compression, the *zeros* correspond to zero phase of the subpulse and the *ones* correspond to π radians phase.

There can be more than one maximal length sequence, depending on the feedback connection. For example, 18 different maximal length sequences, each of length 127, can be obtained with a seven-stage shift register by using different feedback connections. With the proper code, the highest (power) sidelobe can be about $1/2N$ that of the maximum compressed-pulse power. A 24-dB sidelobe can be available with a sequence of length 127. Not all maximal length codes, however, have this low a value of peak sidelobe. For example,[45] with $N = 127$, the highest sidelobe of the various maximal length sequences can vary from 18 to 24 dB below the peak. It is generally said that the more usual maximum sidelobe of a "typical" maximal-length shift register sequence is approximately $1/N$ that of the peak response. In the above example with $N = 127$, this is 21 dB. As mentioned above, a completely random selection of the phases usually results in a sidelobe approximately $2/N$ below the peak; the typical maximal-length shift-register sequence might have a sidelobe of $1/N$, and the best of the maximal-length sequences might approach 1/2N. By comparison, the Barker codes have a peak sidelobe $1/N^2$ below the peak.

Sometimes the term *code* is used and at other times the term *sequence* is used to describe the phases of the individual subpulses of a phase-coded waveform. Both terms are found in the literature and are often interchangeable when discussing pulse compression, as is the practice in this section.

The shift-register codes fit several of the tests for randomness. They are called *pseudo random* since they may appear to be random, but they are actually deterministic once the shift-register length and feedback connections are known. The fact that a pulse compression sequence is random or pseudorandom does not mean it will produce the lowest time-sidelobes at the output of the matched filter. For instance, the Barker code of length 13 in Table 6.4 is a good sequence (for its length) in that it produces a -22.3-dB peak sidelobe, but it is not what is usually thought of as "random." It does not satisfy the *balance* property of a random sequence (the number of ones differs from the number of zeros by at most one); nor does it satisfy the *run* property (among the number of runs of ones and zeros in each sequence, one half are of length two, one quarter of length three, and so forth); nor does it satisfy the *correlation* property (when the sequence is compared term by term with any cyclic shift of itself, the number of agreements differs from the number

of disagreements by at most one). Thus the Barker codes are not random in the above sense, but they produce the lowest sidelobes for their length. It should be no surprise, therefore, to find that there are better binary sequences than the shift-register sequences.

Other Binary Sequences Computer search has shown that the longest code with sidelobe level of 2 is of length 28;[46,47] the longest code with sidelobe level 3 is 51;[48] and the longest codes for levels 4 and 5 are 69 and 88 respectively.[48] It should be noted that the above sidelobe levels are almost 25 dB for code lengths varying from 51 to 88. These sidelobe levels are better than the $1/2N$ values of the best maximal-length sequences.

Doppler Effects The binary phase-coded waveform produces a thumbtack ambiguity diagram so that a bank of matched filters (with each filter tuned to a different doppler frequency) will be needed when the doppler shift of the target echo signal is large. There is, however, a more serious problem with these waveforms when there are large doppler shifts. The sidelobes in the plateau region of the thumbtack can be relatively high and a single target can result in responses from more than one filter to cause ambiguities and/or false target reports at incorrect doppler shifts. Thus the binary phase-coded waveforms might not be suitable when there is a significant doppler shift.

Quadriphase Code[49] Binary phase (biphase) coded signals using rectangular subpulses can result in poor fall-off of the radiated spectrum, mismatch loss in the receiver pulse-compression filter, and loss due to range sampling when the pulse compression is digital. These effects can be reduced by modifying the biphase codes to produce what is called a *quadriphase code.*

To generate the quadriphase code, one first starts with a good biphase code. The binary-code phases, designated as W_k for each subpulse, are transformed to the quadriphase codes, designated V_k, by means of the following transformation:

$$V_k = j^{s(k-1)} W_k \qquad [6.47]$$

where s is fixed and is either $+1$ or -1. Since the phases of the subpulses of a binary code are either 0 or π radians, the above equation shows that the phases of the quadriphase subpulses will be either 0, $\pi/2$, π, or $3\pi/2$ radians. Between subpulses the phase change will be either $+\pi/2$ or $-\pi/2$ radians. Each subpulse of the quadriphase code has a half-cosine shape rather than a rectangular shape. The spectrum of a cosine subpulse decreases more rapidly than that of a rectangular shape, and is therefore less likely to cause interference. The subpulse width τ is measured from the half-power points of the half-cosine. (The base-width of the half-cosine is therefore 2τ.) The overlap of the cosine-shaped subpulses results in an uncompressed pulse that has constant amplitude except for the leading and trailing edges. As mentioned previously in this section, constant amplitude output is desired of high-power transmitters since variations in the amplitude of the pulse can cause loss of transmitter efficiency. The half-cosine shape of the subpulses and the crossover at the half-power points result in constant amplitude and also eliminate phase transients that can cause spectral splatter.

The maximum value of the compressed biphase waveform (the autocorrelation function) is preserved when converted to the quadriphase compressed pulse. The peak

sidelobe level of the quadriphase code, however, can be larger than that of the biphase signal from which it was derived. The increase approaches 1.5 dB when the biphase sidelobe is very large. If, however, the amplitude of the peak sidelobe of the compressed pulse of the biphase code is unity, as with Barker codes, then according to Taylor and Blinchikoff[49] there is no increase in the sidelobe amplitude when transforming to the quadriphase code. When the peak sidelobe of the compressed pulse from a biphase code is two, the peak sidelobe of the compressed quadriphase code is increased by 0.41 dB.

If digital processing is employed, a loss in signal-to-noise ratio occurs when the sampling straddles the peak of the compressed pulse rather than being exactly at the peak. When losses due to random sampling are averaged over all possible locations within the pulse, the range-straddling loss is about 2.3 dB for binary phase codes, but is only 0.8 dB for quadriphase codes.[49] (In both the binary phase and the quadriphase codes, it is assumed in the above that the spacing between samples is the same as the subpulse spacing τ, but can occur anywhere within the subpulse. If the binary phase codes are double sampled, however, the 2.3-dB loss is reduced to 0.8 dB.) The doppler behavior of quadriphase codes is said by Taylor and Blinchikoff to be the same as the doppler behavior of biphase codes. Levanon and Freedman,[50] however, give examples where the ambiguity diagram with a nonzero doppler shift can be significantly different for a quadriphase code than for the biphase code from which it was derived. For example, the ambiguity diagram of a quadriphase code derived from a Barker code of length 13 has a diagonal ridge more like that of a linear-FM ambiguity function rather than the thumbtack ambiguity function of the Barker code. The diagonal ridge, however, is not a general feature of quadriphase codes.

Polyphase Codes The phases of the subpulses in phase-coded pulse compression need not be restricted to the two levels of 0 and π. When other than the binary phases of 0 or π, the coded pulses are called *polyphase codes*. They produce lower sidelobe levels than the binary phase codes and are tolerant to doppler frequency shifts if the doppler frequencies are not too large. An example is the Frank polyphase code[51,52] defined by an M by M matrix as shown on the left side of Table 6.5. The numbers in the matrix are each multiplied by a phase equal to $2\pi/M$ radians (or $360/M$ deg). The polyphase code starts at the upper left-hand corner of the matrix, and a sequence of length M^2 is obtained. The pulse compression ratio is $M^2 = N$, the total number of subpulses. An example of the phases for each of the 25 pulses of a Frank code of $M = 5$ is shown on the right side of Table 6.5. The basic phase increment in this example is $360/5 = 72°$. The phases are shown modulo 360°.

Frank conjectured that for large N, the highest sidelobe of a polyphase code relative to the peak of the compressed pulse is $\pi^2 N \approx 10 \times$ (pulse compression ratio). In the above example with $N = 25$, the peak sidelobe is 23.9 dB. (By comparison, the closest maximal-length shift register sequence, of length 31, has a peak sidelobe of 17.8 dB.)

Since the rate of change of phase is a frequency, examination of the matrix of Table 6.5 indicates that the frequencies of the Frank code change linearly with time in a discrete fashion. The Frank codes can be thought of as approximating a stepped linear-FM waveform. The ambiguity diagram for a polyphase code is similar to that of a linear-FM waveform, but there can be a 3- to 4-dB loss in signal at doppler frequencies that are

Table 6.5 Frank Polyphase Code

$M \times M$ Matrix Defining Frank Polyphase Code	Example of Frank Matrix with $M = 5$ and pulse compression ratio $N = M \times M = 25$
0 0 0 0... 0	0, 0, 0, 0, 0,
0 1 2 3... $N-1$	0, 72, 144, 216, 288,
0 2 4 6.... $2(N-1)$	0, 144, 288, 72, 216,
0 3 6 9.... $3(N-1)$	0, 216, 72, 288, 144,
.	0, 288, 216, 144, 72.
.	
0..... $(N-1)^2$	

The phases of each of the M^2 subpulses are found by starting at the upper left of the matrix and reading each row in succession from left to right.

odd-integer multiples of π radians per pulse.[53] The doppler response of polyphase codes should be satisfactory with aircraft targets but might be a problem when detecting high-speed targets such as satellites and ballistic missiles.

B. Lewis and F. Kretschmer have described variants of the Frank polyphase codes, which they called P-codes.[54] They devised four P-codes that they claim to be more tolerant than the Frank code to receiver bandlimiting prior to pulse compression.

Lewis[55] has also shown that the range, or time, sidelobes of the polyphase codes can be reduced significantly after reception by following the polyphase pulse-compression network with a two-sample sliding-window subtractor for the Frank and P1 codes, and by a two-sample sliding-window adder for the P3 and P4 polyphase codes. The sliding-window subtractor is a one-sample delay whose input and output drive the subtractor. With this additional processing, the sidelobes of a polyphase code of length N are uniform and are $(2/N)^2$ relative to the peak. The sidelobe level is of unit magnitude, just as with the Barker codes. The width of the compressed pulse, however, is doubled so that the pulse compression ratio is reduced to $N/2$. There is a loss because of the doubling that Lewis estimates to be about 1 dB. For example, a polyphase waveform with an original pulse-compression ratio of 400 will have an effective pulse-compression ratio of 200 after the two-sample sliding-window subtractor or adder, and its sidelobe level will be 46 dB below the peak. This is the sidelobe level that would be achieved if there existed a Barker code with a pulse compression ratio of 200. Lewis also states that "tests of the sidelobe suppression with doppler as would be encountered in radar where the codes were useful revealed that the doppler did not significantly reduce the effect of the sidelobe suppression." There exists, however, a range-doppler coupling that is characteristic of linear FM and FM-derived polyphase codes.

Costas Codes A *frequency hopping*, or *time-frequency coded*, waveform is generated by dividing a long pulse of width T into a series of M contiguous subpulses (Fig. 6.19a). The frequency of each subpulse is selected from M contiguous frequencies within a band B (Fig. 6.19b).[56] The frequencies are separated by the reciprocal of the subpulse width (or

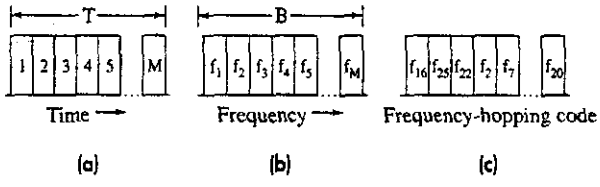

Figure 6.19 Discrete-frequency-coded pulse-compression waveform. (a) Long pulse divided into M subpulses; (b) M contiguous uniformly increasing frequencies covering the band B; (c) a frequency-hopping code.

$\Delta B = M/T$); there are B/M different frequencies to choose for the subpulses; and the width of each subpulse is T/M. If the frequencies of the subpulses were to be selected so as to be monotonically increasing (or decreasing) in frequency from subpulse to subpulse, it would be a stepped-frequency waveform that approximates the linear-FM waveform, especially if the frequency and time steps are small. Its ambiguity diagram will be a ridge, like that of the linear FM. When the frequencies are selected at random, as in Fig. 6.19c, the result is a thumbtack ambiguity diagram. The pulse compression ratio is $BT = (M\ \Delta B)T = M(M/T)T = M^2$. Only $M = \sqrt{BT}$ subpulses are needed instead of the BT subpulses required for binary phase-coded pulses.

Some random selections, however, are better than others for producing an ambiguity diagram with low sidelobes; so it is not wise to choose the frequencies haphazardly. With M choices of frequencies for M subpulses, there are $M!$ different sequences. An exhaustive blind search for the best sequences is not practical except for very small values of M.

J. P. Costas has suggested a procedure for selecting the order of frequencies so as to provide well-controlled range and doppler sidelobes.[57] Costas codes attempt to have a sidelobe no greater than one unit high, so that the maximum (voltage) sidelobe level of the thumbtack ambiguity diagram is $1/M$th the central peak (voltage), where M is the number of subpulses. The sidelobes of the ambiguity diagram (in terms of relative power) are about $(1/M)^2$ relative to the central peak in those regions of the ambiguity diagram away from the central peak, and can be close to $(2/M)^2$ near the central peak.

The waveforms based on the criterion of Costas are described by an array of M rows representing frequency and M columns representing time intervals (subpulses). There is exactly one mark in each row and each column. Such an array is called an $M \times M$ Costas array if the *coincidence function* satisfies $C(r,s) \leq 1$ for all integer pairs $(r,s) \neq (0,0)$ with $|r| \leq M - 1$, $|s| \leq M - 1$. The coincidence function gives the number of coincidences of marks between the original array and its translation along the time and/or frequency axis. It may be regarded as a discrete version of the (unnormalized) ambiguity function. The parameters r and s define the amount of the translation: r is the number of integer shifts to the right or left (translated by columns), and s is the number of integer shifts up or down (translated by rows).

Consider, for example, the 6×6 Costas array of Fig. 6.20.[58] The dashed lines in this figure indicate the translation of the array two time intervals to the right and three frequency intervals up. The Xs locate the frequencies transmitted in the original array, and the Os the same frequencies in the shifted array. From this discrete representation, one point on the ambiguity diagram can be obtained. In the example of Fig. 6.20 there is only one cell in the original array and the shifted array where the X and O marks (signals) coincide. Hence the value for this point (2,3) on the ambiguity diagram is 1. The complete

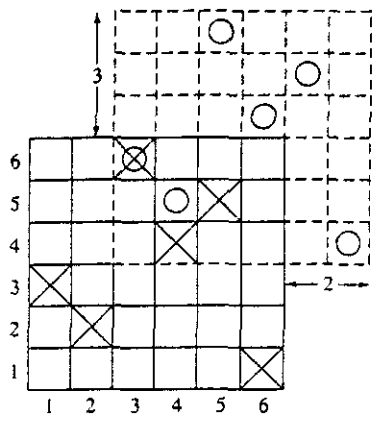

Figure 6.20 A 6 × 6 Costas array indicated by Xs along with its translation two to the right and three up (2,3) shown dashed and indicated by Os. A single coincidence occurs in cell (3,6). (After Chang and Scarbrough.[58] copyright 1989 IEEE.)

ambiguity diagram based on the discrete array is obtained by shifting the two arrays through all values of r and s.

A Costas code is therefore a frequency-hopped signal where there is no more than one coincidence between the original and the translated array. With no translation, there will be M coincidences, which is the peak at the center of the ambiguity diagram. Thus the maximum sidelobe (voltage) ratio is $1/M$. This is only approximate since discrete values are used. A more exact calculation of the ambiguity function, therefore, might have sidelobe levels that can be greater than $1/M$ in the vicinity of the central peak.

Golomb and Taylor[59] have analyzed the Costas codes and conjecture that $M \times M$ Costas arrays exist for every positive integer M. They show that Costas arrays exist when $M = p - 1$, $M = q - 2$, $M = q - 3$, and sometimes when $M = q - 4$ and $M = q - 5$, where p is a prime number and q is any power of a prime number. If lines were to be drawn connecting pairs of marks in the distinct cells of a Costas array, no two of these lines would be equal in both length and slope. Golomb and Taylor list the known Costas arrays for 271 values of M up to 360. They also indicate that there can be a large number of different Costas arrays for a given value of M. If $C(M)$ represents the total number of $M \times M$ Costas arrays, they give $C(M)$ for values from $M = 1$ to 13. For example, when $M = 7$ (pulse-compression ratio of 49) there are 200 different 7×7 arrays that meet the Costas criterion of only one coincidence in the discrete ambiguity diagram. For $M = 13$, there are 12,828 Costas arrays. The probability that a randomly chosen $M \times M$ permutation matrix will be a Costas array is $C(M)/M!$. Golomb and Taylor state that this probability is less than 10^{-21} when $M = 32$. Thus trial and error search is not practical for large M. Figure 6.21 is an example of a Costas array for $M = 24$ and pulse-compression ratio of 576. For this example, the maximum sidelobe in regions of the ambiguity diagram is predicted to be about 27.6 dB below the central peak when not too close to the central peak, and a bit higher in the vicinity of the central peak.

Nonlinear FM Pulse Compression[60,61] Nonlinear FM offers the advantage over linear FM of producing low time-sidelobes using a constant-amplitude waveform and a theoretically lossless matched filter. It does not experience the loss in signal-to-noise ratio associated

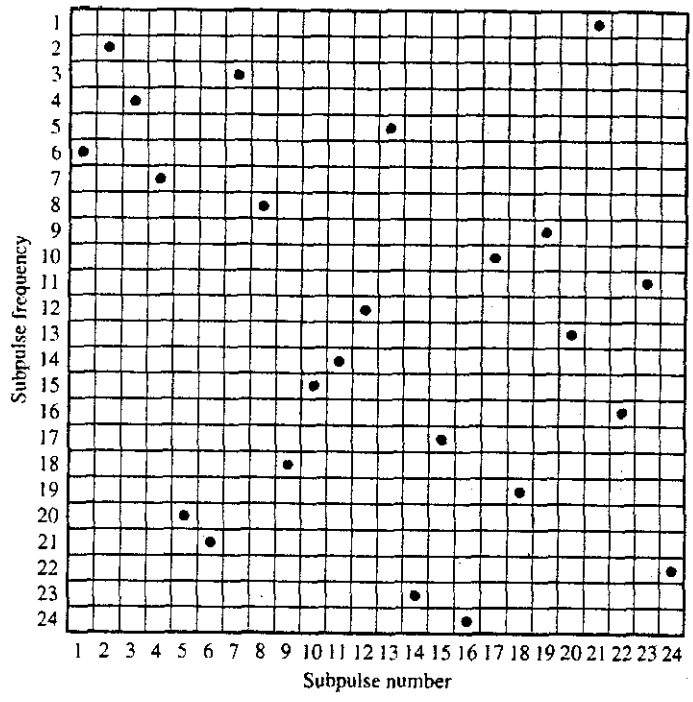

Figure 6.21 Example of frequency-time sequences for a Costas code with $M = 24$, which gives a pulse compression ratio of 576.
[After Golomb and Taylor.[59]]

with the mismatched filter used to reduce sidelobes in a linear-FM pulse-compression system. A constant-amplitude envelope allows efficient generation of high power. The nonlinear rate of change of frequency performs the same role as amplitude weighting of the spectrum. If less time is spent over some part of the spectrum, it is equivalent to reduced amplitude of the spectrum. In addition, there is no significant widening of the compressed pulse. When a symmetrical nonlinear FM is used, the ambiguity diagram is that of a thumbtack; that is, it has a single peak rather than a ridge. (A symmetrical waveform is one where the frequency increases during the first half of the pulse and decreases in a similar manner during the second half of the pulse, or vice versa.) Hence, symmetrical nonlinear FM is more sensitive to large doppler shifts and is not doppler tolerant. A nonsymmetrical waveform utilizes only one half of the symmetrical waveform and has some of the range-doppler coupling characteristic of the linear FM.

Nonlinear FM waveforms result in more system complexity than linear FM. The surface acoustic wave (SAW) dispersive delay line and digital methods can be used to generate and process nonlinear FM. Nonlinear FM waveforms are designed to produce the equivalent of the classical amplitude-weighting functions mentioned previously. Examples of nonlinear FM based on 40-dB Taylor, Hamming, truncated gaussian, and cosine-squared-on-a-pedestal weightings that give low sidelobes (35 to 40 dB, or better) can be found in the literature.[61,62]

Doppler-Tolerant Pulse-Compression Waveforms A *doppler-tolerant waveform* is one whose signal-to-noise ratio out of its matched filter is relatively independent of the doppler

frequency shift (over a wide range of doppler shifts). Thus a single matched filter can be used rather than multiple filters (as in a filter bank). Such waveforms have also been called *doppler invariant.* Several of these have already been encountered in this section.

Short Pulse and Linear-FM A short pulse is doppler tolerant, as can be seen from its ridge ambiguity diagram of Fig. 6.8b. The long pulse of Fig. 6.8a, however, is not doppler tolerant. A bank of matched filters, each tuned to a different doppler shift, is required in order to detect the received signal when its doppler is unknown. The linear-FM is also doppler tolerant, as long as the absolute value of $2(v_r/c)BT$ is not greater than unity, where v_r = radial velocity of the target, c = velocity of propagation, B = bandwidth, and T = pulse duration.[62] When this product exceeds unity the peak-signal out of the matched filter will be significantly reduced and the compressed pulse widened. Except for very high-speed targets and very large values of BT, this restriction is not a concern in most radar applications; but it can be important in sonar since the velocity of acoustic propagation is much lower than that of electromagnetic waves.[63]

Linear Period Modulation The linear-FM waveform is only an approximation to a "true" doppler-tolerant waveform that is not limited by the restriction given in the above paragraph. The doppler-tolerant waveform is[64–66]

$$s(t) = A(t) \cos\left[\frac{2\pi f_0^2 T}{B} \ln\left(1 - \frac{Bt}{f_0 T}\right)\right] \qquad [6.48]$$

The amplitude $A(t)$ represents modulation by a rectangular pulse of width T [sometimes written as rect (t/T)]. The bandwidth is B and the carrier frequency is f_0. This expression for the doppler-tolerant waveform is difficult to interpret as it stands, but if the natural log is expanded using the series $\ln(1 - x) = -(x + x^2/2 + x^3/3 + \cdots)$, for $x^2 < 1$, Eq. (6.48) becomes

$$s(t) = A(t) \cos\left(2\pi f_0 t + \frac{\pi B t^2}{T} + \frac{2\pi B^2 t^3}{3 f_0 T^2} + \cdots\right) \qquad [6.49]$$

When terms greater than the first two can be neglected, Eq. (6.49) is the same as the classical linear-FM (LFM) waveform. Thus the linear FM, or chirp, pulse-compression waveform is a practical approximation to the theoretical doppler-tolerant waveform given by Eq. (6.48).

Differentiating the argument of Eq. (6.48) with respect to time, gives the frequency of the doppler-tolerant waveform as $f_0^2 T/(f_0 T - Bt)$. Inverting to obtain the period, it can be seen that the doppler-tolerant waveform is one whose period is linearly modulated with time; that is, period = $[(1/f_0) - mt]$, where $m = B/f_0^2 T$. This doppler-tolerant waveform has been called *linear-period modulation* (LPM). Because of the logarithm in the argument of Eq. (6.48), it has also been called *logarithmic phase modulation.* It is also known as *hyperbolic frequency modulation* (HFM), since the relationship between frequency and time is hyperbolic. Both the LFM and the LPM waveforms are doppler tolerant in the sense that the signal-to-noise ratio and the compressed pulse width are not significantly changed by a doppler frequency shift. However, with both waveforms there is coupling

between the range and the doppler; and the peak response will be shifted in time so that a range error can result, as evident in the ambiguity diagram of Fig. 6.9 for the LFM waveform.

The time sidelobes of the LPM waveform, after passing through the matched filter, are higher than those of the LFM waveform.[66] It has been said that weighting can reduce the LPM sidelobes to the range of -20 to -30 dB.[67] The spectrum of the LPM is not uniform but falls off exponentially as the frequency increases. The amount of exponential decay depends on the ratio of the highest-to-the-lowest frequency.

LPM pulse-compression is more likely to be important for acoustic (sonar) echolocation applications than for radar. Since the velocity of sound is much smaller than the velocity of light, the acoustic LFM waveform might result in an unacceptable widening of the compressed pulse and a lowering of the output signal-to-noise ratio. Various species of bats have been found to employ acoustic echolocation with LPM waveforms. The LPM is needed rather than LFM since the bandwidth-pulsewidth products are generally high enough to cause the absolute value of $2(v_r/c)BT$ to exceed unity.[68] The bat, which depends on acoustic echolocation to fly through dark caves with impunity and to find and catch insects in flight, has evolved a remarkable pulse compression system during its many years on earth, long before radar or sonar existed.

An accelerating target causes a frequency shift of an LPM signal.[69] The LPM waveform can be made to accommodate accelerating targets if a bank of filters is employed that is matched to the frequency-shifted versions of the received LPM waveform. It has been said, however, that wideband LFM signals "may be quite capable of achieving high acceleration tolerance without the need for separate acceleration-processing channels," even though this waveform is less doppler tolerant than the wideband LPM.[70]

Other Pulse Compression Waveforms There are several other pulse-compression waveforms that have been considered for radar. They each have some interesting characteristics; but as is true of almost everything, they also have some limitations.

Nonlinear Binary Phase-Coded Sequences[71,72] Linear recursive sequences, or shift-register codes, were discussed earlier in this section. They are formed with an n-stage shift register with a feedback logic consisting of modulo-2 additions. The number of different maximal-length sequences that can be obtained with an n-stage shift register with linear feedback logic is approximately $2^n/n$. If nonlinear feedback logic is used instead, the number of maximal length sequences increases to $2^{2^n-1}/2^n$. This large number is of interest when many different codes are desired for such purposes as minimizing mutual interference, providing more security to the code, or making deception jamming more difficult. With a five-stage shift register, for example, only six 31-symbol maximal-length sequences can be obtained when linear feedback logic is used. With nonlinear feedback, 2048 different 32-symbol pseudorandom sequences are available. The length of a nonlinear sequence from an n-stage shift register can be 2^n rather than the $2^n - 1$ for linear sequences.

Complementary Codes It is possible to find pairs of equal-length phase-coded pulses in which the sidelobes of the autocorrelation function of one are the negative of the other. If the autocorrelation functions from the outputs of the two matched filters are added, the algebraic sum of the sidelobes will be zero and the main response will be $2N$, where N

is the number of elements in each of the two codes. These are called *complementary codes,* or *Golay codes* after the person who first reported their existence and described how to construct them.[73] Theoretically, there are no sidelobes on the time axis when complementary codes are employed. Complementary codes can be obtained with either binary or polyphase sequences.[74]

There are two problems, however, that limit the use of complementary codes.[75] The first is that the two codes have to be transmitted on two separate pulses, detected separately, and then subtracted. Any movement of the target or instability in the system that occurs during the time between the two pulses can result in incomplete cancellation of the sidelobes. Transmitting the two codes simultaneously at two different frequencies does not solve the problem since the target response can vary with frequency. The second problem is that the sidelobes are not zero after cancellation when there is a doppler frequency shift so that the ambiguity diagram will contain other regions with high sidelobes. Thus this method of obtaining zero sidelobes has serious practical difficulties and is not as attractive as it might seem at first glance.

Welti Codes[76] These are related to Golay complementary codes in that they are used in pairs that are subtracted from one another to obtain autocorrelation functions with zero time sidelobes. They use four phases (0,90,180,270°) rather than the two phases (0, 180) of the Golay codes. They are a class of polyphase codes but have ambiguity diagrams more like those of biphase codes than the Frank polyphase codes.[77] Welti codes can present the same problems as other complementary codes.

Huffman Codes[78] So far, every pulse-compression waveform discussed in this section is of constant amplitude across the uncompressed pulse. The signal bandwidth is increased by phase or frequency modulation rather than by amplitude modulation. The Huffman codes, on the other hand, consist of elements that vary in amplitude as well as in phase. When the doppler shift is zero, they produce autocorrelation functions with no sidelobes on the time axis except for a single unavoidable sidelobe at both ends of the compressed waveform. The level of these two end-sidelobes is a design tradeoff. In one example,[79] a Huffman code of length 64 with no doppler shift has a sidelobe at each end that is 56 dB below the peak. As with other methods for obtaining zero or low sidelobes, the volume under the ambiguity diagram must remain constant [Eq. (6.46)], which means that higher sidelobes will appear elsewhere in the doppler domain. The sidelobes also degrade if the tolerances in amplitude and phase are not maintained sufficiently high or if there are too few bits in the A/D converter.

Variants of the Barker Code The pulse compression ratio of a conventional Barker code can be increased (beyond the maximum of 13) by making each element of the Barker code itself a Barker code. For example, a Barker code of length 13 in which each element is also a length 13 Barker gives a combined code length of 169 with a pulse compression ratio of 169 and a maximum sidelobe 22.3 dB below the peak.[80] Thus the pulse compression ratio is increased by increasing the length of the uncompressed pulse, but there is no decrease in absolute sidelobe level. This is called a *combined Barker code,* but it has also been known as a *compound Barker* or a *concatenated Barker.*

The sidelobe level of a conventional Barker code can be decreased by extending the time-sidelobe region beyond $2T$, where T = the uncompressed pulse width. This method, suggested many years ago by Key, Fowle, and Haggarty,[81,82] makes use of the fact that the equal-amplitude sidelobes and the main lobe of the autocorrelation function of the Barker codes are of similar shape. Because of this geometric similarity, it is possible to suppress the sidelobes by adding properly weighted and time-shifted replicas of the matched-filter output to the original output of the matched filter. That is, the autocorrelation function of the Barker-13 code, as was shown in Fig. 6.17b, is passed through a transversal filter with delays and weighting designed to eliminate the original sidelobes. If, for example, the six sidelobes that are on each side of the main lobe of a 13-bit Barker are to be removed, there can be six weighted (reduced amplitude) replicas of the Barker code autocorrelation function applied at six different times ahead of the main lobe and six different times behind the main lobe. To accomplish this the Barker code matched filter would be followed by a 13-tap transversal filter with the proper weightings at each tap to completely eliminate (in theory) the original sidelobes. As a result, new sidelobes will appear farther out in time on either side of the original Barker-13 sidelobes. These new sidelobes will be lower than the original. The new maximum sidelobe generated because of the transversal filter will be 32.4 dB below the peak instead of the 22.3 dB of the original. The loss in signal-to-noise ratio is about 0.25 dB, which is small.

Sidelobe Reduction for Phase-Coded Pulse-Compression Signals Suggestions have been made to reduce the sidelobes of phase-coded signals by following the matched filter with a transversal filter with weights that reduce the time sidelobes, similar to that described by Key et al. in the above. The weights are selected according to one of two criteria: (1) minimize the total energy in the sidelobes or (2) minimize the peak sidelobe. The number of bits (taps) in the delay line of the transversal filter can be greater than the length (number of bits) of the phase-coded signal. When the number of bits in the transversal filter is greater than that of the matched filter, the phase-coded signal is zero-padded to the same length as the filter.

One of the first papers to discuss this method was by Ackroyd and Ghani,[83] who determined the weights of a transversal filter so as to give a compressed output signal that approximates the desired output signal in the least-squares sense. The output to be minimized is a sum that represents the "energy" of the difference between the actual sidelobe levels and the desired levels. This is sometimes known as minimizing the integrated sidelobes, or ISL.[84] Starting with a Barker-13 code, Ackroyd and Ghani show that with least-squares filters of lengths 13, 41, 53, and 66, the maximum sidelobe levels below the main peak are 24 dB, 40 dB, 50 dB, and 60 dB, respectively. It is said that when the Barker-13 matched filter is replaced with the least-squares filter, the loss in signal-to-noise ratio is 0.2 dB.

This technique has also been applied to reducing the sidelobe levels of the combined Barker code.[85] A 52-element combined Barker code, for example, can be generated by combining a 4-element Barker code with a 13-element Barker code. When passed through a 200-bit minimum square-error transversal filter, a maximum sidelobe level 40.7 dB below the peak is produced. This mismatched filter results in a computed loss of 1.86 dB.

Similarly, the weights of a transversal filter can be chosen to minimize the peak sidelobe.[86] Baden and Cohen[87] show that the peak sidelobe obtained using this criterion is from one to seven dB less than the peak sidelobe obtained using the minimization of the integrated sidelobes, depending on the particular code and filter length. Loss in signal-to-noise ratio is said to be less than one dB. Compared to the sidelobes of the original output of the matched filter, reductions of 15 dB or more "are readily achieved for reasonable filter lengths." This sidelobe-weighting technique can also be used for generating mismatched filters that produce sidelobe-free regions in the vicinity of the main lobe.

Although there are several methods described for reducing the sidelobes of the output of a matched filter for binary phase-coded signals, apparently they have not had as much application as the nonmatched weighting filter used to reduce the time sidelobes of the linear-FM pulse compression waveform.

Other Aspects of Pulse Compression

Generic Compressed Signal By way of review, the general nature of the compressed pulse produced by a matched filter is sketched in Fig. 6.22. The peak of the compressed pulse is equal to $2E$, where E is the energy of the input signal. (Note, however, that the units of the peak output is in volts, not joules.) The peak value depends only on the input-signal energy and not on the signal shape. The width of the compressed pulse is approximately $1/B$, where B = signal bandwidth, regardless of how the bandwidth is obtained. When the total duration of the uncompressed signal is T, the sidelobes of the compressed pulse extend over a time $2T$. The nature of the sidelobes is determined by the shape of the uncompressed signal, $s(t)$. One of the most important aspects of pulse compression design is the selection of $s(t)$ to minimize the sidelobe level.

The major difference between pulse compression and a short pulse of the same resolution and energy is that the short pulse has no time sidelobes, whereas the pulse compression signal has sidelobes that can be mistaken for real targets or mask the presence of small targets located within the sidelobe region that extends over a time $2T$ in extent.

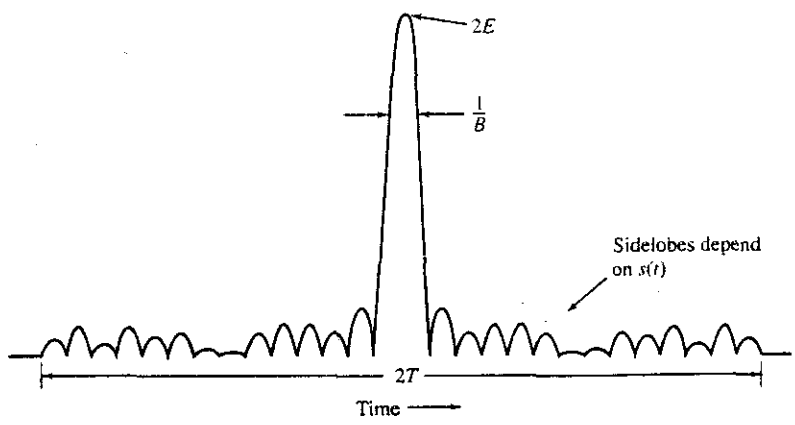

Figure 6.22 Sketch of a generic compressed pulse whose *uncompressed waveform is s(t)*, with bandwidth B, time duration T, and energy E.

Limiting in Pulse Compression Since the amplitude of uncompressed radar waveforms is constant, limiting is sometimes used in the receiver before the matched filter to insure that the input signal to the matched filter is of uniform amplitude or to provide a constant false-alarm rate using CFAR. It was said in Chap. 3 that hard limiting should not be used with MTI radar since it can significantly decrease the improvement factor. If pulse compression is used with MTI, and if hard limiting is desired for pulse compression, the limiter and the pulse compression matched filter can follow the doppler processing rather than precede it. On the other hand, when pulse compression follows the MTI, the MTI processor does not benefit from the reduction in clutter obtained with pulse compression. If there are significant instabilities in the MTI transmitter and oscillators, the use of limiters with pulse compression is different from that assumed here, as will be described later under the heading "Compatibility with Other Processing."

If MTI precedes the pulse-compression matched filter or if MTI is not used at all in the radar, then limiting can be employed with pulse compression. Even so, there are several concerns with the use of a limiter in pulse compression. These include (1) the loss incurred in the signal-to-noise ratio, (2) the suppression of nearby small target signals, and (3) the possibility of spurious (false) targets.

For phase-coded waveforms, the loss in signal-to-noise ratio decreases with the length of the code and the number of pulses integrated. Table 6.6 summarizes the loss due to limiting as given by Castella and Rudie.[88] A hard limiter is one in which the limit level is set low enough (well into the noise) so that there is no variation in the amplitude of the output signal. Phase and frequency modulations, however, are preserved. The hard limiter listed in the table corresponds to analog limiting in the IF. A digital soft limiter is defined by Castella and Rudie as one where the I and Q signal components are quantized to three bits at baseband, with two of these bits allotted to $\pm$ 2 sigma of the noise. The table indicates that one should try to have long code lengths and a large number of pulses integrated if hard limiting is used.

Table 6.6 Loss with phase-coded waveforms due to limiting[88] (probability of detection = 0.5; probability of false alarm = 10^{-6})

Type of Limiter*	Code Length	Number of Pulses Integrated	Loss in Signal-to-Noise Ratio
Hard limiter	16	1	6.4 dB
	16	8	1.8 dB
	128	1	1.4 dB
	128	8	1.1 dB
Digital soft limiter	16 to 128	1 to 8	0.4 to 0.5 dB
Digital hard limiter	16	1	8.6 dB
	16	8	3.0 dB
	128	1	2.4 dB
	128	8	2.0 dB

*See text for descriptions of limiters

The second concern mentioned above, small-signal suppression, involves two uncompressed pulses that overlap. The effect of the limiter is to cause the smaller of the two signals to be suppressed and be less detectable than if limiting were not employed. This can occur with either a linear FM or a phase-coded signal. In the overlap region the weaker signal can be suppressed by as much as 6 dB if the stronger signal has a large signal-to-noise ratio.[89] The noise is also reduced. The net result can be a reduction of the detection probability of the weaker signal, which deteriorates rapidly depending on the amount of overlap.[90]

The third concern is the possibility of generating false targets in addition to the real targets when there is overlap of the uncompressed pulses. Woerrlein[91] states that with two overlapped linear-FM signals there can be an array of false targets that appear on both sides of the two target returns. If the two signals are only partially overlapped, there will be a consequent reduction in the number of false targets. There is, on the other hand, no evidence of any false targets when two binary-phase signals overlap; but when three binary-phase signals overlap, there is a fourth signal that is false. His analysis applies only to large signal-to-noise ratios.

In the above, limiting was assumed to be intentionally included in the radar processing; however, there can be unintentional limiting that can occur when the receiver is driven to saturation by large clutter echoes or interference signals.

Cross-Correlation Properties It is sometimes desirable for more than one radar to operate simultaneously at the same frequency within the same region of coverage. Each radar can employ different pulse-compression waveforms to minimize crosstalk (when one radar accepts signals from another radar as true targets when they are really false alarms). The potential that various waveforms will cause mutual interference or false target-reports can be determined by examining the cross-correlation function (the cross-ambiguity function) between two different signals. In general, the maximum output produced in one radar by a signal from another radar with a different waveform covering the same bandwidth will usually be greater than the sidelobes of the radar's own autocorrelation function (the output of its matched filter).

If there are only two radars each using linear-FM pulse compression, one could have an up-chirp and the other a down-chirp to reduce crosstalk. Nonlinear FM waveforms can also be considered for avoiding crosstalk among various radars.

It is possible to find two Costas (frequency hopped) codes so that the sidelobe power level of the response of one in the other is no greater than $(2/M)^2$ that of the main lobe peak, where M is the number of frequencies and M^2 is the pulse compression ratio.[92] This compares with a maximum sidelobe level of $(1/M)^2$ for the ambiguity function of a Costas code, as mentioned earlier in this section. When more than two signals with Costas codes are present, the maximum cross-ambiguity sidelobes can be much greater than $(2/M)^2$.

For binary phase-coded pulses, H. Deng[93] estimated that the maximum sidelobe (power) level of the cross-correlation function for a set of k binary sequences ($k \geq 2$) is $kM/3(k-1)$ below the peak of the compressed pulse. Each of the k binary sequences is of the same length M. For $k = 2$, this expression predicts a maximum sidelobe $(M/1.5)^2$ below the peak. Thus the cross-correlation sidelobes are not as low as those of the autocorrelation function [which can be $(M)^2$ below the peak]. Using the optimization

technique known as *simulated annealing*, Deng finds sequences of codes with cross-correlation lobes close to that predicted when $k = 2$ or 3. (In his optimization he allowed the autocorrelation maximum sidelobe level to be weighted equally with the cross-correlation maximum sidelobe level.) With increasing k, the expression for estimating the cross-correlation sidelobes predicts better sidelobes than actually obtained by the use of simulated annealing, which is attributed to it being difficult to satisfy the approximations used in the estimate when k is large.

Compatibility with Other Processing Pulse compression may be used in conjunction with MTI radar, as was mentioned previously in this section. Care needs to be taken when they are used together so that if limiting is used for pulse compression it does not degrade the performance of the MTI. The increased range resolution of pulse compression can reduce the amount of clutter the radar sees so that less MTI improvement factor is required. This may be true for an ideal system; but as pointed out by Shrader and Gregers-Hansen,[94] the performance of the MTI may be no better, or even worse, than a system transmitting the same-length uncoded pulse if there are significant system instabilities that cause increased sidelobes.

The sidelobes produced in a pulse compression waveform because of system design or components that are nonlinear with frequency do not vary with time and will therefore cancel in the MTI processor just as would clutter. Instabilities due to noise from the local oscillators, transmitter power supplies, time jitter, and other transmitter noise, however, result in noiselike time-varying sidelobes that are proportional to the clutter amplitude. These noiselike time-sidelobes are not canceled by the MTI and can produce residual clutter that can cross the detection threshold and appear as targets. Shrader and Gregers-Hansen suggest a method for dealing with these noiselike sidelobes. The pulse-compression filter precedes the MTI processor, but a limiter is placed ahead of it. The limiter's dynamic range at its output is set equal to the difference between the peak transmitter power and the transmitter noise within the system bandwidth. A second limiter is placed after the pulse compression filter. The dynamic range at its output is set equal to the expected MTI improvement factor. The MTI processor follows. The two limiters cause the residue due to transmitter noise and other instabilities to be equal to the front-end thermal noise at the input to the MTI processor. The two limiters are adjustable so that when the radar is placed in the field, they can be compensated to allow for differences in clutter and the condition of the radar equipment.

Special consideration has to be given to pulse compression when used in multichannel radars, such as the three receiving channels of a monopulse tracker or the many thousands of channels of an active-aperture phased array radar. Each channel has to be highly matched (almost identical) to all the rest. The reproducibility and precision of SAW devices makes them attractive for applications where precision multiple pulse-compression units are required.[95]

Spread Spectrum Spread spectrum communication systems[96] employ coded waveforms similar to those used in pulse compression radar. The purpose of coded waveforms in communications is different, however, from their purpose in radar pulse compression. Spread spectrum communication waveforms allow multiple simultaneous use of the same frequency band by coding each transmitted signal differently from the others. In military

communications, spread spectrum waveforms also have the capability of rejecting interference as well as reducing the probability of being detected by a hostile electronic-warfare receiver. Sometimes pulse compression radars that use waveforms similar to those of spread spectrum communications have been called *spread spectrum radars*. This terminology, however, is misleading since the purpose of coded waveforms in pulse compression is entirely different from their purpose in spread spectrum communications. It is suggested that the use of the term *spread spectrum* for describing a pulse compression radar be avoided.

Comparison of Pulse Compression Waveforms As seen in this section, there are a number of different pulse compression waveforms with different advantages and limitations. Table 6.7 compares the theoretical sidelobe levels that might be achieved with various

Table 6.7 Maximum sidelobe level for various pulse compression waveforms. (Maximum sidelobe is in dB down from the peak of the compressed signal.)

Pulse Compression Ratio	Pseudorandom Sequences	Computer-Search Binary Phase	Polyphase[1]	Costas[2]
13		22.3		
15	14.0			
16			21.2	12.0
25			23.9	14.0
28		22.9		
31	17.8			
49			26.8	16.9
63	20.4			
64			28.0	18.0
73		25.2		
88		24.7		
100			29.9	20.0
112		25.4		
121			30.8	20.8
127	24			
129		25.3		
144			31.5	21.6
255	25.9			
256			34.0	24.1

[1]For polyphase codes, the maximum sidelobe is taken here to be $\pi^2 N$ down from the central peak, where $N = M \times M$ = pulse compression ratio, and M is the dimension of the matrix.

[2]For Costas codes the maximum sidelobe away from the central peak is taken to be N down from the peak, where $N = M \times M$ = pulse compression ratio and M = number of subpulses (equal to the number of frequencies). Near the central compressed peak, the sidelobes can be larger than indicated in the table.

pulse compression waveforms. The polyphase codes have the lowest predicted sidelobes in this table; but the greater the pulse compression ratio, the smaller the phase increment and the greater must be the precision. A pulse compression ratio of 900, for instance, requires a phase increment of $360/\sqrt{900} = 12°$, and a phase tolerance that is a small fraction of this increment.

Linear FM has been the waveform used most in the past in radar pulse compression. It is less complex than some others, especially if the application permits the use of Stretch. It usually requires weighting on receive to reduce the -13.2 dB sidelobes to the order of -30 dB, with a loss of about one dB. The range-doppler coupling that causes an error in the range measurement when there is a doppler frequency shift is sometimes of little consequence. If not, the true range can be obtained by use of both an up-chirp and a down-chirp. The ridge ambiguity diagram of the linear-FM waveform means that it is doppler tolerant and that a single filter can be used when there is a large doppler shift.

The linear-period waveform is related to the linear FM and is in theory a true doppler-tolerant waveform. In most radar applications, it does not seem necessary to use linear period instead of linear FM.

The nonlinear FM waveform might be more complex than linear FM, but it can give low sidelobes without the loss caused by a mismatched weighting filter. Its thumbtack ambiguity diagram means that a bank of matched filters is needed if there are large doppler shifts, further complicating the processing. In long-range radars where it is important to minimize loss, the nonlinear FM might be considered when low sidelobes are needed.

Binary phase-coded pseudorandom waveforms were sometimes considered in the past for military pulse compression radar when it was originally believed they could provide some degree of security from deception jamming or spoofing. Shift-register codes might appear random, but by examining only a portion of the code, the rest of the code can be readily predicted. Geffe[97] pointed out that the connections of an n-stage shift register that generates binary coded waveforms can be determined by elementary methods from a knowledge of $2n - 1$ successive digits of the shift-register sequence. Thus they have no inherent security. Nonlinear shift-register codes have many more options than linear shift-register codes and for this reason might be a little better for security purposes. Truly random codes might not have the limitation of pseudorandom codes; but even if these codes were fully crypto secure, they would not possess as low sidelobes as other pulse compression waveforms. Processing of binary phase-coded signals is more complex than for linear FM, and they require a filter bank to be employed when the doppler shifts are large.

A brief comparison of the linear FM and the binary phase-coded pulse compression waveforms is given in Table 6.8.

Polyphase codes have lower sidelobes than binary phase codes. They are not very doppler tolerant for large doppler-frequency shifts, but appear to be suitable for detection of targets with aircraft velocities. They could be of interest for pulse compression applications, but have not been widely used. The sliding-window modification suggested by B. Lewis[55] appears to provide significantly lower sidelobes than any other pulse compression method but with a small loss in signal-to-noise ratio.

Costas (frequency-hopping) codes achieve a particular pulse compression ratio with fewer subpulses than phase-coded waveforms. Their sidelobes appear to be almost the same as ordinary binary phase-coded waveforms. Many more different Costas codes of a

Table 6.8 Comparison of Linear Frequency Modulation and Binary Phase-Coded Pulse Compression Waveforms

Property	Linear FM	Binary Phase-Coded Pulse
Time sidelobes	Good (~30 dB) when weighting on receive, and when a loss of about 1 dB can be tolerated	Can be equal to $1/2N$, and are not easy to improve; poor doppler sidelobes
Doppler	Doppler tolerant	Requires filter bank
Ambiguity diagram	Ridge	Thumbtack (but with high sidelobes in plateau)
Pulse compression filter	Single filter can be used for transmit and receive; usually analog for high resolution	Single filter can be used for transmit and receive, but with input at opposite end; usually digital
Complexity	Less complex, especially if Stretch can be used	More complex, (requires filter bank)
Application	High resolution (wide bandwidth)	Long pulses
Other	Range-doppler coupling; has been more widely used than other pulse compression	Bandwidth limited by availability of A/D converter; erroneously thought to be less susceptible to ECM spoofing

given length are available than can be obtained with binary phase codes. This property might be of interest in military radars concerned with operating against some forms of electronic countermeasures.

Complementary codes and Hoffman codes that are supposed to produce zero sidelobes along the zero-doppler time axis have interesting theoretical properties, but have serious practical limitations that make their use in radar less likely.

In engineering design when there is more than one possible method for accomplishing some desired objective, there is seldom one solution that is best for all applications. This applies as well to pulse compression. The radar designer should keep an open mind and examine the options carefully to determine the type of pulse compression waveform to be used for any particular radar application.

6.6 TARGET RECOGNITION

Early radars were "blob" detectors in that they detected the presence of a target and gave its location in range and angle, but could not provide much else about the type of target being detected. As radar resolution in range and cross-range improved over the years, it became possible to resolve the individual scattering centers of a target and infer

something about its nature. Radar began to be more than a blob detector and could provide recognition of one type of target from another.

Even without high resolution, radar has been able to recognize the general nature of a target, or scattering object, based on such information as its behavior in space and time. The frequency dependence of the cross section can also be a useful discriminant in some cases.

The various degrees of target recognition are listed below in increasing order of information required for a decision:

- *General nature of target:* Recognition that the echo on a radar display is that of an aircraft, ship, motor vehicle, bird, person, rain, chaff, clear-air turbulence, land clutter, sea clutter, bare mountains, forested areas, meteors, aurora, ionized media, or other natural phenomena. A trained and experienced radar operator with the right type of radar should be able to sort these broad classes of target echoes from one other.
- *Target type:* This includes recognizing a fighter aircraft from a multi-engine bomber aircraft, a cargo ship from a tanker, a tracked military vehicle from a truck, chaff rather than a ship, a buried rock instead of a mine; or a surface-to-air missile site from a dump site. Sometimes this coarse form of recognition has been called *perceptual classification.*
- *Target class:* This involves determining the particular class to which a target belongs among the many possible classes. For example, if the radar believes it is detecting an aircraft, is it an F-18, F-22, MIG-31, B-2, A-6, Rafale-2000, or something else? If the target is a ship, does it belong to the Aegis destroyer Class DDG-51, Aegis cruiser CG-47, Kara, Sovermeney, or so forth, or is the echo that of a chaff decoy? If it is a bird, is it a starling, mallard, or what else? The process of determining the class of the target is known as *target classification.*

The above definitions are not standardized, so one needs to be careful when hearing or reading such terms to make sure their meanings are clear. Unfortunately, this is not always the case in the literature of target recognition.

The ultimate form of target recognition is *target identification*, which involves determining the actual name of the target, its serial number, or its side number. Identification of a target usually requires a cooperative system; that is, the target must cooperate in some manner with the identification sensor. The target has to have some form of communication system, data link, or transponder system that allows it to identify itself on a regular basis or when asked for its identification by an interrogator. *Noncooperative target recognition* (NCTR) systems, of which radar is an example, obtain target recognition information without any cooperation from the target itself. In the case of radar NCTR, recognition is based on examining the characteristics of the radar echo signal received from the target.

Military cooperative identification systems are called IFF, or *Identification Friend or Foe.* They have also been known as CAI, or *Cooperative Aircraft Identification.* In civil air-traffic control, cooperative identification methods are called ATCRBS, or *Air-Traffic Control Radar Beacon System.* IFF and ATCRBS are examples of *question and answer systems,* in that an interrogator asks the question, "who are you?" and a transponder on the target automatically answers "I am a friend and my name is . . ."

The ability to perform noncooperative target recognition with radar depends on the type of target. Ships, for example, are easier to sort by class than aircraft since ships contain many more individual scatterers with which to recognize one class from another. Target classification generally requires greater signal-to-noise ratio than does target detection since detection depends on the total signal energy, but target recognition depends on discerning the details of the target echo signature. The many small scatterers on a target can sometimes be more important for recognition than the few large scatterers that are more important for detection. The need for large signal-to-nose ratio to detect the small scatterers means that reliable target recognition usually occurs at a shorter range than does detection.

Noncooperative target recognition methods are mainly of interest to the military. By contrast, civilian needs for aircraft target recognition are usually satisfied by cooperative methods, such as the ATCRBS. NCTR sensors, such as radar designed for that purpose, have the task of recognizing one class of target from many others that might be present. Both NCTR and cooperative methods are jointly used for the important military function of *Combat Identification.* When the target is a spacecraft or satellite, target recognition is sometimes called *Space Object Identification,* or SOI. *Automatic Target Recognition,* or ATR, is a name that could apply equally well to NCTR or combat identification, but it appears to be used mainly to describe automatic methods used for the recognition of military land targets. In the civilian sector, the use of radar and other sensors to determine the nature of the natural environment is known as *remote sensing.* Remote sensing radars observe precipitation, atmospheric effects, wind shear, birds and insects; determine the earth's surface topography; explore planets and their moons (such as probing the surface of Venus beneath its ever-present cloud cover); and monitor ice conditions, the mean sea level, and the winds that drive the ocean surface.[98]

There are two aspects to target recognition. The first is to separate the target echo from its surroundings (such as clutter) and extract from the radar echo-signal information about the unique features of a target that can help distinguish one target from another. The second aspect is the method by which one makes the actual decision as to which class or type of target a particular radar signature belongs. The decision is usually, but not always, made automatically and is often based on classical pattern recognition methods or similar decision-making methods. For example, known target signatures can be stored in a computer memory (a library) and when an unknown signature is measured, it is compared with the library of signatures to see which it matches best. (This is an overly simplified statement. The actual algorithms for target recognition can be quite sophisticated.) Only the first aspect, that of information extraction, is considered here.

Target recognition, whether by radar, optics, or the human eye, is not 100 percent accurate. Even cooperative systems do not have accuracies approaching 100 percent.* A target recognition method must be able to recognize one class of target out of many tens of classes with an accuracy of perhaps 85 percent or better before it can be taken seriously. Good target recognition methods might have accuracies of 95 percent or better, which is

*The accuracy of target recognition or identification can be no better than the "availability" of the equipment (where availability is the fraction of the time the equipment can be operable). Thus if a particular IFF or an NCTR has an availability of, for example, 95 percent, the accuracy of target recognition or identification obtained from such an equipment can be no better than 95 percent.

one error out of 20 decisions. There have been many radar target recognition methods proposed and explored; but only a few have been able to achieve the accuracy and reliability required, especially when the total number of targets to be recognized at any one time is large. For this reason, more than one type of recognition method is generally employed in combination to increase the overall probability of a correct decision and approach 100 percent accuracy of a correct recognition decision.

When a target is moving in the presence of clutter, the clutter echoes can be filtered out by doppler processing, as in MTI (moving target indication) radar. If the target is stationary in the midst of clutter, MTI is not applicable and some other technique must be used to separate the target from its surrounding clutter. Some of the target recognition methods mentioned here can be applied for such a purpose. Detection of nonmoving targets is sometimes called *stationary target indication* (STI).

In the remainder of this section, several target recognition methods based on radar will be briefly reviewed. All targets are assumed to be in the clear; or, if clutter is present, the targets are separated by some means from the clutter.

One-Dimensional Imaging with High Range-Resolution Radar A radar with sufficiently high range-resolution can resolve the individual scattering centers of a target and provide the radial profile (the one-dimensional image) of the target. The radial profile might provide a measure of the length of a target in the range dimension, but the true physical target-length usually cannot be determined accurately in this manner. The ends of the target might not always provide large enough echoes to be detected, one of the ends might be masked by other parts of the target, or the aspect angle of the target with respect to the radar might not be known accurately. Even if the length could be measured with accuracy, it is not usually a good means for recognizing the particular class of most targets of interest.

The radial profile of a 757 aircraft obtained with an L-band air-surveillance radar having 1-m range resolution is shown in Fig. 6.23.[99] In the upper portion of the figure are superimposed seven time-aligned pulse-to-pulse radial profiles. The radial velocity of the target can be obtained by measuring the target movement from the first pulse to the last. The average of the seven time-aligned radial profiles is displayed in the lower part of the figure, from which a target dimension can be obtained. With a knowledge of aspect angle, a wingspan or aircraft length can then be estimated. Figure 6.23 is typical for a jet aircraft in that the individual resolved scatterers are relatively constant. A propeller aircraft, on the other hand, can have constant returns from the nose and the tail, but there can be large pulse-to-pulse fluctuations from the propellers, which make it possible to distinuish a propeller aircraft from a jet.

Figure 6.24 is a radial profile of a large naval ship using an X-band radar with a resolution of about 0.3 m. As can be seen, the radial profile of this target remained relatively the same when measurements were obtained a year later.

The radial profile has often been considered a potential method of aircraft target classification. A serious difficulty exists, however, in that the details of the radial profile can change with only a small change in aspect. Masking of one part of the target by another can occur. If there is more than one scattering center within a radar's resolution cell, the relative phases of each scatterer can change with a change in aspect. This causes

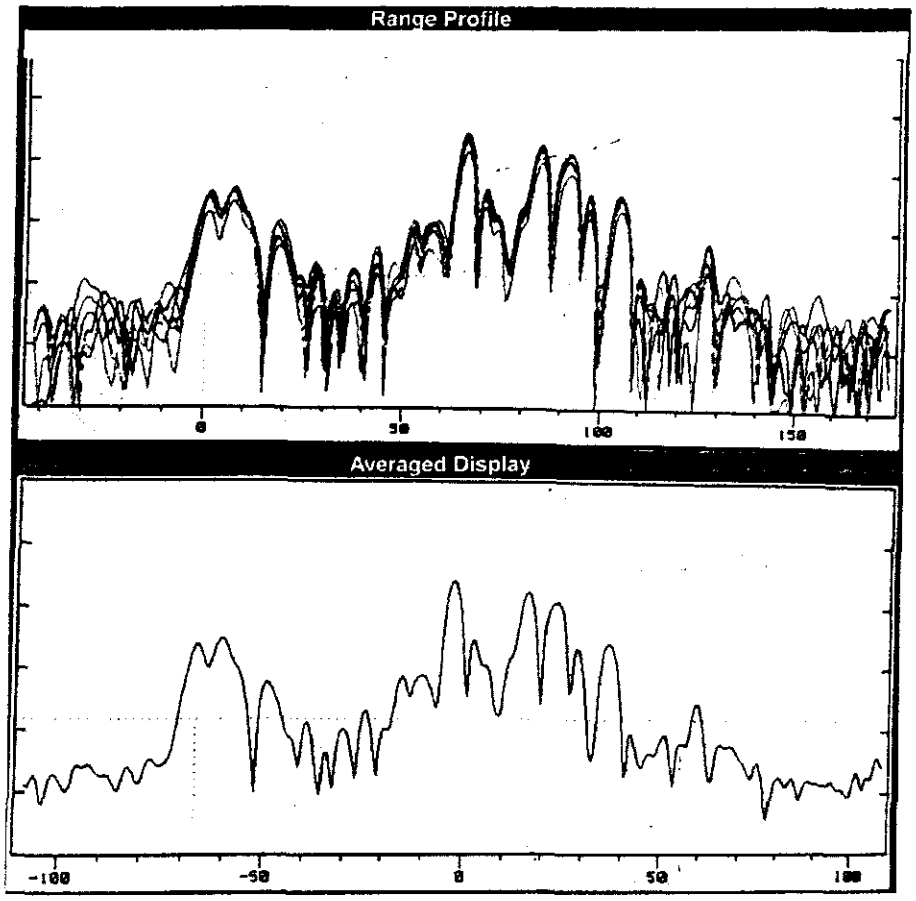

Figure 6.23 Radial profile of a commercial 757 aircraft obtained with an L-band radar with a range resolution of about 1 meter. Upper: the superposition of seven time-aligned pulse-to-pulse radial profiles. Lower: average of the seven profiles. Abscissa is in feet.
[Provided by G. Linde of the Naval Research Laboratory.]

constructive and destructive interference and a change in the resultant cross section of the scatterers within the resolution cell. When creating a library of radial profiles to be used to match to an unknown profile, each target in the library has to be characterized by many reference profiles corresponding to different aspect angles. To make use of this library of reference profiles, the aspect angle of the unknown target must be estimated. (Observing the target's trajectory is one method for estimating the aspect.) There might need to be a large number of reference profiles stored in computer memory for each target. Furthermore, there can be many tens or even hundreds of classes of targets that need to be considered. The use of high range-resolution for target recognition starts out simple but quickly becomes complex. The result is that the use of high-resolution radial profiles for target classification is not easy to achieve in practical situations.[100,101]

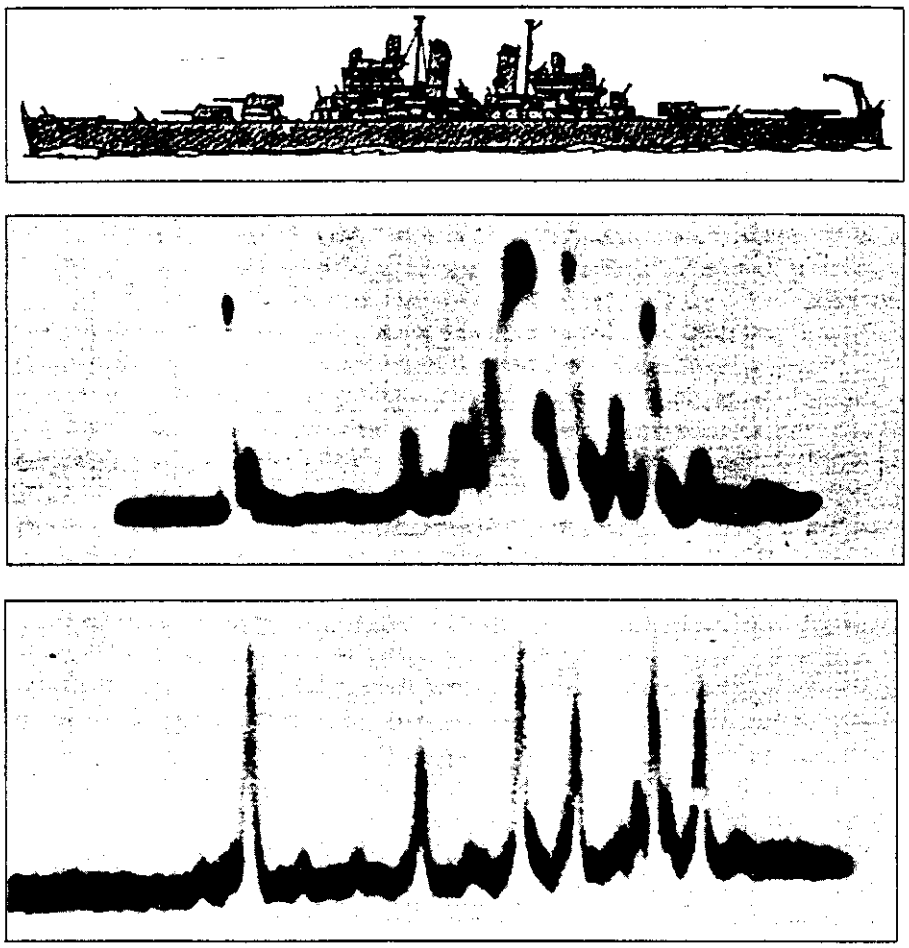

Figure 6.24 Radial profile of the former U.S. Navy gun cruiser USS Baltimore obtained with an X-band radar of 1-ft range resolution. (a) Outline of ship; (b) stern aspect; (c) bow aspect taken one year earlier than in (b).
[Provided by I. W. Fuller, formerly of the Naval Research Laboratory]

Perceptual Classification Although it is difficult to use one-dimensional radial profiles of a target to recognize one class of target from another, it is possible to separate targets into a simpler set of general classes. This has sometimes been called *perceptual classification.* In the case of aircraft, G. Linde and C. Platis[99] were able to show from the radial profile obtained with an L-band radar, having 1-m range resolution, that targets could be separated into the following general categories: small or large jet-engine aircraft, small or large propeller aircraft, helicopters, and missiles. The perceptual classification of aircraft does not always need a dedicated special purpose radar system. It can be achieved, for example, as

demonstrated by Linde, by employing a wideband air-surveillance radar using Stretch pulse compression to obtain high range-resolution as the antenna scans by the target.

When employing high-resolution range-only information for the one-dimensional imaging of ships, it is possible to separate the ships into such categories as large ships, small ships, military ships, commercial ships, tankers, and aircraft carriers. Although perceptual classification is limited in its utility, the requirements on the radar are not as large as when determining the class of target. For reliable target classification other information usually is needed in addition to the radial profile. This added information can be the high-resolution cross-range profile, as discussed next.

Two-Dimensional Radar Imaging of Targets The two-dimensional image of a target (in range and cross-range) can be obtained by use of an imaging radar such as *synthetic aperture radar* (SAR), *inverse synthetic aperture radar* (ISAR), or more conventional high-resolution radars such as the *side-looking airborne radar* (SLAR).

Synthetic Aperture Radar SAR produces a high-resolution image of a scene of the earth's surface in both range and cross-range.[102] It can produce images of scenes at long range and in adverse weather that are not possible with infrared or optical sensors. The theoretical cross-range resolution of SAR is $\Delta x = D/2$, where D is the horizontal dimension of the SAR's real antenna aperture. SAR does not, however, accurately image moving targets. Moving targets can be seriously distorted and displaced from their true location. For instance, a railroad train, if it can be imaged at all, will be displaced from the track it is riding on. The motion of a ship target can be complicated because of its roll, pitch, and yaw. Also, all parts of the ship might not be moving rigidly together. Thus SAR is restricted to the recognition of stationary objects. One application of SAR is its military use for airborne surveillance of the battlefield and for imaging of fixed targets, as in the X-band Joint STARS. An X-band SAR image of a B-52 aircraft sitting on a runway, taken by Metratek, Inc., is shown in Fig. 6.25. Its resolution is about 1 ft. This might be compared with the ISAR image in Fig. 2.18 of a similar aircraft at VHF which has less resolution. (The resolution of published images, such as those in Figs. 6.25 and 2.18, is often degraded by the printing process and is not as good as that available from the original image that emerges from the processor.)

Inverse Synthetic Aperture Radar ISAR can be considered as a radar in which the cross-range resolution is obtained by means of high resolution in the doppler-frequency domain. Each part of a moving target can have a different relative velocity with respect to the radar, especially if there is a large rotational component of the target's motion. Resolution in doppler frequency will allow the various parts of a moving target to be resolved in the cross-range dimension. Resolution in range is obtained with either a short pulse or pulse compression so that a two-dimensional image is obtained. The cross-range resolution can be shown to be $\Delta x = \lambda/(2\ \Delta\theta)$, where $\Delta\theta$ is the change in aspect angle during the ISAR observation time and λ is the radar wavelength. Thus cross-range resolution depends on the amount of angular rotation of the target during the radar observation time. Unlike SAR, ISAR takes advantage of the target's motion to provide a two-dimensional image.

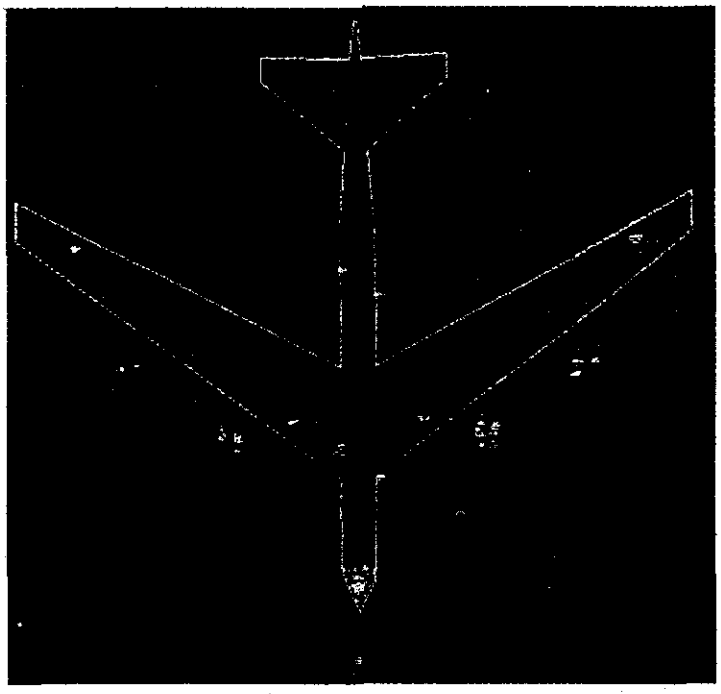

Figure 6.25 *X*-band SAR image of a B-52 aircraft sitting on a runway. Resolution is about 1 ft. The outline of the aircraft is shown for comparison. [Courtesy of Ray Harris of Metratek, Inc.]

SAR and ISAR are related in that they both require a change in the aspect of a target.* In SAR, the target is assumed stationary and the radar is in motion. In ISAR, the target motion provides the changes in relative velocity that cause different doppler shifts to occur across the target. The doppler shifts from the individual scatterers are resolved by filtering. ISAR generally requires that a single large scatterer from the target be tracked to act as the reference.

Figure 6.26 is an example of an ISAR image of a commercial ship obtained with an *X*-band radar with about 2 m resolution in range and cross range.[103] The *pitch* motion of a ship causes the top of the masts to have a higher velocity than the bottom of the masts or the superstructure. These differences in velocity cause different doppler shifts. Resolution in doppler then allows the mast to be imaged. Along with conventional range resolution, the pitching motion of the ship gives a vertical profile of the target along its length dimension. *Roll* motion also provides height information, but in the plane that includes the width of the ship. Roll is not that significant for recognition since the width of a ship is small compared to its length. *Yaw* motion of the ship gives a plan view of the target. As the ship pitches, rolls, and yaws, ISAR might produce a vertical profile along the major axis of the ship, or a vertical profile along the minor axis of the ship, or a horizontal plan

*SAR and ISAR are variations of the same phenomenon. This is seen in ISAR by requiring a change in the target aspect of $\Delta\theta = \lambda/2\Delta x$. In SAR the change in fixed-target aspect is determined by the beamwidth of the real radar aperture $\Delta\theta \approx \lambda/D$. Using this expression for beamwidth in the expression for the SAR cross-range resolution $\Delta x = D/2$, it is found that $\Delta x = \lambda/2\Delta\theta$, which is the same as the ISAR cross-range resolution.

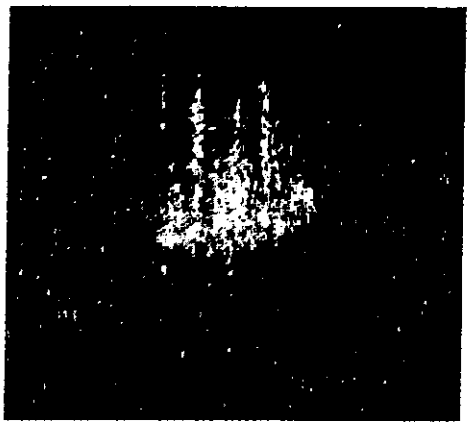

Figure 6.26 ISAR image, before image processing, of a commercial ship (17,000 ton) obtained with an *X*-band radar having 2 m resolution. The vertical scale in this image is slightly exaggerated. Note that "radar eyes" are not like "optical eyes," yet useful information can be obtained from a series of such images.
(Provided by Ronald Lipps of the Naval Research Laboratory)

view, or some combination of the three that results in the image appearing as a perspective view. Since the angular rates of pitch, roll, and yaw are not generally known, an ISAR image does not represent true distances in cross-range, as it does in range. This doesn't seriously limit, however, the ability to recognize one class of ship target from the other.

Since different ISAR images are obtained as the ship pitches, rolls, and yaws it might require many tens of seconds of observation to acquire images suitable for classification. For ship targets, relatively long observation times are not necessarily a serious problem since time is not as urgent as it would be for aircraft recognition. Sometimes an experienced operator can recognize the ship by simply viewing its ISAR image. In most cases, however, the operator has to employ a more structured technique, especially when there are a large number of possible ship classes to which a target might belong. An operator can use a combination of three different techniques: (1) *measurement of the relative locations* of the major scatterers along the bow-stern axis, such as masts, superstructure breaks, guns, and missile launchers; (2) *feature descriptions* which characterize scattering features by their degree of match to descriptive templates such as the shape of the stern (straight, curved, or rounded) or the type of masts (pole, lattice, or solid); and (3) *shape correlation* by visually comparing on the same display a single ISAR image with a superimposed wire-frame model of the candidate target which has been transformed to match the orientation of the target image produced by the ISAR.

Ships are generally large radar targets so that with a good radar the range at which ship recognition can be performed is basically limited by the horizon. It can be tens of miles with a ship radar, 200 miles with an aircraft radar, or much greater ranges with a spaceborne radar.

The classification of aircraft with ISAR is much more difficult than the ISAR classification of ships. First, an aircraft has many fewer scattering centers than does a ship. With fewer scattering centers or features presented by the unknown target, the recognition decision will be less accurate. (ISAR images of an aircraft have seldom been shown in the past without an outline of the aircraft superimposed to allow the viewer to recognize what is being seen.) Second, an aircraft does not usually experience the relatively large pitch, roll, and yaw motions of a ship, so that the cross-range resolution might not

be good enough to isolate the scattering features important for target recognition. Since resolution depends on having a sufficient change of aspect angle, the aircraft must be observed for a relatively long time if it is moving on a straight-line path. Usually a deliberate maneuver by the target aircraft is needed in order to obtain the required change in viewing aspect ($\Delta\theta$) needed for acceptable high-resolution ISAR imaging. Third, aircraft have much smaller radar cross sections than do ships. Therefore, the ranges at which aircraft recognition can be performed, even if the other two limitations are not present, will be much less than those obtained with ships. These difficulties combine to make ISAR imaging of aircraft less attractive than the ISAR imaging of ships.

Although microwave ISAR might not provide aircraft target recognition as well as it does ship recognition, it has been successfully used as a diagnostic tool for understanding the nature of radar scattering from aircraft and the design of low radar cross-section aircraft. Radar images of aircraft in flight can be obtained from both ground-based and airborne radars,[104] so long as sufficient relative motion is achieved between the radar and the target. An ISAR image of a KC 135 jet aircraft (a military version of the Boeing 707) was shown in Fig. 2.18.[105] The aircraft to be imaged flies behind the aircraft carrying the imaging radar in its tail. The radar aircraft maneuvers from one side to the other so that its radar can obtain the relative velocity (and doppler shift) needed to produce an image. Whether one calls this radar an ISAR or a SAR is immaterial. It relies on the relative motion between the imaging radar and the various scatterers that make up the aircraft to be imaged. The advantage of this high-resolution imaging method is that the individual scatterers that contribute to the backscatter echo can be readily recognized and their contributions to the total target cross section can be determined.

An innovative, experimental aircraft-recognition radar is that reported by Steinberg[106,107] to observe commercial aircraft flying into Philadelphia International Airport. It employed a ground-based ISAR to image aircraft passing at relatively close range (typically 3 km). Target aircraft were viewed by the radar in the vicinity of broadside where the rate of change of angle was large so that good cross-range resolution was obtained. A single transmitter was used with two receivers. One receiver was colocated with the transmitter, the other was separated by 25 m. Both were operated as monostatic (single-site) radars. Their physical separation allowed two different target images to be obtained. A third image was obtained by operating the two receiving antennas as an interferometer. The resulting highly processed image of an L-1011 commercial aircraft, with 47-m wingspan and 54-m length, is shown in Fig. 6.27a, along with a plan view drawing of the L-1011 (Fig. 6.27b) for comparison. Figure 6.27a is not that of a single image, as is Fig. 6.27c, but is the superposition of the three images mentioned above (one from each receiver and the two as an interferometer) as well as the inverted images of the three so as to take advantage of the known symmetry of the aircraft about the longitudinal axis. This is an exceptionally good "ISAR" image because of the short range, large signal-to-noise ratio, large change in aspect angle, diversity overlay of multiple images, lack of clutter, and inclusion of the inverted images so as to depict scatterers that might have been masked by the fuselage or the tail. For comparison, several range profiles of the same L-1011 aircraft are shown in Fig. 6.28 at different aspect angles to illustrate the dramatic change in profile with aspect.

Generally, aircraft in normal (nonmaneuvering) flight do not change their aspect angle sufficiently to make good ISAR images with X-band radar. Also there are few

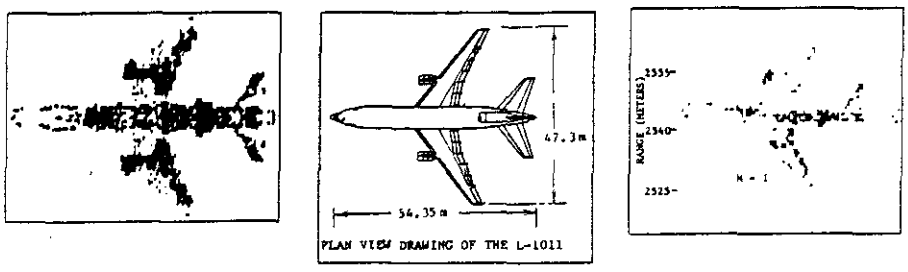

Figure 6.27 (a) ISAR radar image of an L-1011 aircraft made up by superimposing three independent images along with their individual inverted images (see text). (b) Outline drawing of the same aircraft shown for comparison. (c) One of the single images that was used as a part of (a). (Courtesy of Prof. Bernard Steinberg of the Univ. of Pennsylvania.)

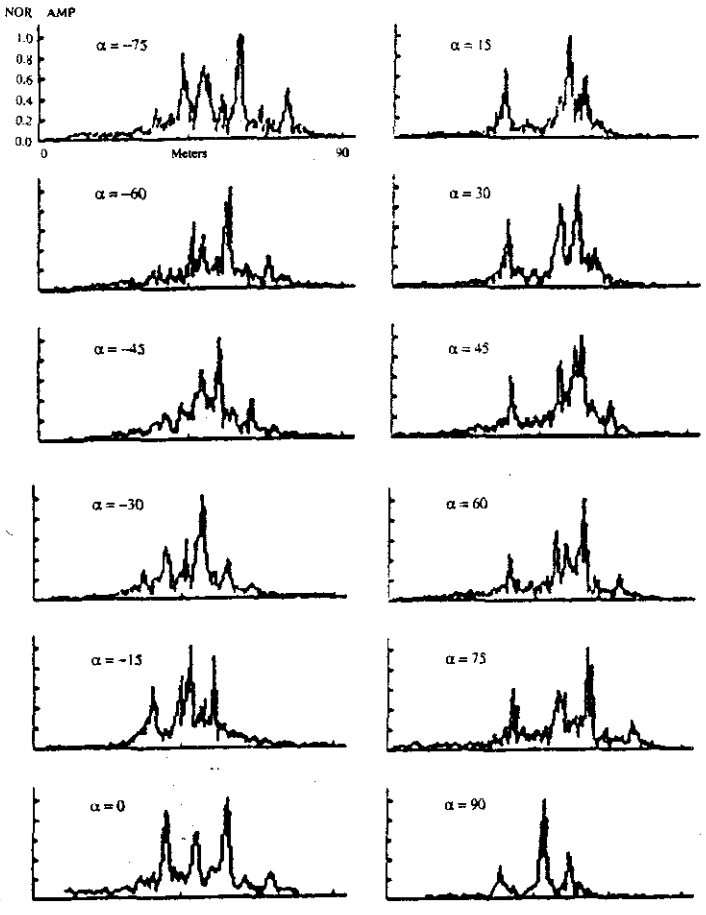

Figure 6.28 One-dimensional profiles of the Lockheed L-1011 as a function of aspect angle, obtained from Fig. 6.27a. Head-on aspect occurs at $\alpha = 0$ deg; positive angles view the port side of the aircraft.
(Courtesy of Prof. Bernard Steinberg of the Univ. of Pennsylvania.)

distinctive features in an aircraft image that allow it to be recognized from other similar aircraft. Thus ISAR imaging of aircraft in normal flight has been disappointing. The ISAR imaging of aircraft at *W* band (94 GHz), however, requires only one tenth the change of target aspect necessary at *X* band for the same resolution. Because scattering occurs from variations in the target surface that are comparable to the radar wavelength, it is also likely there will be more scatterers imaged at millimeter waves than at lower frequencies if the signal-to-noise ratio is high enough. In one experimental investigation,[108] it was found that, compared to ISAR images at *X* band, ISAR images of a small Piper Navajo aircraft made at 49 GHz "showed scattering from small details that tended to fill in the target shape and produce an outline view of the target." Furthermore, the target cross section at 49 GHz, when averaged over 360°, was 8 dB greater than the 9-GHz cross section. The largest increase was 19 dB, and was at nose-on incidence. Millimeter-wave ISAR, therefore, should produce better results than does ISAR at the lower frequencies.

Earth-based radars were used in the past to make ISAR images of the moon, Venus, and Mercury; but this technique has been replaced by planetary SAR radars that can orbit close to a planet and obtain superior resolution than an earth-based radar. ISAR for planetary exploration was called *delay-doppler mapping* by the radar astronomer.[109]

Radar Cross-Section Modulations Radar echoes from moving parts of a target can help recognize one type of target from another or determine the class to which a target belongs. Modulations of the radar backscatter due to propellers, helicopter rotors, jet engines, tank treads, rotating antennas, rotating machinery, the wing beat of birds and insects, and even the heartbeat of a human are examples that might be employed for target recognition. Narrowband (long pulse) as well as wideband (short pulse) waveforms can be used for extracting these modulations.

Propeller Modulation Aircraft propellers cause a distinctive modulation of the echo signal. The modulation depends on the rotation rate of the engine, the aspect angle, the number of blades on the propeller, and the shape of the propeller. An example of the doppler spectrum obtained with a coherent S-band radar is shown in Fig. 6.29 for a DC-7 aircraft,

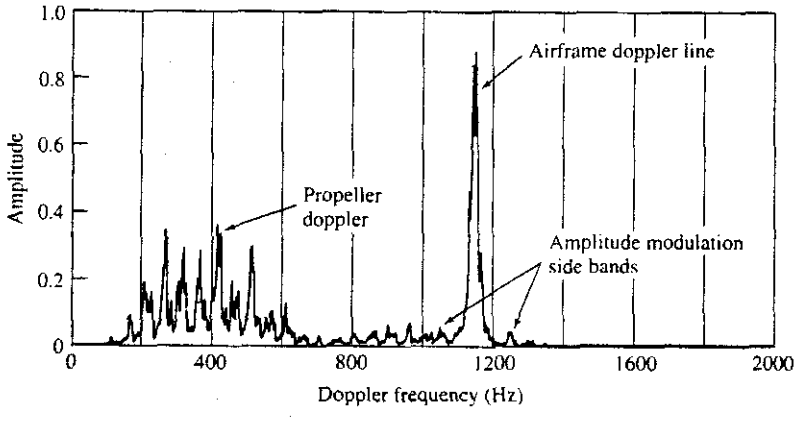

Figure 6.29 Spectrum of the propeller modulation from a DC-7 four-engine commercial aircraft taken with an *S*-band radar and one-second dwell time. (From R. Hynes and R. E. Gardner of the Naval Research Laboratory.[110,116])

a four-engine propeller-driven commercial aircraft.[110,111] The "airframe doppler-line" is the doppler frequency shift from the aircraft itself. The low-level amplitude modulation of the airframe doppler signal is caused by the propeller blade "chopping" a portion of the radar energy reflected from the airframe. At a frequency lower than the airframe line, there are spectral lines due to the radar echo from the rotating propeller blades themselves.

Propeller modulation has not been used to recognize one type of propeller aircraft from another, but its absence can be used to readily distinguish a jet-engine aircraft from a propeller-driven aircraft. In a high-resolution imaging radar, propeller modulation might locate the position of the engines, which could be helpful for target recognition.

Helicopter Blade Modulation Helicopters can be distinguished from fixed-wing aircraft by the characteristic modulation of the radar echo that comes from the rotating blades and the rotating hub structure supporting the blades.

A "blade flash" occurs every time one of the rotating blades is perpendicular to the radar beam direction.[112,113] In this position the radar cross section is a maximum. For a two-blade rotor, there are two flashes per revolution. Rotors with an even number of blades produce a number of flashes per rotation equal to the number of blades. An odd number of blades produce twice the number of flashes per revolution as the number of blades. (This can be verified by drawing a sketch and noting that there will be a separate flash from the front and rear when there are an odd number of blades, but a simultaneous flash from a front and a rear with an even number of blades.) The linear speed at the tip of the blade of helicopter is not highly dependent on the type of helicopter. It varies from about 210 to 230 m/s. If L = the length of the blade in meters, N = number of blades, and the speed of the tip is taken to be 210 m/s, the blade period in seconds for an even number of blades is

$$T_B = \frac{2\pi L}{210N} \qquad [6.50]$$

The period for an odd number of blades is one half that for an even number. Collot[112] points out that the blade period can be used to separate one type of helicopter from another since the rotation speed is constant whatever the type of flight.

Collot also states that the radar cross section, in square meters, for the blade flash is approximately aL^2/λ, where L = length of the blade, λ = wavelength, and the constant $a = 0.5$ for the front edge of the blade and 0.1 for the trailing edge. (The front edge has a higher cross section than the trailing edge since it is blunt and the trailing edge is sharp.[114]) Because of the difference between front and rear cross sections, a rotor with an odd number of blades will have alternating values for the blade flash (since the front edge and rear edge are not seen simultaneously). The echoes from the blade flash with an even number of blades, however, will be the same strength each time. The duration of the blade flash depends on the rotor speed, the length of the blade, and the radar wavelength. Assuming that the reflection from the blades can be approximated by a $(\sin x)/x$ relation and that the angular extent of the reflected echo is λ/L radians, the duration of the blade flash is approximately $t_f = \lambda/420$ for an even number of blades and twice this for an odd number (again assuming that the velocity of the blade tip is 210 m/s). At X band, with λ = 3.2 cm, the duration of the flash with an even number of blades is about 75 μs.

The intermittent nature of the short-duration helicopter blade flash might go unnoticed if the time on target is less than the time between flashes [which is the blade period of Eq. (6.50)]. In order that the helicopter blade flash be intercepted by the radar, a high prf and a long time on target are required.

The frequency spectrum of the radar echo from a helicopter has energy about the airframe doppler line due to reflections from the rotating hub that holds the blades. The helicopter spectrum will be asymmetrical since the echo from the approaching blade will be at a higher frequency than the airframe line and be of a larger amplitude than the echo from the receding blade at a lower frequency. Collot states that recognizing that an echo is from a helicopter and not a fixed wing aircraft is "immediate," and the recognition "of the type of helicopter is given in a very short time with a probability better than 95 percent." (He does not state, however, how many different types of helicopters were involved in obtaining this probability.)

In addition to the characteristic features mentioned above, the classification of helicopters might also include the echo characteristics of the tail rotor, whether there are single or twin rotors, and the configuration of the rotating hub.[115] Bullard and Dowdy[113] point out that to recognize a helicopter based on the spectral characteristics of its echo signal, the radar signal sampling must be at the Nyquist rate or higher to prevent aliasing. For X-band radar they state that a minimum prf of 30 kHz is required.

Jet-Engine Modulation (JEM) The radar echo from a jet-engine aircraft will be modulated by the engine's rotating compressor when looking in the vicinity of the nose. There might also be radar echo modulations from the turbine when looking from the rear of the aircraft; but these usually have a much smaller echo than the echo from the compressor.[110] The characteristic modulations of the radar echoes from aircraft can be used for recognizing one type of aircraft from another, or more correctly, one type of aircraft engine from another. Even though the jet engines are set back at a distance from their air intake and are entirely enclosed except for intake and exhaust ducts, there usually is sufficient propagation down the duct at microwave frequencies to obtain an echo signal from the compressors. Radar echoes from the compressors are sometimes obtained out to angles 60 deg from the head-on.[116]

An example of the *jet-engine modulation* (JEM) produced by a multiple-engine jet viewed head-on by an X-band radar is shown in Fig. 6.30.[110] Shown in this spectrum are the airframe line and the lower frequency sidebands of the compressor modulation. The component labeled c is displaced from the airframe line by a frequency $\Delta f = nb_c$, where n is the number of revolutions per second of the compressor and b_c is the number of blades on the first-stage compressor. There are other engine spectral components that are displaced from the airframe doppler line by integer multiples of Δf. The upper sidebands (not shown here) are symmetrical in frequency with the lower sidebands (with reference to the airframe line), but are lower in amplitude. Because of the high rotation speed of the engine components, aircraft jet-engine modulations are likely to be as high as ten to twenty kilohertz at X band. This requires high sampling frequencies (prfs) to avoid aliasing.

Mathematical analysis of jet-engine modulations indicates that the overall JEM signal can be decomposed into an amplitude modulation component and an angle (phase or frequency) modulation component that can be considered separately. The details of the line spectrum of

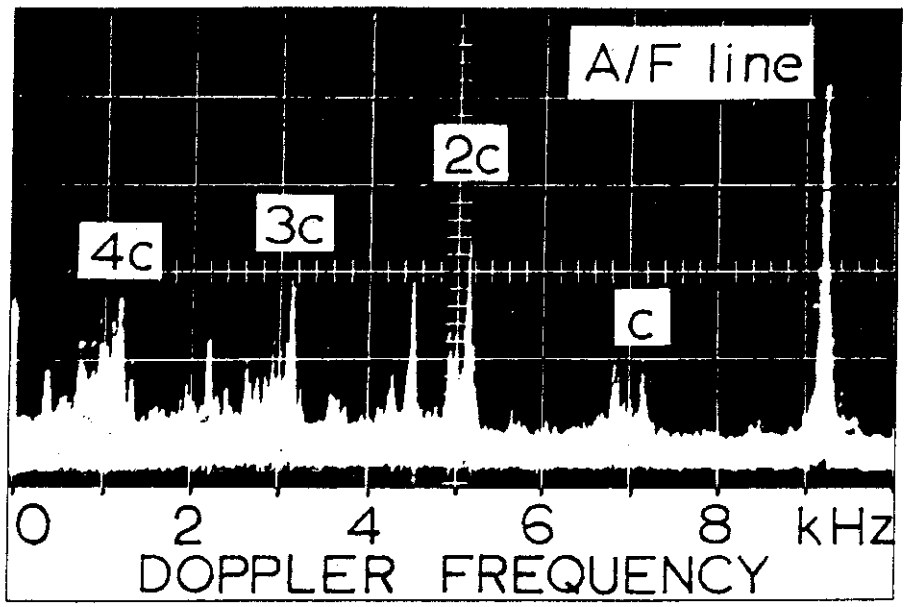

Figure 6.30 Spectrum of a multi-engine jet aircraft taken at 0 deg aspect angle showing the airframe line due to the aircraft's relative velocity and modulations from the compressor. [From R. Hynes and R. E. Gardner of the Naval Research Laboratory.[110,116]]

the echo signal depend on many things including the number of blades on the first and second stages of the compressor. A minimum time of observation is needed to obtain a meaningful spectrum suitable for target recognition, which is said to be at least 25 ms.[117]

Polarization Response and Target Recognition The radar echo from a target can be affected by the polarization of the radar signal. Many research engineers have hoped that the differences in the echo from targets viewed with different polarizations might be used as a means for distinguishing one from another.[118] This is possible in simple cases, as, for example, distinguishing between a long thin rod and a sphere by using a rotating linear polarization (rotating electric field vector).

In the more general situation with realistic targets, such as aircraft, there have been many attempts to use the polarization matrix of the target echo and other polarization descriptors[119–121] for target recognition. Target recognition by means of polarization generally requires measurement of what is called the *polarization matrix.* This is obtained from the radar echo signals received on both horizontal and vertical polarization when horizontal is transmitted, and on the received horizontal and vertical polarization signal when vertical is transmitted. The polarization matrix is a 2×2 complex scattering operator (phase as well as amplitude) that characterizes a target's scattering properties. It may be expressed as

$$S = \begin{bmatrix} S_{HH} & S_{VH} \\ S_{HV} & S_{VV} \end{bmatrix} \qquad [6.51]$$

where the first subscript represents the polarization of the receiving antenna and the second subscript is the transmitted polarization, *H* is for horizontal polarization and *V* is for vertical polarization. For example, S_{HV} is the complex target backscatter signal (amplitude and phase) received with a vertically polarized antenna when a horizontally polarized signal is transmitted. The *HH* and *VV* are both *co-polar* components and the *HV* and *VH* are both *cross-polar* components. In general $HV = VH$.

Although theory might indicate that the polarization response of a target depends on the nature of the target, there has not been the desired success in applying polarimetric methods for practical target recognition. There are several reasons why this has been so: (1) Multipath signals from the surface of the ground or from clutter and structures along the propagation path can modify the polarization of the signal. (2) Practical antennas are limited in the purity of their polarization response, and there is always some finite response to the cross polarization which sometimes might be relatively large. (3) The two orthogonal polarizations (horizontal and vertical) have to be transmitted on different pulses; and if the target changes its aspect during the time between pulses, the polarization response will be distorted. (4) Multiple (unresolved) scatterers or targets within the radar resolution cell will result in a composite signal with a polarization different from any of the individual scatterers. Giuli[122] in his classic paper on polarization diversity states that low-resolution radars "intrinsically provide quite limited classification properties." He points out, however, that wideband radars that can resolve the individual scatterers of a target might make exploitation of the polarization information more profitable by avoiding the changes in echo polarization caused by unresolved scatterers.

Even though the use of polarimetry for target recognition has excited much interest, one can conclude that as a means for recognizing complex targets its effectiveness in the past has been disappointing.

Other Radar Target Recognition Methods Several other radar methods for the recognition of targets are briefly mentioned below. Most can be thought of in terms of aircraft recognition, although they are not limited to aircraft.

High Range-Resolution with Monopulse[123] The use of monopulse radar for target tracking in angle was discussed in Sec. 4.2. If the monopulse radar has sufficiently high range-resolution so as to isolate the major scattering centers of a target, then a measurement of the angular location of each scatter in azimuth and elevation can be made. Thus high range-resolution with monopulse can provide a 3D-like "image" of a target that might be used for target recognition. In addition to requiring high range-resolution, a limitation is that the range must be short enough so that angle measurements can be made with enough accuracy to obtain adequate cross-range measurements of the major scatterers.

Fluctuations of Radar Cross Section with Aspect Angle Section 2.7 indicated that small changes in the aspect angle of complex (multiple scatterer) targets can cause major changes in the radar cross section. This has been considered in the past as a means for target recognition, but it has not had much success. In some respects this method is related to the imaging of moving targets by means of ISAR, discussed previously, except that the highly

successful ISAR technique employs both phase and amplitude. Only amplitude information is available when cross-section variations are observed.

Resonance Region Response There have been several methods proposed for target recognition based on using a number of distinct frequencies in the resonance region of target scattering. (In the resonance region the dimensions of the target are comparable to the radar wavelength.) One method is derived from the ramp response of a target and develops a so-called *feature space* based on the amplitude, phase, and/or polarization of each distinct frequency that observes the target.[124,125] A related method employs the complex *natural resonances*, or *poles*, of the target to characterize the target.[126,127] The *Singularity Expansion Method* has also been applied to the target recognition method that employs frequencies in the resonance region.[128]

These methods have a good theoretical basis; they generally do not depend on knowing the target aspect angle; and they have been tested with computer simulations and experimental model measurements at scaled frequencies. They are not practical, however, for most applications of target recognition since they require frequencies in the resonance region, which for aircraft targets would be in the HF portion of the spectrum. For ships, even lower frequencies would be required. These recognition methods depend on the so-called *late-time scattering* due to creeping waves that travel around the target. Even if long radar wavelengths were no problem, it has been pointed out[129] that the effect of noise can mask the creeping waves that occur beyond the first creeping wave so that there might not be enough information to determine the complex resonances.

Another related method is to transmit a radar waveform that is based on knowing ahead of time the natural resonances of the target so that the desired target echo signal can be readily recognized from the echo signals from targets with a different set of natural resonances. One such method is called *K-pulse;* another is called *E-pulse.*[130] They require that the radar transmit a special signal for each target to be recognized. Rather than transmit special waveforms it might be better to transmit a more normal wideband radar pulse and perform target recognition by convolution processing in the receiver to recognize a particular target signal.[131]

Since they have been difficult to apply in practice, the above resonance region methods have been more of academic interest than for practical target recognition applications.

Nonlinear Scattering Effects When a metal comes into contact with another metal, oxides can form and the junction can act as a nonlinear diode. A radar echo signal reflected from such a metal-to-metal junction will contain higher harmonic components, with the third harmonic usually being the largest.[132–134] Thus if a frequency f_1 is transmitted, detection of the third harmonic, $3f_1$, indicates that the scatterer has metal-to-metal contacts. This nonlinear response has been of interest as a possible method for recognizing certain types of metallic targets. If the third harmonic of the echo signal is used, the transmitted signal must not have significant third-harmonic radiation of its own. A method for avoiding the third harmonic problem is to simultaneously transmit two frequencies f_1 and f_2, and tune the receiver to a strong cross-product such as $2f_1 \pm f_2$. The use of nonlinear target properties for radar has sometimes been called METRRA, which stands for *Metal Reradiating Radar.*

The amount of signal returned from a nonlinear contact at a harmonic frequency is a nonlinear function of the incident field strength. Thus the nonlinear target cross section depends on the peak power. The normal radar equation does not apply.[135,136] The range dependence in the radar equation might be as the sixth power or higher, instead of the usual fourth power. Because of the nonlinearity, in this specialized case high peak power is more important for detection than is high average power.

Although radar detection based on harmonics produced by nonlinear metal-to-metal contacts has some interesting attributes for applications (such as detection of stationary targets in clutter), it is difficult to apply since the echo signals at frequencies other than those transmitted can be very weak.

A related effect is based on the modulation of the scattered signal when metal-to-metal contacts are opened and closed so that the current distribution on a metal target is modified.[137] An example is the intermittent contacts due to the moving wheels of a train. This effect is sometimes called RADAM, which means *Radar Detection of Agitated Metals.*[138] The echo signals from RADAM are usually too weak to be of interest for satisfying the needs of target recognition.

Target Track History In military operations it is important to determine whether a target held in track by a radar is a friend or is a hostile threat. There are several military recognition or identification methods that might be used for separating friend from foe; but the radar itself might be able to assist in the recognition task based on the history of a target's track. If one knew where an aircraft or ship originated, where it has been, and what it is currently doing, it ought to be possible in many cases to determine whether the target is potentially hostile or not. A radar with a good automatic tracking system and with adequate memory is required, as well as logic to recognize the trajectories of potentially hostile targets from ones that are not.

In some cases, military aircraft recognition is accomplished by having friendly aircraft fly in pre-designated corridors in a known manner that the radar is able to observe.

Signal Intercept and Direction Finding Combined with Radar So far, this section has been concerned with radar methods for recognizing one target from another. Sometimes, however, the use of radar with other sensors can have a synergistic effect on the quality of target information. An example is the use of an electronic warfare intercept receiver (a part of ESM, or Electronic Support Measures*) and direction finder (DF) in combination with a radar. The intercept receiver might be able to recognize the type of target by the characteristic signals it radiates. The direction to the target can be obtained by the DF, but electronic warfare equipment usually cannot obtain the target's location in range. Radar, on the other hand, provides target location and track. The two together can locate, track, and obtain target recognition if the radar target track can be properly associated with the DF angle track. The angle accuracy of ESM/DF is often much poorer than the angle accuracy of radar. Nevertheless, algorithms can be developed that allow the ESM/DF information to be associated with a target under track by the radar so that target recognition provided by the ESM can be applied to the radar target under track.[139–141]

*ESM is also known as Electronic Warfare Support, or ES.

Target Recognition Applications There are many areas of application where the radar recognition of a target echo signal is important. Some have already been mentioned previously in this subsection, others are briefly described below. All of these require the intelligent extraction of information from a radar signal, a radar capability which this chapter has tried to introduce.

Military Combat Identification Studies of fratricide, which is the unintentional infliction of casualties on one's own forces, show that fratricide occured in past military hostilities at rates that typically vary from 10 to 20 percent, or greater.[142] Casualties from "friendly fire" have been considered by the military as an unwelcome consequence of war that needs to be kept to a minimum. To minimize the fratricide rate, military forces employ a number of recognition and identification methods as well as strict rules of engagement. Reliable, accurate, and secure combat identification is necessary to reduce fratricide. Both cooperative and noncooperative methods are employed in combination to increase the probability of a correct decision in a timely manner. The particular methods differ depending on whether the target is an aircraft, ship, ground vehicle, or the soldier on the ground. Radar target-recognition methods include engine modulations, track history, SAR, and ISAR.

Ballistic Missile Target Discrimination Defending against a single ballistic missile is a demanding task, but it can be done. The difficulty in ballistic missile defense escalates tremendously when the reentry vehicle carrying the warhead is accompanied by *penetration aids* that might consist of the spent booster tank or the many fragments from the tank after it has been deliberately exploded, the very many pieces of chaff that can be launched in space to accompany the reentry vehicle, solid fuel fragments, separation debris, and the deliberate use of inflated decoys that resemble the reentry vehicle. One of the fundamental challenges in ballistic missile defense, therefore, is to determine which element in the multielement threat complex is the lethal object to be destroyed or made ineffective.[143] If the reentry vehicle is engaged by the defense after it reenters the earth's atmosphere, the drag introduced by the atmosphere causes the lightweight penetration aids to slow down much faster than the heavier high-speed reentry body. Thus the atmosphere separates the warhead from the penetration aids. A serious limitation of this tactic is that it results in a relatively small defended area. If, on the other hand, the ballistic missile threat is engaged outside of the atmosphere so as to achieve a large defended area, then there needs to be some way in which the threatening warhead can be distinguished from the "junk" that accompanies it. The use of radar in such a role is called *ballistic missile target discrimination.*

Meteorological Observation The original weather radars used for many years by the National Weather Service determined the presence of rainfall and estimated the rainfall rate. These were replaced in the early 1990s with the *S*-band Nexrad (WSR-88D) doppler weather radar,[144] which was designed to obtain much more information about the weather, other than it is raining somewhere. In addition to determining rainfall as a function of azimuth and height, Nexrad employs the doppler frequency shift to estimate wind speed as a function of direction and height in order to detect and measure damaging winds, severe turbulence, dangerous wind shear, and recognize the onset of tornadoes. Nexrad

differentiates hail from heavy rainfall, determines the tops of thunderstorms (an indicator of the intensity of such storms), and detects and tracks severe storms and mesocyclones. There are about 40 different weather products that can be generated by the WSR-88D radar.[145] These are processed automatically and displayed to an operator for further action. The extensive processing is such that the trained operator need not be a professional meteorologist to readily employ the information presented by the radar. Nexrad is a good example that radar need no longer be a "blob" detector!

Battlefield Surveillance The *X*-band Joint STARS airborne radar system employs a SAR mode for generating a maplike image of the battlefield and a GMTI mode for detecting moving targets. These two modes allow the recognition of terrain features, roads, fixed structures, military forces, artillery, and stationary as well as moving vehicles. Detection of moving vehicles is readily accomplished with modern GMTI methods. The radar detection of stationary ground targets of military interest is a classical radar application, but recognizing what type of target is being seen by the radar can be difficult. To be useful for target recognition, a radar should be able to distinguish tanks from trucks and from artillery. It would be even better if the type of tank or type of artillery could be determined.

Vehicles are difficult to recognize with radar since they have only a relatively few distinctive scattering centers. This is in contrast to a ship target that has many scattering centers, which makes recognizing one class of ship from many other ship classes achievable based on its ISAR image. Although the writer is not aware of a documented source defining the minimum number of distinctive scatterers needed for classifying targets, it appears that perhaps a dozen (more or less) individual scatterers might be necessary in a target image for reliable classification. The minimum number will depend, of course, on the type of target and the number of different target classes that have to be sorted. The number of scatterers defining a target might have to be greater if there are a large number of different classes of targets that have to be distinguished from one another. With both military aircraft and ships, the number of different classes that might be encountered range from many tens of target classes to more than a hundred if worldwide operation is expected.

As mentioned previously, determining the type of military land target seen by a SAR is called *automatic target recognition*, or ATR.[146] Radar ATR of land targets of military interest is complicated by the military tactic of hiding targets among the trees and other vegetation that can contaminate the target's echo signature as well as interfere with detection when the clutter echo is large. Thus ATR involves some method of STI (stationary target indication) to detect targets in the midst of clutter as well as foliage penetration. Foliage penetration requires operation at the lower radar frequencies, such as VHF, where the attenuation in propagating through trees and underbrush is lower than at microwave frequencies. Recognition of targets also requires very wide bandwidths to isolate the target's scatterers. Wide bandwidth combined with VHF results in ultrawideband (UWB) SAR.[147]

The interpretation of SAR images of terrain and populated areas has also been used in the civilian world for adding to the base of Geographic Information Systems (GIS), which use such information for land usage and planning, urban development, natural resource management, and topography.

Other Applications of Radar Information Extraction Radar has been used for recognizing one species of birds from another by means of the modulation on the bird's radar echo signals thought to be due to the characteristic beating of its wings.[148] Doppler radar can be used to detect the heartbeat and breathing of humans, even when located behind a cinder-block wall.[149,150] Radars can readily detect buried land mines, but the challenge has been to recognize the echo of a mine from the echoes from the many other underground objects that can be present, such as rocks, tree roots, debris, and changes in the underground surface characteristics.

REFERENCES

1. Skolnik, M. I. "Radar Information from the Partial Derivatives of the Echo Signal Phase from a Point Scatterer." Naval Research Laboratory, Washington, D.C., Memorandum Rep. 6148, February 17, 1988.
2. Evans, J. V., and T. Hagfors. *Radar Astronomy,* New York: McGraw-Hill, 1968, Sec. 5.9.
3. Jurgens, R. F. "Earth-Based Radar Studies of Planetary Surfaces and Atmospheres." *IEEE Trans.* GE-20 (July 1982), pp. 293–305.
4. McDonough, R. N., and A. D. Whalen. *Detection of Signals in Noise.* San Diego, CA: Academic, 1995.
5. Goldman, S. *Frequency Analysis, Modulation, and Noise.* New York: McGraw-Hill, 1948, p. 281.
6. Slepian, D. "Estimation of Signal Parameters in the Presence of Noise." *IRE Trans.* no. PGIT-3 (March 1954), pp. 68–89.
7. Manasse, R. "Range and Velocity Accuracy from Radar Measurements," unpublished internal report dated February 1955, MIT Lincoln Laboratory, Lexington, MA. (Not generally available.)
8. Mallinckrodt, A. J., and T. E. Sollenberger. "Optimum Pulse-Time Determination." *IRE Trans.* no. PGIT-3 (March 1954), pp. 151–159.
9. Weiss, A. J. "Composite Bound on Arrival Time Estimation Errors." *IEEE Trans.* AES-22 (November 1986), pp. 751–756.
10. Torrieri, D. J. "Arrival Time Estimation by Adaptive Thresholding." *IEEE Trans.* AES-10 (March 1974), pp. 178–184.
11. Torrieri, D. J. "Adaptive Thresholding Systems." *IEEE Trans.* AES-13 (May 1977), pp. 273–280.
12. Ho, K. C., Y. T. Chan, and R. J. Inkol. "Pulse Arrival Time Estimation Based on Pulse Sample Ratios." *IEE Proc.* 142, Pt. F (August 1995), pp. 153–157.
13. Varian, R. H., W. W. Hansen, and J. R. Woodyard. "Object Detecting and Locating System." U.S. Patent 2,435,615, February 10, 1948.

14. Skolnik, M. *Introduction to Radar Systems*, 2nd ed. New York: McGraw-Hill, 1980, Sec. 3.5.
15. Wadley, T. L. "Electronic Principles of the Tellurometer." *Trans. South African Inst. Elec. Engrs.* 49 (May 1958), pp. 143–161; discussion pp. 161–172.
16. Manasse, R. "Range and Velocity Accuracy from Radar Measurements." Internal memo dated February 1955, MIT Lincoln Laboratory, Lexington, MA. (Not generally available.)
17. *Encyclopaedia Britannica* vol. 12, 15th ed., Chicago, IL, 1991, p. 125.
18. Sinsky, A. I., and C. P. Wang. "Standardization of the Definition of the Radar Ambiguity Function." *IEEE Trans.* AES-10 (July 1974), pp. 532–533.
19. IEEE Standard 686-1990, Radar Definitions, April 20, 1990.
20. Woodward, P. M. *Probability and Information Theory, with Applications to Radar.* New York: McGraw-Hill, 1953, chap. 7.
21. Siebert, W. McC. "A Radar Design Philosophy." *IRE Trans.* IT-2 (September 1956), pp. 204–221.
22. Deley, G. W. "Waveform Design." In *Radar Handbook*, 1st ed., M. Skolnik (Ed.). New York: McGraw-Hill, 1970, p. 3-17.
23. Rihcazek, A. W. *Principles of High-Resolution Radar.* New York: McGraw-Hill, 1969, Sec. 5.3.
24. Woodward, P. M. Ref. 20, Sec. 7.2.
25. Dicke, R. H. "Object Detection System." U.S. patent no. 2,624,876, issued Jan. 6, 1953.
26. Klauder, J. R., et al. "The Theory and Design of Chirp Radars." *Bell System Technical J.* 39 (July 1960), pp. 745–808.
27. Cook, C. E., and M. Bernfeld. *Radar Signals.* Norwood, MA: Artech House, 1993.
28. Skolnik, M. *Introduction to Radar Systems.* 2nd ed. New York: McGraw-Hill, 1980, Sec. 3.3.
29. Borkowski, T. T. "Solid-State Transmitters." In *Radar Handbook*, 2nd ed. M. Skolnik (Ed.) New York: McGraw-Hill, 1990, Chap. 5.
30. Cook, C. E., and M. Bernfeld. Ref. 27, Sec. 7.3.
31. Caputi, W. J., Jr. "Stretch: A Time-Transformation Technique." *IEEE Trans.* AES-7 (March 1971), pp. 269–278.
32. Holt, D. J., and M. B. Fishwick. "Analog Waveform Generation and Processing." *Electronic Progress* 17, no. 1 (Spring 1975), pp. 2–16. (Published by Raytheon, Lexington, MA.)
33. Brookner, E. *Aspects of Modern Radar.* Norwood, MA: Artech House, 1988, pp. 25–28.
34. Farnett, E. C., T. B. Howard, and G. H. Stevens. "Pulse-Compression Radar." In *Radar Handbook*, 1st ed., M. Skolnik (Ed.). New York: McGraw-Hill, 1970, chap. 20.

35. Hartmann, C. S. "SAW Device Technology: Recent Advances and Future Trends." *Microwave J.* 1990 State of the Art Reference, pp. 73–89.

36. Maines, J. D., and E. G. S. Paige. "Surface-Acoustic-Wave Devices for Signal Processing Applications." *Proc. IEEE* 64 (May 1976), pp. 639–652.

37. Cambell, Colin. *Surface Acoustic Wave Devices and Their Signal Processing Applications.* New York: Academic, 1989.

38. Information obtained from Anderson Laboratories, Bloomfield, CT, brochure titled "Dispersive Delay Lines," 1986.

39. Martin, T. A. "Low Sidelobe IMCON Pulse Compression." *Proc. 1976 IEEE Ultrasonics Symposium,* pp. 411–414, IEEE Cat. #76 CH1120-5SU.

40. Farnett, E. C., and G. H. Stevens. "Pulse Compression Radar." In *Radar Handbook,* 2nd ed. M. Skolnik (Ed.). New York: McGraw-Hill, 1990, chap. 10.

41. Wehner, D. R. *High-Resolution Radar,* 2nd ed. Boston, MA: Artech House, 1995, Sec. 4.7.

42. MacWilliams, F. J., and N. J. A. Sloan. "Pseudo-Random Sequences and Arrays." *Proc. IEEE* 64 (December 1976), pp. 1715–1729.

43. Farnett, E. C., and G. H. Stevens. Ref. 40, Sec. 10.6.

44. Golomb, S. W. *Shift Register Sequences.* rev. ed. Laguna Hills, CA: Aegean Park, 1982.

45. Taylor, S. A., and J. L. MacArthur. "Digital Pulse Compression Radar Receiver." *APL Technical Digest* 6 (March/April 1967), pp. 2–10.

46. Turin, R. "Sequences with Small Correlation." In *Error Correcting Codes.* H. B. Mann (Ed.). New York: John Wiley, 1968, pp. 195–228.

47. Linder, J. "Binary Sequences Up to Length 40 With Best Possible Autocorrelation Function." *Electron. Lett.* 11 (October 10, 1975), p. 507.

48. Kerdock, A. M., R. Mayer, and D. Bass. "Longest Binary Pulse Compression Codes with Given Peak Sidelobe Levels." *Proc. IEEE* 74 (February 1986) p. 366.

49. Taylor, J. W., Jr., and H. J. Blinchikoff. "Quadriphase Code—A Radar Pulse Compression Signal with Unique Characteristics." *IEEE Trans.* AES-24 (March 1988), pp. 156–170.

50. Levanon, N., and A. Freedman. "Ambiguity Function of Quadriphase Coded Radar Pulse." *IEEE Trans.* AES-25 (November 1989), pp. 848–853.

51. Frank, F. L. "Polyphase Codes with Good Nonperiodic Correlation Properties." *IEEE Trans.* IT-9 (January 1963), pp. 43–45.

52. Cook and Bernfeld, Ref. 27, Sec. 8.4.

53. Nathanson, F. E. *Radar Design Principles.* 2nd ed. New York: McGraw-Hill, 1991, Sec. 12.5.

54. Lewis, B. L., F. F. Kretschmer, Jr., and W. W. Shelton. *Aspects of Radar Signal Processing.* Norwood, MA: Artech House, 1986, Chap. 2.

55. Lewis, B. L. "Range-Time Sidelobe Reduction Technique for FM-Derived Polyphase PC Codes." *IEEE Trans.* AES-29 (July 1993), pp. 834–840.

56. Nathanson, F. E. Ref. 53, Sec. 13.5.

57. Costas, J. P. "A Study of a Class of Detection Waveforms Having Nearly Ideal Range-Doppler Ambiguity Properties." *Proc. IEEE* 72 (August 1984), pp. 996–1009.

58. Chang, W., and K. Scarbrough. "Costas Arrays with Small Number of Cross-Coincidences." *IEEE Trans.* AES-25 (January 1989), pp. 109–112.

59. Golomb, S. W., and H. Taylor. "Constructions and Properties of Costas Arrays." *Proc. IEEE* 72 (September 1984), pp. 1143–1163.

60. Nathanson, F. E. Ref. 53, Sec. 13.11.

61. Farnett, E. C., and G. H. Stevens. Ref. 40, Sec. 10.4.

62. Cook, C. E., and M. Bernfeld. Ref. 27, Sec. 6.8.

63. Minkoff, J. *Signals, Noise, and Active Sensors.* New York: John Wiley, 1992, Sec. 9.2.

64. Thor, R. C. "A Large Time-Bandwidth Pulse-Compression Technique." *IEEE Trans.* MIL-6 (April 1962), pp. 169–173. Reprinted in *Radars* vol. 5, Pulse Compression, D. K. Barton (Ed.). Boston, MA: Artech House, 1875.

65. Kroszcynski, J. J. "Pulse-Compression by Means of Linear-Period Modulation." *Proc. IEEE* 57 (July 1969), pp. 1260–1266.

66. Minkoff, J. Ref. 63, Sec. 9.3.

67. Rowlands, R. O. "Detection of a Doppler-Invariant FM Signal by Means of a Tapped Delay Line." *J. Acoust. Soc. Am.* 37 (April 1965), pp. 608–615.

68. Altes, R. A., and E. L. Titlebaum. "Bat Signals as Optimally Doppler Tolerant Waveforms." *J. Acoust. Soc. Am.* 48 (1970), pp. 1014–1020.

69. Altes, R. A. "Radar/Sonar Acceleration Estimation with Linear-Period Modulated Waveforms." *IEEE Trans.* AES-26 (November 1990), pp. 914–923.

70. Kramer, S. A. "Doppler and Acceleration Tolerances of High-Gain, Wideband Linear FM Correlation Sonars." *Proc. IEEE* 55 (May 1967), pp. 627–636.

71. Golomb, S. W. Ref. 44, Chap. VI.

72. Belyayev, V. S. "A New Pseuodorandom, Phase-Controlled Signal Based Upon a Nonlinear Sequence and the Possibilities for Generating It." *Radiophysics and Quantum Electronics* 34 (March 1991), pp. 285–287.

73. Golay, M. J. E. "Complementary Series." *IRE Trans.* IT-7 (June 1960), pp. 82–87.

74. Levanon, N. *Radar Principles.* New York: John Wiley, 1988, pp. 159–162.

75. Cloke, J. A. "Ambiguity Function of Complementary Series." *IEE International Conf., Radar-82,* October 18–20, 1982, pp. 477–481.

76. Welti, G. R. "Quaternary Codes for Pulse Radar." *IRE Trans.* IT-7 (June 1960), pp. 400–408.

77. Nathanson, F. E. Ref. 53, p. 564.

78. Cook, C. E., and M. Bernfeld. Ref. 27, pp. 264–269.

79. Kretschmer, F. F., and F. C. Lin. "Huffman-Coded Pulse Compression Waveforms." Naval Research Laboratory, Washington, D.C., Report 8894, May 23, 1985.

80. Eves, J. L., and E. K. Reedy. *Principles of Modern Radar.* Van Nostrand Reinhold, New York, 1987, Sec. 15.3.2.

81. Key, E. L., E. N. Fowle, and R. D. Haggarty. "A Method of Sidelobe Suppression in Phase-Coded Pulse Compression Systems." MIT Lincoln Laboratory, Lexington, MA, TR-209, August 28, 1959.

82. Nathanson, F. E. Ref. 53, Sec. 12.4.

83. Ackroyd, M. H., and F. Ghani. "Optimum Mismatched Filters for Sidelobe Suppression." *IEEE Trans.* AES-9 (March 1973), pp. 214–218.

84. Eves and Reedy, Ref. 80, Sec. 15.5.2.

85. Morgan, G. B., P. Dassanayake, and O. A. Liberg. "The Design and Performance of Transversal Filters for Sidelobe Reduction of Pulses Compressed from Combined Barker Phase Codes." *The Radio and Electronic Engineer* 51 (June 1981), pp. 272–280.

86. Nathanson, F. E. Ref. 53, pp. 556–557.

87. Baden, J. M., and M. N. Cohen. "Optimal Peak Sidelobe Filters for Biphase Pulse Compression." *Record of the 1995 IEEE International Radar Conf.*, IEEE Catalog No. 90CH2882-9, pp. 249–252.

88. Castella, F. R., and S. A. Rudie. "Detection Performance of Phase-Coded Radar Waveforms with Various Types of Limiting." *IEE Proc.* 136, Pt. F (June 1989), pp. 118–121.

89. Cahn, C. R. "A Note on Signal-to-Noise Ratio in Band-Pass Limiters." *IEEE Trans.* IT-7 (January 1961), pp. 39–43.

90. Bogotch, S. E., and C. E. Cook. "The Effect of Limiting on the Detectability of Partially Time-Coincident Pulse Compression Signals." *IRE Trans.* MIL-9 (January 1965), pp. 17–24.

91. Woerrlein, H. H. "Capture and Spurious Target Generation Due to Hard Limiting in Large Time-Bandwidth Product Radars." Naval Research Laboratory, Washington, D.C., Report 7001, December 22, 1969.

92. Maric, S. V., I. Seskar, and E. L. Titlebaum. "On Cross-Ambiguity Properties of Welsh-Costas Arrays." *IEEE Trans.* AES-30 (October 1994), pp. 1063–1071.

93. Deng, H. "Synthesis of Binary Sequences with Good Autocorrelation and Cross-correlation Properties by Simulated Annealing." *IEEE Trans.* AES-32 (January 1996), pp. 98–107.

94. Shrader, W. W., and V. Gregers-Hansen. *Radar Handbook*, M. Skolnik (Ed.). New York: McGraw-Hill, 1990, "MTI Radar," Chap. 15, pp. 15.55–15.57.

95. Arthur, J. W. "SAW Pulse Compression in Modern Multi-Channel Radar Applications." *Microwave J.* 29 (January 1986), pp. 159–169.

96. Dixon, R. C. *Spread Spectrum Systems.* New York: Wiley Interscience, 1976.

97. Geffe, P. R. "Open Letter to Communications Engineers." *Proc. IEEE* 55 (December 1967), p. 2173.

98. Skolnik, M. I. "Radar's Environmental Role." *IEEE Potentials* 10 (April 1991), pp. 13–16.

99. Linde, G. J. "Use of Wideband Waveforms for Target Recognition with Surveillance Radars." *Record of the IEEE 2000 International Radar Conf.* May 7–12, 2000, Washington, D.C., pp. 128–133. See also Linde, G. J., and C. V. Platis. "Target Recognition with Surveillance Radar." *NRL Review.* Naval Research Laboratory, Washington, D.C., pp. 118–120, 1995.

100. Hudson, S., and D. Psaltis. "Correlation Filters for Aircraft Identification from Radar Range Profiles." *IEEE Trans.* AES-29 (July 1993), pp. 741–748.

101. Zyweck, A., and R. E. Bogner. "Radar Target Classification of Commercial Aircraft." *IEEE Trans.* AES-32 (April 1996), pp. 598–606.

102. Cutrona, L. J. "Synthetic Aperture Radar." *Radar Handbook,* M. Skolnik (Ed.). New York: McGraw-Hill, 1990, Chap. 21.

103. Kerr, D., S. Musman, and C. Bachmann. "Automatic Recognition of ISAR Ship Images." *IEEE Trans.* AES-32 (October 1996), pp. 1392–1404.

104. Jain, A., and I. Patel. "Dynamic Imaging and RCS Measurements of Aircraft." *IEEE Trans.* AES-31 (January 1995), pp. 211–226.

105. Harris, et al. "Dynamic Air-to-Air Imaging Measurement System." *Conf. Proceedings of the 14th Annual Meeting of the Antenna Measurements Techniques Association,* October 19–23, 1992, pp. 6-11 to 6-16.

106. Steinberg, B. D. "Microwave Imaging of Aircraft." *Proc. IEEE* 76 (December 1988), pp. 1578–1592.

107. Steinberg, B. D., D. L. Carlson, and W. Lee. "Experimental Localized Radar Cross Sections of Aircraft." *Proc. IEEE* 77 (May 1989), pp. 663–669.

108. Dinger, R., et al. "Measurements of the Radar Cross Section and Inverse Synthetic Aperture Radar (ISAR) Images of a Piper Navajo at 9.5 GHz and 49 GHz." Naval Command Control and Ocean Surveillance Center (NRaD), Tech. Rep. 1569, January 1993.

109. Pettengill, G. H. "Radar Astronomy." In *Radar Handbook,* 1st ed. M. Skolnik (Ed.). New York: McGraw-Hill, 1970, chap. 33.

110. Hynes, R., and R. E. Gardner. "Doppler Spectra of S-Band and X-Band Signals." Supplement to *IEEE Trans.* AES-3 (November 1967), pp. 356–365. Also, *Report of NRL Progress* (January 1968), pp. 1–10.

111. Dunn, J. H., and D. D. Howard. "Target Noise." *Radar Handbook,* 1st ed. M. Skolnik (Ed.). New York: McGraw-Hill, 1970, Chap. 28, Sec. 28.5.

112. Collot, G. "Fixed/Rotary Wings Classification/Recognition." *Proc. of the CIE International Conf. on Radar,* Beijing, China, October 22–24, 1991, pp. 610–612.

113. Bullard, B. D., and P. C. Dowdy. "Pulse Doppler Signature of a Rotary-Wing Aircraft." *Proc. 1991 IEEE National Radar Conf.*, Los Angeles, CA, March 12–13, 1991, pp. 160–163.

114. Fliss, G. G., and D. L. Mensa. "Instrumentation for RCS Measurements of Modulation Spectra of Aircraft Blades." *Proc. IEEE 1986 National Radar Conf.*, pp. 95–99.

115. Kulpa, K., Z. Czekala, J. Misiurewicz, and J. Falkiewicz. "Parametric Detection of the Helicopter Hub Echo." *Proc. 1999 IEEE Radar Conf.*, Waltham, MA, pp. 262–266, IEEE Catalog No. 99CH36249.

116. Gardner, R. E. "Doppler Spectral Characteristics of Aircraft Radar Targets at S-Band." Naval Reserach Laboratory, Washington, D.C., Report 5656, August 3, 1961.

117. Bell, M. R., and R. A. Grubbs. "JEM Modeling and Measurement for Radar Target Identification." *IEEE Trans.* AES-29 (January 1993), pp. 73–87.

118. Copeland, J. R. "Radar Target Classification by Polarization Properties." *Proc. IRE* 48 (July 1960), pp. 1290–1296.

119. Holm, W. A. "Polarimetric Fundamentals and Techniques." *Principles of Modern Radar*, J. L. Eaves and E. K. Reedy (Eds.). New York: Van Nostrand Reinhold, 1987, chap. 20.

120. Evans, D. L., T. G. Farr, J. J. Van Zyl, and H. A. Zebker. "Radar Polarimetry: Analysis Tools and Applications." *IEEE Trans.* GRS-26 (November 1988), pp. 774–789.

121. Boerner, W. M., W-L Yan, A-Q Xi, and Y. Yamaguchi. "On the Basic Principles of Radar Polarimetry: the Target Characteristic Polarization State Theory of Kennaugh, Huynen's Polarization Fork Concept, and Its Extension to the Partially Polarized Case." *Proc. IEEE* 79 (October 1991), pp. 1538–1550.

122. Giuli, D. "Polarization Diversity in Radars." *Proc. IEEE* 74 (February 1986), pp. 245–269.

123. Howard, D. D. "High Range-Resolution Monopulse Radar." *IEEE Trans.* AES-11 (September 1975), pp. 749–755.

124. Ksienski, A. A., Y. T. Lin, and L. J. White. "Low-Frequency Approach to Target Identification." *Proc. IEEE* 63 (December 1975), pp. 1651–1660.

125. Lin, H., and A. A. Ksienski. "Optimum Frequencies for Aircraft Classification." *IEEE Trans.* AES-17 (September 1981), pp. 656–665.

126. Chuang, C. W., and D. L. Moffatt. "Natural Resonances of Radar Targets via Prony's Method and Target Discrimination." *IEEE Trans.* AES-12 (November 1976), pp. 583–589.

127. Moffatt, D. L., and R. K. Mains. "Detection and Discrimination of Radar Targets." *IEEE Trans.* AP-23 (May 1975), pp. 358–367.

128. Baum, C. E., E. J. Rothwell, K-M Chen, and D. P. Nyquist. "The Singularity Expansion Method and Its Application to Target Identification." *Proc. IEEE* 79 (October 1991), pp. 1481–1492.

129. Dudley, D. G. "Progress in Identification of Electromagnetic Systems." *IEEE Ant. and Prop. Society Newsletter* (August 1988), pp. 5–11.

130. Fok, F. Y. S., and D. L. Moffatt. "The K-Pulse and E-Pulse." *IEEE Trans.* AP-35 (November 1987), pp. 1325–1326.

131. Chen, K-M, D. P. Nyquist, E. J. Rothwell, L. L. Webb, and B. Drachman. "Radar Target Discrimination by Convolution of Radar Return with Extinction-Pulse and Single-Mode Extraction Signals." *IEEE Trans.* AP-34 (July 1986), pp. 896–904.

132. Optiz, C. L. "Metal-Detecting Radar Rejects Clutter Naturally." *Microwaves* 15 (August 1976), pp. 12–14.

133. Harger, R. G. "Harmonic Radar Systems for Near-Ground In-Foliage Nonlinear Scatterers." *IEEE Trans.* AES-12 (March 1976), pp. 230–245.

134. Flemming, M. A., F. H. Mullins, and A. W. D. Watson. "Harmonic Radar Detection Systems." *IEE RADAR-77 International Conf.,* October 25–28, pp. 552–554, 1977.

135. Powers, E. J., J. Y. Hong, and Y. C. Kim. "Cross Sections and Radar Equation for Nonlinear Scatterers." *IEEE Trans.* AES-17 (July 1981), pp. 602–605.

136. Hong, J. Y., and E. J. Powers. "Detection of Weak Third Harmonic Backscatter from Nonlinear Metal Targets." *IEEE Eascon-83,* September 19–21, 1983, pp. 169–175, 83CH1967-9, ISSN:0531-6863.

137. Bahr, A. J., and J. P. Petro. "On the RF Frequency Dependence of the Scattered Spectral Energy Produced by Intermittent Contacts Among the Elements of a Target." *IEEE Trans.* AP-25 (July 1978), pp. 618–621.

138. Newburgh, R. G. "Basic Investigation of the RADAM Effect." Rome Air Development Center, Rome, N.Y., Report RADC-TR-151, June 1978.

139. Trunk, G. V., and J. D. Wilson. "Association of DF Bearing Measurements With Radar Tracks." *IEEE Trans.* AES-23 (July 1987), pp. 438–447.

140. Saha, R. K. "Analytical Evaluation of an ESM/Radar Track Association Algorithm." *SPIE* 1698, "Signal and Data Processing of Small Targets." (1992), pp. 338–347.

141. Farina, A., and B. La Scala. "Methods for the Association of Active and Passive Tracks for Airborne Sensors." *International Radar Symposium,* Munich, Germany, September, 1998.

142. Hawkins, C. F. "Friendly Fire: Facts, Myths and Misperceptions." *Proc. U.S. Naval Institute* 120 (June 1994), pp. 54–59.

143. Silberman, G. L. "Parametric Classification Techniques for Theater Ballistic Missile Defense." *Johns Hopkins APL Technical Digest* 19, no. 3 (1998), pp. 322–339.

144. Heiss, W. H., D. L. McGrew, and D. Sirmans. "Nexrad: Next Generation Weather Radar (WSR-88D)." *Microwave J.* 33 (January 1990), pp. 79–98.

145. Crum, T. D., and R. L. Alberty. "The WSR-88D and the WSR-88D Operational Support Facility." *Bulletin of the American Meteorological Society* 74 (September 1993), pp. 1669–1687.

146. Dudgen, D. E., and R. T. Lacoss. "An Overview of Automatic Target Recognition." MIT Lincoln Laboratory Journal, "Special Issue on Automatic Target Recognition," vol. 6, pp. 3–10, Spring 1993.

147. Sheen, D. R. et al. "The P-3 Ultra-Wideband SAR: Description and Examples." *Proc. 1996 IEEE National Radar Conf.*, pp. 50–53, IEEE Catalog no. 96CH35891.

148. Vaughn, C. R. "Birds and Insects as Radar Targets: A Review." *Proc. IEEE* 73 (February 1985), pp. 205–227.

149. Chen, K-M, et al. "An X-Band Microwave Life-Detection System." *IEEE Trans.* BME-33 (July 1986), pp. 697–701.

150. Geisheimer, J. "A Radar System for Monitoring Human Vital Signs." *IEEE Potentials* 17 (January 1999), pp. 21–24.

PROBLEMS

6.1 (a) Sketch the rms range error (in meters) for a quasi-rectangular pulse with a half-power pulse width of 2 μs, as a function of the peak-signal-to-mean-noise ratio ($2E/N_0$) over the range of values from 10 to 60 dB. (b) Why might it not be appropriate to consider signal-to-noise ratios below 10 dB and above 60 dB?

6.2 Derive the rms error in measuring the time delay for a gaussian pulse of half-power width τ [Eq. (6.17)].

6.3 Based on the measurement of doppler frequency shift, sketch the rms error of the radial velocity (in meters) as a function of the width τ of a rectangular pulse when the pulse width varies from 1 μs to 10 ms for (a) constant pulse energy and (b) constant peak power. The frequency is 5400 MHz. Assume in both cases that $2E/N_0 = 36$ when the pulse width is 1 μs.

6.4 (a) What is the minimum width τ of a rectangular pulse that can be used with an X-band radar (9375 MHz) if it is desired to achieve a 10 kt radial velocity accuracy (based on the doppler frequency measured by a single pulse), when $2E/N_0 = 23$ dB? (b) What is the minimum range (in nautical miles) that corresponds to this pulse width? (c) In part (a) of this question, what should be the value of $2E/N_0$ (in dB) to achieve a 10 kt radial velocity accuracy if the pulse width can be no longer than 10 μs? (d) What would be the minimum pulse width in (a) if the radar operated at W band (94 GHz)? (e) Comment on the utility of accurately measuring the velocity with a single short pulse.

6.5 There are two methods for finding the radial velocity of a target. One is based on the doppler shift $f_d = 2v_r/\lambda$; the other is based on the rate of change of range with time $\Delta R/\Delta t$. They give different measurement accuracies. (a) What is the expression for the radial velocity error, δv_d, found by measuring the doppler frequency shift of a long quasi-rectangular pulse of width τ and RF frequency f_0? (b) What is the expression for the radial velocity error, δv_r, found from the rate of change of range based on two range measurements R_1 and R_2 separated by a time τ, so that the velocity is $v_r = (R_2 - R_1)/\tau$, and τ is

the same as the pulse width of the doppler measurements? The pulses in this range-rate measurement are of gaussian shape with a half-power bandwidth B [use right-hand side of Eq. (6.17)]. Assume the total value of $2E/N_0$ in each of these two methods for radial velocity measurement [(a) and (b)] is the same. (c) What is the value of $\delta v_d/\delta v_r$? (d) Based on your answer in (c), which is the more accurate method of velocity measurement, the doppler method or the range-rate method? (e) Under what conditions will these two methods give comparable accuracies (assuming the same total $2E/N_0$)? (f) Why do you think the doppler method has not been used very often for a velocity measurement?

6.6 (a) What value of $2E/N_0$ (in dB) is required to achieve an angular accuracy of 0.3 mrad when the antenna beamwidth is one deg, assuming the antenna has a cosine aperture illumination? (b) If the signal received by this radar antenna has a value of $2E/N_0 = 23$ dB for a particular target at a range of 150 nmi, at what range will the radar first be capable of obtaining an angular accuracy of 0.3 mrad?

6.7 Determine $\beta\alpha$ (the product of the effective pulse width β and the effective time duration α) for the following: (a) gaussian pulse, (b) triangular pulse, and (c) quasi-rectangular pulse. (Use the expressions for β and α already given in the text.) (d) Based on the above answers, how much flexibility is there in selecting one of these simple waveforms to achieve a large value of $\beta\alpha$ for the purpose of making an accurate measurement of both time delay and frequency? (e) What option, other than a large $\beta\alpha$, is available for obtaining an accurate measurement of both time delay and frequency simultaneously?

6.8 Derive the rms error in measuring frequency for a rectangular pulse of width τ (Eq. 6.24).

6.9 How is the rms error in measuring frequency affected when the width of a rectangular pulse is increased by a factor of four, with the peak power remaining constant?

6.10 (a) A K-band (24.15 GHz) radar speed-gun, used for measuring the speed of an auto or a baseball, has a claimed accuracy of 0.1 statute mile/hour. If the signal-to-noise ratio ($2E/N_0$) is 17 dB, what observation time is needed to achieve this accuracy? (b) How far does a car with a speed of 60 mph travel during this time? (c) Assuming the same obervation time and value of $2E/N_0$ as in part (a), what would be the accuracy of an X-band (10.525 GHz) radar speed-gun?

6.11 Using the first part of Eq. 6.21, $\beta^2 E = \int_{-\infty}^{\infty} [s'(t)]^2\, dt$, show that the rms error in measuring the time delay of a trapezoidal pulse is the same as that given by Eq. (6.14).

6.12 Find the values of the effective bandwidth β and the effective time duration α for a different quasi-rectangular pulse formed by taking the bandwidth B_s [in Fig. 6.2 and Eq. (6.9)] extending from $-2/\tau_r$ to $+2/\tau_r$, where τ_r is the width of the original rectangular pulse. Thus $B_s\tau_r = 4$. (You will have to look up values of the sine integral function.) Estimate the half-power width τ of the time waveform given for this case (you might have to plot the output pulse). Express β and α in terms of the half-power width τ.

6.13 Using the definition of β [Eq. (6.8)], definition of α [Eq. (6.23)], Eq. (6.21), Parseval's relation [Eq. (5.13)], Schwartz inequality, [Eq. (5.11)], and performing integration by parts, show that $\beta\alpha \geq \pi$ and that the equality holds for the gaussian function. (Only for those who enjoy a mathematical exercise.)

6.14 Show that $\int (2\pi f)^2 |S(f)|^2\, df = -\int s''(t)s(t)dt = \int [s'(t)]^2\, dt$, which is Eq. (6.21). The limits of all integrals are from $-\infty$ to $+\infty$. (Start with $s(t)$ expressed as an inverse Fourier transform of $S(f)$, and differentiate $s(t)$ twice.)

6.15 What is the message of the radar "uncertainty principle"?

6.16 Show that the rms error for the measurement of the phase of a sinewave is $\delta\phi = (2S/N)^{-1/2}$, where S/N is the signal-to-noise ratio. [This can be obtained from the error in making a measurement of the time when a sinewave crosses the time axis. Note that phase ϕ is equal to $2\pi ft$, so that $\delta\phi = 2\pi f\, \delta t$. The derivation is similar to that given for the rectangular pulse that led to Eq. (6.4), except that the time is measured when the sinewave crosses the time axis once.]

6.17 What information about the radar waveform can be obtained from the ambiguity diagram?

6.18 The amplitude of the peak of the signal out of a matched filter is $2E$, where E is the signal energy. This can be seen from Eq. (6.42). A peak output of $2E$ implies that the output has units of energy [(volts)^2 $\times$ time], but this cannot be so since the output of a filter should have volts as the unit. Show that the unit for the output of the matched filter is actually volts and not energy. (This is related to problem 5.6.)

6.19 Explain qualitatively (no derivation needed) why the ambiguity diagram shown in Fig. 6.9 is that of a down-chirp; i. e., frequency of the linear FM waveform decreases with time.

6.20 (a) Why might one want to use both an up-chirp and a down-chirp waveform on two successive pulses in a linear-FM pulse-compression radar system? (b) When might one use a waveform with the following three contiguous parts: (1) an unmodulated CW waveform, (2) a down-chirp and (3) an up-chirp? (c) Why might one want a radar to operate with an up-chirp when another similar nearby radar operates with a down-chirp?

6.21 A C-band (5.5 GHz) ballistic-missile detection radar employs a linear-FM pulse-compression radar with a 1.0-ms uncompressed pulse-width having a down-chirp covering a bandwidth of 200 MHz. If the target has a radial velocity of 2 km/s, what is the error in range (km) due to the doppler shift of the target? What is the range error in terms of the resolution of the compressed pulse?

6.22 Determine the shift in the time delay ΔT_r with a linear-FM pulse-compression waveform whose bandwidth is B and time duration is T when the target experiences a doppler frequency shift f_d for the following two cases: (a) Ballistic-missile-detection radar with $B = 1$ MHz and $T = 1$ ms, when $f_d = 100$ kHz. (b) Aircraft-detection radar with $B = 100$ MHz and $T = 10$ μs, when $f_d = 1$ kHz. In each of the two cases: (c) What is the doppler-caused time-shift error, measured in meters of range? (d) What is the ratio of the doppler-caused time shift and the resolution in time delay of the waveform (which you may assume to be $1/B$)?

6.23 How can one find the true range and true doppler frequency shift of a target when using linear-FM pulse-compression waveforms?

6.24 In this problem two nearby aircraft are both located within the antenna beam, but one is trailing slightly behind the other. The trailing aircraft has a slower speed than the leading

aircraft. They are being detected by a linear-FM pulse-compression radar. Describe why, in this case, it is better to use an up-chirp rather than a down-chirp when it is desired to provide a wide separation between the two output echo signals.

6.25 (a) Show that the tapped delay line that generates a Barker code of length 5 can be used as a matched filter if the receive signal is inserted from the opposite end. (This can be shown by sketching the output of the matched filter.) (b) How can the dispersive filter used to generate a linear-FM (chirp) signal be used as the matched filter to receive the echo signal?

6.26 Show (simple diagrams are okay) that the two different Barker codes of length 4 in Table 6.4 are also complementary codes.

6.27 *Background:* Generally, one can assume that the doppler shift is constant across the spectrum of the echo signal. There are cases, however, where this is not so, as in the current problem. *Problem:* A ballistic missile detection radar is attempting to detect a target moving with a radial velocity of 2 nmi/s. The radar employs a linear-FM pulse-compression waveform with a bandwidth of 100 MHz. What is the longest pulse width that can be used before significant degradation of the compressed pulse width occurs? (See the discussion in the subsection *Doppler-Tolerant Pulse-Compression Waveforms.*)

6.28 In the previous problem, one might have used the criterion that $2BTv_r/c$ must not exceed unity. This criterion is based on the doppler at the leading edge of a long FM pulse of length T and bandwidth B being significantly different from the doppler at the trailing edge of the pulse when the target radial velocity is v_r. Derive the expression $2BTv_r/c < 1$. [One criterion that might be applied is to require the spread in the time-delay measurements caused by the difference in the doppler shifts at the leading and trailing edges of the pulse of duration T to be no greater than the spread $(1/B)$ in the time-delay measurement when the target is stationary (no doppler shift).]

6.29 A linear-FM pulse-compression radar has a bandwidth B and an uncompressed pulse duration T. The matched filter is followed by a sidelobe-reduction filter whose weighting function is

$$W(f) = \cos(\pi f/B)\ \text{rect}(f/B)$$

where $\text{rect}(x) = 1$ for $|x| < 1/2$ and equals 0 for $|x| > 1/2$. The signal spectrum at the output of the matched filter is rectangular and is given as

$$S_m(f) = \sqrt{T/B}\ \text{rect}(f/B)$$

and the noise spectrum at the matched filter output is

$$N(f) = (N_0/2)\ \text{rect}(f/B)$$

Find:

a. The signal waveform $s_w(t)$ at the output of the sidelobe-reduction filter.
b. The loss in signal-to-noise ratio due to the sidelobe-reduction filter.
c. The level of the first sidelobe of the output waveform $s_w(t)$.

(Acknowledgment: This problem was generously given to the author by an instructor of a radar course in Huntsville, Alabama many years ago. He used it as part of a take-home exam. Unfortunately, over the years I lost his name, but wish to acknowledge, with gratitude, my use of his problem here and throughout the years in my own radar course.)

6.30 An *X*-band (9.5 GHz) ground-based ISAR (inverse synthetic aperture radar) is imaging an aircraft at a range of 20 nmi. The aircraft is traveling at a speed of 250 kt and is on a tangential trajectory (i.e., it is perpendicular to the radar line of sight). The ISAR image is obtained as the aircraft is viewed broadside to the radar line of sight, so that the viewing aspect is 90° or in close vicinity to it. What must the total radar observation time be in order to obtain an image with a cross-range resolution of 1 m?

6.31 What effect might the echo from a rapidly rotating antenna located within a range-resolution cell of an ISAR have on the ISAR image of the target?

6.32 A ground-based *S*-band (3.2 GHz) radar is observing a helicopter. One may assume that the velocity of the tip of the blade of a helicopter is 210 m/s and that the length of a blade is 6 m.

a. What is the time between blade flashes for a two-blade and a three-blade helicopter?
b. What is the time duration of the blade flash for a two-blade and a three-blade helicopter?
c. If the radar antenna has an azimuth beamwidth of 3°, at what rpm must the antenna be rotated in order to insure that the blade flash will be detected on each scan of the antenna?
d. What must the prf of the radar be to insure that there are at least five pulses received from the blade flash?
e. What is the radar cross section of the blade flash for an odd number of blades?
f. If the helicopter is hovering, what is the maximum doppler shift that might be obtained from the helicopter blades?
g. What is the maximum forward speed (kt) that a helicopter can have if the actual velocity of the tip is to be less than 0.8 of Mach 1? (Mach 1 can be assumed to be 343 m/s.) What is the maximum doppler shift of the radar echo from the helicopter blade?

6.33 (a) What options are available for reliably recognizing one aircraft target from another by noncooperative methods? (b) Describe how one might reliably recognize a ship target by noncooperative methods. (c) Describe how one might reliably recognize a helicopter target by noncooperative methods.

6.34 It has sometimes been said that two pulse signals, one at frequency f_1 and the other at frequency f_2, each of width τ, can be resolved (separated by filters) by a radar if the number of cycles within the pulse width τ at frequency f_1 differs by at least one from the number of cycles within the pulse width τ at frequency f_2. (a) Show that this criterion for resolution is equivalent to the more usual criterion that $|f_1 - f_2| \geq 1/\tau$. (b) A long-range UHF radar (440 MHz) for the detection of satellites is assumed to have a pulse width of

2 ms. What is the minimum difference in radial velocity of two targets that will allow them to be separated by doppler filtering?

6.35 A linear-FM waveform and a $(\sin \pi ft)/\pi ft$ waveform both have a uniform power spectrum. Does that mean they both can use the same pulse compression filter? (More than a simple yes or no answer would be nice.)

6.36 It was said in Sec. 6.5 in the discussion of linear-FM pulse-compression that the true range of a target can be found by using both an up-chirp and a down-chirp waveform, and taking the average of the two time delays. It is also possible to obtain the true doppler frequency shift using the same two measurements of time delay from the up-chirp and down-chirp waveforms. (This was Problem 6.23.) Derive an expression for the rms accuracy of the frequency measurement found from the two time delay measurements when the frequency extent of the linear FM is B and the time duration is T.